NASA SP-50

N64-30251 N64-30302
(ACCESSION NUMBER) (THRU) 51
433 1
(PAGES) (CODE)
28
(NASA CR OR TMX OR AD NUMBER) (CATEGORY)
FACILITY FORM 602

THE PHYSICS OF SOLAR FLARES

GODDARD SPACE FLIGHT CENTER
GREENBELT, MARYLAND
OCTOBER 28-30
1963

52

NASA SP-50

AAS-NASA SYMPOSIUM ON THE PHYSICS OF SOLAR FLARES

Proceedings of a symposium held at the Goddard Space Flight Center, Greenbelt, Maryland, October 28-30, 1963.

Edited by
Wilmot N. Hess
Goddard Space Flight Center

Scientific and Technical Information Division 1964
NATIONAL AERONAUTICS AND SPACE ADMINISTRATION
Washington, D.C.

For sale by the Superintendent of Documents, U.S. Government Printing Office
Washington, D.C., 20402 Price $3.25

CONTENTS

PAGE

INTRODUCTION, by W. N. Hess vii

OCTOBER 28

I. OBSERVATIONS ON FLARES

Session A

Chairman: John Firor

STRUCTURE, MOTION, AND DEVELOPMENT OF FLARES

1. Solar Flares: Their Structure, Development, and Motion, by H. J. Smith 1
2. Moving Material Accompanying the Flare of 1959 July $16^d21^h14^m$ UT, by H. W. Dodson and E. R. Hedeman 15
3. Optical Characteristics of Chromospheric Flares Associated With Type IV Radio Bursts or Noise Storms, by Y. Avignon, C. Caroubalos, M. Martres-Tropé, and M. Pick 25
4. Flare Importance Ratings—Some Hope for Improvement, by C. S. Warwick 27

Summaries of Two Recent Publications by J. M. Slonim and S. I. Gopasyuk et al., contributed by E. R. Mustel 29

SPECTROGRAPHIC OBSERVATIONS

5. Spectrographic Observations, by H. Zirin 33
6. Time Variations in the Solar Extreme Ultraviolet Spectrum Observed by OSO I, by W. M. Neupert 49
7. Solar Flares in the Light of Hydrogen Lyman-Alpha, by K. L. Hallam 63
8. Broadening and Asymmetry of the Emission Lines in Flares, by M. C. Ballario 65
9. Solar Flares and the Loop Prominence Mechanism, by J. T. Jefferies and F. Q. Orrall 71
10. Mass Balance in Flare Loops, by J. Kleczek 77
11. On the Stark Broadening of High Balmer Lines Emitted by Solar Flares, by L. D. de Feiter 81

MAGNETIC OBSERVATIONS

12. Magnetic Observations Relating to Solar Flares, by R. Howard 89
13. On the Behavior of Magnetic Fields Associated with Solar Flares, by A. B. Severny 95
14. Association of Flares With Stationary Points of Zero Magnetic Field, by J. Weddell 103
15. On the Observable Effects of Magnetic Energy Storage and Release Connected With Solar Flares, by H. U. Schmidt 107

Session B

Chairman: Frederick T. Haddock

X-RAY AND GAMMA RAY BURSTS

16. Energetic X-Ray Bursts From Solar Flares, by J. R. Winckler 117
17. Solar X Rays: A Comparison With Microwave Radiation, by W. A. White 131
18. Comments on High Energy X-Ray Bursts Observed by OSO I, by K. J. Frost 139
19. Comments on Gamma Rays, by G. G. Fazio 145
20. Solar X-Ray Emission—NRL Results, by H. Friedman 147

RADIO BURSTS

21. Radio Observations of Solar Flares, by J. P. Wild 161
22. The Slowly Varying Component of Solar Radio Emission, by G. Swarup 179

PAGE

23. Study of Solar Noise Storms at 169 Mc/s With the Aid of the Nancay Interferometer, by A. M. Le Squeren 199
24. Study of the Slowly Varying Component at 9400 Mc/s as a Function of Solar Activity, by C. Caroubalos 203
25. Active Dark Filaments and Type III Bursts, by T. Takakura and T. Tlamicha 207
26. The Association of Bremsstrahlung X Rays With Explosive Flares, by G. E. Moreton 209

OCTOBER 29

I. OBSERVATIONS ON FLARES—Continued

Session C

Chairman: Frank B. McDonald

ENERGETIC PARTICLES

27. A Review of Solar Cosmic Ray Events, by W. R. Webber 215
28. The Association of Energetic Particles With Solar Flares, by J. M. Malville 257
29. Charge Composition of Energetic Solar Particles, by C. E. Fichtel 263
30. Mariner Solar Wind Measurement, by C. W. Snyder 273
31. Solar Surface Nuclear Reactions, by E. L. Fireman 279
32. Some Properties of Corpuscular Streams From the Chromospheric Flares, by E. R. Mustel and N. B. Egorova 285
33. On the Possible Role of Flare-Like Nonstationary Processes in the Origin of Solar Wind, by E. R. Mustel 287
34. Velocity Dependence and Source Spectra of Solar Proton Events, by D. A. Bryant, T. L. Cline, U. D. Desai, and F. B. McDonald 289

Session D

Chairman: John C. Lindsay

COMBINATIONS OF OBSERVATIONS

35. Case Histories of Flares: The Large Flares of July 11, 12, 18, and 20, 1961, by A. Bruzek 301
36. An Assembly of Flare Observations as Related to Theory, by K. O. Kiepenheuer 323

OCTOBER 30

II. THEORY OF FLARES

Session A

Chairman: William C. Erickson

RADIO AND X-RAY EMISSION

37. A Survey of the Interpretations of Radio and X-Ray Bursts, by M. R. Kundu 335
38. On the Generation of Solar Radio Bursts, by S. F. Smerd 343
39. Type III Solar Radio Bursts, by P. A. Sturrock 357
40. Some Notes on the Relations of X-Ray, Particle, and Radio Emission of the Sun During Flares, by G. Elwert 365
41. Radiofrequency Radiation and Particle Acceleration From Solar Flare Filaments Due to Collective Motion at Multiples of the Cyclotron Frequency, by R. L. Moore and J. R. Johnston 371
42. Electromagnetic Radiation From Plasma Oscillations, by L. Oster and M. Altschuler 377
43. Type II Bursts and the Magnetic Field in the Corona, by T. Takakura 383

Session B

Chairman: Leo Goldberg

ORIGIN AND PARTICLE ACCELERATION

44. Magnetic Energy Shedding in the Solar Atmosphere, by T. Gold 389

CONTENTS

PAGE

45. The Origin of Solar Flares and the Acceleration of Charged Particles, by D. G. Wentzel ---- 397
46. Instability Problems in the Origin of Sclar Flares, by P. A. Sweet ---- 409
47. Remarks on the Discharge Theory of Flares, by J. W. Dungey ---- 415
48. Comments on Understanding the Solar Flare, by E. N. Parker ---- 417
49. A Mechanism for the Dissipation of the Magnetic Field in Solar Flares, by R. K. Jaggi ---- 419
50. Magnetic Field Annihilation, by H. E. Petschek ---- 425
51. Stability of the Solar Magnetic Field in the Region of Flares, by J. W. Warwick ---- 441
52. Solar Magnetic Fields and Spacecraft Observations, by L. Davis, Jr. ---- 443
53. Production of Gamma Rays and Neutrons in Solar Flare Regions, by E. L. Chupp ---- 445
54. A Process for Flares, by H. Carmichael ---- 451

Summary of a Recent Publication by E. E. Dubov, contributed by E. R. Mustel ---- 457

APPENDIX

Attendees at the Symposium on Solar Flares ---- 459

INTRODUCTION

The study of solar flares is a field of continually increasing interest pursued by more and more people. The subject is over 100 years old, but it has been expanding considerably of late. A brief chronology of the subject will show the motivation for calling the conference held at The Goddard Space Flight Center on October 28–30, 1963.

Optical observations of flares have been made since 1859, when Carrington and Hodgson observed the first solar flare in white light. In the 1860's spectroscopic flare studies were begun, and in 1926 the spectroheliograph was introduced by Hale to give pictures of the sun in one wavelength. Optical measurements have been used in international solar flare patrols since the early 1930's, when the International Astronomical Union (IAU) organized a patrol. The efforts during the International Geophysical Year (IGY) in 1958–1959 made the existing patrol nearly complete, helped standardize data collections and analysis, and provided a worldwide flare monitoring service to researchers.

In the past few years since the IGY, optical work has progressed to include on- and off-line spectroheliographs to study motions by the Doppler shift; spectroheliographic cinematography to study motions and time histories of flares; large wavelength range spectrographs to study line profiles, relative line intensities, and time variations of these parameters; and the use of Zeeman splitting to study the photospheric magnetic fields, both longitudinal and (more rarely) transverse, associated with flares.

Radio emission from the sun has been studied since 1942, but especially in the last 10 years the different kinds of radio bursts have been sorted out and their relation to flares established. The tentative identification of bremsstrahlung and synchrotron radiation from fast electrons as well as plasma radiation ties this subject closely to other fields of flare study.

In the late 1940's the Naval Research Laboratory (NRL) group started using rockets to study flares and found a large increase of soft x rays at the time of flares. Eclipse measurements and a pin-hole-camera x-ray photograph showed the relation of x-ray emission to active areas. In 1958 Winckler observed x rays of greater than 20 kev associated with flares using balloon-borne detectors. For large flares, later balloon flights showed x rays extending above 100 kev.

In 1946 it was recognized that the sun could produce energetic particles at the time of flares and on February 23, 1956, a large cosmic ray event was studied in considerable detail by ground-based and balloon-borne detectors. Starting with the IGY, many measurements have been made on the more frequent medium-energy solar cosmic rays ($10<E<500$ Mev) by balloons, rockets, and satellites. Their energy spectra, charge composition, and time histories related to flares have been measured for many events.

Satellites have contributed substantially to the knowledge of flare processes. The Solar Radiation I satellite of NRL launched in 1960 and SR III in 1961 showed the relation between soft x-ray and flare occurrence. Several satellites including Explorers VI, VII, XII, and XIV have studied solar proton events in great detail. The NASA OSO I satellite launched on March 7, 1962, has made

extensive measurements of the sun in the UV and x-ray region and shows details of solar emission at the time of flares in these energy intervals. The NASA AOSO satellite, which is planned for launching in 1967, will be able to point to any location on the solar disk to an accuracy of ± 5 seconds of arc. Instruments on this vehicle aimed at flares should help considerably in our understanding of them.

The first theoretical model of a flare that viewed the process as electromagnetic in nature was by Giovanelli in 1946. Extensions and amplifications of this and other models by Hoyle, Dungey, Gold, Sweet, Severny, and Parker are still coming out regularly.

This short and incomplete history of flare studies was included here, first, to show how many different areas of research are included in flare investigations and, second, to show how recent much of the data available on flares is. A large fraction of current flare information is less than 10 years old. Because of the rapid recent development of the field it seemed appropriate to call together specialists from several disciplines to produce a status report on the subject. To this end, a symposium was organized jointly by NASA and the American Astronomical Society and was held at Goddard on October 28–30, 1963. The organizing committee consisted of:

Dr. W. Hess (Chairman), Goddard Space Flight Center
Prof. L. Goldberg, Harvard College Observatory
Prof. F. Haddock, University of Michigan
Dr. J. Firor, High Altitude Observatory
Dr. A. Cameron, Institute for Space Studies
Dr. F. McDonald, Goddard Space Flight Center
Dr. J. Lindsay, Goddard Space Flight Center

This document is the proceedings of the symposium, with several papers added.

In reviewing these proceedings, it will be obvious that the flare problem is not solved. A frequently used definition of a solar flare is "a sudden short-lived brightening of a localized area of the chromosphere." The qualitative and fragmentary nature of this statement is some indication of the state of the subject. We know that flares are complex phenomena involving several forms of strong radio emission, hard x rays, protons of energies up to a few Bev, energetic electrons, and shock waves. The visible flare may well be a secondary effect, and the real flare process invisible by our present observational techniques. This situation allows the theorist a fair amount of freedom. He can and does talk about discharges of meters thickness at magnetic neutral points and also about large scale motion of energetic particles up through the photosphere in an invisible fashion.

We are clearly a long way from understanding about flares in detail, but this conference served the very useful purpose of outlining the important problem areas and framing a number of questions for future work.

WILMOT N. HESS

I OBSERVATIONS ON FLARES

SESSION A

Chairman, Dr. JOHN FIROR

N64 30252

1 SOLAR FLARES: THEIR STRUCTURE, DEVELOPMENT, and MOTION

HENRY J. SMITH
National Aeronautics and Space Administration
Washington, D.C.

To begin this symposium on the physics of solar flares, it would be well to have a working definition of what we mean by the term *flare*. Our French and German colleagues use the word *eruption*, which Hale employed first some 71 years ago. To some of us, however, this term connotes the explosive ejection of material, which is not a conspicuous feature of all flares. Richardson, therefore, 2 solar cycles ago, encouraged the use of the word *flare*, which the dictionary defines as an "unsteady glaring light." An astronomer using a conventional monochromatic photoheliocinematograph might be content with the following simple operational definition: "A flare is a sudden transient localized brightening of the chromosphere."

Some flares are found to be accompanied by bursts of soft x rays, or of energetic particles, or of certain spectral types of radio emission—separately, or together, or sometimes not at all. We shall all doubtless wish to continue using the word *flare* to describe the totality of the phenomenon, or sometimes some non-optical parts of it. But *invisible flares*, according to this definition, are an impossibility. We must be constantly aware of those chromospheric brightenings not accompanied by radio frequency or energetic photon emission. Perhaps the word *eruption* ought to be re-established to deal with the other class of energetic solar events which proceed without chromospheric visible counterpart.

About 30 years ago Hale organized a number of astronomical observatories around the world to participate in an international cooperative program to patrol the occurrence of solar flares. With the exception of an interruption during the years of World War II, this patrol has continued successfully since its founding. The results, a monumental record of the devotion of two generations of observers to this demanding goal, are available to all of us in the "Quarterly Bulletin of Solar Activity" published by the International Astronomical Union. From the many tens of thousands of individual reports of chromospheric flares, we can derive some simple but basic data describing the essential characteristics of flares and the circumstances of their occurrence. The Quarterly Bulletins provide information on the following observable parameters of each flare:

1. A flare's position is reported in *heliographic latitude* and *central-meridian distance*.
2. The *times* of first brightening, of maximum brightness, and at which the event is essentially concluded.
3. The *area* of maximum brightness of the flare, quoted in square equatorial heliographic degrees ($1° = 12{,}140$ kilometers). (Usually the time of maximum brightness coincides with the time of maximum area, but in some flares these times are not coincident.)
4. Some observatories measure and report the *brightness* of flares. These measures refer to the most intense part of the flare and are generally quoted in terms of the brightness of an undisturbed region near the center of the disk, either in terms of chromospheric brightness seen through the monochromator, or of the continuum at approximately the wavelength of H-alpha ($H\alpha$).
5. The *importance* of the flare is a complicated function of the above parameters (location, area, and brightness) but also of some ill defined subjective impression of the observer of its energetic character. Importance, as strictly

defined, is a measure of the area of a flare as if it were seen at the center of the disk. The largest flares are called Importance 3 and 3+; smaller flares of Importance 2 and Importance 1, in succession; and the most minute events (not reported completely except by a few observatories) are subflares of Importance 1−.

The very abundant data on flares provided by the Quarterly Bulletins suffer from rather severe inhomogeneities. These result in part from limitations of observations through narrow bandwidth monochromators. Quite startling systematic differences in the appearance and behavior of flares result from rather subtle changes not only in the total width but even of the shape of the pass band of a monochromator. In addition, flare or *ejecta* motions in the line of sight produce a Doppler shift which drastically changes the morphological character of some chromospheric events.

The simple statistical analysis of the data on positions of flares reveals that they occur mostly in connection with, and close to, centers of solar activity. For example, Figure 1–1 shows the distribution in latitude of chromospheric flares observed during the International Geophysical Year (IGY). Flares, we know, occur mostly within a few tens of thousands of kilometers from a sunspot. (Sunspots occur in the zone about 15 degrees wide, centered at a latitude that migrates from 30 degrees at the beginning of a solar cycle to about 8 degrees latitude at the end of the cycle.) In consequence, flares occur at latitudes mainly between plus and minus 40 degrees relative to the sun's equator. Flares appear with slightly higher frequency either north or south of the equator, depending on which solar cycle is studied. The same north–south asymmetry has been detected in sunspots; like spots, the flare asymmetry varies in amplitude and even size from one extended period to another. The significance of this asymmetry is greater for spot physics than for flare physics.

The distribution of flare incidence in longitude, or rather meridional distance from the central meridian of the sun's apparent disk, shows on the contrary some significant facts about flares. Figure 1–2 shows flare incidence in 10 degree wide lines, separately for three different size groups of flares. The largest flares show a pronounced concentration near the central meridian. The smaller flares still exhibit this tendency; but the smallest ones, the subflares, reveal a central defect if anything at all. Right at the limb, on the contrary, there is a local enhancement of incidence for flares of all sizes, which is more pronounced for the smaller events. These distributive properties of flares can be accounted for simply enough by recognizing the essential geometric shapes of flares. The average flare is a flattened, slightly convex structure, subject to a varying measure of geometrical foreshortening as it is viewed from a slant perspective. Smaller flares preserve essentially the same heights as larger flares and

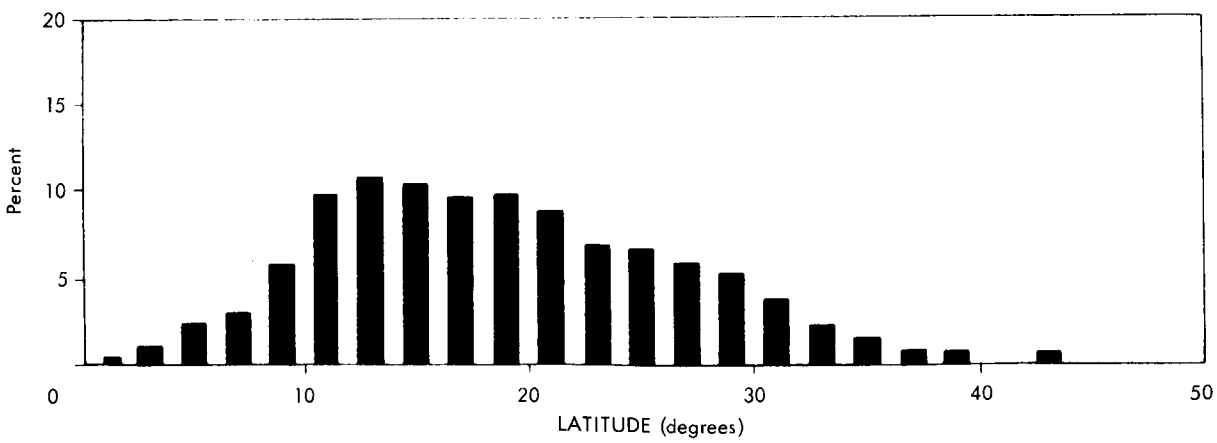

FIGURE 1–1. Distribution of flares in heliographic latitude.

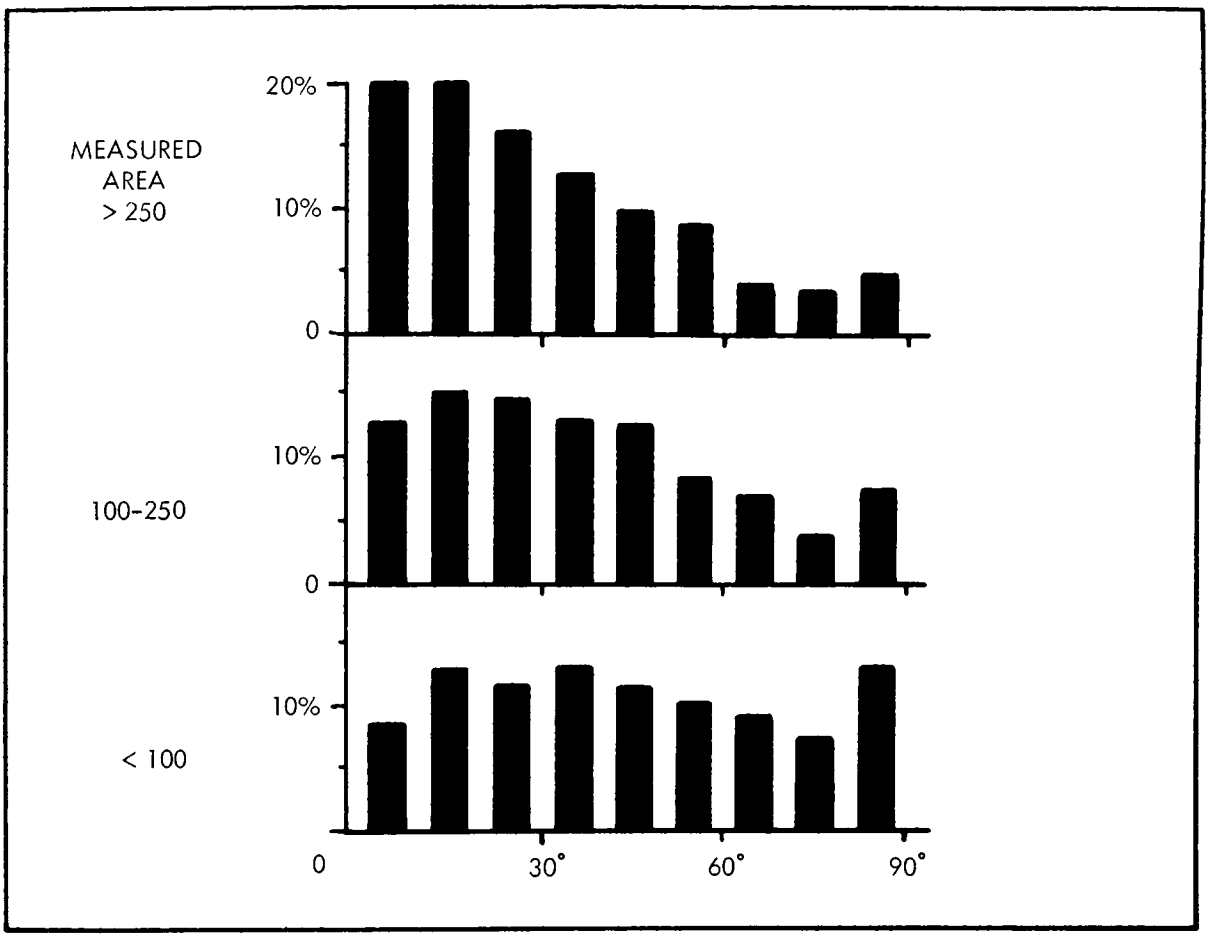

FIGURE 1–2. Distribution of flares in heliographic longitude.

therefore are less affected by foreshortening. The visibility functions in Figure 1–2 thus reveal evidence for the finite radial heights of flares but do not, in fact, suffice for the determinations of these heights. The excess of flares at the limb similarly bears testimony to flare heights, for we obviously are counting as smaller flares the tops of flares situated some distances beyond the limb.

Observers occasionally report the discovery of an asymmetry in the distribution of flares east or west of the meridian. Depending on the data sample used, slightly more flares are detected on the east or west half of the sun's disk. The usual proof of alleged reality is frequently based on an unsound argument of statistical theory, which does not adequately account for the tendency of flares to be congregated about active centers. This aggregating tendency lessens the improbability of the observed asymmetry, and this raises doubt as to its reality. In consequence, we need not feel compelled to entertain elaborate and implausible ideas of an average inclination of peculiarly shaped flares.

Flares occur close to activity centers; therefore, it is of interest to see how the flare incidence relates to some measurable parameters of these centers. During the IGY some 1556 spot groups were noted, but the Quarterly Bulletin tabulates only 652 active regions. We conclude at once that some regions at least produce not one but a multiplicity of spot groups. Observations reveal that these may appear either simultaneously or consecutively. The total lifespan of an active region is closely related to the measure of

activity associated with it, particularly its flare production. Not only do flares occur in proportion to the total lifetime of the associated regions but, most important, the probability of a large flare occurring is a strong function of total life. The following table illustrates this fact:

Region duration (rotations)	0–½	½–1½	1½–2½	3
Frequency (percent)	30	43	23	3. 4
Probability of great flare	0	0. 025	0. 07	0. 4

The region 57–JG produced a record performance during the IGY— four major flares in two successive rotations. In general (though not without exception) the occurrence of very large flares is associated in time with the frequent occurrence of numerous smaller flares. When one very large flare has erupted, the probability is very large that a second one will occur within the following fortnight or two. We note, however, that about 20 percent of small spot groups last less than 2 days and produce few or no flares at all. Flare incidence I^*, measured for instance as the monthly average number of flares per hour inferred to occur on the visible hemisphere, correlates moderately well with the monthly average sunspot number R (Figure 1–3). This correla-

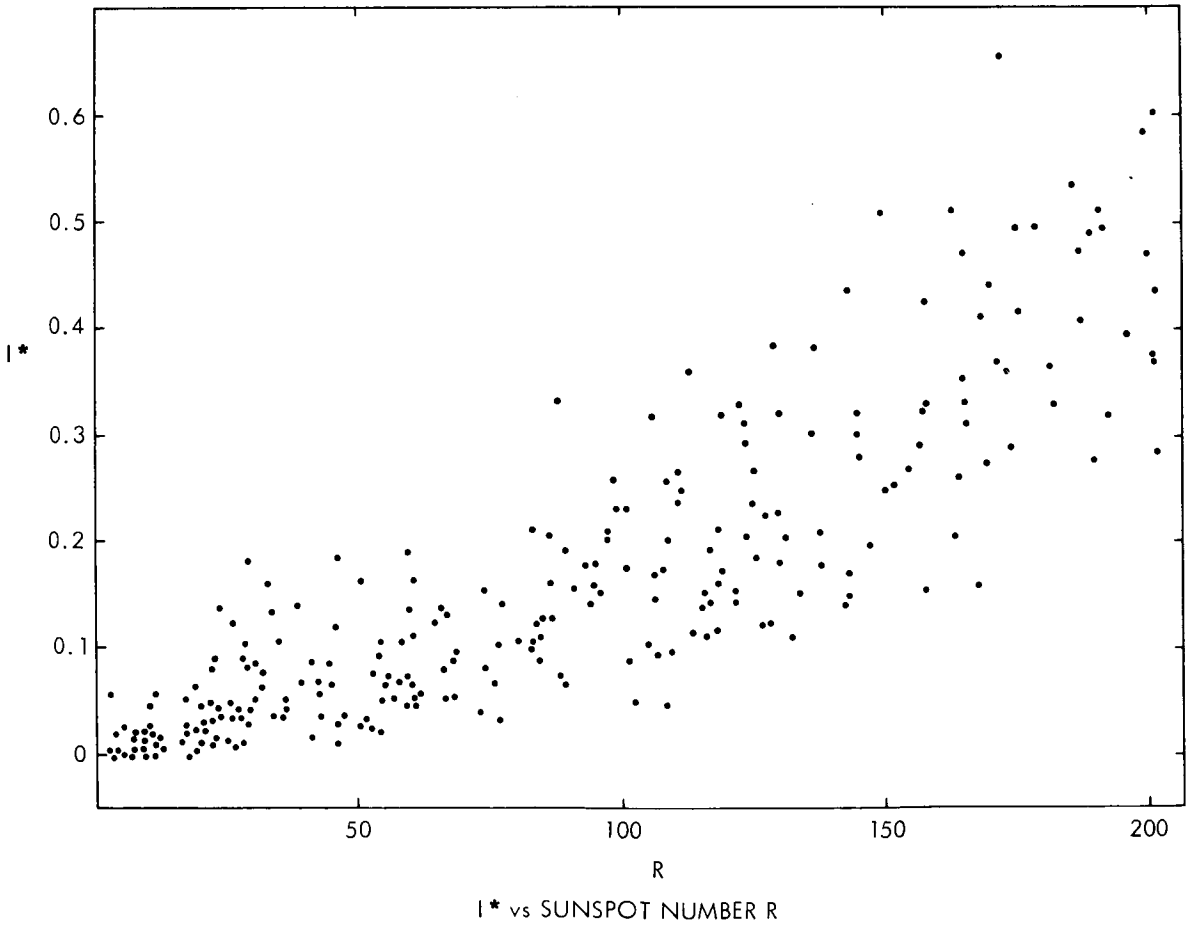

FIGURE 1–3. Monthly average flare incidence per hour.

tion would be improved by the omission of all shorter lived spot groups, but would never be near perfect. From Figure 1–3 we see that, near sunspot maximum, flares occur at the average rate of one every 20 to 30 minutes; the smaller ones are in no sense a rare phenomenon.

Another important factor relating to flare incidence in active regions concerns the magnetic configuration of the associated sunspots. The magnetically complex (gamma-type) spot groups, though relatively rare, are much more prolific flare producers than the more numerous bipolar (beta-type) or unipolar (alpha) groups. Indeed, the appearance of a large complex gamma group almost certainly will herald a higher flare incidence, with a greatly enhanced probability of a major flare event.

Statements on the total number of flares, and the relative frequency of flares of different sizes, must be qualified by comments on the effects of geometrical foreshortening—mentioned earlier. If flares had no thickness at all, the rectification of foreshortened flares could be accomplished perfectly by multiplying the apparent area with the secant of the central distance angle of a judiciously chosen mean position in the flare. Unfortunately this procedure does not work perfectly because flares are not geometrically thin. We can, however, ignore foreshortening effects near the center of the disk. Figure 1–4 shows the area frequency distributions for both central and limb zones. Foreshortening does two things: The number of large flares is diminished as the large flares move into smaller area classes, and the total number of flares above a certain threshold of size diminishes as small flares are lost from our limited range of detection. Clearly, the very large flares are quite rare, and the very small flares very numerous. By extrapolating data for the central zone to the entire hemisphere (taking account of the latitude distribution of flares), we can estimate fairly precisely the global incidence of flares of intrinsic area classes. For convenience we divide flares into four importance classes. Excluding the smallest (the subflares, called Importance 1−), some 40,000 flares were reported in the Quarterly Bulletin between 1936 and 1960.

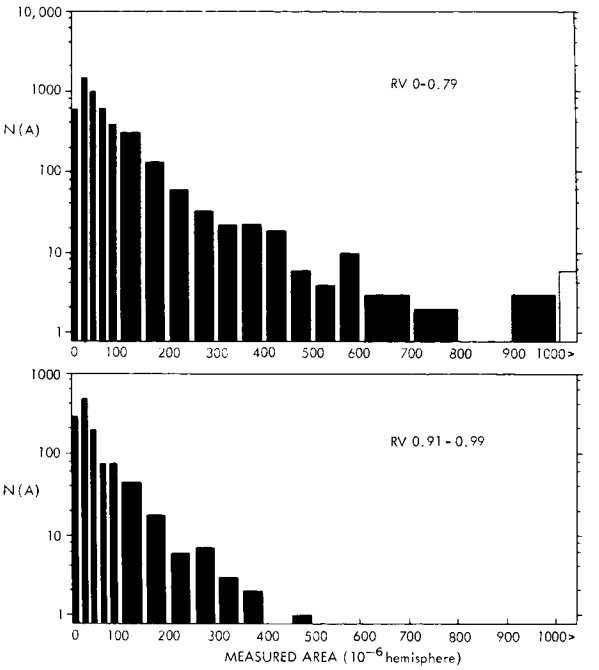

FIGURE 1–4. Area-frequency functions of flares.

Of these, about 250 were in the class of Importance 3. The relative populations of the three importance classes (1, 2, and 3) have varied through the years. In 1936 the ratio was roughly 73:22:5 percent; in 1960 it changed to 91:8:1 percent, reflecting the greater thoroughness with which we detect smaller flares. These data exclude subflares, which account for three out of four of all the flare events detected by a modern cinematographic patrol. An obvious question is: "How much smaller can a flare be than the threshold of our detection capability, and at what point do their numbers begin diminishing?" Needless to say, the most refined observational techniques do reveal numerous events smaller than the subflares; but counts are not available. This question merits considerably more attention than it has received, for one of the important new results from OSO I (1962 ζ1) was the detection of very frequent, very small bursts of soft x rays, which may very well have microflare counterparts.

The durations of flares relate only very loosely to their areas. This is clearly seen in Figure 1–5, which presents the frequency distributions

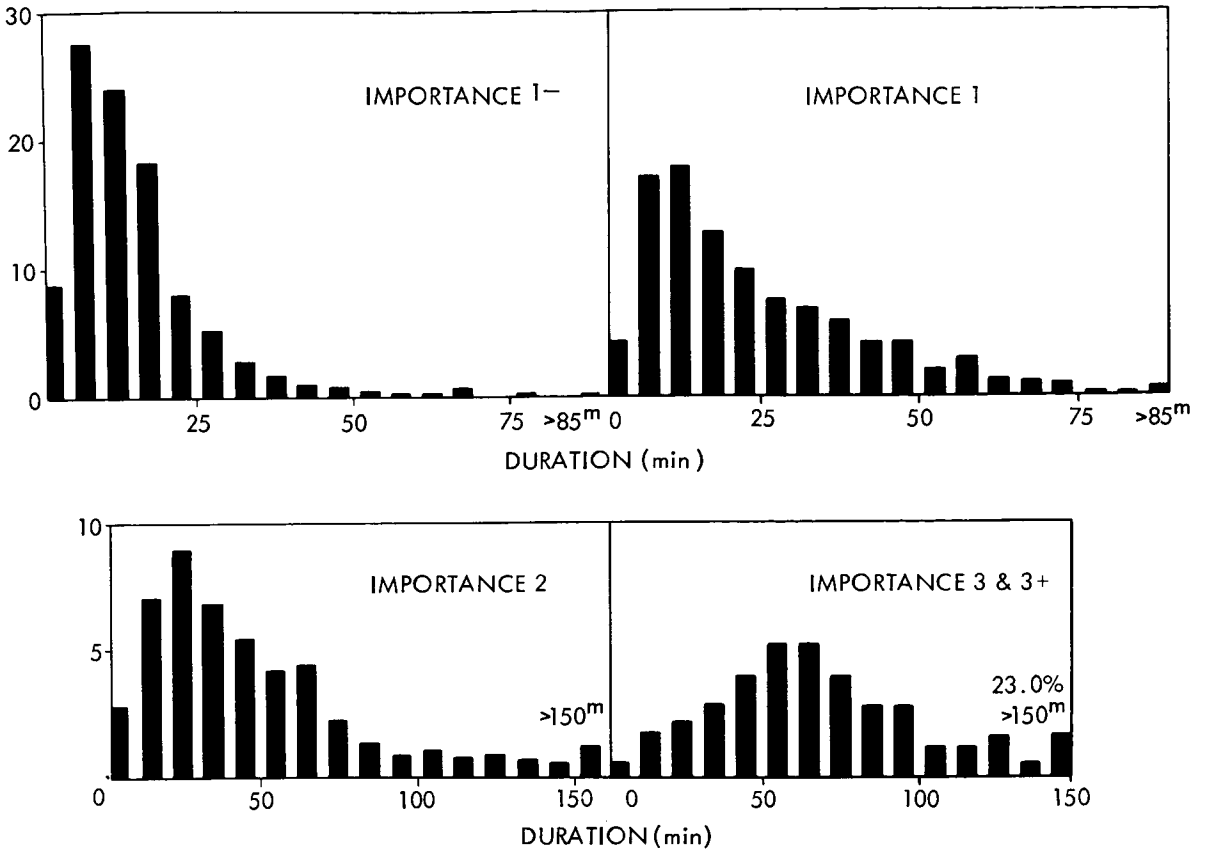

FIGURE 1–5. Frequency distribution of flare durations.

for each of the four classes of flare importance. There is overlap between the durations of all sizes of flares, so that some Importance 3 flares persist less than some subflares. The great dispersion is notable. Probably the chromosphere itself defines the relaxation time of a flare, with the total energy or the time variation of its impulsive release only partly governing the shape of the declining part of the flare light curve. The duration of a single flare is no guide at all to the event's area or importance. This is true because of the loose relations shown in Figure 1–5, but *a fortiori* because of the ill-defined ending time of a flare. The logarithmic decay of the light curve seldom allows precise definition of the end of a chromospheric flare.

A discussion of the shapes of flares, and of their morphological development, must begin with the recognition of pre-existent structures in the chromosphere. High resolution, high contrast pictures of the chromosphere disclose a very complex stippling and striation in the chromosphere; near an active center the dark features (*mottles*) become elongated (*fibrilles*) and form partly organized structures (Figure 1–6). Sometimes in the vicinity of a spot the fibrilles define a vortical pattern, which obeys a cyclonic law of rotational sense. These structures evolve rather slowly and can be recognized from one day to the next. The individual fibrilles and mottles appear and disappear over the course of 10 to 20 minutes, but with a distinct recurrence tendency. They are small, ranging from 2,000 to 10,000 km average, and require greater angular resolution than the normal small-scale patrol telescopes provide (Figure 1–7). The images made by such photoheliographs often do not reveal the essential details of flare structures, so that not all the remarks which follow pertain to the majority of existing observations.

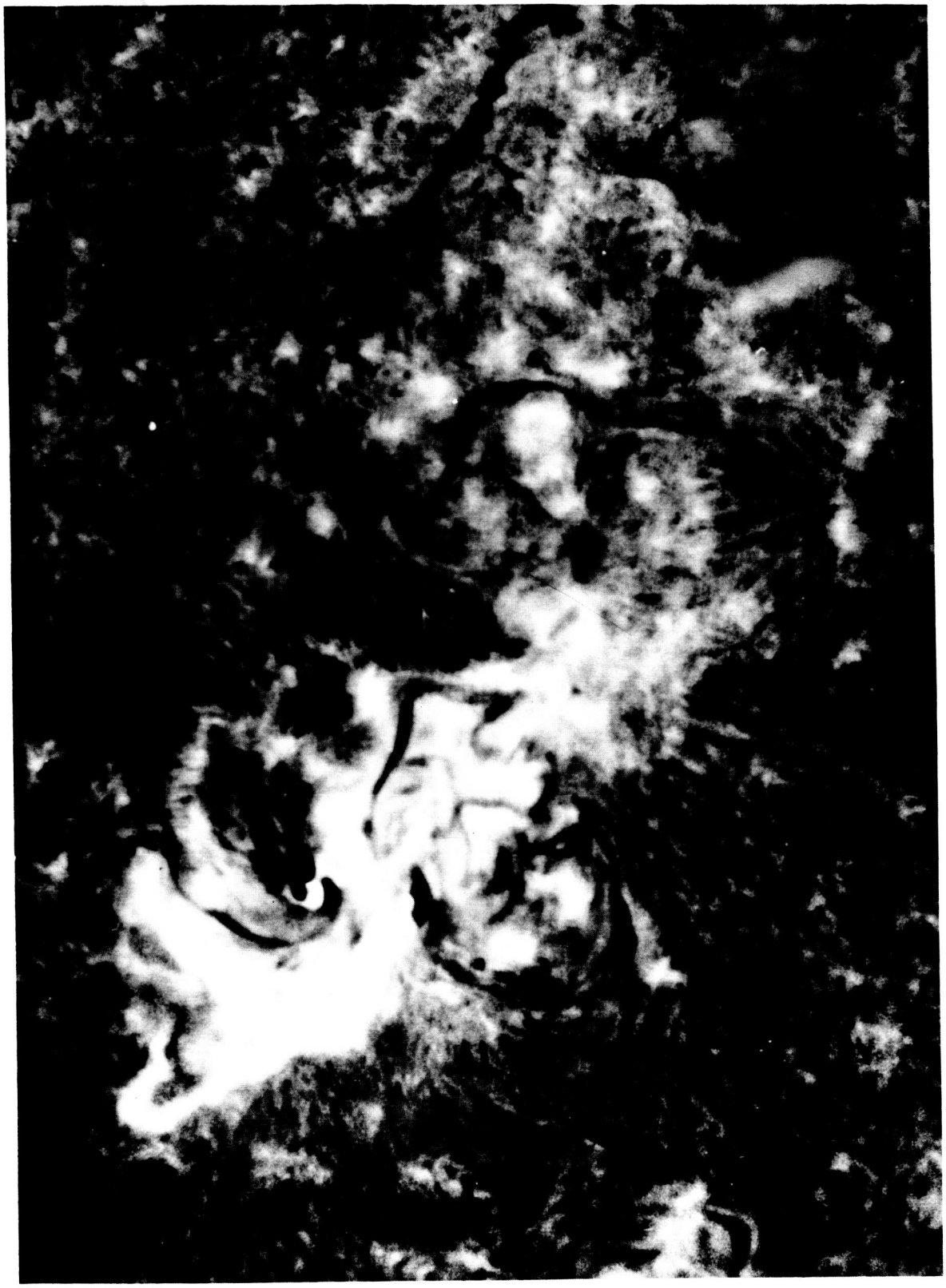

FIGURE 1–6. Importance 2 flare.

728–629 O—64——2

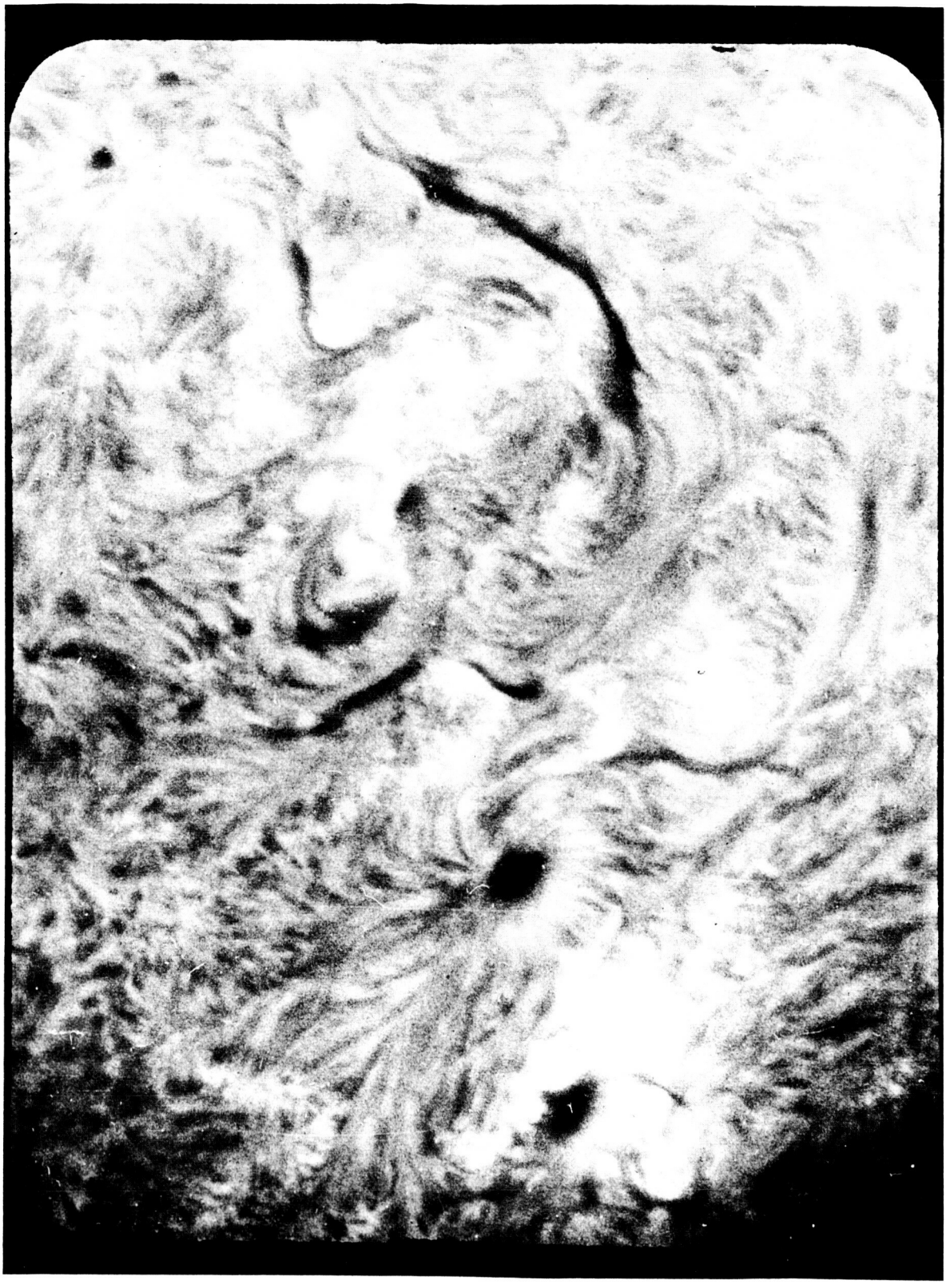

FIGURE 1–7. Chromospheric structure near sunspots

Most flares begin as one or more points which brighten rather suddenly. Soon larger features emerge as flare components from the *plage*, that is, the generally concentrated bright chromospheric constituent of the chromospheric structure which surrounds activity centers. The intensities of individual points rise rapidly in the initial phase. During this brightening, the affected areas grow at first along the local fibrille structure, then seem to swell as if escaping the constraints that define the outlines of individual fibrilles. At this phase, adjoining parts usually merge to form intensely bright areas that only partly follow the configuration of the pre-flare chromospheric structure. The flare does not always grow by extension of such bright features; sometimes an extensive area will brighten simultaneously all over. The brightest features are often likened to ropes, but their varying thickness and kinks more resemble ribbons.

Flares in general are not kinematic phenomena. The growth of the bright parts of flares is a slow process as judged by the Doppler effects seen in spectrograms. Usually the radial velocities measured amount to about 10 km/sec; but, in the tangential direction, motions as fast as 200 km/sec are sometimes recorded. However, the *apparent* rate of growth, especially in explosive flares, reveals the propagation of some disturbance at rates up to a few hundred kilometers per second. Even after the brightest phase of a flare is attained, the involved area continues to swell slowly, as the main parts appear to disperse at a typical velocity of 10 km/sec.

In prolific flare-producing regions we can detect a strong tendency for flares to recur at nearly the same place in the chromospheric structure, and therefore with respect to the general configuration of sunspots. The *homology* phenomenon, as Ellison described it, persists through the x-ray emission bursts, too. Smaller flares share in homology, as only small parts of a recurrently flaring area brighten up successively rather than simultaneously. Ellison discovered a mysterious influence of flares upon the underlying chromosphere, which he called the *nimbus*. This is a hazy, slightly obscuring layer which obliterates the fibrilles and mottles temporarily. We cannot say how this relates to the hydromagnetic process which delineates the chromospheric structure.

Flares, as seen at the limb, present another dimension to our knowledge of their morphology. Figure 1–8 shows several examples of each of a variety of limb flare shapes. A majority of small limb flares are rounded convex features, called *mounds* in the illustration. Often, however, the tops will be pointed to a varying degree (*cones* or *spikes*). These events have been cited as visible evidence for the hydromagnetic pinch effect. Loop structures (which we must carefully distinguish from the post-flare sunspot loop prominences) are yet another variety of limb flare shapes. Finally, there are many limb flares which we must frankly admit are irregular. Figure 1–9 illustrates the time development of some limb flares. Each has an initial ejective phase. The example of August 6, 1960, continued its development by withdrawal, as it were, of the coronal excrescence. The other two small flares formed loop structures, which merely faded to disappearance. Expansive growth of flares in the radial direction proceeds at velocities up to a few hundred kilometers per second. The peak heights attained by limb flares amount to about 50,000 km; most range 2000 to 10,000 with a mean of about 7000 km.

Some observers have publicized the case of the *sympathetic flare*, a flare which apparently is started by the propagation of some disturbance originating from a prior-starting flare. Descriptions of some individual cases of sympathetic cases offer very convincing testimony of their reality. By assuming a time of origin of some stimulus, as for example during the flash or explosive phase of a flare, we can calculate a propagation velocity of the order of 1000 km/sec. Some statistical tests have been applied to very large samples of flares, to see whether the incidence of sympathetic flares is numerically significant. Usually one asserts that the onset of flare events will exhibit a Poisson distribution of successive intervals. Such tests generally conclude that sympathetic flares are rare, and statistically insignificant.

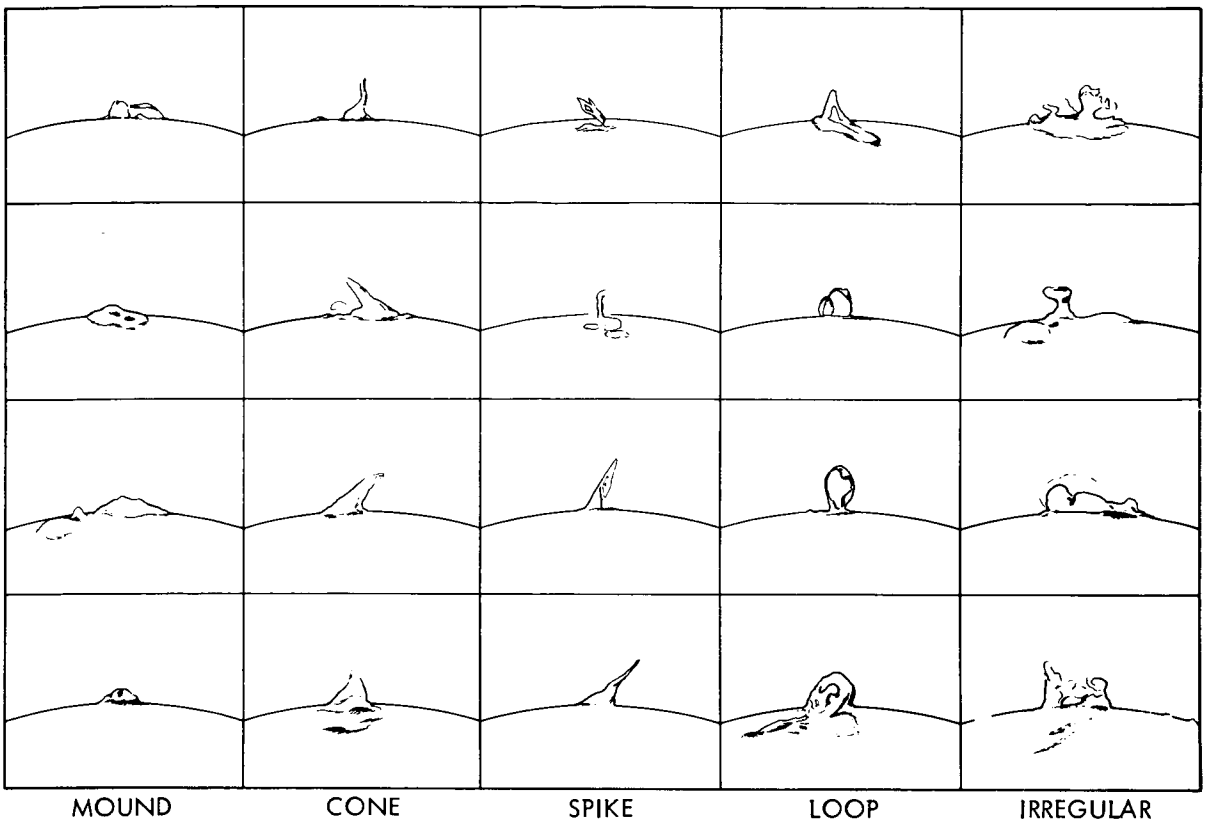

FIGURE 1–8. Shapes of limb flares.

This kind of analysis is prone to criticism, for the Poisson law is not strictly applicable. However, it sets less stringent conditions than the real situation; so the conclusion remains valid.

The photometry of solar flares is only rarely performed for the patrol task, and even then the procedures used are not always adequate for the purpose. The most careful work exhibits a loose correlation between peak intensity in the center of Hα and the corrected area of the flare at maximum (Figure 1–10). The scatter within one importance class is quite large, and it is only by massive averages that a functional relation emerges from such data. Roughly speaking, the peak brightness is 0.5 (times the quiet sun continuum) for subflares, up to 1.5 for Importance 1 or 2, and as large as 3.5 for Importance 3. Since the chromosphere has an undisturbed brightness of 0.14, the largest flares brighten monochromatically by a factor of about 25 times. This is really a lower limit, set by the restricted resolution attainable in our ground-based telescopes.

Light curves typically exhibit rapid rise and slower decline, but no well-defined relations exist between these rates, or total amplitude or duration of flares. Most events reach maximum amplitude within 5 to 10 minutes of onset. No ordinary flare declines more rapidly than it rises, although the rising phase of some flares may exceed in duration the decay phase of others.

Although the fundamental chromospheric brightening we have discussed as the flare proper is not a kinematic event, many flares do have an aspect involving dynamic motion. This is the ejection of jets of visible gas, in the form of surges or spray prominences. The latter are generally the higher energy, faster ejections seen best at the limb but sometimes on the disk, too. Figure 1–11 shows the devel-

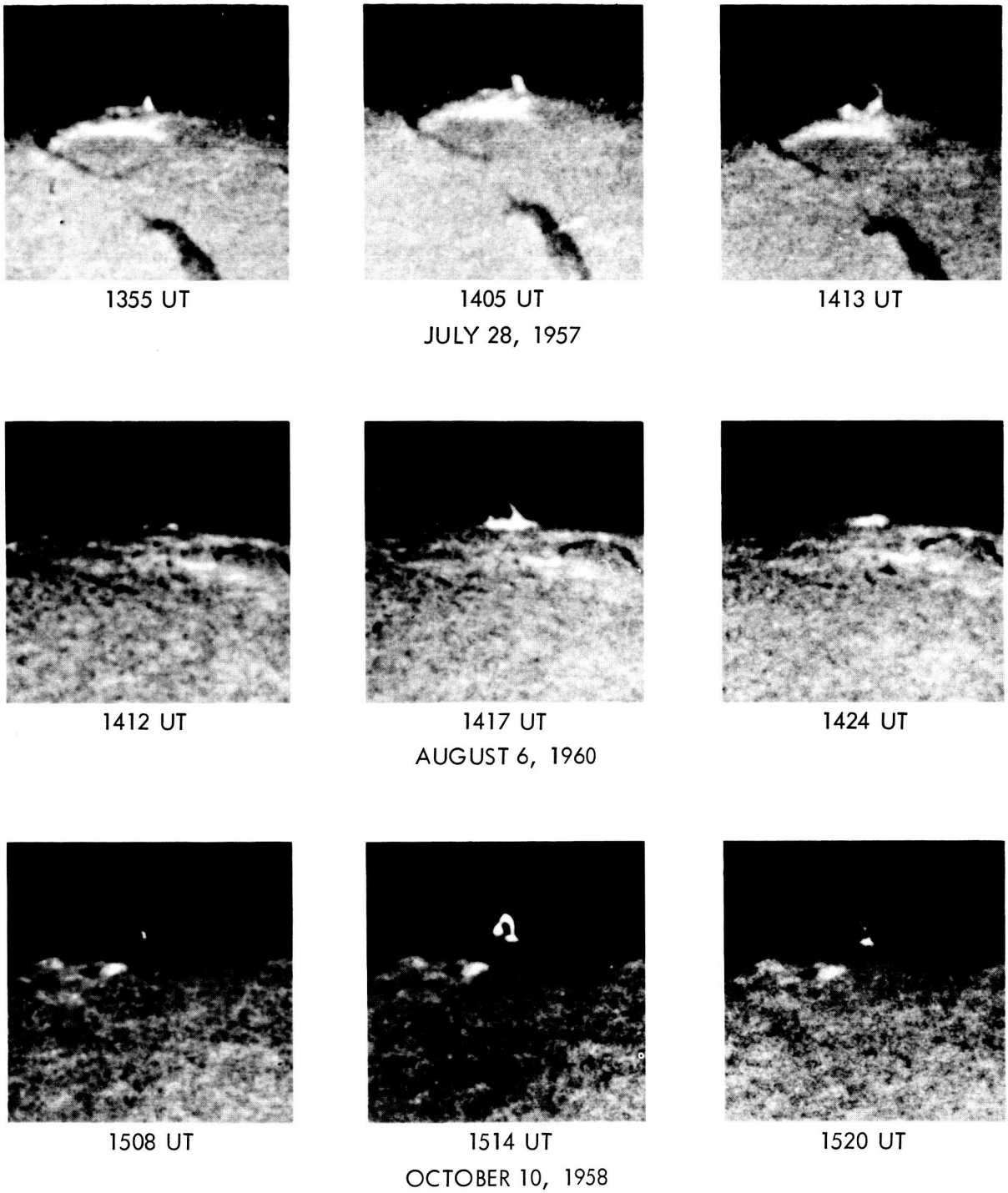

FIGURE 1–9. Development of three limb flares.

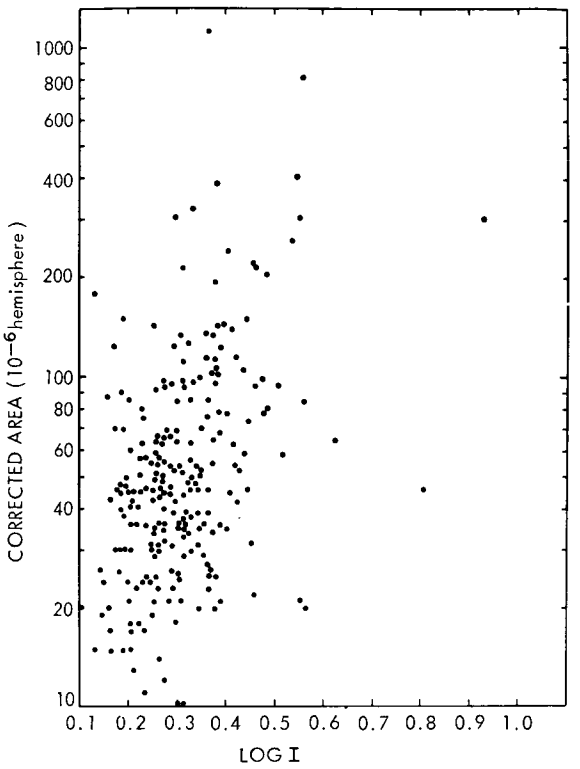

FIGURE 1–10. Correlation of area with Hα central intensity.

opment of the examples. The surge usually issues from a small swelling excrescence, a *puff*. The material moves along twisting trajectories, but constrained overall to a narrow-angle cone, like water issuing at high velocity from a hose. The peak heights at which they remain visible range between 20,000 and 100,000 km. The ejection velocity will range from 50 to about 200 km/second for typical surges. Sprays disclose velocities as high as 1500 km/sec. The lifetimes of surges and sprays range from 5 to about 150 minutes; very often the greatest events are also the most rapid. The high velocities of flare ejections in the line of sight often produce a complex change in the pattern of visibility. Material becomes invisible in a narrow-band monochromator as it curves around in a spiraling trajectory, so that our pictures of spray prominences and surges are often fragmentary. The impact of flare ejections upon the quasi-enduring structures in the corona is not well known. Rapid flashing responses are sometimes seen above flares, in the Fe [XV] radiation, for example (Figure 1–12). The pursuit of more such observations is a necessary preliminary to an understanding of the dynamic coupling between the corona and the chromosphere.

Other contributions to this symposium will discuss the radio frequency radiation of the corona in relation to flares, and the informative facts deducible from spectroscopic studies. The complicated interactions between flares and prominences, particularly the sunspot loops, although elucidated by monochromatic observations such as we have discussed, will likewise be taken up later.

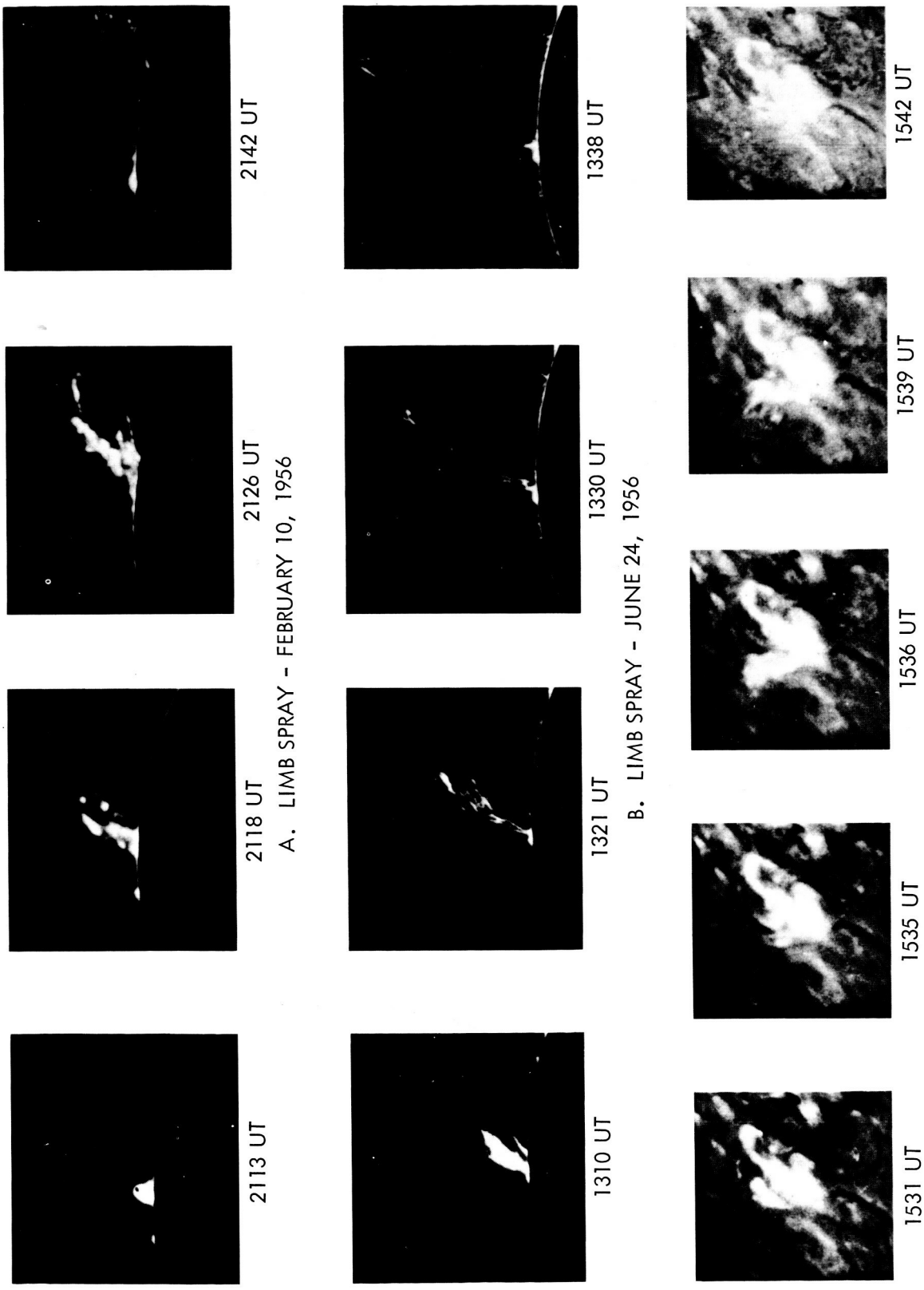

FIGURE 1-11. Flare sprays.

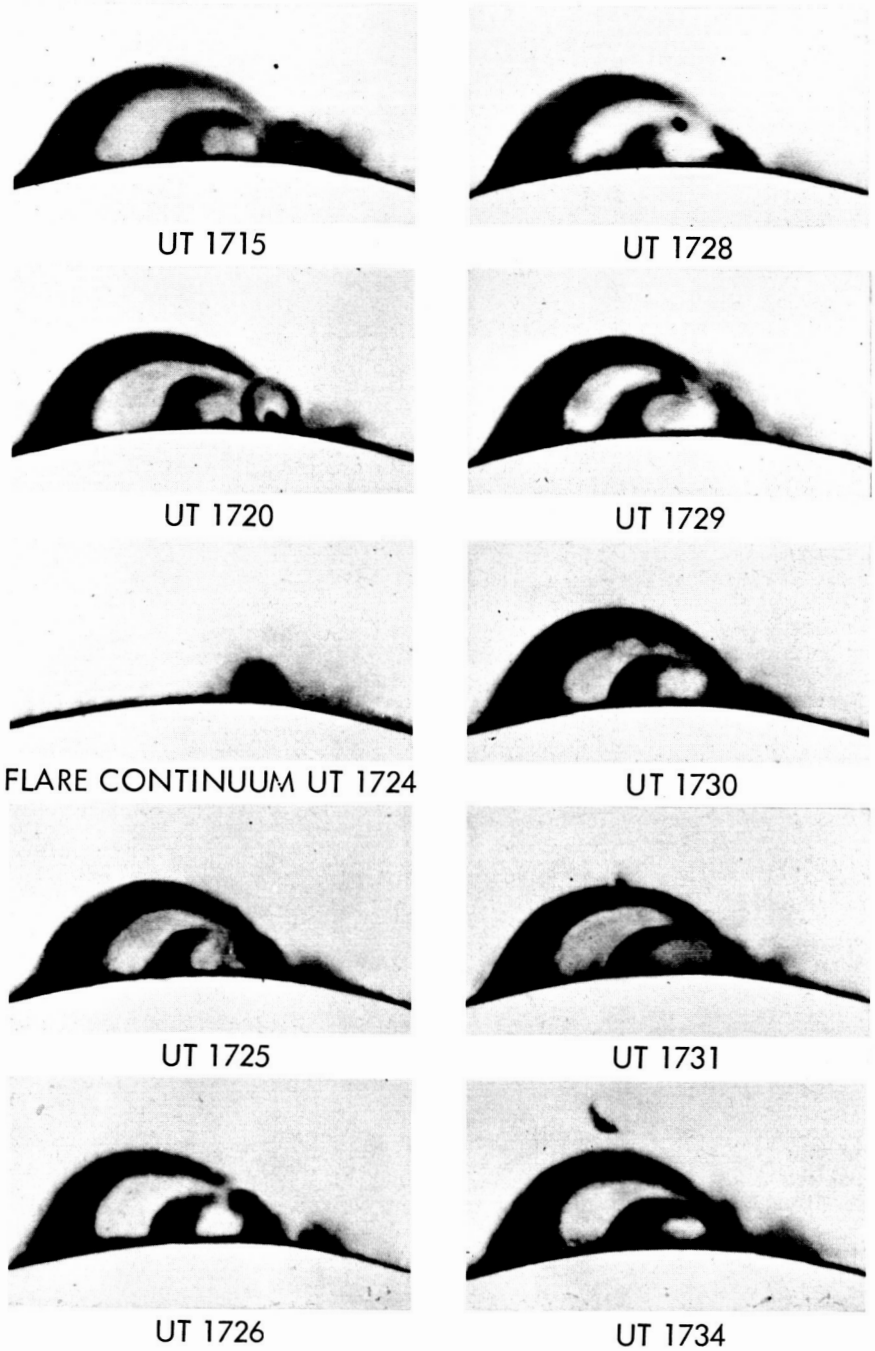

FIGURE 1–12. Motion of a flare spray through the corona.

N64-30253

2 MOVING MATERIAL ACCOMPANYING THE FLARE OF 1959 JULY $16^d21^h14^m$ UT*

HELEN W. DODSON and E. RUTH HEDEMAN
McMath-Hulbert Observatory of the University of Michigan
Pontiac, Mich.

The important (3+) Hα flare of 1959 July $16^d21^h14^m$ UT took place at N16°W31°. The flare was associated with severe ionospheric and geomagnetic disturbances and with the emission of high-energy particles, including enhancement of cosmic rays at the surface of the earth (see Figure 2–1). The McMath-Hulbert Observatory's center-of-Hα flare patrol records of the flare are supplemented by more than 500 spectroheliograms in 25 "series" or λ-sweeps made throughout the course of the flare by small systematic changes of wavelength from at least 3A on the violet side of the center of Hα to at least 3A to the redward. Since the flare was relatively close to the center of the solar disk, ascending and descending motions of the hydrogen atoms resulted in Doppler shifts and introduced differences in the spectroheliograms made with radiation from the red and violet sides of the center of Hα.

PRE-MAXIMUM AND EARLY PHASE OF FLARE

The first 60 spectroheliograms (three λ-sweeps) were secured during the rise to maximum intensity, between $21^h24^m20^s$ and $21^h33^m45^s$ UT. In this interval, the brightest parts of the flare showed in emission over the full 6A range of the λ-sweeps.

In general, the emission images were similar in form and brightness on spectroheliograms made in symmetrical positions in the wings of Hα. If there is an asymmetry, it is in the sense that the Hα emission was wider on the redward side.

The spectroheliograms provide evidence for two ejections during the rise to maximum intensity. They were in progress as early as $21^h24^m53^s$ and continued to $21^h41^m41^s$. The ejections occurred at the outer extremities of the two very bright segments and apparently emerged from the portions of the flare that showed maximum curvature on center-of-Hα images. The velocities were ≥200 km/sec, the observational limit (see Figure 2–2).

A third ejection was in progress at $21^h40^m39^s$. The velocity was as great as 200 km/sec. It apparently was a surge since it "returned" in the same location 8 minutes later, showing Doppler shifts to the redward side.

LATE PHASE OF FLARE

Dark, curvilinear descending features, interpreted as systems of loop-type prominences in projection, developed in the post-maximum phase of the Hα flare, and as the 10 cm emission was rapidly diminishing. The curved absorption features were detectable as early as 21^h52^m, were clearly developed by 22^h06^m, and were still in progress at the close of observations at 23^h10^m.

The system of dark loop-type prominences showed certain relationships to the flare emission. First, as nearly as can be determined, the loops had their *feet* near the regions of the concomitant, bright flare emission (Reference 1). Secondly, during the July 16, 1959, flare the pattern or locus of dark material at +1A was similar in shape and position to the parts of the flare with emission extending at least 1A to the redward, approximately three-quarters of an hour earlier. The distribution of descending material in the systems of loop-type prominences appears to have been influenced by the location of the widest parts of the Hα

*Presented by Dr. Dodson-Prince.

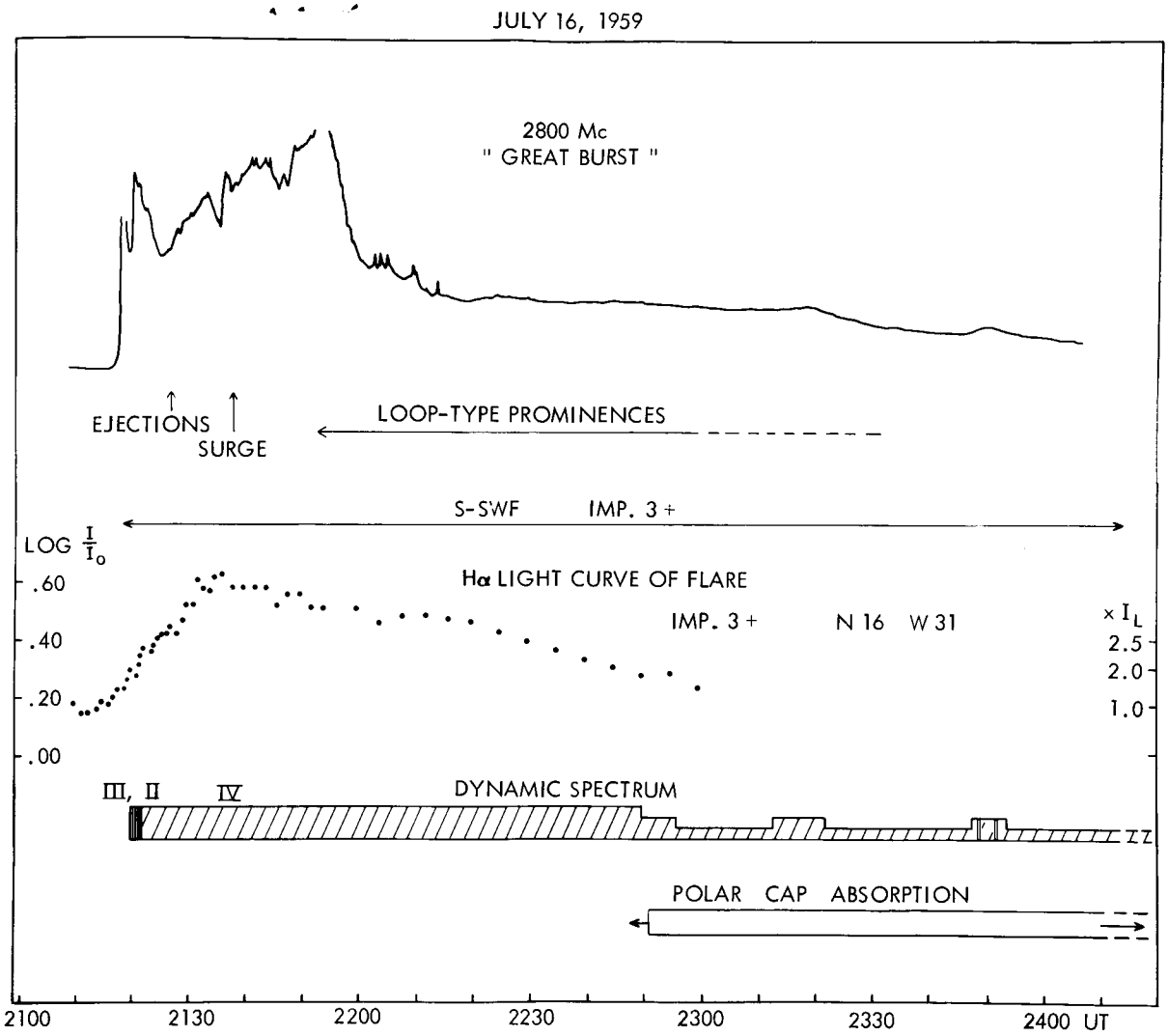

FIGURE 2–1. Summary of phenomena relating to the flare on 1959 July 16^d 21^h 14^m UT.

(The photometric light curve and information about ejections and loop-type prominences are based on observations at the McMath-Hulbert Observatory. The 2800 Mc/s record was kindly made available by A. E. Covington, National Research Council, Ottawa. Other information is based on data in the *Quarterly Bulletin of Solar Activity* and the F-Series publications of CRPL.)

flare emission during earlier stages of the flare (see Figure 2–3).

If the foregoing interpretation of the spectroheliograms is correct, the inferred prominence motions during the disk flare of July 16, 1959, are consistent with observations of prominence activity during certain major flares at the limb; that is, ejections in the pre-maximum and early stages and systems of loop-type prominences and descending material in the post-maximum or late phase. The loops often continue after the Hα flare and associated ionospheric disturbances have ceased.

"ACTIVATION" OF RELATIVELY DISTANT FILAMENTS

The familiar "winking" of filaments near the start of flares as shown on center-of-Hα records was exhibited by the July 16, 1959, flare (Reference 2). The λ-sweep records reveal what

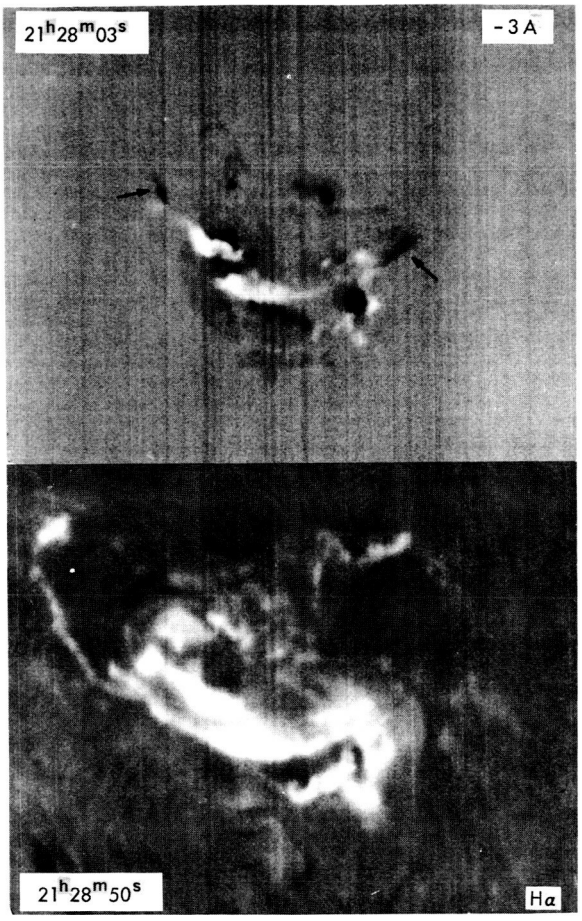

FIGURE 2–2. Ejections during the rise to maximum intensity of the flare on July 16, 1959.

(Spectroheliograms show the site of the flare as recorded in radiation 3A to the violet of Hα (upper picture) and in the center of Hα (lower picture). Arrows point to absorption features that were visible on spectroheliograms taken with radiation on the violet side of Hα but not recorded on similar records taken on the red side of Hα. These features are interpreted as indicating "ejections." The observations extend to 4½A to the violet side of Hα, and the "ejections" are visible to the limit of the λ-sweep.)

happened to a part of the filament during the interval of transient activation.

At $21^h25^m54^s$ the filament was not visible in the center of Hα but appeared, apparently intact, on the redward side of Hα with Doppler displacements of the order of 1A. Three minutes later the filament segment, still intact, showed a similar displacement, but at this time to the violet side of Hα (see Figure 2–4). The entire process was repeated before the filament became relatively stable at 21^h40^m. With Doppler shifts of the order of 1A and duration of motion about 5 minutes, the translation of the prominence material apparently was of the order of 13,000 km.

Wavelength sweep spectroheliograms show that similar "down-up" motions occurred in the filaments activated during the flare of 1960 June $25^d20^h39^m$. Filaments *A*, *C*, and *E*, with distances from the flare of the order of 150,000, 210,000, and 330,000 km respectively, were displaced, first to the red and then to the violet sides of Hα. (See Figures 2–5 and 2–6.) During the primary displacement to the redward, a small portion of filament *A* can be seen on the —0.75A spectroheliogram taken at approximately $20^h47^m55^s$ in agreement with "activation" reported for this feature by Athay and Moreton (Reference 2) from examination of records made on the violet side of Hα.

Interpretation of these Doppler shifts is not obvious, but they seem to represent a temporary disturbance of the mechanism by which a prominence is supported. The cause of the disturbance apparently moves outward from the site of the flare with a velocity of the order of 600 km/sec. When the disturbance reaches them, entire filaments—or large portions of them—appear to be "activated" almost simultaneously. For the activation on July 16, 1959, Athay and Moreton (Reference 2) have reported a propagation velocity of ≈570 km/sec and write, "Filament activated as unit." For the activations observed during the flare of June $25^d20^h39^m$ the Athay-Moreton study suggests velocities of ≈1000 to 3000 km/sec. It is possible that these high velocities are correct, but according to our records the filament activations on this date can be interpreted as a result of a single traveling disturbance with a much slower velocity.

In order to supplement the data from the λ-sweep and offband records, we have measured, photometrically, the filament activations as recorded on center-of-Hα filtroheliograms (see Figure 2–7). According to these measurements, activation of filament *A*, which was ≈150,000 km from the center of gravity of the flare, started at 20^h45^m. Activation of filament *E*—

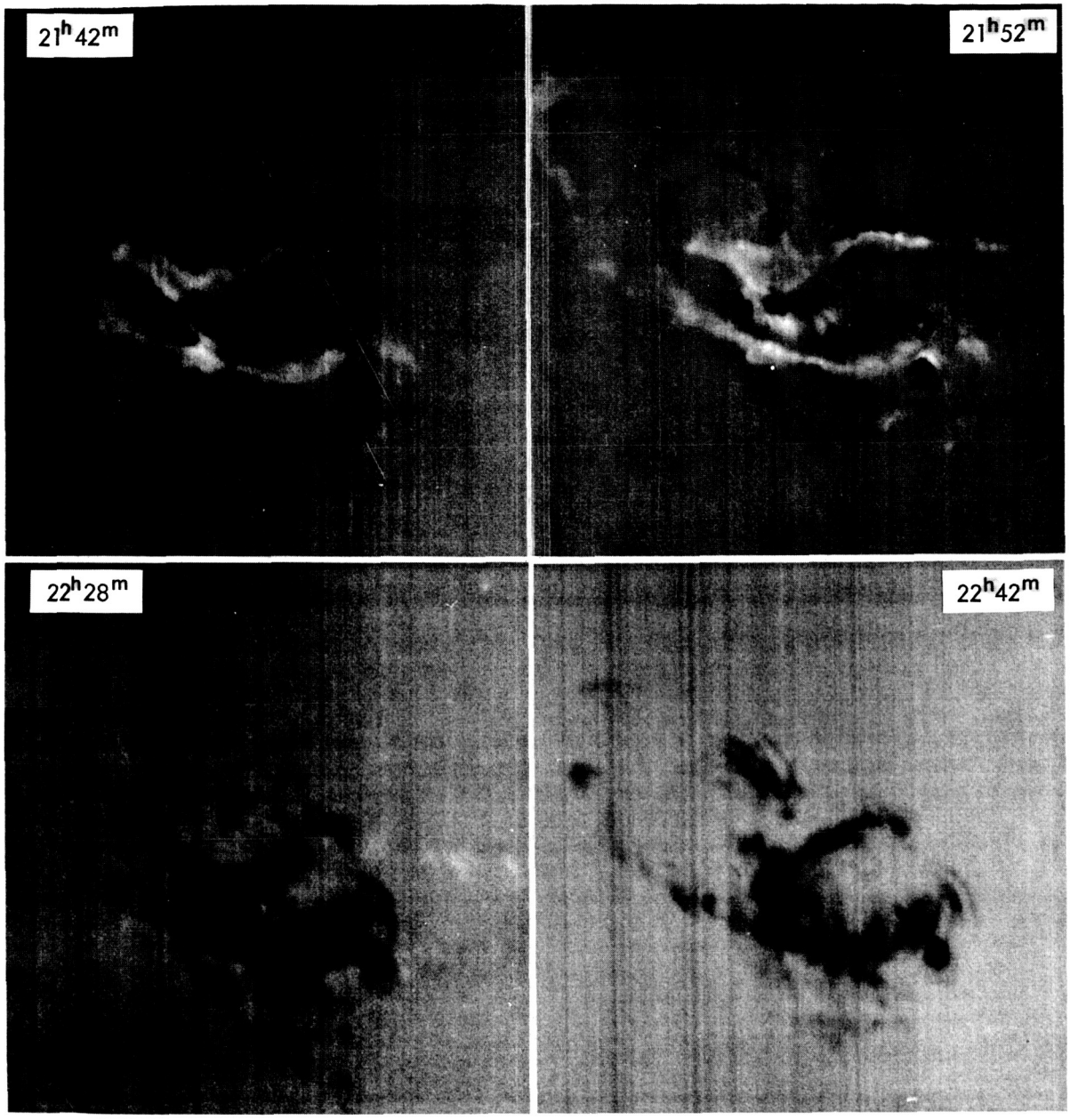

FIGURE 2–3. Comparison of position of Hα flare emission with locus of descending dark material (identified as portions of loop-type prominences) approximately ¾ hour later.

(The top two pictures show the location of bright flare emission on spectroheliograms recorded 1A to the redward of Hα on 1959 July 16^d 21^h 42^m and 21^h 52^m UT. The lower two pictures show spectroheliograms recorded 1A to the redward of Hα, 46^m and 50^m later, respectively.)

180,000 km more distant from the flare than *A*—started at 20^h50^m. These distances and times indicate a propagation velocity of the order of 600 km/sec. In turn, this velocity suggests that the disturbance began near the site of the flare 250 seconds prior to *A*'s activation, or at 20^h41^m (see Figure 2–7). This is the time of the start of the sudden increase in

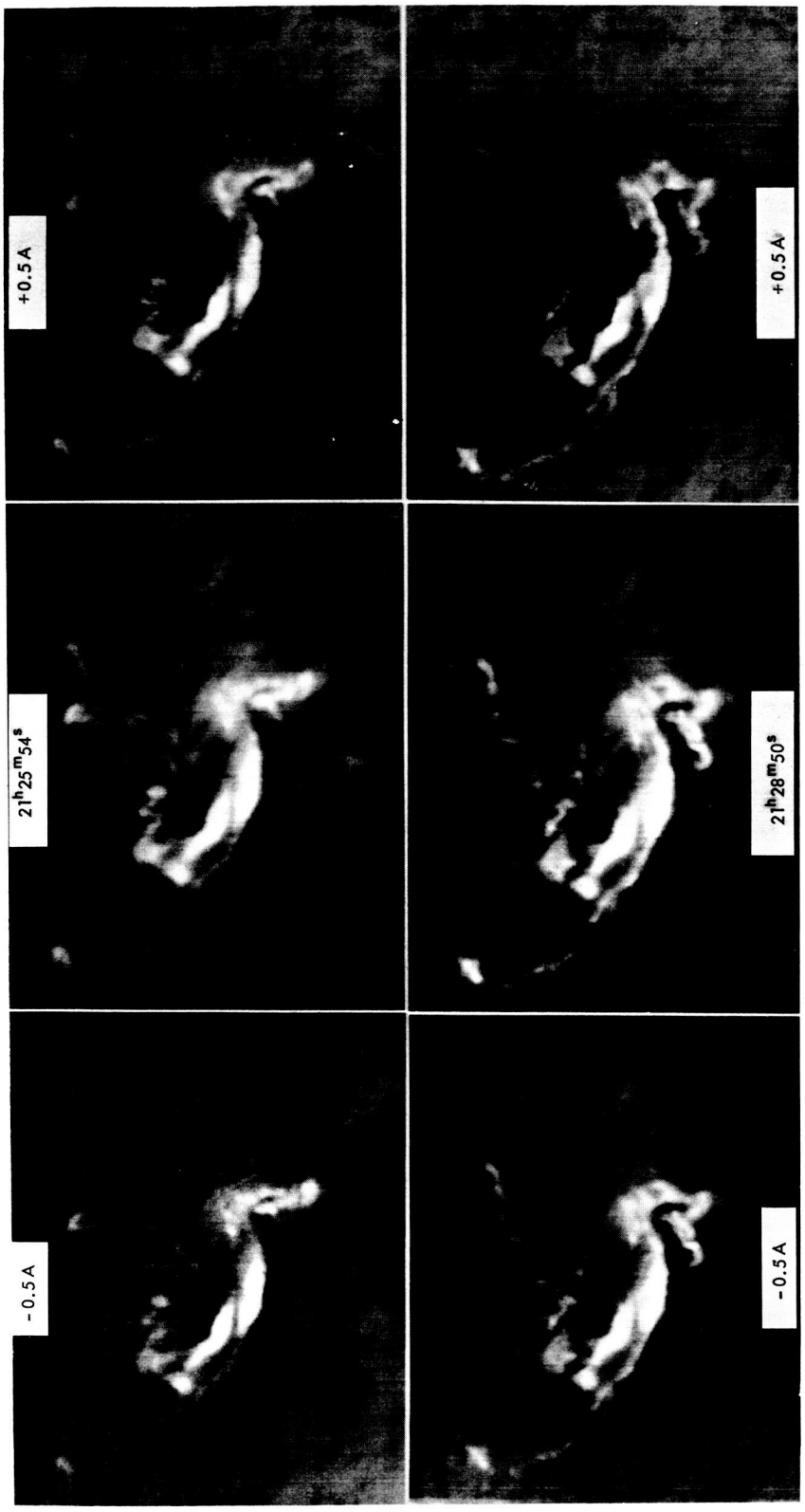

FIGURE 2–4. Spectroheliograms showing the "down-up" motion of part of an activated filament during the flare of 1959 July 16^d 21^h.

(The three pictures at the top were recorded at approximately 21^h 25^m 54^s; the three lower pictures at 21^h 28^m 50^s. The central pictures were made with radiation from the center of Hα; those to the left with radiation 0.5A to the violet of Hα, and those to the right with radiation 0.5A to the redward. The position of the activated filament is the lower left-hand corner of each of the six pictures.)

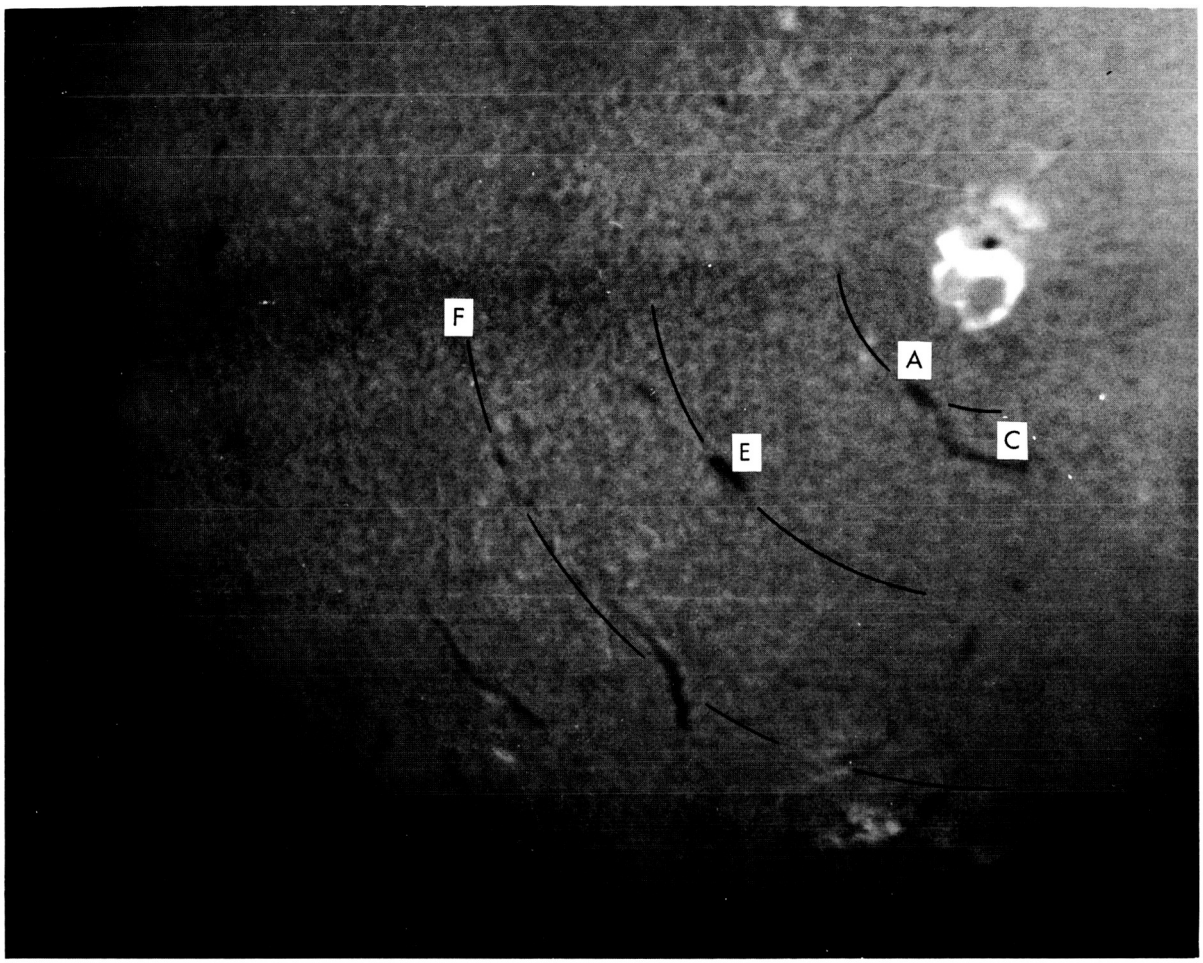

FIGURE 2–5. Hα filtroheliogram of a portion of the solar disk during the flare of 1960 June 25^d 20^h 39^m with a guide to the location of activated filaments.

(Circles with radii corresponding to approximately 150,000; 330,000; and 410,000 km have been drawn centered on the starting position of the flare. Locations of filaments called *A*, *C*, and *E* are indicated. The filament at distance of 410,000 km reported (Reference 2) as activated should lie along circle *F*. This feature could not be identified clearly on our filtroheliograms.)

brightness or flash phase of the flare. Furthermore, using the 600 km/sec velocity, the disturbance would have reached filament *F*—410,000 km from the flare—at $20^h52.4^m$. Athay and Moreton report activation of this filament on violet-side records at $20^h56^m20^s$. It probably began earlier on the redward side.

That whole filaments may undergo almost simultaneous activation is borne out by the similarity of time of activation of filament segments *A* and *C* on June 25, 1960, (see Figure 2–7), even though they were at rather different distances from the flare. Detailed study of the long filament activated by a flare on 1949 May $10^d20^h00^m$ (Reference 3) provides further evidence. This latter filament, more than 200,000 km in length, was as close to the flare as 180,000 km and as distant as 265,000 km. Activation began apparently simultaneously in all parts of the filament at $20^h13^m30^s$ and lasted for 12 minutes. (Cadence of record was 1 frame per minute.) The start of the activation was 12 minutes after the sudden increase in brightness or flash phase, 8 minutes after the

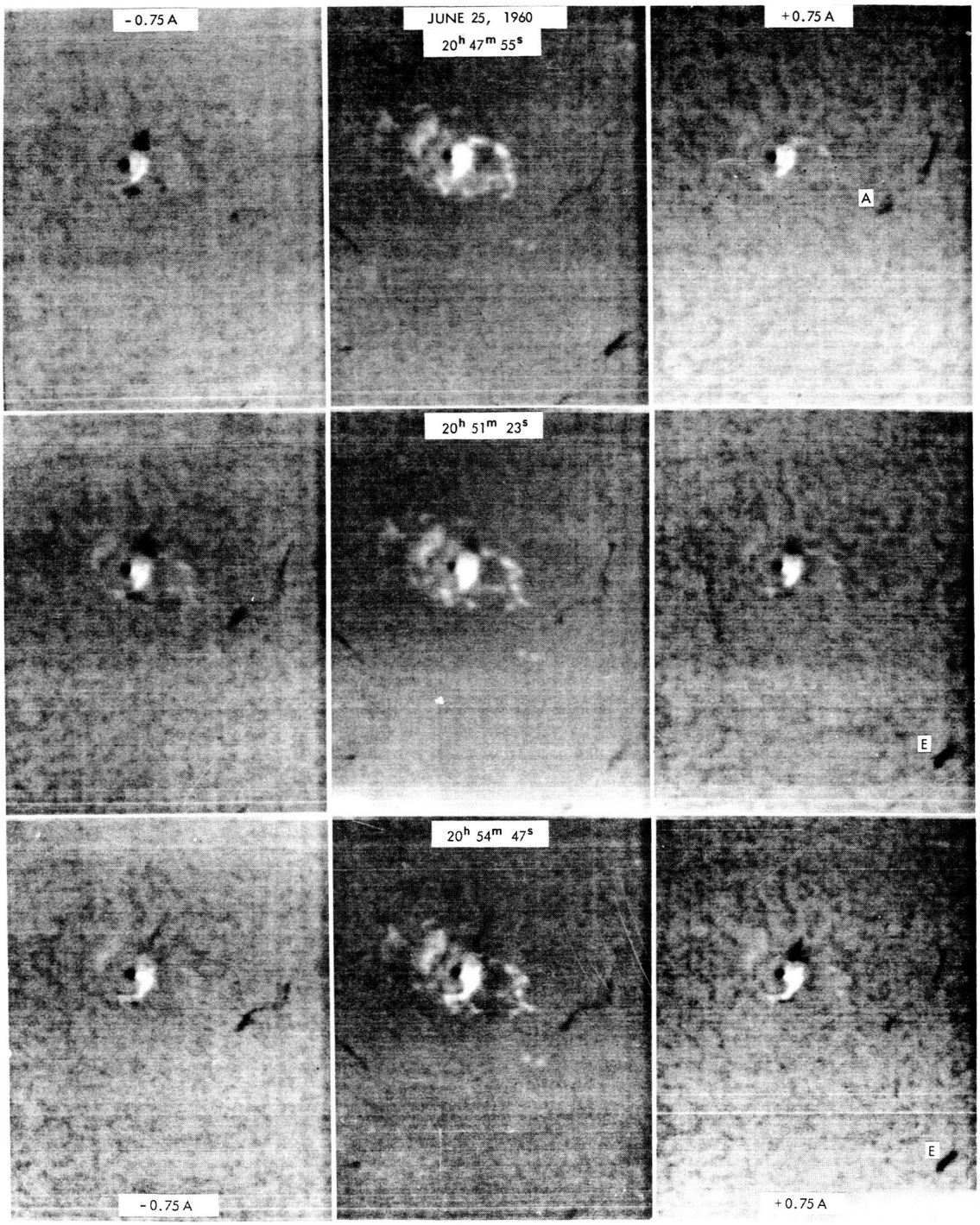

FIGURE 2–6. Hα spectroheliograms showing the "down-up" motion of filaments activated during the flare of 1960 June $25^d 20^h 39^m$. (The pictures in the top row were made at approximately $20^h 47^m 55^s$. The central picture in this row was recorded with light from the center of Hα; the picture to the left with radiation 0.75A to the violet of Hα, and the one to the right with radiation 0.75A to the redward of the center of Hα. The pictures in the central and bottom rows were made in a similar way at $20^h 51^m 23^s$ and $20^h 54^m 47^s$, respectively. The locations of filaments *A* and *E* are indicated in the right-hand column.)

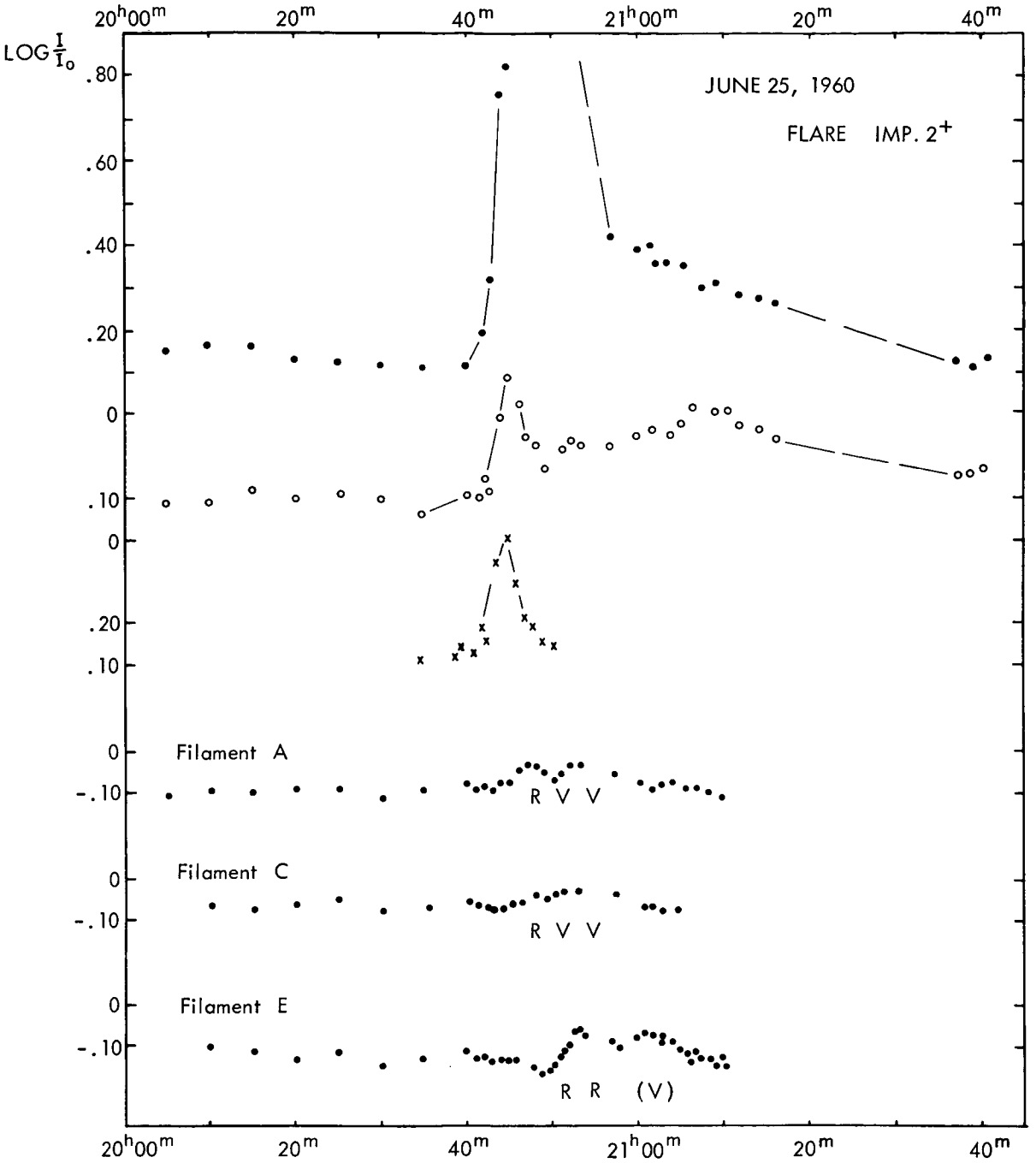

FIGURE 2–7. Photometric measurements of flare and activated filaments on center-of-Hα filtroheliograms, 1960 June 25^d.

(The three top curves are photometric light curves for three different parts of the flare. The three bottom curves show the "winking" of filament segments *A*, *C*, and *E*. The symbols *R* and *V* indicate the times when λ-sweep spectroheliograms showed Doppler shifts to the red and violet sides of Hα, respectively. The symbol (*V*) indicates violet displacement on λ-sweep filtroheliograms.)

beginning of an ejection, and 6 minutes after the start of a large 480 Mc/s burst. If the disturbance traversed the intervening 180,000 km in these intervals of time, the respective velocities were of the order of 250, 375, and 500 km/sec.

The meaning of these observations is still far from clear; but, if prominences are supported by magnetic fields, then these observations may provide evidence for a traveling disturbance in the magnetic fields surrounding spots and plages at the time of certain flares.

REFERENCES

1. Dodson, H. W., 1961, *Proc. Nat. Acad. Sci.*, 47: 901.
2. Athay, R. G., and Moreton, G. E., 1961, *Astrophys. Jour.*, 133: 935.
3. Dodson, H. W., 1949, *Astrophys. Jour.*, 110: 382.

DISCUSSION

Dr. Prince: May I recall, for Dr. Bruzek, the flare film that we showed in Dublin in 1955. With the flare of May 10, 1949, we said, "Watch it wink." Miss Hedeman has made measurements for that long filament which crossed the equator. The distance from the flare to the different parts of the filament varies by more than 100,000 kilometers. The activation of the filament starts all over at once—"from stem to stern"—as though, once activated, that particular filament became activated all together. It is very difficult to know how to interpret the phenomenon or what the zero point is. We will be happy to share what little we know about it with anyone who is interested.

Dr. Moreton: I would like to comment on this excellent observation discussed by Dr. Prince. New Lockheed results, from observations made by sequentially displacing our filter bandpass 0.5A into the H wings, confirms the down-up motion of winking filaments.

It also may be of interest that both of the flares discussed by Dr. Prince were of the "homologous" type mentioned in Dr. Henry Smith's paper; that is, each event was preceded a few hours earlier by a flare that showed similar optical characteristics and also caused filament activations.

I wish to emphasize that in the case of the June 25 flare the high velocity obtained for outward motion is *not* inferred from the time of filament activations. Instead, 10-second-interval filtergrams show a well defined wave- or front-like feature that propagates from the flare at the time of the explosive phase. A transverse velocity component of 2000 km/sec is determined by direct measurement of the displacement of the feature with time. Two other disturbances that propagate with speeds of 1000 km/sec and 500 km/sec are initiated 3 and 8 minutes after the faster disturbance. These latter speeds also are determined directly by measuring their displacement on the filtergrams.

Dr. Prince: Our records do show the occurrence of three actively moving dark features in the neighborhood of the flare. These may or may not be associated with the activation of the filaments. In our judgment, the activations of the three closest filament segments as shown on λ-sweep and center-of-Hα records are consistent with a single disturbance moving outward from the flare with a velocity of the order of 600 km/sec.

728-629 O—64——3

NW-30254

3 OPTICAL CHARACTERISTICS OF CHROMOSPHERIC FLARES ASSOCIATED WITH TYPE IV RADIO BURSTS OR NOISE STORMS*

Y. Avignon, C. Caroubalos, M. J. Martres-Tropé, and M. Pick
Observatoire de Paris, Section d'Astrophysique
Meudon (Seine et Oise), France

We shall summarize some characteristics of these chromospheric flares and of the associated optical regions which are accompanied by radio emissions: long-lasting type IV radio bursts observed on meter wavelengths, or type I storm activity. These two types of events are distinguished by the importance of high-frequency emissions accompanying them.

We have considered, first of all, 16 chromospheric flares associated with polar cap absorption (PCA) and, consequently, with intense type IV radio bursts. The characteristics common to these flares allow the following definition of a new class of flare which we shall designate as "type A configuration," Figure 3–1 (Reference 1): The centers of activity are made up of two rows of spots of opposite polarity; the minimum distance between these two rows is generally less than 1 heliographic degree.

The flares are constituted by two approximately parallel, bright filaments—each covering a row of spots of the same polarity.

This structure was also described by Ellison et al., who studied the flares leading to an increase of cosmic rays measured at ground level (Reference 2). Moreover, we have varified that the type A configuration did not correspond to all the accompanied type IV bursts but was, in fact, only related to those accompanied by proton events.

Subsequently, we examined the chromospheric flares associated with meter wavelength radio events: metric type IV, or noise storm (Reference 3). For all cases not associated with a PCA it was found that the position of the flares lies partly along the position of filaments which are present in the interior of centers of activity—the "plage filaments." These are very small: 2 to 3 heliographic degrees. Their lifetime is relatively short—from a few hours to 2 or 3 days. Their position in the center is fairly stable, and in most cases they seem to occupy one of two privileged positions: Either they "point" between two spots of opposite polarity (configuration A′), or they surround one or several spots of the same polarity (configuration B).

The plage filament indicates a peculiar structure of the magnetic field, probably corresponding to a large horizontal component.

Finally, we have shown that the total area of the umbra and penumbra covered by the flare is the characteristic quantity which defines the importance of the high-frequency radiation (2800 to 9400 Mc/s) associated with it (References 3, 4, and 5).

* Caractères optiques des éruptions chromosphériques associées à des sursauts de type IV ou à des recrudescences d'orage. This paper was given by Dr. André Boischot, Observatoire de Paris, Section d'Astrophysique, Meudon (Seine et Oise), France.

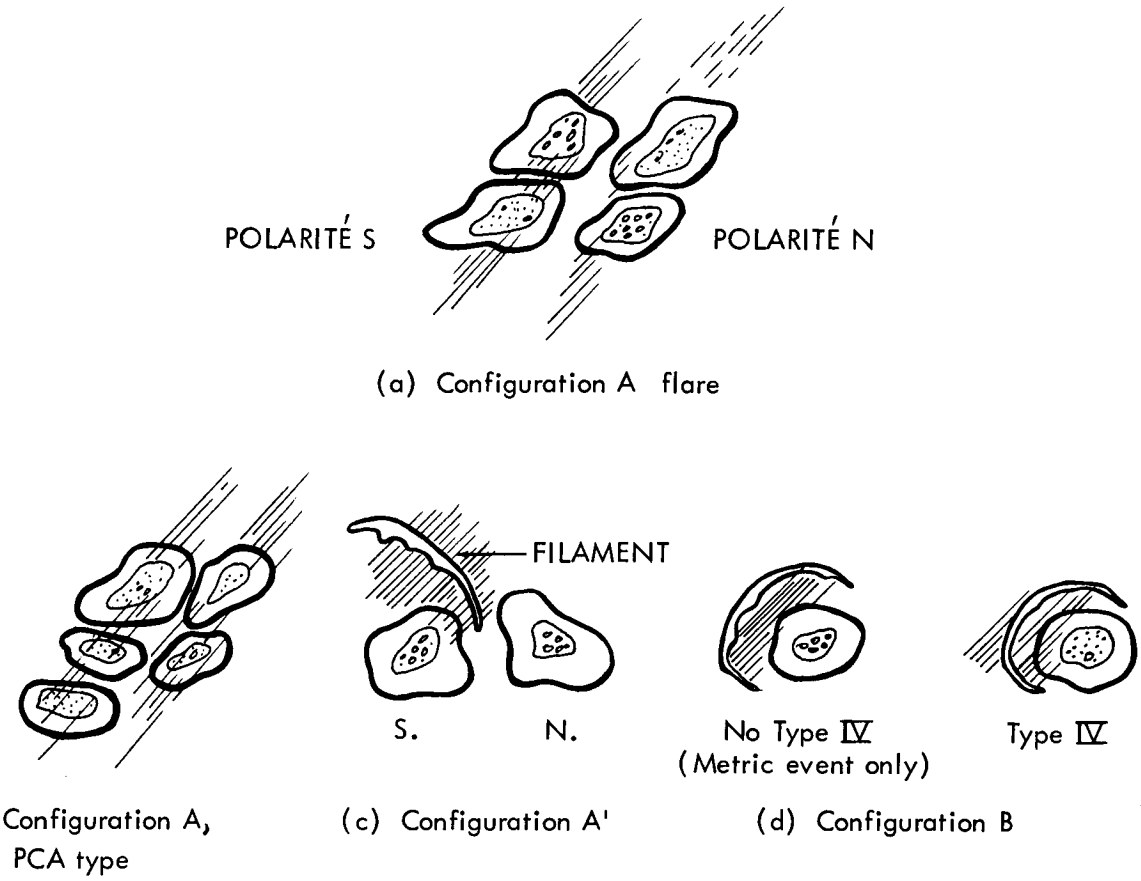

FIGURE 3–1.

REFERENCES

1. AVIGNON, Y., MARTRES-TROPÉ, M. J., and PICK-GUTMANN, M., 1963, *C.R. Ac. Sc.*, 256: 2112.
2. ELLISON, M. A., MCKENNA, S., and REID, J. M., 1961, "Cosmic Ray Flares," *Dunsink Observatory Public.*, 1(3).
3. MARTRES, M. V., and PICK, M., 1962, *Ann. Astrophys.*, T. 25(5): 4.
4. DODSON, H. W., and HEIDMAN, 1960, *Astronom. J.*, 65: 51.
5. MALVILLE, J. M., and SMITH, S. F., 1963, *J. Geophys. Res.*, 68: 3181.

DISCUSSION

Dr. Firor: May I ask, the 25 other events which did not have type IV, did they also cover some of the penumbra or umbra?

Dr. Boischot: Out of 61 flares which were studied, only 6 gave type IV events. The others did not give type IV and not once covered a penumbra.

N64-30255

4 FLARE IMPORTANCE RATINGS—SOME HOPE FOR IMPROVEMENT

CONSTANCE S. WARWICK
Central Radio Propagation Laboratory, National Bureau of Standards
Boulder Laboratories, Boulder, Colo.

All of you who have used published flare data are aware of inconsistencies among reports of a given flare from various observatories. The published data fail to reveal the full extent of these discrepancies because the observatories that disagree most drastically and most consistently are widely separated in longitude and seldom see the same flare. Dodson and Hedeman showed that about four times as many flares of Importance 2 are reported to begin at 8 to 10 hours Universal Time (UT), as at 18 to 20 hours. The distribution of subflares is no more uniform but has its maximum at a different hour. Clearly, the problem is not that flares are not observed at 18^h UT but that what looks like a perfectly good flare in Paris or Rome is called a subflare in Colorado or California. Another serious error that does not show up in a comparison of published reports is the center limb variation in the importance scale. Twice as many flares are reported in a 10-degree interval of central meridian distance near the center of the disk as in a similar interval at the limb, and this is true for the large flares as well as for the smaller ones.

Although we detect these errors through the nonuniformity of distributions in UT and in CMD—distributions that we expect to be uniform—the errors actually depend on the reporting observatory and on the distance of the flare from the center of the disk. What we really want to know is something like this: If Monte Fortissimo reports a class 3 flare 30 degrees from the center of the disk, then it probably is really class 2; and if Peaceful Peak reports an Importance 1 limb flare, it is more likely 1^+.

At the National Bureau of Standards we are trying to carry out such a program, grouping together reports that pertain to a given flare, and applying corrections to each reported importance rating to derive final values that are free from these systematic errors. The project is far from complete, but we are far enough along the way to have discovered some pitfalls and to be able to estimate what kind of success is attainable. For IGY, the number of flares per UT observing hour can be made uniform for flares of Importance ≥ 2. The center-limb distribution is uniform for flares of corrected Importance 1 or greater. Although the systematic errors can be removed, at least for the larger flares, the more or less random disagreement among reports of a given flare, as measured by the sum of the squared deviations from the mean, is only slightly improved. The corrected values offer an improvement over the original values, mainly because they cannot introduce spurious and misleading relations into solar or geophysical studies utilizing flare data.

DISCUSSION

Dr. Lindsay: Is there a unique flare phenomenon? May it not be that this phenomenon which we have associated with flares may be occurring in centers of activity all the time, or more or less all the time, and that the sensitivity level is such that we call only certain things flares?

Dr. C. Warwick: If you are suggesting that we are not seeing everything that might be called a flare in Hα, I certainly agree with you.

Dr. Lindsay: I am really asking the question: Is there a unique flare phenomenon, or is this phenomenon occurring fairly generally at low levels that we don't observe?

The reason I raise this question is: If we take some of the OSO data, which I hate to mention because I may be speaking of something that someone else is going to talk about, the x-ray flux apparently from centers of activity is almost continuously varying. Whether these rapid variations in x-ray emission from a plage give a different phenomenon from that occurring in flares (except that it is more intense in flares) we have no way of knowing. It may well be the same phenomenon.

I am wondering whether other flare phenomena may not be occurring in plage activity more or less regularly but below the threshold of our observations.

Dr. C. Warwick: I should think that might well be so. Certainly, as a station lowers its threshold, or reports smaller and smaller flares, then it must see more and more small, short-lived phenomena.

Dr. H. Smith: Will it always be necessary to pursue massive statistical rectification of flare area reports, or have we perhaps—from your study—learned some things that will enable the reporters to improve their techniques and the quality of the raw data they report?

Dr. C. Warwick: I am sure they could and will be improved, but I think it is always going to be useful to have a comparison of the data, such as this I have described.

Dr. Zirin: I think the Lindsay and White OSO observations show how we are "prisoners of history" in this respect. We have only been studying Hα for many years. We are stuck with having to clarify a phenomenon which is observed in one line, indeed quite an important line, but only in one way, which may or may not be a pale reflection of what is going on. We might have been more fortunate if we had no Lyot filters or spectroheliographs and could observe flares only in 2800 Mc. We would have a much more quantitative measure of the importance of these things.

I think some time after the conclusion of a colossal study of this type you should perhaps be able to set up final criteria so that we can compare things and decide what it really is we want to class in importance.

Are we really interested in the area or the Hα brightness? Are we perhaps more interested in the 2800 Mc intensity, or the depth of the ionospheric absorption? It is really questionable whether we are truly interested in the Hα brightness, or have we gotten into that corner through historical reasons?

Dr. C. Warwick: Perhaps.

Dr. Giovanelli: This raises the rather broader question that was brought out by Dr. Boischot's talk and must, in any case, be obvious to many other people who have been studying the relations between flares and other phenomena: that it is not primarily area or importance that counts, but other things.

For example, by going to the little 1— flares, one can often find things happening that are associated with type III radio bursts, that are associated with the ejection of particles across or out from the surface of the sun.

We ought to be considering more the characteristics that enable us to class flares into a common physical type. For example, we have seen that flares which cover sunspots have certain characteristics. They produce other things on the surface of the sun. They may cause the ejection of high-speed particles.

We can characterize flares that break out in filaments, flares that break out bordering filaments; and no doubt we ought to be able to classify other sorts of flares, not by their size so much as by other identifiable characteristics.

I suggest that this is one of the most important things that the observers can do, to get together and sort out ways of telling the non-solar people just which flares have common optical characteristics. I think that this would be quite a help.

The radio people already have done this. They have classified their bursts into various types, and they understand one another when they are speaking of these things.

I am afraid that, with our longer history, the optical people have not done this as yet. I would urge this as an urgent matter.

Dr. Firor: I would suggest, as an ex-radio man, that Dr. Giovanelli underestimates the agreement among radio observers.

SUMMARIES OF TWO RECENT PUBLICATIONS BY J. M. SLONIM AND S. I. GOPASYUK ET AL.

Contributed by E. R. Mustel

Prof. Mustel has supplied the following summaries of two recent Soviet publications.

J. M. Slonim: *Solnetchnye Dannye (Solar Data)*, 1963, 4: 67; and *Sov. Astr. Journ.*, 1962, 39: 798.

It is possible on the basis of existing observations to divide the chromospheric flares into three types:

A. Sharp and short impulses of emission. They are accompanied by ejection of chromospheric gases (in particular, by surges).

B. Strong and slow bursts of emission. They are accompanied by the upward outflow of chromospheric gases with a constant velocity of the order of 10 km/sec and by an appearance of prominences which are similar to the loop prominences.

C. Chromospheric flares of long duration with a small amplitude of the light curve. These flares are characterized by a pulsating brightness; they are accompanied by an inflow of loops, streams, and jets of coronal prominences.

The width of the Hα line and the maximum brightness of the flares of types A and B depend on the area of the flare emission, whereas the brightness amplitude and the width of Hα line for type C are small and are not connected with the area of flare emission. The flares of A and B types are observed mostly on the descending phase of development of the active region, while the flares of type C are observed on the ascending phase.

The nature of the chromospheric flares of types A, B, and C is different. The flares of types A and B are chromospheric phenomena, whereas the flares of type C arise inside the solar corona and gradually diffuse toward the lower layers.

Some facts which speak about the relatively high (coronal) localization of the flares of type C are indicated.

S. I. Gopasyuk, M. B. Ogir, and T. T. Tsap: *Solnetchnye Dannye (Solar Data)*, 1963, 4: 77.

It is found that the ejections from the chromospheric flares (which produce dark areas on the solar surface in the Hα line) possess the following properties: (a) They appear during the whole lifetime of the chromospheric flare; (b) the appearance of an ejection is always accompanied by an increase of Hα brightness of an already existing knot of the flare or by the rise of a new knot; and (c) ejections proceed from the penumbra or from the umbra of sunspots.

A comparison of the number of atoms contained in the flare with the total number of atoms in the whole chromosphere or in the whole corona seems to indicate that the gases of the flare itself and of the ejections come mostly from the photosphere. This is corroborated by the fact that, during the chromospheric flare, the upward radial velocities at the photospheric level are increased. In this connection the authors suggest that this strong enhancement of the mass of gases lifting from the photosphere, the ejection of chromospheric gases above the sunspots, and the appearance of the chromospheric flares themselves—all this is a result of the same *primary* process which takes place in the photosphere or in the subphotospheric layers.

Spectrographic Observations

N64-30256

5 SPECTROGRAPHIC OBSERVATIONS

HAROLD ZIRIN
High Altitude Observatory
Boulder, Colo.

Spectrographic observation of solar flares has been heavily influenced by observational factors. The fact that the spectrograph is not an automatic instrument but must carefully be set on a flare when it occurs has severely limited the number of flare spectra that have been obtained. It is almost impossible to anticipate the region in which a flare will occur, and most of the spectra we have were obtained in the late phases of flares. Further, activity in this field was not strong until after 1950.

Even when a spectrogram of a flare has been obtained, it is not exactly clear to what we are referring. When an observation is made on the disk, the spectrum is obtained superimposed on the spectrum of the photosphere, which is normally excited by the flare. It is very difficult to decide which portion of the spectrum is due to the flare itself and which is due to the excited background. When we are fortunate enough to obtain the spectrum of a flare on the limb, we can feel satisfied that we have separated the flare radiation from the radiation of the sun itself. However, there is some question as to the relation of the bright cloud of material that appears above the limb and the flare that we see on the disk in Hα. Certain spectral characteristics are common to both limb and disk flares, however, so that we may avoid this problem for part of the observations.

Some of the problems of observing the spectra of flares are illustrated by Figure 5–1, which is a Sacramento Peak Hα filter photograph of a large ascending or eruptive prominence on June 14, 1956. We see that there are two small prominences visible on the limb. Figure 5–2 shows spectra obtained in Hα at Climax at the same time at various heights. The spectra made at 1515 UT were made in the lower part of the eruption, while those at 1531 were made at a series of heights higher up. We see in the 1515 spectra that, although the prominence *A* is a quiescent prominence (because it shows a narrow emission line), the prominence *C* shows the broad Hα emission of a flare and indeed was a flare, probably responsible for the ejection of the eruptive prominence *B*. Radial velocities have shifted its emission out of the pass band of the filter. In the 1531 UT spectrum, remarkable radial velocities are observed at the top of the eruption. Separations of 11A are observed, indicating that the top of the loop is flying apart at 800 km/sec.

The limb observations show us the faintest lines, so we begin with them. Figure 5–3 shows the spectrum of a limb flare November 20, 1960. This is after the maximum of the flare but still during a phase when energetic radiation was being produced. The spectrum of the flare is more or less similar to that of a B-star. It is dominated by the lines of hydrogen and helium. There also is strong radiation from ionized helium at 4686. The lines of the ionized metals, although weak, may still be observed. Relative to the hydrogen and helium lines, they are quite weak as compared with their strength in the chromospheric spectrum. In addition to these line emissions, we see a strong continuum, which in this case appears to be the same color as the sun. We also see one coronal line, the 4412 line of argon XIV.

In Figure 5–4 we see the spectrum of the flare in the region between 5400 and 5800A. In this region only three strong emission lines are seen: two lines of Ca XV, and a line of ionized helium. In this part of the spectrum the flare might be said to exhibit the spectrum of a recurrent nova, like RS Ophiuchi. The only

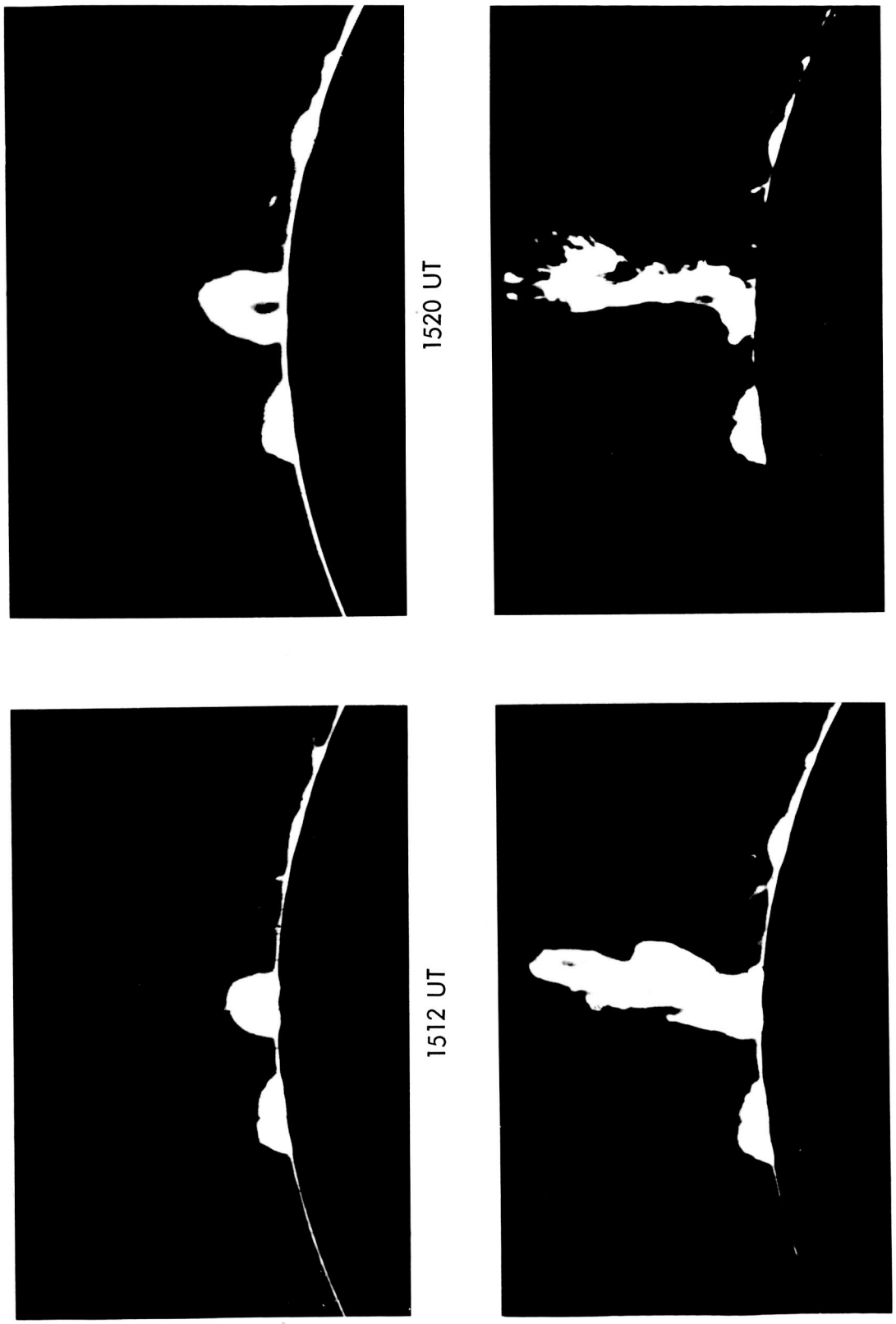

FIGURE 5–1. Flare and eruption, June 14, 1956, observed with Hα filter at Sacramento Peak.

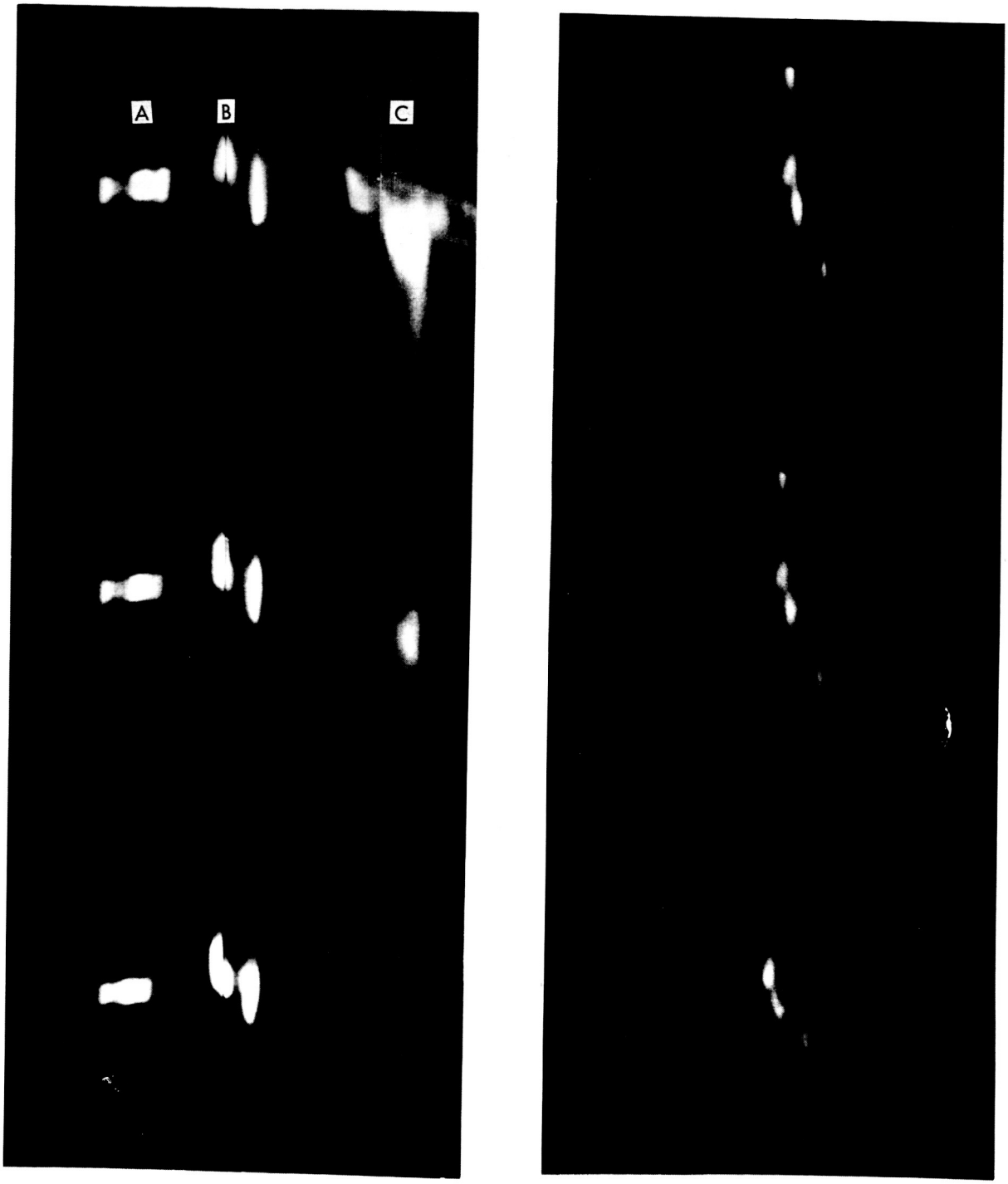

FIGURE 5–2. Hα spectra of same flare (Figure 5–1) at various heights, obtained at Climax. 1515 UT spectra are at lower heights; 1531 spectra are higher. (Height intervals, 4500 km)

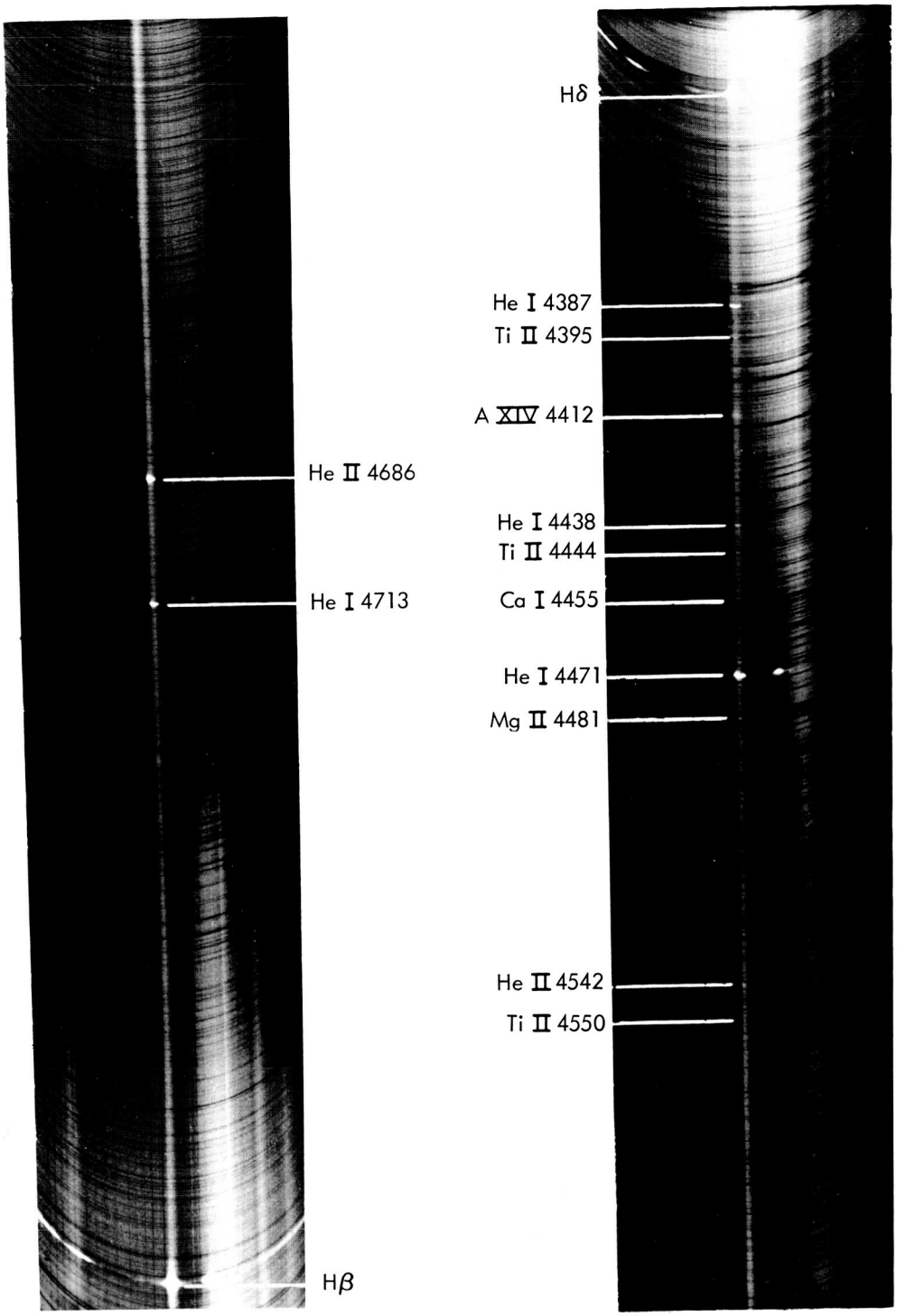

20 NOV. 1960

FIGURE 5–3. Spectrum of limb flare November 20, 1960; 4500A region, 2145 UT. Dark curved lines are the spectrum of the sky; bright streak across middle is continuum emission, probably due to electron scattering.

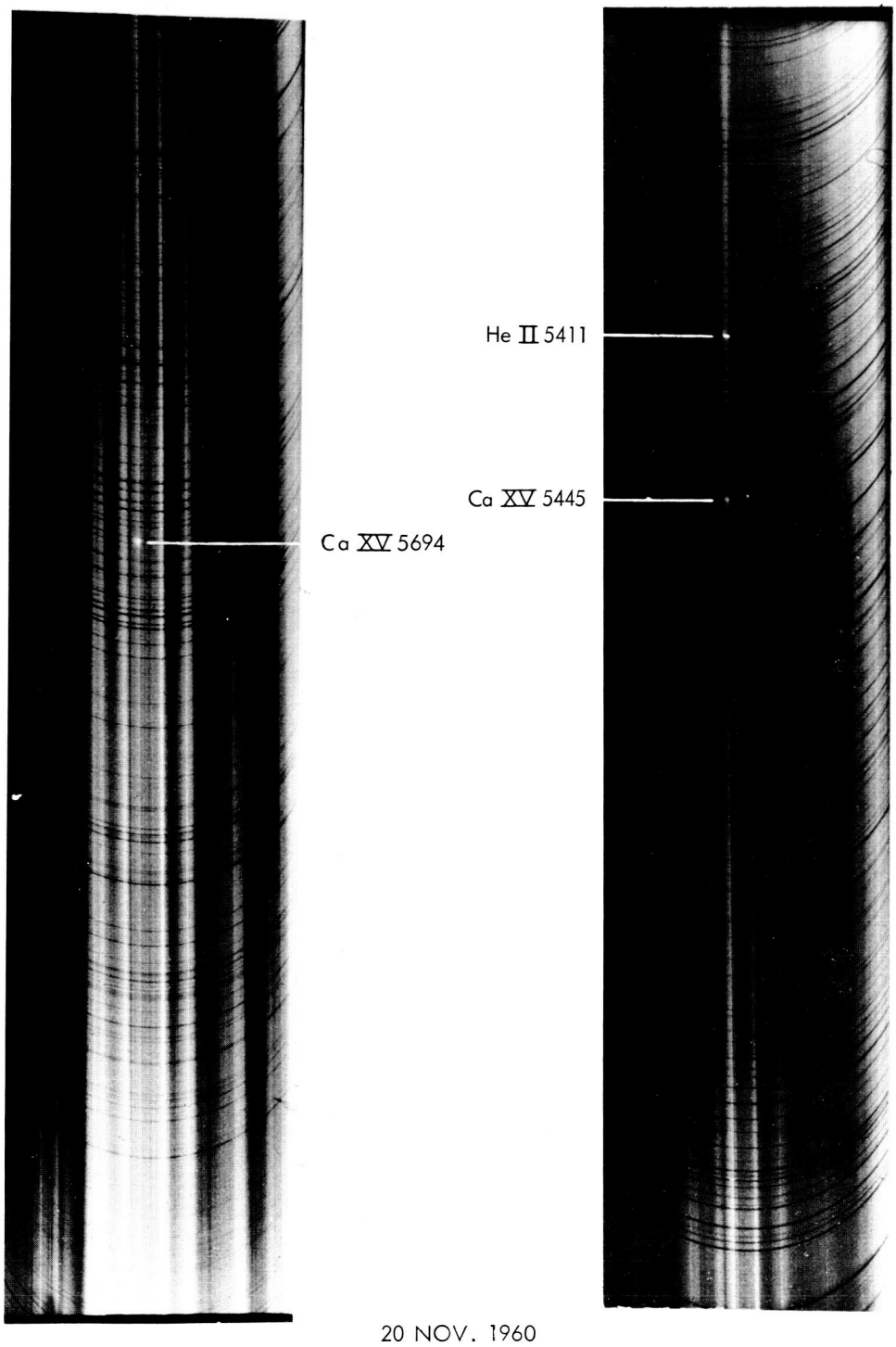

FIGURE 5–4. Spectrum of same flare in yellow region, 2227 UT. Stray light at sides is photospheric light which got around the occulting disk because of chromatic aberration in the coronograph.

metallic line that we have found to be enhanced in the spectrum of the flare is the 4481 line of Mg II, which is a high excitation line.

Figures 5–5 and 5–6 show the spectra of two limb flares—on December 18 and 19, 1956—in the region between 3900 and 4100A. This spectral region is fairly rich in lines, although there are no strong ionized helium lines. In addition to the H and K lines of ionized calcium and the hydrogen lines, the spectrum is dominated by strong neutral helium lines. One important criterion is the ratio of the Sr II line at 4077 to the neutral helium line at 4026. In quiescent prominences and the low chromosphere these lines are about equal in intensity; but in flares the helium line is much stronger.

The December 18, 1956, flare was really a bright condensation from the corona—in fact, it appeared suspended above the limb. It shows the emission of the 4086 line of Ca XIII, indicating the high temperature. By contrast, the December 19, 1956, flare was a bright mound projecting upward from the surface, and shows no coronal line. Probably connected with this is the fact that the first flare was associated with an ionospheric fadeout, presumably caused by coronal radiation, while the second was not.

At this point we have no spectra of the explosive phases of flares—most of our observations are of necessity of the post-flare loops or the strong coronal condensation that appears to be produced by the explosion. There are spectra, however, of nonexplosive flares.

When a flare is observed on the disk, we may no longer see the faint helium and coronal lines; and the continuum is relatively more difficult to detect. Figures 5–7 and 5–8 show two spectra of disk flares obtained by Jefferies, Smith, and Smith with the universal spectrograph at Sacramento Peak. One may often see a great number of metallic lines of considerable intensity, which are more easily visible because they fill in deep absorption lines. These often are somewhat displaced from the position of the bright hydrogen and helium emission and have quite narrow profiles. However, their intensity relative to the hydrogen and helium lines is much stronger than that seen in the limb flares. They appear to come

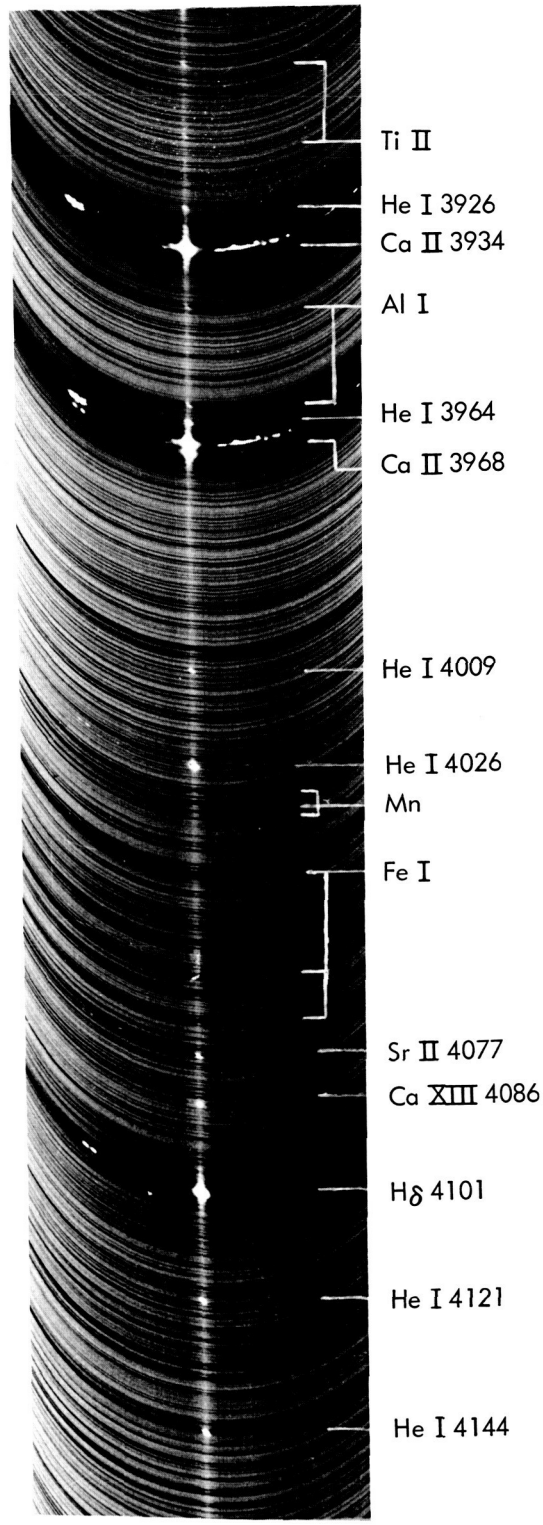

FIGURE 5–5. Spectrum of limb flare December 18, 1956; 4000A region.

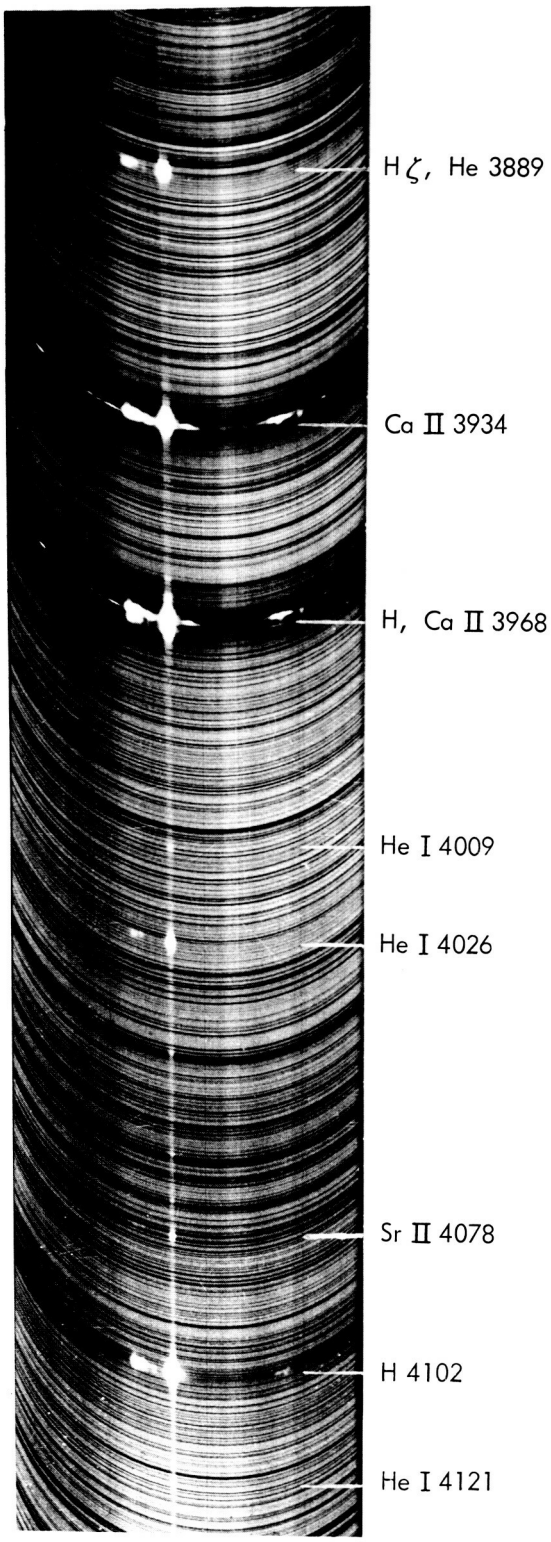

FIGURE 5–6. Spectrum of limb flare December 19, 1956; 4000A region.

from a chromospheric region which is excited by the radiation of the flare. More careful investigation of such lines should give us much more information on the relation between the flare and the underlying chromosphere.

The continuum radiation from flares is of great interest. If we see continuum at the limb, it is tempting to ascribe it to Thomson scattering of photosphere radiation. This is true for all of the continuum to the red side of the Balmer limit. On the far side of the Balmer limit, however, one often finds strong emission in the Balmer continuum. The comparison of this emission with the scattered continuum to the longward side of the Balmer limit has given important information on density and temperature in flares. When we observe flare continuum emission on the disk, we must find a different explanation. Thomson scattering could only lead to absorption, and not emission, from a flare region seen projected against the bright photosphere. Thus the continuum seen on the disk in the visual region must be due to free-free emission and free-bound continua of elements other than hydrogen, as well as possibly Paschen continuum. It may also be connected with the excitation of deeper lying chromospheric layers by the flare. There has been the suggestion that the continuum emitted by disk flares is due to synchrotron radiation. To my knowledge, no conclusive measurements of the polarization have been made. Presumably, even if polarization were not found, the backers of the synchrotron hypothesis would be able to devise an explanation for that situation as well.

It is important that the flare spectra obtained so far differ only in brightness from that of the loop prominences that condense from the corona after flares. This suggests that what we see in the spectrum is just the cooler part of the flare, probably what has cooled from coronal temperature.

The spectrum of flares in the extreme ultraviolet will be discussed by Dr. Neupert in the next paper, and I only note that in the ultraviolet we see the resonance lines of the same coronal ions observed in the visible. In the x-ray region we are not certain whether the emission of the flares is due to lines or

728–629 O—64——4

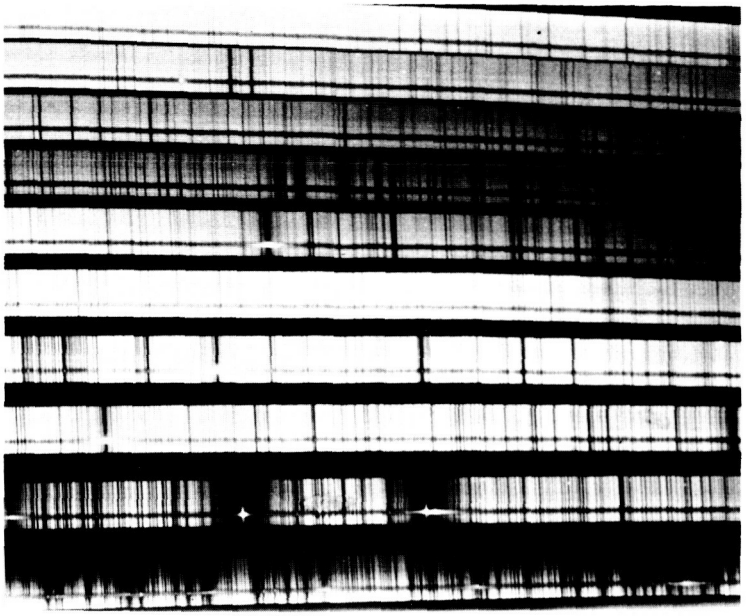

FIGURE 5–7. Section of Universal Spectrogram of disk flare September 2, 1960. Note prominent broad emission of Balmer lines, Ca II H and K lines, and He I D_3. Many metal lines, especially of Fe I, appear as sharp emission peaks. (E. Smith, Sacramento Peak Observatory)

FIGURE 5–8. Universal Spectrogram of disk flare of September 18, 1957. (Jefferies, Smith, and Smith, Sacramento Peak Observatory)

continuum. Although Blake recently has found line emission down to 13A in the spectrum of the quiet sun, it is not clear what is the relative strength of the emission lines and of the continuum. Of course, we know nothing at all about how they behave during a flare. There is strong evidence that different flares have different spectra in the x-ray region. This is shown by the fact that some flares which produce observed increases in the spectrum in the 10 to 20A region do not produce ionospheric effects, which require x-rays in

the 2 or 3A region. Observations with various satellites certainly have indicated such a variability.

We turn to the analysis of the various radiations in the flare spectrum. The analysis of the continuum is most straightforward. When we observe scattered continuum above the limb, we attribute it to Thomson scattering. This cross section is well known, and we may assume the condensation we are looking at to be cylindrically symmetric. All electrons must scatter with the Thomson cross section no matter what their temperature. For a condensation of cross section L and intensity $I/I_{\odot}$ (measured in terms of the intensity of the center of the disk) the electron density is given by

$$N_e = \frac{0.6 \times 10^{25}}{L} \frac{I}{I_{\odot}}.$$

We may use this formula only for limb flares. We have used it in the case of a number of limb flares and obtained densities between 3×10^{10} and 3×10^{11} near the maximum phase of flares. If there is filamentation in the object at which we are looking, then this density is too low—although the observed value for the total number of electrons along the line of sight must be correct no matter what the filamentation situation. If there is considerable free-free emission, this estimate is too high. Free-free emission is important only in cases of high density, which would imply greater filamentation. These two effects would therefore balance one another, so that we have a reasonably good value.

The determination of electron densities and temperatures from the ratio of the Balmer continuum to the continuum longward of the Balmer limit has been studied by Jefferies and Orrall. The emission on the long side is predominately due to electron scattering, and hence proportional to n_e. The emission in the Balmer continuum is proportional to $n_e^2\ T^{-3/2}$. The ratio of the emissions on either side of the Balmer limit, after subtracting the electron scattering component on the shortward side, is approximately proportional to $n_e\ T^{-3/2}$. The method therefore lends the greatest weight to regions of high density and low temperature. The ratio has been measured in a number of cases by Jefferies and Orrall, who find combinations of densities and temperatures like 20,000° and $n_e = 10^{11}$. Just as we shall indicate in the discussion of line emission, one should be most careful in the interpretation of these temperatures and densities. They effectively compare the free-bound recombination from the cooler parts of the flare with the scattered continuum from the entire flare. The temperatures obtained appear, indeed, to be appropriate to the temperatures at which hydrogen would be recombining from the flare cloud.

A completely different picture is given by the analysis of the coronal lines in the flare. The lines that are characteristically observed to be enhanced are the two lines of Ca XV at 5445 and 5694A, the line of Ca XIII at 4086A, and the line of A XIV at 4412A. All these lines have ionization potentials over 650 volts. Thus, observations of them refer only to the hot part of the flare, just as the Balmer continuum must arise in the cooler part. The fact that these lines are observed at all gives us a rough temperature to begin with, since the ionization equilibrium in the corona is such that they should be observed only at temperatures above 3 million degrees. Measurements of the line widths of these four lines in various flares always give values between 3 and 4 million degrees. These are the only two clear-cut measurements of the temperature which may be made in this case.

The intensity of the lines may be used to estimate the density in the flare coronal condensation as well. This may be done in two ways: Under conditions of fairly high density, any coronal line is excited primarily by electron collisions, with a smaller contribution due to photospheric excitation. Since the electron scattering continuum is proportional to n_e and the collisionally excited line emission will be proportional to n_e^2, the ratio line/continuum is proportional to the electron density along with constant factors, such as the abundance of the element in question. Of course, for any line there is also dependence on ionization equilibrium; but, if we observe two stages of ionization, such as in calcium, we can assume that a certain fraction of the element is in a stage of

ionization observed. A second method of determining the electron density is to measure the ratio of two lines from different levels in the same ion, as in the case of Ca XV. One may make an equilibrium calculation of the dependence of the intensity of the two yellow lines on electron density and use this to determine the electron density when a certain ratio is observed.

Both methods discussed above depend critically on the collision cross sections, because that is the way in which the density enters the calculations. Therefore, if we use collision cross sections that are 10 times too great, we will get a density that is 10 times too small. One way of checking this is to normalize the method by comparing the results with the results from measurement of the electron scattering continuum. Further, the line intensity methods measure the true local electron density at the point where the line is produced, whereas the continuum methods measure the total density along the line of sight. So another discrepancy is introduced in this way. So far, the preliminary results indicate that the cross sections calculated from Fe XIV by Blaha must be decreased by about a factor of 10 when applied to Ca XV.

The analysis of the x-ray spectrum goes pretty much like the analysis of the continuum except that there is hardly any spectrum to observe. The published observations indicate that the intensity in the 10 to 20A region corresponds to emission from material at 4 million degrees. In the shorter wavelength region the contribution must be due to a much more energetic source, and probably can be explained only by bremsstrahlung from high energy electrons with energies over 20 kev.

A key question is: What does this coronal part have to do with the flare? Is it the real flare, or is it a hot side-effect? The photos of the November 20, 1960, flare shed some light on this point. This flare occurred when the November sunspot group had gone around the limb of the sun, but its upper parts still could be seen above the limb. Figure 5–9 shows six phases of the flare, which began at 2023 UT. Figure 5–10 shows radio and ionospheric effects. The peak ionospheric effect was at 2045 UT, but nothing is visible in Hα.

This large flare, which gave a ground level cosmic ray increase, is a typical explosive flare. First, a large bright cloud of material appeared above the limb, starting at 1940. This is called the "first flare" in the caption, but it probably was all one phenomenon. The first cloud was accompanied by an increase in the microwave emission at 1940 and by a mild dip in the cosmic noise radiation received at the earth's surface, produced by an increase in the ionospheric absorption. At 2022 the explosive phase began. Typically these explosive phases seem to be triggered by small surges or flares in other parts of the active region, from which hydromagnetic waves propagate and set off the explosion.

When the explosive phase occurred at 2023, there was a sharp increase in the 2800 Mc/s emission observed by Covington and a major ionospheric fadeout and cosmic noise absorption. The peak ionospheric effect, which corresponds to the peak x-ray emission, took place at 2040 UT, at which time nothing was visible above the limb in Hα except a small surge. For this reason no Climax spectra were obtained at this time. The fact that such a large ionospheric effect is produced with the sunspot 15,000 km below the limb and no Hα to speak of proves that the x-ray emission comes from the corona high above the surface.

At 2117 a bright loop formation appeared above the limb, of which the spectra shown in Figures 5–3 and 5–4 were obtained. Although the Hα loop was of flare brightness and is called the "second flare" in the figure, it was really the cool recombined part of the coronal material still present and still producing the ionospheric absorption (which lasted till 2300 UT, at least). This fact is graphically illustrated by Figure 5–11, which shows the spectrum lines 5411 of He II and 5445 of Ca XV at four different heights at 2155 UT. Comparing these two lines, which represent the extremes of temperature in the flare, with the continuum gives us a measure of the total number of electrons at all temperatures. Microphotometer measurements show that the continuum intensity and the coronal line

LIMB FLARE OF NOV. 20, 1960

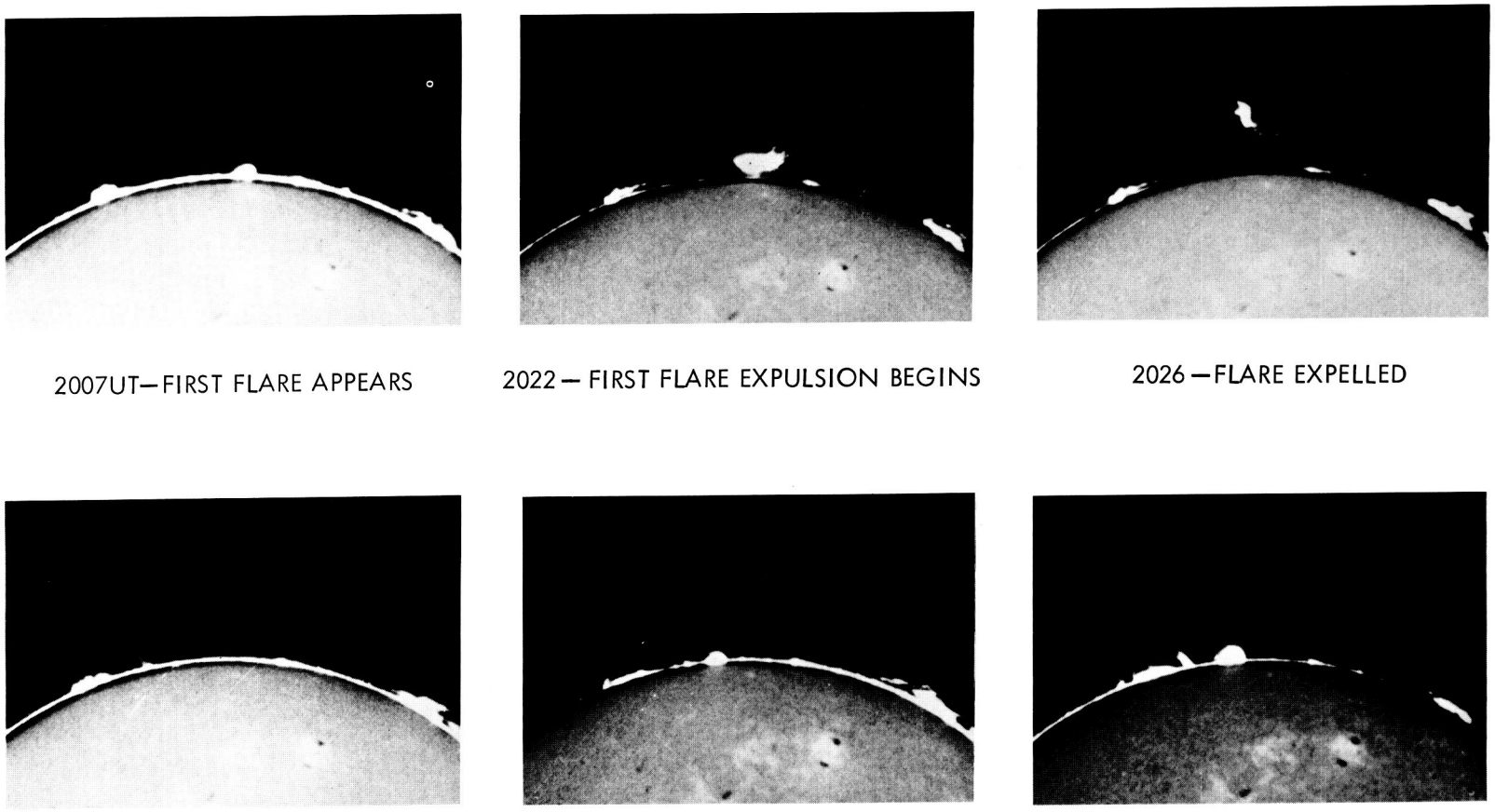

2007UT—FIRST FLARE APPEARS

2022—FIRST FLARE EXPULSION BEGINS

2026—FLARE EXPELLED

2040—SMALL SURGE; PEAK OF SSWF

2145—2nd FLARE, WHICH FIRST APPEARED 2117, RISES ABOVE LIMB

2245—2nd FLARE MAXIMUM

FIGURE 5–9. Sequence of events on November 20, 1960. A limb picture with 3A bandpass and the sun occulted is superposed on a 0.75A pass band disk picture (both Hα).

NOVEMBER 20, 1960

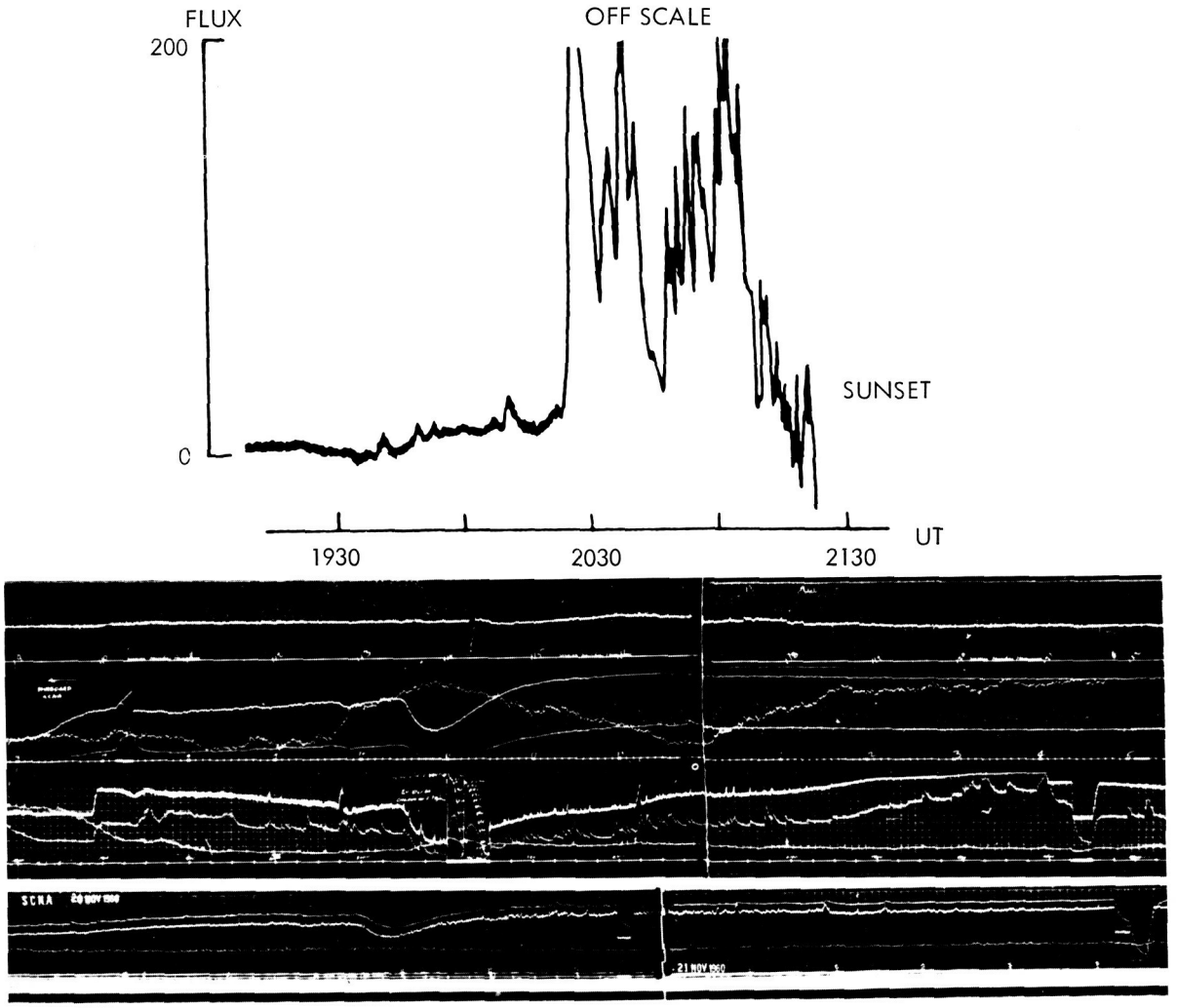

FIGURE 5–10. Upper half: 2800 Mc/s radio observations by Covington, November 20, 1960. Lower half: Records of cosmic radio noise at 18 Mc/s from (top to bottom) Sacremento Peak, HAO Boulder, Hawaii, and McMath-Hulbert. (Boulder record shows 27 kc atmospherics as well.)

intensities vary little with height, while the He II emission increases sharply close to the surface. This means that a large amount of ionized helium emission can come from a very small fraction of the flare material, and leads us to conclude that the preponderance of the flare material above the limb is at coronal temperatures.

Finally, Figure 5–12 shows a very interesting spectrum obtained by accident at 2007 UT during the beginning of the flare by the routine Climax coronal survey. The pre-flare is marked at point B by extremely strong Hα emission as well as continuum. It is strongly shifted to the blue, which accounts for the fact that narrow-band Hα filters did not pick it up. At point A, however, which coincides with the probable position of the spot group, there is strong continuum but no Hα emission. It was at point A that the flare loops appeared

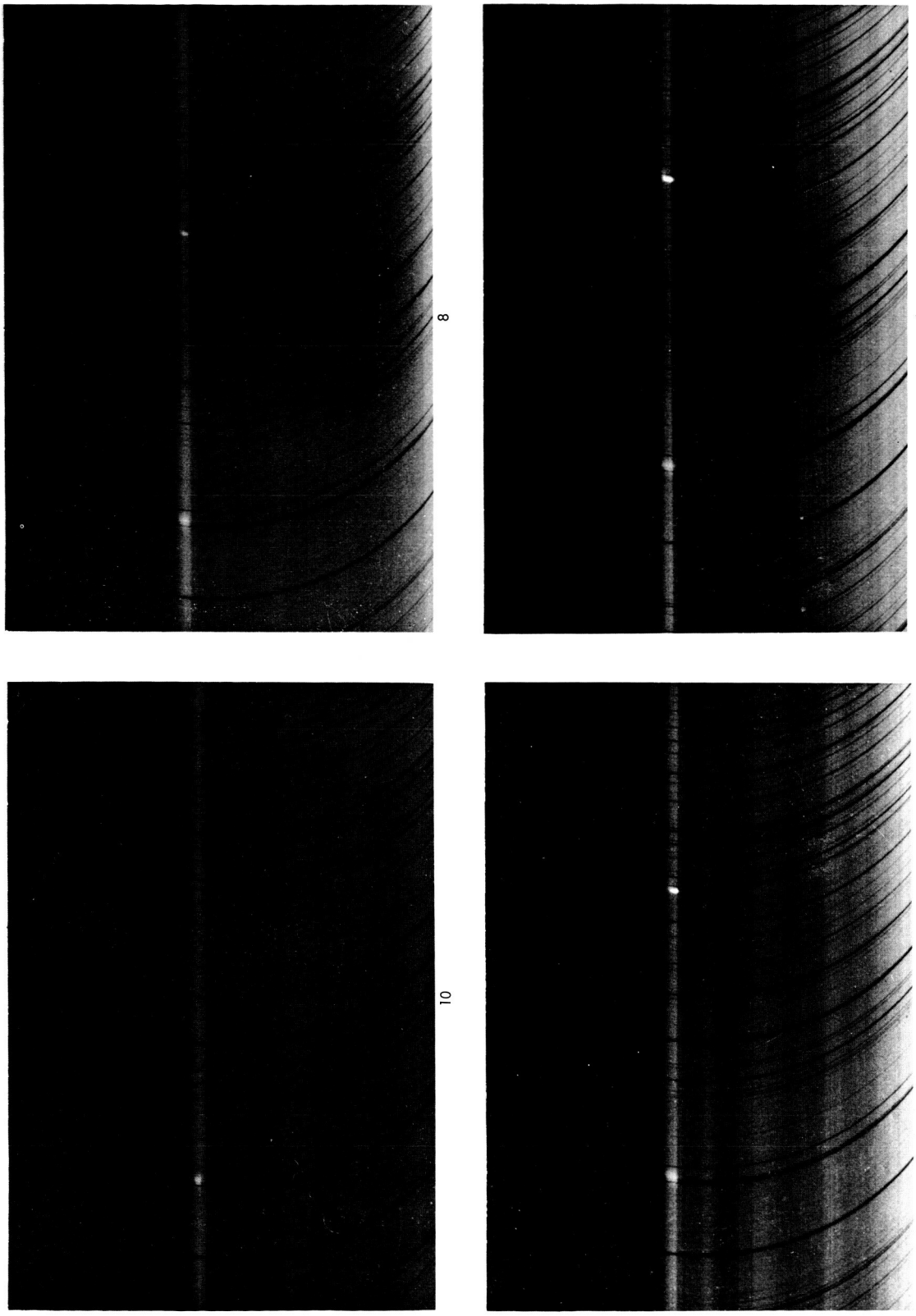

FIGURE 5–11. Spectrum of November 20, 1960, flare at various heights (4, 6, 8, and 10×2200 km) 2155 UT, showing 5411 (He II) and 5445 (Ca XV)

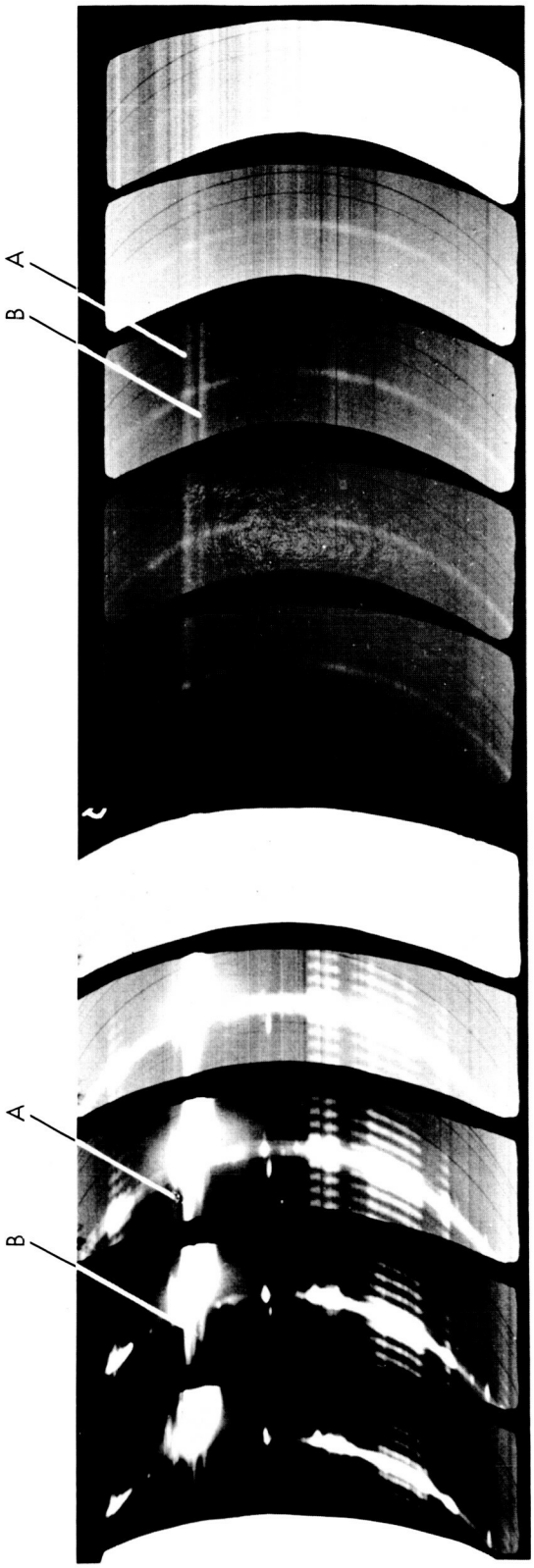

FIGURE 5–12. Spectrum of limb flare November 20, 1960, 2007 UT, in Hα and red coronal line of Fe X, 6374.

at 2117 UT. Such pre-flare continuum has been observed a number of times.

Much study has been devoted to the non-coronal emission lines. They are easy to observe and complicated to explain, so the theoreticians have had a field day. The principal conclusion that one seems to find is that each emission line tells us about the peculiar conditions under which it alone is emitted, and is not so informative about the condition of the rest of the material. An example would be the lines of ionized helium. These, except for the corona lines, are the highest excitation lines that we observe; and their intensification in flare spectra is a measure of the high excitation present (at least in the region where these lines are emitted).

We have conducted a program for a number of years for photographing these lines in limb flares and, in particular, of comparing the neutral helium line 4713 with ionized helium 4686. Although 4686 is normally about 10 times weaker than 4713, it usually exceeds it in brightness in flares. In every case in which we have been able to measure these lines, we find that the Doppler width of the ionized helium line exceeds that of the neutral helium line. This means that the ionized helium emission comes either from a hotter region or from one where there are greater microscopic velocities. Neither result is surprising. But it shows clearly that it is pointless to try to derive temperatures in the flare by comparison of the ionized and neutral helium emission. We may decide only on the relative proportion of the flare material of higher and lower excitation.

Furthermore, since we are also looking at many filaments, we are performing a kind of time-averaging. Some filaments along the line of sight may have started cooling from the coronal condensation earlier than others, and the brightest lines will be those which last the longest and thus are present in the largest fraction of the material along the line of sight. The importance of this point is shown by the ionized helium observations. We may observe three lines of helium: 4686, 5411, and 4542, due to the transitions 4 to 3, 7 to 4, and 9 to 4, respectively. The ratio of intensity of these lines is far from what one would get under normal conditions of static excitation. They may be explained only if the helium is continually recombining from the corona, so that each ionized helium atom radiates just once and drains downward to neutral helium. An example is shown by the flare of November 20, 1960. In Figure 5–3 we show the spectrum of 5411 and 5445 as observed in this flare at different heights. At the higher level, the ionized helium line is seen as a line quite similar in distribution and line width to the corona line. This line is clearly due to recombination from the corona. At the lower heights there is a very large increase in the intensity of this line without corresponding change in the continuum or corona line intensity. Presumably in these lower heights the excitation mechanism is much more efficient, and a small amount of material at fairly low temperature and perhaps higher density suffices to produce the greatly enhanced emission in a line. This also convinces one that the material whose electron scattering we measure by the continuum observation is predominately at coronal temperatures, since the intensity of the coronal line is more or less the same throughout the flare; and the low excitation line emission can be explained by the emission of a fairly small part of the material, as in Figure 5–11.

A great deal of effort has been put into the interpretations of the hydrogen lines in the solar flare. These are the easiest lines to observe and the most complicated to explain. Hydrogen occupies a curious position in the ionization scheme. It is easy to ionize but very difficult to ionize more than once. Therefore, there is always recombination emission of hydrogen lines at almost all temperatures, and the hydrogen emission may take place at quite a range of temperature. The observational evidence, however, indicates that most of the emission observed is in the 20,000 to 30,000 range. The hydrogen lines are particularly sensitive to Stark broadening, and there has been a spirited controversy over whether this broadening was important in the profiles of the Balmer series. The early Balmer lines are usually broadened by self-absorption, whereas the higher members

would be particularly sensitive to the Stark broadening.

One example of the detailed study of the Hα line was that by Svestka of the flare of August 7, 1960, notable for its intense x-ray emission. This flare showed a very strong self-absorption, in the course of the Balmer lines, which is not always observed. In this case the higher Balmer lines were clearly broadened by the Stark effect, and the rather high value for the electron density of about 5×10^{13} cubic centimeter was derived. The temperature of the height of the Balmer-line emitting region was found to be of the order of 10,000 or 20,000 degrees, as is a common result in all studies of this type. A most interesting result of Svestka's investigation is that it was possible to deduce the geometrical thickness of the radiating layer. From the hydrogen lines, resulting thicknesses of the order of several kilometers were obtained; from the absence of any Balmer continuum emission, a value of less than 4 kilometers was found. Of course this latter value depended on an assumption of 10,000° for the temperature. In any event, in many of the cases it is possible to explain the observed hydrogen line emission from extremely thin geometrical thicknesses of material. A similar result is obtained by Suemoto and Hiei. This is equivalent to saying that we can get the observed hydrogen line emission from only a small fraction of the material in the flare which is cool enough to produce this radiation. Of course we must, at the same time, place a great deal of emphasis on the filamentary structure of the flares.

There are many other interesting facets of the investigation of the hydrogen line spectra of flares, but obviously we cannot discuss all of them. One of the most interesting is the observation of the deuterium line in several flares by Severny. This line is a satellite of Hα and is occasionally observable as a small bump in the wing of the Hα line. It would be extremely difficult to use these observations to deduce the ratio of deuteriums to protons in flares, because we are far from having any satisfactory theory of the total number of Hα emitting atoms along the line of sight. But further investigation of this effect may give us more information.

The spectroscopic investigation of flares has been greatly advanced since the days of the early observations of Richardson and Minkowski, and the construction of large new spectrographs which obtain spectra in many lines simultaneously with great resolving power will advance it even further. At the present time, there are already a great number of observations which we cannot explain, but which might be understood with more concentrated consideration.

N64-30257

6 TIME VARIATIONS IN THE SOLAR EXTREME ULTRAVIOLET SPECTRUM OBSERVED BY OSO I

WERNER M. NEUPERT
Goddard Space Flight Center, NASA
Greenbelt, Md.

A grazing incidence spectrometer (Reference 1) was flown as a pointed experiment on OSO I (1962 ζ1) to monitor the extreme ultraviolet (EUV) spectrum of the sun. Over 6000 spectra were obtained at the rate of about 100 per day over a period of time from March through May 1962, corresponding to nearly 3 solar revolutions. Intermittent operation has subsequently provided spectra for a period of greater than 1 year. This paper presents, in a condensed form, the variations observed in three of the more reliably identified lines of the spectrum: 284A (Fe XV), 304A (He II), and 335A (Fe XVI).

The solar EUV observations may be considered as falling into three categories: (1) quiet corona; (2) slowly varying components; and (3) transient phenomena, such as flares. These categories are also listed in the order of increasing difficulty of making reliable observations. This paper will review some of the observations of slowly varying components that have been made, and then present several instances in which transient phenomena have been observed.

DESCRIPTION OF SPECTROMETER

During operation the spectrometer was pointed at the center of the solar disk within approximately 2 minutes of arc. In this orientation, radiation from the entire solar disk and inner corona passed directly through the entrance slit and struck a concave grating mounted in grazing incidence, the angle of incidence being 88 degrees. The exit slit and detector were mounted on a carriage which was driven on a circular rail so that the exit slit scanned along the Rowland Circle, where the spectrum was focused, from 10 to 400A. The 50 micron entrance and exit slits provided a spectral passband of 1.7A and permitted resolution of lines 0.85A apart. The detector was a windowless photomultiplier developed by the Bendix Corporation specifically for use in this spectrometer. A tungsten photocathode was chosen to minimize response to wavelengths above 1500A and to reduce changes in sensitivity due to variations of the emission properties of the cathode.

The instrument calibration was performed by (1) exposing the entire spectrometer to a beam of monochromatic radiation of known intensity, and (2) evaluating the essential components of the spectrometer (grating, detector, etc.) and then computing the sensitivity of the instrument. The first method was used at 44A using a proportional counter for determining the source intensity. The second method was applied at longer wavelengths (80–400A). In addition, a comparison was made of the solar fluxes obtained against the fluxes measured by Hall, Damon, and Hinteregger (Reference 2) with a calibrated rocket instrument. The comparison could be made only in the region of overlap, 250A to 400A, and would be meaningful only if the solar radiation was the same. The 2800 Mc mean daily flux recorded by the National Research Council, Ottawa, Canada, was used as an independent estimate of solar flux to choose the satellite data for the comparison. A best fit made between these methods of obtaining a calibration yielded values of 8.0×10^5 photons cm^{-2} count^{-1} at 335A and 4.2×10^5 photons cm^{-2} count^{-1} at 284A. These values are useful for comparing the intensities of the lines at these two wavelengths, but their use to obtain absolute solar fluxes is not recommended.

PRESENTATION OF DATA

Figure 6–1 presents a typical scan obtained over the region of 170 to 400A. Several factors reduce the usable spectral range of the spectrometer from its nominal range of 10 to 400A. At wavelengths below 100A, the decreasing sensitivity of the spectrometer, combined with an increase in scattered light upon approaching the central image, made it impossible to distinguish a reliable spectrum on a single scan. However, a combination of several scans, using cross-correlation techniques, has shown the apparent existence of a line-emission spectrum in the region from 50 to 100A (Reference 3). At wavelengths above 342A the second-order images of intense spectral lines observed in first order above 171A obscure a considerable amount of interesting data. This effect is illustrated in Figure 6–1, which indicates, by cross-hatching, those first-order lines which have strong second-order counterparts in the recorded spectrum. These second-order images were less prominent in earlier rocket results, leading to considerable dissimilarity between the rocket and satellite spectra above 342A (Reference 4). For these reasons the obviously usable range of the instrument can be considered to be from 170 to 340A, a range which can be extended, with spectral precautions, to cover the interval from 50 to 400A.

The brightest emission line in the region from 170 to 340A is the Lyman-alpha line of ionized helium at 304A. In addition, numerous other emission lines appear with combined flux comparable with, or somewhat greater than, that of the helium line. Resonance lines of heavy ions (Mg through Fe) are expected in this region, leading to attempts (References 4 and 5) to identify the more prominent features of the spectrum in terms of such lines. The difficulty of positive identification can be appreciated more if, for example, we realize that the resonance lines of all stages of ionization of iron from Fe X through Fe XVI, with the exception of Fe XV, are expected in the small wavelength interval from 335 to 390A. The overlapping of these resonance multiplets, combined with second-order radiation of shorter wavelengths, makes positive identification a formidable task. The resonance lines of Fe X through Fe XIV have not been identified in the extreme ultraviolet (EUV) spectrum, although their intensity as predicted by Ivanov-Kholodny and Nikolsky (Reference 6) should permit their observation. Tousey (Reference 7), working with a spectrum having higher resolution, reports that no Fe XIV multiplet can be found in his record. Because of these difficulties, discussion will center around three of the more intense and more reliably identified lines of the spectrum: the Fe XV ($3s^2\ {}^1S_0$—$3s\,3p\ {}^1P_1{}^\circ$) line at 284A, the Fe XVI ($3s\ {}^2S_{\frac{1}{2}}$—$3p\ {}^2P^0_{3/2}$) line at 335A, and the He II ($1s\ {}^2S_{\frac{1}{2}}$—$2p\ {}^2P^0_{3/2,1/2}$) line at 304A. The location of these lines is indicated in Figure 6–2.

SLOWLY VARYING COMPONENTS OF THE EUV SPECTRUM

The months of March and April 1962 were auspicious for a study of the solar EUV spectra

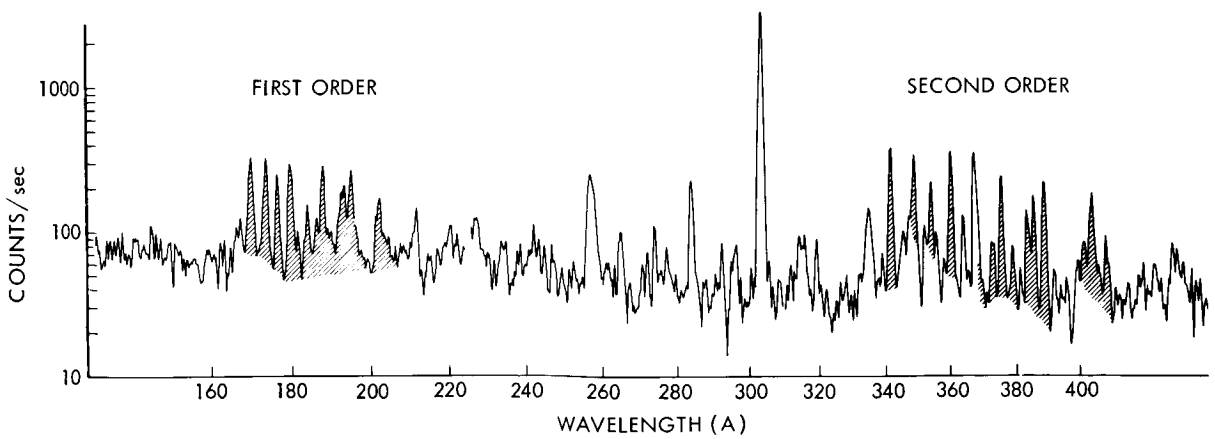

FIGURE 6–1. Solar spectrum from 170 to 400A with second-order line images indicated.

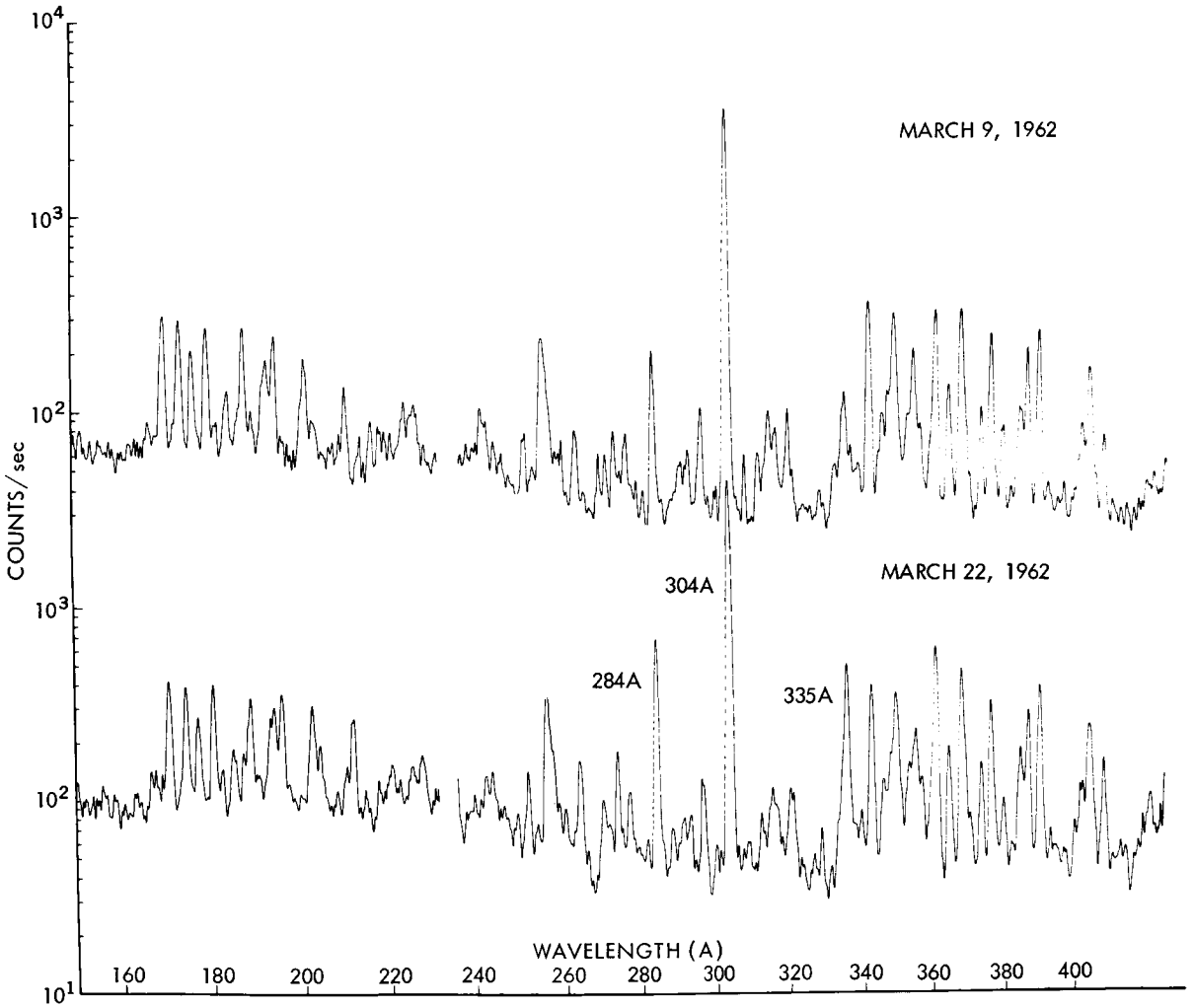

FIGURE 6–2. Comparison of two spectral scans taken under different solar conditions.

in that observations could be made on both a quiescent and a disturbed solar atmosphere. During the second week in March the sun was especially quiet, the Zurich Provisional Relative Sunspot Number being zero on 11 March. As the month progressed, solar rotation carried several centers of activity across the visible hemisphere of the sun. Definite enhancements in the solar spectrum were associated with these centers of activity.

Figure 6–2 presents two scans of the EUV spectrum taken approximately 10 days apart. During the first of these observations (March 9) only one small region of activity was present on the solar disk. In spite of this low level of activity it is observed that the Fe XV and Fe XVI lines persist as two of the more prominent features of the spectrum. The second spectrum (March 22) was obtained while several large and well-developed centers of activity were present on the disk. Comparing these two spectra, we observe that the emission lines have increased in intensity but not all by the same amount. The Fe XV and XVI lines, already prominent even in the near absence of solar activity, have increased in intensity appreciably more than any other line observed with certainty in this spectral range. The He II line has also increased, but by a lesser amount.

Time variations of these three lines as observed for the first 1066 orbits of operation are given in Figure 6–3, in which each datum point represents the average of one orbit's observations (6 to 8 scans). Errors bars indicating one standard deviation in the data are given for each wavelength. Also indicated are the times of appearance and disappearance of the major plage areas as catalogued by the McMath-Hulbert Observatory. The first increase in the counting rates above the "quiet sun" values is associated with the appearance of McMath Plage No. 6366 on the east limb on March 11. The counting rate for the He II (304A) line increases gradually to a maximum on March 23, after which it drops rather abruptly to an apparent plateau. This sudden drop cannot be unambiguously attributed to the disappearance of plage region 6366 on the west limb, for it follows quite directly after an unusual flare of Importance 3 observed in plage region 6370 on March 22, for which data are not given in the figure. A gradual decline in readings is observed from March 29 to April 7. A similar enhancement, followed by a return to near preplage rates, occurred in April. Since the spectrometer did not carry an internal standard, it is impossible to state positively that its counting characteristics did not change over the period of observations. The consistent behavior of the data however, as demonstrated in Figure 6–3, leads to the conclusion that no significant change in sensitivity occurred throughout the period of observation. (Subsequent analysis of real-time data after 1 year in orbit supports this conclusion, even for the longer time interval.)

Also shown in the figure are the variations with solar activity of the coronal Fe XV (284A) and Fe XVI (335A) lines, the relative increases being considerably larger than for the He II (304A) line. A definite, although small, enhancement associated with the appearance of plage 6366 is observed in both the Fe XVI and Fe XV lines. The possibility exists that the coronal emissions appear slightly earlier as might be expected, since the coronal emission must take place at greater heights than the emission of ionized calcium radiation. The most obvious increase in intensity of these lines is associated with the appearance, in succession, of plage areas 6370, 6369, and 6373 on March 17 through 19. The counting rates then increased gradually throughout this period, indicating that the enhanced emission was not from a point source but rather from an extended volume having as its base an area at least as large as the underlying calcium plage. The disappearance of area 6366 on March 25 results in a slight decrease in counting rates, followed by a general decline from March 29 through April 3 as the other plage areas are carried off the visible hemisphere of the sun by the solar rotation.

DISCUSSION OF SLOWLY VARYING COMPONENTS

The relation of these observed counting rates to several ground-based measurements of solar activity is presented in Figures 6–4 and 6–6. In Figure 6–4 the He II radiation is compared with daily values of the solar flux at 2800 Mc and with the Zurich Provisional Relative Sunspot Number (ZPRSN). Also shown is an estimate of the calcium plage area, each area being weighted by the estimated intensity of the area on a scale from 1 to 5 and by the cosine of its longitude from the central meridian. Values for this computation were supplied by the McMath-Hulbert Observatory.

A more detailed comparison is made in Figure 6–5, in which the radio and He II fluxes have been adjusted by dividing each observation by the rate observed for the "quiet sun." In addition, the weighted Ca^+ plage intensity has been adjusted to coincide with the 2800 Mc enhancement on March 21. This plot shows more clearly the close relation which has been known for some time between the 2800 Mc radiation and the plage areas and also shows the divergences of the He II (304A) line from both of these. A better agreement between plages and the 304A line is obtained if only the plage areas, with no weighting factors for intensity or longitude from central meridian passage, is used. In Figure 6–6 the daily values of solar flux at 2800 Mc and the ZPRSN are compared with the coronal lines of Fe XV (284A) and Fe XVI (335A). The estimated weighted calcium plage area is also shown.

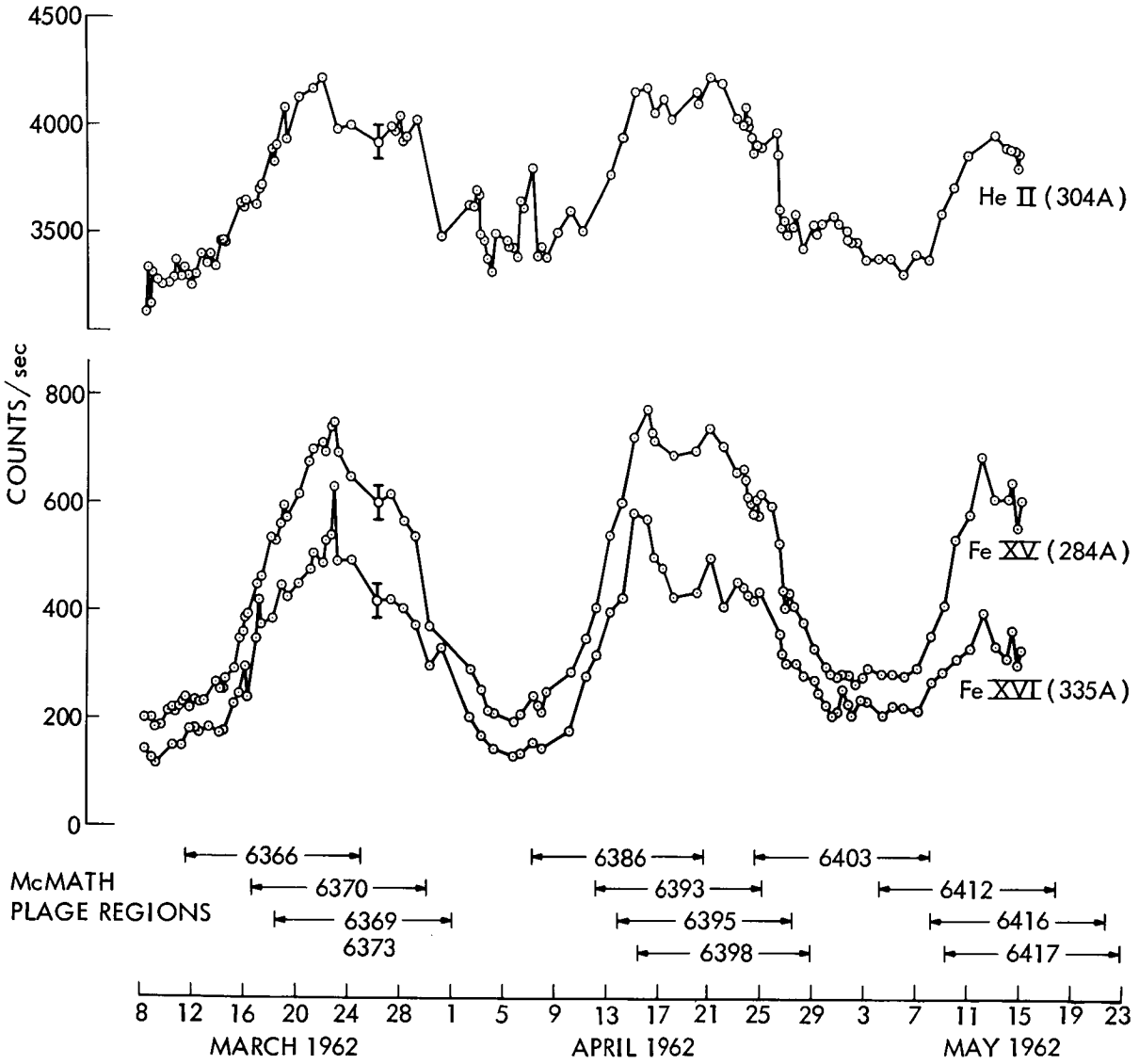

FIGURE 6–3. OSO I data for three spectral lines compared with appearance and disappearance of major plage areas.

The spectral lines chosen for presentation here were selected because they are reliably identified with particular ions and not because they convey, more than any other line in the spectrum, changes in solar flux which occur with the appearance of plage areas. These three lines represent the extremes which have thus far been observed in the spectral region from 171A to 400A; only a few faint lines have smaller non-flare variations than the He II Lyman-alpha ine, while no other outstanding lines have increases as great as those observed for 284 and 335A.

An attempt has been made to compute an electron temperature for the corona, as nearly as possible undisturbed by centers of activity, from the observed ratio of intensities of the Fe XV and Fe XVI lines. Such a calculation has validity only if both radiations originate in the same region of the corona at some well-defined electron temperature and only if an ionization-recombination equilibrium, as as-

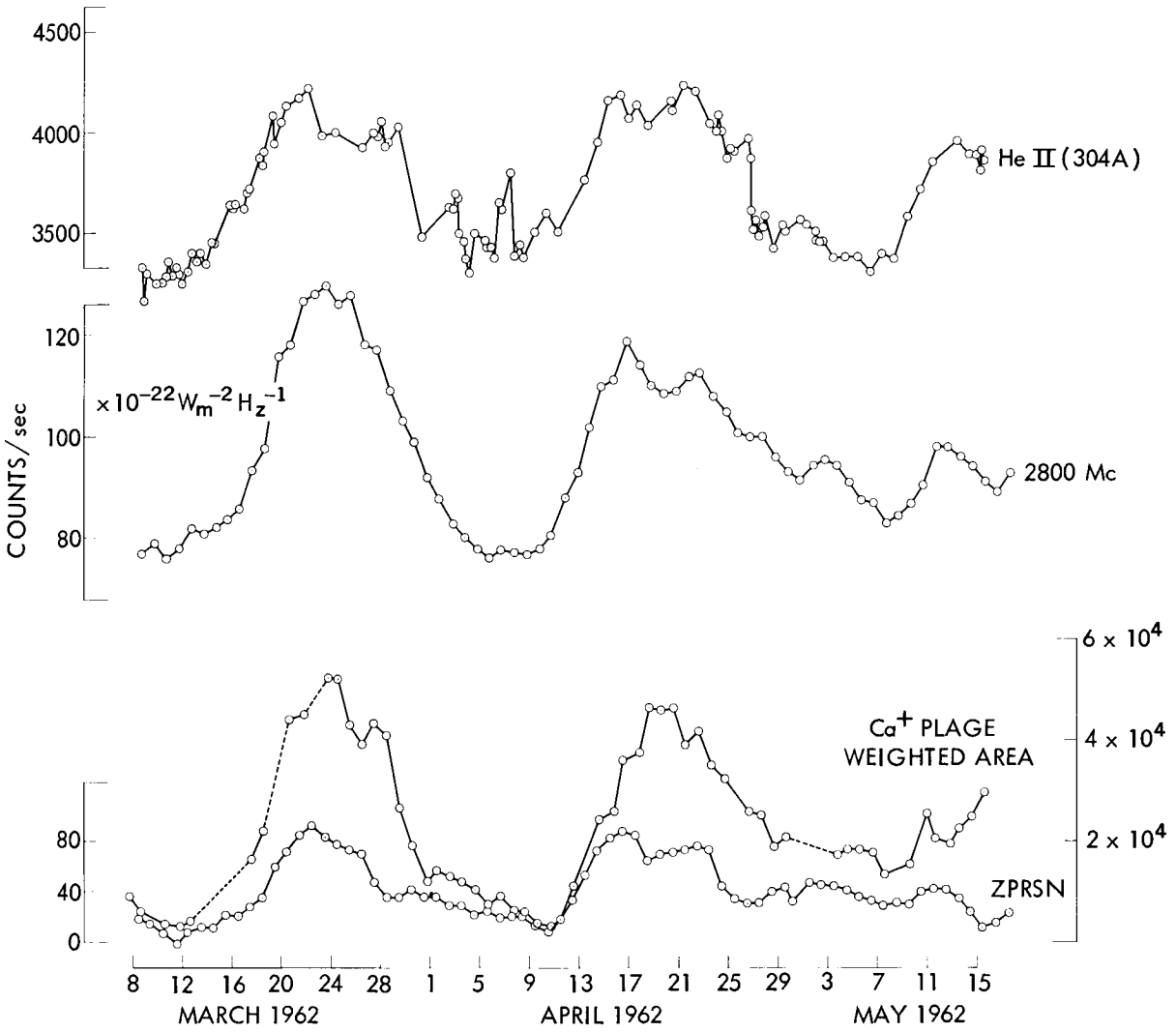

FIGURE 6–4. Relation of observed counting rates for the He II Lyman-alpha line to ground-based measurements of solar activity.

sumed by theory, is actually present. It is found that an electron temperature of 1.75± 0.10 million degrees in that part of the corona assumed to be the source of both Fe XV and Fe XVI best fits the observed data. This result contrasts sharply with the value of 800,000 °K usually obtained from observation of the forbidden lines of Fe X and Fe XIV.

It has been estimated that the emission of Fe XV and Fe XVI radiation associated with a plage area is approximately 150 to 200 times that of an equivalent area of the quiet sun. The corresponding value for the 304A line is 15. Assuming that the increase in emission is due to a density increase only, we find it necessary to hypothesize an increase in electron density by a factor of 12 to 14 over each plage for the two iron lines. The fact that a large range of intensity variations is observed demonstrates, however, that an increase in electron density alone is not sufficient to explain the behavior of the spectrum. On the other hand, the constancy of the ratio Fe XVI/Fe XV as we extrapolate to zero plage area argues against a significant change in electron temperature over plages. We can only conclude, at this time,

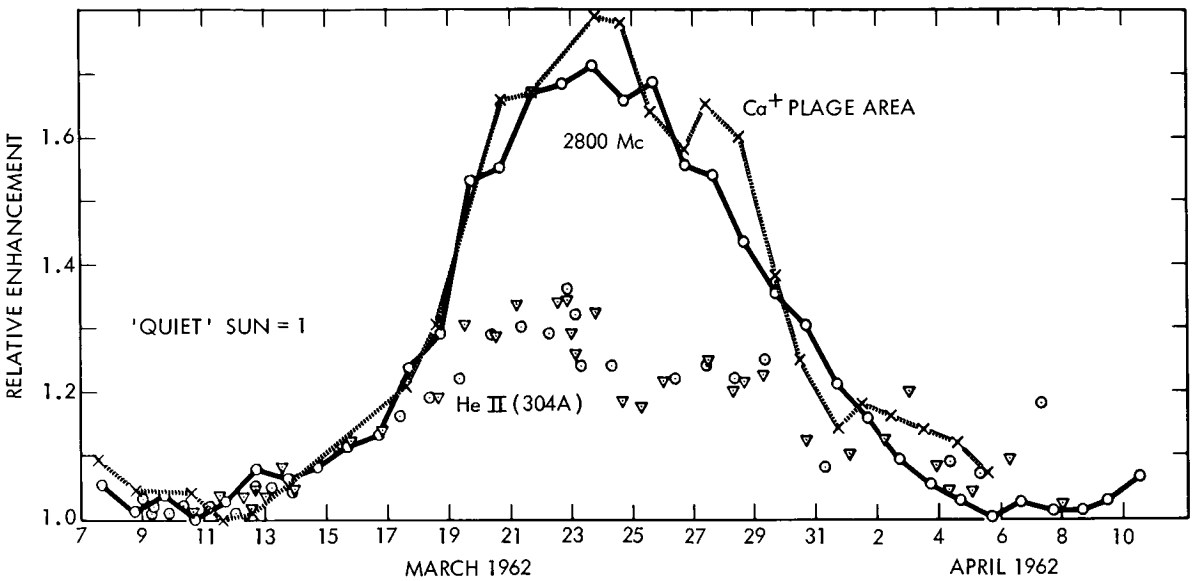

FIGURE 6–5. Comparison of 304A data, normalized to a "quiet sun" value of 1, with weighted calcium plage data and 2800 Mc radio observations.

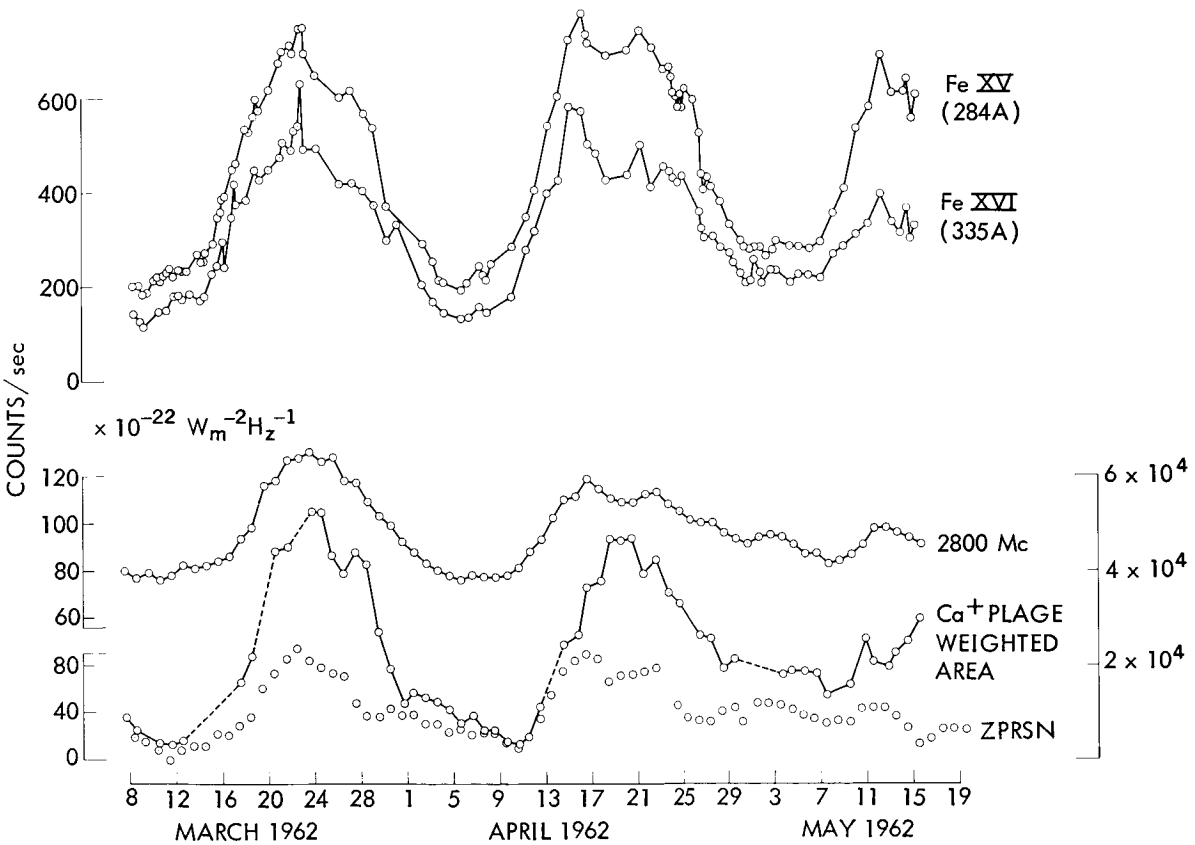

FIGURE 6–6. Relation of observed counting rates for the 284A and 335A lines to ground-based observations.

728–629 O—64——5

that those regions (or region) of the corona emitting Fe XV and Fe XVI radiation occupy a relatively greater volume of the corona over plages and centers of activity.

The initial analysis of only three lines (He II, 304A; Fe XV, 284A; Fe XVI, 335A) indicates that the relative prominence of spectral lines may depend on the age of the center of activity which is responsible for the increased radiation. As an example of this, one may observe (Figure 6–6) that the maximum emission in the Fe XV line apparently occurs later in time than the maximum for the 2800 Mc flux—or for the plage areas—observed during March, April, and May. In addition to such a slowly changing effect, one may note that localized perturbations appear (March 7–9 and April 16–17) for which the relative increases in the helium and the iron lines are considerably different. In these instances we are apparently observing phenomena localized at particular levels in the solar atmosphere.

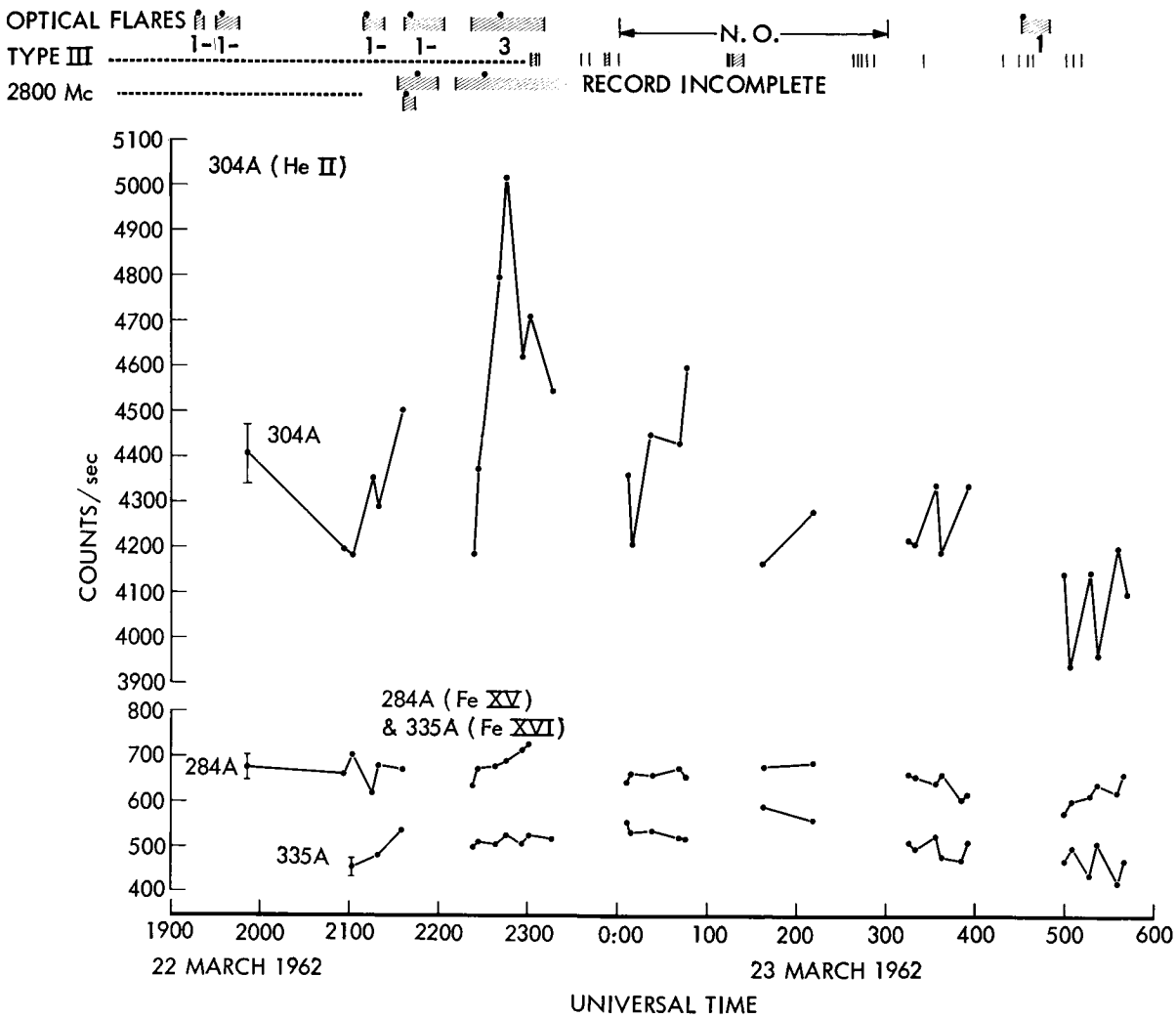

FIGURE 6–7. Increases in EUV line emission associated with optical flares: EUV flare observations March 22, 1962.

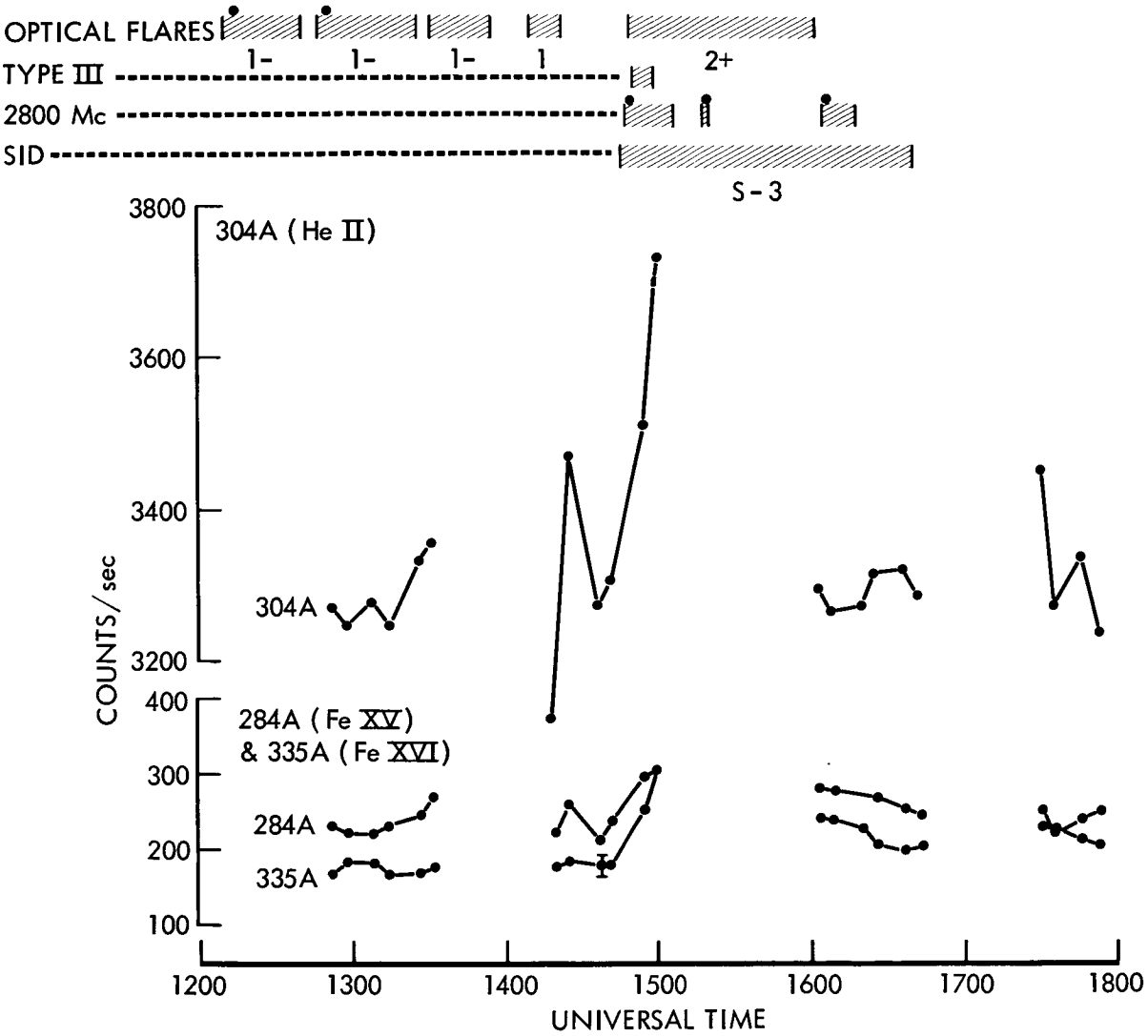

FIGURE 6–8. Increases in EUV line emission associated with optical flares: EUV flare observations March 13, 1962

EUV FLARE OBSERVATIONS

It is difficult to obtain reliable EUV flare observations with the type of spectrometer used in OSO I because the flare radiation is seen as only a small increase in the radiation from the entire solar disk and because the long time required to scan the spectrum (8 min) severely limits the time resolution with which the flare can be observed. In spite of these difficulties, several increases in the EUV radiation have been associated with flares. Three such instances are shown in Figures 6–7, 6–8, and 6–9. Supplementary information for these events is given in Table 6–1.

March 22, 1962 (Flare of Importance 3)

From the observations of the He II line at 304A made 1 minute before and 3 minutes after maximum in Hα, we may conclude that the maximum at 304A certainly occurs no earlier than Hα maximum and may occur later. No changes at 284 and 335A can be associated with this flare, optically of Importance 3 but geophysically of much less importance.

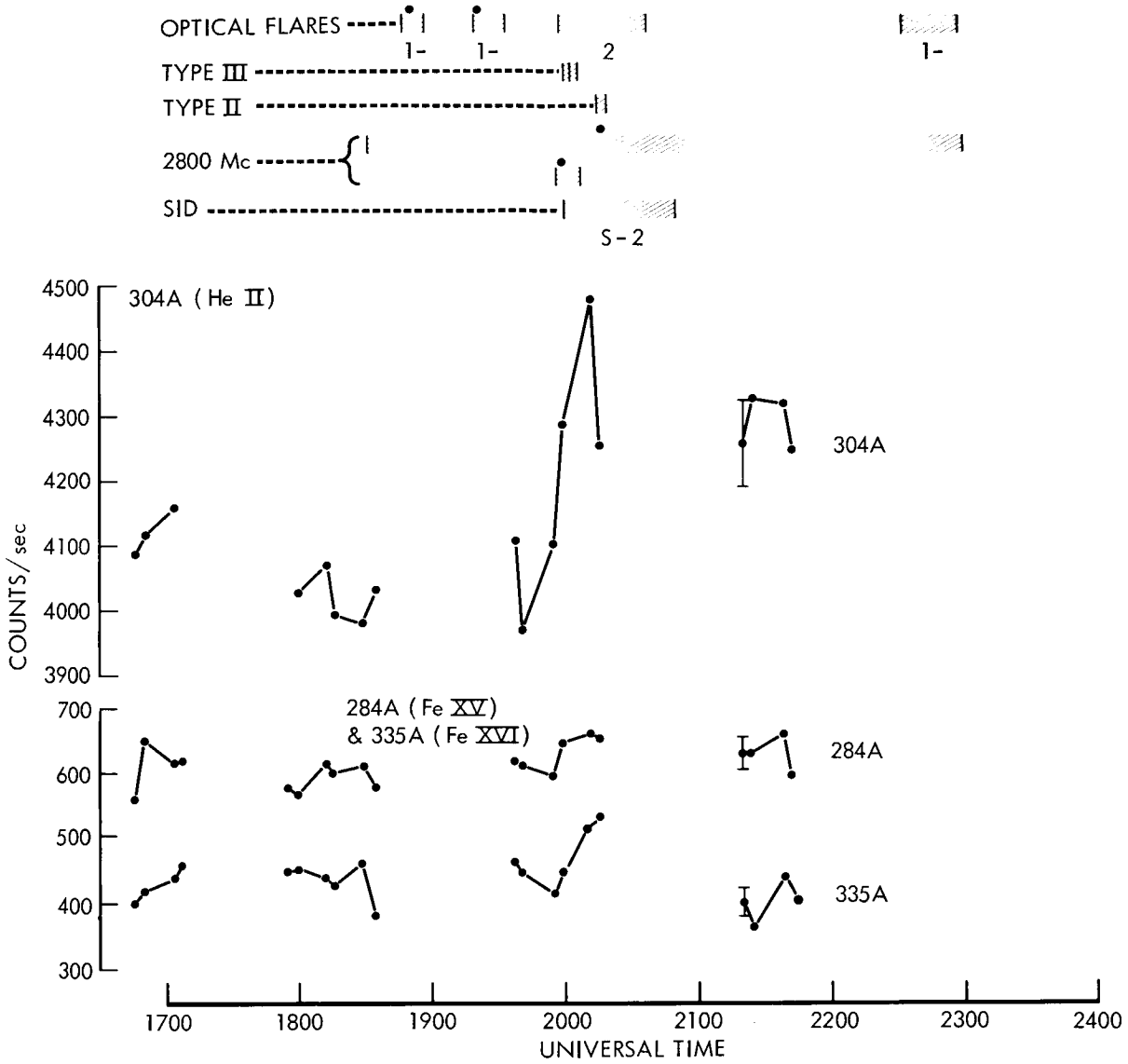

FIGURE 6–9. Increases in EUV line emission associated with optical flares: EUV flare observations April 20, 1962.

March 13, 1962 (Flare of Importance 2+)

Peak phase of this flare apparently occurred near satellite sunset. The last valid observations before sunset indicate that the EUV flare radiation reaches a maximum after the 2800 Mc radio burst. Increases are noted for all three lines, with the ratio 335A/284A apparently increasing at or near maximum phase of the optical flare. The enhancement in the coronal lines may continue after cessation of the visible flare.

April 20, 1962 (Flare of Importance 2+)

EUV observations are poorly situated in time relative to the optical maximum of this flare. It appears, therefore, that the EUV emission maxima may have been significantly greater than the maximum reading actually recorded. In spite of this shortcoming, an increase in the

Fe XVI radiation, relative to Fe XV, can again be observed.

DISCUSSION OF FLARE OBSERVATIONS

A considerable number of additional events apparently have been observed—some associated with optical flares, others not. However, the data for these events have not been sufficiently analyzed to establish their validity. The increase of the ratio Fe XVI/Fe XV is most frequently associated with solar events producing ionospheric disturbances. The increase in this ratio suggests that some volume of the solar atmosphere, associated with the flare, has been raised to a higher electron temperature.

It is interesting to note that the EUV maxima coincide more closely with the optical maxima and with ionospheric effects than they do with centimetric radio bursts. The association with ionospheric effects is understandable if we assume that the hard x rays, which themselves may be line emission at short wavelengths and which are causing these ionospheric disturbances, have the same common thermal origin in flares as does EUV flare radiation observed by the OSO I spectrometer. On the other hand, the coincidence with optical Hα maxima cannot be explained in the same manner, since the hydrogen radiation must originate in a cooler region of the solar atmosphere.

TABLE 6–1

Supplementary Flare Observations

(a) March 22, 1962

Event	Start	Max.	End	Importance
Optical flare	22:20?	22:41	23:10?	3
2800 Mc bursts	Gradual rise 22:00 to sunset (22:40) Short bursts at 22:31, 22:33.5, 22:38			35 flux units
Type III bursts	None observed			----------
Type II bursts	None observed			----------
SID (HAO preliminary report)				
SCNA	22:33	----------	23:02	1–
SEA	22:35	----------	23:25	1–
Approximate EUV Observation Times (UT) at Peak of Flare March 22–23				
		(Peak)		
304A (He II)	22:40:23	22:44:10	22:58:00	
284A (Fe XV)	22:40:03	22:43:50	22:57:40	
335A (Fe XVI)	22:40:53	22:43:20	22:58:30	

TABLE 6-1—Continued

Supplementary Flare Observations—Continued

(*b*) *March 13, 1962*

Event	Start	Max.	End	Importance
Optical flare	14:48 (earlier than)	15:05	16:01 (later than)	2+
SID (CRPL-F Bulletin, NBS)				
SCNA	14:50	15:00	15:45	1
SEA	14:50	----------	15:55	2
SPA	14:45	15:05	16:40	----------
2800 Mc bursts	14:47. 5	14:50. 5	15:07	470 flux units
Type III bursts	14:50	----------	14:58	Group of bursts

Approximate EUV Observation Times (UT)			
304A (He II)	14:40:05	14:53:55	(Peak) 14:57:10
284A (Fe XV)	14:40:25	14:53:35	14:57:30
335A (Fe XVI)	14:39:35	14:54:25	14:56:40

(*c*) *April 20, 1962*

Event	Start	Max.	End	Importance
Optical flare	19:58	20:02	20:40	2+
SID (CRPL-F Bulletin, NBS)				
SCNA	20:00	20:04	20:35	2
SEA	20:01	----------	20:50	2
SPA	20:02	20:07	20:50	2
2800 Mc burst	19:57. 3	19:59	20:09	80 flux units
Type III bursts	20:00. 6	----------	20:02	(Harvard)
	20:00	----------	20:04. 15	(HAO)
	20:05. 15	----------	20:07. 30	(HAO)
Type II bursts	20:04. 6	----------	20:19	(Harvard)
	20:16	----------	20:20. 3	(HAO)

Approximate EUV Observation Times (UT)			
304A (He II)	19:58:00	(Peak) 20:11:50	20:15:00
284A (Fe XV)	19:58:20	20:11:30	20:15:20
335A (Fe XVI)	19:57:30	20:12:20	20:14:30

REFERENCES

1. Behring, W. E., Neupert, W. M., and Nichols, W. A., 1962, *J. Opt. Soc. Amer.*, 52(5): 597.
2. Hall, L. A., Damon, K. R., and Hinteregger, H. W., 1963, "Space Research III," ed. W. Priester (Amsterdam, North-Holland Publ. Co.), 745.
3. Neupert, W. M., Behring, W. E., White, W. A., and Lindsay, J. C., 1962, GSFC Publ. X-614-62-156.
4. Neupert, W. M., and Behring, W. E., 1962, *J. Quant. Rad. Transf.*, 2: 257.
5. Zirin, H., Hall, L. A., and Hinteregger, H. E., 1963, "Space Research III," ed. W. Priester (Amsterdam, North-Holland Publ. Co.), 760.
6. Ivanov-Kholodny, G. S., and Nikolsky, G. M., 1961, *Astronom. Zhurn.*, 38: 828.
7. Tousey, R., 1963, *Space Science Reviews* (to be published).

DISCUSSION

Mr. Maran: In comparing the fluxes from the active and quiet sun, is it your finding that the lines from the higher ionization states of iron vary with greater amplitude than do the lines from the lower ionization states?

Is this not most simply interpreted by saying that the relative density changes in the corona are greater in the regions or at the levels where the temperature is higher?

Dr. Neupert: Yes, that is a possible conclusion. However, we cannot discriminate between this hypothesis and one in which the electron temperature profile of the corona changes above the active region in such a manner that a greater relative volume is at the higher temperature.

Dr. Zirin: I have the impression that you have essentially a factor-of-2 increase in the total radiation from the whole sun coming from a flare which essentially is 0.1 percent of the area. This impresses me as a very large change. Is that so, would you say?

Dr. Neupert: We can associate changes of 50 percent or more during flares only with the Fe XVI and Fe XV lines. Many lines show no statistically reliable change. For the event on March 13, we can demonstrate, by averaging our data over one complete orbit, that several other lines do show changes. Rapid variations of 10 to 20 percent in the faint lines would be unobservable because of statistical fluctuations. We probably should use the Hα area of a flare only as a lower limit in estimating the size of the EUV emitting region.

Dr. Gerjuoy: Would you clarify for me how long and how large an area of the sun you are looking at?

Dr. Neupert: We are looking at the entire solar disk, out to about one quarter of a solar radius from the limb. So we are looking at the entire disk plus the inner corona with this instrument. Since our measurements cover an extended period of time, we can get information on the quiet sun. Then, by correlating with ground-based observations, we can conclude that the enhancements come from localized regions.

Dr. Chubb: Can you say something about how the variability of the lines around 170A is as compared with, say, the 304A and the iron lines?

Dr. Neupert: The variations with solar plage area of the lines between 170A and 200A are less than those of the 284A and 335A lines. They are comparable with, or somewhat more than, that of the helium line. We have not analyzed flare data for these lines, but it is our experience that lines which increase most because of the presence of a center of activity also increase the most during flares.

Dr. Lindsay: I believe that you have averaged about 60 lines in this region over a period of about a month. Why don't you report at least the integrated or the average of these line variations?

Dr. Neupert: We have made integrations over the spectrum for 2 days. Not for March 13 and March 23, but for 2 days on which activity was similar to those which we had in the second figure (Figure 6–2). The increase in counting rate was of the order of 50 to 80 percent. This is an increase due to the presence of centers of activities on the sun's disk, not an increase due to flares.

N64-30258

7 SOLAR FLARES IN THE LIGHT OF HYDROGEN LYMAN-ALPHA

KENNETH L. HALLAM
Goddard Space Flight Center, NASA
Greenbelt, Md.

The total solar flux of hydrogen Lyman-alpha was monitored on OSO I (1962 $\zeta 1$) by means of a spectrally selective gas ionization chamber. Useful data were obtained from the date of launch, March 7, 1962, until April 28, 1962. One reading of the flux was obtained every 136 seconds while the satellite was on the sunlit side of the earth. This gave about 20 measurements of the Lyman α flux per orbit. Fluctuations of the detector signal from the orbital mean were typically about ± 1 percent peak-to-peak in March. Only those events with sustained enhancements greater than the fluctuating part of the signal could be detected.

During this observing period of 53 days, five flares of optical Importance 2 or greater were associated with detectable enhancements in Lyman α. No class 1 flares were ever detected, whereas three of seven class 2 flares and both class 3 flares which occurred during satellite observing periods were detected. Table 7–1 summarizes this Lyman α observational rate, where E is the percent Lyman α enhancement. The particulars of the detected flares are given in Table 7–2.

TABLE 7–1

Lyman-Alpha Observational Rate for Solar Flares

Class	Total Reported	No. with E>3	No. with 1<E<3	Not Detectable, E<1
1	----------	0	0	----------
2	7	2	1	4
3	2	2	0	0

TABLE 7–2

Circumstances of Lyman-Alpha Flares

1962 Date	Position	Optical Class	Fraction of Time Observed in Lα	Percent Average Observed Lα Enhancement	Percent Peak Observed Lα Enhancement	Optical Duration (min)
March 13	N10 E66	2+	0.6	2	4	86
March 16	N10 E32	1+	.4	2	2	86
March 22	N07 E36	3	.9	3	6	50
April 18	N10 E05	3	.6	3	5	236
April 22	N07 W48	2+	.2	7	10	160

All Lyman α enhancements occurred mostly within the duration of the Hα flare. There is apparently no typical time dependence of the variation in Lyman α. The time of peak Lyman α enhancement does not necessarily coincide with the Hα flare maximum, but usually precedes it slightly.

The flare of March 22 provided the best observed Lyman α enhancement. It is unique among all the events in that the Lyman α enhancement profile behaves in a way very similar to that of a "classic" Hα flare. In this particular instance, the time of Lyman α maximum coincides exactly with the reported optical flare maximum.

It is of interest to consider the spatial contrast on the surface of the sun that such an event as this would be expected to give in Lyman α. Assuming the area of the Lyman α flare is the same as that for Hα, then—depending on the circumstances of the distribution of the rest of the Lyman α radiation over the solar surface—the Lyman α surface brightness contrast of the flare to the surrounding background would be between 5 and 150. This is easily sufficient to allow good resolution of such flare activity even in broadband Lyman α photography.

N64-30259

8 BROADENING AND ASYMMETRY OF THE EMISSION LINES IN FLARES

MARIA C. BALLARIO
Osservatorio Astrofisico di Arcetri
Firenze, Italy

Papers of Jefferies and Orrall (Reference 1), Svestka (Reference 2), Fritzova (Reference 3), and Michard (Reference 4) suggested to me that perhaps the two phenomena of broadening and asymmetry of the emission lines in flares may be due to the same cause, that is, to macroscopic motions in the flare itself.

Since in a paper of 1962 (Reference 5) I found that a flare may have a loop structure with the two branches diverging from the solar surface and inclined at an angle of 50 degrees to the solar radius (Figure 8–1), I have assumed a macroscopic motion inside this loop and have examined the effect of this motion on the emission lines.

If V_1, V_2, V_3, are the velocities in the three different parts of the loop, the sight-line components V_1^*, V_2^*, V_3^* are a function of the heliocentric angle v and of the motion direction inside the flare. But in every case there are, in this model, two components of opposite sign; for instance,

$$V_1^*=V_b^* \text{ (sign}-\text{)},$$
$$V_2^*=V_r' \text{ (sign}+\text{)}, \quad V_3^*=V_r''^* \text{ (sign}+\text{)}.$$

Then I have assumed that broadening and asymmetry may be due to a double mechanism:

1. The absorption line is filled up and broadened by Doppler thermal effect or Stark effect, damping, etc. I call this broadened line the *basic line* and its effective width L (Figure 8–2).

2. The basic line is displaced toward the red and toward the blue by Doppler shifts, due to the sight-line components, by the quantities:

$$\Delta'\lambda_r=\frac{\lambda}{c}V_r'^*, \qquad \Delta''\lambda_r=\frac{\lambda}{c}V_r''^*, \qquad \Delta\lambda_b=\frac{\lambda}{c}V_b^*.$$

Let us suppose that

$$\Delta\lambda_r'>\Delta\lambda_r''.$$

Then the effective width W of the line (Figure 8–3) is

$$W(v)=\frac{\lambda}{c}(V_r'^*+V_b^*)+L,$$

and the asymmetry is

$$\Delta W(v)=\frac{\lambda}{c}(V_r'^*-V_b^*).$$

The third component, whose displacement is $\Delta''\lambda_r$, will contribute only to the reconstruction of the profile.

First, I have examined the Hα line (Reference 6). The calculated values of $W(v)$ and $\Delta W(v)$ for different v values are in agreement with the experimental results, that is, in the loop model:

1. The broadening increases with the increasing values of v (Figure 8–4) in agreement with the results given by Goldberg, Dodson, Müller (Reference 7) and Fritzova's (Reference 3) experimental data.

2. The asymmetry decreases with the increasing values of v (Figure 8–5) in accordance with Fritzova's experimental results (Reference 3).

3. The asymmetry is prevalently red asymmetry [Waldmeier (Reference 8), Svestka (Reference 2)].

4. The center of the blended line has small displacements from the normal Hα center in

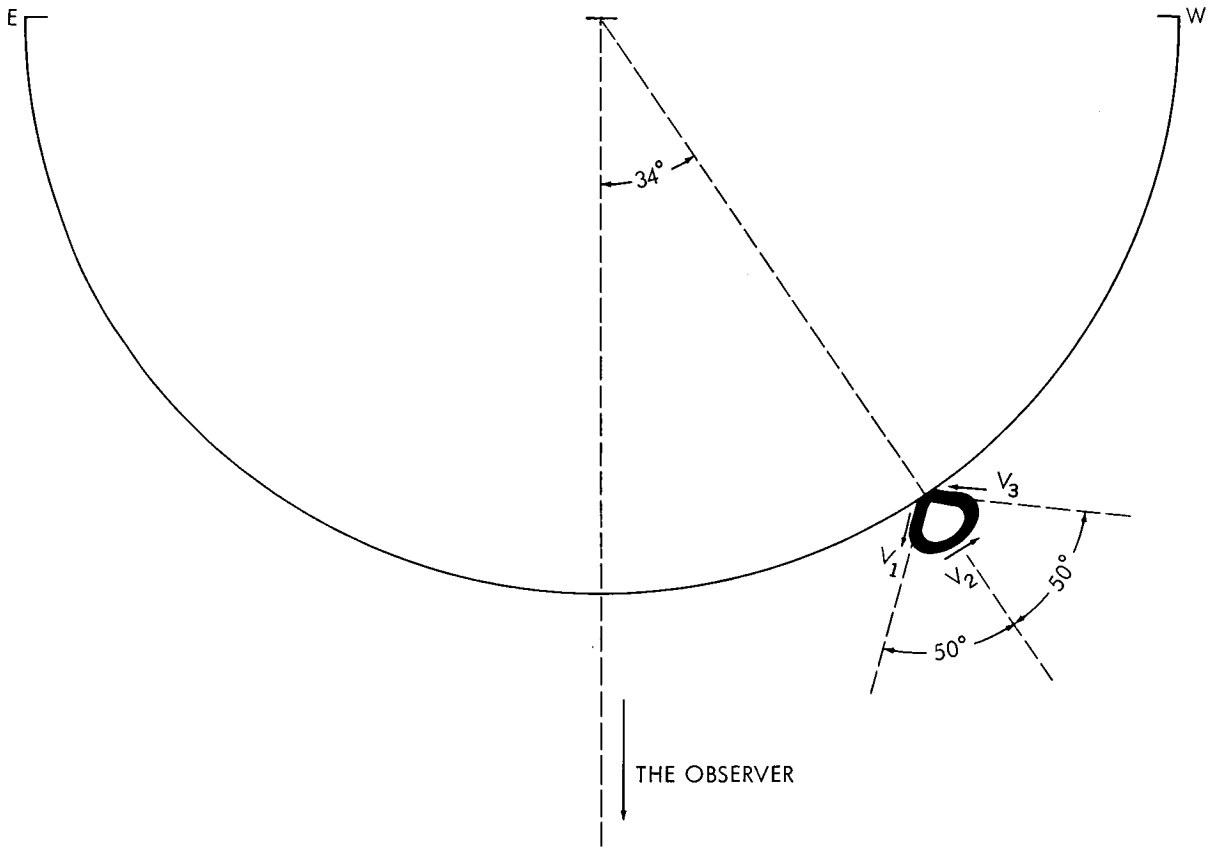

FIGURE 8–1. The loop model for the flare of September 2, 1960.

accordance with the results supplied by Waldmeier (Reference 8), Ellison (Reference 9), and Giovanelli (Reference 10).

5. The lines are broadened because they consist of superposed components in accordance with the statements of Jefferies and Orrall (Reference 1).

Then I examined the other Balmer lines (Reference 11). Since the Balmer lines originate in the same region of the flare, I ought to obtain analogous expressions for Hβ, Hγ, etc. That is,

$$\Delta W_n = \frac{\lambda_n}{c}(V_r'^* - V_b^*)$$

and

$$W_n = \frac{\lambda_n}{c}(V_r'^* + V_b^*) + L_n,$$

where $n = \alpha, \beta, \gamma, \ldots$. Thus

(a) $$\frac{\Delta W_n}{\lambda_n} = \text{const.},$$

(b) $$\frac{W_n - L_n}{\lambda_n} = \text{const.}$$

For checking (a), it would be sufficient to know the values of the asymmetry ΔW_n of the various Balmer emission lines in a flare, but

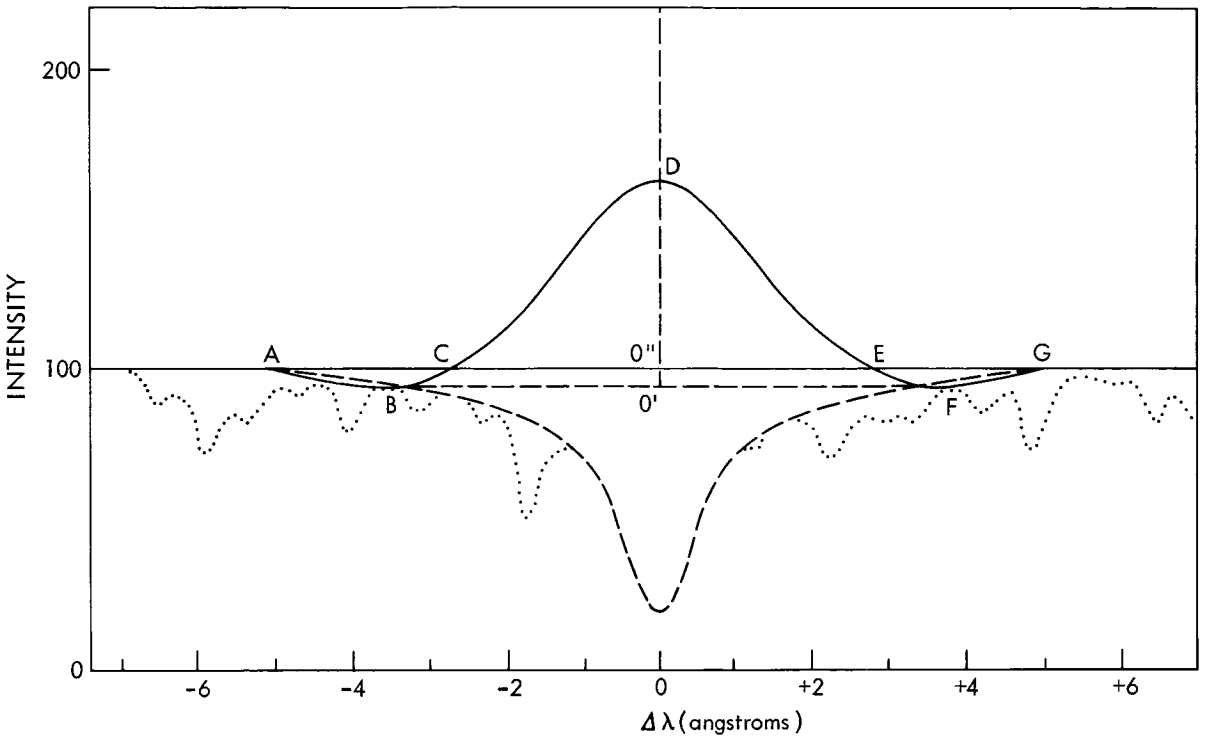

FIGURE 8–2. The basic line for the flare of September 2, 1960.

such data are not generally given even in the most detailed studies on the profiles of hydrogen lines. But in the loop model the asymmetry is twice the displacement $\Delta\lambda_n$ of the line emission center with respect to the normal line center (Reference 11):

$$\Delta W_n = 2\Delta\lambda_n.$$

Thus it will be sufficient to prove that

$$\Delta\lambda_n/\lambda_n = \text{const.},$$

and the experimental research of many observers [Severny (Reference 12), Fritzova (Reference 13), v. P. Smith (Reference 14)] proves that this relation is valid.

It is more difficult to check relation (b) because the experimental data W and ΔW are lacking and the values L_n of the basic lines are not known.

I have tried to deduce these data from the profiles given by Svestka (Reference 15): Hα, Hβ, Hγ, Hϵ, Hζ for the flare of July 30, 1958. The results are satisfactory (Reference 11), but the check is very approximate; therefore, I can conclude only that relation (b) might also be valid.

Finally, I have tried to reproduce the emission line profiles as a blend of three superposed components (Reference 16). I have chosen the profile of Hβ given by v. P. Smith (Reference 14) for the flare of September 2, 1960, because in her paper she notes that macroscopic motions apparently dominated this flare.

Figure 8–2 gives the Hβ basic line and Figure 8–3 reproduces the blend of the three components. The full line is the observed profile given by v. P. Smith, and the circles represent the calculated blend. The basic line has a gaussian shape whose equation is

$$y = 70e^{-0.28\Delta\lambda^2};$$

and the velocities, deduced from the values $\Delta'\lambda_r$, $\Delta''\lambda_r$, $\Delta\lambda_b$, are (in km/sec):

$$V_1 = 80$$
$$V_2 = 197$$
$$V_3 = 92$$

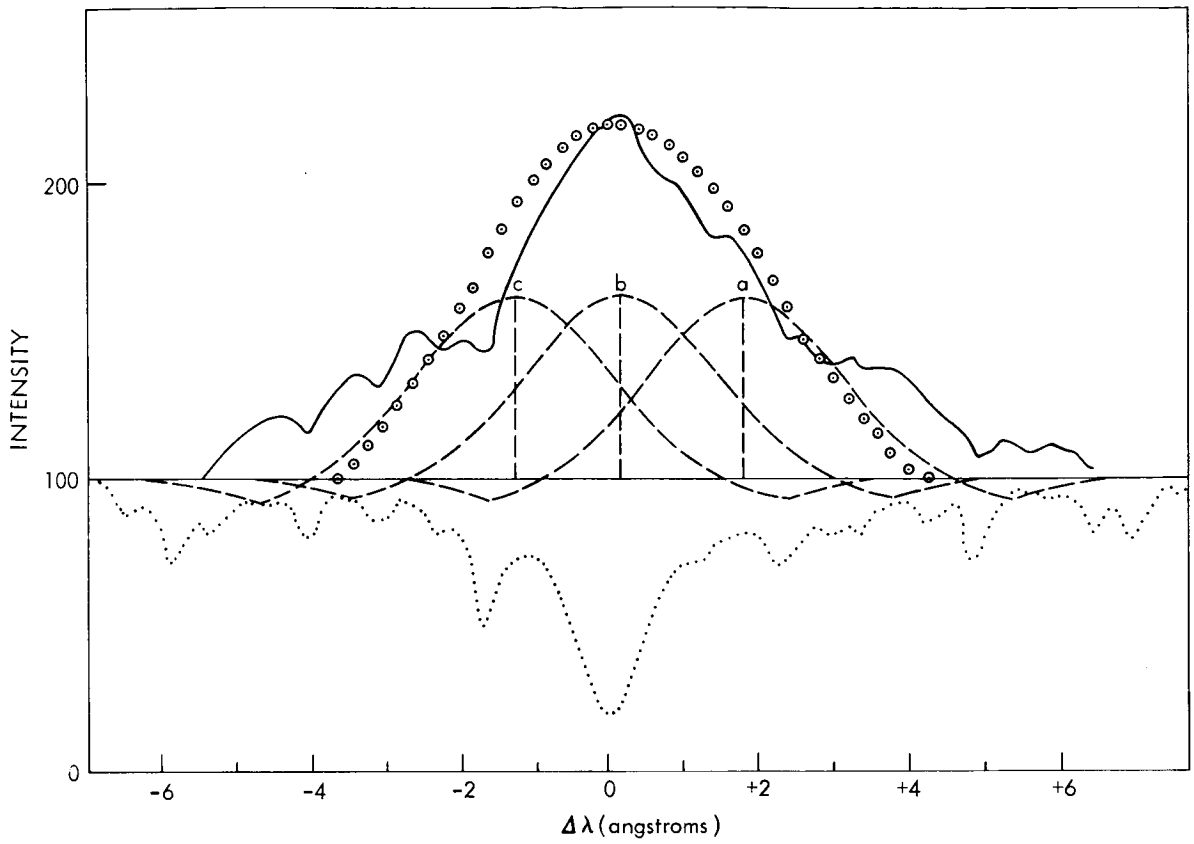

FIGURE 8–3. The blend of three superposed basic lines. The full line is the observed Hβ profile given by E. v. P. Smith (Reference 14) for the flare of September 2, 1960; the circles represent the calculated profile.

The values of the velocities found by v. P. Smith in a different way (Reference 14) are, in km/sec:

$$V_r = 178$$
$$V_b = 164$$

Concerning metallic lines, I have only a few points to note. According to Severny (Reference 12), $\Delta\lambda_n/\lambda_n$=const. for Balmer lines and metallic lines. On the other hand, according to Fritzova (Reference 13), this ratio is constant for the Balmer lines but assumes a different value for metallic lines. I think that perhaps in some flares the Balmer and metallic lines originate in the same zone. In other flares, as suggested by Svestka (Reference 17), they originate in different zones—for instance, in different loops having different velocities.

Another experimental result might be explained by the loop model. Svestka (Reference 18) has observed that in some flares metallic lines are doubled. In the loop model, when the displacements $\Delta''\lambda_r + \Delta\lambda_b > L$, the profile consists of two separate parts, one of which is larger and more intense than the other.

In conclusion I should like to emphasize that the loop model, although in agreement with many experimental results, is only a model and that the phenomenon may develop differently. According to many authors (Reference 19) solar flares occur mostly in magnetically complex spot groups and optical flares occur in the region F which (Figure 8–6) might be similar to the loop model I have studied.

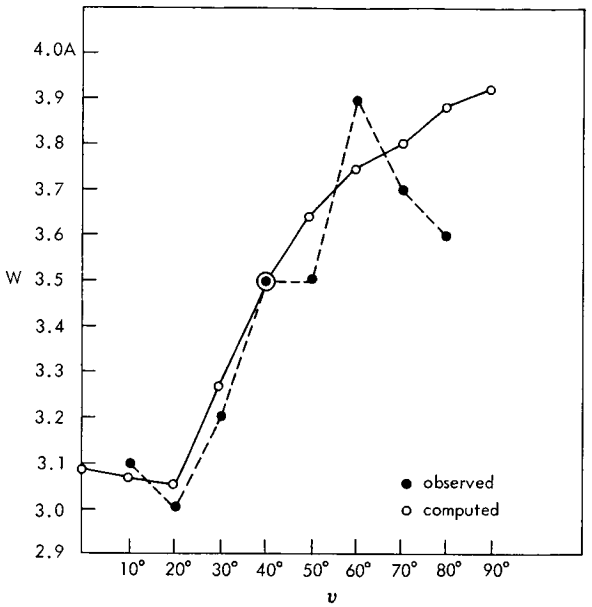

FIGURE 8–4. Comparison between the computed values of the mean effective width of the broadened Hα in the loop model and Fritzova's experimental data.

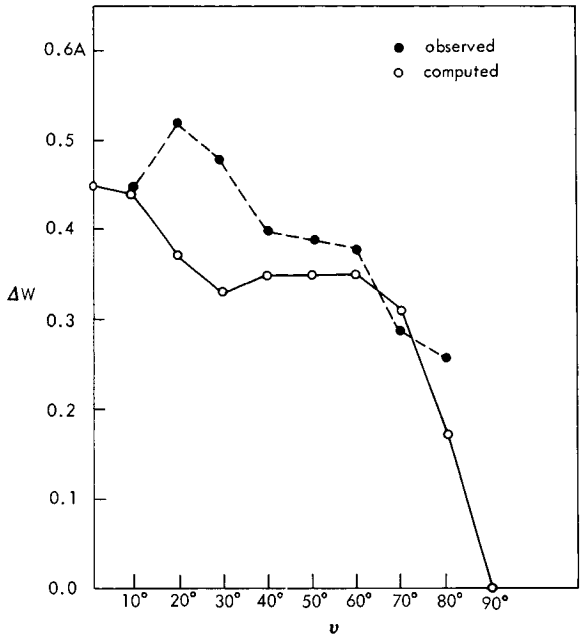

FIGURE 8–5. Comparison between the computed values of the mean asymmetry of the broadened Hα in the loop model and Fritzova's experimental data.

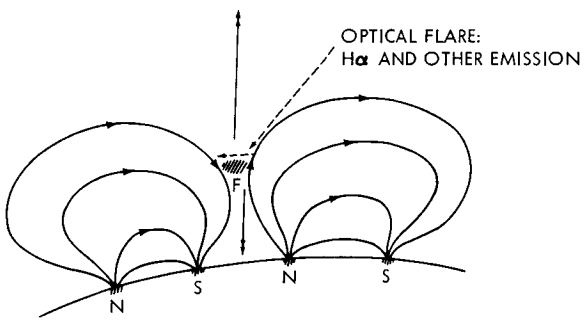

FIGURE 8–6. Two bipolar spot groups and the optical flare.

REFERENCES

1. Jefferies, J. T., and Orrall, F. Q., 1961, *Ap. J.*, 133: 946.
2. Svestka, Z., 1962, *BAC*, 13: 37.
3. Fritzova, L., 1961, *BAC*, 12: 254.
4. Michard, R., 1959, *Ann. Astroph.*, 22: 887.
5. Ballario, M. C., 1962, *Mem. S.A.I.*, vol. XXXIII, fasc. 4.
6. Ballario, M. C., 1963, *Mem. S.A.I.*, vol. XXXIV, fasc. 2.
7. Goldberg, L., Dodson, H. W., Müller, E., 1954, *Ap. J.*, 120: 83.
8. Waldmeier, M., 1940, *Zs. fur Ap.*, 20: 46.
9. Ellison, M. A., 1940, *M.N.*, 109: 3.
10. Giovanelli, R. G., 1940, *Ap. J.*, 91: 340.
11. Ballario, M. C., 1963, *Mem. S.A.I.*, vol. XXXIV, fasc. 4.
12. Severny, A. B., 1959, *Izv. Krym. A.O.*, XXI: 131.
13. Fritzova, L., 1960, *BAC*, 11: 117.
14. Smith, E. v. P., 1963, *Ap. J.*, 137: 580.
15. Svestka, Z., 1960, *BAC*, 11: 167.
16. Ballario, M. C., 1963, *Mem. S.A.I.* (in press).
17. Svestka, Z., 1961, *BAC*, 12: 73.
18. Svestka, Z., 1962, *BAC*, 13: 85.
19. de Jager, C., 1962, *Space Science Reviews*, Utrecht.

DISCUSSION

Dr. Prince: I think you have brought together much observational material; you have organized it and can say something about it. The flare model that you suggest is not contrary to what is observed, and you should be highly encouraged to continue the investigation.

There are flares now and then at the limb for which confusion, I believe, does not exist as to what is flare and what is something else. There was one long ago (May 8, 1951); in its initial stages it was small and looked like the fingers in a clenched hand—perhaps similar to the loops that you suggest. This feature was as bright at the limb as any flare we have observed on the disk. During the first 90 seconds there were great radial velocities, going in opposite directions in the two parts of the event.

N64-30260

9 SOLAR FLARES AND THE LOOP PROMINENCE MECHANISM*

JOHN T. JEFFERIES
Joint Institute for Laboratory Astrophysics
Boulder, Colo.
and
FRANK Q. ORRALL
Sacramento Peak Observatory, AFCRL
Sunspot, N. Mex.

LOOP PROMINENCES AND SOLAR FLARES

Loop prominences sometimes form above solar flares during their decline from maximum and may exist for several hours following the flare, but it is clear that all flares do not produce loop prominences (Reference 1). Indeed, Bruzek (Reference 2) has suggested that all loop prominences are preceded by great flares. Of the eight loop prominences observed against the disk by Dodson (Reference 3) and Bruzek (Reference 4), all followed important flares. Not all loops at the limb are accompanied by visible flares, but here the accompanying flare may be over the limb. We may thus consider the loop prominence as a rather rare post-flare phenomenon.

The profile of the core of the Hα line emitted by loop prominences is usually broadened by mass motions corresponding to velocities of about 50 to 100 km/sec (that is, velocities near that of free fall). But, in addition to this broad core, the line shows extended wings that cannot be explained by instrumental effects, damping, or by Stark effect (see Figure 9–1). When the loop is observed with the coronagraph against a good sky, the wings may sometimes be followed 10 angstroms or more from the line center. It seems inescapable that these wings are caused by fast neutral atoms in the prominence having energies in the kev range, some of which are probably produced from equally energetic protons by charge transfer. In one loop prominence (February 19, 1962) the wings could be observed out to ± 60A from the line center, corresponding to proton energies of 40 kev (Reference 5).

There is evidence that large numbers of energetic electrons and protons remain stored in the coronal magnetic field for hours following some flares. Thus the stationary component of the type IV radio emission has been attributed to energetic electrons trapped in the magnetic field of the inner corona, and the observation that proton cosmic ray events often last as long as their accompanying noise storm has been attributed to a similar storage of energetic protons. Further, some of these particles are believed to be stored at rather low levels, even within the coronal condensation overlying the flare. Thus the type IV microwave emission is thought to originate below 0.05 $R_\odot$ (Reference 6). Of the eight loop prominences and flares observed against the disk (References 3 and 4), all were accompanied by type IV bursts and six were accompanied by proton cosmic ray events. Several authors have suggested in passing that loop prominences and sporadic condensations may be a manifestation of these stored particles (References 6 and 7). Since we have observed kev hydrogen atoms in loop prominences, it is natural to ask whether these are related to the more energetic protons and electrons stored at higher levels in the corona.

First of all, we must ask how long kev protons can exist in the coronal condensation or loop

*Presented by Dr. Orrall.

728-629 O—64——6

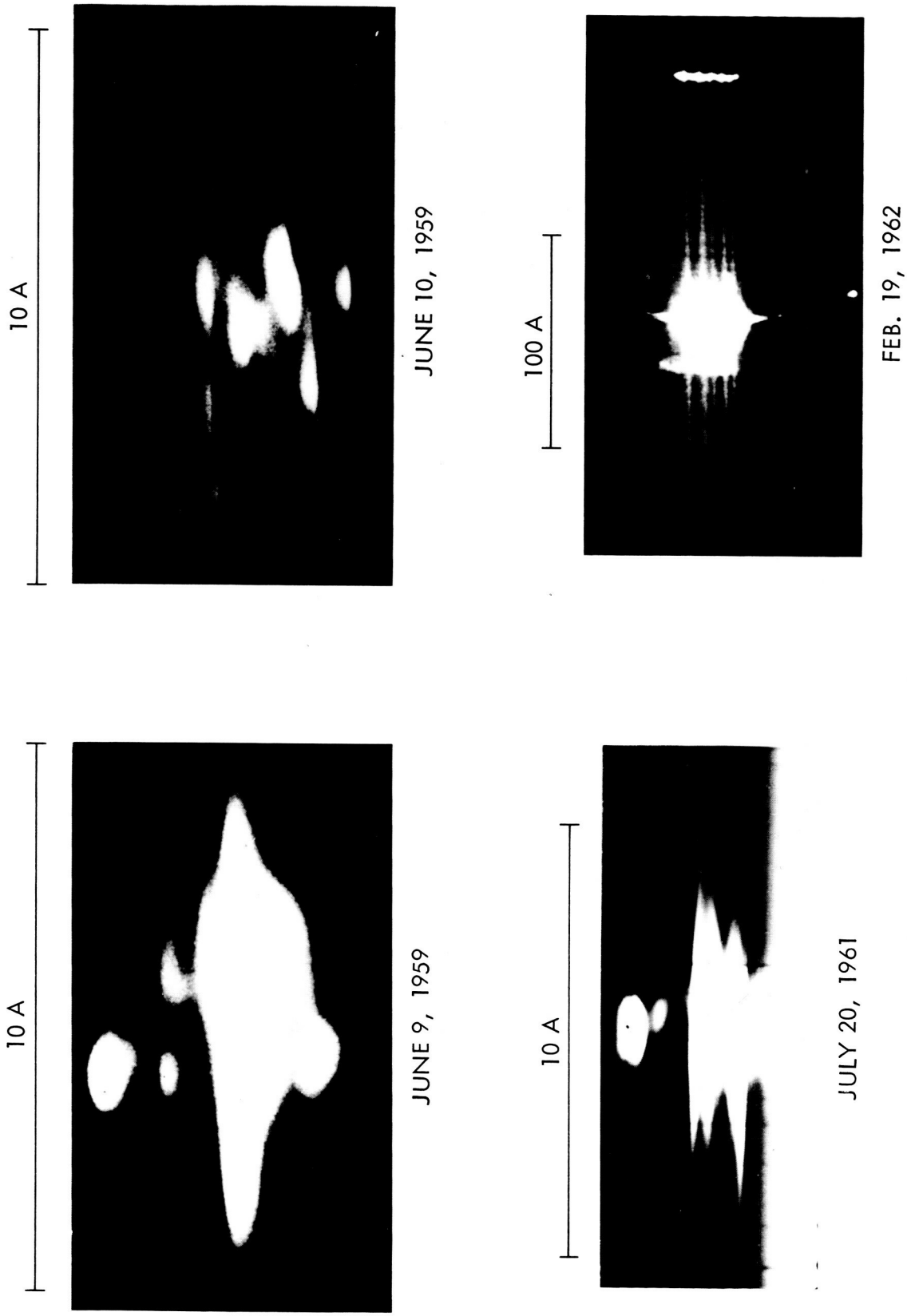

FIGURE 9–1. Examples of the Hα line emitted by loop prominences.

prominence without giving up their energy to the thermal field. Using the theory of Butler and Buckingham (Reference 8), we have computed the time t_1 for a fast proton injected into a plasma to have its velocity reduced by a factor e^{-1} by coulomb collisions. For the loop prominence we have taken $T_e \approx 2\times10^4$ °K and $N_e \approx 10^{11}\text{cm}^{-3}$. For the coronal condensation in which it is imbedded, $T_e \approx 2\times10^6$ °K and $N_e \approx 2\times10^9$ cm^{-3}. The results are shown in Table 9–1. Since the extended wings are observed in loops for hours after the flare, it is clear that the kev protons cannot be stored in the coronal condensation. Thus, if they are produced by the initial flare event, they must be stored elsewhere in the corona and fed into the condensation or they must be produced indirectly from more energetic particles. To proceed further, we must look at the observed loop prominence velocity distribution.

TABLE 9–1

Stopping Time t_1 for Fast Protons in a Plasma

Initial Proton Energy (kev)	Initial Proton Velocity (10^8 cm/sec)	t_1(sec)	
		Loop Prominence, $T_e=2\times10^4$ °K $N_e=10^{11}$ cm^{-3}	Coronal Condensation, $T_e=2\times10^6$ °K $N_e=2\times10^9$ cm^{-3}
1	0. 45	0. 001	2. 4
10	1. 4	0. 002	22. 0
40	2. 8	0. 013	34. 0
100	4. 5	0. 051	36. 0
1000	14. 0	1. 6	40. 0

THE HYDROGEN-ALPHA LINE PROFILE IN LOOP PROMINENCES

We observe $I(\Delta\lambda)$, the Hα line profile, and from this infer the number of three-state hydrogen atoms moving with a given velocity in the line of sight. These fast three-state hydrogen atoms presumably result from fast protons, but the velocity distribution of these fast protons cannot be inferred from the line profile without further assumptions. We therefore shall consider the consequences of two limiting assumptions about the nature of the fast particle distribution:

1. *The velocity distribution is isotropic:* We may now find the distribution of *speeds* of the three-state hydrogen atoms. These fast three-state atoms are most probably produced from fast protons by charge exchange; and, since the probability for charge transfer to the various excited levels of hydrogen is known, we can determine the fast proton speed distribution that is consistent with the observed profile and with our assumption of isotropy. We have calculated this distribution and find that it contains 10^3 times as much energy as the thermal energy of the prominence. Most of this energy is in the slower protons with energies less than 10 kev. Clearly, such a distribution cannot be maintained unless the fast protons escape into the corona before they are thermalized. The distribution would relax in $<10^{-2}$ second unless maintained by a continual input of fast protons. But the required input of fast protons would also supply 10^5 times the thermal energy content of the prominence each second, which is about 10^6 times the rate at which the prominence loses energy by radiation and other processes.

However, it is hard to see how kev protons can escape from a loop prominence. The fast neutral hydrogen can cross the magnetic field of the loop, but most of it still will be thermalized before it escapes into the corona unless the diameters of the individual threads of the loop are less than 10 km. Until we have other evidence for such a fine structure, we must suppose that the particles that are less energetic than 100 kev cannot escape, so that an isotropic distribution consistent with the observed profiles could last for only a fraction of a second.

2. *There is a stream flow with a velocity gradient:* We may account for the line shape in its entirety by invoking a physical picture similar to that of Severny (Reference 9), who supposed a velocity gradient to exist in the gas, as would be expected if it were forced through a nozzle or were subjected to a pinch. Hα emission in a loop prominence is usually first seen at the top of the loop and thereafter spreads downward. This suggests that any acceleration of the prominence material takes place near the top of the loop. Severny suggested that the acceleration mechanism in the

flare was the pinch effect. We do not think that the acceleration of material at the top of loop prominences is caused by the pinch effect, but the analysis will be similar. He supposed that material was ejected with an initial velocity V_0 and was stopped within a length X_0, producing a velocity gradient. Pairs of values of V_0 and X_0 consistent with the observed line profile can be found, but no unique pair can be determined by the line profile alone. We have considered several possible flows; and it is clear that all of them must contain 10^2 to 10^3 times the thermal energy of the Hα prominence, although we do not know how much of this energy will be converted to heat and how much will be delivered to the chromosphere and lost to the prominence without calculations based on a more specific model of the prominence and the sporadic condensation in which it is imbedded.

THE LOOP PROMINENCE MECHANISM

J. W. Warwick (unpublished) has suggested that both the energy and mass of loop prominences are supplied from below in the form of energetic particles which are generated at the photospheric levels and move up the magnetic lines of force that presumably outline the loops. We do not think it possible that these particles are generated at the *photospheric* level, but otherwise this picture seems to us preferable to the alternate and more frequently discussed process in which the prominence material is thought to condense from the surrounding corona. Independent estimates of the mass delivered to the chromosphere by large loop prominences (References 5 and 10) agree that more than 10^{16} grams must be supplied, and this is 10 times the mass of the Waldmeier-Müller coronal condensation. Further, the total thermal energy content of the coronal condensation is inadequate to provide the radiative losses of the loop system, also by about a factor of 10. It is of course possible that the mass and energy of the coronal condensation are continually resupplied at the proper rate, but it is difficult to see how either the mass or energy can be delivered to the loops across the magnetic field.

We therefore favor Warwick's hypothesis and suggest that energetic particles injected into the bottom of the loop are rapidly thermalized at the top, producing a dense high temperature region. This region expands rapidly but is contained by the magnetic field and so accelerates material along the loop, causing much of the motion evidenced by the wide wings and displacements of the Hα line. This rapid heating also causes the radio bursts and x-ray emission that accompany rapid changes in loop prominences (References 11 and 12).

The following quantities are typical of a large loop prominence event (such as that of February 19, 1963). The total mass delivered to the photosphere by the loop system during its lifetime is

$$M_T \approx 10^{16} \text{ gm},$$

corresponding to N_T protons where

$$N_T \approx 6 \times 10^{39}.$$

The total lifetime of the system is

$$t_T \geq 1.6 \times 10^4 \text{ sec},$$

while the lifetime of an individual loop is

$$t_L \approx 1.5 \times 10^3 \text{ sec}.$$

We may use these figures to estimate the radiative energy losses of the system. The *net* radiative emission ϵ from an optically thin plasma has been calculated by Orrall and Zirker (1961), who find that

$$\epsilon = 1.75 \times 10^{-23} \eta_e^2 \text{ erg cm}^{-3} \text{ sec}^{-1}.$$

The total energy E_R lost by the system during its lifetime is then

$$E_R = \frac{\epsilon}{\eta_e} N_T t_L \approx 2 \times 10^{20} \eta_e \text{ ergs}.$$

Here we have assumed that the proton and electron densities are equal and have used the values of N_T and t_L given above. We have used t_L rather than t_T, since t_L is the time during which any particular bit of material can radiate. Using $\eta_e = 10^{11}$ cm^{-3} (this is probably a lower limit), we find the total radiative loss $\approx 2 \times 10^{31}$ ergs.

We have used the line profiles to estimate the total kinetic energy delivered to the photo-

sphere by streaming and jet flow, and find $\approx 10^{31}$ ergs. This is very uncertain and is probably an upper limit, as some of it will be returned to the prominence as thermal energy.

The total energy loss of the loop system is thus $\approx 3\times 10^{31}$ ergs. If the entire mass M_T is to be supplied by energetic ions of initial velocity V_0, then the total energy E_T supplied to the prominence by their kinetic energy is

$$E_T=\frac{1}{2}M_T V_0^2.$$

We see that, for $V_0=10^8$ cm, $E_T=5\times 10^{31}$ ergs—or about the right amount of energy to maintain the system.

The occurrence of sprays and surges in active regions shows that there are mechanisms available at the chromospheric level for accelerating matter in large quantities to 10^8 cm sec^{-1} and, indeed, surges are sometimes seen to follow preexisting prominence loops.

But, since loop prominences are believed to follow large flares (Reference 2), it seems reasonable to look for the source of energetic particles in the coronal reservoir of energetic particles that these flares produce. A suggested model for this process is shown in Figure 9–2: (a) Following a large flare, the coronal magnetic field contains many trapped energetic flare particles (see, for example, Reference 6, p. 125). (b) Energetic ions from time to time drift or are transferred from the outer field lines to the inner field lines within the coronal condensation. (c) If the density becomes high enough, the less energetic ions may become thermalized and the density and temperature rapidly increase as more and more particles become trapped. This process begins near the top of the loop as the coronal density is observed to be higher there. (d) The hot, dense region thus produced ($N_e>10^{11}$ cm^{-3}; $T_e>4\times 10^6$ °K) cools by radiation and expansion to loop prominence temperature (2×10^4 °K). This process goes on irregularly in various loops of the system throughout its lifetime. The loop prominence is thus one way in which the corona discards the trapped flare plasma.

The energy and mass required seem somewhat high, but not at all unreasonable. Total energies of 10^{32} to 10^{33} ergs have been estimated for some large flares (Reference 2). Parker (Reference 13) estimates that 2×10^{15} gm were accellerated to 1500 km sec^{-1} by one large flare, which is about what we require.

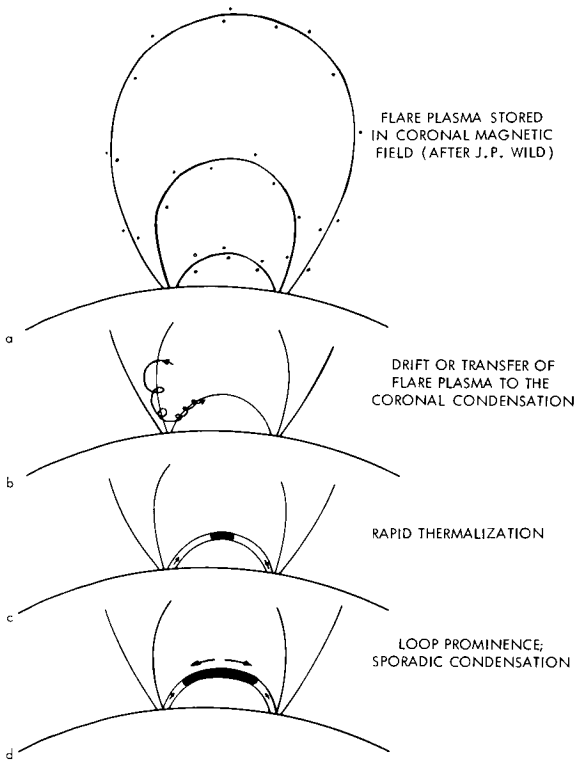

FIGURE 9–2. A suggested mechanism for the formation of loop prominences.

Finally, we point out that the fast protons implied by the most extended Hα wings observed (that is, those having energies in excess of 10 kev) cannot be produced in the explosion accompanying the rapid thermalization at the top of the loops unless the temperature of this explosion exceeds 10^8 °K. This is perhaps possible, but it seems more likely that these fast protons are some of the injected flare particles that emit Hα in the process of thermalization.

ACKNOWLEDGMENTS

We have had the benefit of numerous discussions on the subject of loop prominences with A. Bruzek, J. Kleczek, H. Schmidt, and J. B. Zirker.

REFERENCES

1. SMITH, H. J., and BOOTON, W. D., 1962, *Sacramento Peak Observatory Cont.*, No. 49.
2. BRUZEK, A., 1963, *these Proceedings*, paper no. 35.
3. DODSON, H. W., 1961, *Proc. Nat. Acad. Sci.*, 47: 901–905.
4. BRUZEK, A., 1962, *Zs. f. Ap.*, 54: 225-233.
5. JEFFERIES, J. T., and ORRALL, F. Q., 1963, *Symposium on the Solar Spectrum*, Utrecht.
6. WILD, J. P., 1963, "The Solar Corona," p. 125 (ed. J. W. Evans, Academic Press, New York).
7. ZIRIN, H., 1963, "The Solar Corona," p. 231 (ed. J. W. Evans, Academic Press, New York).
8. BUTLER, S. T., and BUCKINGHAM, M. J., 1962, *Phys. Rev.*, 126: 1.
9. SEVERNY, A B., 1962, *Izv. Krim. Astrophys. Obs.*, 27: 71.
10. KLECZEK, J., 1963, *Bull. Ast. Inst. Czech.*, 14: 167.
11. KLECZEK, J., 1963, *these Proceedings*, paper no. 10.
12. KLECZEK, J., and KRIVSKY, L., 1960, *Bull. Ast. Inst. Czech.*, 11: 165.
13. PARKER, E. N., 1963, *Ap. J. Supp.*, Series 8, No. 77: 177.

W64-30261

10 MASS BALANCE IN FLARE LOOPS

JOSIP KLECZEK
Sacramento Peak Observatory
Sunspot, N. Mex.

Solar flares are sometimes followed by loop prominences. The phenomenon is described in detail in Dr. Bruzek's papers (References 1 and 2). In these loops, a large amount of Hα material is condensed and then streams into the chromosphere. What does one mean by condensation? Where does this material come from? Is the material of the surrounding coronal condensation enough to supply sufficient material for formation of the loops?

To answer the questions, we measured the size, height, and velocity of all of the streamers of several loop systems through their lifetimes; for example, events such as those of May 8, 1956; September 11, 1956; and October 22, 1956. We have used Richard Dunn's large-scale prominence movies of the Sacramento Peak Observatory for this purpose, as they show the greatest detail.

CONDENSATION PROCESS

By condensation we mean the appearance of of knots and streamers in Hα over the solar limb. (We must not confuse this word *condensation* with the *coronal condensation*, the name given by Waldmeier to the coronal structure in which the loops are embedded.) A faint, nearly circular cloud appears first. Soon the cloud grows brighter as it grows. As a rule the initial growth is in all directions, but one direction or two opposite directions prevail. The following evolution shows that the preferred direction of growth is along a looplike trajectory. Often two or more neighboring loops develop simultaneously. This description applies to the evolution of the top of a loop.

The loops are rooted in flare ribbons or sunspots (References 1, 3, and 4). The growth of some of the studied loop system is not a continuous one. In some cases it is obvious that the growth of the loop system proceeds in jumps and *not* in expansion of individual loops. A new loop appears above a previous one. When the system reaches the height of 6 to 8×10^4 km, the condensation process fades and a new system is formed nearby.

MASS OF THE LOOP SYSTEM

The volume of each streamer was calculated from its length and width. The shape of the fine streamers was taken to be cylindrical. For the broader streamers, their width was measured and their thickness was taken to be that of normal streamers, so that the resulting volume is an underestimate. The densities of active prominences are generally higher than in quiescent prominences, and different values are found in literature. We have used densities of $\approx10^{-12}$ gm cm^{-3}, consistent with continuum observations of Jefferies and Orrall (Reference 5).

Hα Mass Condensed in Loops, 1956	Total Volumes of Loops (cm^3)	Total Mass of Loops (gm)
May 8	2×10^{27}	2×10^{15}
Sept. 11	1×10^{28}	1×10^{16}
Oct. 22	2.3×10^{27}	2.3×10^{15}

Results for three events are shown in the above table. Several other loops systems were measured in this way. The total mass delivered to the chromosphere by the loop system is in the interval 10^{15} to 10^{16} grams, depending on the duration and intensity of the loops; 10^{15} grams seems to be the lower limit, and the values near to 10^{16} grams are more representative. Expressed in particle density, 10^{39} to 10^{40} particles participate in a flare-loop system.

MASS OF THE CORONAL CONDENSATION

The loops are imbedded always in a coronal condensation, with volume about 10^{30} cm^3, that is, $(10^5 \text{ km})^3$. With densities 10^8 to 10^9 electrons per cm^3, this gives 10^{14} to 10^{15} grams in one condensation. Integrating the model of Waldmeier and Müller (Reference 6), we receive the mass of 1×10^{15} grams in a coronal condensation.

The loops occupy only a small fraction of the whole coronal condensation, a few thousandths only. That means that only a mass 10^{12} to 10^{13} grams of coronal plasma is at disposal for the condensation process. The coronal movies and coronal spectra do *not* indicate any exhaustion of coronal plasma by a loop system.

On the contrary, sporadic condensations in the inner part of the coronal condensation form during flare loops, as may be seen on Hα and 5303A movies from November 22, 1956 (Reference 7). The sporadic condensations represent an *increase* of density, as may be inferred from increase of brightness in visual as well as radio bands.

CONCLUSION AND IMPLICATIONS

Coronal condensations therefore cannot supply enough material for the loops' formation. A powerful mechanism must exist for transporting material from lower, denser atmospheric layers during and after some flares.

The loop prominences certainly seem to outline magnetic tubes of force. The observations show that the condensation process proceeds at the top of loops. Do the 10^{39} to 10^{40} particles get there in the form of corpuscular radiation? This would agree with Jefferies' and Orrall's (Reference 8) observations of energetic particles in loops and with Warwick's theory of flares (Reference 9). If so, how are the particles captured and thermalized? The yellow line emission might indicate the *lower limit* of the energy of the incoming particles.

REFERENCES

1. Bruzek, A., 1962, *ZfA.*, 54: 225.
2. Bruzek, A., 1963, *these Proceedings*, paper no. 35.
3. Bumba, V., and Kleczek, J., 1961, *Transactions IAU*, XI B: 430.
4. Dodson, H. W., 1961, *Proceedings Nat. Acad. Sciences*, 47: 901.
5. Jefferies, J. T., and Orrall, F. Q., 1961, *Ap. J.*, 133: 963.
6. Waldmeier, M., and Müller, H., 1950, *ZfA.*, 27: 58.
7. Newkirk, G., 1957, *Ann. Astroph.*, 20: 127.
8. Jefferies, J. T., and Orrall, F. Q., 1963, *Symposium on the Solar Spectrum*, Utrecht.
9. Warwick, J. W., 1962, *PASP*, 74: 302.

DISCUSSION

Dr. Kiepenheuer: I quite agree with Dr. Orrall and Dr. Kleczek that it is very difficult to supply material for these loops from the corona. But I do not quite see how you explain the lifting of this material without its being visible, because there are no Doppler shifts observed in that sense.

Dr. Kleczek: One explanation could be the explanation of Dr. Warwick. I think his picture of a flare is consistent with the idea that the mass is supplied in the form of corpuscular radiation. In this case we could not observe it in the optical region.

Dr. Kiepenheuer: Yes, but is it really possible to transport 10^{15} or 10^{17} grams in the form of corpuscular radiation without any trace? I really do not believe it. We are not able to compute that in detail.

Dr. Kleczek: Maybe you are right, but I think the estimates of Parker agree well with our results also. There is evidence that enough material to supply the loop prominences is emitted as corpuscular radiation by the flare. Only one part of the corpuscular radiation is captured by the overlying magnetic fields, thermalized, cooled to about 10^4 °K and returned sunward as loop prominence. The other part escapes into interplanetary space. Both parts seem roughly equal. We certainly would not see the corpuscular radiation in Hα, and it seems unlikely that we would see it even in the 5303A line.

Dr. Orrall: I didn't show another figure for want of time. In this figure, one could see above the loop, evidence of material that was being injected into even higher coronal loops. If the particles are injected into the loops at 1000 km/sec, we should not expect to see these in the corona—that is, in the coronograph—against the sky. We shouldn't expect to see them at all.

Dr. Prince: As we consider loop-type prominences, perhaps we should remember that they are indeed very rare solar phenomena and that, while they are taking place, very great things often are happening on the earth. While the loop-type prominences are occurring on the sun, very often protons are arriving at the polar regions of the earth.

I cannot help but look upon the great systems of loop-type prominences on the sun as a consequence of something very great that has happened. I also cannot forget two things: In Professor Kiepenheuer's book on the sun, he reproduces Waldmeier's drawings of loop-type prominences and the corona. He shows them to be intimately connected. I also remember the words of Monsieur Bernard Lyot, who enioyed looking at the sun and seeing what he could see. Apparently one of the most amazing observations that he shared with us informally was that, as he looked at the sun and saw loop-type prominences in Hα, his concomitant coronal observations indicated that the loop-type prominences had a sort of "skin" of coronal emission. These observations suggest a very intimate association between loop-type prominences and coronal emission. Is it possible that, in watching the formation of loop-type prominences, we also may be watching the growth of some aspect of the corona?

Dr. Moreton: Dr. Prince has brought up a good point, regarding loops being rare phenomena.

We recently have begun new observations of the limb, and I am surprised at the number of loop displays we observe.

Are loop prominences really rare, or is this because of observational problems?

Dr. Zirin: I think, besides this question, there are very many beautiful cases of large—extravagant, one might say—loops following a flare. These are brighter and stronger than most types. I also think that, just about every time we observe a large active region on the limb under good conditions, we will see fine, faint loops of some sort above them. I hope to show some pictures of them tomorrow.

So it may be that these even are two different things. I don't know. Certainly the brightest, strongest loops seem to follow flares. But not all loop prominences follow flares.

Dr. Prince: My comments have referred to the great systems of loop-type prominences.

Dr. Zirin: Yes, that is what I mean; these great, big, extravagant loops seem almost to follow flares. You also will get very nice loops when these are no flares. Maybe this is because there are always little surges or flares in progress.

I would like to make two points about Dr. Kleczek's paper. First of all, I think one could push the total mass involved in the Waldmeier-Müller condensation up perhaps to 10^{16} grams, since we have often observed densities of 10^{10} and 10^{11} in the post-flare loop phenomenon. We also have a number of observations of cases—I think the best was November 10, 1961—where a beautiful loop system followed a flare and one could watch the coronal density decrease as the loops died out.

And, finally, I would like to bring up this difficult question: How do you determine the density of material on the loops? Do you really understand the excitation of Hα in these loops? Can you, therefore, really give a number that is all right to a factor of 10 for the amount of material in the loops?

Dr. Kleczek: I think Frank Orrall or John Jefferies could comment on this question.

Dr. Jefferies: The electron density is derived from an observation of the integrated emission along the line of sight. We cannot, in this way, distinguish between the presence of clumps of high density material and a uniform distribution of lower density. Some limit to the clumpiness is presumably given, however, by a simple comparison of the scale lengths of the emitting gas in the sky plane and an estimate of the scale length resolvable by the tele-

scope and the associated observing equipment with the given seeing conditions.

In this way, I believe we are safe in saying that the *mean* electron density has been found to better than a factor of 2. I do not believe that observations are compatible with local concentrations of density more than about twice this mean density. A way to decide this question is through observation of the Stark-broadened lines of hydrogen (this gives a measure of the *local* electron density); however, different attempts to use this principle have not always given consistent results. The matter needs further study.

Dr. J. Warwick: I want to respond to the point that Dr. Moreton made a moment ago, about the occurrence frequency of the great loop systems.

I support Helen Dodson Prince's remark about the great loops and their rarity on the basis of some 3 years of experience with a full limb patrol of the sun of the type that you are describing.

The second point I would like to emphasize, in anticipation of some remarks I will make tomorrow, is a very important point made by Mrs. Prince concerning the relation between post-flare loops and the flare bright structure itself. For example, in the July 16, 1959, event the loop system has a very close topological similarity to the bright filaments of the flare.

N64-30262

11 ON THE STARK BROADENING OF HIGH BALMER LINES EMITTED BY SOLAR FLARES*

L. D. DE FEITER
Netherlands Foundation for Radio Astronomy
Sterrenwacht Sonnenborgh, Utrecht, Netherlands

30262

In 1959 Suemoto and Hiei showed that the Balmer line spectra of solar flares could be interpreted only when it was assumed that the emission takes place in small filamentary structures. This conclusion was confirmed by Svestka in 1962. In their analysis these authors treated the Stark broadening according to the classical Holtsmark theory. It is shown in this paper that the conclusions remain valid when the effects of the electrons on the Stark-broadening parameters is taken into account.

Auth.

The study of Balmer line spectra, emitted by solar flares, has led to controversial conclusions with regard to the importance of Stark broadening in the formation of these lines; see, for instance, the discussion by Smith and Smith (Reference 1). In many flares macroscopic motions seem to be more important than the linear Stark effect in producing the broad Balmer lines. This conclusion, however, has been derived from a study of the intensity profile in the wings of Hα and a few other low Balmer lines. It should be noted that in these lines the influence of Stark broadening on the intensity profile may easily be masked by the effects of macroscopic motions. Since the importance of Stark broadening grows with increasing quantum number n, higher Balmer lines should be used in a study of this broadening mechanism. This fact has been recognized by Redman and Suemoto (Reference 2) in their analysis of the Balmer lines in eclipse spectra. In these spectra the halfwidths first decrease with increasing quantum number because of the decreasing influence of self-absorption; for $n \geq 20$, the halfwidths increase as a consequence of the growing influence of Stark broadening.

*This research was made possible by the financial support of the Netherlands Foundation for Pure Research.

This method of halfwidth analysis has been applied to the spectra of solar flares by Suemoto and Hiei (Reference 3), by Hirayama (Reference 4), and by Svestka (References 5 and 6). In these spectra the turning point lies at a quantum number $n=9$, indicating that the electron density in flares is higher than in the undisturbed chromosphere. From the upgoing part of the halfwidth curve these authors derived electron densities for the flares investigated which, indeed, are higher than in the chromosphere by a factor of 10 to 100. The descending part of the curve has been used by the Japanese investigators to derive an estimate of the total number of hydrogen atoms in the second quantum state, in a column of 1 cm^2 area, above the base of the flare: N_2z. Since this method depends rather critically on assumptions which possibly are not fulfilled in flares—such as the constancy of the source function with depth, and no influence of the flare radiation on the underlying chromosphere—the outcome of this estimate is open to some doubt. Being aware of this fact, Svestka chose the lines investigated in such a way that a small influence of self-absorption on their halfwidth is still present. This enabled him to use these lines also for obtaining an estimate for N_2z. In order to separate the density of the hydrogen atoms in the second quantum state from the thickness of the emitting layer, a third relation is needed. For this Suemoto and his coworkers used the Saha-Boltzmann equation and showed that the thickness could not exceed 10 km. From the unobservably low intensity of the Balmer continuum in the flare of August 7, 1960,

Svestka showed that the values of N_e and N_2z would lead to an effective thickness of 4 km only. These results have led to the hypothesis that the Balmer line emission originates in very small structures, which have not yet been observed directly.

This conclusion is attractive from the theoretical point of view, because of the serious difficulties met in explaining the origin of solar flares as a process of converting the magnetic energy stored in the large-scale magnetic fields near sunspots into the kinetic energy and radiation. A reduction of the scale of the magnetic field elements to the values derived above would greatly help in reducing the time necessary for such a conversion (References 7 and 8).

Before this working model is adopted, however, one should examine critically the assumptions underlying the method of analysis used to obtain the values of N_e and N_2z. One of the factors that could reduce the estimated electron density is the introduction of electron broadening in the computation of the halfwidths of the high members of the Balmer series. It is the purpose of this paper to present the results of a revised analysis which examines the treatment of the electron broadening.

THE CALCULATION OF STARK-BROADENED PROFILES

According to Griem (Reference 9), a good approximation to the combined broadening action of both ions and electrons can be obtained by computing these contributions separately—the first according to the usual quasi-static theory, and the second according to the impact theory—and then folding the two profiles so obtained. In addition, it was stated in his paper that the contribution of the ionic fields can be computed with sufficient accuracy by using an average Stark profile for almost all lines, provided that suitable scaling factors K_{mn} are introduced for every transition $m \rightarrow n$. It can be shown that this is equivalent to the application of Pannekoek's approximation (Reference 10). In fact, Griem's scaling factors K_{mn}, which are the factors K_{ab} in his notation, are (apart from a constant factor which is approximately 2.94) the same as the factors s_{mn} derived by De Jager (Reference 11) from the tables of Stark profiles published by Underhill and Waddell (Reference 12). When the only broadening mechanism operative in the formation of the hydrogen line $m \rightarrow n$ is the Stark broadening produced by the fields of the ions, the absorption coefficient can be approximated very well by the expression:

$$\ell(\Delta\lambda)d\Delta\lambda = \frac{\pi e^2}{mc^2}\lambda^2 f_{mn}\frac{T^H(\beta)}{K_{mn}F_0}d\Delta\lambda, \qquad (1)$$

where the symbols $\pi e^2/mc^2$, λ, f_{mn} have their usual meaning; $F_0 = 1.25\times10^{-9}N_e^{2/3}$, $\beta = \Delta\lambda/K_{mn}F_0$, and T^H is the standard Stark function introduced by Griem.

This profile is folded with a damping profile to take into account the broadening due to the rapidly changing fields of the electrons. In his second paper Griem (Reference 13) gave a revision of the formula to be used in the computation of the damping constant γ_e. This revision, which is based on the modified impact theory developed by Lewis (Reference 14), makes this damping constant dependent on the position within the line where the absorption coefficient has to be calculated. As a good approximation to the complicated exact formulas, Griem suggests the use of the following interpolation formulas (the position in the line is denoted by the dimensionless quantity β):

For $\beta < \beta_p$, where

$$\beta_p = 3.61\times10^4\frac{N_e^{-1/6}}{n^2-m^2},$$

$$\gamma_e = 5.6\times10^{-6}N_e^{1/3}T^{-1/2}\frac{n^5+m^5}{n^2-m^2}\log\frac{4.6\times10^6 T}{n^2N_e^{1/2}} + 1.5\pi\beta_w^{-1/2}$$

$$= \gamma_w + \gamma_s. \qquad (2)$$

Here

$$\beta_w = 8.38\times10^{10}\frac{T}{n^4N_e^{2/3}}.$$

We denote the two terms in Equation 2 as γ_w and γ_s, respectively, and their sum as γ_e.

For $\beta_p < \beta < \beta_w$:

$$\gamma_e = \frac{\log\beta_w/\beta}{\log\beta_w/\beta_p}\gamma_w + \gamma_s.$$

When $\beta > \beta_w$, the usual quasi-static theory is valid also for the electron broadening.

These formulas cannot be used directly for the computation of the central parts of the lines. The variation of the damping constant in the line produces a deviation from the Lorentz profile, which destroys the normalization. When we compute the central parts of the line, we must specify the value of β to be inserted in Equation 3. In our computations we have substituted a real damping profile for the profile of the electron broadening instead of the one with the variable damping constant. The halfwidths of both profiles have been made equal. So the effective value of the damping constant γ_{eff} has been taken equal to the halfwidth of the actual electron-broadening profile. From this definition and Griem's interpolation formula, it follows that

$$\gamma_{eff} = \gamma_w + \gamma_s,$$

when

$$\gamma_w + \gamma_s < \beta_p;$$

and

$$\gamma_{eff} = x_{1/2}$$

with

$$x_{1/2} = [2(\gamma_w + \gamma_s)\gamma(x_{1/2}) - \gamma^2(x_{1/2})]^{1/2},$$

when

$$\beta_p < \gamma_w + \gamma_s < [2\gamma_w\gamma_s + \gamma_s^2]^{1/2}.$$

When $\gamma_w + \gamma_s > [2\gamma_w + \gamma_s^2]^{1/2}$, the halfwidth of the electron-broadening profile is larger than β_w; and, consequently, almost the entire profile must be calculated according to the quasi-static theory.

In Figure 11–1 the computed values of the damping constants are given for a number of Balmer lines as a function of electron density. A value of 10,000 °K has been taken for the kinetic temperature. The damping constants reduced for the Lewis correction in the manner described above and those derived from the formulas given in Griem's first paper are given.

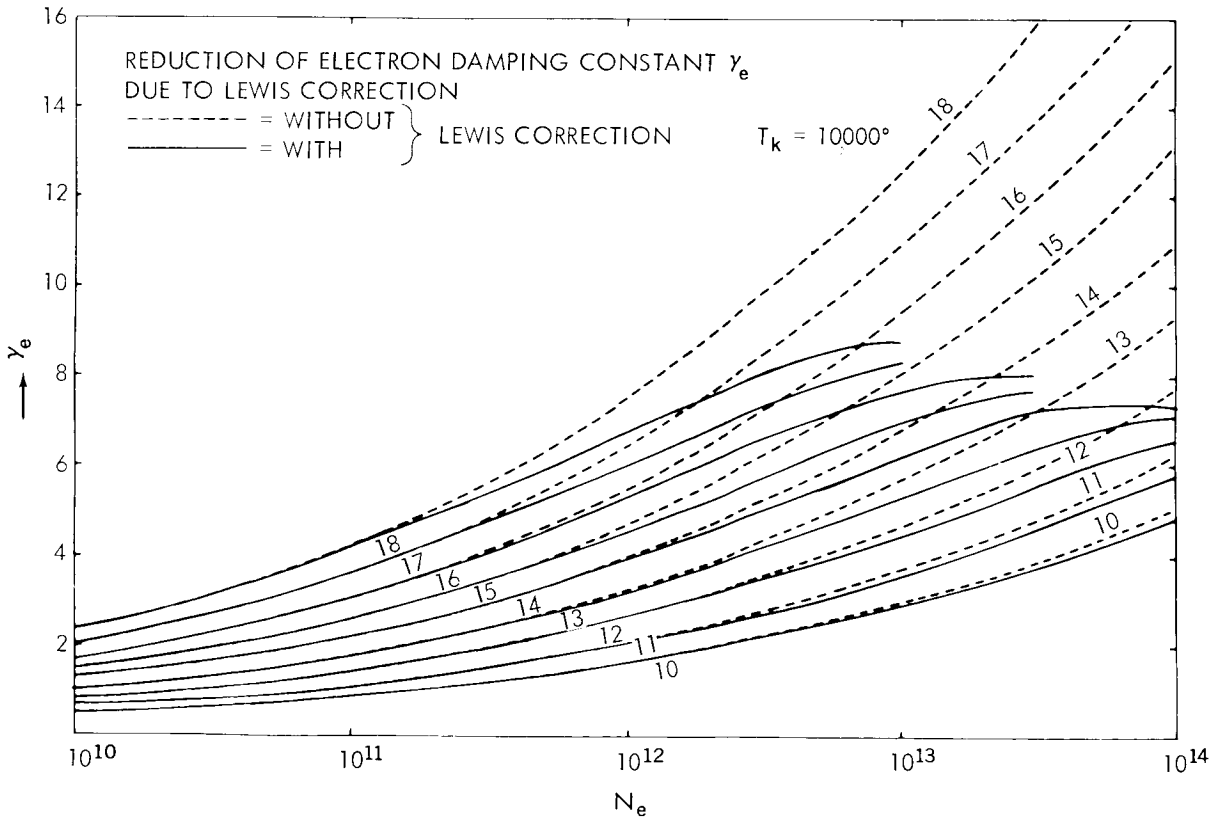

FIGURE 11–1. Electron damping constants for the Balmer lines H_{10}–H_{18} as a function of electron density. $T_k \pm 10{,}000°$.

With the values so obtained, the halfwidths of the lines can be computed. For low values of the electron density the thermal broadening also should be taken into account. If this is done in an exact way, one quickly runs into laborious computations which are hardly justified. The computational procedure adopted by Redman and Suemoto (Reference 2) is advantageous. It consists of approximating the average Stark profile by a Voigt profile, which gives—when folded with either a Doppler or a damping profile—again a Voigt profile. The parameters of this new profile can be calculated quite easily.

TABLE 11–1

The Folding of the Stark Profile with a Damping Profile; Comparison of Central Intensities and Halfwidths for Exact and Approximate Computations

γ	Exact Values		Approximate Values	
	Central Intensity	Halfwidth	Central Intensity	Halfwidth
0	0. 0976	4. 15	0. 0974	4. 2
1	0. 0791	4. 9	0. 0790	4. 8
2	0. 0661	5. 7	0. 0660	5. 5
3	0. 0564	6. 5	0. 0558	6. 3
4	0. 0490	7. 3	0. 0487	7. 1
5	0. 0432	8. 1	0. 0427	8. 0
7	0. 0347	9. 8	0. 0345	9. 7
10	0. 0267	12. 5	0. 0262	12. 5

In table 11–1 the central intensities and halfwidths, computed according to the Voigt profile method, and those derived from Griem's tables of the function $T(\beta,\gamma)$ are given. From this table it follows that the approximate method is completely justified. The folding with a Doppler profile, for which exact computations have been published by De Jager and Neven (Reference 15), can equally well be performed with the aid of the Voigt functions, as is demonstrated in Table 11–2. For comparison with the original data given by De Jager and Neven, it should be noted that their β-scale must be multiplied by 2.94 to bring it into accordance with the scale used by Griem. The halfwidths presented in Figures 11–2 and 11–3 are computed according to this approximate method. For the conversion of the Voigt parameter a into the halfwidth the

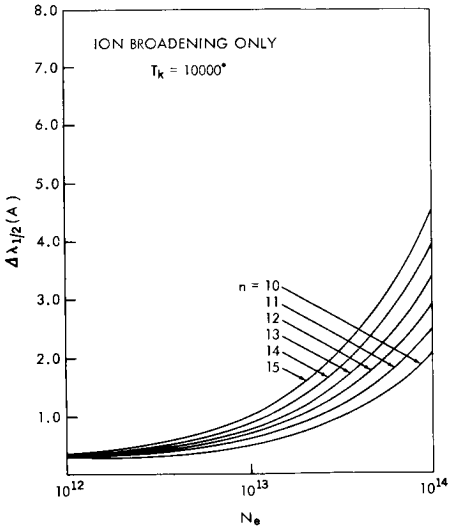

FIGURE 11–2. Halfwidths of the Balmer lines H_{10}–H_{15} as a function of electron density. $T_k=10{,}000°$. Broadening by thermal Doppler effects and Stark effect of ionic fields only.

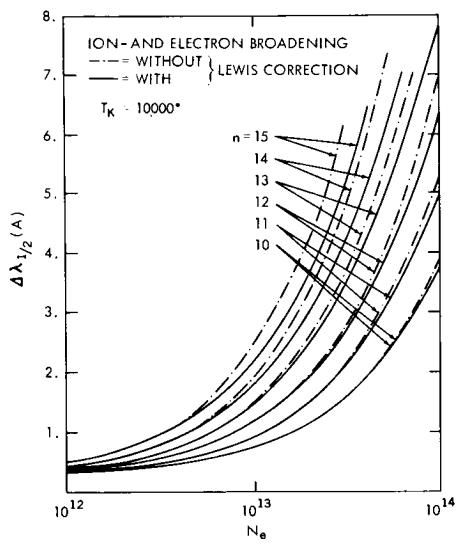

FIGURE 11–3. Halfwidths of the Balmer lines H_{10}–H_{15} as a function of electron density. $T_k=10{,}000°$. Broadening by thermal Doppler effects, Stark effect of ionic fields and electron damping.

following formula should be used:

$$\Delta\lambda_{1/2}=2W(a)(\beta_S^2+\beta_D^2)^{1/2}K_{mn}F_0,$$

where

$$\beta_D=\Delta\lambda_D/K_{mn}F_0 \qquad (4)$$

Here the function $W(a)$ can be derived from the tables given by Posener (Reference 16).

TABLE 11–2

The Folding of the Stark Profile with a Doppler Profile; Comparison of Central Intensities and Halfwidths for Exact and Approximate Computations

β_D	Exact Values		Approximate Values	
	Central Intensity	Halfwidth	Central Intensity	Halfwidth
0	0. 0960	4. 15	0. 0965	4. 15
1	0. 0835	4. 3	0. 0828	4. 2
2	0. 0635	4. 8	0. 0630	4. 5
3	0. 0502	5. 3	0. 0492	4. 9
5	0. 0340	6. 3	0. 0316	6. 2
7	0. 0253	7. 7	0. 0248	7. 5
10	0. 0182	10. 1	0. 0179	9. 9

DISCUSSION

From the curves of Figure 11–3 the electron density necessary to produce a certain observed halfwidth of H_n with $10 \leq n \leq 15$ can be derived. The results of the estimate of N_e in this way are compared with the values derived by Suemoto et al. and by Svestka in Table 11–3. It is immediately clear from this table that the electron density, which is derived with electron broadening, is only a factor 2 or 3 lower than the estimates of this quantity when these effects are not considered. This leaves unaffected the conclusion regarding the filamentary structure, at least for the parts of the flare emitting the Balmer lines. It seems very difficult indeed to find a way to interpret these observations without invoking these subtelescopic structures.

TABLE 11–3

Electron Densities in Some Flares, Derived from the Observed Halfwidths of High Balmer Lines, Taking the Electron Broadening into Account (for comparison, the values derived with Holtsmark's theory are also given).

Flare Discussed	N_e Derived Without Electron Broadening	N_e Derived With Electron Broadening	Author
Jan. 5, 1957, Imp. 2+ Dec. 29, 1956, Imp. 1+	2×10^{13}	6×10^{12}	Suemoto & Hiei
July 12, 1961, Imp. 3-+	7×10^{13}	3×10^{13}	Svestka
Aug. 7, 1960, Imp. 1	6×10^{13}	2×10^{13}	Svestka

REFERENCES

1. SMITH, H. J., and SMITH, E. v. P., 1963, "Solar Flares," Macmillan.
2. REDMAN, R. O., and SUEMOTO, Z., 1954, *Mon. Not. Roy. Astr. Soc.*, 114: 524.
3. SUEMOTO, Z., and HIEI, E., 1959, *Pub. Astr. Soc. Japan*, 11: 185.
4. HIRAYAMA, T., 1961, *Pub. Astr. Soc. Japan*, 13: 152.
5. SVESTKA, Z., 1962, *Bull. Astr. Inst. Czech.*, 13: 236.
6. SVESTKA, Z., 1964, to appear in *Bull. Astr. Inst. Czech.*
7. PARKER, E. N., 1963, *Astroph. J. Suppl.*, Series 8: 177.
8. KIEPENHEUER, K. O., 1963, *Symposium on the Solar Spectrum*, Utrecht.
9. GRIEM, H. R., 1960, *Astroph. J.*, 132: 883.
10. DE FEITER, L. D., 1964, to be published.
11. DE JAGER, C., 1960, *Ann. d'Astroph.*, 23: 889.
12. UNDERHILL, A. B., and WADDELL, J., 1959, N.B.S. Circular No. 637.
13. GRIEM, H. R., 1962, *Astroph. J.*, 136: 422.
14. LEWIS, M., 1961, *Phys. Rev.*, 121: 501.
15. DE JAGER, C., and NEVEN, L., 1962, *Ann. Obs. Roy. de Belgique*, 9: 47.
16. POSENER, D. W., 1959, *Aust. J. of Phys.*, 12: 184.

Magnetic Observations

728-629 O—64——7

N64-30263

12 MAGNETIC OBSERVATIONS RELATING TO SOLAR FLARES

ROBERT HOWARD
Mount Wilson and Palomar Observatories
Carnegie Institution of Washington, California Institute of Technology
Pasadena, Calif.

Solar flares always occur near measurable magnetic fields—although not always near sunspots. Recent theories of the flare process have relied on the interaction of magnetic fields and the chromospheric matter to supply a large amount of energy in a small volume to produce a flare. Because of the paucity of observations of magnetic fields on the surface of the sun, especially observations with good time resolution in the neighborhood of flares, the task of the theoreticians has been a difficult one. It is the purpose of this paper to discuss the magnetic observations that are available to help in an understanding of the solar flare phenomenon.

SUNSPOT MAGNETIC FIELDS, CLASSIFICATIONS, AND AREAS

Sunspot magnetic fields, areas, and Zürich spot classifications are useful parameters in correlation studies of solar flare frequency. These data are available for a period of many years. The Zürich classifications give an indication of the size and the stage of development of the spot group.

Giovanelli (Reference 1) made one of the earliest statistical studies of the relation between flare frequency and parameters of the spot group. He found that Mount Wilson type γ spot groups (complex) showed the highest frequency of flare incidence. A γ spot group produced on the average 2.05×10^{-3} flare per day per spot area in millionths of the solar hemisphere. The next highest frequency (1.20×10^{-3}) was found for $\beta\gamma$ groups; next came β groups (0.96×10^{-3}); and, finally, α (0.81×10^{-3}).

He found a very well defined relation between probability of a flare occurrence and spot group area. The probability is proportional to the spot area. The factor of proportionality for all groups combined is 2.5×10^{-3}, where the probability is per spot group per day and the area is measured in millionths of the solar hemisphere.

Giovanelli also found that flares are more likely to occur when a spot group is increasing its area than when it is decreasing its area, and flares are more likely to occur when a spot group is decreasing its size than when its area is not changing.

Kleczek (Reference 2), from a study of 5000 flares, found that the mean frequency of flares per unit time in a spot group depended on the classification of the spot group. The greatest frequency of flares (22.93 in 100 hours) was found in spot groups of Zürich type F. This held true for all importance classes, and the effect was most striking for the flares of greatest importance. The spot groups with the next lowest flare frequency were class E. The frequency of flares in class E groups is less by a factor 3 than that for class F. Zürich type F spot groups are very large groups with many individual spots and dimensions in longitude of at least 15 degrees. Zürich type E spot groups are also large groups with dimensions in longitude of at least 10 degrees. These two classifications represent the largest sunspot groups seen on the disk. Often included as E or F are groups which are magnetically more or less complex.

Künzel (Reference 3), from a study of more than 14,000 flares, also found that the magnetic

classification of the region is an important parameter in the determination of the probability of flare occurrence. He found that flares were more likely to occur in group types F, E, and D when the spot magnetic fields were arranged in a complex pattern than when the pattern was the simple β one. In turn, for each of these Zürich classifications the probability of flare occurrence was greater when one of the spots contained both a north and a south magnetic polarity than when the group was complex, but no spots contained two polarities. The greatest probability for the occurrence of a flare is in a type F group, where one spot contains two polarities. In such a group one can expect about 4 flares per day.

A similar study by Bell and Glazer (Reference 4), using Mount Wilson sunspot classifications and flare results from the IAU Quarterly Bulletin, for the period 1937–1953, gives the following results:

The average number of flares per γ spot group per rotation across the visible disk is 19.1, and for $\beta\gamma$ groups it is 11.20. The average number of flares for β groups is 1.85, and for α, 0.68. The expected frequency of flare incidence depends in addition on the maximum magnetic field strength in the spot group. For example, for γ groups with maximum fields greater than 2000 gauss the average number of flares is 22.70, while for γ groups with maximum fields between 1000 and 2000 gauss the average number of flares is 8.7. Bell and Glazer also found a relation between probability of flare occurrence and sunspot group area. They concluded that for the largest spots the relation was logarithmic; that is, the probability of flare occurrence did not increase as rapidly with the area for the larger groups as for the smaller groups.

These statistical studies indicate quite definitely that the probability of flare occurrence increases with the area of the spot group, the complexity of the magnetic configuration—and possibly with the maximum value of the spot fields, although whether this is true as separate from the dependence on area is in doubt. That there is not good agreement between the actual numerical results of the studies is not surprising. The investigators used data from different periods and, in some cases, different sources. The completeness of the flare data, particularly the older data, is poor. Kleczek is the only one of these authors who has taken into account the duration of the available flare observations. His results consequently give the highest probability of flare occurrence and are the most accurate.

STUDIES OF INDIVIDUAL FLARES AND ASSOCIATED SPOT FIELDS

Bumba (Reference 5), from a study of 69 flares in 10 spot groups, concludes that in general the location of earliest development of flares occurs on the boundaries between polarities. He also found that the main portion of the flare is usually found where spots of opposite polarity approach closest—sometimes the sudden development of a spot near another of opposite polarity immediately precedes the flare. In some cases the development of the flare seems to depend on the magnetic configuration. Sometimes flares occupied the position of filaments.

Bruzek (Reference 6) studied the large complex active region responsible for the great flares of June and July 1959. These flares occurred during gradual changes in the structure of the spot group. Bruzek could find no connection between the occurrence of the flares and any particular phase of development of the spot group. Despite the changes in appearance of the group, all the flares originated at the same point relative to the positions of the spot umbrae, and all the flares had nearly the same shape. The great flares and most of the smaller ones originated on or near the neutral line separating umbrae of different polarities. This was not a neutral point of the field because the transverse component was frequently strong at this position.

Gopasyuk (Reference 7), from a study of several flares of Importance 1 and 2, found that with the appearance and development of flares a shift of nearby spots is observed toward the flare. The spot observations were made with relatively good time resolution. The velocity of this motion is about 0.5 km/sec. The motion of the spots and the flare start within about 5 minutes of each other. The spot motion con-

tinues for 2 to 3 hours after the end of the Hα flare. The motion is not uniform; the translational velocity seems to vary roughly sinusoidally. The amplitude of the sinusoidal variation increases with the importance of the flare.

A recent study of flare and spot positions by Wolbach (Reference 8) shows that, for the 11 spot groups and 288 flares which he investigated, the flares tended to occupy regions where there were two magnetic polarities rather than unipolar areas. He could find no correlation between the occurrence of flares and spot activity, such as a change in magnetic classification or the disappearance of spots. About 10 percent show evidence of covering some part (usually a small part) of a spot umbra.

Ellison et al. (Reference 9) have found that the 10 great flares which produced cosmic rays recorded at ground level tended to occur directly over spot groups. Moreover, these were γ or $\beta\gamma$ regions. The flares occurred around the time of the maximum area of the group. The flares consisted of two roughly parallel filaments positioned along the line dividing the two polarities. The emission in these filaments was most intense over the spots.

Observers of spot fields and flare positions seem to be in good agreement that flares originate and tend to stay in regions where opposite spot polarities are close to each other. It does not seem that most flares can be correlated with any particular changes taking place within the group, although some motion of nearby spots toward the flare during and after the flare seems established. The larger flares are more likely to occur directly over spots than are the smaller flares.

MAGNETOGRAPH STUDIES

The development of the solar magnetograph by Babcock (Reference 10) enabled observers to actually map magnetic fields on the surface of the sun. This has proved to be a valuable tool in the study of flares and active regions, although as yet both spatial and time resolution have not been as great as they should be. Further improvements in instrumentation, such as the recent measures of the transverse component of the magnetic field by Stepanov and Severny (Reference 11), will undoubtedly help us toward an understanding of the phenomenon known as an active region.

Severny (References 12, 13, and 14) in a series of papers has discussed the relation of solar flares and magnetic fields in active regions. At the Crimean Observatory one or two magnetic maps per day are made of each spot group as a part of a routine flare patrol program. In general, during the first years only the strongest fields—mostly in spots—were recorded. Severny found that in the majority of cases flares originate near what are probably neutral points in the magnetic field. The relation between flares and neutral points is improved if one considers only the magnetic maps made with the core of Hβ, which may be considered to represent more accurately the chromospheric field. Severny concludes from studying magnetograms made before and after flares that, in general, the flares result in a decrease in the magnetic gradients around the neutral point. Sometimes this results from a decrease in the magnitude of the fields and sometimes from a displacement of the magnetic poles away from the flare.

Table 12–1 shows the results of a study of 51 flares (Reference 15). The gradients are those measured at the neutral point in the vicinity of the flare. These gradients were measured from models constructed using the measured spot fields.

Some recent measures of the transverse component of solar magnetic fields in active regions (Reference 14) seem to indicate that flares originate in regions where there are peculiar

TABLE 12–1

Flare Importance	Number	Gradient at Neutral Point (gauss/km)	
		Before	After
3+ (Balloon cosmic ray)	13	0. 73	0. 25
3 and 3+ (PCA)	11	0. 46	0. 27
3 (No geophys. effects)	12	0. 18	0. 13
2 and 2+	15	0. 054	0. 038

branchings of the transverse component. This is the configuration one would expect to measure at a neutral point. However, detailed results of measures of transverse fields must be treated cautiously. Öhman (Reference 16) has pointed out that the formation of an absorption line in the presence of a magnetic field is really a very complicated process, and there are effects which can cause an apparent rotation of the plane of polarization.

An investigation of the weaker (plage) fields associated with the great cosmic ray flare of July 16, 1959, (Reference 17) failed to show any changes in the fields during the course of the flare. Fourteen magnetograms of the active region with a resolution of 7500 km were made starting a few minutes after the start of the flare. No changes could be detected in the strength or configuration of the magnetic fields other than those which could be attributed to imperfections in seeing or scanning. The highest field strength distinguishable in these observations was 40 gauss.

Bappu and Punetha (Reference 18) have examined calcium spectroheliograms covering periods before and after four large flares. It is well known that the correspondence between the position of photospheric magnetic fields and calcium *plages* is a very good one. These authors found no changes in the pattern of the plage which could be attributed to the occurrence of the flare.

A subsequent investigation of the Crimean Observatory records of the same active region (Reference 19) indicates that the spot fields decreased in magnitude from the day before to the day after the July 16, 1959, flare. The central field strength of the spots as measured photographically or visually did not show an appreciable change, but the spot group did decrease in area from the day before to the day after the flare. The 7000 km resolution of the Crimean Observatory magnetograph would show, as a result, a decrease in the strength of the measured spot fields. It may be (Reference 20) that a decrease in area of the spot group is an effect characteristic of the largest (cosmic ray) flares. Giovanelli (Reference 1) has shown that flares are more likely to occur during a decrease in area of the spot group, but unfortunately he did not distinguish between flares of various importance classes.

Gopasyuk (Reference 21) has studied the relation of the development of flares and the longitudinal component of the magnetic field. From a study of 3 years of Crimean Observatory data, he finds that flares tend to originate at neutral points of the magnetic field. During the initial stages of development, the expansion of the flare does not depend on the local magnetic field configuration, but later the magnetic field seems to determine the development. During these later stages, the expansion of the flare is characterized by two types of dependence on the local magnetic fields: (1) expansion along the zero line of the magnetic field, and (2) expansion along a wide front within a region of one magnetic polarity.

SUMMARY

There is little doubt that the existence, the importance, and to some extent the development of solar flares are dependent on the configuration of local magnetic fields. Flares are more likely to occur in magnetically complex active regions than in magnetically simple active regions. This dependence on the complexity of the magnetic configuration is much greater for the more important flares. In general, flares tend to occur during the stages of growth of the sunspot group, although there is evidence that the flares with the greatest geophysical effects occur in decaying spot groups. Many flares originate near what may be neutral points in the magnetic field. Generally the occurrence of a flare results in the decrease of the magnetic gradients in the vicinity of the neutral point—either because of a decrease of the fields, or because of a separation of the nearby spots. However during, and for an hour or two after, the flare the nearby spots approach the flare. It is impossible with the present observations to pinpoint the exact time of the changes in the magnetic fields. The only magnetic observations with reasonably good time resolution are of weaker fields ($<$40 gauss), and these showed no changes during a very large flare.

It should be pointed out that all these observations refer to magnetic fields which are

measured in the photosphere or the low chromosphere in the vicinity of flares. The only observations of magnetic fields *in* flares are those of Blaha, Kopecky, and Svestka (Reference 22), who detected a broadening of the D_1 line of sodium in two flares, which they attributed to the Zeeman effect. Although calibration is difficult with a method that does not use polarizing analyzers, they estimated the fields to be between 2500 and 3000 gauss—roughly the same as the field strengths in nearby spots.

It should be possible during the next solar maximum to obtain magnetic observations of active regions with improved time resolution. It is important to determine the time of the occurrence of changes in the local magnetic fields. Since it appears that the important changes occur in the sunspot fields rather than the weaker *plage* fields, and since there are already some interesting results from a study of the positions of spots associated with only a few flares (Reference 7), it seems worthwhile to maintain a white-light patrol to look for changes in sunspots.

The measurement of magnetic fields on the surface of the sun has already produced new results to help in our understanding of the phenomenon of an active region. It seems likely that in the years ahead improved techniques will provide additional data to help in the solution of the problem of solar activity.

REFERENCES

1. Giovanelli, R. G., 1939, *Ap. J.*, 89, 555.
2. Kleczek, J., 1953, *B.A.C.*, 4: 9.
3. Künzel, H., 1960, *A.N.*, 285: 271.
4. Bell, B., and Glazer, H., 1959, *Smithson. Contr. Astrophys.*, 3(4).
5. Bumba, V., 1958, *Izv. Crim. Astrophys. Obs.*, 19: 105.
6. Bruzek, A., 1960, *Zs. f. Astr.*, 50: 110.
7. Gopasyuk, S. I., 1962, *Isv. Crim. Astrophys. Obs.*, 27: 110.
8. Wolbach, J. G., 1963, *Smithson. Contr. Astrophys.*, 8(2).
9. Ellison, M. A., McKenna, S. M. P., and Reid, J. H., 1961, *Dunsink Obs. Publ.*, 1(3).
10. Babcock, H. W., 1953, *Ap. J.*, 118: 387.
11. Stepanov, V. E., and Severny, A. B., 1962, *Izv. Crim. Astrophys. Obs.*, 28: 166.
12. Severny, A. B., 1958, *Izv. Crim. Astrophys. Obs.*, 20: 22.
13. Severny, A. B., 1960, *Izv. Crim. Astrophys. Obs.*, 22: 12.
14. Severny, A. B., 1962, *Astr. Zhurn.*, 39: 961.
15. Gopasyuk, S. I., Ogir, M. B., Severny, A. B., and Shaposhnikova, E. F., 1962. *Izv. Crim. Astrophys. Obs.*, 29: 15.
16. Öhman, Y., 1958, *I.A.U. Symp.*, No. 6, p. 166.
17. Howard, R., and Babcock, H. W., 1960, *Ap. J.*, 132: 218.
18. Bappu, M. K. V., and Punetha, L. M., 1962, *Observatory*, 82: 170
19. Howard R., and Severny, A. B., 1963, *Ap. J.*, 137: 1242.
20. Howard, R., 1963. *Ap. J.*, 138: 1312.
21. Gopasyuk, S. I., 1961 *Izv. Crim. Astrophys. Obs.*, 25: 114.
22. Blaha, M., Kopecky, M., and Svestka Z., 1960, *Nature*, 187: 224.

DISCUSSION

Dr. Jefferies: Is any change seen in the ionized calcium line configuration at the same time as the magnetic field configuration is observed to change?

Dr. Howard: For the flare on July 16, 1959, and for a few others for which there is coverage for the weaker fields, we do not have the calcium measurements ourselves. Dr. Bappu and Dr. Punetha, who observed the calcium measurements, found no changes before, during, or after several very large flares. This is evidence that the changes, if there are any in the smaller field, are too small to be noticeable.

Dr. Suemoto: Would it be possible to make a magnetograph to work for coronal fields, using a coronal emission line?

Dr. Howard: I don't know. I haven't done it. In principle, it probably is not impossible.

Dr. Noyes: I wonder whether the solar magneticians—Dr. Howard, Dr. Severny, or others—can sometime in the future visualize a different magnetic classification more quantitative than the Zurich system or the alpha-beta-gamma system, perhaps in terms of field strengths of field gradients, or whether there is not enough unanimity or enough observations yet.

My second question would be related to that. You had shown that many of the large flares, cosmic-ray-producing flares, had very large field gradients before the flare, which decreased after it. Have there been observed large field gradients without flares, or is there a unique relation between a high gradient and a large flare?

Dr. Howard: Certainly large gradients exist at times without large flares. That is, the spots can remain relatively unchanged for a period of some days or weeks without producing a large flare.

Whether there is a case of a very large gradient which did not produce a large flare, I don't know.

I think that it may not depend entirely on the gradient. It may depend on the complexity of the magnetic configuration more than the gradient, the fact that there is a neutral point and that there is some complexity in the field.

In answer to your first question, although we had not thought specifically about a simple classification scheme that would give us more information, we have looked at magnetic regions. For example, in the case that I have shown here, the sunspot group—the alpha group—is the very simplest kind of group; yet there was some magnetic complexity involved in the photospheric configuration. In fact there was a flare, which I described.

It may be, for example, that such a configuration is necessary for a flare in an alpha group.

What we are doing is to go back through many years of magnetograms and classify magnetic regions and look in some detail at what we can expect in the way of a correlation between flares and magnetic region classifications rather than the classification of the spot group itself.

Dr. Hess: Did I understand correctly? The observations in the Crimea on the July 1959 event showed a decrease in the field, while the Mt. Wilson observations did not. But these are not necessarily in disagreement because the Crimean measurements are for considerably higher fields than the Mt. Wilson ones?

Dr. Howard: Yes. The Crimean measurements showed a decrease in field strengths, and the Mt. Wilson magnetograph measurements did not show any change during the course of the flare. Of course, the measurements made at the Crimea and at Mt. Wilson were made at different times; and it is possible, for example, that there was a change in the field strengths before we started observing at Mt. Wilson.

Also this change, as I mentioned, was not noticed in the visual sunspot field measurements. There may be several reasons for this. One is that these measurements are very inaccurate. Even if that is not taken into account, the change in size of the spot group is sufficient to account, I think, for the change in the measured Crimean fields because of the angular resolution of the magnetograph.

N64-30264

13 ON THE BEHAVIOR OF MAGNETIC FIELDS ASSOCIATED WITH SOLAR FLARES

A. B. Severny
Crimean Astrophysical Observatory
P/O Nauchny, Crimea, U.S.S.R.

In 1958 we observed that the density of isogauss lines on the contour maps of longitudinal field decreased in the region where a flare appeared (Reference 1). This fact forced us to consider in more detail all available maps of longitudinal field $H_{\parallel}$ in cases where we had magnetographic records *before* and *after* a flare. In seven cases out of eight, the gradients of $H_{\parallel}$ being $0.1 \div 0.05$ gm/km before the flare are reduced to the lower values ($\approx 0.02 \div 0.01$ gm/km) after the event. The simplification of field was found to be the most characteristic phenomenon accompanying solar flares (Reference 2); and this process includes not only the diminution of field but also some changes of magnetic configuration—the shifts of magnetic "hills" of magnetic relief (Reference 3); see below. Some observers noted the temporary drop of field strength of nearby spots occurring during flares (References 4 and 5). The temporary diminution of field gradients associated with flares is also pointed out in Reference 6.

We can also expect the changes or disappearance of the Hα fibrile structure of the chromosphere during the flare if one assumes that this structure is closely connected with magnetic fields as shown in References 7 and 8. Such changes were actually observed in several big flares, according to Reference 9, and attributed to changes of magnetic field. However, this structure recovered after the end of the flare, showing that the magnetic field also can be recovered to pre-flare state.

The recent progress in recording transversal magnetic fields with the aid of the Crimean magnetograph (see References 10 and 11) permitted us to compare the observed pattern with that produced by corresponding magnetic configuration of dipoles—sunspots. By magnetic configuration we mean the *position* of the main magnetic poles (sunspots) and their *magnetic "charges"* m, $m = H_m S$, where H_m is maximal field strength and S is area, which can be identified with the area of sunspot umbra. This configuration can be constructed by computing the run of the lines of force with the aid of a electroric computer or, more simply, by using a laboratory model or analog—a set of solenoidal magnets arranged in a proper way with corresponding field strengths and covered by the glass plate with iron filing (see Reference 12). The possibility of using such a laboratory analog comes from the invariancy of the expression for the magnetic force of dipole interaction to the similarity transformations, provided that sunspots can be considered as rigid magnets placed in a nonmagnetic medium. In most of the cases it seems possible to construct such an artificial analog configuration which shows the *general*, and sometimes even detailed, agreement with the observed pattern (for examples of such a comparison, see Reference 11).

This circumstance permitted us to use the routine observations of magnetic fields made during IGY–IGC (compiled in Reference 13) to trace the possible changes of magnetic fields associated with many flares. Fifty-two configurations of magnetic fields of sunspot groups *before* and *after* flares of Importance ≥ 2, and especially those associated with cosmic ray flares, were examined in the Crimean Observatory by using all available data. In most of the cases the configuration consisted of three or four different and separate polarities. We found that all large cosmic ray flares are associated with quite a pronounced change

in the configuration of sunspots; namely, in most of the cases one of two or three separate polarities of the same sense is pushed out while the polarities of opposite sense are attracted a little after the flare, or the whole configuration is expanded.

The most typical changes observed, for instance, in cases of the great flares 12.XI.60 and 3.VII.57 are presented in Figure 13–1. We found that the gradient of the transversal field near neutral point $(\nabla H_{\perp})_0$ is the most sensitive indicator of the possible appearance of a flare irrespective of the question of where the flare actually appears—in neutral points (lines), or not. If the real magnetic field can be described approximately as dipole fields (and we have just considered this possibility), we should expect that the possible changes of the gradient $(\nabla H_{\perp})_0$ due to the change of *distance* between dipoles r_{ik} must be large compared with the changes due to the possible change of magnetic masses m_i (field strength of sunspots); the force and gradients are $\propto m_i/r^3_{ik}$. This explains the fact why the real changes of field are mainly connected with the changes in the *position* of sunspots or with the field *between* spots but not with the change of their own magnetic fields. Sometimes we cannot observe appreciable diminution of the H_m;* moreover, the slight increase of H_m can take place instead; but nevertheless the gradient decreases considerably because of increase of *distances* between spots. This is quite natural since one could hardly expect considerable destructions of magnetic fields inside sunspots themselves because of the extremely large time of diffusion.

*These changes of H_m are frequently within the limits of errors of usual determinations of magnetic fields.

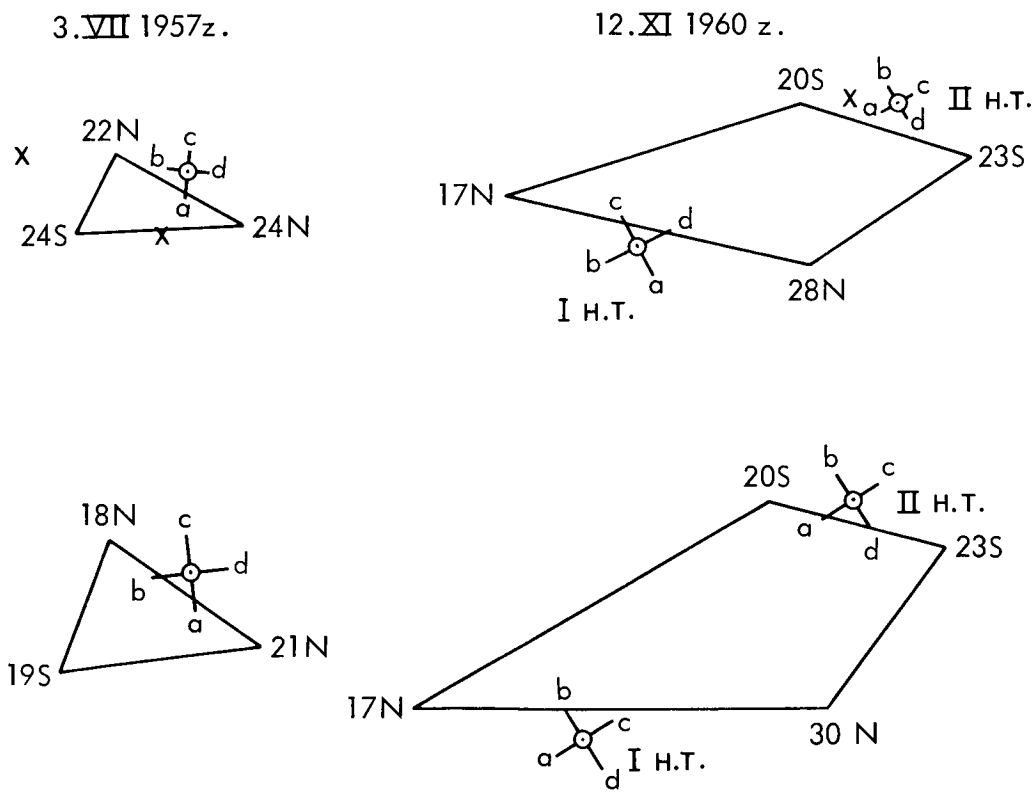

FIGURE 13–1. The typical configurations of sunspots before (top) and after (bottom) the great flares July 3, 1957 (left), and November 12, 1960 (right). The neutral points around which the field gradients were measured are denoted by crosses with dot.

Figure 13–2 is an illustration of how the gradients $(\nabla H_{\perp})_0$ are changing if we compare them before and after the flare in the case of great cosmic ray flares. (Heavy part of the straight line joining moment of the first nearest measurement before the flare with the second nearest to the end of the flare denotes the interval of the flare event; see Reference 12. In the great majority of the cases we have diminution of gradients $(\nabla H_{\perp})_0$, and this effect is greater with larger flare importance, as regards cosmic ray effects. Figure 13–3 shows the mean gradients $(\nabla H_{\perp})_0$ and the changes of these gradients as a function of the duration of flares (dots are gradients before, open circle the same after the flare, in brackets—the number of cases). The most pronounced of these changes are for great cosmic ray flares (13

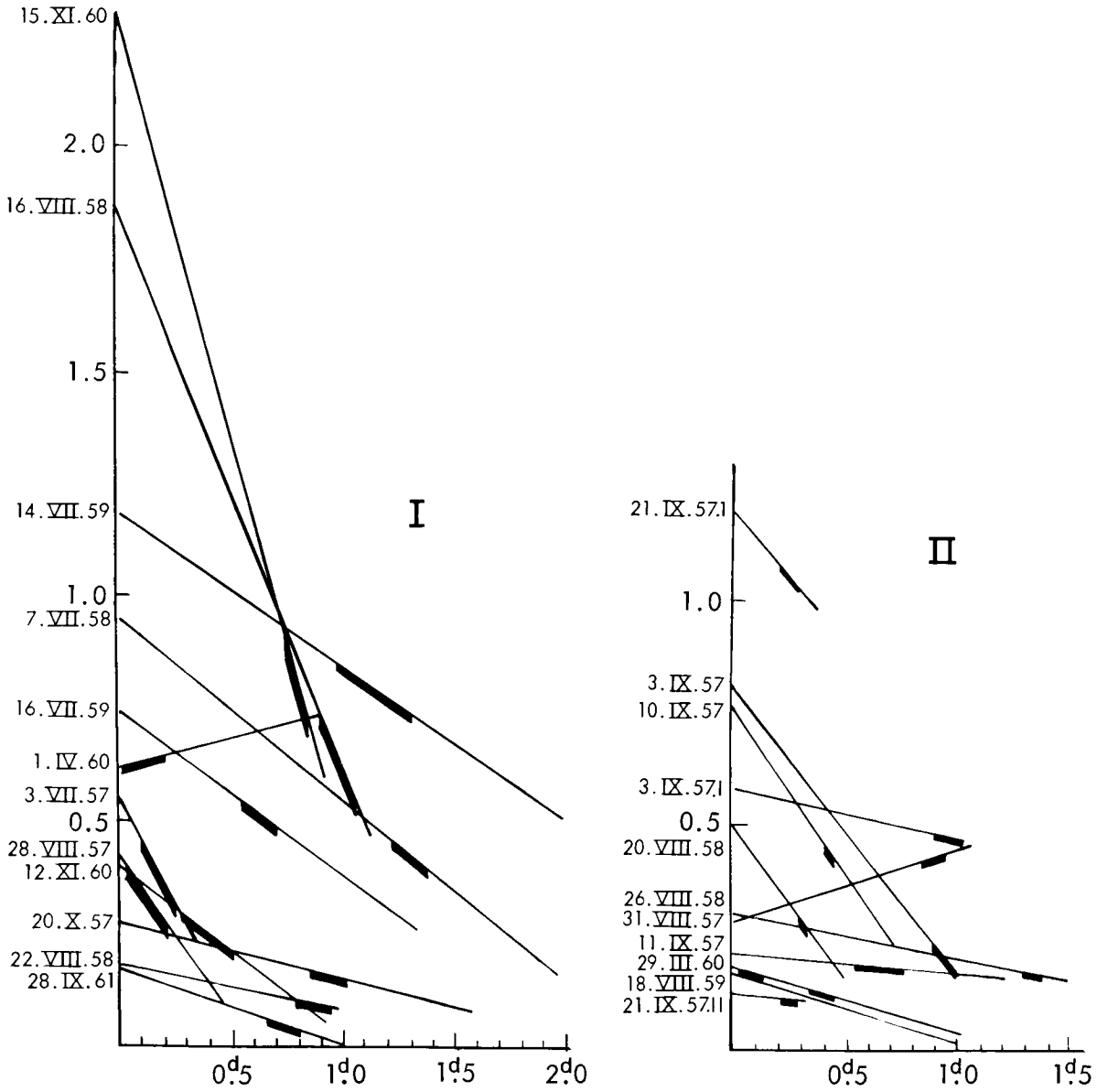

FIGURE 13–2. The gradients of different cosmic ray (left, group I) and PCA (right, group II) flares before (0^d0) and after the flare, in gauss/km.

cases), and the smallest but appreciable effect shows flares of Importance 2+ and 2 (15 cases). The polar cap absorption flares (11 cases) and those of Importance 3 but without geophysical effects (12 cases) are in between these two extremes.

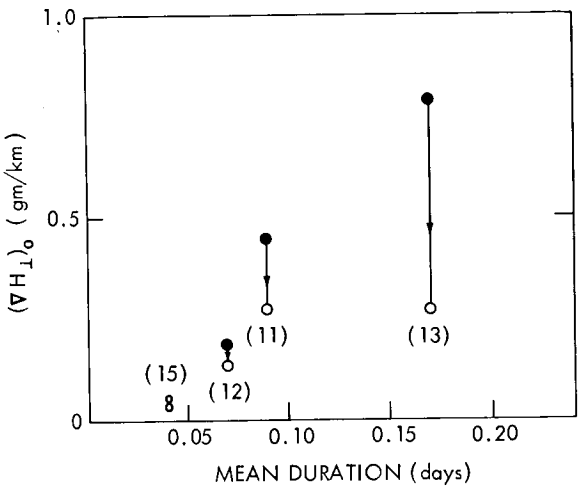

FIGURE 13–3. The mean gradients near neutral points before (solid dots) and after (open circles) the flare (see text).

It is also worth mentioning that the mean observed relative change of distances between dipoles—sunspots, $\delta R/R=+0.32$, corresponds to the change of magnetic interaction energy

$$\delta W=-\frac{3m_1m_2}{R^3}\frac{\delta R}{R}=0.3\times10^{32}\text{ ergs},$$

which practically coincides with the energy loss of big flares by cosmic rays (we assume

$$m_1=m_2=HSh\approx10^3(10^9)^2\times h=10^{31},$$

where S is area and h is the length of dipole $\approx R=10^{10}$cm). Thus we come again, as before in Reference 2, to the conclusion that high gradients of magnetic fields are favorable for the appearance of flares. Since these gradients are due mostly to the close approach of sunspots, we should expect the most frequent occurrence of large flares inside groups with separate spots in close contact; and this is a probable explanation of why large cosmic ray flares sometimes cover the umbra of sunspots. However, this effect of umbra coverage by flares is probably not so typical for large flares and can be observed also for small flares, as a recent statistical study showed (Reference 14). The close approach of large spots is found also to be in good correlation with the appearance of type IV radio bursts as it follows from recent considerations of French astrophysicists (Reference 15).

If a flare results from the close approach of at least three spots of different polarities, we should watch for the evolution of a configuration leading to such a situation. The attempt to trace such an evolution in 23 cases of groups without appreciable flares, for the whole period of the passage of groups on the visible disk, has been made recently in Reference 16. The results were that the configurations in these cases are simple, show but slow or minor changes of mutual distances, and show no close approach of sunspots of different polarities (except the simple bipolar groups), the mean $\delta R/R$ being $+0.054$.

These statistical results also have been confirmed in several cases by the study of magnetic contour (isogauss) maps obtained from strip-chart records made with the aid of the Crimean magnetograph. These maps of longitudinal fields $H_{\parallel}$ were examined before and after the following great flares: 3.07.1957; 22–23.08.58; 14–17.07.59; 18.08.59; and 1.04.60. The run of gradients of $H_{\parallel}$ and magnetic energies $H_{\parallel}^2/8\pi$ during the July 1959 events are considered in detail in Reference 17; the other cases are described in Reference 12.

The examination of the behavior of the transversal (as well as $H_{\parallel}$) field associated with flares was started in 1962 with the modified-for-this-purpose magnetograph, and on several occasions we found convincing evidence of very remarkable changes in these fields associated with flares (Reference 18). In Figure 13–4 we present an example of such changes for the case of flare Importance 2, which appeared June 22, $12^h\ 05^m$–$12^h\ 55^m$ Mosc. T. We have here the combined maps of isogauss $H_{\parallel}=$ const. and the arrows showing the directions and amplitudes of transversal vibration. At the bottom of these figures we have the approximate pattern of lines of force constructed by drawing continuous lines parallel to the direc-

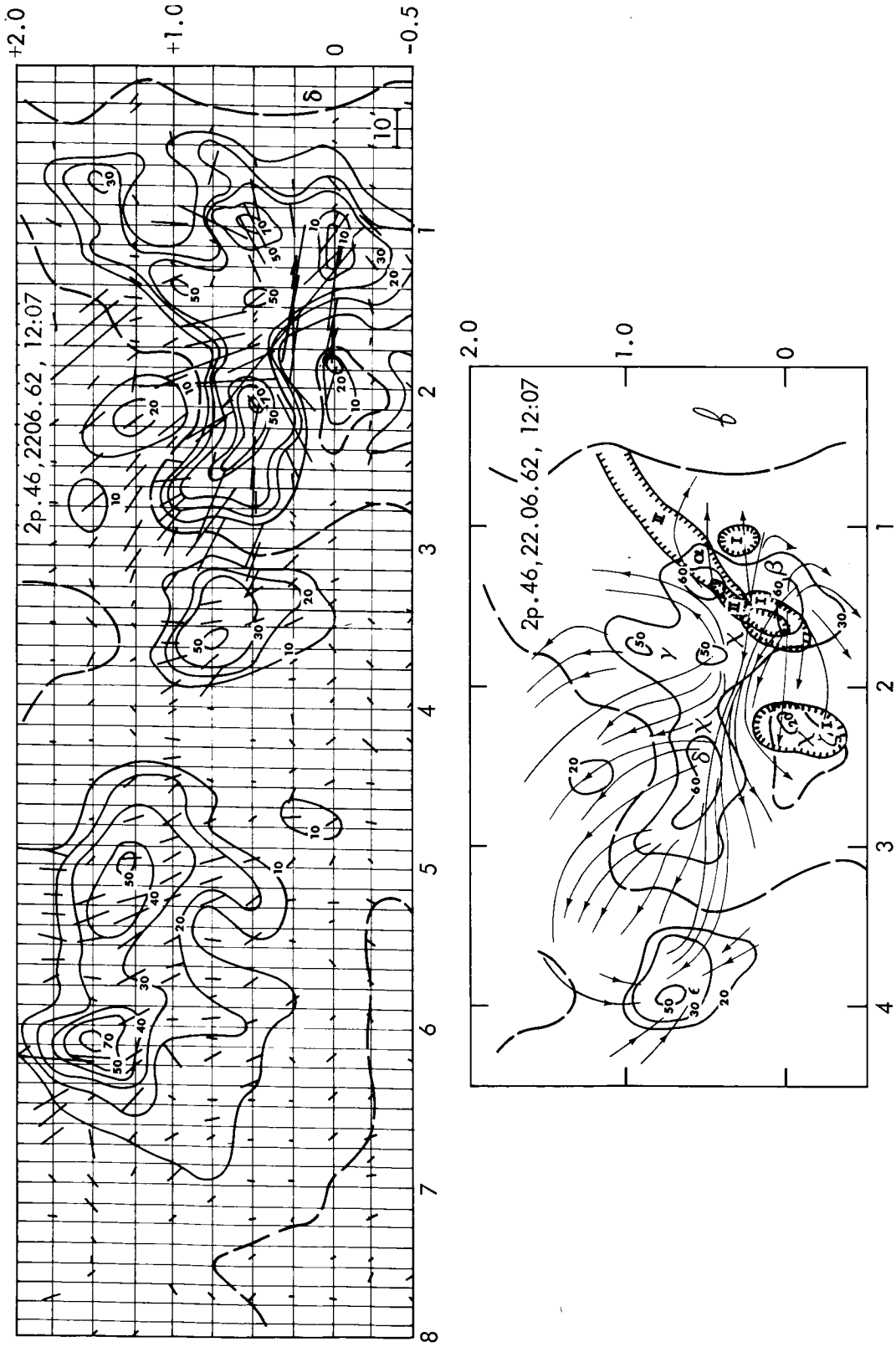

FIGURE 13–4(a). The combined isogauss contour map and the map of transversal field (top) obtained at the Crimean magnetograph June 22, 1962, at 12:07 Mosc.T. The length of the arrow is a measure of the strength of transversal field, one unit of longitudinal field = 5g. Flare of Importance 2 appeared at 12:10 Mosc.T. (areas with dashed boundary from inside). Dashed line is the line $H_{\parallel}=0$. At the bottom, the approximate picture of lines of force.

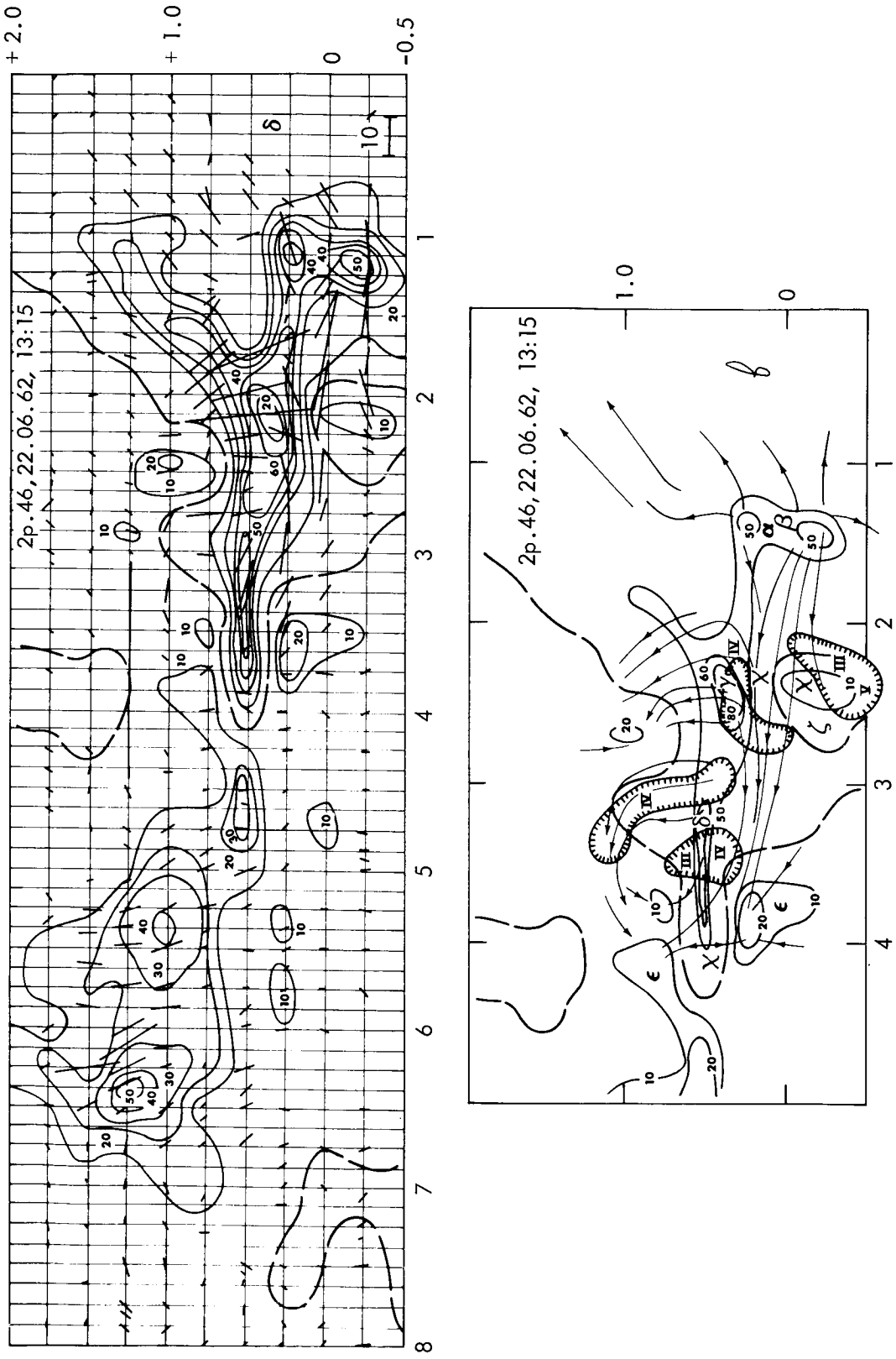

FIGURE 13–4(b). The same as Figure 13–4(a) but for the moment 13:15 Mosc.T. The comparision with 13–4(a) shows considerable changes in magnetic field during the flare.

tions of the first map. The first map relates to the configuration just at the start of the flare at 12:07 Mosc. T., and the second to the moment 14:00—about 1 hour after the end of the flare. We see how the polarities γ and δ are pushed out to the east as under the action of repulsive force between poles α, and γ and δ; and this process is connected with the formation of an elongated tongue which split the polarity ϵ into two pieces. The velocity of propagation of isogauss 30 (the front of this tongue) in west-east direction was ≥ 5 km/sec, and the full amount of kinetic energy connected with this deformation is more than 10^{29} ergs.

But not only the transversal dilatations or contractions of the areas occupied by one polarity are observed during flares. The upward motions on the large area and, in particular, inside sunspots were recorded in several cases (Reference 19)—for instance, in the case of the great flare of July 14, 1959, and in some others (Reference 20), showing that the rearrangement of magnetic configuration displays itself in specific motions of photospheric plasma.

REFERENCES

1. Severny, A., 1958, *Izv. Krim. Astrophys. Obs.*, 20: 22.
2. Severny, A., 1960, *Izv. Krim. Astrophys. Obs.*, 22: 12.
3. Gopasyuk, S., 1961, *Astr. Zhurn.*, 38: 209.
4. Evans, J., 1959, *Astr. J.*, 64 (N8): 330.
5. Chistyakov, V., 1960, *Solnechn. Dannye*, N9: 81, 1959.
6. Michard, R., Mouradain, Z., and Semel, M., 1961, *Ann. d'Aph.*, 24: 54.
7. Stepanov, V., 1958, *Izv. Krim. Astrophys. Obs.*, 20: 52.
8. Tsap, T., 1964, *Izv. Krim. Astrophys. Obs.*, 31: 200.
9. Ellison, M., McKenna, S., and Reid, J., 1960, 1961; *Observatory*, 80: 149, 1960; *Dunsink Obs. Publ.*, 1: 2, 1961.
10. Stepanov, V., and Severny, A., 1962, *Publ. Crim. Astrophys. Obs.*, 28: 166.
11. Severny, A., 1963, "Magnetic Fields of Sunspot Groups," Sympos. 22, Rottach (in press).
12. Gopasyuk, S., Ogir, M., Severny, A., and Shaposhnikova, E., 1963, *Izv. Krim. Astrophys. Obs.*, 29: 15.
13. Petrova, N., Shaposhnikova, E., and Stepanov, V., 1962, "The Catalogue of Field Strengths and Polarities of Sunspots for the Period IGY," Ann. IGY, vol. XXIII Pergamon Press.
14. Wolbach, J., 1963, *Smithson. Contr. to Astroph.*, 8: N2.
15. Michard, R., 1963, Commun. at Sympos. 22, Rottach (in press).
16. Ogir, M., and Shaposhnikova, E., 1963, *Izv. Krim. Astrophys Obs.*, 31 (in press).
17. Howard, R., and Severny, A., 1963, *Ap. J.*, 137: 1242.
18. Severny, A., 1964, *Izv. Krim. Astrophys. Obs.*, 31: 159.
19. Gopasyuk, S., Ogir, M., and Tsap, T., 1963, *Solnechn. Dannye*, N4: 77.
20. Vasilyeva, G., 1961, *Solnechn. Dannye*, N12: 64.

N64-30265

14 ASSOCIATION OF FLARES WITH STATIONARY POINTS OF ZERO MAGNETIC FIELD

JAMES WEDDELL
Space and Information Systems Division, North American Aviation, Inc.
Downey, Calif.

30265

ABST

The positions at which solar flares originate have been correlated with measurements of the photospheric magnetic field made on the day of each flare and, at times, as much as 35 days before each flare. The 51 flares considered occurred in 1959 and 1960, had corrected areas at least $100\mu_{\odot}$ (millionths of the solar hemisphere), and were associated with calcium plage regions which were making their first disk passages. The flares were measured ~~at Sacra-~~ mento Peak Observatory. Author

It has been shown previously (Reference 1) that 72 percent of flares with areas greater than 100 $\mu_{\odot}$ were associated with plages which had made at least one previous disk passage. Observation of the optical characteristics of plages was found to permit prediction, from 21 to 35 days in advance, of flares which occur on the next disk passage of each plage. Such predictions have the expectation 0.95 of being correct. One objective of the present work is prediction of flares which cannot be predicted on the basis of optical observation of plages.

The positions on the solar disk occupied by 51 points which later became sites of flares were calculated for dates, on or before each flare date, on which Mount Wilson Observatory magnetograms were produced; 140 different magnetograms were used. The calculations accounted for differential solar rotation and for the inclination of the solar equator to the ecliptic.

The magnetic field component $B_{\parallel}$, parallel to the line of sight, at each computed position was plotted versus the time before the first flare at that position. Only computed positions within 45 degrees of the central meridian were considered, so that $B_{\parallel}$ is in all cases a fair approximation of the radial field component. In 22 cases, $B_{\parallel}$ was zero on at least two consecutive observations, 3 days or more apart, and on the solar rotation previous to the flare.

In these 22 cases, $B_{\parallel}$ was large ($\gtrsim 10$ gauss) and positive on one side of a line through the zero-field point, and large and negative on the other side. In all but one case, $B_{\parallel} \lesssim 10$ gauss at all times during the rotation preceding the flare.

The results also confirm those of Severny (Reference 2) that large flares tend to occur between regions of strong and opposite magnetic polarity, at points where $B_{\parallel}$ is locally zero at the time of the flare. Severny's results concern the magnetic configuration at a flare position near the time of the flare; the present work is based on the magnetic configuration on the solar rotation preceding the flare. In 45 of the 51 cases, $B_{\parallel}$ was zero on the day of the flare at a point within 0.5 heliographic degree of the flare. This result shows that the stationarity of a zero-field point is an almost sufficient condition for a flare.

As a control on the analysis just described, 80 points were considered at which $B_{\parallel}=0$ on at least one observation and at which no flare with area greater than $100\mu_{\odot}$ occurred for at least 40 days (1.5 solar rotations) following such an observation. In 62 of these cases, $B_{\parallel}=0$ on two or more consecutive observations, 3 days or more apart. This result shows that the stationarity of a zero-field

728-629 O—64——8

point may prove to be a necessary condition for the occurrence of a flare.

The simultaneous magnetic field conditions listed below are followed, with probability 0.43, by at least one flare with an area greater than $100\mu_{\odot}$ on the next disk passage of the given magnetic region:

1. $|B_{\|}| \lesssim 4$ gauss for 3 days or longer
2. $|\partial B_{\|}/\partial t| \lesssim 1$ gauss/day
3. $|\nabla B_{\|}| \gtrsim 10$ gauss/heliographic degree

The gradient of $B_{\|}$ is understood to be the component normal to the line of sight of $\nabla (\boldsymbol{B} \cdot \boldsymbol{n})$ where $\boldsymbol{n}$ is a vector of unit length parallel to the line of sight. This result can be applied to flares not predictable from optical observations of plages. The combined optical and magnetic prediction methods have the expectation 0.79 of being correct: the expectation of a "false alarm" is 0.04. Some physical implications of the stationarity of zero-field points beneath flare position have been discussed elsewhere (Reference 3).

ACKNOWLEDGMENTS

The magnetograms used in this work were provided by Dr. R. F. Howard of Mount Wilson Observatory, whose cooperation is gratefully acknowledged. The assistance of Miss P. J. Leavell with the data analysis is appreciated.

REFERENCES

1. Weddell, J. B., 1963, *Bull. Am. Phys. Soc.*, Series II, 8: 480.
2. Severny, A. B., 1957, *Astron. Zhurn.*, 34(5); *Soviet Astron.*, 1: 668.
3. Weddell, J. B., 1962, *Proceedings of the Symposium on Protection Against Radiation Hazards in Space*, TID 7652, pp. 88–95.

DISCUSSION

Dr. Evans: I think this suggestion that we might be able to predict the occurrence of flares with a probability of 79 percent would be very exciting, but I must say I am doubtful about some of these observations. I don't think that the IBM card Sacramento Peak observations you used are good enough to pinpoint a region where the field is less than 10 gauss when you have a gradient greater than 10 gauss per degree on the sun. I wonder how you located these positions so accurately after a full rotation.

Dr. Weddell: First, we will assume that the position at which the flare occurred, as reported from Sacramento Peak, is an exact position. Granted, there is an experimental error. The motion of the position corresponding to the flare during the previous solar rotation is a purely kinematic one.

In other words, the purely kinematic motion of this position during 0.5 to 1.5 solar rotation periods before the flare is an entirely geometric calculation. It is based entirely on the number of degrees which the sun rotates at a given heliographic latitude between the time that the magnetic field is measured and the time at which the flare occurs.

Then these transformed points are compared with the magnetogram patterns.

Dr. Evans: The Sacramento Peak flare patrol positional data, I think, are typical in accuracy and are probably no better than 2 or 3 degrees in position for the small events.

Dr. Weddell: I might remark again that this analysis was confined to flares which had corrected areas of 100 millionths of a hemisphere. A similar analysis was repeated with a sample confined to flares with areas of 200 millionths of a hemisphere and larger, with similar results. However, the statistics were not very good, and the fact that the results did confirm the ones for 100 millionths is made less valid by the smallness of the sample of flares of this size, which were associated with the magnetograms that were available.

Dr. Wilcox: What was the size of the area that you used when you said less than 4 gauss? What size area did that refer to?

Dr. Weddell: The resolution of this area is the resolution of the magnetogram. Dr. Howard can describe this. I believe it is about ½ to 1 heliographic degree. The resolution of the magnetogram is about 23 seconds of arc.

Dr. Wilcox: So you just counted it as a point?

Dr. Weddell: I counted the center of each of the rectangles of area as a point. The resolution of the gradient of the magnetic field, of course, is limited by the distance on the disk from the center of one parallelogram to the next, which is about 1 degree.

Dr. Goldberg: Could you say what part of the sunspot cycle your observations covered?

Dr. Weddell: 1959 to 1960, just past the last maximum.

Dr. J. Warwick: I have a point I would like you to clarify. When you speak of a zero field point, you really mean zero longitudinal field component, do you not?

Dr. Weddell: That is right. Maybe I didn't make this clear enough. Throughout all of this I am talking only about the component of the field which is parallel to the direction of propagation of light, or anti-parallel to it.

Dr. J. Warwick: So the substitution of magnetic Reynolds numbers should be put into the context that the field could be of any strength, say 3000 gauss, at these points?

Dr. Weddell: That is true if we wish to be completely arbitrary about the unknown horizontal component. It would be surprising if it were several orders of magnitude larger than the parallel component.

Dr. Prince: I have struggled very hard with your paper, and I do not understand exactly what you have done. Do I understand correctly that, after having used our calcium plage data, you have identified the flares that occurred in regions in their first rotation; you then took the positions of these flares and counted backward an appropriate number of days or degrees and arrived at corresponding positions on the sun for the preceding rotations; you then looked at magnetograms and found in these corresponding positions no magnetic fields? Is that correct?

Dr. Weddell: That is correct, or we found whatever the magnetic field was at these previous points in time.

Dr. Prince: In other words, the plages that we call "new" corresponded to portions of the solar disk for which you find that in the preceding rotation the magnetic fields were not very great. In this respect, your magnetographic information and our plage observations are in agreement. You found no great magnetic field where we found no plage.

Dr. Weddell: Just off the zero field positions with which the zero field was associated, the field was not necessarily small. There may have been a bipolar or multipolar magnetically active region which had made its appearance at least a few days earlier than the enhancement of the calcium line which is manifested as a plage.

Certainly a plage would appear soon after this, because a plage has always developed by the time the first flares occur.

Dr. Prince: I believe that the plage normally is observed before the spot and that magnetic fields appear along with the plages and the spots. If, in your studies, you have found strong magnetic fields in the prior-rotation-positions of flares in plages that we have called "new," then I am afraid that we may have made mistakes in our identifications or descriptions of the calcium plages. We will be glad to check our data.

Dr. Weddell: No, we cannot say that the fields were large at these points. They may have been 10 or 20 gauss. In these magnetograms, using the high resolution instrument which has relatively low saturation (about 50 or 60 gauss), the strongest field in the region might have been 10, 20, 40, not over 60 gauss at the outside—much weaker than the fields associated even with very small sunspot umbra.

Question: To continue that line of questions, after going back 1 rotation, we go back another rotation, so you cover almost 2 rotations?

Dr. Weddell: One and one-half at the maximum.

Question: Doesn't anything happen to the correlation from a theoretical point of view if you have a spot group and the spots have proper motions?

Dr. Weddell: The spots, which are the regions of the most intense magnetic fields, probably do have proper motions on the disks. One of the points here is that, if a point on the zero field line which passes between the two bipolar spots has no proper motion, this is a condition favorable to the occurrence of a flare at such a point in the future.

Dr. Zirin: Flares seem to me to cover quite large areas. They extend from the umbra of the spot quite some distance out. I really don't understand how you decide what the position of the flare really is. I have the impression that the field gradients near spots are quite large and the field may vary quite a bit over the area where the flare takes place.

Dr. Weddell: We use the positions of the flares reported from Sacramento Peak, which is presumably about the centroid of area of the flare. There is certainly a question of the comparison of the zero field line to different points of the flare. By using a homogeneous data sample, that is, data obtained at a single observatory, any discrepancy would cancel out. Hopefully, this condition would refer to the point of origin of the flare rather than the condition at some point to which the flare spreads as it develops.

NIH-302666

15 ON THE OBSERVABLE EFFECTS OF MAGNETIC ENERGY STORAGE AND RELEASE CONNECTED WITH SOLAR FLARES*

HERMANN U. SCHMIDT†
Sacramento Peak Observatory, AFCRL
Sunspot, N. Mex.

ABST

302666

A classification of the possible magnetic changes in the solar atmosphere in terms of their observable effects is proposed.

Ten magnetograms taken before and after the great flare of July 16, 1959, are used to compute the changes of the total flux and of the total magnetic energy in a current-free approximation. Large and rapid changes are found. Two independent characteristic lengths of the field in this region are also derived. These do not exhibit comparable changes, but only a moderate expansion. This would suggest the existence of major changes in the total flux without corresponding changes in the geometrical distribution of this flux. Since the conductivity does not allow any appreciable dissipation or diffusion of flux, this interpretation implies an improbable coupling between the velocity field and the magnetic field. This discrepancy stresses the need for further observations.

The energy output of a solar flare may well be balanced by a sudden release of magnetic energy in the solar atmosphere. This magnetic energy in turn originates in the convective motions of the solar plasma below the photosphere. Most of the possible changes in the magnetic field will imply some changes in the photospheric magnetic field, which may be observed. So the information contained in observations of the inverse Zeeman effect in Fraunhofer lines may give some insight into the energy balance of a flare. The purpose of this paper is a discussion of some aspects of this relation.

CLASSIFICATION OF MAGNETIC CHANGES

Since the solar plasma is a good conductor and conserves the magnetic flux very well (Reference 1), all changes in the magnetic field are either coupled with material motions or they imply dissipation and diffusion, which are relatively slow unless they occur in thin current-carrying layers. In the active parts of the solar atmosphere, the magnetic stresses are generally strong enough to enforce an approximately force-free configuration of the field (Reference 2). This implies that the field with its conserved flux may not store appreciable energies by local compression but may do so by a twisting of the field lines coupled with rotatory motions in the plasma. The possible changes of the magnetic energy in the solar atmosphere may be described in terms of the following types of changes in the underlying photosphere:‡

(1) Changes of the total flux crossing the photosphere due to diffusion, dissipation, or vertical motions in that layer:

$$\frac{d}{dt}\int |B_n|\,da \neq 0.$$

*This research was performed under Contract AF 19(604)-6664 with the Air Force Cambridge Research Laboratories.

†Member of High Altitude Observatory Solar Project at Sacramento Peak, on leave from Max Planck Institut für Physik und Astrophysik, Munich, Germany.

‡Throughout this paper the term "photosphere" labels the level to which the magnetographic measurements refer. **B**, **j**, and **v** are the vectors of the magnetic field, the electric current density, and material velocity, respectively; and the subscripts n and h mark the normal and horizontal components in and with respect to the photosphere; da is the area differential in that layer.

(2) Changes in the geometrical distribution of the conserved flux within the photosphere, occurring simultaneously with horizontal motions in the photosphere:

$$\frac{d}{dt} B_n \neq 0, \quad \frac{d}{dt} \int |B_n| da = 0.$$

(3) Changes in the electrical currents crossing the photosphere, that is, changes in the curl of the horizontal photospheric field, if they are due to the rotatory horizontal motions in the photosphere. Such motions do not necessarily cause (2) at the same time, but they do produce a change of twist in the magnetic field above:

$$\frac{d}{dt} \mathbf{j}_n \sim \frac{d}{dt} \operatorname{curl} \mathbf{B}_h \neq 0, \quad \operatorname{curl} \mathbf{v}_h \neq 0.$$

(4) Changes in the electrical currents crossing the photosphere, if they are due to dissipation and subsequent or independent rotatory motions in the atmosphere. Such processes generally will tend to diminish the currents and the twist of the field, and they will release more energy than they actually dissipate:

$$\frac{d}{dt} \operatorname{curl} \mathbf{B}_h \neq 0, \quad \operatorname{curl} \mathbf{v}_h = 0.$$

(5) Other changes in the horizontal field in the photosphere which are due to dissipation and subsequent or independent motions in the atmosphere. Such processes must not necessarily cause (4) at the same time. If they do not, energy will be released mainly by dissipation:

$$\frac{d}{dt} \mathbf{B}_h \neq 0, \quad \frac{d}{dt} \operatorname{curl} \mathbf{B}_h = 0, \quad \frac{d}{dt} B_n = 0.$$

(6) Changes in the atmosphere, which do not noticeably affect the photospheric level. They will be due to the same processes as the preceding two categories:

$$\frac{d}{dt} B_n = \frac{d}{dt} \mathbf{B}_h = 0.$$

The first three types describe energy changes in the atmosphere involving an energy flow through the underlying photospheric boundary. By these processes the convective motions below the photosphere are capable of storing magnetic energy in the overlying atmosphere. Normally these processes are comparatively slow, since they are controlled by the observable photospheric motions or by the even larger time scales of magnetic diffusion and dissipation. But occasionally they might be produced more rapidly by major changes of the types (4) and (5).

The last three types describe changes in the atmosphere due to conversion of magnetic energy into thermal energy and due to exchange with ordered kinetic energy. By such changes, magnetic energy release may contribute to the energy balance of flares or of other transient or stationary phenomena, such as solar corpuscular emission. Many mechanisms which are capable of producing such changes, especially those describing a locally enlarged dissipation, have been discussed in the literature (see, e.g., Reference 3). Types (1) and (2) affect the magnetic flux in the photosphere, so that near the center of the disk they may be investigated by means of a magnetograph measuring the line-of-sight or longitudinal component of the photospheric field. Types (3), (4), and (5) involve correlated changes in the two horizontal components of the photospheric field. Therefore their investigation needs more refined techniques, and not too many observations have been made in this field so far. Types (3) and (4) can be separated only if information about the horizontal motions in the photosphere is available. But, in general, only type (3) will be accompanied by type (2).

EVALUATION OF MAGNETOGRAMS BY MEANS OF POTENTIAL THEORY

The most comprehensive data on photospheric magnetic fields in active regions are the magnetograms of the longitudinal component obtained at the Crimean and Mt. Wilson Observatories.

These observations contain almost exclusively information about the distribution of magnetic flux crossing the solar surface, but they do not give useful information about the horizontal components of the field. Therefore, we expect them to give direct evidence only of the types

(1) and (2) of magnetic energy changes. Since the flux through a surface (of single connection) contains just the correct information needed to determine a potential field, it is expedient to discuss magnetographic observations in terms of potential theory. The solar atmosphere is certainly not free of currents, but the magnetogram does not contain any information bearing on the current distribution. The flux of current crossing the photosphere is observable in the curl of the horizontal field only.

A magnetogram furnishes the distribution of magnetic flux over a finite region of the solar photosphere if this region lies near the center of the disk. It can cover the complete area of an active region, and in this case we may assume that all the flux which is of importance in the overlying atmosphere originates in the region covered by the magnetogram. If we neglect the curvature of the photosphere, we can consider the potential field above this region for our purposes as originating entirely from artificial surface sources in the photosphere. To show this and to calculate the proper surface charges, we may use the mirror principle, assuming arbitrarily a potential field below the photosphere, which is symmetrical to the wanted field above the photosphere. The local density of surface charge in the photosphere must then be consistent with the divergence of the combined field **B** in this plane interface. This surface divergence equals twice the density of flux, that is, the normal component B_n leaving the photosphere on either side. Using gaussian units throughout, we have

$$4\pi\sigma = \mathrm{Div}\,\mathbf{B} = \left[\mathbf{B}\cdot\mathbf{n}\right] = 2B_n. \qquad (1)$$

The potential field above the photosphere may now be calculated from a potential $\psi(\mathbf{r})$ which originates from these sources in the photosphere:

$$\psi(\mathbf{r}) = \int \frac{\sigma'}{|\mathbf{r}-\mathbf{r}'|}\,\mathrm{d}a' = \frac{1}{2\pi}\int \frac{B'_n}{|\mathbf{r}-\mathbf{r}'|}\,\mathrm{d}a' \qquad (2)$$

where **r** is the location vector and the prime refers to the location where the integrand is taken. Since the field

$$\mathbf{B} = -\nabla\psi \qquad (3)$$

fulfills the boundary condition at the upper edge of the photosphere, it furnishes the solution for the atmosphere above. The proof of existence of the integrals in Equation 2 and in the following Equation 4 may be found in Stratton (Reference 4).

Equations 2 and 3 can be used for construction of current-free approximations to field configurations in the solar atmosphere, using flux measurements in the photosphere. Thereby no meaningful information from the observations will be lost, and no implicit assumptions about spurious current distributions are made.

We may now determine the total energy content U of the atmospheric field. In order to do so, we do not need to integrate the energy density $B^2/8\pi$ of the evaluated field **B** over all space above the photosphere. Instead, we may conveniently calculate the energy content of the total field **B**, including the spurious subphotospheric part by integration of the potential energy which is needed to bring into place all the surface charge under the influence of its own integrated potential. This would be twice the energy U, so that we get

$$2U = \frac{1}{2}\int \sigma\psi\,\mathrm{d}a = \frac{1}{8\pi^2}\int B_n\left(\int \frac{B'_n}{|\mathbf{r}-\mathbf{r}'|}\,\mathrm{d}a'\right)\mathrm{d}a. \qquad (4)$$

Therefore a double integration over the observable longitudinal field immediately yields the total energy content of that potential field in the atmosphere, which is consistent with the observations.

MAGNETIC CHANGES CONNECTED WITH THE SOLAR FLARE OF JULY 16, 1959

We shall now apply these methods to a set of 10 magnetograms covering a very active region from July 14 through 18, 1959. During this interval this region produced three major flares. The 3+ flare of July 16 was one of the largest of the last solar maximum. The magnetograms

were taken at the Crimean Observatory, and they were published by Gopasyuk (Reference 5), Howard and Severny (Reference 6), and Gopasyuk, Ogir, Severny, and Shaposhnikova (Reference 7). Mt. Wilson magnetograms were also taken during the flare of July 16 (Reference 8). Other data about this flare are given by Ellison, McKenna, and Reid (Reference 9). Howard and Severny (Reference 6) estimate from the evaluation of the Crimean magnetograms that during a 15 hour period including the great flare the total magnetic energy may have dropped to 1/10 of its original value. They state that apparently "sunspot groups are not always quiet features where magnetic fields dissipate slowly from diffusion of the field." Therefore these data seem to be very useful for our purpose.

In Table 15–1 we give a list of the evaluated magnetograms with starting time, calibration units, and the linear foreshortening of the region on the disk. The recording time for each magnetogram is about 45 minutes as given by Howard and Severny (Reference 6). All the magnetograms present the distribution of the longitudinal component in isogauss lines. These data were digitized in the following manner. First, the magnetograms were covered with a rectangular grid having a mesh width of 12.5″ near the center of the disk, but foreshortened by cos θ in the direction perpendicular to the limb. This procedure corrects not only for the foreshortened area but also for the foreshortening of the distances, which are important in the evaluation of integral Equation 4. Then the total flux or average B_n in each rectangle was estimated. Of course, no correction can be made for the deviations between longitudinal and normal components, which may be large near the limb. Care was taken against systematic errors by independent cross-checks. These data were then processed on an IBM 1620 to evaluate the following integrals:

$$\phi=\int |B_n| \mathrm{d}a+\left|\int B_n \mathrm{d}a\right|,$$

$$\Delta\phi=\left|\int B_n \mathrm{d}a\right|,$$

$$W=\frac{1}{8\pi}\int B_n^2 \mathrm{d}a,$$

$$U=\frac{1}{16\pi^2}\int B_n\left(\int \frac{B_n'}{|\mathbf{r}-\mathbf{r}'|}\mathrm{d}_a'\right)\mathrm{d}a.$$

TABLE 15-1

List of Evaluated Magnetograms

No.	Date, July 1959	Starting Time* (UT)	Source*	Calibration Unit* (gauss)	Cos θ†	Remarks
1	14	*G* 0654 (*H* 710)	*G* 5 a, (*H* 1)	13. 6	0. 975	---------
2	14	0803	*G* 5 b, (*H* 2)	16. 4	0. 975	---------
3	14	0856	*G* 5 c, *H* 3	13. 4	0. 975	---------
4	14	*G* 1355 (*H* 1410)	*G* 5 d, (*H* 4)	*G* 37. 6, (*H* 18. 8)	0. 980	(‡)
5	15	1310	*G* 6, *H* 5	*G* 29. 2, *H* 24. 2	0. 953	(‡,**)
6	16	1135	*G* 7 a, *H* 6	16. 5	0. 898	---------
7	16	1500	*G* 7 b, *H* 7	26. 3	0. 893	---------
8	17	0600	*G* 8, (*H* 8)	8. 7	0. 800	(**)
9	17	0800	*H* 9	9. 5	0. 800	---------
10	18	0847	*H* 10	7. 1	0. 660	---------

*G refers to Gopasyuk, Ogir, Severny, and Shaposhnikova (Reference 7, Table 12). H refers to Howard and Severny (Reference 6, Table 1). If the H numbers appear in parenthesis, these magnetograms are not reproduced in the paper of Howard and Severny for reason of similarity with adjacent data.

† Cos θ is the linear foreshortening of the active region on the solar disk.

‡In our Figure 15-1 the calibration units H are used in order to allow comparison with the results of Reference 6. When the calibration units G are used, all the corresponding ordinates are raised by a factor of 4 for magnetogram no. 4 and by a factor of 1.46 for magnetogram no. 5. There will be no change in our Figure 15-2.

**We assume that in Reference 7 the captions of Figures 21 and 23 showing magnetograms 5 and 8 have been interchanged by misprint.

The quantity ϕ is the total flux counted twice, that is, leaving and reentering the photosphere. This formula corrects for that part of the flux which may not be covered by the magnetogram, assuming that this missing flux has only one sign. Then $\Delta\phi$ is just this missing flux. Howard and Severny (Reference 6) derived for their energy estimates the integrated energy density of the longitudinal field in the photosphere—that is, the quantity labeled W here—and multiplied this by 10^4 km as an assumed average for the extension of the field in the vertical direction. We have calculated the quantity W from our estimated flux data to

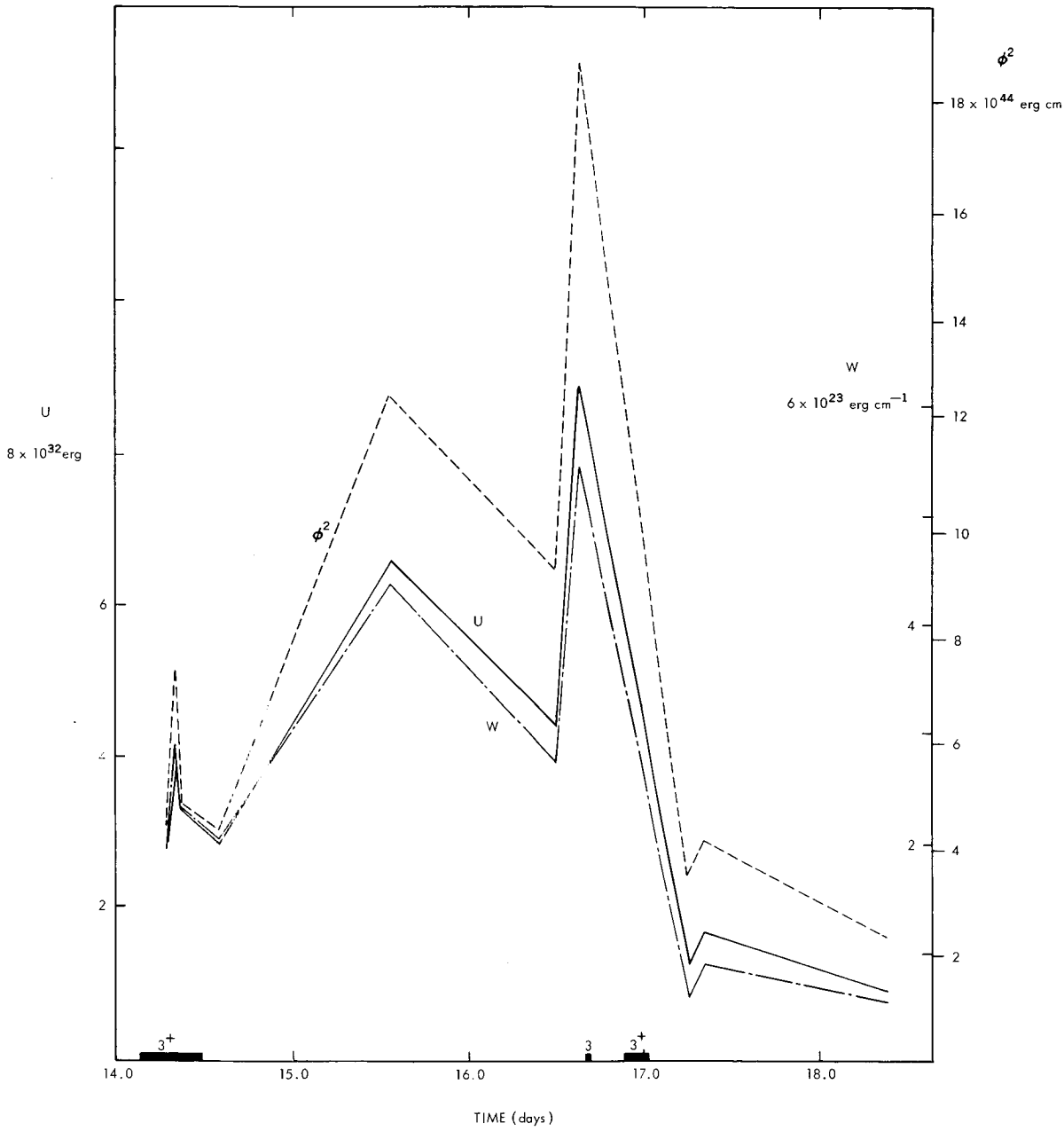

FIGURE 15–1. The total energy U, the surface energy W, and the total flux ϕ (squared) as functions of time.

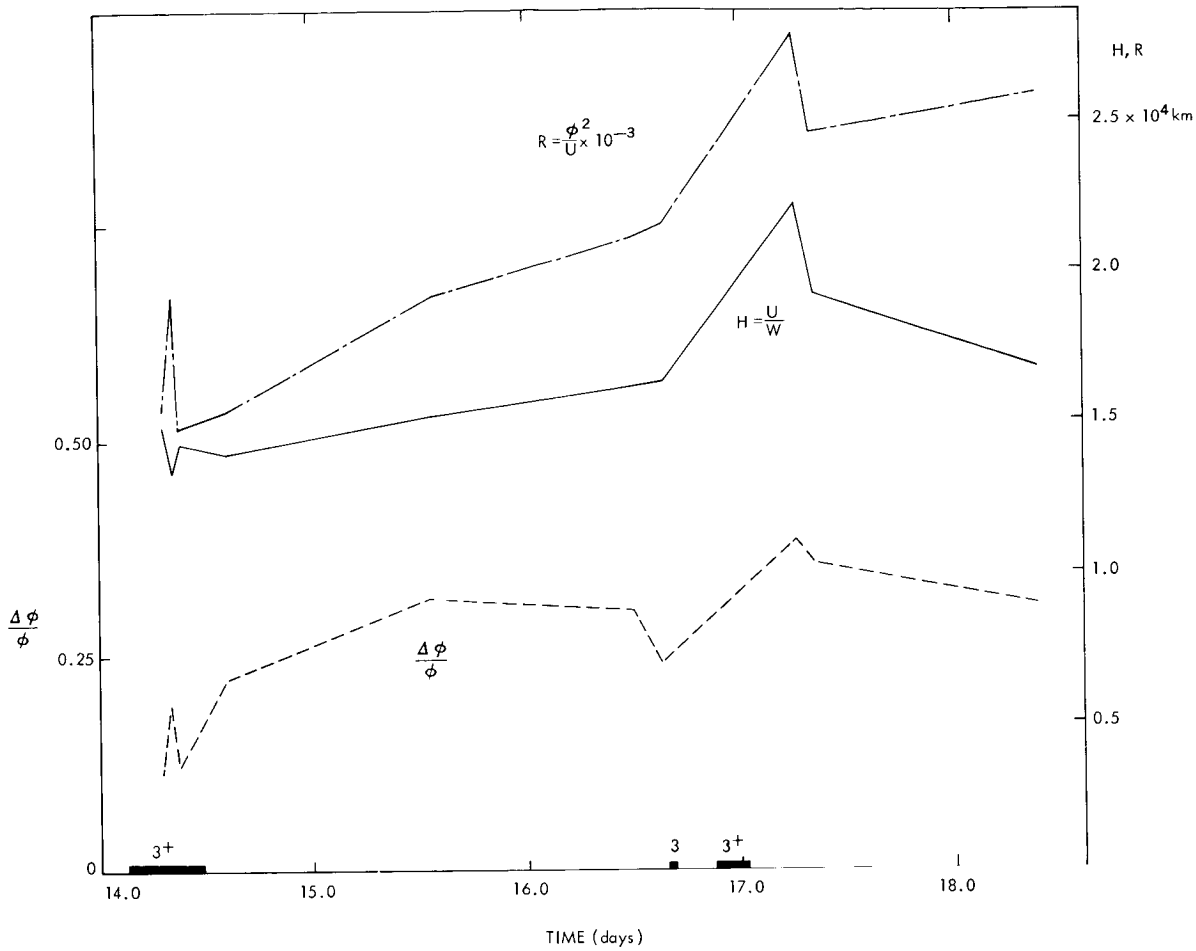

FIGURE 15–2. The two characteristic lengths R and H and the relative omission of flux $\Delta\phi/\phi$ as functions of time.

check for consistency with their results. Finally, U is the actual energy for the potential field.

These integrations took about 10 hours of actual running time on the computer. The results are presented in Figures 15–1 and 15–2 as functions of time. The values of the surface energy W in Figure 15–1 fit very accurately the corresponding values of Howard and Severny (Reference 6, Figure 7) if a general factor of 0.7 is applied. This factor probably characterizes the arbitrariness in estimating flux data from a set of isolines.

The relative values of missing flux in Figure 15–2 range from 11 to 38 percent. A comparison of successive pairs of magnetograms indicates that at the northern and western edges varying amounts of flux having exclusively the polarity of spots A and B should fall beyond the boundaries of the magnetograms. Rough estimates of this flux are proportional to $\Delta\phi$, though somewhat smaller. This justifies roughly our assumption that $\phi = \int |B_n| da + |\int B_n da|$ should represent a measure of the total flux of the active region. The missing flux should not distort the values of the energies U and W too much, because both quantities integrate essentially over the square of the local field strengths which are relatively weak in the occasionally excluded outer parts of the active region.

The most astonishing result is that both the total energy U and the squared flux ϕ^2 almost resemble the surface energy W as functions of

time. They all show the rapid changes and especially the drop in W by a full order of magnitude as found by Howard and Severny (Reference 6). Other rapid changes in W during a flare were observed by Evans (Reference 10).

It should be emphasized that the actual values for the three quantities U, ϕ^2, and W depend on the square of the calibration units given in Table 15–1. If we had used the calibration units given by Gopasyuk et al. (Reference 7) instead of those given by Howard and Severny (Reference 6), then the three curves in Figure 15–1 would have been changed in shape, since for magnetogram no. 4 (July 14.6) all three values would have been enlarged by a factor of 4 and for magnetogram no. 5 (July 15.55), by a factor of 1.46. However, the three curves still would resemble each other very closely, since the ratios between these quantities do not depend on the calibration.

These ratios represent two independent lengths, which characterize the total field configuration: $H=U/W$ is an average of the extension of the field in the vertical direction (multiplied by an average B^2/B_n^2), as was implied earlier; and $R=\phi^2/U$ may be called a weighted average of the denominator in the innermost integrand of U, that is, some measure of the concentration of the flux in the photospheric level. If the flux is conserved, R is inversely proportional to the total energy. The two lengths are given in Figure 15–2 as functions of time.

Both H and R show a general but slow expansion with a time scale of days plus some faster and smaller changes, but nothing comparable with the large rapid changes of the energies U and W and of the total flux ϕ shown in Figure 15–1. The faster and smaller changes in both lengths on July 14 and 17 coincide with changes in the missing flux, so that their actual shape is somewhat doubtful. Near the great flare an expansion of 30 percent may have occurred, corresponding to an energy decrease of 23 percent. The expansion in the overall flux distribution of the active region as derived from the magnetograms must be separated from the aging or the contraction of the sunspots proper as observed for this and other flares (Reference 11). The latter may not be shown properly by the magnetograms (see, e.g., Reference 12). Both phenomena together might well be consistent with overall flux conservation. They cannot account for a change in energy by a full order of magnitude or in flux by a factor of 3.

These results, then, imply that the large rapid changes apparent in Figure 15–1 would have to be attributed almost exclusively to changes of type (1) described earlier as a change of the total flux through the photosphere without changes in its relative distribution. A redistribution of the flux in the photosphere —that is, changes of type (2)—will of course change the characteristic lengths R and H arbitrarily. Minor changes of this kind obviously are present, but they are not comparable with those of type (1).

DISCUSSION

We have found that the observed large changes in the solar magnetic field accompanying the great flare of July 16, 1959, were changes in the total flux crossing the underlying photosphere rather than changes in the geometrical distribution of that flux. Since the dissipation as well as the (ambipolar) diffusion of photospheric flux with a characteristic cross section in the range of $(10^4 \text{ km})^2$ needs more than 10^9 sec (Reference 1 and 3), the only possibility to have such a change would be to assume that the flux was transported through the photosphere by a peculiar velocity field in the local solar plasma. A photospheric velocity field that transports magnetic field lines so that it changes the flux through the photosphere but does not change the geometry of the flux distribution in this layer would have to have a divergence in its two components perpendicular to the field, which must be everywhere the same at a time. The transverse velocity should vanish at the outer boundary, and it should have a consistent vertical component wherever the flux changes sign. This homogeneous divergence in the transverse velocity only would couple the magnetic and the velocity field in a way which is hard to understand, especially since it must be applied to a very active region with a complex magnetic configuration. But

the observations actually seem to imply that the photosphere below this active region manages to soak up ⅔ of its magnetic flux within 15 hours, and does so without deviating from this homogeneous divergence in the transverse velocity more than is demonstrated by the relatively weak configurational changes in the magnetograms. This is not impossible, but it is improbable. It is hoped that further observations may clarify this near discrepancy.

Because of the transport of essential parts of the total flux below the photosphere, the actual energy release within the atmosphere will be substantially smaller than the difference in the total energy before and after the flare. This constitutes a downward flow of magnetic energy, and compression of the lost magnetic flux even may require additional energy from other sources. It is possible that the observed flux changes represent only the wake of the proper magnetic or other energy release in the flare. They also may be connected with the sudden aging of spot groups when they have produced major flares (Reference 11).

It is often assumed that the most probable magnetic source of energy supply for the flare losses is the twisting of a force-free, but not current-free, magnetic field. Observation of photospheric changes of types (3) and (4) might prove or disprove this widespread assumption. So far, observations of the transverse Zeeman effect do not cover enough flare material. They often show a rotary structure around spots, but it is hard to prove that a substantial large-scale current exists (References 13, 14, 15, and 16). The larger twists and energies may well be connected with smaller cross sections, which are not yet resolved.

REFERENCES

1. Cowling, T. G., 1953, "The Sun," ed. G. P. Kuiper (Chicago: University of Chicago Press).
2. Lüst, R., and Schlüter, A., 1954, *Zs. F. Ap.*, 34: 263.
3. Parker, E. N., 1963, *Ap. J. Suppl.*, 8(77): 177.
4. Stratton, J. A., 1941, "Electromagnetic Theory" (New York: McGraw-Hill).
5. Gopasyuk, S. I., 1961, *Pub. Crim. Ap. Obs.*, 25: 114.
6. Howard, R., and Severny, A. B., 1963, *Ap. J.*, 137: 1242.
7. Gopasyuk, S. I., Ogir, M. B., Severny, A. B., and Shaposhnikova, E. F., 1963, *Pub. Crim. Ap. Obs.*, 29: 15.
8. Howard, R., and Babcock, H. W., 1960, *Ap. J.*, 132: 218.
9. Ellison, M. A., McKenna, S. M. P., and Reid, J. H., 1961, *Dunsink Obs. Pub.*, 1.
10. Evans, J. W., 1959, *A.J.*, 64: 330.
11. Howard, R., 1963, *Ap. J.*, 138: 1312.
12. Teske, R. G., Dodson, H. W., and Hedeman, E. R., 1963, submitted to *Ap. J.*
13. Leroy, J. L., 1962, theses presentèes a la faculte des sciences del' Univ. de Paris.
14. Severny, A. B., 1962, *Astr. J. U.S.S.R.*, 39: 961.
15. Stepanov, V. E., and Severny, A. B., 1962. *Pub. Crim. Ap. Obs.*, 28: 166.
16. Stepanov, V. E., and Gopasyuk, S. I., 1962, *Pub. Crim. Ap. Obs.*, 28: 194.

I OBSERVATIONS ON FLARES

SESSION B

Chairman, Prof. Fred Haddock

NLM 30267

16 ENERGETIC X-RAY BURSTS FROM SOLAR FLARES

JOHN R. WINCKLER
School of Physics, University of Minnesota
Minneapolis, Minn.

The purpose of this paper is not to make a complete survey of the subject of solar x rays but to deal with the energetic solar flare x-ray emissions, which have been studied in recent years with high altitude balloons and rockets. An excellent summary by Friedman (Reference 1) of the entire subject of x rays and ultraviolet emissions from the sun is available to this conference. A summary of the relation between the energetic x rays and microwave emissions also has been provided by Kundu and is likewise available to this conference (Reference 2). The main purpose of my remarks is to summarize the recent cases of the energetic x rays and their relation to high energy processes in solar flares.

These flare x-ray events constitute the most energetic electromagnetic radiation that we receive from the sun. They are observed by balloons floating at high altitudes during flares, by rocket launches during flares, and more recently by satellites continuously observing the sun. The first event of this energetic type was observed during a balloon flight over Cuba in 1958 during a class 2 explosive-type flare. A photograph of this flare from the Meudon Observatory is shown in Figure 16–1. It occurs between two sunspots, and the appearance of

FIGURE 16–1. Flare x-ray event observed in 1958.

the flare has some of the characteristics of a mirror magnetic geometry with a bright filament coming out of the side. This filament appeared close to the time of the flare maximum. During the rapidly developing phase of this flare, we observed in ionization chambers and counters carried in the balloon at an 8 gm/cm^2 depth below the top of the atmosphere a burst of radiation which could only be photonic in nature. This radiation cannot consist of charged particles because the magnetic field of the earth would exclude all but the most energetic particles traveling from the sun at the low geomagnetic latitude of the measurement. It is known that such very energetic particles were not present in this event. The ionization and Geiger counter increase is shown in Figure 16–2 and correlates exactly with radio frequency emissions from the flare. These radio emissions were also very rapid bursts and were not seen at frequencies below 800 Mc. An analysis of this event has been carried out by Peterson and Winckler (Reference 3). The basis of the analysis was that the balloon observations are bremsstrahlung x rays caused by electrons accelerated in this flare. The analysis shows that approximately 10^{35} electrons were involved in this event—having energies around ½ Mev and producing the x rays by plunging into the solar chromosphere.

Figure 16–3 demonstrates how the bremsstrahlung spectrum produced by monoenergetic electrons of several chosen energies is altered after filtering through the earth's atmosphere to reach the balloon, taking proper account of the angle of the sun. This bremsstrahlung is produced in hydrogen. We see that the effect of the earth's atmosphere is to harden the photons which are observed, although the spectrum leaving the sun contains the usual distribution of photons characteristic of thick-target x-ray production. However, at the balloon the event appears to have a characteristic high energy. We do not believe this observation is unique, but is probably basically the same as other x-ray bursts of nonthermal origin arising during the explosive phase of flares.

Certainly the assumption of monoenergetic electrons used in the analysis of Peterson and Winckler is not correct, but some kind of a spectral distribution must be involved of which there is no knowledge directly from the data. A monoenergetic spectrum has been used as a simplifying assumption.

Peterson and Winckler speculated whether the electrons generated in the flare which produced the x-ray bursts could also produce the high frequency radio emission through the synchrotron process. A calculation was made, assuming the same number of electrons responsible for the bremsstrahlung to be radiating synchrotron radiation in a field of 500 gauss. It was found that this would give 10^4 more radio emission than was actually observed.

Takakura suggested that the discrepancy could be accounted for, as shown in Figure 16–4, by a process in which the electrons were produced high in the photosphere where the density is low and would then travel down the dipole-like magnetic field of the sunspot groups and would produce synchrotron radiation while passing through a layer at approximately 20,000 km above the photosphere. We see, therefore, that it is not impossible that the electrons which account for the x-ray bursts are also those which produce the wide-band microwave portion of the radio spectrum of flares which is observed to occur in close time correlation.

Figure 16–5 shows the spectrum of x rays from a class 2+ flare obtained by Friedman in August 1959 (Reference 1). It has the advantage over the previous observation that it was made from a rocket above the atmosphere and there is a spectral measurement of the photons. The spectrum changes with time between the two curves shown in the figure, and the measurement was made shortly after the beginning of the flare.

If one must account for such a spectrum of photons by thermal emission, then extraordinarily high temperatures of the order of 10^8 degrees are required; and this would result in complete ionization of the hydrogen. It is generally concluded that events of this type come from superthermal processes in which the electrons gain energies well above the thermal region by various mechanisms.

A much improved calculation of the synchrotron emission from electrons in flares has been made recently by Ney and Stein of the

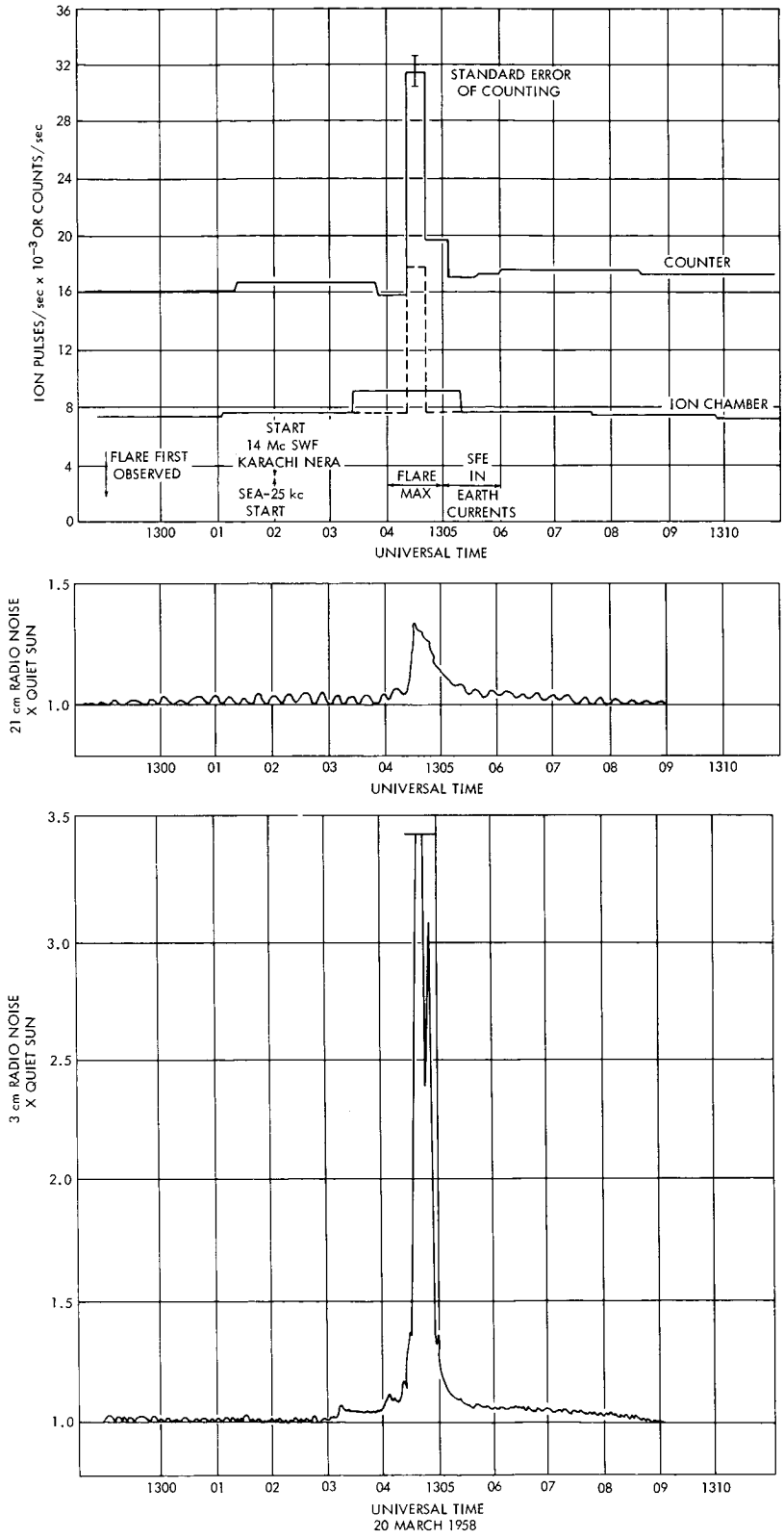

FIGURE 16–2. Ionization and Geiger counter increase observed during flare shown in Figure 16–1.

728–629 O—64——9

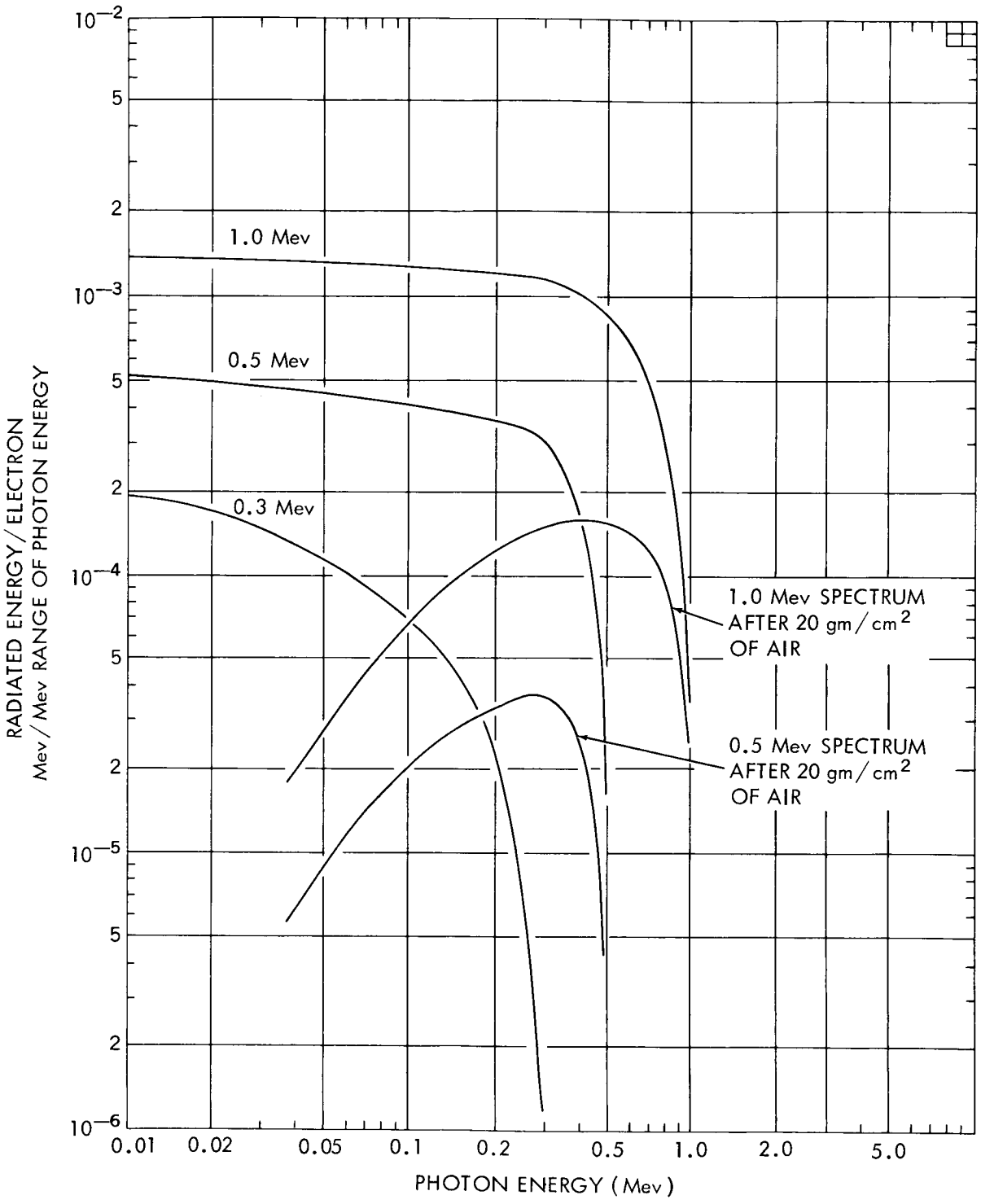

FIGURE 16–3. Differential energy spectra bremsstrahlung from electrons stopping in hydrogen.

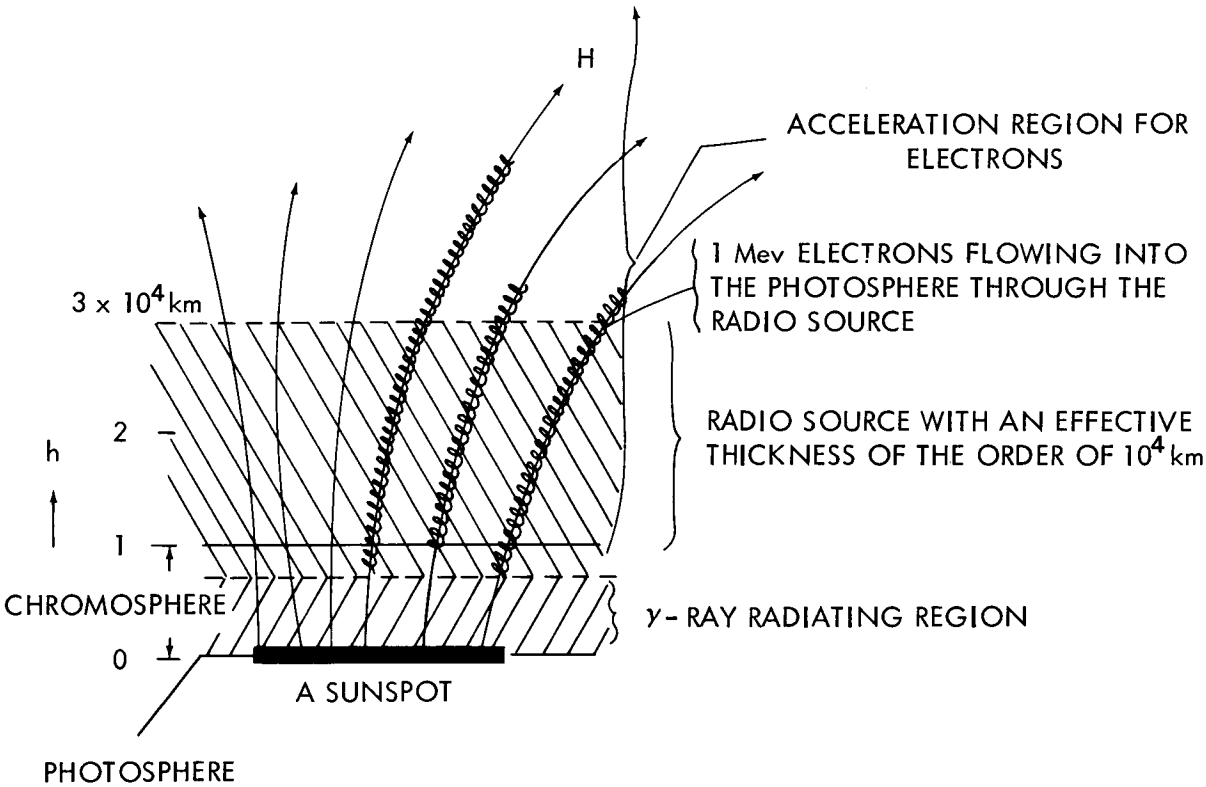

FIGURE 16–4. Relativistic electrons accelerated in the lower corona are flowing into the chromosphere through a radio source. Fractional energy loss of the electrons due to synchrotron radiation in the radio source is very small, so that they flow into the middle chromosphere in which they lose their energy by γ-ray radiation and/or ionization. Synchrotron radiation is weaker in the layer above 3×10^4 km, since the magnetic field becomes weaker; this results in weaker emissivity and lower concentration of the electrons, since $\nu_{\parallel}$ increases. The radiation cannot escape from the middle of the chromosphere because of the absorption.

University of Minnesota (Reference 4). They found that an exponential rigidity spectrum for the flare electrons could account for both the radio emission and the white-light continuum seen in flares on rare occasions. The form of the spectrum which fitted the observations was given by the equation $I=I_0e^{-R/R_0}$. This spectrum gave a suitable amount of white-light continuum to be consistent with estimates of the visually observed white-light continuum; and, also, the spectrum did not contain too many low energy electrons to account for the radio emission. However, it seemed impossible to account for the energetic x-ray bursts as very high energy synchrotron radiation. This would require extremely high energy electrons outside the range of energies which were plausible for flares.

While on the subject of other possible origins of these energetic photons of flares, it does not seem very likely that they are of nuclear origin. There are various reasons for this, although one can never be sure that there is not a small contribution of nuclear gamma rays in the spectrum. The spectrum is too soft, and it resembles too much the bremsstrahlung spectrum to be considered as of nuclear origin. We have observed nuclear gamma rays produced by natural causes, such as the polar-cap protons striking the top of the atmosphere, with essentially the same instruments used for observing the solar x-ray bursts (Reference 5). The mean energy and other characteristics are different, so that it is easy to separate these higher energy gamma rays. Also, there is no other evidence obtained on balloon flights

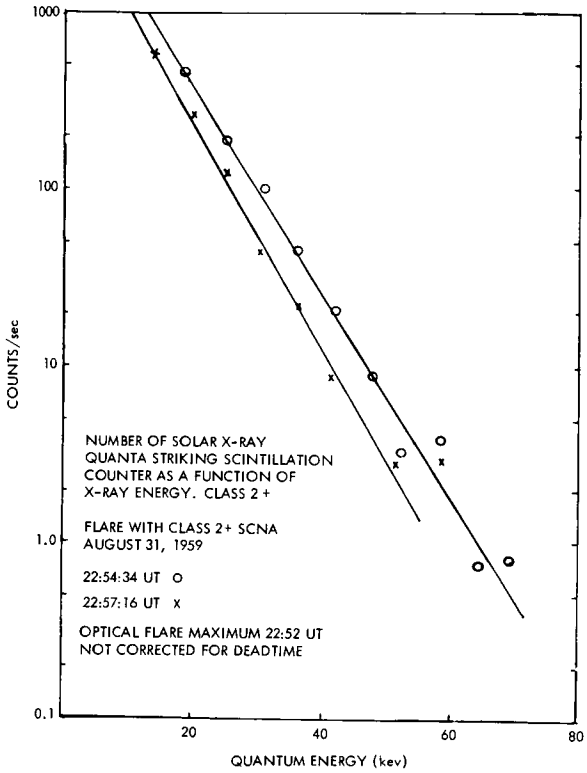

FIGURE 16–5. Spectra of x rays from a class 2+ flare.

showing nuclear physics in flares, such as neutrons or gamma rays directly.

Another event observed with high altitude balloons occurred on August 11, 1960. This is shown in Figure 16–6. It was observed simultaneously with balloons at two latitudes, and both balloon flights gave essentially the same profile of radiation; thus, there can be no question that the effect is of photonic origin. The x-ray burst began simultaneously with an explosive class 2 flare. The dynamic spectra shown in Figure 16–6 is from the Fort Davis Radio Astronomy Station, and the photographs of the flare are from Lockheed Solar Observatory. Again, this is a rather short x-ray burst. It appeared to have some connection with the type III radio bursts, which are seen in the first part of the radio spectrum. In an analysis of this event by Winckler, May, and Masley (Reference 6), it was suggested that possibly the electrons associated by Wild with the fast drift bursts and which have relativistic speeds might be the same electrons that cause the bremsstrahlung. However, even in this case there is also a wide-band microwave radiation present, so that there is again the possibility of the associations described above being substantially correct for this event.

In the next figure, Figure 16–7, we show another event which is to date the best one observed with balloons. This observation was made by Kinsey Anderson in a high altitude balloon flight over southern Canada on September 28, 1961 (Reference 7). The figure, from a paper by Maxwell (Reference 8), shows also the dynamic spectra of the flares that accompanied this x-ray burst. Again, there are type III bursts visible here at various times. There is also wide-band emission reaching high frequencies, which is time synchronous with the main part of the x-ray bursts. Figure 16–8 shows some additional details of the time history of this solar flare x-ray event. It was observed simultaneously with balloons floating at different latitudes, which were already at high altitude during the flare, including the Anderson balloon at Flin Flon, Canada, and one over Minneapolis. This figure shows that the time structure was the same in both places. Thus, the simultaneous observations are important, as at times one sees x rays produced by electrons precipitating from the geomagnetic field; and it is possible to confuse such x rays with solar flare x rays. In fact, in this case there were weak auroral x rays in progress prior to the solar x-ray bursts. It is clear from Figure 16–8 that the time history of this event, however, is of direct solar origin.

Figure 16–9 is significant because it shows the history of the x-ray spectra for this September 28, 1961, event. The main feature is that the spectra measured with a scintillation counter with several energy channels show that the spectra remains more or less constant throughout the event although the intensity rises and falls again during the time of the burst. There are no gross changes in the photon spectrum during the time history of the event seen in balloons. This spectrum, which has been corrected for the effects of the residual atmosphere above the balloon, is a typical bremsstrahlung spectrum. We do not know specifically what

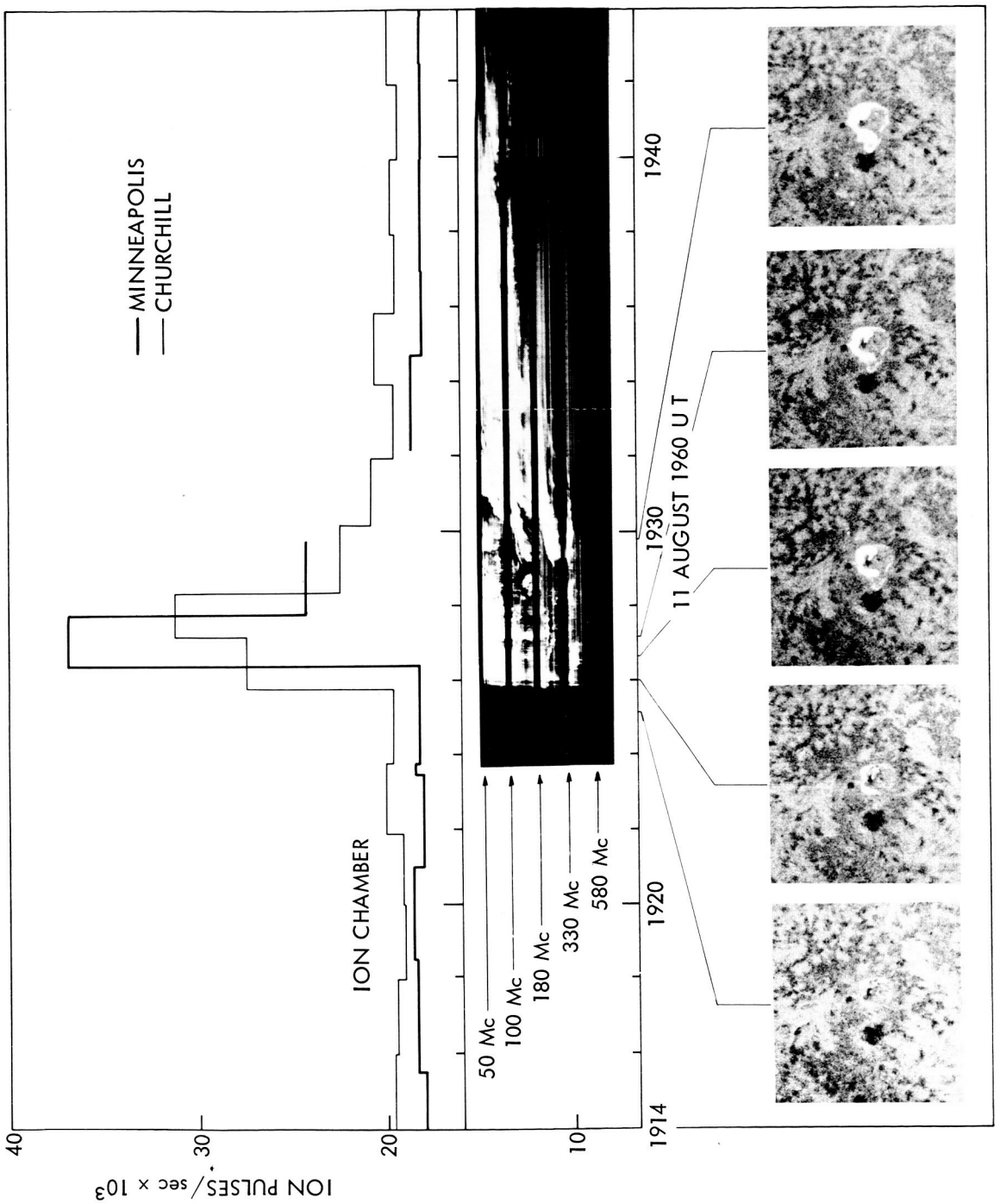

FIGURE 16-6. Flare x-ray event observed August 11, 1960.

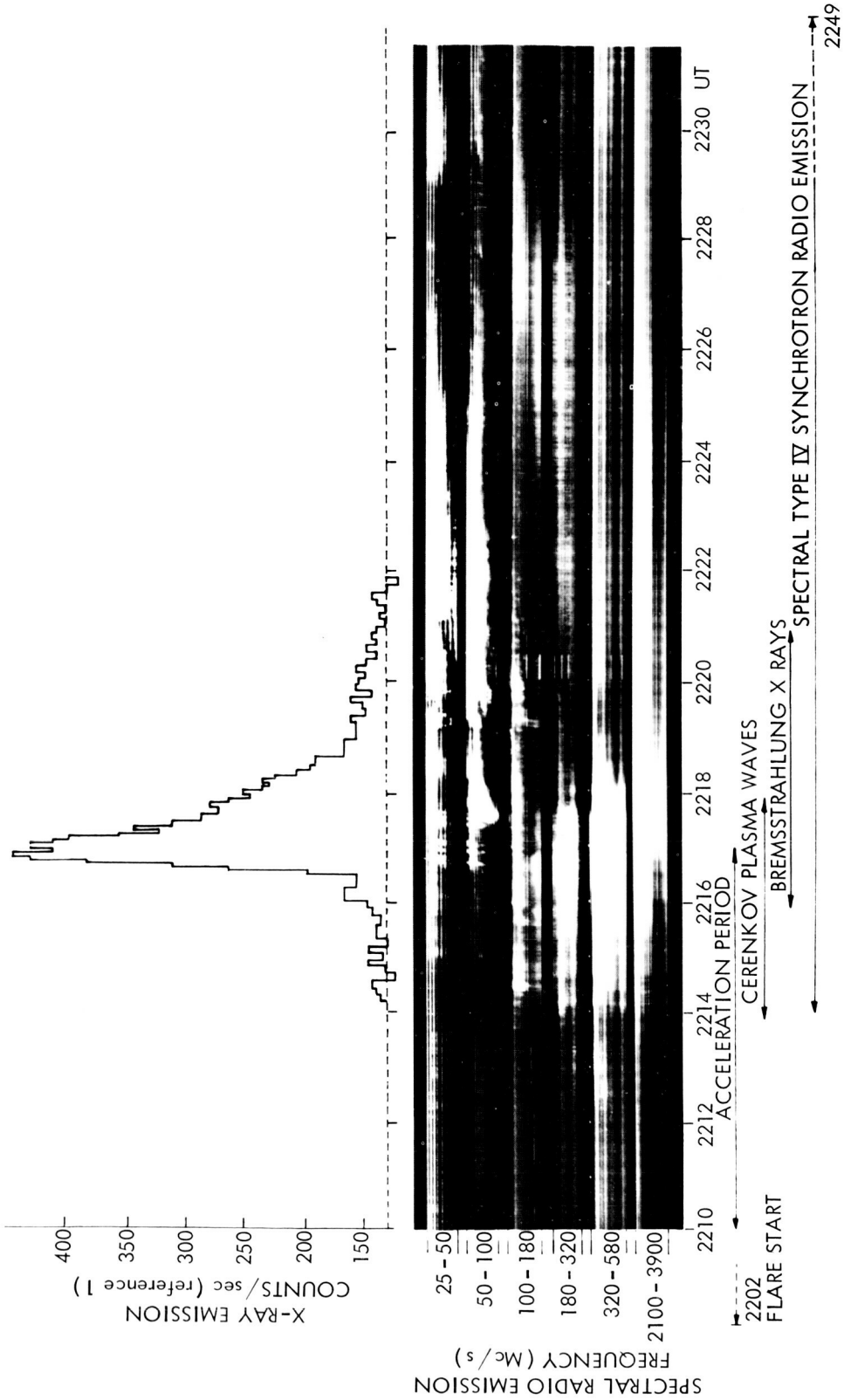

FIGURE 16–7. Flare x-ray event observed September 28, 1961.

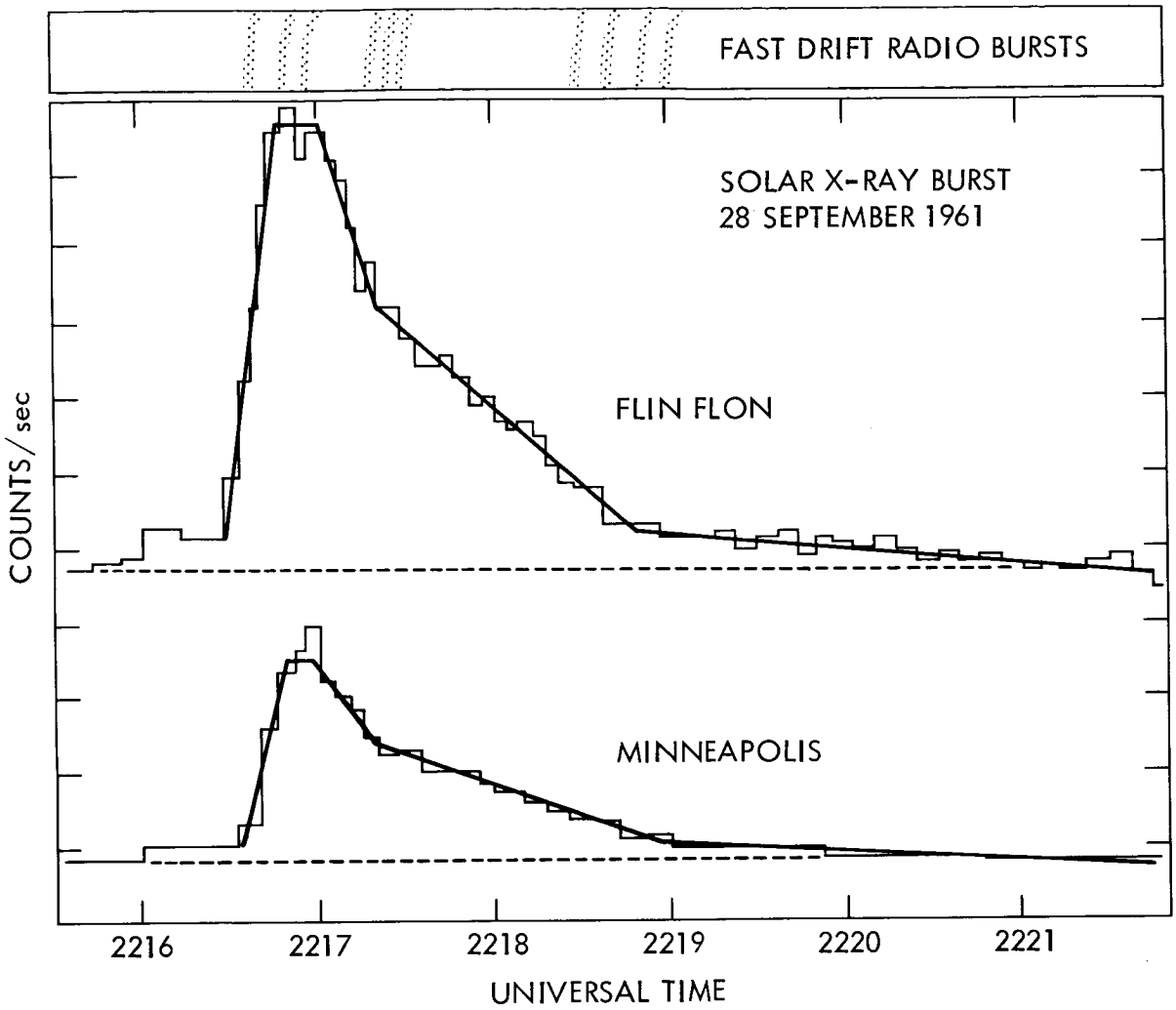

FIGURE 16–8. Additional details of Figure 16–7 time history.

kind of an electron spectrum produced the photons, but we can take suitable choices for this and can get reasonable spectra resulting. For example, a power-law spectrum would do, but other kinds of spectra would also be suitable. The conclusions from this event, which has considerably more information than other balloon events, are tentatively that the electrons were produced first and then fed their energy into the bremsstrahlung process without changing the basic spectrum. This particular flare of September 28, 1961, also produced solar cosmic rays, which were observed in many ways. It was not a typical explosive-type flare; the x-ray burst occurred during the Hα increase phase of the flare event.

Figure 16–10 shows the possibility that the time history of the x rays may be broken down into three separate events, which are possibly associated with fast drift bursts seen on a dynamic spectra record. Anderson has suggested that these three sub-events might be associated with electron bunches which have been accelerated and then oscillate back and forth in the magnetic loop fields above the sunspot group to produce the fast drift bursts when the electrons arch up into the upper region and the x rays when the electrons came down to the mirror points. I don't think one is forced uniquely to this conclusion, but it suggests a

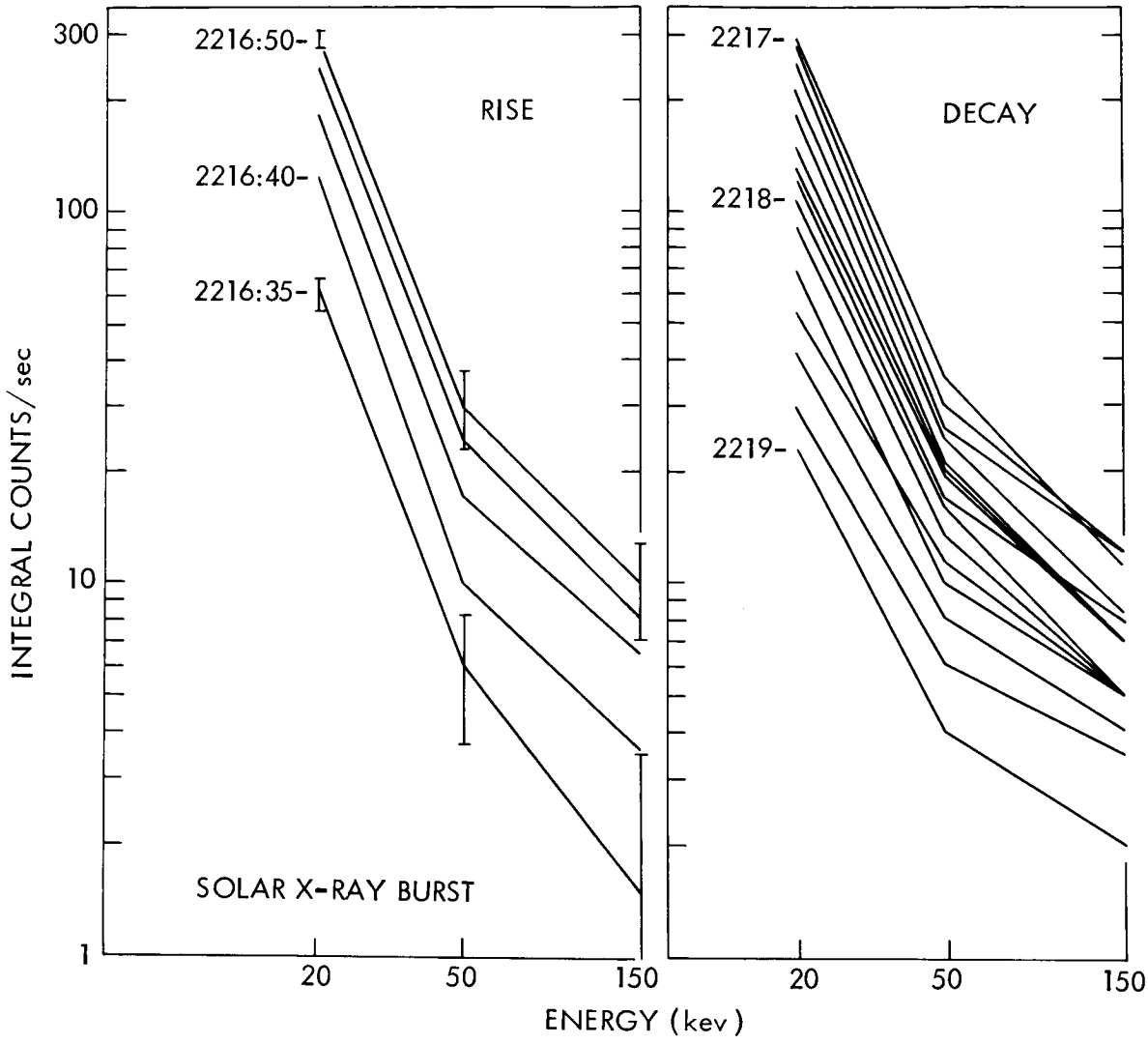

FIGURE 16–9. History of x-ray spectra for the September 28, 1961, event.

means of reconciling type III bursts with x rays.

In conclusion, I should like to mention the association between x rays and the energetic particles produced in flares. A total of six cosmic ray flares has been observed with balloons floating at high altitude during the time of the flare. Of these six, two produced an x-ray burst of this type, two did not, and in two cases the sun was not visible to the balloon so one could not expect to see an x-ray burst. We can tentatively conclude that the appearance of energetic particles is not a necessary condition for the observation of a very intense x-ray burst. However, a recent event showing a case in which x rays did accompany the cosmic ray event is shown in Figure 16–11. This record of the radiation instruments on a high altitude balloon over Fort Churchill shows the x-ray bursts, the time of the occurrence of the class 3 optical flare, and the incidence of the cosmic ray protons. Hofmann and Winckler have examined the intensity increase of the solar flare protons from the standpoint of the simple diffusion model analysis as a means of understanding

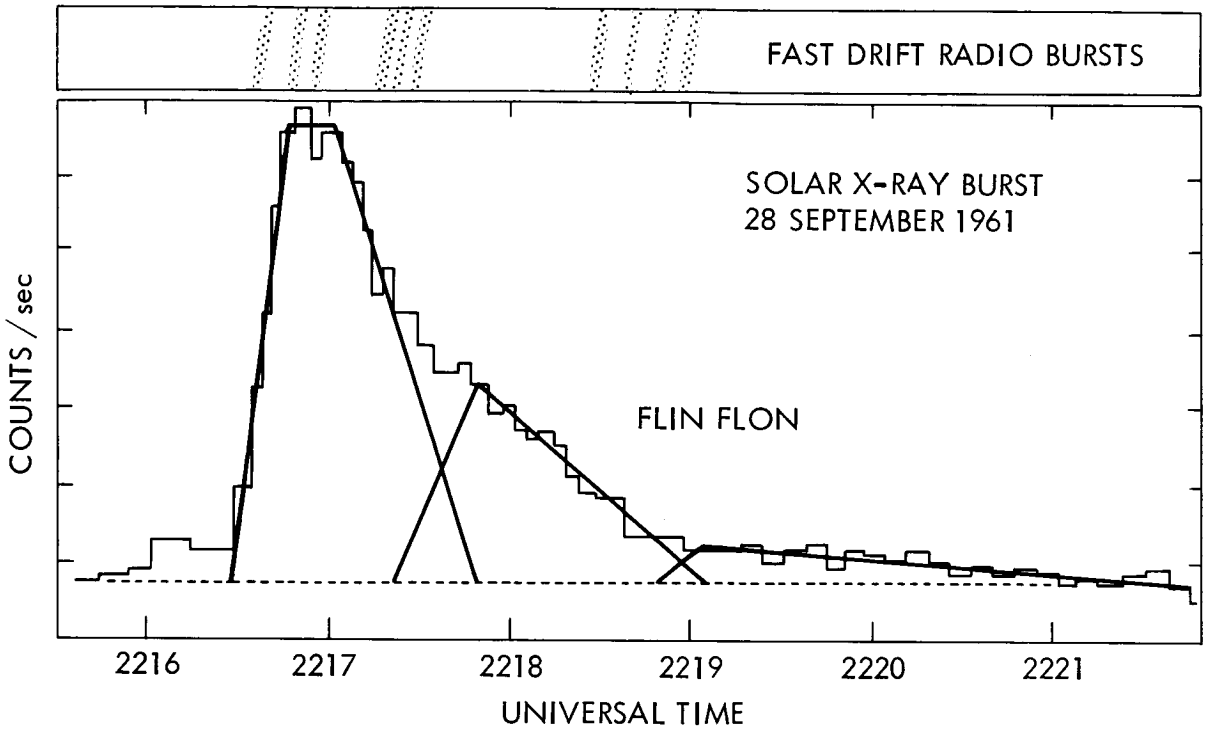

FIGURE 16–10. Time history of September 28, 1961, x rays broken down into three events.

the time variation of the solar protons; this analysis is presented in detail elsewhere. The application of the diffusion equation to the increase in intensity is sensitive to the time of origin of the cosmic ray particles. Assuming that the particles left the sun 8 minutes before the x-ray bursts were observed at the earth—in other words, the particles generated simultaneously in the sun with the x rays—a satisfactory straight-line theoretical fit is given. The error in this fit is certainly as much as 5 minutes or so; thus, at least the cosmic ray time behavior from the flare is consistent with the generation of the cosmic rays at the time of the energetic x-ray burst. From balloon observations, however, we cannot say at this time that this is a necessary condition. However, the acceleration of the cosmic rays for some hours following the explosive phase of the flare seems ruled out.

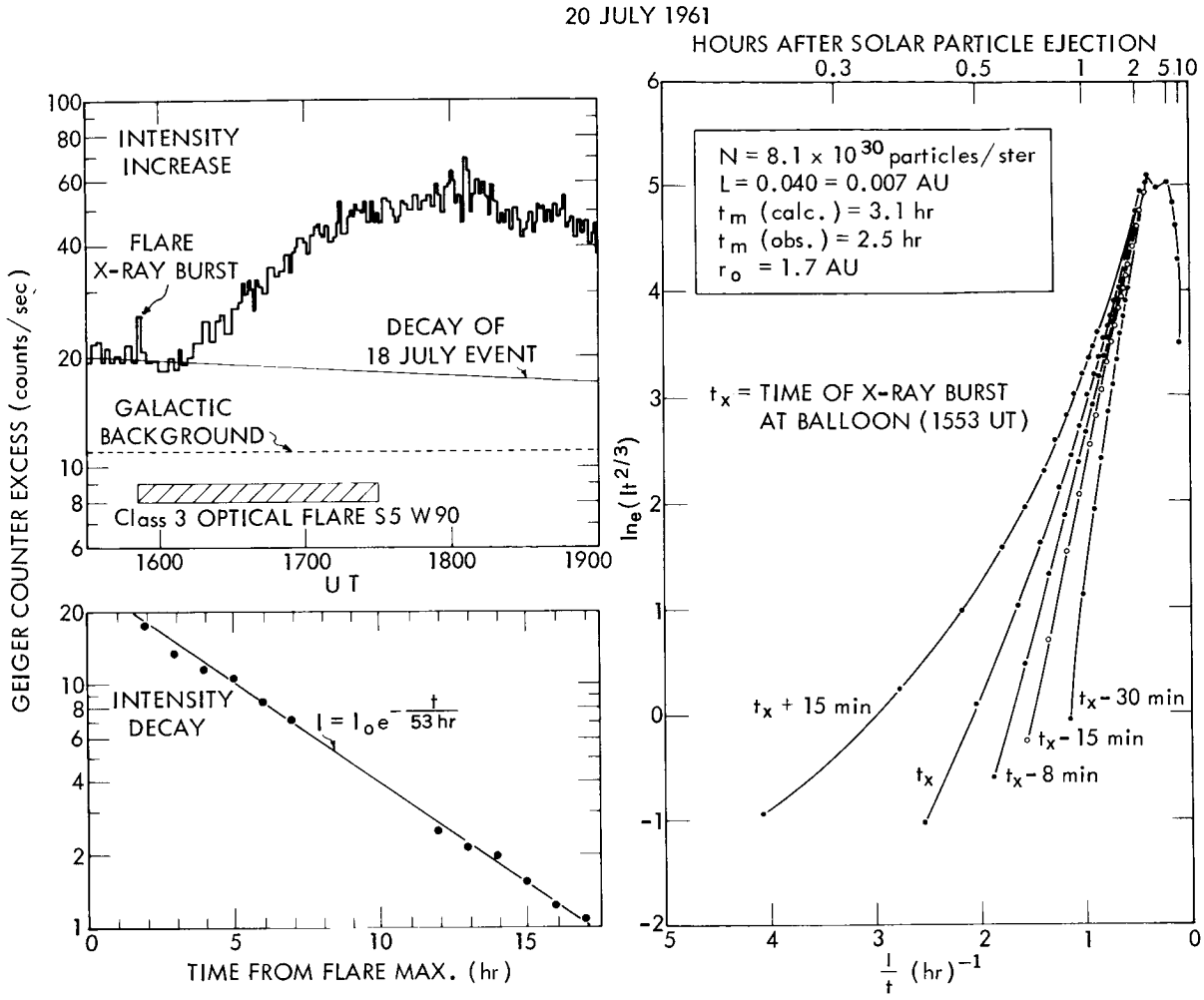

FIGURE 16–11. Flare event observed July 20, 1961.

REFERENCES

1. FRIEDMAN, H., 1963, "Ultraviolet and X Rays from the Sun," *Ann. Rev. of Astron. and Astrophys.*, 1: 59.
2. KUNDU, M. R., 1961, "Bursts of Centimeter-Wave Emission and the Region of Origin of X Rays from Solar Flares," *J. Geophys. Res.*, 66: 4308.
3. PETERSON, L. E., and WINCKLER, J. R., 1959, "Gamma-Ray Burst from a Solar Flare," *J. Geophys. Res.*, 64: 697.
4. STEIN, W. A., and NEY, E. P., 1963, "Continuum Electromagnetic Radiation from Solar Flares," *J. Geophys. Res.*, 68: 65.
5. HOFMANN, D. J., and WINCKLER, J. R., 1963, "Simultaneous Balloon Observations at Fort Churchill and Minneapolis during the Solar Cosmic Ray Events of July 1961," *J. Geophys. Res.*, 68: 2067.
6. WINCKLER, J. R., MAY, T. C., and MASLEY, A. J., 1961, "Observation of a Solar Bremsstrahlung Burst of 1926 UT, August 11, 1960," *J. Geophys. Res.*, 66: 316.
7. ANDERSON, K. A., and WINCKLER, J. R., 1962, "Solar Flare X-Ray Burst on September 28, 1961," *J. Geophys. Res.*, 67: 4103.
8. MAXWELL, A., "Generation of Radio Waves and Acceleration of Particles by the Class 3 Solar Flare of 1961 September 28," Harvard University.

DISCUSSION

Dr. Fireman: You made the statement that there is no evidence for nuclear reactions in flares. I don't think that statement is true. There is a paper by O. A. Schaefer and J. Zähringer [*Phys. Rev. Letters*. 8: 389 (1960)] which measured a large helium 3 flux in the November 12, 1960, flare.

There are three papers by E. L. Fireman, J. DeFelice, and D. Tilles [*Phys. Rev.*, 123: 1935 (1961); *JGR*, 67: 1660 (1962); and Radioactive Dating IAEA, 323 (1963)] which measured tritium in the November 12, 1960, flare. I think that these papers are strong evidence for nuclear interactions that occur during the late stages of the November 12, 1960, flare. This is the first statement. Would you like to comment on this evidence?

Dr. Winckler: According to our discussion before the meeting, I would like to talk with you about this further. We don't have any evidence from particles observed with balloons which are of nuclear origin. I would say we have no direct evidence at this time of the emission of gamma rays or neutrons by flares.

Dr. Fireman: I would say perhaps the measurements don't overlap enough for one to check the other. I think that would be a fairer statement of the situation. Either with the gamma rays or with your particles, or with the nuclear waves.

Dr. Winckler: I would like to ask a question: Is it absolutely certain that the abundance of helium 3 and tritium was not produced in the apparatus by the very large flux of protons which are incident near the earth?

Dr. Fireman: I think the tritium abundance is more than 2 orders of magnitude too large to be explained in this way.

With regard to the helium 3, it is closer to 4 orders of magnitude too large to be explained in this way.

Dr. Winckler: I would like to ask about the flux values you used in your protons?

Dr. Fireman: That is quite all right.

Dr. Hess: Have you ever seen a good type IV radio event where you did not get x rays? When you were aloft?

Dr. Winckler: Yes. There are a number of cases where there were type IV and solar cosmic rays produced. We have a balloon at high altitude able to see the sun, and we did not see one of these bursts. But I think it is a question of one's sensitivity threshold, whether he sees energetic particles or not from a flare. We know that the lower the threshold becomes, the more flares are seen to give energetic particles; for instance, the Mariner data and Pioneer V data. I think the same thing could well be true of these energetic x rays.

Dr. Hess: To turn the question around, did you ever see an x-ray event where you didn't have type IV?

Dr. Winckler: Yes, I think so. There was wide-band microwave emission. I don't think that is the same as type IV.

Dr. Kundu: I have two questions regarding the September 28, 1961, event. First, on the spectrum record produced by Dr. Maxwell, I think there are more than three groups of type III bursts which you have chosen (I think rather conveniently) to coincide with the change in decay of the intensity slope of the x-ray burst.

Second, if you think that the same electron streams produced type III bursts and x-ray bremsstrahlung bursts by oscillating back and forth several times, then one should be able to observe type III bursts of different senses of drift in frequency—that is, one sense of drift—while going from lower levels to higher levels. Then, during passage of electron streams in the opposite direction, one should observe the opposite sense of drift. This was not observed in your case. But I am surprised that you people are still sticking to that idea of type III bursts being generated by the same electron streams as those producing x-ray bremsstrahlung bursts.

Dr. Winckler: I don't think I am sticking to it, but it is fun to speculate about it!

N64-30268

17 SOLAR X RAYS: A COMPARISON WITH MICROWAVE RADIATION

W. A. White
Goddard Space Flight Center, NASA
Greenbelt, Md.

30268

Analysis of data from the OSO I satellite shows that solar x rays shortward of 10 angstroms exhibit a violent dynamic behavior which, however, contains within it counterparts of the somewhat less dramatic behavior of the solar microwave flux. Specifically, the solar x-ray flux contains: (1) a slowly varying component, (2) "gradual rise and fall" bursts, and (3) impulsive bursts. The OSO I data show the first two to be related to their microwave counterparts, and the empirical relations are given in this paper. Observations at 10A of the third component (impulsive bursts) could not be associated directly with microwave observations because of the extreme disparity in sensitivities of the two methods of observing this phenomenon. However, observations by Frost (reported at this Symposium) of solar x rays in the 20 to 100 kev region do show a direct counterpart of the microwave impulsive burst.

With the launching of the OSO I (1962 $\zeta 1$) on March 7, 1962, it became possible for the first time to point instruments at the sun accurately and continuously for entire daylight portions of a satellite orbit; for the 550-km orbit of OSO I these observing time intervals were the order of 1 hour each, separated by darkness intervals of about ⅔ hour. The observing periods were long enough to disclose some interesting dynamic effects which would be difficult to study otherwise.

SENSOR CHARACTERISTICS

OSO I provided coverage of the solar x ray radiation near a wavelength of 10A by means of an ion chamber whose characteristics are given in the following list:

Window material	Beryllium
Window thickness	0.005 in.
Total window area (2 chambers in parallel)	3.38 cm²
Absorbing gas	Xenon
Gas pressure	780 mm
Ion chamber depth at normal incidence	2.19 cm
Ion pairs per erg	2.8 $(10)^{10}$

The conversion efficiency as a function of wavelength is shown in Figure 17–1.

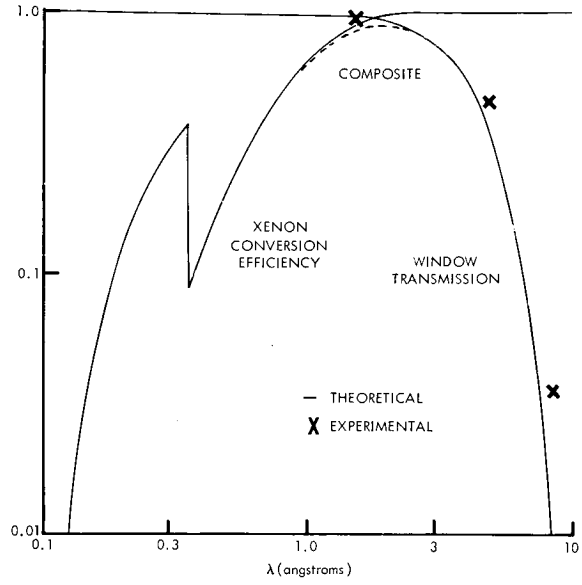

FIGURE 17–1. OSO I ion chamber conversion efficiency as function of wave length.

Amplified ion-chamber current was sampled for 2 seconds every 20 seconds by the telemetry.

The full-scale sensitivity of such a broadband sensor is, of course, dependent on the shape of the input spectrum. It has been shown (Reference 1) that for non-flare periods it is reasonable to assume a spectral shape consistent with a $2.8(10)^6$ °K plasma composed of ionized hydrogen and helium in the ratio of their solar abundances. Over the frequently used band

limits of 2 to 8A, the full-scale sensitivity is then $3.6(10)^{-4}$ ergs cm^{-2} sec^{-1}.

COMPONENTS OF THE SOLAR X-RAY FLUX

Changes in the solar x-ray flux as observed by OSO I occurred over a broad range of time scales, from fractions of a second to many weeks. In particular, counterparts to the microwave slowly varying component and to the microwave "gradual rise and fall" burst are clearly seen.

The markedly dynamic character of the solar x-ray flux as contrasted with the 2800-Mc radiation should be emphasized; for instance, on only 3 occasions out of 70 days (March 7 through May 15, 1962) was the x-ray flux "quiet"—that is, free from bursts—for an interval of as much as 8 hours.

Slowly Varying Component

Solar rotation markedly affects the x-ray flux. In fact, if we define the non-burst x-ray flux background as the minimum flux reached in a 6-hour interval and evaluate this for a succession of such intervals, we find that for the spring of 1962 the OSO I data empirically fit the relation

$$\Phi_{2-8A}=k_1\ (\Phi-\Phi_0)_{2800\ Mc}\ \text{erg cm}^{-2}\ \text{sec}^{-1}. \qquad (1)$$

That is, the daily mean non-burst x-ray flux is proportional to the difference between the daily mean of the 2800-Mc flux and a value of 2800-Mc flux which is presumably a "quiet sun" asymptote for the appropriate phase of the solar cycle (Reference 2). Note that any such quiet sun asymptote in the x-ray flux is *zero*, at least to the sensitivity and accuracy of this empirical fit. Apparently a truly quiet sun, stripped of plage, would be dark in x rays while still emitting an appreciable 2800-Mc flux. Figure 17–2 shows the measured mean non-burst x-ray flux and the index values calculated from Equation 1 with $k_1=1.4(10)^{-5}$, $(\Phi)_{2800\ Mc}$

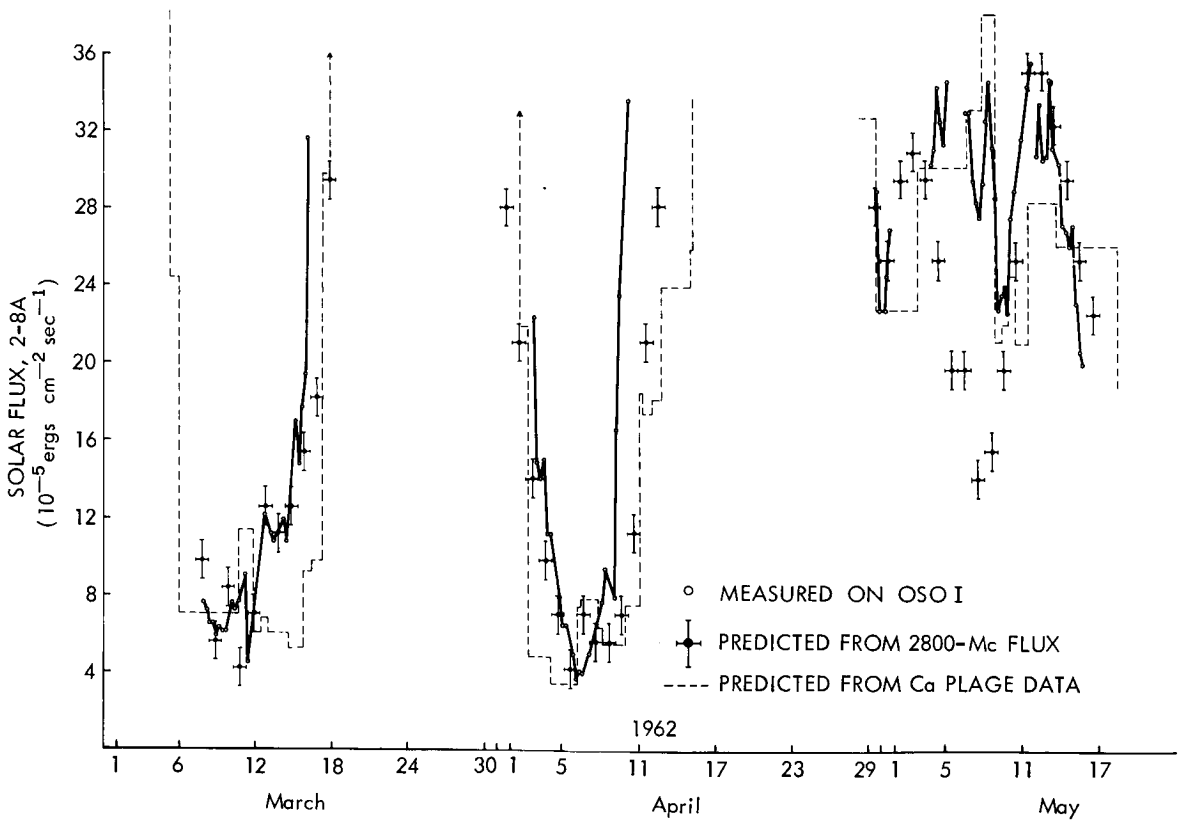

FIGURE 17–2. Slowly varying component of solar x-ray flux.

in units of 10^{-22} w m^{-2} (c/s)$^{-1}$; and $(\Phi_0)_{2800\ \mathrm{Mc}}=$ 73 such units.

It is fruitful to look in more detail at the relation between the calcium plages and the x-ray flux. For example, is the brightness of a plage in Ca emission a measure of its brightness in x rays? If so, we might expect a relation somewhat as follows:

The brightness of a plage in Ca-K emission is expressed by an intensity number assigned by the McMath-Hulburt Observatory apparently on the basis of a subjective estimate of relative densities on a patrol photograph; as such, it is likely to be approximately logarithmic.

The other routinely reported parameter characterizing a Ca plage is its area. Since we are dealing at x-ray wavelengths with a volume source, an assumption has to be made regarding the dependence of the x-ray source volume upon the area of the plage. It is found from the OSO I data that it is much better to assume that the thickness of the x-ray source is proportional to the mean plage diameter than to assume a constant thickness. The volume of the ith plage is then given by

$$(\mathrm{d}V)_i \propto (A_i)^{3/2},$$

where A_i is the reported area.

The hypothesis that the x-ray flux arises from such a plage-associated volume sources with x-ray brightness proportional to Ca-K brightness can be written as

$$\Phi_{2-8\mathrm{A}}=k_2\sum_i (A_i)^{3/2}(b)^{I_i} \quad \mathrm{erg\ cm^{-2}\,sec^{-1}}, \qquad (2)$$

where A_i is the area of the ith plage in thousandths, I_i is the McMath Ca-K intensity number, and k_2 and b are constants to be empirically determined from the OSO I data.

The best fit to date is plotted in Figure 17–2, for plages of area ≥ 1 thousandth, for

$$k_2=0.134(10)^{-5}$$

and for

$$b=2.$$

Plage data reported by the McMath-Hulburt Observatory and published in the CRPL Bulletin were used, with times of rising and setting of the x-ray sources calculated from plage Central Meridian Passage minus and plus 7.8 days, respectively. This corresponds to an assumed source height extending to some 21,000 km above the photosphere.

Two types of gross discrepancy can be seen between the x-ray flux and the hypothetical indices derived from plage and 2800-Mc data. The first type, exemplified by the periods March 12–14, April 10–14, and May 1–2, shows too low a value for the plage-derived index. Each of these periods saw the birth of one or more small plages upon the disk which were not included in the index combination of Figure 17–2. The second type of discrepancy is seen during the period May 3–7 for which the index derived from the 2800-Mc flux is low. This period included a large plage (McMath 6412) which was reported to be declining in Ca-K intensity; this plage contained a single sunspot which was seen to die on the disk.

Gradual Rise and Fall Bursts

Superimposed upon the x-ray slowly varying component, and occurring so frequently as to make difficult the finding of intervals completely free from their effects, are x-ray bursts analogous to the "gradual rise and fall" bursts seen in solar microwave radiation. A complete statistical analysis of the x-ray bursts observed by OSO I has not yet been made, but typical on-scale bursts (see Figure 17–3) have rise times of 2 to 4 minutes and fall times of 10 to 20 minutes. However, many bursts carry the experiment output off scale; for these, the duration of the event can be as long as 6 hours. A comparison of the x-ray data with 2800-Mc records (kindly made available by A. E. Covington) taken at Ottawa shows that all 2800-Mc gradual bursts had a time-coincident counterpart in the x-ray data. A peak amplitude of only 1 or 2 units of 10^{-22} w m^{-2} sec^{-1} at 2800 Mc was in all cases accompanied by an off-scale x-ray burst. Larger bursts at 2800 Mc were, of course, also off scale in x rays; but, again, times of onset and recovery were found to agree with the corresponding times for the accompanying x-ray burst.

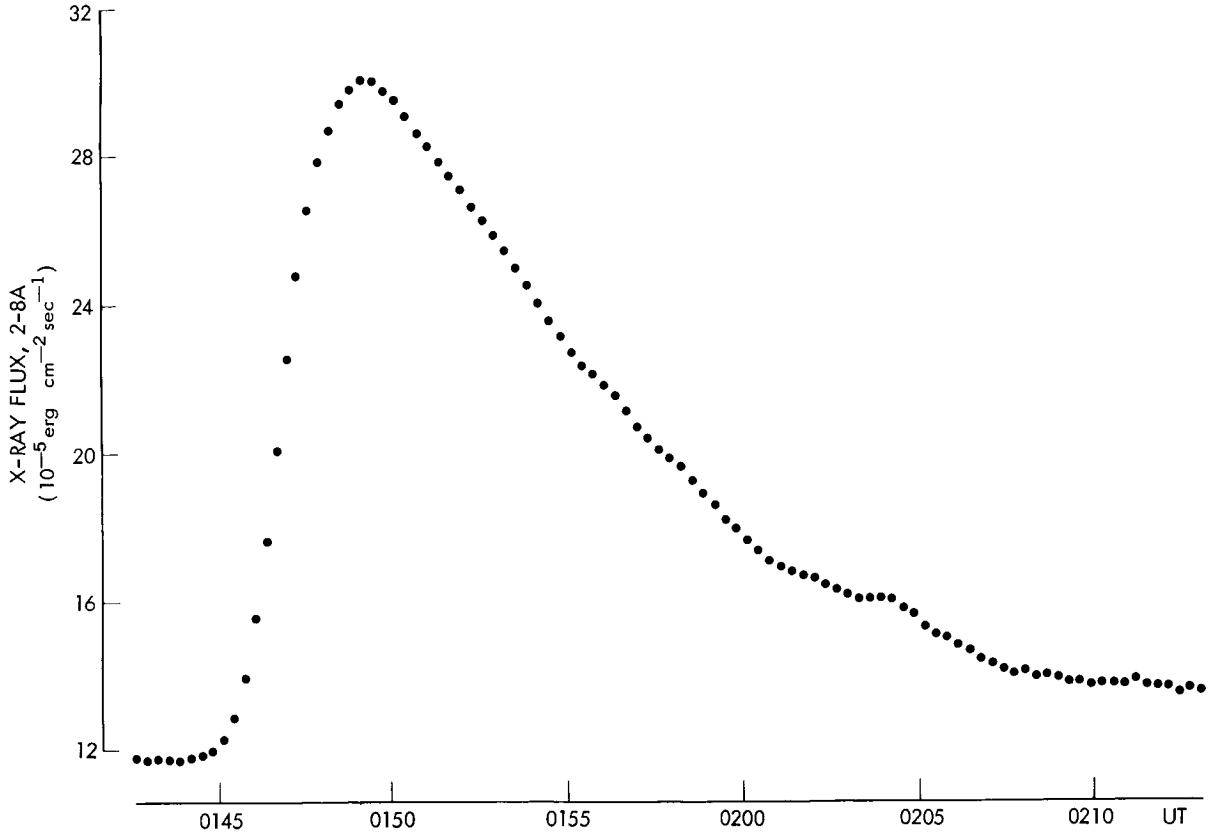

FIGURE 17–3. X-ray burst, OSO I; March 8, 1962.

It is important to note that the relation between burst flux at 2800 Mc and at 2–8A is different from the relation between the slowly varying component at 2800 Mc and at 2–8A. As has been shown (Equation 1), a change in the 2800-Mc slowly varying component of .1 flux unit is accompanied by a change in 2–8A flux of about $1.4(10)^{-5}$ erg cm^{-2} sec^{-1}; whereas a burst type change at 2800 Mc of 1 flux unit is accompanied by a change in 2–8A flux of at least $30(10)^{-5}$ erg cm^{-2} sec^{-1}. This increase in the x-ray/microwave ratio of more than 20 times is suggestive of a different physical process being responsible for the two phenomena.

Several apparent associations of certain x-ray bursts into groups displaying a definite pattern were observed; Figure 17–4 shows such grouping. Similar groupings are present in the data for the first week in April 1962; in fact, the one particular March group shown in Figure 17–4 appears to have an exact April counterpart 27.1 days later with identical time separations between events and with identical peak excursions above mean background level. In addition to these two groups, two others each having 4 members and one other having 3 members were found. For all five groups, the envelope joining the peaks of the bursts within a group is a straight line of slope $\pm 1.51(10)^{-9}$ erg cm^{-2} sec^{-2} for wavelengths between 2 and 8A; three groups displayed positive slopes, two groups negative.

Impulsive Bursts

Several instances of very fast bursts (entire duration less than 2 minutes) were seen by Frost (reported at this Symposium) from an OSO I sensor responsive to photons of energy greater than 20 kev. For every one of these instances the lower energy ion-chamber channel was off-scale prior to and during the time in-

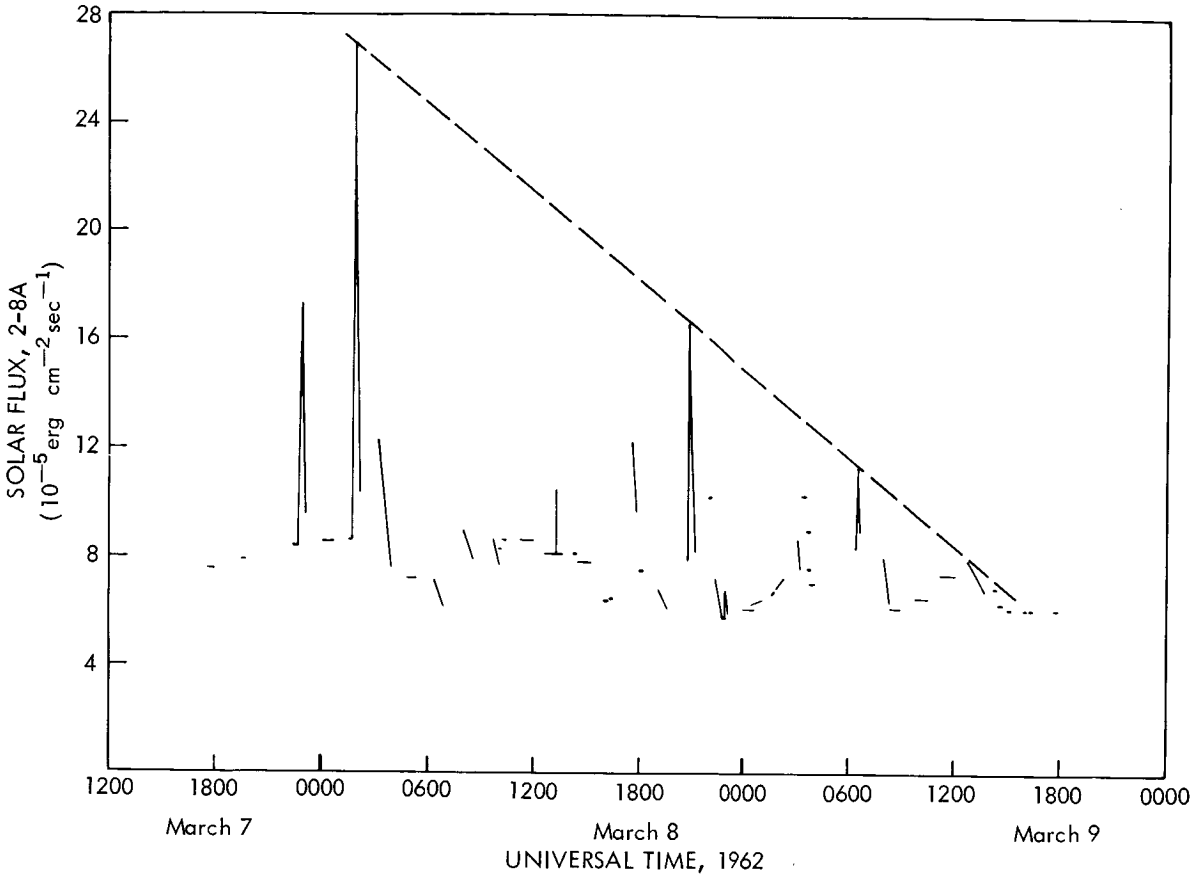

FIGURE 17–4. Solar x rays (2–8A) showing grouping of x-ray bursts.

terval of the impulsive burst. It is indeed unfortunate that we are thus unable to obtain an x-ray/microwave ratio for an impulsive burst to compare with the values obtained for gradual bursts and for the slowly varying component.

REFERENCES

1. WHITE, W. A., 1963, "Solar X-Rays: Slow Variations and Transient Events," COSPAR IV, Warsaw, June 1963.
2. COVINGTON, A. E., and HARVEY, G. A., 1960, *Astrophys. Jour.*, 132: 435.

DISCUSSION

EDITOR'S NOTE: As a continuation of Dr. White's paper, Dr. Lindsay discussed, on the second morning, the extreme variability of solar x-ray emission. Figure 17–5 was shown by Dr. Lindsay. The following discussion ensued:

Dr. Oster: It seems in Figure 17–5 the sensitivity is going up. It seems to me that you have a continuous slope of your receiver. How do you calibrate during the whole flight?

Dr. Lindsay: If you recall the data shown in which three solar rotations of x-ray data were plotted, it did correlate extremely well with the 2800 Mc and plage activity.

The system can hardly get more sensitive. The ion chamber may go dead, but it is not going to become more sensitive.

The only component in the system that can vary and change the sensitivity—actually,

728–629 O—64——10

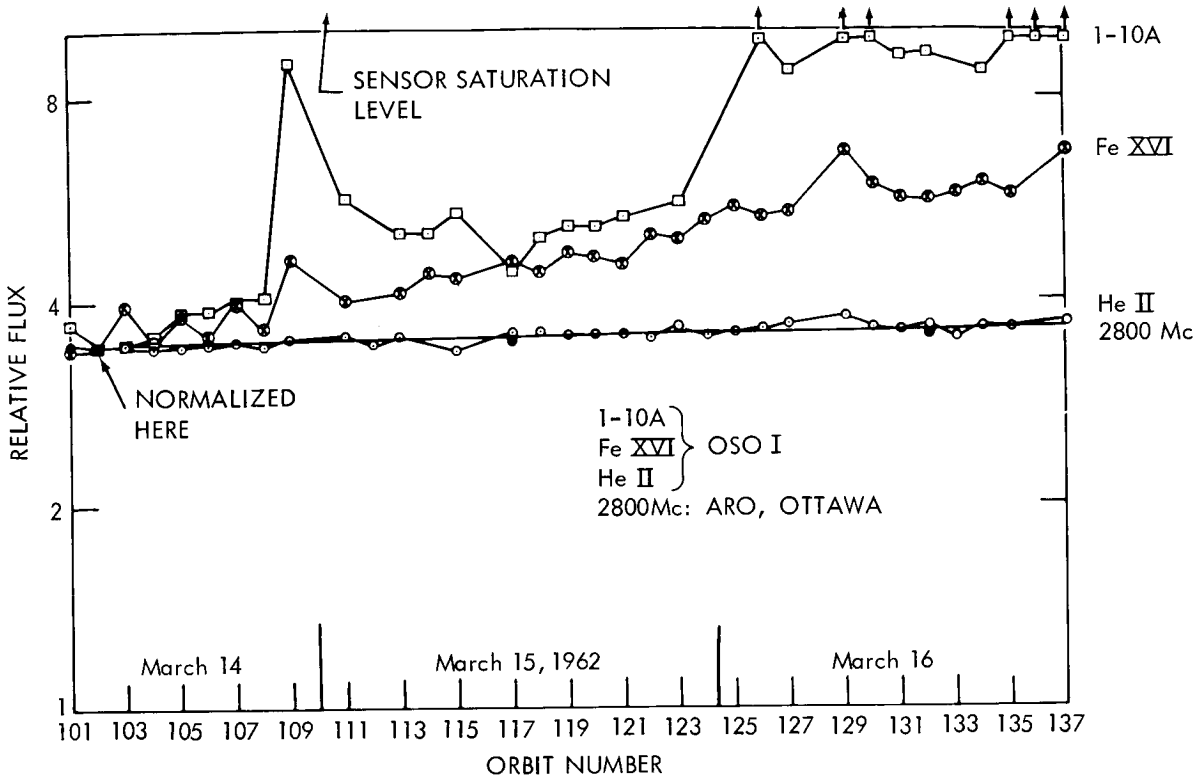

FIGURE 17-5. Solar fluxes, relative values for selected radiations.

we would be aware of that, too—the only component that can vary is the high resistance in the electrometer. This electrometer has a 100 percent feedback to give it high speed. If that resistor changes, the rise time of the system will change. We very carefully checked the rise time, and the rise time remains constant. In fact, it was the same even after the satellite had been in orbit for 1 year.

The point is, though, that we came down when the plage activity disappeared to the same level.

Dr. Leighton: I am not quite sure what we were looking at in Figure 17-4. I am sure you must have considered that any two of those peaks determine a straight line; and it is only a question then of how many possible combinations of two you have to look at on this figure on which you would, by accident or by design, find a third point or more which would tend to lie in the same line. There should be a fairly simple statistical test to make for something like that.

Dr. Lindsay: I think that there is another point that I didn't mention. We have had—in the second case, in fact—say three members of a series, and not the fourth one. That is, the data were not available to us. We calculated where it should occur; asked that those data be reduced; and, when we looked at the data, it was there.

Dr. Leighton: Was that true even when the one that you were missing was a very high peak? Or was it only true when it was a low peak at the other end?

Dr. Lindsay: We have several of them. In the first place, I don't think the amplitude is as significant as the time might be. It is obvious that we have a limit to how high we can go. In one case, we looked for two events on an ascending group, when we would expect it to be saturated. The event was there, but it was off-scale.

Dr. Leighton: At the right time?

Dr. Lindsay: Right.

Dr. Leighton: If you aren't concerned about the amplitude, I am not quite sure what the significance is of those pretty lines we saw.

Dr. Lindsay. This is the thing that, of course, called them to our attention; but of even more interest was the time relation.

Dr. Leighton: I am really mystified by that.

Dr. Lindsay: We are, too. And, in fact, I am not standing up here saying this is the absolute truth, because I think it is amazing. It may well be an accident. But, on the other hand, I think it is an observation.

N64-30269

18 COMMENTS ON HIGH ENERGY X-RAY BURSTS OBSERVED BY OSO I

KENNETH J. FROST
Goddard Space Flight Center, NASA
Greenbelt, Md.

30269

Instrumentation aboard the first Orbiting Solar Observatory observed five separate instances of high energy x-ray bursts accompanying solar flares. The x-ray bursts were observed in the 20 to 100 kev range. Data on the types of flares producing the x-ray bursts and the associated microwave radio bursts are presented.

Among the experiments carried by OSO I (1962ζ1) in the pointed section was a scintillation counter designed to detect hard solar x-ray bursts in the 20 to 100 kev energy range. The scintillation counter consisted of a cylindrical NaI(Tℓ) crystal 0.3 cm high and 2.24 cm in diameter and an RCA C–7151 photomultiplier tube. The photomultiplier tube and crystal assembly was placed in a cylindrical copper shield which, through an opening in the front end, provided a field of view of 0.3 steradian. The copper shield had a wall thickness of 1 cm. The 3.8 cm^2 area of the front surface of the crystal was held normal to the solar direction by the pointing of the satellite. An aluminum disk of 0.08 cm thickness was placed over the front surface of the crystal. The efficiency of the detector in the 20 to 100 kev interval was approximately 0.90.

The electronics associated with the detector consisted of lower and upper level discriminator circuits and a logarithmic ratemeter. The lower and upper level discriminator circuits were set to select only those pulses from the photomultiplier tube which correspond to an energy loss of between 20 and 100 kev in the crystal. The pulses accepted by the discriminator circuits were then passed on to the logarithmic ratemeter. The output of the ratemeter was a voltage level between 0 and 5 volts which corresponded to an input count rate between 10 and 10^4 counts/second. The output of the ratemeter was able to respond to changes in count rate that occurred in a time longer than 10 milliseconds.

The satellite telemetry system sampled the voltage level at the output of the ratemeter continuously for 2 seconds once every 20 seconds. This sampling format was operative during the entire daylight part of an orbit.

DATA

With the return of the first hundred orbits of reduced data, the response of the detector to the general spacecraft x-ray background and the response to the regions of trapped radiation were determined. In addition it was found that the experiment responded to the electron warm spots detected by an electron-proton spectrometer placed aboard the spacecraft by Schrader et al. (Reference 1). When passing through regions not including trapped radiation or electron warm spots, the detector was found to produce a count rate for a 2-second sample that consistently fell between limits of 10.5 to 14.5 counts/second.

On March 17, 1962, a short-lived increase in count rate occurred while the satellite was passing through a region where the count rate normally fell in the background range of 10.5 to 14.5 counts/second. The increase in count rate started at 19:39:49 UT and ended at 19:40:08 UT. A record of the satellite telemetry signal for the orbit containing this time period indicated conclusively that the fluctuation in count rate was real and could not be attributed to telemetry noise that had been erroneously digitized by the automatic data reduction

system. Reference to the available solar data revealed that a solar flare had been observed by the McMath-Hulbert and Lockheed Observatories between the times of 1934 to 1959 UT and 1936 to 2003 UT, respectively. The flare was observed on the east limb of the sun and was classified by McMath-Hulbert as an Importance 1 flare and by Lockheed as an Importance 2 flare. Also at this time an impulsive radio burst of 3-minute duration, beginning at 19:39 UT and reaching maximum at 19:40:12 UT, was observed at 2800 Mc/s by Ottawa. Furthermore, an SID accompanied the flare beginning at 19:40 UT and reaching maximum at 19:44 UT. The very close correlation in the time of these events and the fluctuation of the 20 to 100 kev count rate suggested that the most plausible explanation of the fluctuation was a burst of energetic x rays produced by the flare.

During succeeding orbits of the spacecraft, four more instances of rapid excursions in count rate were observed during the presence of a flare on the sun which produced an impulsive radio burst in the microwave range and an SID. These excursions in count rate were also interpreted as solar flare x-ray bursts. The history of these five events is presented graphically in Figures 18–1 through 18–5 (Reference 2).

DISCUSSION

Prior to the launch of OSO I eight occurrences of high energy x-ray bursts accompanying solar flares had been observed (References 3 to 7). Kundu has analyzed the radio data associated with each of these events (Reference 8). He found that an impulsive microwave burst was associated with every x-ray burst, whereas type III bursts and other meter wave events did not show as strong a correlation. Furthermore the general character of the microwave spectrum was found to be such that the peak flux observed at wavelengths in the 3 to 10 cm range was stronger than that observed at wavelengths in the 10 to 20 cm range. The radio data associated with the OSO I x-ray bursts, as indicated in Figures 18–1 through 18–5, appear to lend strong support to Kundu's analysis. Additional information of interest to this analysis is the fact that, as far as can be determined from spectral observations in the meter wave range, no type III bursts occurred during the x-ray events.

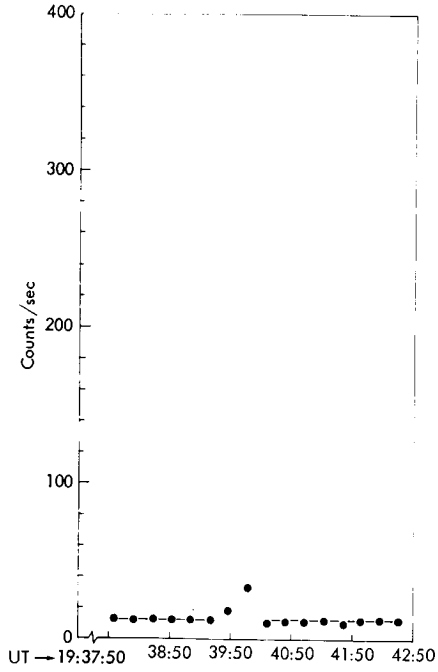

1+ FLARE 1 SID

RADIO DATA

Mc/s	Start UT	Max. UT	Duration	Type	Peak Flux*
2800 OTT	1939	2000	101 min	S	2
2800 OTT	1939	1940.2	3 min	S	6
18 NBS	1940	1949	135 min		

* In units of $10^{-22} w\ m^{-2} (c/s)^{-1}$

FIGURE 18–1. High energy x-ray burst, OSO I; $20 < E\gamma < 100$ kev, March 17, 1962.

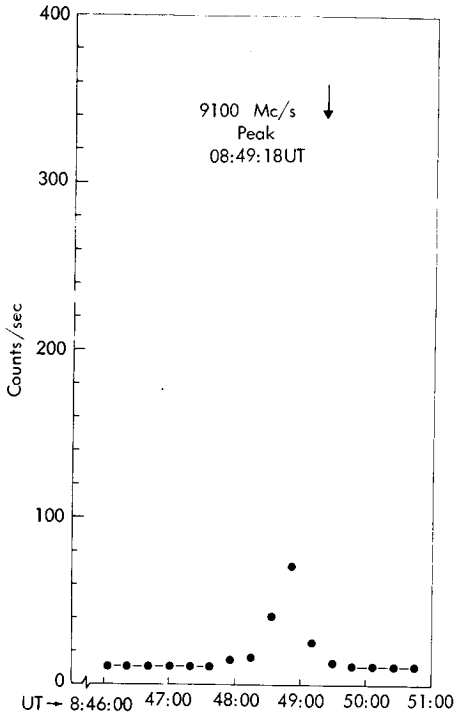

1^+ FLARE 1 SID
RADIO DATA

Mc/s	Start UT	Max. UT	Duration	Type	Peak Flux*
9100 NED	0848.1	0849.2	4.5 min	S	102
2980 NED	0848.0	0849.2	4.5 min	S	122
1500 HHI	0848.0	0849.6	22.0 min	S	38

* In units of 10^{-22} w m^{-2} $(c/s)^{-1}$

FIGURE 18–2. High energy x-ray burst, OSO I; $20 < E\gamma < 100$ kev, April 13, 1962.

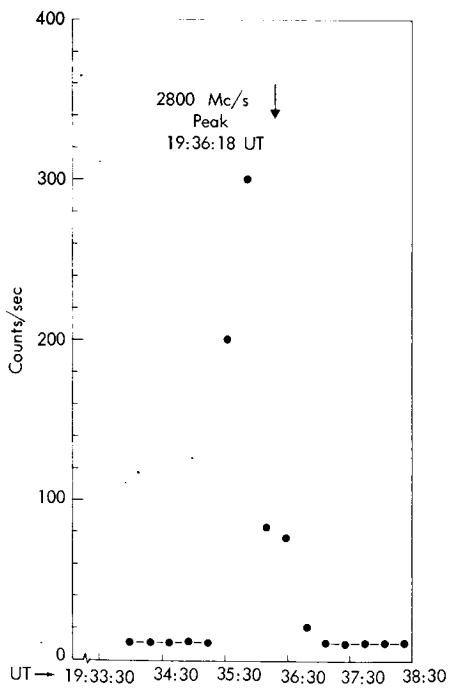

1^+ FLARE 1 SID
RADIO DATA

Mc/s	Start UT	Max. UT	Duration	Type	Peak Flux*
2800 OTT	1935	1936.3	8 min	S	165

* In units of 10^{-22} w m^{-2} $(c/s)^{-1}$

FIGURE 18–3. High energy x-ray burst, OSO I; $20 < E\gamma < 100$ kev, April 19, 1962.

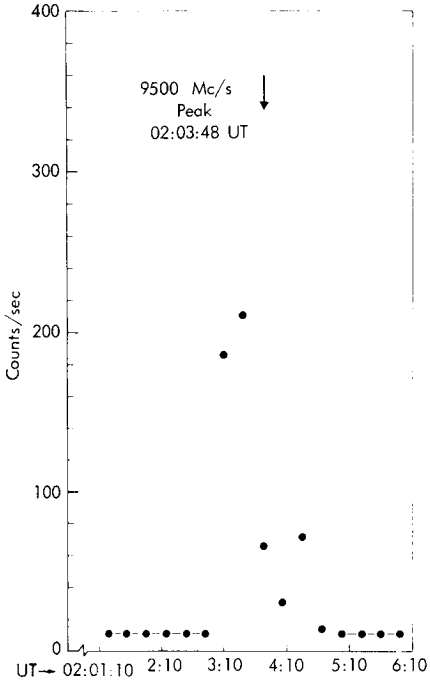

1^+ FLARE 1 SID
RADIO DATA

Mc/s	Start UT	Max. UT	Duration	Type	Peak Flux *
9500 TOK	0203.5	0203.8	1 min	C	419
3750 NAG	0203.5	0204.2	2.5 min	C	330
2000 NAG	0203.5	0204.2	2.5 min	C	73
1000 NAG	0203.5	0204.3	2.5 min	S	37
222 SEA	0203.5	0204.0	1 min	S	110

*In units of 10^{-22} w m^{-2} $(c/s)^{-1}$

FIGURE 18–4. High energy x-ray burst, OSO I; $20 < E\gamma < 100$ kev, April 21, 1962.

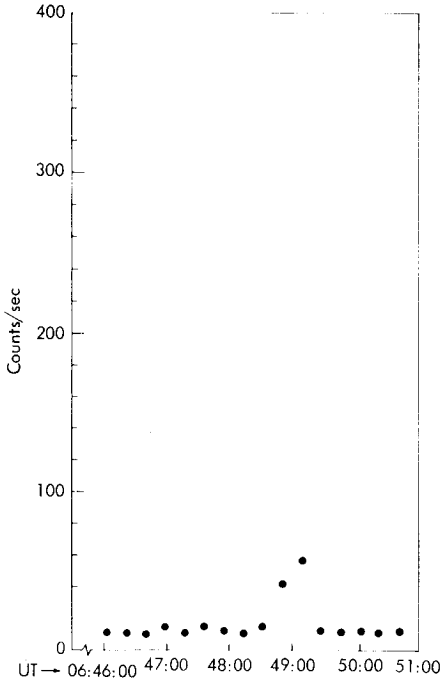

2 FLARE 2 SID
RADIO DATA

Mc/s	Start UT	Max. UT	Duration	Type	Peak Flux*
9400 NAG	0647.5	—	5 min	—	>80
3750 NAG	0647.5	0650.2	5	C	270
2000 NAG	0647.5	0654.9	10	C	80
1500 HHI	0643	0650.0	16.7	f	73
1000 NAG	0647.5	0654.3	10	C	30
545 NED	0648	—	0.8	C	70
200 NED	0648	0649.7	15	C	65

*In units of 10^{-22}w $m^{-2}(c/s)^{-1}$

FIGURE 18–5. High energy x-ray burst, OSO I; $20 < E\gamma < 100$ kev, May 1, 1963.

REFERENCES

1. SCHRADER, C., KAIFER, R. C., WAGNER, J. A., ZINGER, J. H., and BLOOM, S., University of California, Lawrence Radiation Laboratory, 1963, "Proton, Electron Fluxes (75 Kev) from OSO," presented at AGU Spring Meeting, April 1963.
2. Flare, SID, and Radio Data taken from Quarterly Bulletin on Solar Activity No. 137, January/March 1962, and No. 138, April/June 1962.
3. PETERSON, L. E., and WINCKLER, J. R., 1959, *J. Geophys. Research*, 64: 697.
4. CHUBB, T. A., FRIEDMAN, H., and KREPLIN, R. W., 1960, *Proceedings of International Space Science Symposium, Nice*, p. 695.
5. WINCKLER, J. R., MAY, T. C., and MASLEY, A. J., 1961, *J. Geophys. Research*, 66: 316.
6. VETTE, J. I., and CASAL, F. G., 1961, *Phys. Rev. Letters*, 6: 334.
7. ANDERSON, K. A., and WINCKLER, J. R., 1962, *J. Geophys. Res.*, 67: 4103.
8. KUNDU, M. R., 1963, *Space Science Reviews* 2, 438–469.

DISCUSSION

Dr. Zirin: Would you care to say what the photon flux corresponds to?

Mr. Frost: Let's take the burst on April 19, which reached a peak counting rate of 300 counts. The area of the detector is 3.8 cm^2. For the peak counting rate of 300 counts/sec we have 79 counts/cm^2 sec. The average efficiency over the 20 to 100 kev band is 0.90. Therefore we are talking about 88 photons/cm^2 sec in the peak.

I can't give you any idea of what the energy distribution is. I can say it definitely doesn't go above 100 kilovolts for that day.

Dr. Maxwell: I think it is quite clear from the set of data presented in this paper that the small microwave radio bursts are not to be described as type IV bursts, nor are they synchrotron radiation. Presumably we have electrons with energies up to 100 kev threading a magnetoactive plasma. These may possibly set up Cerenkov plasma waves, which will radiate energy in electromagnetic modes by scattering at thermal fluctuations in the medium, or by bremsstrahlung. I think Dr. Kundu probably will agree with me that these microwave radio bursts are not type IV synchrotron radiation.

Dr. Kundu: I think Dr. Takakura wants to explain centimeter wave bursts by synchrotron radiation, including even the impulsive microwave bursts. He assumes that its very short duration can be ascribed to very heavy radiation damping. On the other hand, I think the bremsstrahlung, with nonthermal electrons, has been proposed by many people, including Wild, Weiss, and Smerd in a recent article. I don't think anybody has explained this Cerenkov radiation as the cause of this small microwave burst.

N64-30270

19 COMMENTS ON GAMMA RAYS

GIOVANNI G. FAZIO
Astrophysical Observatory, Smithsonian Institution
Cambridge, Mass.

Two brief comments will be made. The first concerns the high energy gamma ray detector aboard the first Orbiting Solar Observatory (1962ζ1). This experiment was a joint project with Dr. E. M. Hafner, University of Rochester, to search for gamma rays, with energy greater than 100 Mev, from the sun. The principal source of this radiation on the sun is the decay of π-mesons which are produced in proton-proton reactions. Detection of such radiation would indicate the presence of solar protons with billion electron volt energy. Partial reduction of the data has indicated no evidence for this radiation from the sun. The upper limit to the flux from the quiet sun is 2×10^{-3} photon/cm^2 sec, and the upper limit during a flare (e.g., type 3 flare, March 22, 1962) was 10^{-2} photon/cm^2 sec.

The second comment concerns theoretical calculations which Mr. Joseph Dolan, Harvard University, and I have performed in an attempt to predict the gamma ray spectrum of the sun and thus determine what portions of the spectrum would be most interesting to investigate. In the energy region from 10 kev to 1 Mev electron bremsstrahlung radiation is the most important source. Another region which is very important, but which has not been experimentally investigated, is the spectrum between 1 and 10 Mev. The predominant radiation in this region results from the de-excitation of excited states of carbon, nitrogen, and oxygen nuclei produced by proton inelastic scattering. Crude estimates of the flux indicate that this radiation certainly should be detected in a large flare. Future solar observatory satellites should have experiments to search this region of the spectrum. The spectrum above 50 Mev should be pursued further, even though present results are negative. The flux of this radiation is very sensitive to the proton energy spectrum in the flare.

N64 30270

20 SOLAR X-RAY EMISSION—NRL RESULTS

HERBERT FRIEDMAN
*E. O. Hulburt Center for Space Research**
U.S. Naval Research Laboratory, Washington, D.C.

Until very recently, the spectrum of the sun below 100A was known only in broad outline as defined by filter photometers covering various wavelength intervals, that is, 2–8A, 8–20A, 44–60A, and 44–100A. Over a solar cycle these results showed a marked extension of emission to shorter wavelengths and an overall enhancement of emission with increasing sunspot number. X-ray observations at the eclipse of October 12, 1958, and the x-ray pinhole photograph of June 1960 identified the source of x-ray emission with the inner corona—below 40,000 km—and with coronal condensations over chromospheric plages, the same regions responsible for the slowly varying component of radio decimeter wave emission.

At times of large solar flares (class 2+), emission was observed to extend to energies above 100 kev; and increases in the 1–10A emission were adequate to account for sudden ionospheric disturbances. In the flare measurements, pulse amplitude scintillation spectrometers were successfully employed to define the shape of the spectral continuum above 20 kev. X-ray monitor experiments carried in the NRL series of small solar radiation (SR) satellites have established that x-ray enhancements are a most sensitive index of solar activity and that optical classifications of flares are a relatively unreliable index of x-ray emission. The observational bases for these summarized statements are treated in detail in References 1 to 8.

Within the past year new results have added to our detailed knowledge of the solar spectrum and the distribution of x-ray sources in the solar atmosphere. These include measurements of the line spectrum from 1–25A, fan beam scans to resolve the dimensions of active regions, and spectroheliograms in the ultraviolet lines of highly ionized coronal ions. With respect to flare spectra, previously unpublished data in the 2 to 20 kev region are presented below and interpreted in terms of possible thermal mechanisms.

X-RAY SPECTRA, 1–25A

Although steady progress has been made in pushing the optical techniques of grazing incidence ruled grating spectroscopy to extremely short wavelengths, the difficulties grow enormously at wavelengths below 25A. On the other hand, crystal analyzers are now available which can be employed very effectively in the simple Bragg spectrometer for wavelengths below 25A. Using a potassium acid phthalate (KAP) crystal and Geiger counter detector, the spectrum was scanned from an Aerobee rocket on April 4, 1963. The results are listed in Table 20–1 (Reference 9).

X-RAY SPECTROHELIOGRAMS

X-ray pinhole photographs have shown that emission below 50A is concentrated largely in coronal condensations above the plage areas. To define the dimensions of the enhanced regions and their brightnesses relative to the general disk background, fan beam scans have been made (Reference 9) with slit telescopes in wavelength bands 44–60A, 8–20A, and 8–15A. Figure 20–1 is an example of the kind of information derived from such measurements. At the longer wavelengths the background sun contributed substantially to the total flux even though the active region was markedly brighter. At 8–15A, however, the background disk in-

*Jointly supported by the Office of Naval Research and the National Science Foundation.

TABLE 20–1

Wavelengths Below 25A

λ, Observed A (Reference 9)	λ, Predicted or Laboratory Measured A (Reference 10)	I_0, Intensity Above Atm. ($h\nu$ cm^{-2} sec^{-1})	Ion	Transition
13. 7	13. 820	1. 4×10^4	Fe XVII	2p $^1S_0$–3p′ $^1P_1$
15. 0	15. 012	11. 7	Fe XVII	2p $^1S_0$–3d $^3D_1$
15. 25	15. 261	7. 2	Fe XVII	2p $^1S_0$–3d $^1P_1$
16. 0	16. 006	4. 2	O VIII	1s $^2S_{1/2}$–3p $^2P_{3/2,\,1/2}$
16. 72	16. 774	11. 1	Fe XVII	2p $^1S_0$–3s $^1P_1$
17. 03	17. 051	14. 7	Fe XVII	2p $^1S_0$–3s $^3P_1$
17. 7	17. 768	3. 5	O VII	1s^2 $^1S_0$–1s4p $^1P_1$
18. 6	18. 627	5. 0	O VII	1s^2 $^1S_0$–1s3p $^1P_1$
18. 9	18. 969	23. 2	O VIII	1s $^2S_{1/2}$–2p $^2P_{3/2,\,1/2}$
20. 8	20. 910	Very weak	N VII	1s $^2S_{1/2}$–3p $^2P_{3/2,\,1/2}$
21. 55	21. 602	78. 0	O VII	1s^2 $^1S_0$–1s2p $^1P_1$
21. 70	21. 804	36. 2	O VII	1s^2 $^1S_0$–1s2p $^3P_1$
24. 8	24. 781	16. 6	N VII	1s $^2S_{1/2}$–2p $^2P_{3/2,\,1/2}$

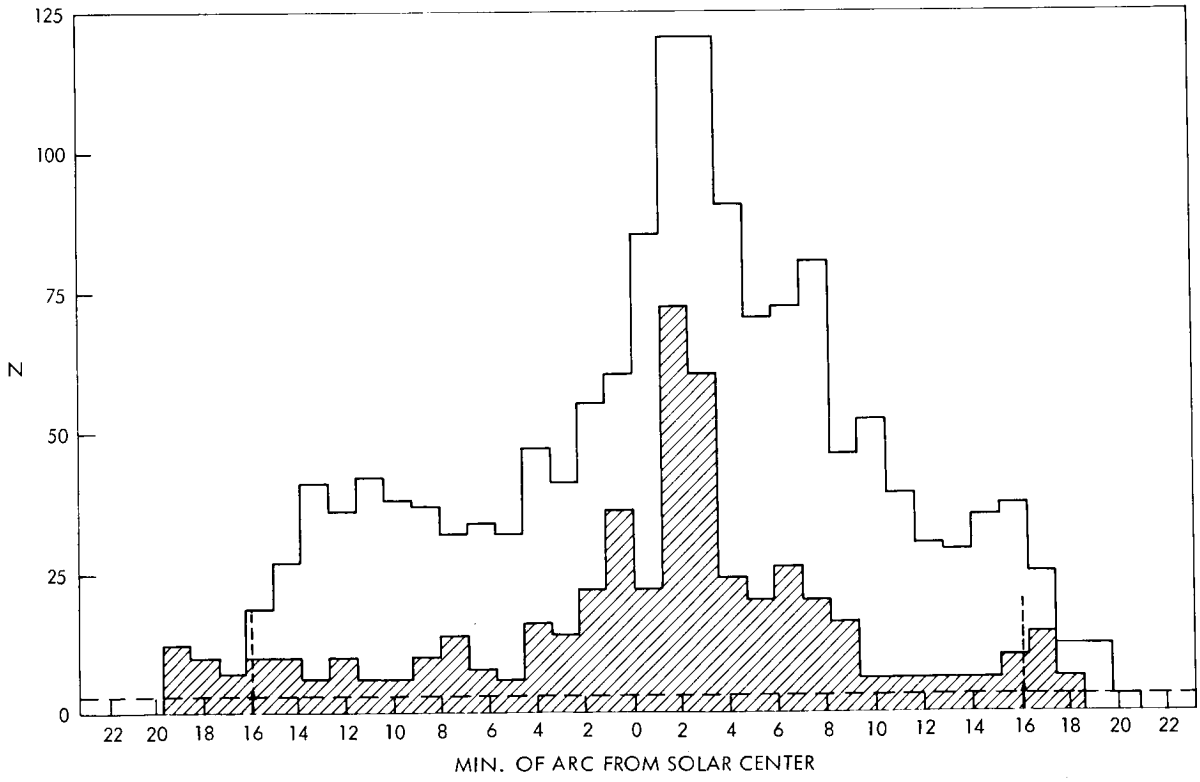

FIGURE 20–1. Scans showing numbers of counts measured per 1 minute interval of scan across the solar disk with fan beam telescope. Instrumental resolution at 8–15A was 1 minute of arc; at 44–60A, 0.6 minute of arc. Limbs of sun are indicated by arrows at plus and minus 16 minutes from center.

tensity was almost negligible and the active region provided nearly all the flux. The fan beam width was 1 minute of arc at 8–15A and 0.5 minute at 44–60A. It is clear that the finest structure at 8–15A is smaller than the instrumental resolution. Furthermore, with reference to the wavelengths of Table 20–1, the interval 8–15A contains only the Fe XVII lines. In association with plages of average brightness it has been found typically that the x-ray brightness ratios of active regions to quiet disk are as follows:

44–60A, 4 : 1
8–20A, 10 : 1
8–15A, 25 : 1

This picture of concentrated emission regions at wavelengths below 50A is duplicated in recent ultraviolet spectroheliograms at wavelengths near 300A. Figure 20–2 shows a series of overlapping spectroheliograms (Reference 11) in two exposures with a grazing incidence spectrum of the sun sandwiched between and printed to the same scale of dispersion. The bright He II (304A) line can be seen to produce an image of the full disk with enhancement in the plages, which are identified with the Ca-K and Hα images at the right. Six major plage regions are present, aligned approximately in two diagonal rows.

In contrast to the He II, 304A image are the images corresponding to Fe XV, 284.1A, and Fe XVI, 335.4A, which are restricted almost exclusively to the plages as was observed for Fe XVII in the x-ray region. It appears, therefore, that with increasing energy of ionization the emission becomes more and more confined to active centers of presumably higher temperature.

X-RAY FLARES

The study of x-ray emission during the course of solar flares began with a pre-IGY series of Rockoon experiments (Reference 2) in 1956. A pronounced increase in x-ray emission accompanying a class 1 flare was observed by means of a GM counter sensitive to a wavelength band from 1 to 10A. The Rockoon technique was superseded during the IGY by the two-stage Nike-Deacon combination of solid propellant motors, which could be launched to ionospheric heights from the ground. Photon counters with windows of different filtration characteristics provided some measure of spectral definition. By 1959, during the IGC, scintillation and proportional counter techniques had been developed to give more detailed spectral information based on pulse amplitude distributions. The results of the scintillation counter measurements in the energy range above 20 kev have been published (Reference 5) and interpreted in terms of various thermal and nonthermal models of the flare regime. The present paper presents some results of proportional counter measurements in the 2 to 20 kev range obtained during the same series of experiments.

Proportional counters were carried on three Nike-Asp rockets, launched during the summer of 1959 as part of the IGC solar flare program of the U.S. Naval Research Laboratory. The detector was a side-window tube of conventional geometry equipped with a beryllium window. Two such detectors were filled with krypton and methane; the third with krypton and methylamine. Figure 20–3 shows the variation of efficiency with photon energy. The pulse amplitude distribution under excitation by Fe^{55} (5.9 kev) had a width at half-maximum of about 25 percent.

In Table 20–2 are listed the times of launch of the three flights and the condition of solar activity. Flight NN 8.68 CF was launched at 1705 UT on August 7, 1959. Solar activity reports from the High Altitude Observatory listed a class 2 flare, beginning at 1551 and ending at 1605 UT. A subflare from the same plage was observed, beginning at 1732 UT and ending at 1759 UT. The Central Radio Propagation Laboratory (CRPL) compilations of solar geophysical data (1959) list sightings of subflares by both the Sacramento Peak and Lockheed Observatories, beginning at 1659 and 1716 UT. The flare at 1551 UT and the subflare at 1732 UT produced sudden ionospheric disturbances (SID) in the form of short-wave fadeouts (SWF). Weak radio noise at 18 Mc/s ended at 1701 UT and resumed again at 1734 UT with moderate intensity. A burst ending at 1630 UT was accompanied by a

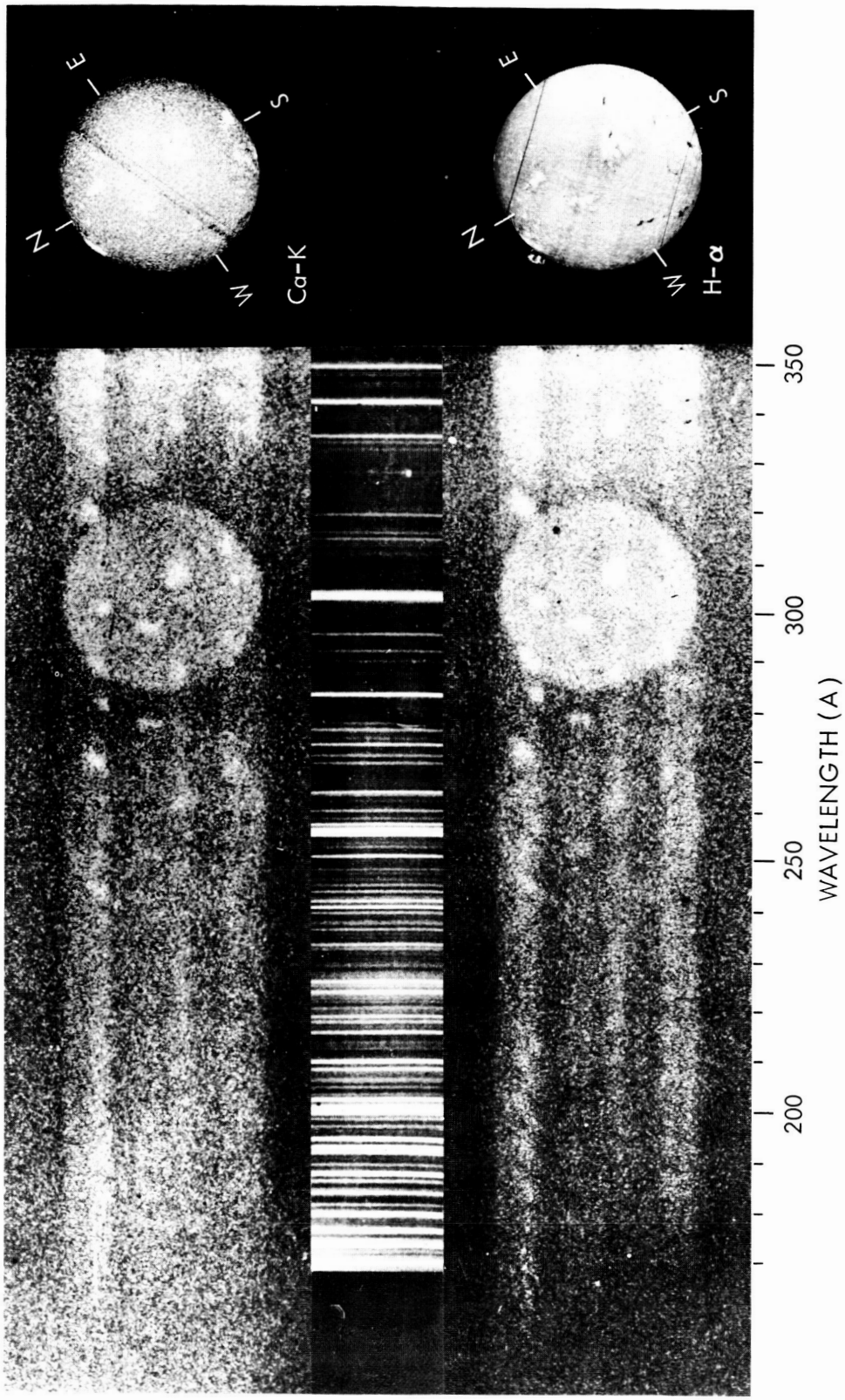

FIGURE 20–2. Spectroheliograms of the sun in the wavelength region 200–350A, obtained with instrument described in text. (J. D. Purcell, D. L. Garrett, and R. Tousey, NRL)

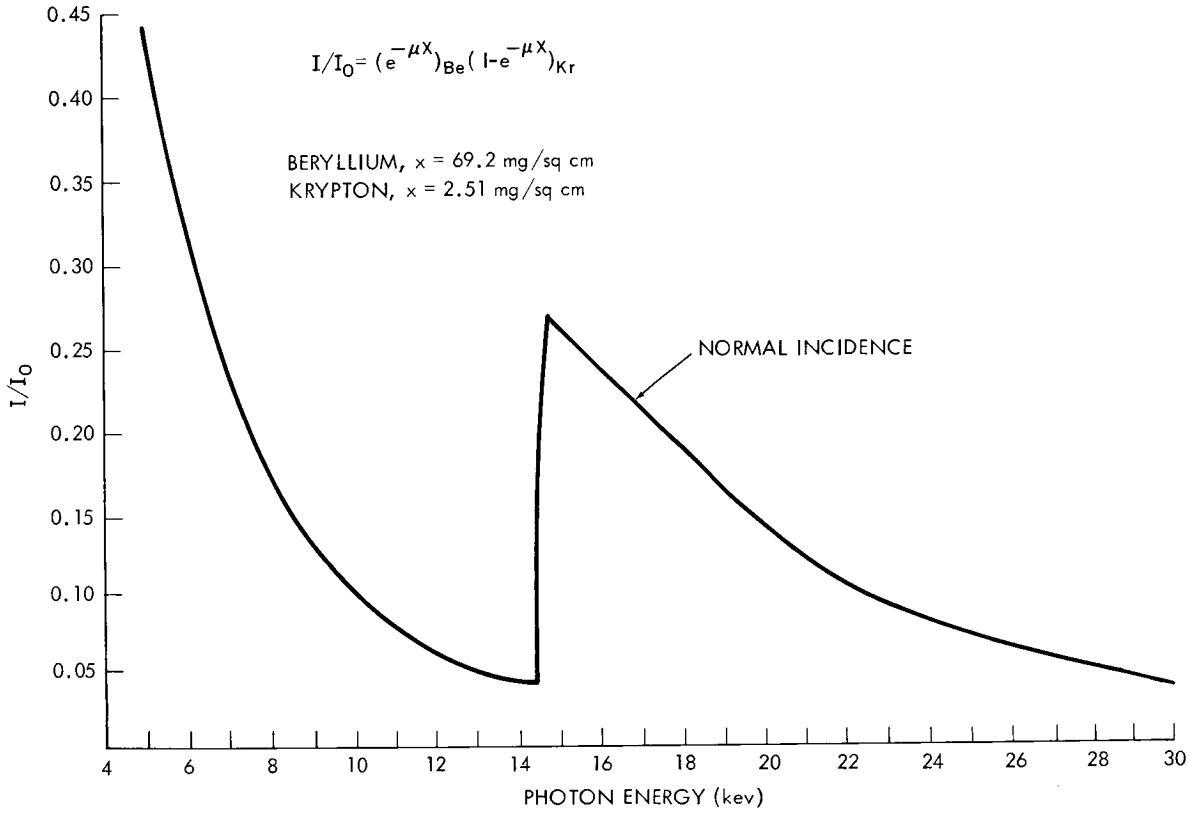

FIGURE 20–3. Efficiency of krypton-gas-filled proportional counter.

TABLE 20–2

Proportional Counter Observations

Date	Launch (UT)	Rocket No.	Solar Flare Classification			
			Importance	Began	Ended	Max.
Aug. 7, 1959	1705	NN 8.68 CF	1—	1659	------	------
Aug. 14, 1959	1600	NN 8.69 CF	-----	Background	------	------
Aug. 28, 1959	1610	NN 8.72 CF	1—	1556	------	------

SCNA class 1 (20 percent cosmic noise absorption). Continuum solar radio emission at 25 to 580 Mc/s was recorded at Fort Davis, Tex., from 1657 to 1700 UT at moderate intensity, and from 1734 to 1738 UT strongly.

Flight NN 8.69 CF was launched 1 week later under relatively quiet conditions. No flares or subflares were reported during the flight, which began at about 1600 UT. A class 1 flare ended at 1450 UT, and a class 1+ flare began at 1804 UT. A subflare was observed at the Wendelstein Observatory at 1629 UT, which may have begun earlier. No ionospheric disturbances were reported within 12 hours of the flight. Moderately intense radio continuum emissions were recorded at Fort Davis on 25 to 580 Mc/s at 1512 and 1609 UT. Faint single bursts of type III solar radio noise were detected at 1538 and 1716 UT. A moderate intensity outburst at 18 Mc began at 1905 UT.

728–629 O—64——11

Flight NN 8.72 CF was launched at 1610 UT on August 28, 1959. A class 1 flare was in progress from before 1656 to at least 1720 UT, and a subflare was reported at 1550 UT. Another subflare was reported at 1556 UT and again at 1630 UT. A widespread, moderately strong solar noise storm on 18 Mc/s began 2 hours before launch and continued until early the next day. Fort Davis reported faint continuum emission (25–580 Mc/s) throughout the time of flight, with a single type III burst occurring exactly at launch time.

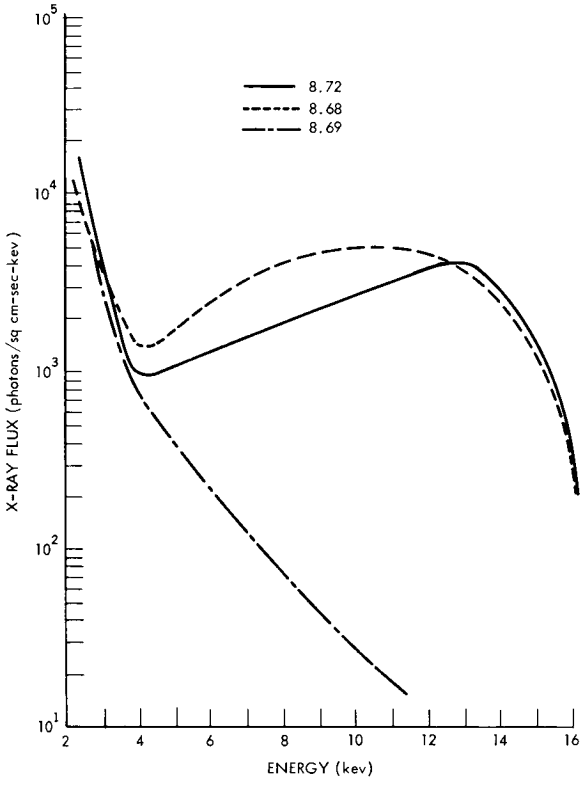

FIGURE 20–4. Comparison of spectra obtained from proportional counters on three different flights.

Figure 20–4 summarizes the results of the three flights. Under quiet conditions Flight 8.72 revealed an intensity decreasing monotonically with increasing energy. The spectrum from 2 to 4 kev roughly fits a 4×10^{6}°K Planckian distribution. In contrast, Flights 8.68 and 8.69 show a marked increase in flux above 4 kev, maximizing in the 10 to 13 kev range and then fading out rapidly toward higher energies. Figures 20–5 and 20–6 show that the spectrum undergoes marked variations even during the few minutes duration of each rocket flight.

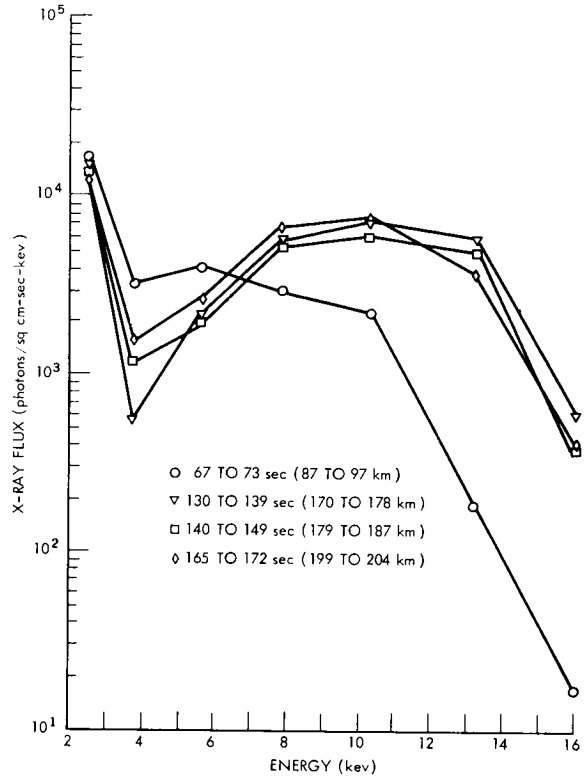

FIGURE 20–5. Spectral variation with time—Flight NN 8.68 CF.

In interpreting these results, only qualitative significance should be attached to the position of the spectral peak. The experiments were performed under relatively primitive conditions by today's standards. Instrumentation packages were checked out at the launching site and then invariably remained stored in the field for relatively long periods without recalibration. No in-flight calibration was provided. It is characteristic of the proportional counters that slight changes in operating voltage produce large changes in gain, which are reflected by shifts in the energy versus pulse-height calibration. The voltage supplies were stabilized by corona discharge tubes, and it is entirely possible that serious shifts occurred between the original calibrations and flight times. We may therefore conclude that the data

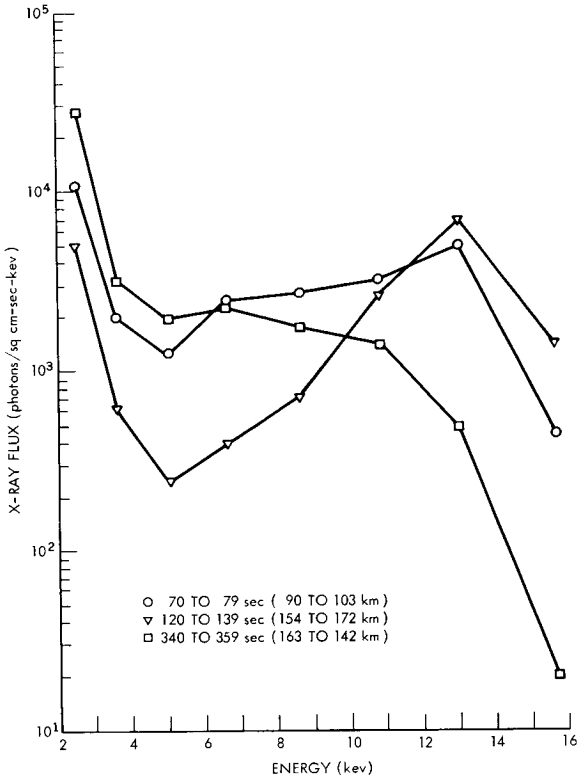

FIGURE 20–6. Spectral variation with time—Flight NN 8.72 CF.

indicate a pronounced peak in the 5 to 15 kev region but cannot specify the maximum energy with any better definition. Table 20–3 lists the wavelengths and relative intensities of x-ray emission lines to be expected at various solar plasma temperatures, according to Elwert's theory (Reference 12). The Fe XXV and XXVI emission lines near 7 kev become relatively intense at the higher temperatures. The series limit of Fe XXVI is 1.37A, and its recombination radiation should therefore exhibit a pronounced edge at about 9 kev. Since the resolution of the proportional counter was only about 25 percent, an emission line or recombination limit would appear as a broad peak in the pulse amplitude spectrum.

According to Kawabata (Reference 13) the spectral distribution of x-ray emission should vary with temperature as shown in Figures 20–7, 20–8, and 20–9 for free-free, free-bound, and line emission. From 2 to 8A, x-ray emission is predominantly the result of free-bound transitions to the K-shells of carbon, nitrogen, oxygen, and neon if the temperature is less than about 3×10^7 °K. Above this temperature, free-free transitions rapidly become more important. The integral of line emission is always less than the continuum flux above 10^7 °K. These calculations suggest that the recombination limit at Fe XXV may show up prominently at temperatures of a few tens of millions of degrees. When scanned with the relatively broad resolution of a proportional counter, the increased radiation to the high energy side of the limit may account for a hump in the spectral distribution with an apparent peak at 10 to 12 kev. Although line emission from Fe XXV and Fe XXVI would come up

TABLE 20–3

Relative Intensities of X-Ray Lines

Emission Lines	λ (A)	10^7 °K	2×10^7 °K	5×10^7 °K	10^8 °K
Fe XXIII	12.0	5.2	1.5	--------	--------
Fe XXIV	11.0	2.1	3.6	0.1	--------
Mg XI	9.3	0.6	--------	--------	--------
Mg XII	8.4	1.3	0.9	0.2	--------
Si XIII	6.7	2.2	0.6	--------	--------
Si XIV	6.3	0.6	1.9	0.7	--------
S XV	5.2	0.5	1.0	--------	--------
S XVI	4.3	-------	0.6	0.5	0.007
Fe XXV	1.9	-------	0.39	8.3	10.0
Fe XXVI	1.7	-------	0.10	0.64	5.0

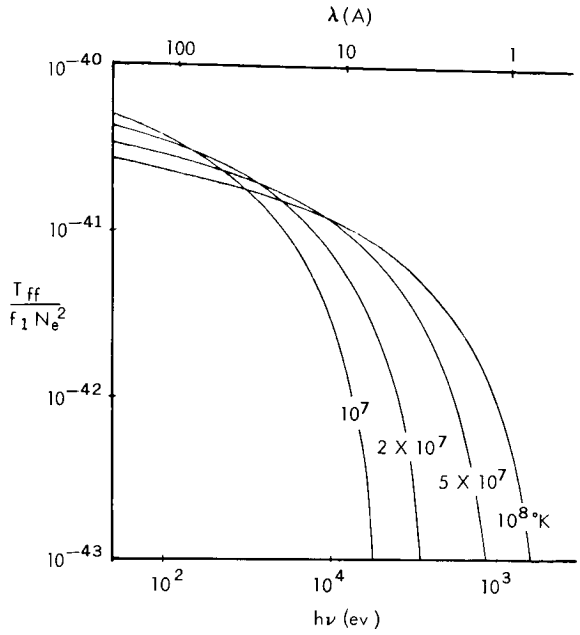

FIGURE 20-7. Computed x-ray spectra of free-free emission. (After Kawabata, 1960)

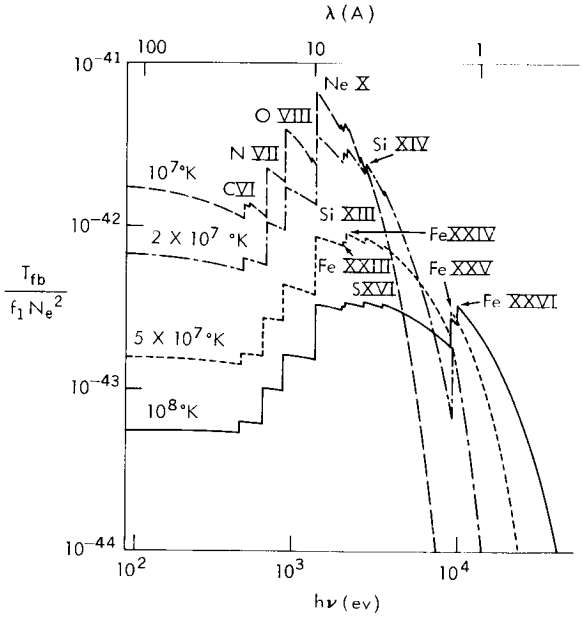

FIGURE 20-8. Computed x-ray spectra of free-bound emission. (After Kawabata, 1960)

sharply at temperatures greater than 5×10^7 degrees, it would be swamped by continuum radiation when scanned with the resolution of the proportional counter. In summary, the measurements and theory are suggestive of local temperatures of 20 to 30 million degrees in active regions characterized by subflare activity. High resolution line spectroscopy could resolve the question of the existence of such thermal regimes because of the strong temperature dependence of ion abundances and their resulting line intensities. Such spectroscopy is being planned for future OSO satellites.

It is interesting to consider the evidence for spectral variations in solar x-ray flux in relation to ionospheric behavior. Taubenheim (Reference 14) has used analyses of oblique incidence field strength records and simultaneous observations of solar microwave radio noise to derive a model of the absorbing region responsible for sudden ionospheric disturbances. From a study of the rate of change of the excess total absorption with time during a short-wave fadeout, Taubenheim concluded that the absorbing layer had a thickness of about 10 km. Although absorption data do not by themselves indicate the height level at which absorption takes place, the coincidence of short-wave fadeout with long-wave and very low frequency (VLF) effects supports the hypothesis that the flare radiation ionizes a layer centered between 70 and 75 km. According to Volland (Reference 15), comparison of SWF and VLF effects shows that at least 50 percent of the excess absorption produced by flare radiation takes place below 80 km. To produce a thin layer for the short-wave fadeout, the ionizing radiation must be largely monochromatic. Since the scale height in D-region is 6 km, a simple Chapman layer would be consistent with Taubenheim's model. He estimates that x rays of wavelength 2.5 to 3A are required to produce a layer at 70 to 75 km.

Radio observations also may contain information about the temporal behavior of the ionizing flux. Statistical studies by Hachenberg and Kruger (Reference 16) have shown a strong coincidence between 3.2 cm bursts and SWF. Of eighteen SWF effects, Taubenheim found that the radio burst at 3.2 cm had ended before the exponential decrease in radio absorption

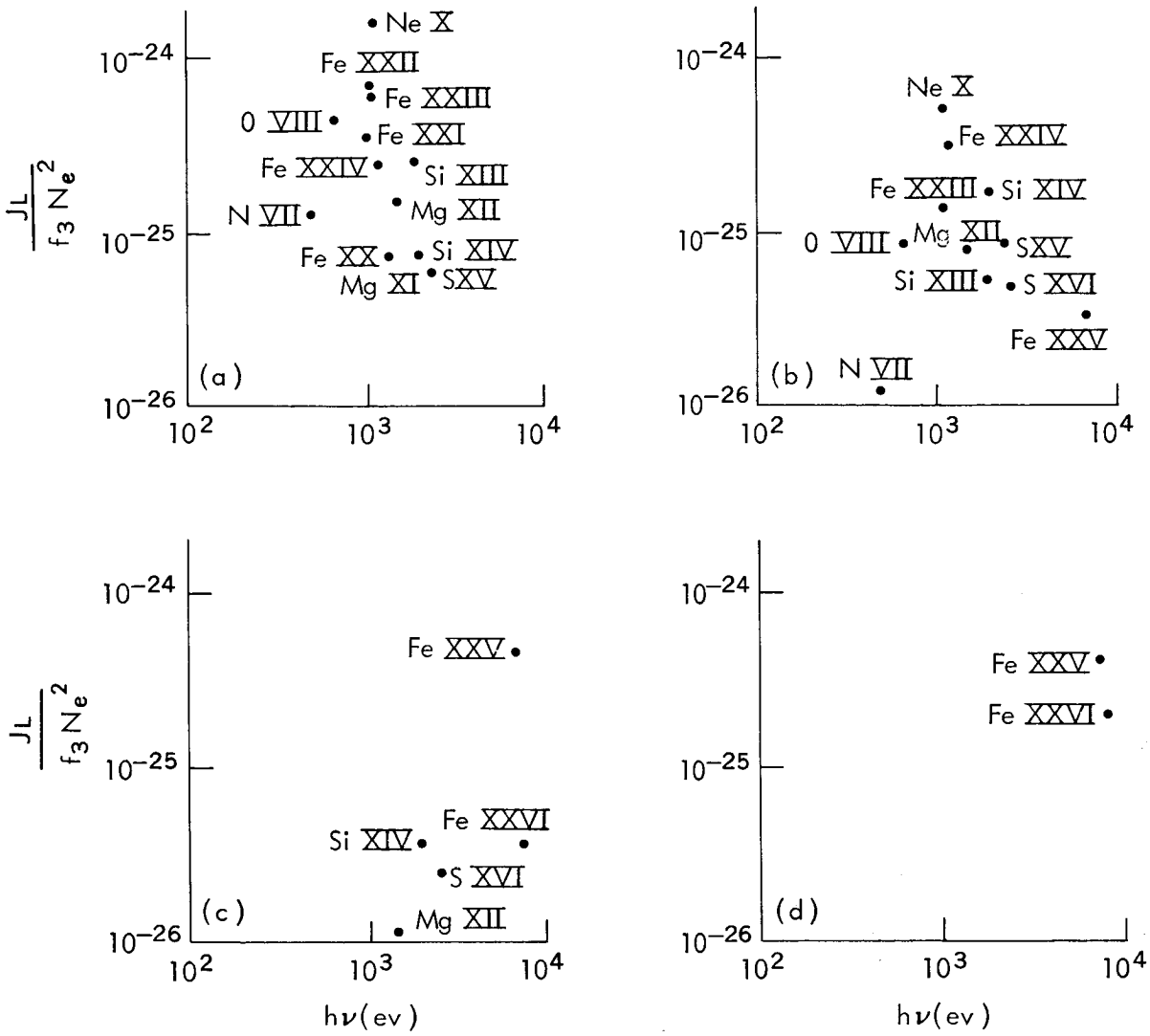

FIGURE 20–9. Computed x-ray spectra of line emission: (a) 10^7 °K, (b) 2×10^7 °K, (c) 5×10^7 °K, (d) 10^8 °K. (After Kawabata, 1960)

had begun. In the remaining cases, the exponential decay began when the radio burst had decreased in intensity to a few percent of its maximum value and continued beyond the end of the microwave burst. Maximum absorption was delayed by an average of 5 minutes after the burst maximum. Assuming a simple attachment law, Taubenheim calculated the radiation intensity versus time from the absorption. Some of the computed intensity curves exhibited a complex form, corresponding to similar complexity in the radio bursts. At other times, the computed intensity distribution with time showed a simple maximum similar to the 3.2 cm burst curve. A common feature in all cases was a sharp maximum of the ionizing radiation generally coinciding with the peak of the radio burst. This coincidence was not always precise—the x-ray peak sometimes being delayed up to 3 minutes beyond the 3 cm peak.

Various investigators have proposed models of a sudden ionospheric disturbance based on flashes of radiation ionizing the lower portion of the D-region. Warwick and Zirin (Reference 17), by fitting ionization and recombination

rates to the observed time variation of electron density during a short-wave fadeout, concluded that the excess ionizing radiation appears as an instantaneous flash. Swift's model (Reference 18) proposes a short burst of hard radiation at about 13 kev, lasting for only 6 minutes in a typical SID.

Analysis of events corresponding to ionization at different levels of D-region indicates complex time variations in the ionization at different levels. Bureau (Reference 19) has pointed out that the different types of SID have quite different temporal distributions. The sudden enhancement of atmospherics (SEA) on 8 to 16 km wavelengths is associated with reflection at a height of about 85 km. The SEA phenomenon starts to recover later and persists beyond the effects of the sudden phase anomaly (SPA) at longer wavelengths and the short-wave fadeout at shorter wavelengths. The SPA presumably occurs at lower and the SWF at higher altitudes than the SEA. Gregory's observations (Reference 20) of fixed frequency soundings at 1.75 Mc/s during two SID's showed that, in one case, echoes from the lowest level disappeared first and were replaced at maximum of the fadeout by echoes which were displaced downward by a few kilometers and, in the second case, high E-region echoes disappeared first. The echoes moved progressively to lower levels as they faded away, leaving lowest level echoes at the maximum of the SID. During the recovery phase, the echoes returned from the bottom up with the lowest levels recovering first and the E-region echoes last. These observations suggest that temporal variations in the spectrum and, therefore, the penetrating power of the flare x-ray emission may be an important factor in the shifting levels of ionization.

The evidence presented here from rocket experiments is very fragmentary, but it appears that complex spectral variations in the radiation affecting D-region do occur during the course of even a small flare. The emission detected at energies above 20 kev during class 2+ flares (Reference 5) is undoubtedly bremsstrahlung produced by thermalized electrons, although it is not clear whether the original production of high energy electrons is by a thermal or nonthermal process. If the observed spectrum (Figure 20–10) is extrapolated back to lower energies, the flux falls one to two orders of magnitude short of that required to produce the ionization deduced by Taubenheim at 70 to 75 km. On the other hand, an emission peak such as observed in the proportional counter measurements would produce adequate ionization at the required level.

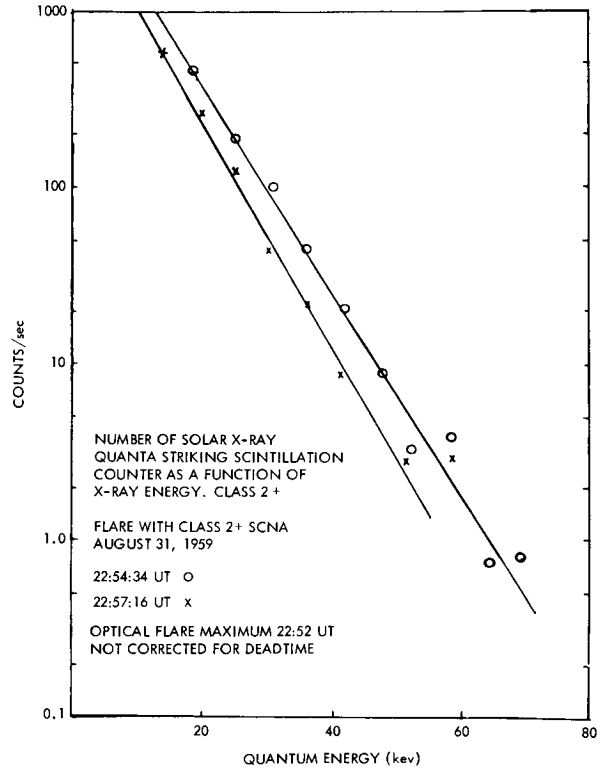

FIGURE 20–10. Spectra of flare x-ray emission 20–80 kev.

REFERENCES

1. FRIEDMAN, H., 1963, "Ultraviolet and X-Rays from the Sun," *Annual Review of Astronomy and Astrophysics*, Vol. 1, ed. L. Goldberg, pp. 59–96.
2. FRIEDMAN, H., 1962, "Solar Observations Obtained from Vertical Sounding," *Reports on Progress in Physics*, Vol. XXV, ed. A. C. Stickland, pp. 163–217.

3. FRIEDMAN, H., 1963, "Ionospheric Constitution and Ionizing Radiations," *Proc. of Internatl. Conf. on the Ionosphere*, London, July 1962, publ. by Inst. of Physics and The Phys. Soc., pp. 3–18.
4. KREPLIN, R. W., 1961, *Annales de Geophysique*, 17(2): 151.
5. CHUBB, T. A., FRIEDMAN, H., and KREPLIN, R. W., 1960, *J. Geophys. Res.*, 65: 1831.
6. KREPLIN, R. W., CHUBB, T. A., and FRIEDMAN, H., 1962, *J. Geophys. Res.*, 67: 2231.
7. BLAKE, R. L., CHUBB, T. A., FRIEDMAN, H., and UNZICKER, A. E., 1963, *Astrophys. J.* 137: 3.
8. ACTON, L. W., KREPLIN, R. W., CHUBB, T. A., MEEKINS, J. F., 1963, *J. Geophys. Res.*, 68: 3335.
9. BLAKE, R. L., CHUBB, T. A., FRIEDMAN H., and UNZICKER, A. E., 1963, unpublished.
10. TYREN, F., 1938, *Z. Physik*, 111: 314.
11. PURCELL, J. D., and TOUSEY, R., 1963, unpublished.
12. ELWERT, G., 1961, *J. Geophys. Res.*, 66: 391.
13. KAWABATA, K., 1960, *Rept. Ion. Space Res. Japan*, XIV: 405.
14. TAUBENHEIM, J., 1962, *J. Atmos. Terr. Phys.*, 24: 191.
15. VOLLAND, H., 1960, Tech. Ber. Nr. 37, Heinrich-Hertz Institut, Berlin-Charlottenburg.
16. HACHENBERG, O., and KRUGER, A., 1959, *J. Atmos. Terr. Phys.*, 17: 20.
17. WARWICK, J., and ZIRIN, H., 1957, High Altitude Observatory Scientific Report No. 7.
18. SWIFT, D. W., 1961, *J. Atmos. Terr. Phys.*, 23: 29.
19. BUREAU, R., 1947, *L'Onde Electrique*, 27: 45.
20. GREGORY, J. B., 1958, *J. Geophys. Res.*, 63: 273.

DISCUSSION

Dr. Lindsay: The point I wanted to raise was a word of caution concerning this pinhole camera photograph. Recently Giovanni and I flew an x-ray telescope using a filter that was as closely identical to the one that NRL flew as I believe one can be made.

Actually, this should have been some 20 or more times more sensitive than the pinhole system. Amazingly enough, the light from the sun came barreling through this filter.

We tested the filter before flight and after flight, exposing it in the telescope to the white-light sun for 10 minutes with no darkening of the film. We were wondering what caused this.

We don't have a conclusive answer, but we have estimates of the transmission of this filter in the extreme UEV above 170A; and it turns out that the best estimate is that it is about 1/20,000. In the 44 to 60A region this filter should have a transmission of about 1/20th. So, if we have a thousand times more flux above 170A, this is probably what we are seeing.

Dr. Friedman: I am very confident that the filters we have used in our experiments were transmitting x rays, and the pictures were produced by x-ray emission. The experiments have been repeated several times. Filters of the same material and different thicknesses have been used, and the densities have varied according to the predicted transmission as a function of thickness.

We have tested the filters as thoroughly as we can by exposure to the full spectrum of ultraviolet light and to x-ray sources, and I have no reason to believe that they were not transmitting as calculated and as measured.

Direct measurements have shown that the flux from 170A to 1000A is of the order of 1 erg cm^{-2} sec^{-1}, a factor of at most 10 rather than 1000 times the flux below 60 A.

N64-30271

21 RADIO OBSERVATIONS OF SOLAR FLARES

J. P. Wild
Radiophysics Laboratory
CSIRO, Sydney, Australia

30271

ABST

Solar flares have been observed on the earth throughout the range of radio wavelengths capable of penetrating the earth's atmosphere—that is, from $\lambda \approx 4$ mm to $\lambda \approx 60$ m. The bursts of solar radiation recorded in this vast range seem to fall phenomenologically into three distinct, though perhaps overlapping, wavelength ranges. We refer to these ranges as the *microwaves* ($\lesssim 20$ cm), the *decimeter waves* (10 cm–1 mm), and the *meter waves* ($\gtrsim 1$ m). Broadly, the physical distinction between phenomena in the different ranges can be traced to the region of origin of the radiation—microwaves mainly in the chromosphere, meter waves in the corona, and decimeter waves presumably in the region of transition though often confused by overlapping coronal and chromospheric effects.

We shall here give emphasis to the division between microwave and meter waves and say less about the intermediate decimeter waves, which are at present more difficult to interpret physically.

Author

GRADUAL EFFECTS

Flares originate in active regions which initially appear in the microwave spectrum as fairly stable bright patches roughly covering the areas of optical plages. Their microwave intensity is enhanced because they are rather hotter and much denser than their surroundings. It is well known optically that sometimes minor flares or the preludes of other flares begin by a gradual brightening of part of a plage region. A somewhat similar phenomenon occurs in the microwave spectrum [e.g., Figure 21–1 (a)].

Part of the radio plage, or a region close to it, gradually intensifies; for example, the brightness temperature at 3 cm wavelength increases from perhaps 5×10^5 °K to 10^6 °K in a period of 5 to 10 minutes.

In some events of minor significance no further developments take place, and the intensity gradually decreases to its former level after 10 to 30 minutes. Covington called this phenomenon the *gradual rise and fall;* it is thought to be thermal in origin, presumably due to the combined effects of magnetic compression and heating in a localized region. The dominant microscopic mechanism of emission and absorption is probably the free-free transitions of electrons in the field of protons (*bremsstrahlung*).

THE FLASH PHASE

The Microwave Impulsive Burst

Many optical flares are known to exhibit a *sudden* intensification and expansion—the so-called "flash phase"—which may be additional to the more gradual increases described above. The flash phase characteristically marks the onset of the main radio emission. At microwavelengths (Figure 21–1) a source region subtending 1′ to 2′ arc rises suddenly to a maximum brightness temperature sometimes exceeding 10^8 °K within a period of as little as 1 minute. Further peaks may appear before the level subsides, a few minutes after the start. This Covington called the microwave *impulsive burst.* Striking examples have been reported by Kundu and by Anderson and Winckler (e.g., Figure 21–2) in which the burst coincides accurately in time of commencement, and even in detailed features, with the burst of "hard" (20–500 kev) x rays.

According to Tanaka, the microwave emission may be weakly circularly polarized in the

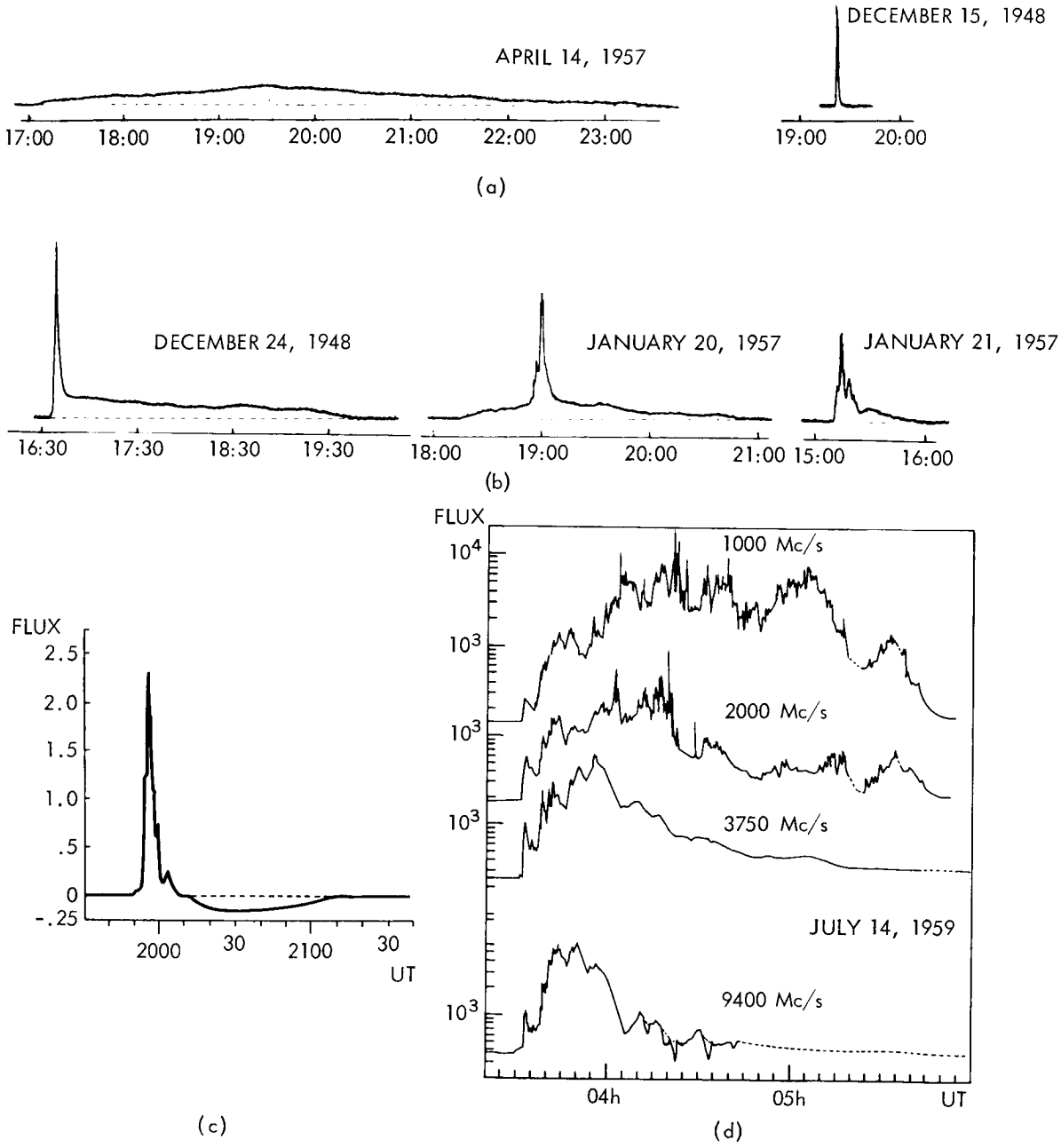

FIGURE 21-1. Types of microwave bursts: (a) the basic types: gradual rise and fall (left) and impulsive, (b) combinations of the basic types, (c) absorption following an impulsive burst, and (d) outburst (type IV). [(a) to (c): from Covington, and (d): Kakinuma and Hatanaka]

sense corresponding to the extraordinary mode. Its spectrum is a continuum whose envelope differs from one event to another; but there appear to be characteristic patterns, two of which are shown in Figure 21-3 (due to Hachenburg and Wallis). In case (a) the curve reaches a flat maximum extending into the upper frequency limit; in the case (b) there is a distinct maximum and the curve falls off rapidly towards the higher frequencies. Any

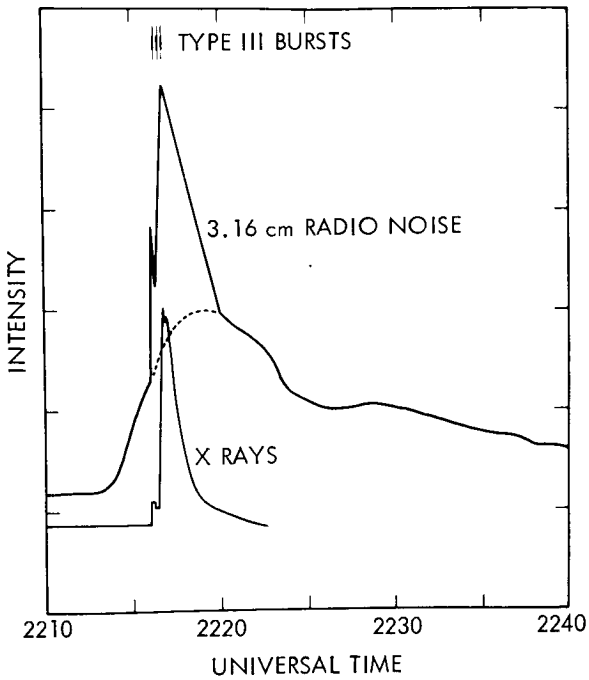

FIGURE 21–2. Coincident occurrence of x-ray burst, microwave impulsive burst, and meter-wave type III bursts at the flash phase of a flare: September 28, 1961. (Anderson and Winckler; radio data from Tokyo Astronomical Observatory)

one of the curves of the first class is reminiscent of the bremsstrahlung spectrum of a slab of isothermal plasma, the gas being optically thick in the (roughly square-law) rising part and optically thin in the flat part; however, the same model would predict that, as the radiation temperature rises, the flux of the optically thick part should rise while that of the optically thin part should fall—that is, successive curves should cross one another before flattening. This effect is not observed, nor, invoking the angular size observations of Kundu, could one account for the rise in flux in terms of a constant-temperature bremsstrahlung source of varying area. It is possible that some strict combination of concurrent increases in both temperature and density could account for the observations by the bremsstrahlung process, but the requirement seems artificial and improbable.

Hence the evidence is against bremsstrahlung being the dominant mechanism. The suggested alternative, which covers all spectral patterns, is the synchrotron mechanism; Takakura has thus accounted for the general character of the observed intensity, lifetime, bandwidth, and polarization in terms of electrons with energy $\approx 10^5$ electron volts in a magnetic field of $\approx 10^3$ gauss.

At the same time Anderson, Winckler, and Peterson have demonstrated that electrons with similar energy can account for the simultaneous x-ray burst by bremsstrahlung. Some 10^{33} fast electrons injected from the source region into chromospheric gas of density 10^{12} cm^{-3} are required in a typical case; if the source region is assumed to have a volume of 10^{28} cm^3 and an electron density of 3×10^{10} cm^{-3}, only one electron in 3×10^5 need be accelerated to energies above 20 kev. Such electrons are comfortably adequate to account for the microwave emission so that on present evidence we can, by postulating their existence, account satisfactorily for the combined microwave/x-ray event.

The Meter-Wave Type III Bursts

Further elucidation of the flash phase is obtained from meter wave observations, where, coincident with the time of maximum expansion, the type III bursts occur. (Only 1 in perhaps 7 flares and subflares produce type III bursts, but of those flares and subflares which show a *distinctive* flash phase the ratio is probably closer to 1 in 2.)

On dynamic spectrum records an individual type III burst appears as a broad spectral maximum which drifts rapidly from high to low frequencies at rates of ≈ 10–10^2 Mc/s per sec. (Examples of type III spectra are to be found in Figures 21–5 and 21–8.) Some type III bursts span the whole wavelength range between about 1 m and the longest wavelengths that penetrate the ionosphere (≈ 60 m); others are confined to part of this range. In some, the frequency drift decreases, vanishes, or even reverses—the latter yielding the "inverted U" dynamic spectrum.

In some type III bursts one can recognize a 2:1 harmonic structure. Their *apparent* angular size (the contribution of scattering is unknown) increases with wavelength from 1′ or 2′ arc near 1 meter (300 Mc/s) to 10′ arc or more near 6 meters (50 Mc/s). It was shown by

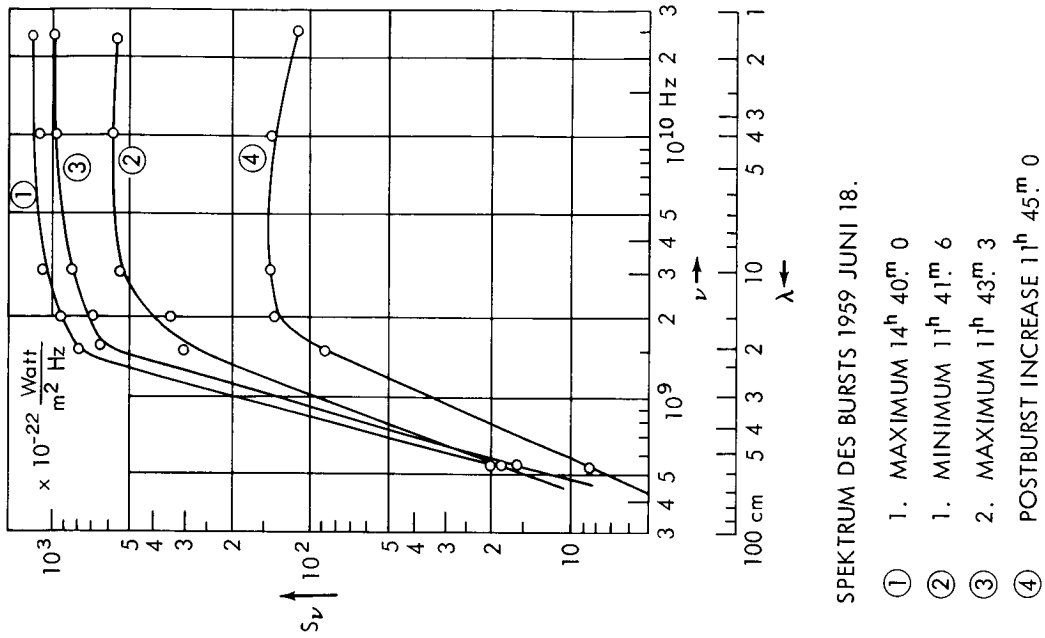

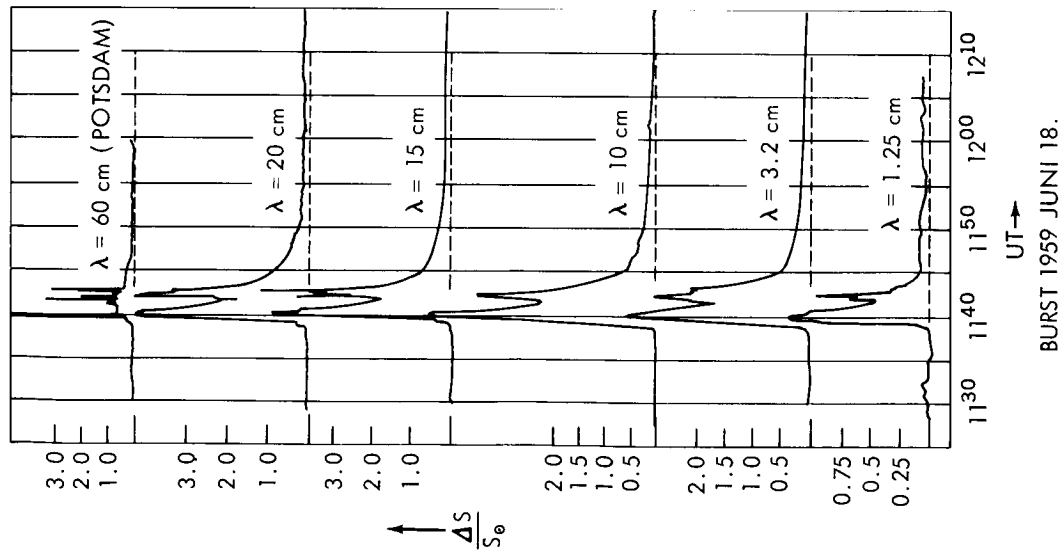

(a) A burst whose spectrum flattens in the centimeter range.

FIGURE 21–3. Time profiles and spectra of two mocrowave bursts. (Hachenburg and Wallis)

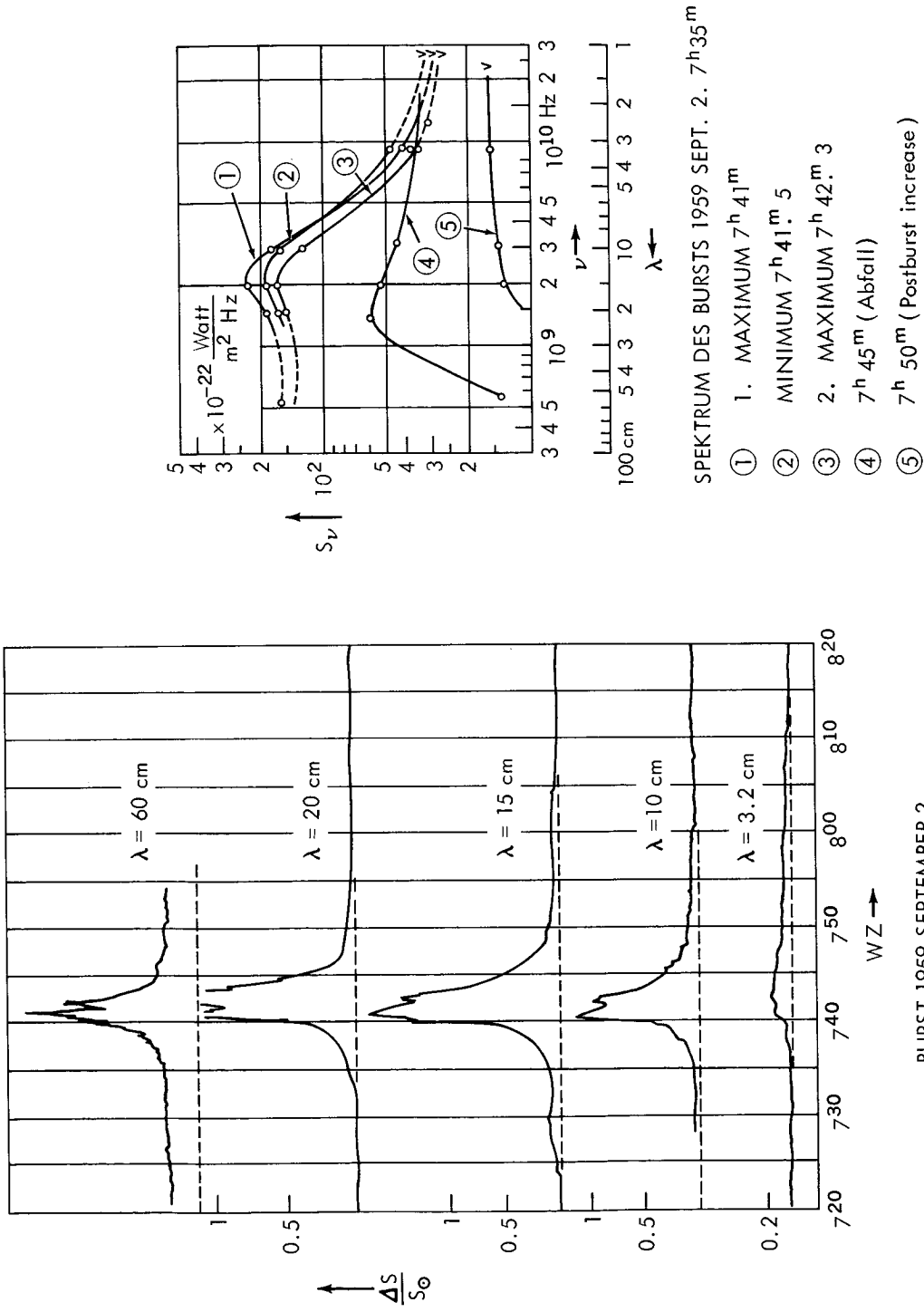

(b) A burst whose spectrum decreases with frequency in the centimeter range.

FIGURE 21–3. Concluded.

Wild, Sheridan, and Neylan that, when observed over limb flares, the height of origin increases with wavelength. On current evidence the height rises from about 0.3 R_0 at 1.5 m (200 Mc/s) to 1.0 R_0 near 7 m ($\approx$40 Mc/s). The bursts, which last a few seconds individually, appear in groups of 1 to 100, typically $\sim$10, and are often associated with short periods ($\sim$1 minute) of continuum radiation known as type V bursts. Their brightness temperature ranges up to $\sim 10^{11}$ °K.

The observed characteristics of type III bursts are consistent with the interpretation known as the "plasma hypothesis," which asserts that their source is a burst of electrons traveling out from the inner corona along coronal streamers at speeds of $\approx$0.2–0.7c, exciting in their path the successively decreasing local coronal plasma frequencies. This velocity range corresponds to the energy range 10 to 200 kev. The existence of 2:1 harmonics greatly restricts the possible processes of radio wave generation; the favoured mechanism is one in which the electron stream excites coherent Cerenkov plasma waves which generate radio waves at the first two harmonics of the plasma frequency by scattering on local coronal inhomogeneities.

Calculations based on Bohm and Gross's expression for the intensity of coherent plasma waves (stabilized by collisional damping) and Ginzburg and Zhelezniakov's expression for the radiat on efficiency of the scattering process show that, for electrons with type III energies, the observed radio emission near 100 Mc/s requires a stream density of about 1 percent of that of the local plasma frequency. Hence, assuming a source area of 10^{10} cm$\times 10^{10}$ cm, a source depth of 10^9 cm, and a local plasma frequency of 10^8 cm^{-3}, we find that 10^{35} stream electrons are required. A group of 10 bursts would thus require 10^{36} electrons.

Viewing the meter wave, microwave, and x-ray results as a whole, the most significant point is that the whole of the flash-phase phenomenon can be attributed to the sudden acceleration of electrons to energies in the 10 to 100 kev range. Those escaping freely outward generate type III bursts, those traveling downward from or trapped in the neighborhood of the flare region generate the microwaves and x rays. Rather more electrons may be required to explain the meter waves. It seems most unlikely that the electrons, traveling at $\sim$½ c, are accompanied by protons (whose energy would then approach the Bev range), since type III bursts are often observed with the most trivial (or even unobserved) optical flares.

The process of acceleration is not known. The most enlightening evidence comes from type III bursts by which we see the electrons as a series of discrete pulses separated in time by a few seconds. The acceleration time must be $\lesssim$1 sec; and hence, adopting calculations by Parker, the Fermi process seems to be eliminated. Acceleration by the pinch effect, often suggested in the past in connection with flares, seems worth investigating if only to explain the flash-phase electrons. The observation of quasi regularity of type III bursts within a group is distinctly suggestive of the repeated pinches observed in laboratory experiments.

A further vital problem is posed by the apparent freedom with which many type III bursts escape roughly radially from the sun and with nearly uniform speed despite the complex magnetic spot fields to which electrons must remain tightly bound. One must postulate either a highly radial field structure or that escape occurs within neutral planes. The latter alternative is attractive in the light of some current flare theories and observations (controversial though they may be). My colleague Dr. A. A. Weiss and I recently have calculated the effect of injecting instantaneously a bunch of electrons with gaussian velocity distribution into a neutral plane configuration such that the field outside the plane falls off exponentially in the "vertical" direction. The result, shown in Figure 21–4, shows that the densities of electrons crossing successive height layers bear a general resemblance to the time profiles of type III bursts at spaced frequencies. A detailed correspondence would not necessarily be expected, since a variety of effects other than electron content will modify the radiation profiles. No difficulty has yet appeared in applying the neutral plane theory, although a rather similar result might be expected for

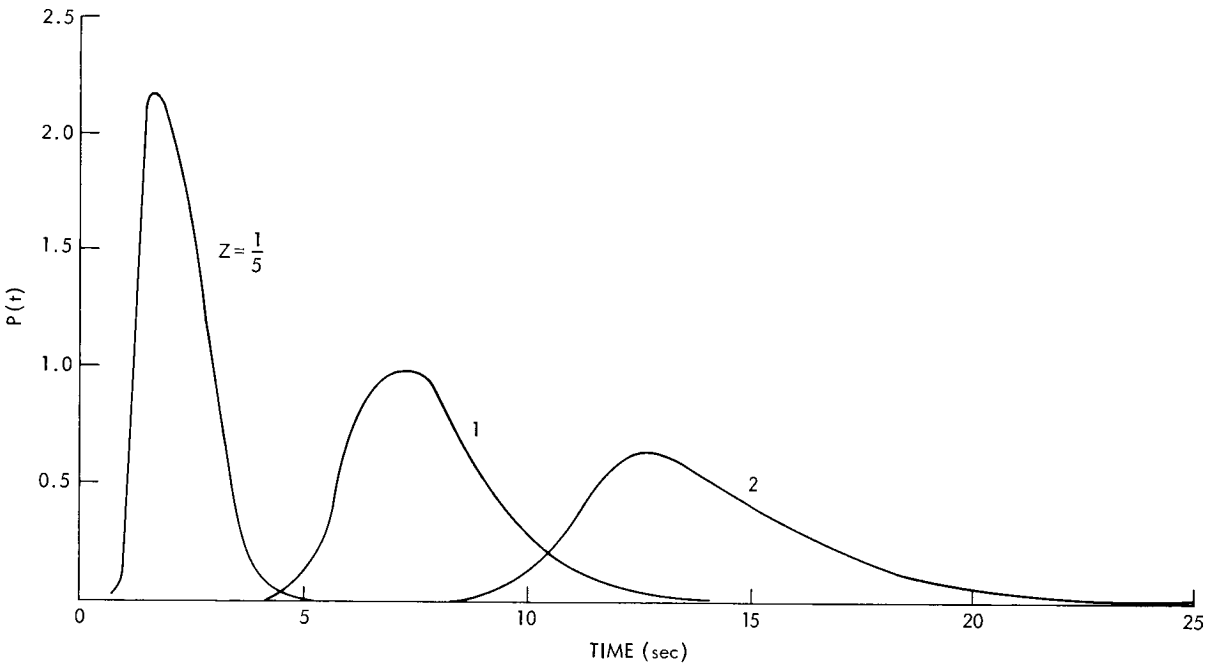

FIGURE 21–4. Result of a calculation relating to a model of a type III burst. An isotropic flux of electrons with gaussian velocity distribution ($\Delta v_{rms}/v = 1/6$) is assumed to emanate from a point on the neutral plane of a simple magnetic-field configuration at time $t=0$. Along a line parallel to the z-axis, which lies in the neutral plane, the magnetic field decreases exponentially with z. The three curves show the relative number of electrons crossing successive planes of constant z, and are intended to simulate the number of electrons crossing plasma levels in the solar atmosphere. Quantities have been chosen to suit solar conditions as far as these are known. (Similar results are obtained for magnetic fields decreasing exponentially in the z-direction in the absence of a neutral plane.) (Weiss and Wild)

electrons escaping along radial field lines, in the absence of neutral planes.

THE SECOND PHASE

Meter Waves

Most flares, especially small ones of Importance 1 or 1−, exhibit no more in the radio spectrum than the flash-phase phenomena described above. With certain large flares, however, a radio "outburst" occurs involving a second more energetic and more complex phase in addition to part or all of the flash-phase accompaniments. In current perspective we may identify such outbursts with eruptions of sufficient energy to cause the mass movement of ions, as well as electrons, far beyond the tight, magnetically bounded region round the flare.

The distinction between the two phases is most marked at meter wavelengths, where the second phase is characteristically introduced by a type II burst, beginning several minutes after the type III bursts have subsided (see Figure 21–5). Type II bursts are defined by the slow frequency drift ($\lesssim 1$ Mc/s per sec) of their spectral features; their duration is of the order of 10 minutes; their angular size ($\sim 10'$ arc) and intensity indicate brightness temperatures up to about 10^{11} °K; their polarization is random; they often show pronounced 2:1 harmonic structure, while their spectral form varies from simple narrow-band—sometimes showing a characteristic frequency split of a few Mc/s (e.g., Figure 21–5)—to highly complex structures. Position measurements at different frequencies indicate a behavior similar to those of type III bursts, and again are consistent with the plasma hypothesis.

Type II, like type III, bursts are interpreted in terms of plasma radiation excited

728–629 O—64——12

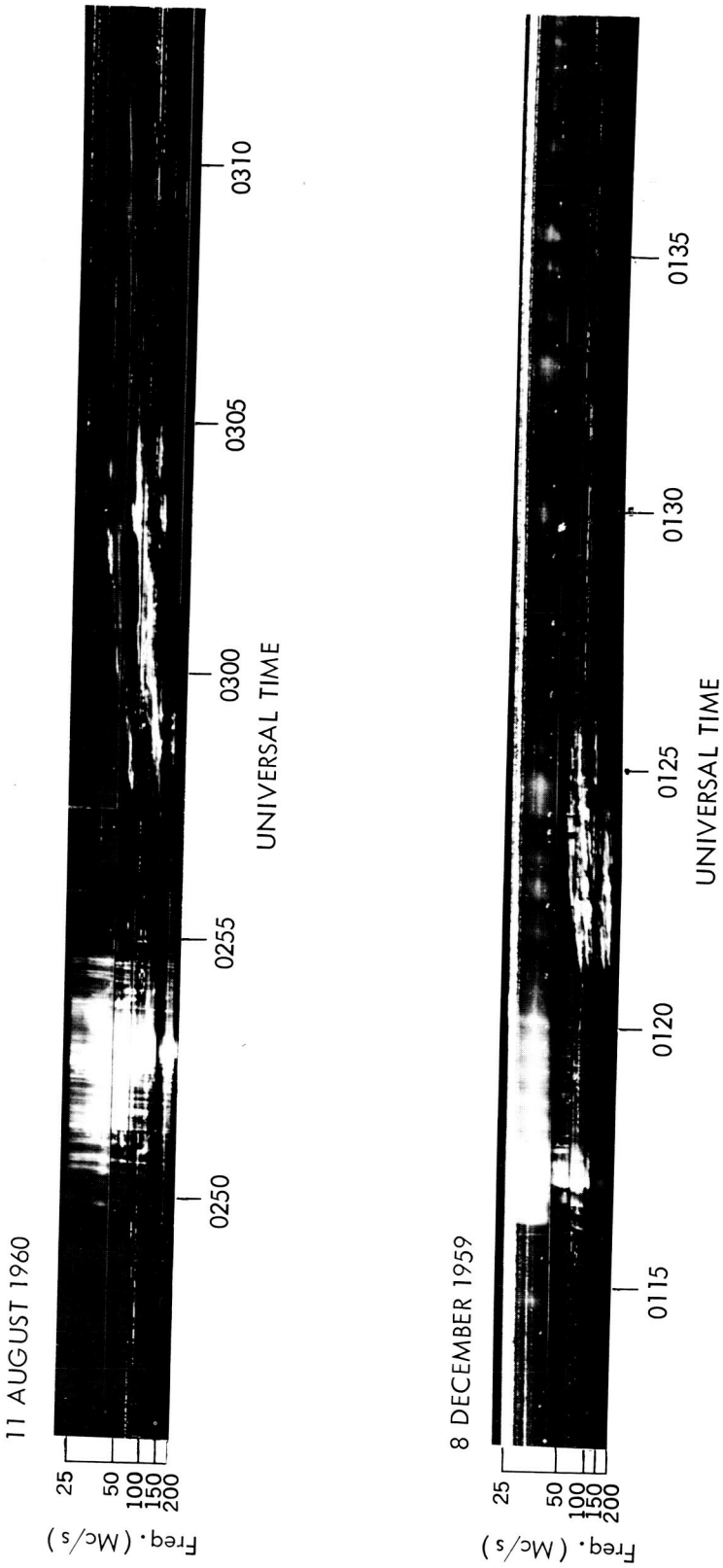

FIGURE 21–5. Dynamic spectra of meter wave bursts showing the distinction between flash phase (type III bursts) and second phase (type II burst). No type IV emission occurred in either event. (CSIRO Division of Radiophysics)

by an outward moving agency, but the frequency drift corresponds to much lower velocities ($\sim$1000 km/sec). The evidence is consistent with the supposition that the agency is a shock wave which is initiated at the time of the flash phase and which travels through the corona at several times the local velocity of sound. The observations imply that the shock wave is sharp-fronted and hence magnetohydrodynamic in character.

A recent analysis by Weiss indicates that the burst sources are often multiple—that is, within the same burst, they are located at widely separated positions on the sun's disk (e.g., Figure 21–6); the shock fronts evidently propagate as fragments shot out in different directions, reminiscent of Moreton's Hα observations.

An important clue to the structure of type II sources comes from the observation that the drifting spectral bands seen on dynamic spectra sometimes appear to issue a succession of short-lived features similar to type III bursts which extend out toward the low frequency domain; occasionally there occur simultaneously similar features with reverse drift extending in toward the high frequencies (the "herring-bone effect"—see Figure 21–7). Weiss has recently found that bursts showing these effects tend to be of very low or vanishing frequency drift and that in some cases, as in Figure 21–7, they show pronounced transverse motion across the disk at a given frequency (in contrast to the " normal" narrow bands). This whole observational pattern is consistent with the idea that the type II shock fronts propagate normal to the magnetic field and continuously eject bunches of fast electrons along the field—that is, normal to the direction of motion. Indeed the ejection of fast electrons previously had been postulated to account for the generation of the radio emission in a manner similar to that for type III bursts.

A detailed theory of type II bursts does not exist, and the evidence provides several puzzling features. In particular we require a theory—presumably in terms of shock waves—to account for the following distinctive phenomena:

1. The existence of first and second harmonics, and the observation of second harmonics from positions on the disk *inside* those of fundamentals,

2. The existence of split bands within each main harmonic band,

3. The "herring-bone" effects outlined above.

In certain large outbursts (e.g., Figure 21–8) the type II burst is characteristically followed by long periods (tens of minutes, hours, or even days) of continuum radiation (spectral type IV), which is general cover almost the whole expanse of the observable radio spectrum. At meter waves Boischot, Denisse, and Pick-Gutmann have recognized two distinct components:

Type IVmA—A component which has been recognized conclusively on a small number of occasions only and then only at frequencies below 200 Mc/s: events lasting $\sim$10 minutes with sources of large angular size ($\sim$10′ arc) which show marked transverse motions at speeds of up to 3000 km/sec to heights of up to 5 solar radii. The radiation is emitted within a wide cone of angles (quasi-isotropic) and may be weakly circularly polarized in the sense of the extraordinary mode. The radiation is attributed to synchrotron radiation from electrons with energy $\sim$3 Mev in fields of $\sim$1 gauss, some 4×10^{32} electrons being needed to radiate the observed maximum intensity. The transverse motions may be explained by supposing that the electrons, accompanied by the less mobile positive ions, swarm out from the sun and drag with them parts of the coronal magnetic field, which becomes elongated into a magnetic "bottle."

Type IVmB—Events lasting hours or days with sources of small angular size ($\sim$3′ arc) fixed on the disk and situated low in the solar atmosphere, near the plasma level. The radiation is emitted within a narrow cone and may be strongly circularly polarized in the sense of the ordinary mode. The radiation is believed due to fast electrons trapped in the magnetic loops of sunspot fields; the electrons excite Cerenkov plasma waves which can couple directly with the ordinary mode of the electromagnetic field over part of their downward trajectories.

These second-phase events depict the widespread deployment of ionized material above the flare. Indeed their effects appear to extend

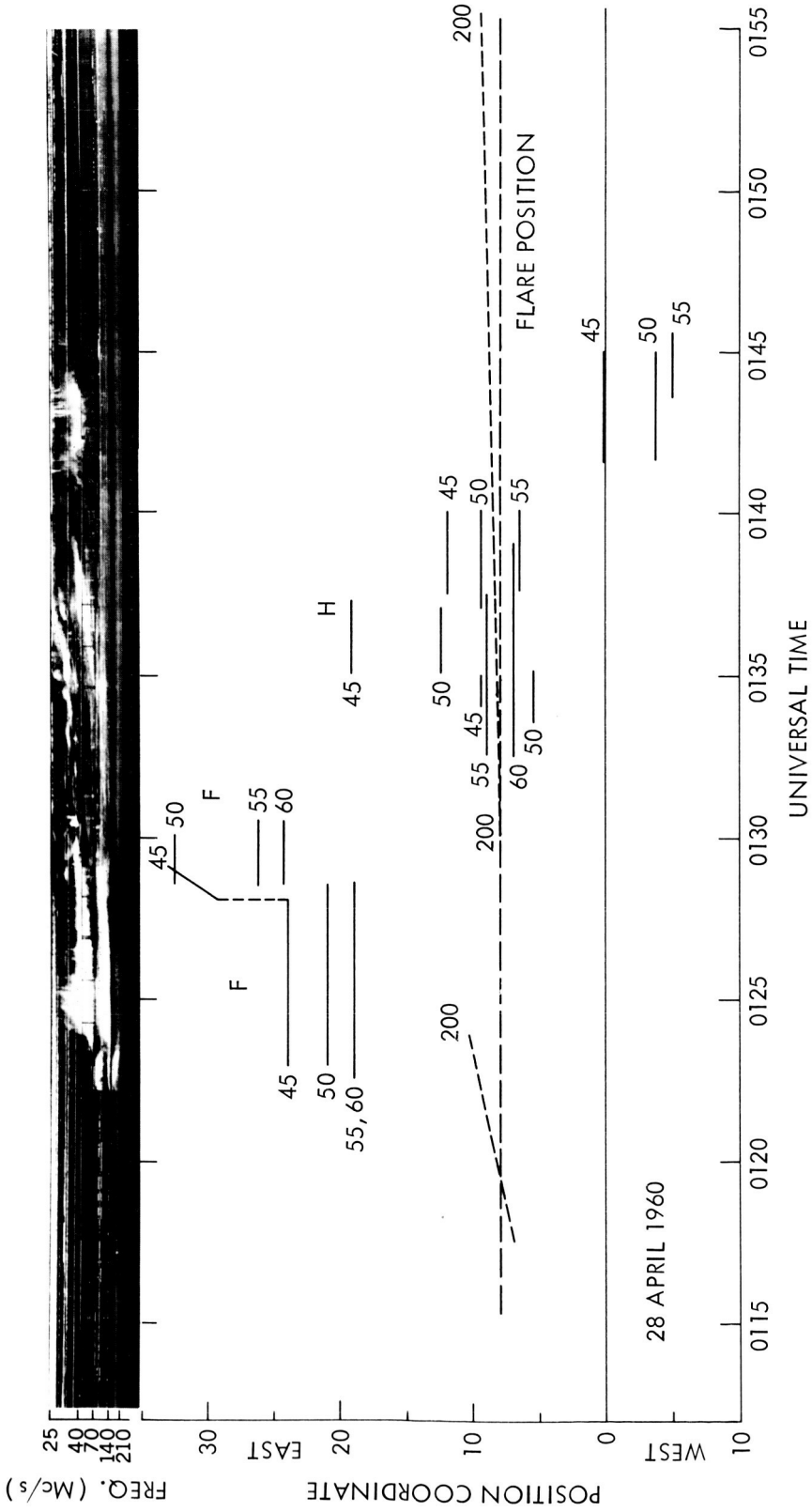

FIGURE 21–6. Simultaneous records taken at Dapto (Sydney) of the spectrum and position of a complex type II burst, illustrating how different spectral branches can occur at widely separated positions on the sun's disk. Positions refer to the east-west displacement in minutes of arc of the centroid of the source from the center of the sun's disk. Position measurements are made at different frequencies, indicated on the lines in Mc/s. Fundamental and second-harmonic bands are labeled F and H, respectively. The 200 Mc/s data are Tokyo observations. (Weiss)

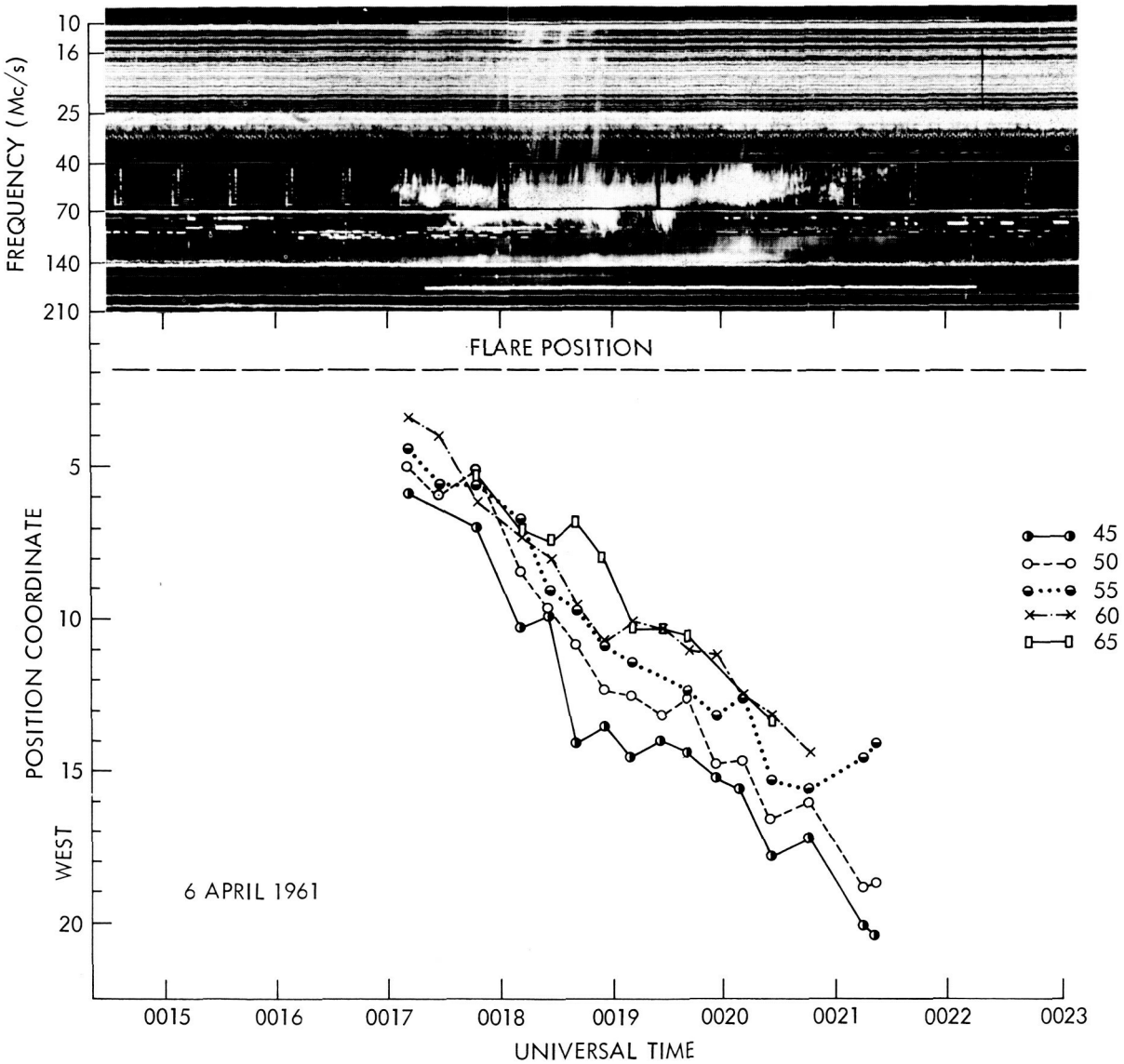

FIGURE 21–7. Observations of a type II burst with little or no frequency drift and with pronounced herring-bone effect. The position measurements (see legend on Figure 21–6) indicate pronounced movement across the disk at each frequency. (Weiss)

at least as far as the earth's orbit, since the best known indicator of a sudden-commencement geomagnetic storm is the occurrence on the sun some 30 to 40 hours previously of a combined type II–IV event.

Microwave and Decimeter Waves

A microwave outburst consists of a prolonged (e.g., ½ hour) continuum, often with multiple peaks but otherwise relatively smooth [e.g., Figure 21–1(d) at 3750 Mc/s]. In many cases the distinction between the two phases is at the best a subjective one: The two appear to merge together and apart from duration possess similar if not identical characteristics. The second phase, being a prolonged continuum, is now regarded as of spectral type IV and termed "type IVμ." Like the impulsive bursts that constitute simple events, it is attributed to synchrotron radiation from electrons in the 100

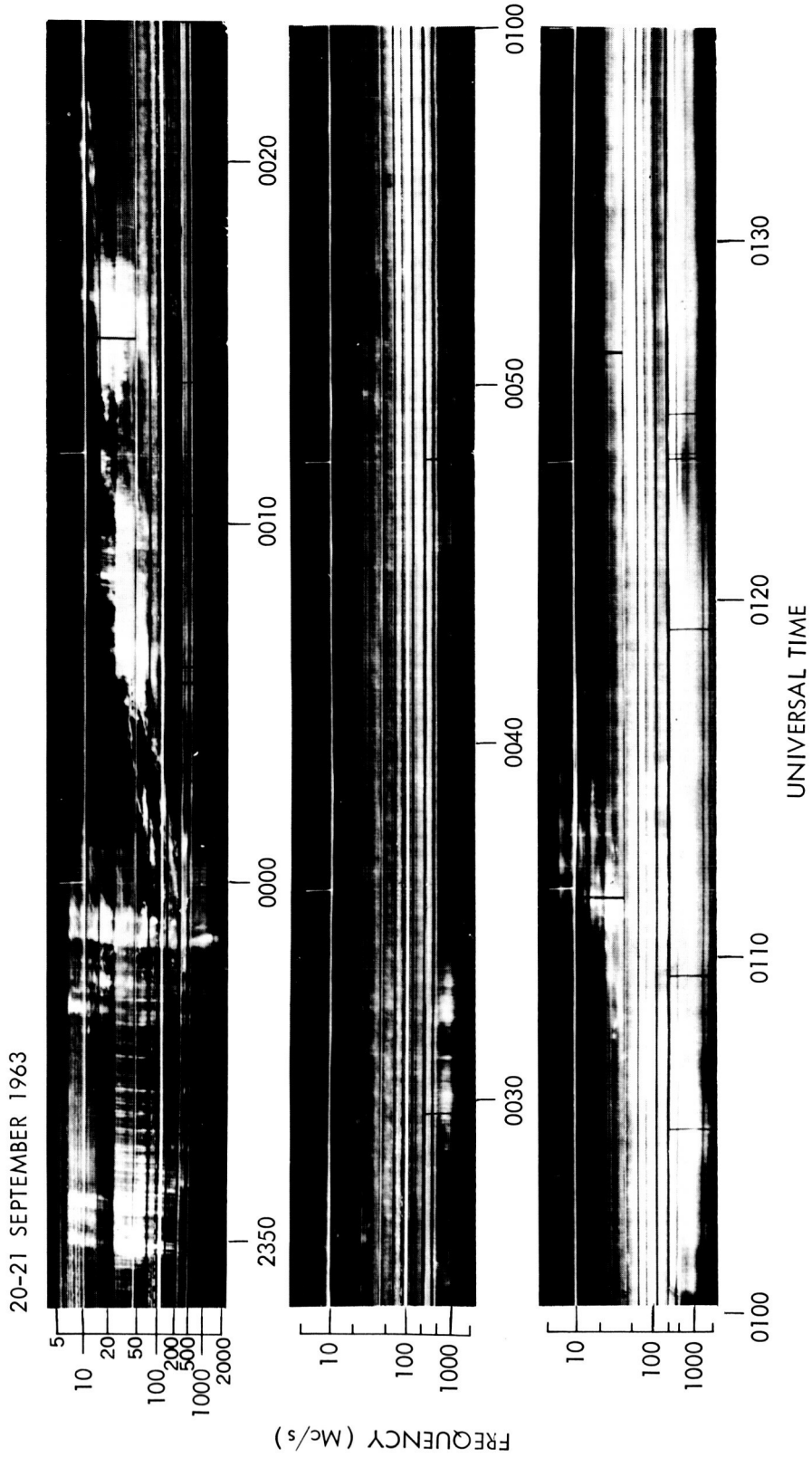

FIGURE 21-8. Record of a large outburst, taken over the frequency range 5–2000 Mc/s, showing type III, type II, and type IV events. (Suzuki, Attwood, and Sheridan)

kev range in magnetic fields of ~ 1000 gauss. These electrons are presumably trapped in the low-lying magnetic loops of sunspot fields.

Of great significance is the remarkably close association between the occurrence of a microwave outburst and the emission of solar protons capable of delayed detection at the earth.

Following investigations by Kundu and Haddock and by Sakurai, it is generally presumed that the radio emitting electrons and the solar protons are accelerated in the same region, perhaps by the same process. The ample time (~ 5 min) between the flash phase of the flare and that part of the outburst which can be deemed the "second phase" allows one to accept the Fermi process as possibly responsible for the acceleration.

Between the microwave and meter-wave components of the type IV burst, characteristic phenomena occur at decimeter wavelengths (sometimes called type IVdm). To some extent one may here be observing the superimposed overflow of meter wave and microwave continuum, but there exists also variable radiation, sometimes possessing bursty structure rather resembling a rapid succession of type III bursts; the latter is strongly circularly polarized in the sense (assuming the usual leading spot hypothesis) of the ordinary mode. Its physical interpretation is obscure: One suggestion by Takakura invokes Doppler-shifted gyro radiation from a source region associated with the *following* spot of a group.

SUMMARY OF THE COMPLETE FLARE EVENT

The sequence of events in a major flare as revealed by the radio evidence currently available may be summarized as follows:

1. Preliminary heating, presumably due to magnetic compression, causes the microwave intensity from part of the active center to increase gradually, giving the *gradual rise and fall.*

2. Minutes later the flash phase occurs; materially this constitutes the sudden ejection, from the chromosphere or lower corona, of several packets of electrons with energy in the range 20 to 200 kev—each packet containing some 10^{33} to 10^{35} electrons. Of those traveling upward into the corona, some escape freely along radial field lines or neutral planes and generate plasma radiation to give the *type III bursts,* others are trapped in or bent round enclosed loops to give the *type V* and *U bursts.* Those traveling down into or trapped within the surrounding chromosphere cause the microwave *impulsive burst* and *x-ray burst* by the synchrotron and bremsstrahlung processes, respectively.

3. The same eruption initiates also shock waves which propagate in fragmentary form in various directions; those moving out through the corona issue bunches of fast electrons which in turn generate the *type II burst* by plasma radiation. The shock is also responsible for exciting Alfvén waves within the field structure, and these waves cause acceleration of the electrons and protons trapped in the field. The electrons thus accelerated generate the various components of the *type IV burst* by synchrotron and plasma processes, while some of the protons, accelerated to much greater energies, are those responsible for the *solar proton event* detected at the earth.

The suggested coordination of these phenomena is indicated diagrammatically in Figure 21–9.

Generally speaking, the first-phase phenomena are understood better than the second phase and seem to give a clear affirmative answer to the controversial question of the existence of "runaway" electrons explosively ejected.

NOTE ON BIBLIOGRAPHY

The account given here represents a mere skeleton of the intricate mass of results available in the literature, and I am aware of the many important omissions and generalizations which have been imposed by space. Even so the account is based on the work of a great number of contributions, and specific mention of the work of individual investigations has been made only where special investigations or an element of controversy is involved. For an introduction to the complete bibliography the reader is referred to a recently completed review by J. P. Wild, S. F. Smerd, and A. A. Weiss in *Annual Review of Astronomy and Astrophysics,* 1: 291 (1963).

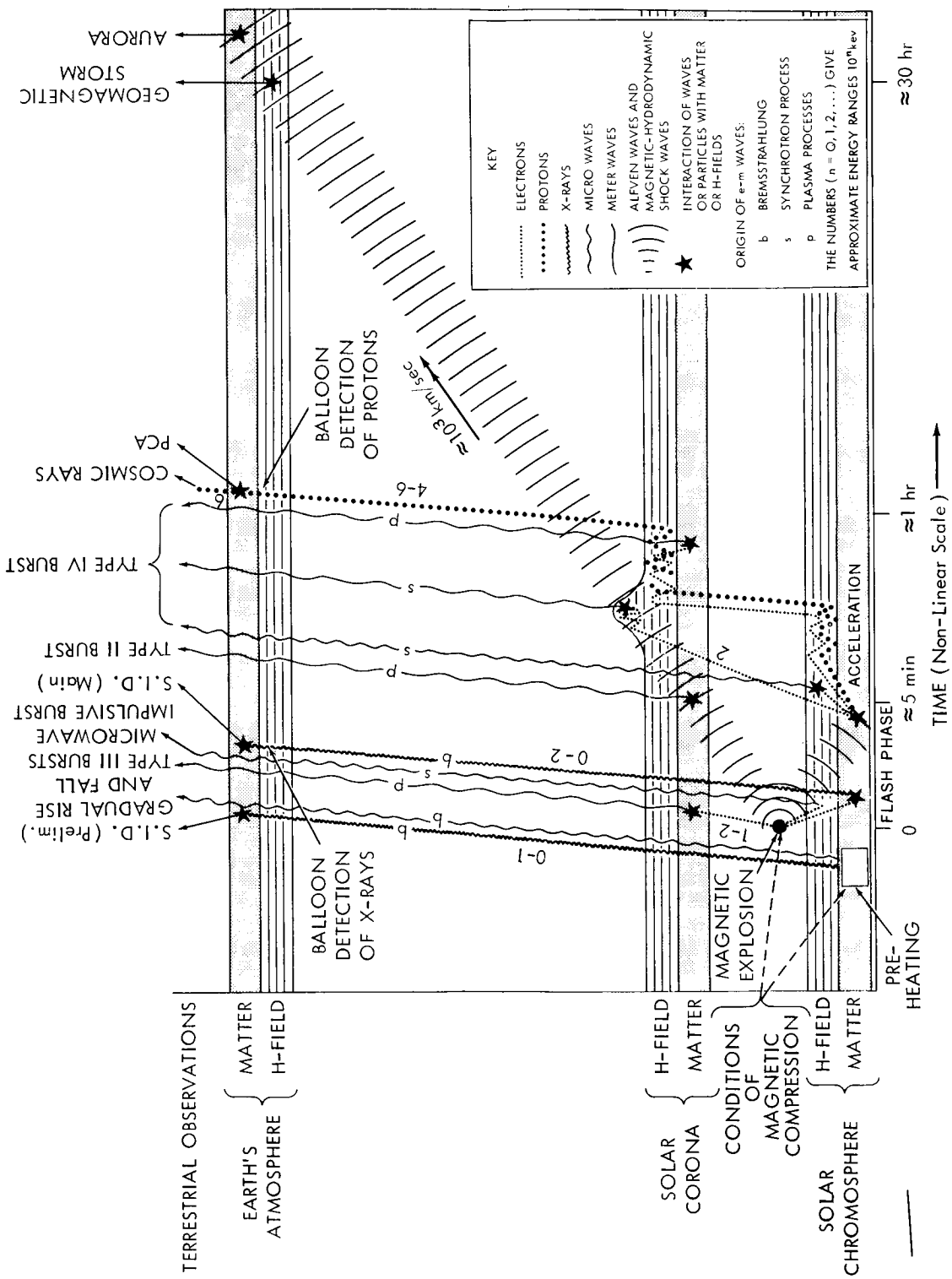

FIGURE 21-9. Diagram showing the origin of the radio emission, x rays, and corpuscular effects of great solar flares according to the ideas favored in this review.

DISCUSSION

Dr. Ney: If you say that synchrotron radiation adequately accounts for the microwave bursts, it seems to me you must also add the condition that the spectrum of the electrons be very sharp, almost monoenergetic, because any power law spectrum will give you too much low frequency, and you won't have flux density increasing with frequency; you will have it the other way around.

I think the spectrum must be at least as sharp as exponential.

Dr. Wild: I would like to refer this question directly to Dr. Takakura.

Dr. Takakura: I have shown that, if the spectrum of electrons is given by the power law E^{-2}, or something similar, we can expect this kind of spectrum. Because, if the energy of the electron is lower than, say, 20 kev, the frequency band which such electrons contribute is very small. If the energy of electrons is too high, the number of electrons is too small. So, the most effective range of electrons which contributes to the synchrotron radiation is given by the range I have specified.

Dr. Maxwell: The thing that worries me is how you can describe electrons of energy 20 to 100 kev, which are non-relativistic, as radiating by synchrotron mechanism. Presumably this is really cyclotron radiation with very few harmonics.

Then a question arises: How much energy can escape in the form of electromagnetic radiation? One recalls the analysis of Twiss which shows that, at these very low energies, the energy radiated is very low. The other thing that worries me is the 1000 gauss, which is a very high figure for 3000 Mc radiation.

Dr. Takakura: I made a numerical computation of the intensity spectrum of synchrotron radiations, assuming a power law distribution of electron energy in a uniform magnetic field. In that case the frequency at which the intensity is maximum became nearly twice the frequency of gyro-frequency.

I think, however, if we take into account the resonance absorption at the harmonics of gyro-frequency, which was pointed out by Ginsburg and Zhelezniakov, the field strength may be half the value which I gave before. The field may be 500 gauss at a height, say, 3×10^4 km from the photosphere.

Dr. Maxwell: The point is that you have radio sources which have spectra that decrease in intensity with increasing frequency.

Dr. Takakura: Bursts on microwaves have a maximum in intensity generally at about 3 to 10 cm. Then the intensity decreases with increasing frequency. However, the spectra of type IVμ bursts in millimeter range are not known. The bursts which have spectra that decrease in intensity with increasing frequency in a whole microwave range are not microwave bursts, but may be bursts in dm range.

Dr. Sturrock: I wish to make the following comments on your discussion of Type II bursts, which are generally agreed to be produced by shock waves. You propose that these are MHD shock waves which propagate normally to the magnetic field lines. Another possibility is that these are acoustic shock waves. It is sometimes said that the mean free path is too long for this interpretation to be tenable; but, at a height where the density is 10^8 particles/cm, the mean free path is about 10^8 centimeters, which seems to me to be sufficiently small to be consistent with the sharply defined spectrum.

In your picture of type II bursts, you proposed that the shock wave propagates vertically upward and normal to the magnetic field, so that the field lines are taken to be parallel to the surface of the sun. In discussing type II bursts, you interpret these as propagating vertically upward and parallel to the field lines, which must therefore be radial. From this picture, I would conclude that, when a normal type II burst is observed (one which does not display the herringbone structure), one would not observe type III bursts. Is this so?

Dr. Wild: I am not quite sure that you aren't just agreeing with me. The picture is this: If we have the magnetic field lines, quasi-radial, a type III burst originates in a burst of electrons which travels along the field lines. When we are dealing with a type II burst, we are dealing with a motion of ions, as well as electrons, which can propagate at right angles to the field. In

the case of a radial field, we have a type II burst of zero drift and electrons shooting up, thus producing the herringbone effect.

Dr. Sturrock: My point was that a normal type II burst does have drift and therefore, according to your picture, is moving radially, which implies that the field lines are more or less horizontal. If one observes a normal type III burst, the field lines are more or less vertical. If one observes a normal type II and a normal type III at the same time, then—according to your picture—there is something wrong.

Dr. Wild: For simplicity I had idealized and oversimplified the field configuration in terms of strictly radial and strictly horizontal fields. In practice, the field shapes are complex archtype structures combining the two extreme kinds; and I envisage the type III burst taking place in one part of the field where the lines are predominately radial, and the type II in another where the lines may be horizontal.

Dr. Moreton: The 1000 km/sec disturbances that we detect optically propagate across the chromospheric backgound to distances as great as half a solar radius. If these disturbances are some type of optical counterpart of the type II burst, then it seems more likely that the agency is an MHD wave rather than an acoustic wave.

Dr. Wild: I think the nature of the shock wave remains an open question. The evidence I have shown here that the phenomenon is consistent with an MHD shock wave gives no more than an indication. I think the whole subject is theoretically confused, and it has to be cleared up before we can really interpret these shock-wave phenomena.

Dr. Zirin: I suppose I shouldn't bring up something that you had to skip over because of time, but I am really confused as to what these decimeter bursts are. I can see that the microwave bursts are the things that Dr. Covington observes, and the meter bursts are the type II bursts, and so forth. But what are the decimeter bursts?

Dr. Wild: Decimeter bursts have a whole range of characteristics which were explored by the Convair spectrograph. Many details of a number of characteristic features are, to my knowledge, completely unexplained at the present time. But, then, we have to leave something for the next solar cycle!

Dr. Maxwell: For a Fermi acceleration mechanism operating in the region of a solar flare, Parker estimates that the characteristic time required to bring particles to relativistic energies is approximately 2 minutes. Schatzman has stated that the characteristic acceleration time is probably the same for both protons and electrons. Could you describe your acceleration mechanism in which the characteristic acceleration time for electrons is only 1 second?

Dr. Wild: I think this is a very important point indeed. In the case of the flash phase phenomenon, we need deal with electrons only. If one is dealing with electrons only, and with relatively low energies, I think the theoretical problem of finding an accelerating mechanism to act in 1 second may be a very much simpler one than the problem that Sweet, Gold, and Hoyle (and so on) have been trying to tackle when they attempt to explain the energy of the whole flare. I think it is possible that their neutral plane theories involving merging magnetic fields might be much more easily adapted to explaining simply the flash phase electrons. These processes may give fast accelerations in a very short time.

Dr. Chubb: I have one question. How does one explain the fact that these type III bursts, when they occur in a sequence, all have the same velocity?

Dr. Wild: I think the implication of the observations is, first of all, that the electrons are following the same path. That is to say, they come from the same point in the same magnetic field configuration.

Secondly, we don't know how they are accelerated. We don't know how they are generated; but they are generated apparently as one pulse after another with very similar characteristics.

Dr. Chubb: In other words, you think that each pulse represents a separate generation of particles in a region?

Dr. Wild: Yes.

Dr. Chubb: And each time they get the same energy?

Dr. Wild: Essentially the same particle energy, yes, but not necessarily the same total energy.

Dr. Schmidt: Just a comment to the last remark about the possibilities which might make the neutral plane theories adapted to smaller energies, but faster time scales. I would think it is just the other way around; the difficulties of all neutral plane theories lie with the time scales, not with the energies.

22 THE SLOWLY VARYING COMPONENT OF SOLAR RADIO EMISSION

N64-30272

G. SWARUP
Tata Institute of Fundamental Research
Colaba, Bombay, India

Measurements of solar radio emission at centimeter and decimeter wavelengths made by Covington (Reference 1) and Lehany and Yabsley (Reference 2) revealed a component which varied slowly from day to day and showed a good correlation with the total visible sunspot area. It has been called the slowly varying component, or *S*-component, and is superimposed on a steady background level that is attributed to thermal emission from the quiet sun. These two components were first separated from each other by means of scatter diagrams by Pawsey and Yabsley (Reference 3) and Denisse (Reference 4). The *S*-component is distinguished from rapidly varying components which have burstlike characteristics and have duration of a few seconds to some hours (Reference 5). It is most prominent in the wavelength range of about 3 to 60 cm but can still be recognized at longer as well as shorter wavelengths (at 88 cm by Firor, Reference 6; at 176 cm by Moutot and Boischot, Reference 7; and at 8 mm by Salomonovitch, Reference 8).

Eclipse observations by Covington (Reference 9) and Christiansen, Yabsley, and Mills (Reference 10) provided the first important clues about the sources responsible for the *S*-component. It was established that the radio emission originated in localized bright regions lying close to positions where either sunspots were still visible or had occurred during previous rotations of the sun. Also, the *S*-component was found by Covington to show a small degree of circular polarization at 10 cm wavelength. In view of the above facts and because of the observed steadiness of the *S*-component over periods of hours or days, it usually has been postulated that it originates thermally in regions of high electron densities and magnetic fields that exist in the vicinity of sunspots and chromospheric plages (References 2, 11, 12, 13, 14, and 15).

Soon after the discovery of the slowly varying component it became clear that its detailed observations will provide us with a new means for determining physical parameters of the solar atmosphere overlying active regions. This prompted Christiansen and Warburton (Reference 16) and Tanaka and Kakinuma (References 17 and 18) to construct multi-element interferometers having 3′ arc and 4.5′ arc wide east–west fan beams at 21 and 7.5 cm wavelengths, respectively. Simultaneously, Covington and Broten (Reference 19) studied brightness distribution across the sun at 10.7 cm wavelength with a waveguide array which provided 8′ arc fan beam. Since then a number of new interferometers have been constructed in various parts of the world, including the 3′ arc pencil-beam instruments which are located at Sydney (Christiansen et al., Reference 20) and Stanford (Reference 21), and operate at 21 and 9.1 cm wavelengths, respectively. Pencil-beam maps of the radio sun also have been obtained on a few occasions at 3.2 cm by Vitkevitch et al. (Reference 22) and at 8 mm by Salomonovitch (Reference 8) using single paraboloidal antennas. Also, very high resolution instruments which provide 1′ arc wide fan beams have been constructed for operation at wavelengths of 3.2, 9.1, and 10.7 cm.

In the next section of this paper, we shall summarize the observations of the slowly varying component for a "strong" radio source (area of the associated sunspot group > about 500 millionths of visible hemisphere) and a "weak" source (sunspot area <200 millionths), with an emphasis on their wavelength dependence. This will be followed by a discussion of various theories of the origin of the radio emission. We then shall describe some results concerning the observed association between the strength of the *S*-component and the flare activity of a solar active region. Although most of the results described in this paper already have been published, some new results—not yet reported—are also included.

OBSERVATIONS OF THE S-COMPONENT

Source Brightness Distribution and Correlation With Optical Activity

The solar radio emission at cm-dcm wavelengths shows a high degree of correlation with sunspot area, as can be seen from Figure 22–1. However, this relation is only a partial one. High resolution observations have shown that the localized sources of solar radio emission have a longer lifetime than associated sunspots and are connected closely with the chromospheric plage (References 19, 23, 24, 25, 26, and 27). During the growth of a solar active region, radio emission increases with sunspot area but with a lag of about 1 or 2 days (References 23, 24, and 27). However, during its decay while the sunspot area decreases to about 1/30th after two rotations, the radio emission decreases to only about 1/6th of the maximum value at 21 cm and about 1/10th at 9.1 cm wavelength. Therefore, although the correlation between radio flux density and sunspot area is high during the period of maximum activity of a solar active region, it is small when the region is new or old. Since the stronger radio sources predominate in the picture, the measured values of correlation coefficient are found to have high values of about 0.8 to 0.9 at 10 and 21 cm. At longer wavelengths, the contrast between stronger and weaker sources is smaller so that the correlation coefficient is lower; for example, it has a value of 0.6 at 60 cm wavelength (Reference 24). The correlation with sunspot area is also lower at 3.2 cm than at 7.5 or 9.1 cm, as can be seen from Figure 22–2 (Reference 15).

At a wavelength of 21 cm, the size and shape of the radio source correspond closely to that of the chromospheric plage as has been shown by Christiansen et al. (References 23 and 28) and Christiansen and Mathewson (Reference 29) from observations made with 3′ arc fan- and pencil-beam interferometers. This close correspondence is shown clearly in Figure 22–3, which shows contours of radio brightness at 21 cm, chromospheric plage, and 5 gauss magnetic field for the case of a large sunspot group. In Figure 22–4, a 21 cm radio map is compared with a Fraunhofer Institute optical map for the same day. These observations indicated that a typical 21 cm source seen during sunspot maximum has a width of about 5′ arc. The sizes of the radio sources at 21 cm vary from about 4′ arc to more than 8′ arc and show a good correlation with diameters of associated Hα plage.

On the other hand, by means of 3′ arc pencil-beam observations, Swarup (Reference 30) and Swarup et al. (Reference 31) have determined that the center of a strong 9.1 cm source coincides with the centroid of the associated sunspot group within $\pm$½′ arc or less. Also, it is found that the size of a 9.1 cm source is smaller than that of the associated plage. Measurements by Covington with a 1.2′ arc fan beam have indicated that a strong radio source has a width of about 2.5′ arc at 10.7 cm wavelength (References 31 and 32). Figure 22–5(a) shows the brightness distribution across a strong 10.7 cm source for four successive days.

Kundu (Reference 33) has made high resolution (1.8′ arc) observations at 3.2 cm wavelength with a variable spacing 2-element interferometer. It was concluded that a 3.2 cm radio source consisted of [see Figure 22–5(b)]: (1) a very intense region of small diameter ($\approx$1.5′ arc), and (2) a weak diffuse region of large diameter ($\approx$5′–8′ arc). The intense regions were seen only during periods of very strong solar acitivity (several days). According to observations made by Ikhsanova (Refer-

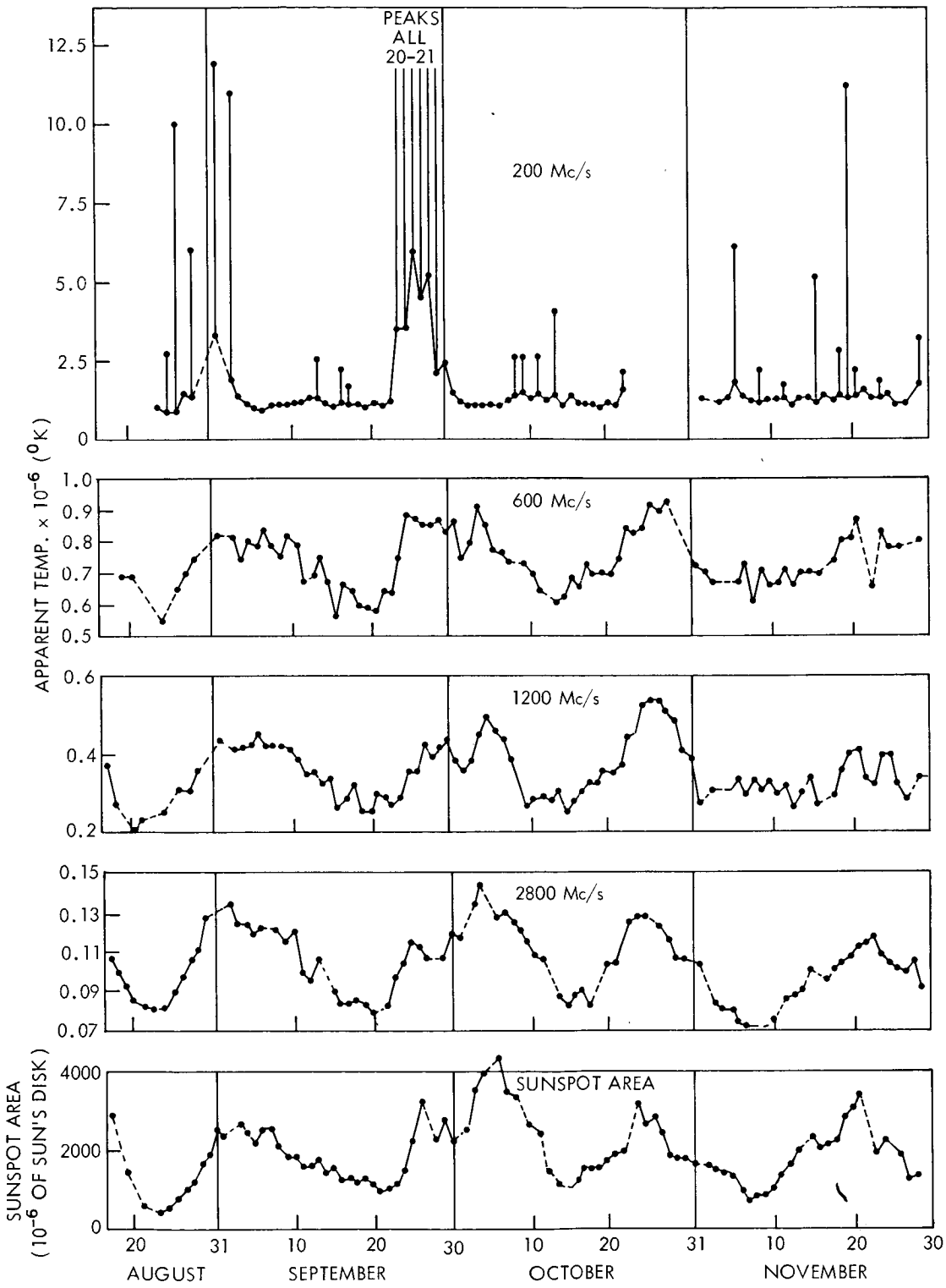

FIGURE 22–1. The variation with time of the apparent disk temperature of the sun at frequencies of 200, 600, 1200, and 2800 Mc/s together with sunspot area for the period. (Piddington and Minnett, Reference 11)

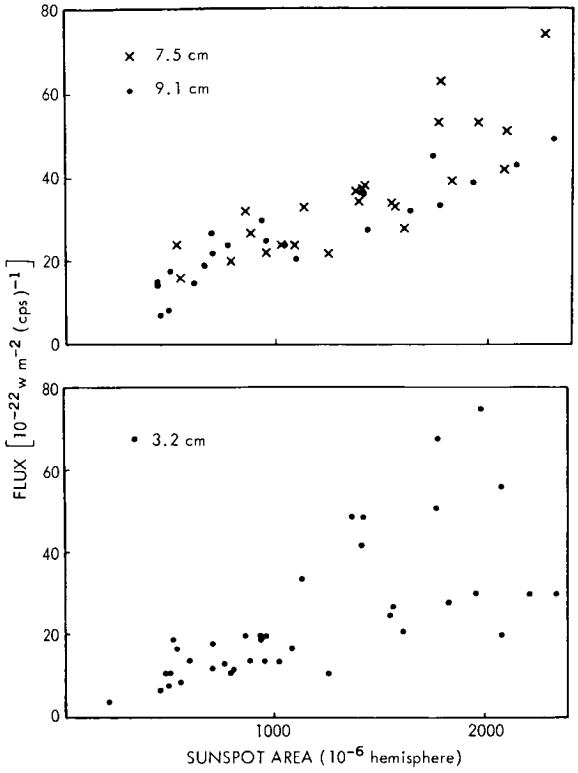

FIGURE 22–2. Scatter diagram of the flux density of radio sources versus their associated sunspot area. (Kakinuma and Swarup, Reference 15)

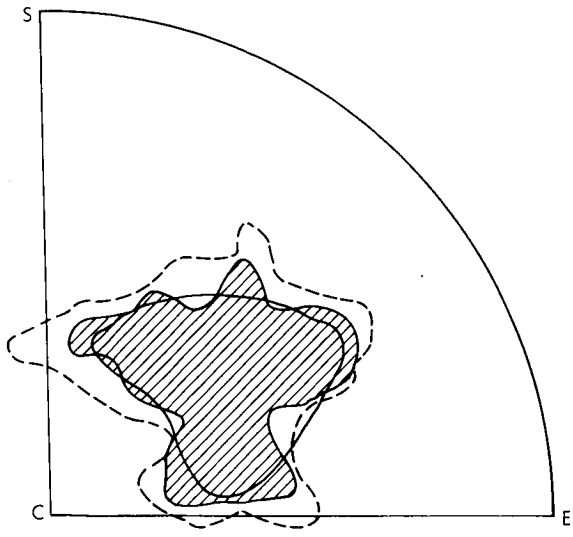

FIGURE 22–3. Comparison of sizes and shapes of (a) radio source at $\lambda = 21$ cm, half power contour (full line); (b) 5 gauss magnetic contour (dotted line); (c) plage (shaded area) on December 1, 1957. (Christiansen et al., Reference 28)

ence 34) with a 1.2′ fan beam, the dimensions of the radio sources at 3.2 cm are the same as those of the accompanying sunspot groups and are usually less than 1.3′ to 3.0′ arc. Since Kundu's instrument was of a fan-beam type, and also since no phase measurements were made, it could be that a part of the broad diffuse region seen by him was due to superimposition of several weak sources located elsewhere and not connected with the intense source. However, the general picture of a fairly bright radio source connected with sunspots and a surrounding weak diffuse region with nearly the same dimension as that of the associated chromospheric plage is probably the correct one at centimeter wavelengths, and is also supported by eclipse measurements (Reference 35 and 36). A similar distribution was observed at 8 mm by Salomonovitch (Reference 8), who used a 2′ arc pencil beam, but the bright nucleus was found to be less prominent at 8 mm than at centimeter wavelengths.

Spectrum of Flux Density

From eclipse, interferometric, and statistical investigations, Tanaka and Kakinuma (References 36, 37, and 38) have found that flux densities of many strong sources of the slowly varying component are higher near 8 cm than at shorter or longer wavelengths. In Figure 22–6(a), curves *A* and *B* show spectrum of flux density (corresponding sunspot area $= 10^{-3}$ hemisphere) obtained statistically, and curve *C* shows the spectrum for a strong source observed during the eclipse of April 19, 1958. A similar spectrum has been derived by Molchanov (Reference 39) and Smerd (Reference 40). Figure 22–6(b) shows a comparison of Russian and Japanese data for the above eclipse.

Recently, Swarup et al. (Reference 31) studied 10 solar active regions by combining interferometric observations made at wavelengths of 3.2, 7.5, 9.1, 10.7, and 21 cm with an aim to determine wavelength dependence of the slowly varying component. Figure 22–7 shows the flux densities for the 10 regions. It is seen that, for 2 out of the 10 sources, flux density increases with decreasing wavelength; but, for 7 sources, it is higher around 10 cm than at 3 or 21 cm wavelengths. The interferometric

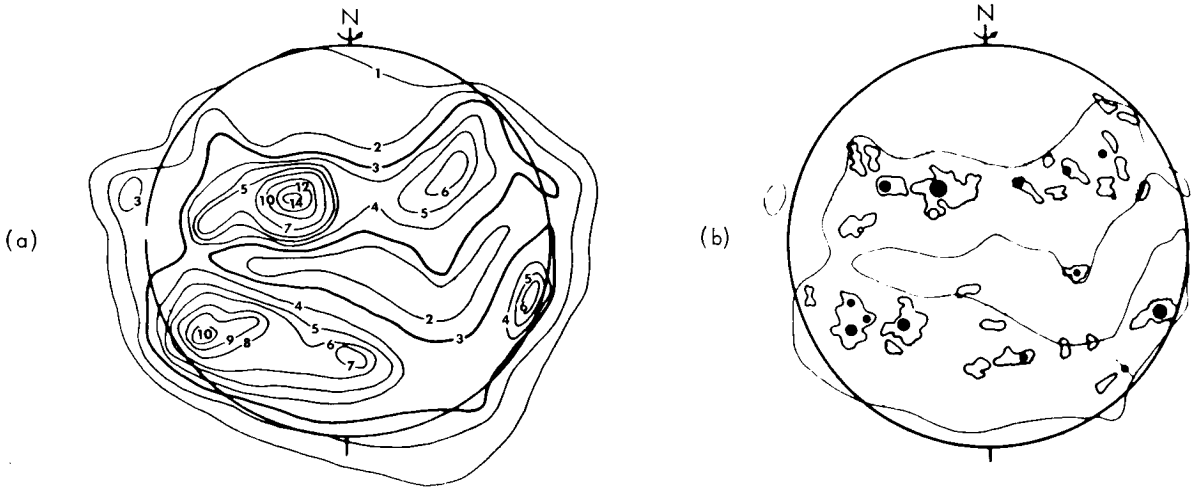

FIGURE 22–4. Solar observations on November 11, 1957 (corrected for solar rotation to a common time at 03^h00^m UT). (a) Radio brightness contours ($\lambda=21$ cm) (contour unit is 7.5×10^4 °K); (b) Fraunhofer Institute solar map showing plage and position of sunspot groups. (Christiansen and Mathewson, Reference 29)

data were calibrated by referring to the daily whole-sun flux density values measured at Toyokawa and Ottawa at frequencies of 1000, 2000, 2800, 3750, and 9400 Mc/s.

It appears, therefore, that for many strong radio sources, the spectrum of flux density has a peak around 5 to 10 cm wavelength. This result is unlikely to have been caused by calibration errors, because in several cases flux densities at 3 cm have been found to be smaller than those at longer wavelengths by a factor of about 2, whereas the errors of measurement were estimated to be less than about 20 percent.

Brightness Temperature

The pencil-beam observations provide a direct measurement of the radio brightness temperature T_b, but in case of the fan-beam observations T_b is calculated by using the relation

$$S=\frac{2kT_b}{\lambda^2}\,\Omega_s,$$

where S and Ω are measured values of flux density and size of the radio source.

At a wavelength of 21 cm, Christiansen and Mathewson (Reference 29) found from 3′ arc pencil-beam observations that the temperatures ranged from small values up to a cutoff at about 1.5×10^6 °K, the most commonly found value being at 0.6×10^6 °K (see Figure 22–8). Since the measured upper limit of 1.5×10^6 °K was close to the commonly accepted temperature of the corona, it was concluded that the sources of S-component are simply optically dense parts of the corona. It was pointed out that the median value of 0.6×10^6 °K, which was lower than the accepted coronal temperature, could be due to the smoothing effect of the relatively broad antenna beam (3′ arc).

Measurements at 3 cm by Kundu (Reference 33) and Ikhsanova (Reference 34) have shown that weak radio sources have $T_b\approx50{,}000°$ to 100,000°K, and a very intense source (lifetime, several days) has $T_b\approx500{,}000$°K.

The 9.1 cm radio maps obtained by Swarup (Reference 30) during April to August 1960 with a beam of about $3.1'\times3.4'$ showed a most commonly found value of 4.5×10^5 °K and a maximum value of about 1.3×10^6 °K. However, observations made at Ottawa (References 31 and 32) with a 1.2′ fan beam at 10.7 cm have shown that the average width of a strong source seen during this period was smaller than the width of the above pencil beam, and was about 2.5′ arc. Therefore, values of brightness temperature given by the 9.1 cm maps are lower than true peak values.

At 10.7 cm, the calculated values for a strong radio source range from 1.6 to 3.8×10^6 °K

728–629 O—64——13

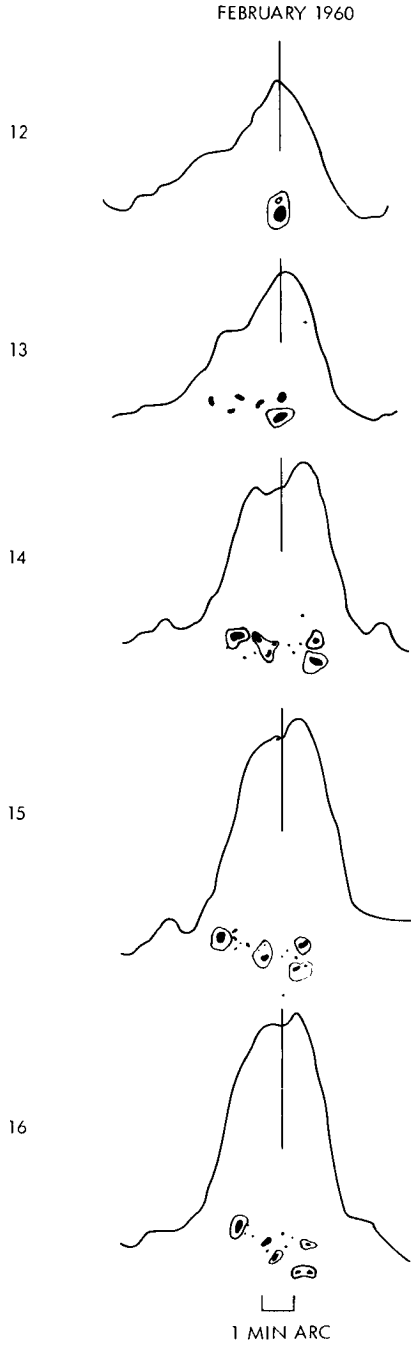

FIGURE 22–5(a). East-west strip scans across a strong radio source made with a 1.2′ arc wide beam during Feb. 12–16, 1960, at 10 cm wavelength. Associated sunspot group is also shown. Eastern part (left) of the profile is associated with growth of the following member of the spot region. (Covington et al., Reference 32)

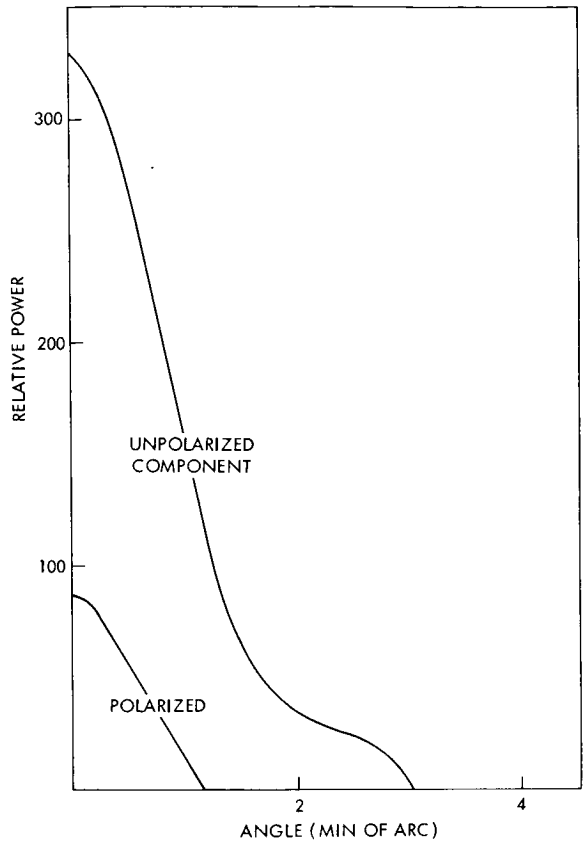

FIGURE 22–5(b). The distribution of brightness across a strong radio source at 3.2 cm wavelength. (Kundu, Reference 44)

when it is assumed that the north–south extent of the sources are equal to the measured east–west extent (Reference 31). These values could have been overestimated by about 30 percent. But, on the other hand, if one assumes that the north–south extent is smaller than the observed east–west extent—as is true for the sunspot groups and plages—one will obtain even higher values than given above. As shown in Figure 22–9, values of T_b at 10.7 cm are closely correlated with sunspot area and peak values of photospheric magnetic fields.

Heights

The heights of the sources of solar radio emission may be determined from their rate of travel across the solar disk. The measured values of height for a source of S-component range from 20,000 to 100,000 km at 21 cm,

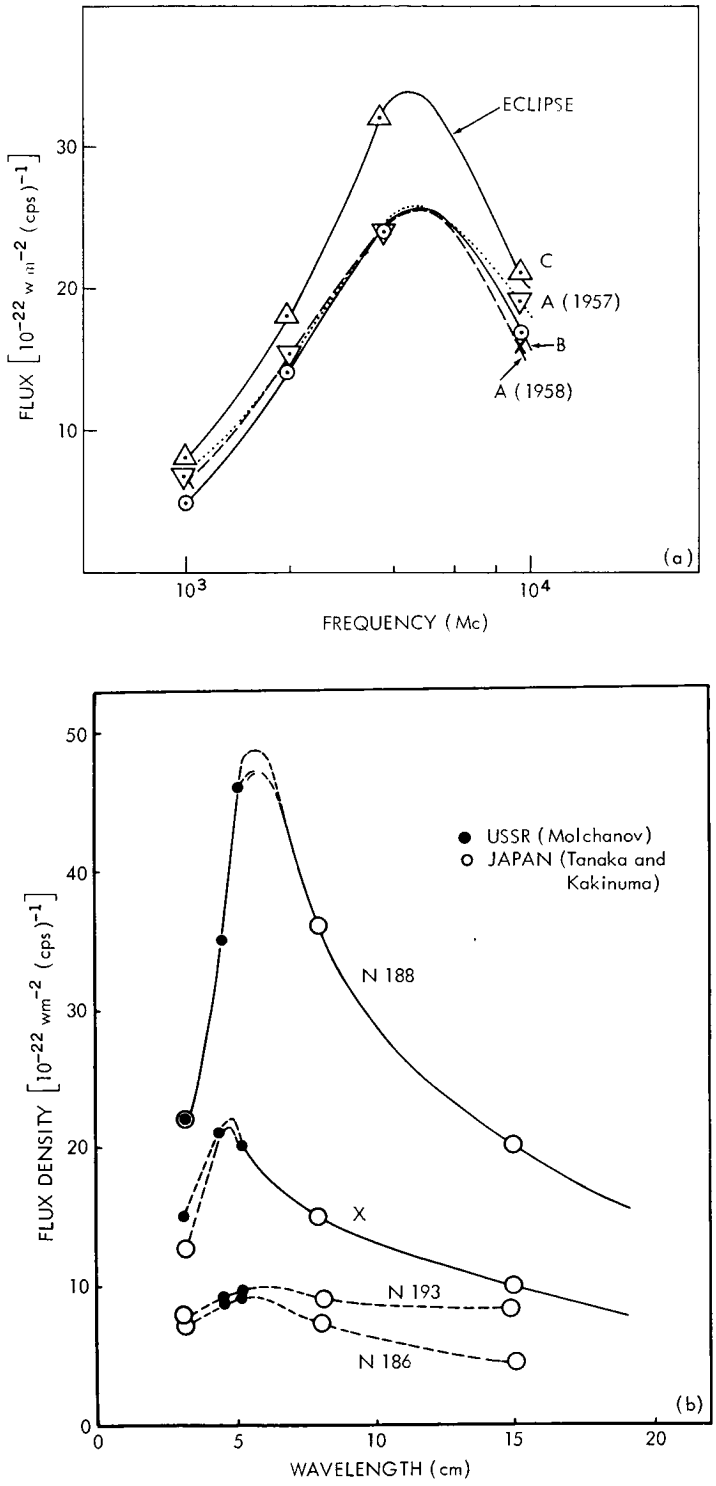

FIGURE 22–6. Spectra of flux density (a) obtained from statistical and eclipse investigations. (Kakinuma and Swarup, Reference 15); (b) determined from eclipse observations of April 19, 1958, for four different sources (Molchanov, private communication).

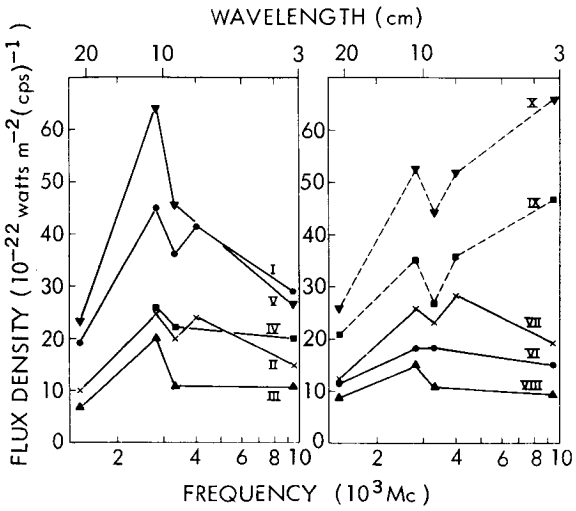

FIGURE 22–7. Spectra of the flux density of 10 solar active regions determined from interferometric data. (Swarup et al., Reference 31)

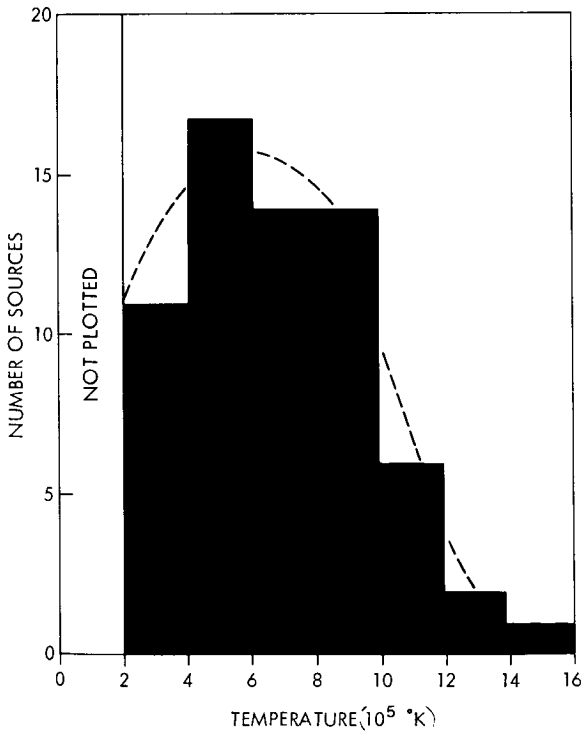

FIGURE 22–8. The distribution of the peak brightness temperature of 65 radio sources observed with a 3′ arc wide beam during September 1957 to January 1958 at 21 cm wavelength. (Christiansen and Mathewson, Reference 29)

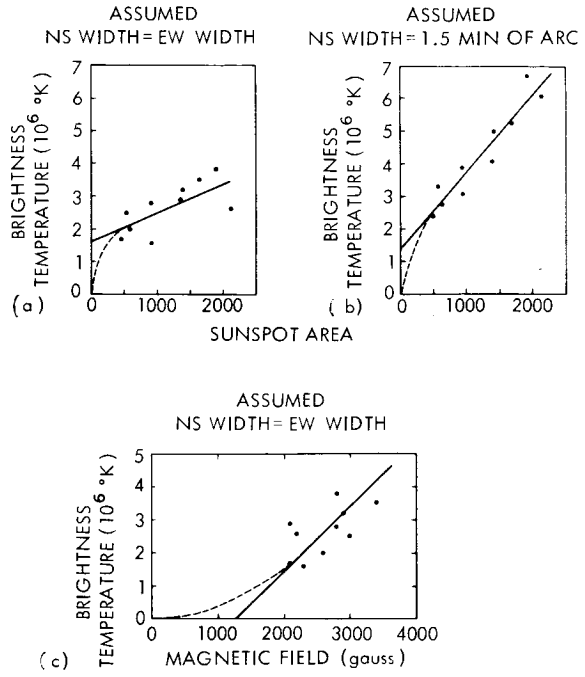

FIGURE 22–9. Radio brightness temperatures at 10.7 cm wavelength plotted against sunspot areas in units of millionths of the solar hemisphere and against magnetic fields in gauss. (Swarup et al., Reference 31)

and from <10,000 to about 40,000 km near 3 to 10 cm (References 29, 30, 31, 32, 34, and 38). The average values are about 40,000 km at 21 cm, and 15,000 km in the range 3 to 10 cm.

Center-to-Limb Variation

The flux density of a radio source decreases as it rotates from the central meridian to the limb. Figure 22–10(a) summarizes the results obtained by various investigators on the basis of high resolution observations (References 23, 24, and 41); in addition to curves given in the figure also refer to Covington and Harvey, Reference 27; Vauquis, Reference 42; and; Waldmeier and Muller, Reference 13. It is seen that the directivity of the radio sources increases with increasing wavelength. The 21 and 60 cm curves correspond to observations near sunspot minimum. At 21 cm the radio flux follows a cosine law, showing that the emitting regions have a disk-like shape. According to Christiansen and Mathewson (Ref-

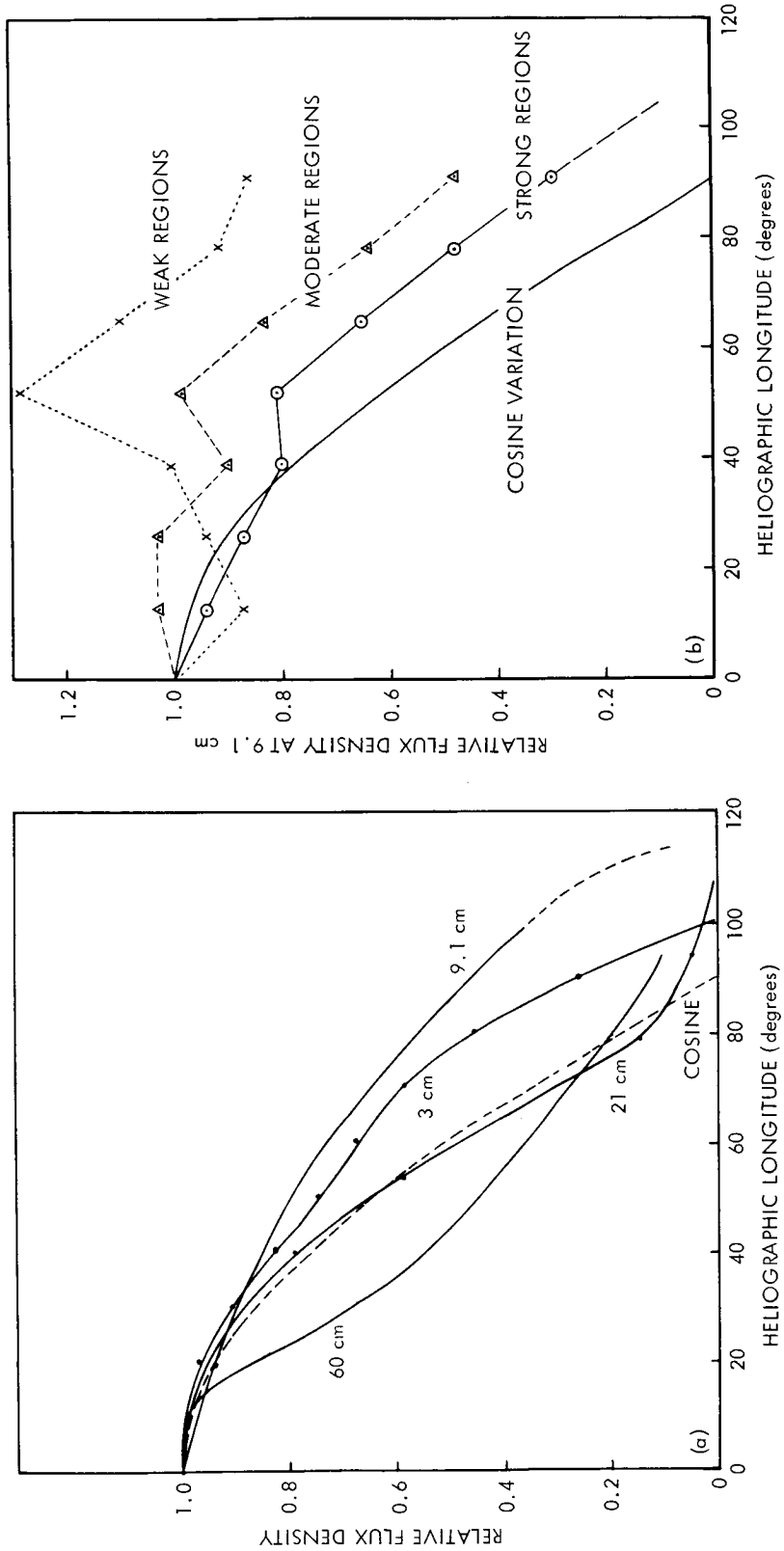

FIGURE 22–10. Center-to-limb variation of the flux density of a radio source. (a) At different wavelengths; (b) at 9.1 cm wavelength for a strong, moderate, and weak radio source.

erence 29), a similar variation is found near sunspot maximum. However, several strong sources have somewhat broader directivity as can be seen from 21 cm maps published in the *IAU Quarterly Solar Bulletins*.

We have recently determined center-to-limb variation at 9.1 cm for a strong, moderate, and weak radio source (flux density being >15, 8–15, and $3\text{–}8\times10^{-22}$ w m^{-2} $(cps)^{-1}$ during 3 days around CMP). The results are shown in Figure 22–10(b). About sixty radio sources were studied. Flux densities were determined from pencil-beam maps obtained by the author during 1960 to 1962 (see *CRPL Solar Geophysical Data Bulletins*). For the weak radio sources, radio flux is seen to be nearly constant from center to limb, indicating that their optical depth $\tau<1$ at 9.1 cm wavelength. The directivity of the strong 9.1 cm sources indicates that $\tau>1$, and horizontal extent is approximately four times the vertical extent. This is consistent with measured values of 10^5 km (2.5′ arc) for the diameter and 15,000 km for the mean height of the emitting region. The still narrower directivity at 21 and 60 cm may be partly due to broader dimensions and partly due to refraction effects and masking effect produced by the limb brightening of the quiet corona.

Polarization

As mentioned in the introduction, Covington (Reference 43) discovered that sources of *S*-component have a small degree of circular polarization at 2800 Mc/s. Piddington and Minnett (Reference 11) showed that the sense of polarization reversed as a large sunspot group crossed the central meridian. Kundu (Reference 44) showed that the size of the polarized component was $<1.5'$ arc. A more detailed picture about the brightness distribution of the polarized component has emerged from the eclipse and interferometric observations by Tanaka and Kakinuma (References 36 and 38), Tanaka (Reference 45), Korolkov, Soboleva, and Gelfreikh (Reference 46), and Kakinuma and Swarup (Reference 15). It has been found that a bipolar group located near CMP has two centers of polarization. The source over the S-pole radiates the excess of the left-handed circularly polarized wave, and the source over the N-pole radiates the excess of the right-handed circularly polarized wave (see Figure 22–11). The sense of polarization corresponds to that of the extraordinary wave of the magneto-ionic theory. The degree of polarization of the two centers is nearly equal when the center is located near CMP but becomes unequal before and after CMP, thus appearing lower for the center away from the observer. This fact accounts for the observed reversal of the net polarization of the whole source.

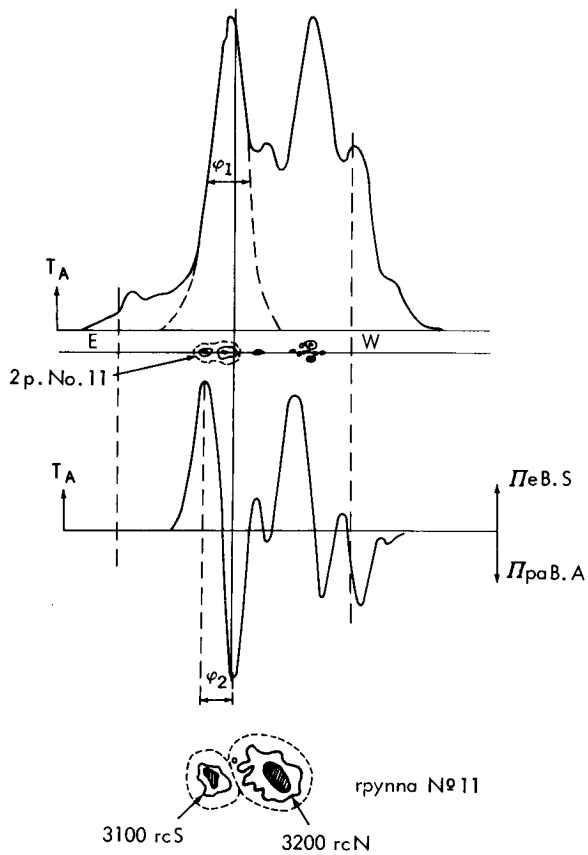

FIGURE 22–11. East-west strip scan across the sun obtained at 10.6 cm wavelength with 4′ arc wide beam of the Pulkova radio telescope. E and W denote edges of the solar disk. The upper graph shows total flux excluding the "quiet sun" level; the middle, circularly polarized flux; and the lower, sunspot group no. 11 on an enlarged scale. (Korolkov et al., Reference 46)

The above investigations and that by Christiansen and Mathewson (Reference 29) have shown that the degree of polarization of a strong source of the S-component is $\gtrsim 30$ percent at 3 cm, ≈ 10 percent at 10 cm, and <2 percent at 21 cm. Eclipse observations by Tanaka and Kakinuma (Reference 36) revealed a strong source with polarization of 60 percent at 3.2 cm and 18 percent at 8 cm. Also, the flux density of the source was found to be higher at 8 cm than at 3.2 cm.

S-Component at Meter Wavelengths

So far we have not described the observations of the S-component which have been made by Firor (Reference 6) at 88 cm with a 4.8′ fan beam, and by Mutot and Boischot (Reference 7) at 176 cm with a 3.5′ fan beam. At these wavelengths it is difficult to recognize the S-component because of two reasons. Firstly, the contrast between brightness of the quiet sun and that of the sources of the S-component is small because of the relatively large optical depth ($\tau \approx 1$) of the quiet corona. Secondly, many solar active regions are accompanied by rapidly variable noise storms. However, it has been possible to identify the S-component at meter wavelengths on some relatively calm days with the aid of high resolution arrays (see Figure 22–12).

At 176 cm wavelength, the sources of the S-component are found to have a size of about 10′ arc, brightness temperature of 1.2×10^6 °K ± 15 percent, and height of about 150,000 km. The directivity of the source is very narrow. The sources of the S-component are visible at this wavelength only up to a distance of nearly 10′ arc from the central meridian. This may be explained as follows: The optical depth of the quiet corona is larger near its limb than at central meridian, and therefore any enhancement of electron density has much less influence on the brightness temperature near the limb than at the center. Also, the emerging ray near the limb will be deviated away from the coronal condensation because of refraction effects.

At 88 cm, the size of the radio sources is about 6′ to 8′ arc, and the height is about 130,000 km (References 6 and 28).

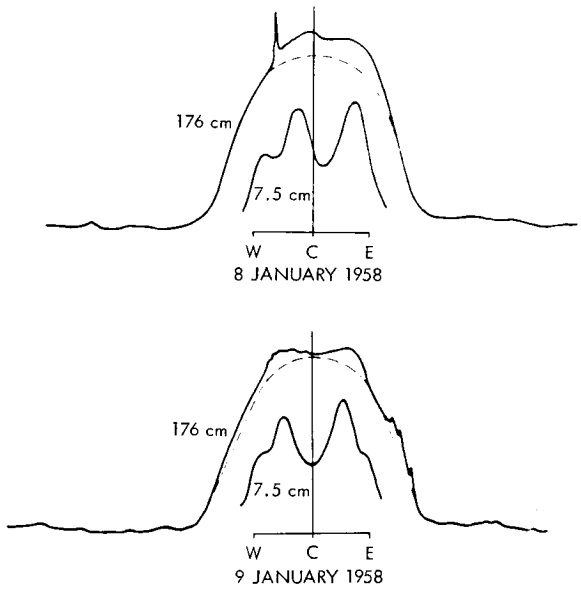

FIGURE 22–12. A comparison of the strip scans across the sun at $\lambda = 176$ cm and $\lambda = 7.5$ cm. (Christiansen et al., Reference 28)

Summary of Observations

The main results concerning the characteristics of a strong source of the S-component are summarized in Figures 22–9, 22–10, 22–11, and 22–13.

The intensity of a source of S-component varies considerably during its lifetime of a few months. For weak sources which remain visible for several months after disappearance of sunspots, the excess flux density over the background has a value of about 2 to 4 units (1 unit$=10^{-22}$ w m^{-2} (cps)$^{-1}$), and this increase is nearly independent of wavelength. For strong sources, the observed range of flux densities is about 7 to 30 units at 21 cm, and about 10 to 70 units at 3 and 10 cm. Most of the strong sources show a peak in their spectrum around 5 to 10 cm. However, for some very intense sources it has been noted that the flux density is higher at 3 than at 10 cm. For comparison, the flux density of the quiet sun near sunspot minimum is about 20, 30, 70, and 235 units at 60, 21, 10, and 3 cm.

The weak sources are associated very closely with the chromospheric plages. For strong sources, the size is smaller at cm than at dcm wavelengths. The height of the emitting region

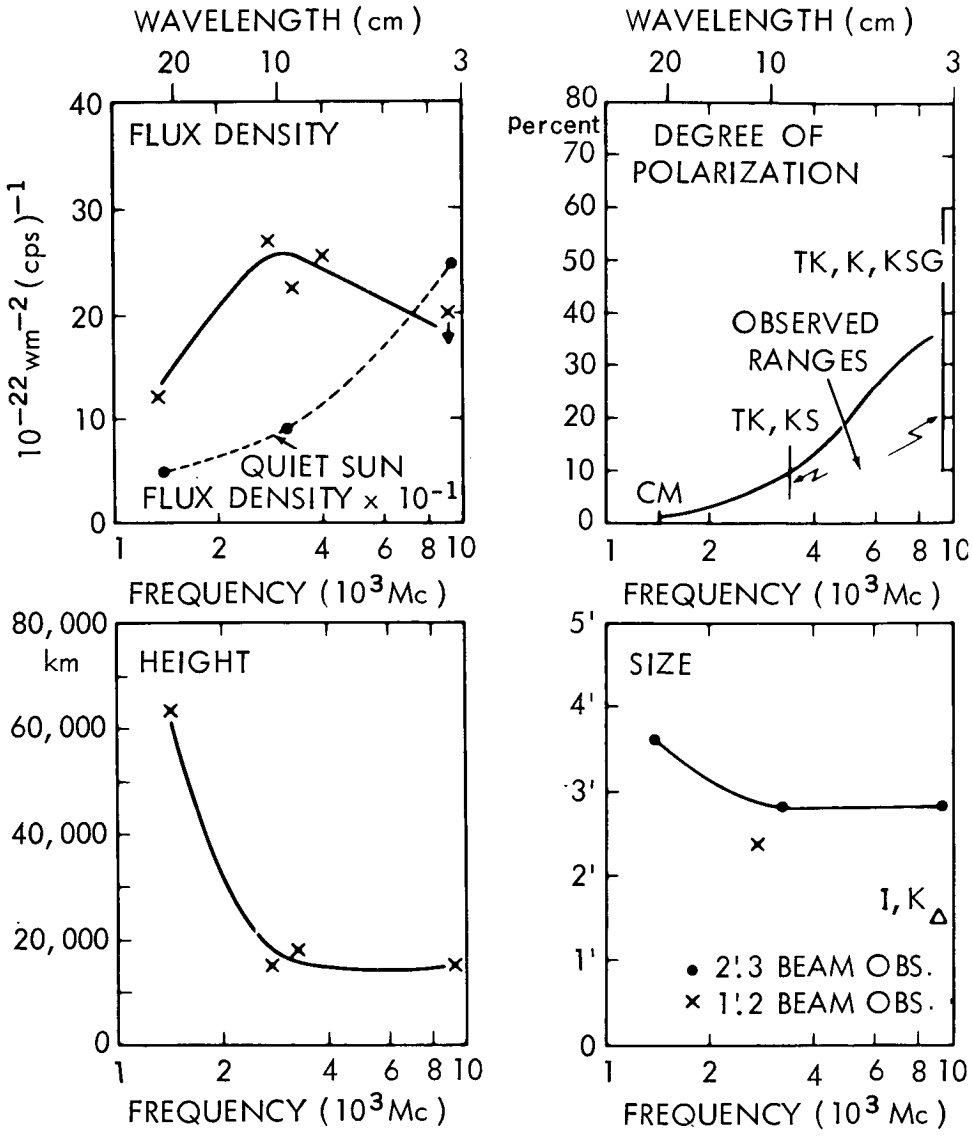

FIGURE 22–13. Variation of the characteristics of a strong source of the slowly varying component with wavelength. (Swarup et al., Reference 31)

is, on an average, about 40,000 km at 21 cm and about 15,000 km at 3 and 10 cm. The measurements of height have not yet revealed any systematic dependence on the activity of the emitting regions.

The measured values of brightness temperature lie in the range of about 3×10^4 to about 5×10^5 °K at 3 cm, about 5×10^4 to 4×10^6 °K at 10 cm, and about 2×10^5 to 1.5×10^6 °K at 21 cm. Observations made with a 1.2′ beam show that the brightness temperature at 10.7 cm exceeds 1.5×10^6 °K not just for a day or two, but during nearly all the period when the area of the associated sunspot group is larger than about 500 millionths (Reference 31). On the other hand, observations with a 3′ beam at 21 cm show a cutoff at about 1.5×10^6 °K (Reference 29). According to our expectations, the peak values of brightness temperature should be nearly the same at 10 and 21 cm. It may be that a strong source at 21 cm has a core of higher brightness temperature of about

2 to 4×10^6 °K which was not resolved by the 3′ arc pencil beam. Observations with a 1′ arc beam at 21 cm are needed to resolve this question.

The radio emission from a strong source shows a small degree of circular polarization which is $\gtrsim$30 percent at 3 cm, $\approx$10 percent at 10 cm, and $<$2 percent at 21 cm.

As will be shown in the next section, the above characteristics can be explained by assuming that the radio emission originates thermally in regions of enhanced electron densities and magnetic fields that lie over sunspots or plages. Optical observations have indicated that, above a complex sunspot group of type E or F, the electron density may increase for a few days to about 20 times the normal (References 13 and 47); but for most plage regions the values are about 5 times the normal (Reference 14). The close connection noted by Babcock (Reference 48) between chromospheric plages and photospheric magnetic fields suggests that the high densities are produced by a magnetic "bag" effect due to localized fields.

Denisse and Kundu (Reference 49) have shown that there exists a close correlation between the ionization of the E-layer of the earth's ionosphere and the slowly varying component of radio emission. This is in accord with the earlier findings of Allen (Reference 50), who demonstrated an association between the E-layer ionization and chromospheric plage. The connection arises because both the x-ray emission, which produces the ionization, and the radio emission are dependent on the square of the electron density. Blake et al. (Reference 51) have compared an x-ray map of the sun obtained during a rocket flight with a 9.1 cm map obtained by the author at the Stanford University. As shown in Figure 22–14, there exists a close correlation between the x-ray and the radio map.

THE ORIGIN OF THE SLOWLY VARYING COMPONENT

The first theory proposed (References 2 and 12) to explain the origin of the slowly varying component was that the magnetic field associated with sunspots raised the reflection level of the extraordinary ray from the cool chromosphere into the hot corona. Waldmeier and Muller (Reference 13) postulated that the radio emission is due to collision of electrons with ions (free-free transitions) in regions of abnormally dense "coronal condensations" which have been observed optically. An explanation given by Piddington and Minnett (Reference 11) considered collisional absorption from hot and dense regions in the presence of magnetic fields.

From optical observations, Newkirk (Reference 14) has deduced that the average densities above plages are about 5 times that of Van de Hulst's model for equatorial regions at sunspot maxima. He has computed characteristics of radio emission from these dense regions, assuming a temperature of $1\text{–}2\times10^6$ °K, and found reasonable agreement with the observations available at that time.

Recent, high resolution observations have shown that, while the flux density of a strong source decreases with decreasing wavelength in nearly 10 to 3 cm wave region, the degree of polarization increases. Kakinuma and Swarup (Reference 15) have shown that it is difficult to explain this result if we consider only the effect of electron-ion collisional absorption, and have suggested that resonance absorption by a thermal electron at the gyro-frequency and its harmonics also should be taken into account, The mechanism of resonance absorption has been independently proposed by Zheleznyakov (Reference 52), who argued for it on the basis of high values of brightness temperature at 3.2 cm ($\approx0.5\times10^6$ °K) that have been observed by Kundu and Ikhsanova. Earlier, Ginzburg and Zheleznyakov (Reference 53) had suggested that this mechanism might be significant for the theory of radio bursts.

It therefore appears that, while it may be sufficient to consider only the collisional-absorption theory for sources of the *S*-component with weak or moderate strength, we should also consider the resonance-absorption mechanism for the case of strong sources, particularly in the range of about 3 to 10 cm. Brief details of the two theories are presented below.

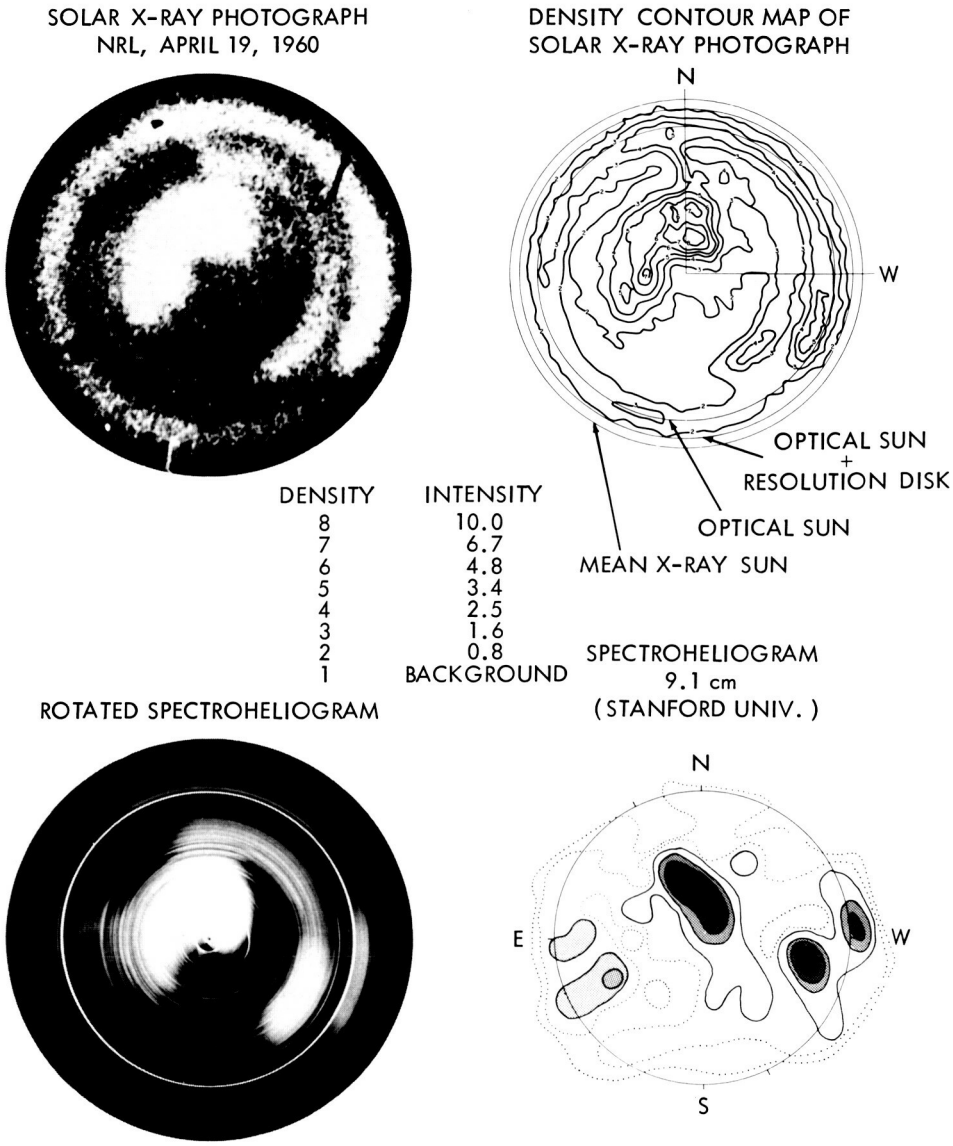

FIGURE 22–14. Comparison of an x-ray photograph obtained on April 19, 1960, with a 9.1 cm spectroheliogram obtained by Swarup on the same day. The x-ray camera got rotated during the rocket flight, and therefore the 9.1 cm map was for comparison purposes artificially smeared by rotation. (Blake et al., Reference 51)

Collisional Absorption Theory

The absorption coefficient in nepers per cm is approximately (Reference 54)

$$\mathcal{K}=\frac{\zeta N^2}{f^2\mu T_e^{3/2}},$$

where N is the electron density (cm^{-3}), ζ equals 0.16 in the corona and 0.11 in the chromosphere, f is the frequency of the radio radiation, μ is the refractive index of the medium, and T_e is the electron temperature. In the absence of a magnetic field the refractive index is

$$\mu=\sqrt{\left(1-\frac{f_0^2}{f^2}\right)},$$

where $f_0=(81\times10^6\,N)^{1/2}$ is the plasma frequency

of the medium. The optical depth of the emerging ray is

$$\tau=\int_s^\infty \mathcal{K}(s)\,\mathrm{d}s,$$

where s is the path length along the ray. The apparent brightness temperature observed for any path is

$$T_b=\int_0^\tau T_e(\tau)e^{-\tau}\,\mathrm{d}\tau.$$

If the chromospheric contribution is given by T_{CH}, and the corona is at a constant temperature of T_c, the above equation becomes

$$T_b=T_c(1-e^{-\tau})+T_{CH}e^{-\tau},$$

where τ is the optical depth of the corona.

Recently Christiansen et al. (Reference 28) combined high resolution observations of one solar active region obtained at wavelengths of 7.5, 21, 88, and 176 cm and derived physical conditions in the solar atmosphere by applying the following two equations:

$$T_b=\int_0^{\tau_{max}} Te^{-\tau}\mathrm{d}\tau$$

and

$$\bar{\rho}=\frac{\int_0^{\tau_{max}} \rho\mathrm{d}T_b}{\int_0^{\tau_{max}} \mathrm{d}T_b},$$

where $\bar{\rho}$=mean height of the origin of emergent radiation. Their model is shown in Figure 22–15.

For the case of thermal emission from an ionized gas without a magnetic field, it has been shown by Piddington (Reference 55) that the flux density does not decrease with decreasing wavelength except near plasma frequency, which in solar corona is much lower than the frequencies corresponding to cm wavelengths. In the presence of a magnetic field, however, it can be shown (References 11 and 15) by magneto-ionic theory that the optical depth of the extraordinary wave increases for both quasi-transverse and quasi-longitudinal cases, and that of the ordinary wave remains the same for the former case and decreases for the latter. It may be argued that this accounts for

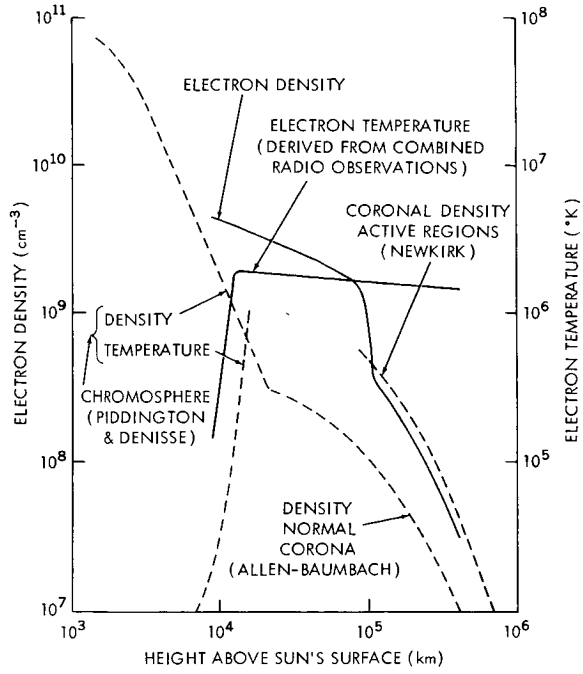

FIGURE 22–15. The variation of electron density and temperature with height, derived from radio observations of a selected active region on the sun. (Christiansen et al., Reference 28)

the increase of flux density near 10 cm because the value of magneto-ionic parameter $Y=f_H/f$, where f_H is the gyro-frequency, is larger at 10 than at 3 cm. But it can be shown (Reference 15) that this increase would be expected to be accompanied by a larger degree of polarization at 10 than at 3 cm, which is contrary to observations. It is therefore concluded that it is not sufficient to consider only the effect of electron-ion collisions for deriving a model of a strong source at centimeter wavelengths.

Resonance Absorption Theory

In the presence of a magnetic field, the thermal electrons of the solar atmosphere produce absorption not only due to electron-ion collisions but also due to resonance radiation at the gyro-frequency and its harmonics. At the fundamental frequency it is sufficient to consider only the resonance absorption for the ordinary wave, since the extraordinary would not escape because of reflection at $Y=1-X$ level, which lies at a greater height than $Y=1$ level. Sitenko and Stepanov (Reference 56)

have derived a dispersion equation of the ionized gas with a magnetic field using kinetic equations and have also derived an expression for the absorption coefficient for the ordinary ray. Expressions giving the absorption coefficients for the harmonics of gyro-frequency have been derived from the above dispersion equation by several workers (References 15, 52, 53, and 57), who have used different approximations.

It has been shown by the above workers that the absorption coefficients for the fundamental $\omega=\omega_H$ and the second harmonic $\omega=2\omega_H$ are proportional to the square root of the electron temperature T_e, and for the third harmonic to $T_e^{3/2}$. The absorption coefficients increase with electron density and wavelength both for the fundamental and harmonics; further, they show an approximate proportionality in the case of harmonics. Assuming that $N_e=10^9/\text{cm}^3$ and $T_e=2\times10^6$ °K, the absorption coefficients at 8 cm have been calculated by Kakinuma and Swarup (Reference 15) as a function of the angle θ between directions of magnetic field and ray propagation for the fundamental as well as for the second and third harmonics; and the calculated values are shown in Figure 22–16. When the frequency ω of the propagating ray is a little different from $2\omega_H$ or $3\omega_H$, the absorption coefficients decrease rapidly. The effective thickness of the absorbing layer is (Reference 53)

$$L=h_0\left(\frac{2\pi}{3}\right)^{\frac{1}{2}}\mu\left(\frac{v}{c}\right)\cos\theta,$$

where h_0 is the scale of the magnetic field, v is the thermal velocity of the electron, and θ the angle between the magnetic field and direction of propagation. Assuming $h_0=4\times10^4$ km, we find that L is about 700 km. The optical depth is given by $\tau=\kappa L$. Approximate values of the optical depth may be obtained from the scales shown on the right-hand side of Figure 22–16. It is seen that values of optical depth due to resonance absorption are much greater than those due to collisional absorption. A schematic model showing resonance absorption layers and size of polarized regions is shown in Figure 22–17.

In the case of a large sunspot group, the $\omega=2\omega_H$ level for a 10 cm wavelength might lie in the solar corona. This requires that $H=550$ gauss at a height of nearly 15,000 km—which is the observed height for the 10 cm source. Since the optical depth of the $2\omega_H$ level is greater than 1 for both ordinary and extraordinary rays (except for small values of θ) the brightness temperature of the 10 cm source is equal to the coronal temperature and the source has a small degree of polarization. However, the $\omega=2\omega_H$ level of 3.2 cm requires a high value of 1700 gauss and therefore lies mostly in the cooler chromosphere except, perhaps, for some very intense regions. Therefore, for most of the 3.2 cm sources it is sufficient to consider the collisional absorption theory only. Even if the electron density is 20 times the normal, the optical depth at 3.2 cm wavelength due to collisional absorption in a coronal condensation is less than 1 for both extraordinary and ordinary rays, although it is larger for the former than the latter. Consequently the flux density decreases with decreasing wavelength in the range 10 to 3 cm, but the degree of polarization increases.

The theory of resonance absorption not only explains the observed spectra of flux and polarization but also accounts for the small size and high brightness temperature of the source at centimeter wavelengths. The theory predicts a lot of fine structure, with peculiar peaks and dips, in the brightness distribution across the radio sources at cm wavelengths for both polarized and random components. Also, we expect a sudden change in the brightness distribution in the range of about 3 to 6 cm, where the 2 ω_H level may emerge from the cooler chromosphere into the hot corona. In order to verify the theory and to determine electron densities, temperatures, and magnetic fields in inner corona, it will be desirable to construct arrays with beamwidths of less than 0.5′ arc.

ASSOCIATION WITH FLARE ACTIVITY

Measurements made by Kundu (Reference 58) with a two-antenna interferometer in 1957 have shown that there exists a good correlation between the amplitude of observed fringes, which is a measure of amplitude of sources of

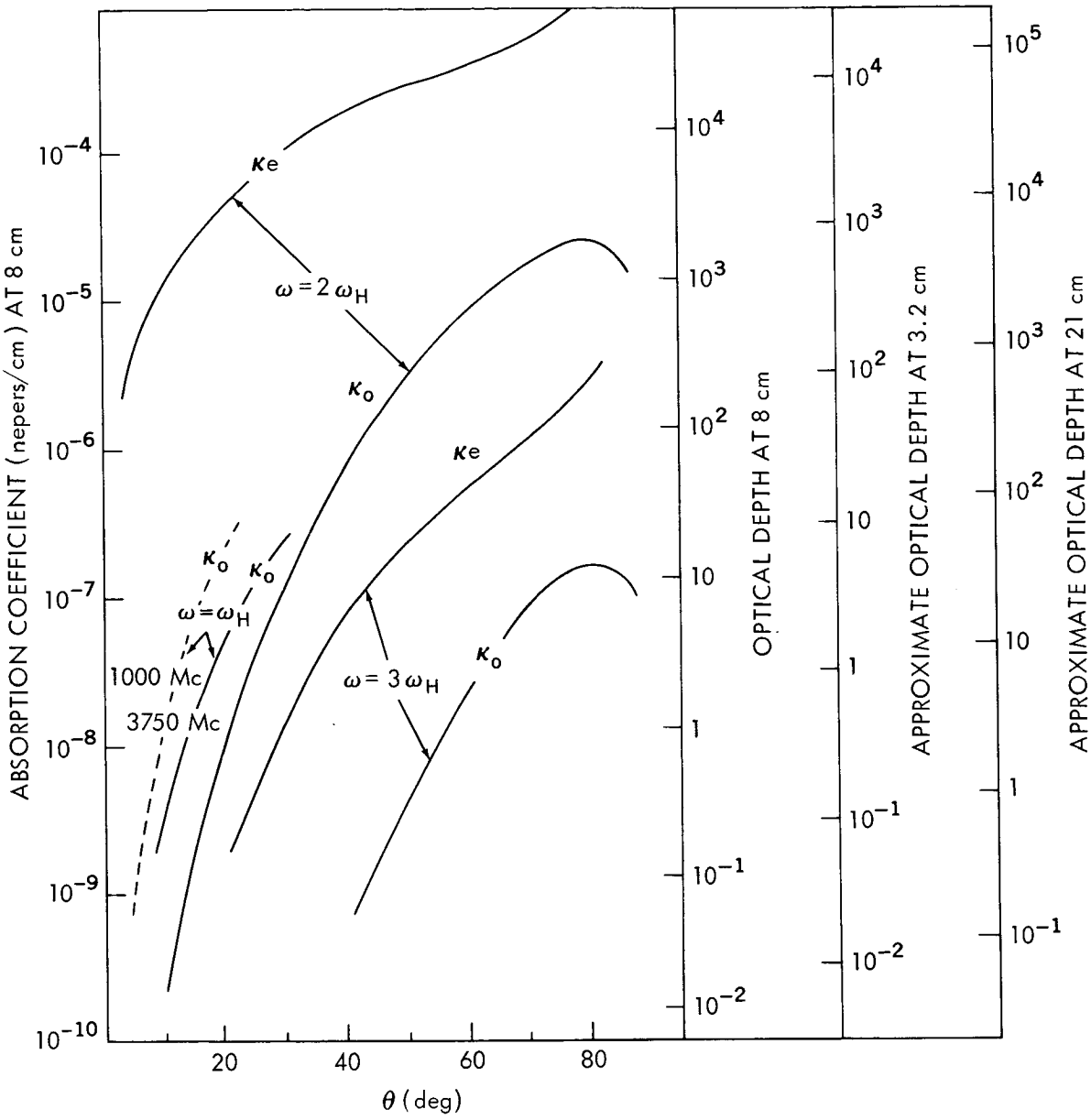

FIGURE 22–16. Resonance absorption coefficients at 8 cm wavelength for the ordinary (κ_0) and extraordinary rays (κ_e) in an ionized gas with $N_e = 10^9/\text{cm}^3$; $T_e = 2 \times 10^6$ °K; and magnetic fields corresponding to $\omega = \omega_H$, $2\omega_H$, or $3\omega_H$. The scales on right-hand side show optical depths at 3.2, 8, and 21 cm for an effective layer thickness of 700 km. (Kakinuma and Swarup, Reference 15)

diameter less than about 2′ arc, and the number of bursts observed on 3 cm wavelength on the same day (see Figure 22–18). It was suggested that this relation might be used for a certain form of forecast of chromospheric flares. This tendency of intense sources of small diameter to give rise to bursts has been verified by Pick (Reference 59) from observations made with a 4.5′ arc fan beam at 3.2 cm during the years 1958 and 1959. It was found, as shown in Table 22–1, that the 3.2 cm sources which had flux density of greater than 60×10^{-22} w m^{-2} (cps)$^{-1}$ were associated with many times more cm wave outbursts (identified as Type IV) than

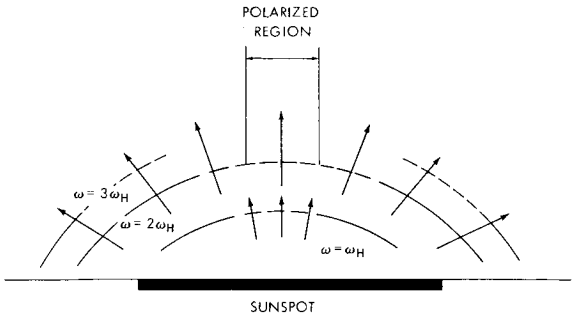

FIGURE 22–17. Schematic model showing resonance absorption layers and regions of circular polarization over a sunspot group. (Kakinuma and Swarup, Reference 15)

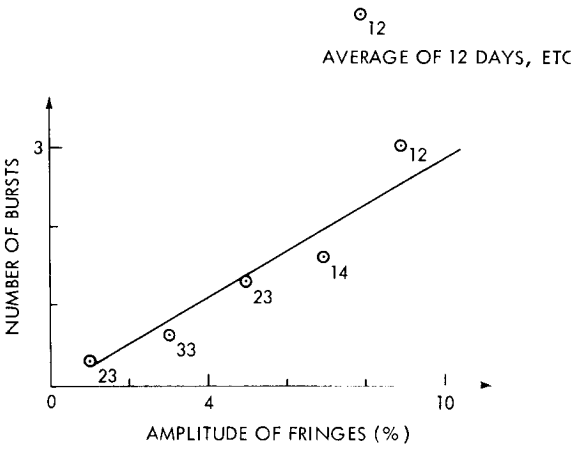

FIGURE 22–18. Number of bursts observed per day plotted against mean amplitude of interferometric fringes (expressed in percentage of total solar radiation) observed around noon. The number of days on which a given range of amplitude was observed are indicated besides each point. (Kundu, Reference 58)

TABLE 22–1

3 cm=λ Radio Source		Number of cm—λ Outbursts (Type IV)
Flux Density S [10^{-22} w m^{-2} (cps)$^{-1}$]	Number	
$S<30$	24	1
$30\leq S<60$	26	6
$S\geq 60$	6	20

those with smaller flux-density. However, the above authors did not make any comments on the question of whether or not this relation is simply a result of the fact that large sunspot groups have high flux density at cm-dcm wavelengths. For example, we have plotted scatter diagrams of the number of flares of importance greater than 1+ against sunspot area, and also against 9.1 cm flux density of solar active regions, and we find that there is no appreciable difference in the two scatter diagrams.

Recently, the French workers (Reference 60) have shown that there exists a higher tendency for a solar active region with a given optical importance to give rise to type IV bursts if its 3.2 cm flux density is higher than the average value of flux density for that optical importance. It is known that 14 out of 26 PCA events which have been seen since July 1959 came from four solar active regions with CMP on July 15, 1959; April 1, 1960; November 12, 1960; and July 14, 1961. All these four regions had flux density near CMP of more than about 60 units at 3.2 cm wavelength. From examination of 3.2 cm records obtained at Toyokawa with a 2.2′ arc fan beam, we have found that the high flux density preceded the occurrence of the first type IV burst by more than a day for at least 2 out of the above 4 regions. Further, the 3.2 cm flux density did not show any appreciable variations from day to day, so that we can rule out the possibility that the high flux density is caused by some high-energy electrons remaining trapped in the active region after type IV bursts. It would be interesting to examine the radio and optical data of these four regions in more detail.

It is suggested that the very intense sources of the S-component at 3.2 cm are due to high magnetic fields which raise the third or even second harmonic gyro-frequency level from the cool chromosphere into the hot corona. This requires that the magnetic field is more than 1200 gauss at the base of the corona above very active regions, and it may be that this high magnetic field is associated with more chromospheric eruptions.

CONCLUSIONS

By means of high resolution observations, it has been established that the slowly varying component originates at heights of about 10^4 to 10^5 km above the photosphere in regions of high coronal densities and magnetic fields that lie above sunspots and plages.

It appears that the radio emission is due to two different thermal mechanisms: electron-ion collisional absorption, and resonance absorption at harmonics of gyro-magnetic frequency. The latter mechanism becomes effective when sunspots and magnetic fields appear in a solar active region. By combining the two mechanisms we can explain satisfactorily observations of both weak and strong sources. This explanation requires (Reference 15) that the electron densities of the corona above a large sunspot group have values of about 5 to 10 times the normal, and the average strength of the magnetic field is about 600 and 250 gauss at heights of 2×10^4 km and 4×10^4 km, respectively. Because of the observed steadiness of the *S*-component over periods of days, it has been postulated that it originates thermally. This requires that the value of the electron temperature in the inner solar corona above a large sunspot group is about $2\text{–}4\times10^6$ °K.

REFERENCES

1. Covington, A. E., 1948, *Proc. IRE*, 37: 407.
2. Lehany, F. J., and Yabsley, D. E., 1949, *Aust. J. Sci. Res.*, A2: 48.
3. Pawsey, J. L., and Yabsley, D. E., 1949, *Aust. J. Sci. Res.*, A2: 198.
4. Denisse, J. F., 1949, *C.R. Acad Sci., Paris*, 228: 1571.
5. Wild, J. P., 1963, *these Proceedings*, paper no. 21.
6. Firor, J., 1959, *Paris Symp. on Radio Astronomy*, ed. R. N. Bracewell (Stanford, Calif.: Stanford University Press), 136.
7. Moutot, M., and Boischot, A., 1961, *Ann. d'Astrophys.*, 24: 171.
8. Salomonovitch, A. E., 1962, *Astr. Zhurn.* 39: 260 (*Sov. Astron.–AJ*, 6: 202).
9. Covington, A. E., 1947, *Nature*, 159: 405.
10. Christiansen, W. N., Yabsley, D. E., and Mills, B. Y., 1949, *Aust. J. Sci. Res.*, A2: 506.
11. Piddington, J. H., and Minnett, H. C., 1951, *Aust. J. Sci. Res.*, A4: 131.
12. Denisse, J. F., 1950, *Ann. d'Astrophys.*, 13: 181.
13. Waldmeier, M., and Muller, H., 1950, *Zs. f. Ap.*, 27: 58.
14. Newkirk, G., Jr., 1961, *Astrophys. J.*, 133: 983.
15. Kakinuma, T., and Swarup, G., 1962, *Astrophys. J.*, 136: 975.
16. Christiansen, W. N., and Warburton, J. A., 1953, *Aust. J. Phys.*, 6: 190.
17. Tanaka, H., and Kakinuma, T., 1953, *Proc. Res. Inst. Atmosph., Nagoya U.*, 2: 53.
18. Tanaka, H., and Kakinuma, T., 1955, *Proc. Res. Inst. Atmosph., Nagoya U.*, 3: 102.
19. Covington, A. E., and Broten, N. W., 1954, *Astrophys. J.*, 119: 569.
20. Christiansen, W. N., Labrum, N. R., McAlister, K. R., and Mathewson, D. S., 1961, *Proc. IEE*, 108B: 48.
21. Bracewell, R. N., and Swarup, G., 1961, *Trans. IRE Antennas Propagation*, AP 9: 22.
22. Vitkevitch, V. V., Kuzmin, A. D., and Salomonovitch, A. E., 1958, *Aked. Nauk S.S.S.R., Doklady*, 118: 1091.
23. Christiansen, W. N., Warburton, J. A., and Davies, R. D., 1957, *Aust. J. Phys.*, 10: 491
24. Swarup, G., and Parthasarathy, R., 1958, *Aust. J. Phys.*, 11: 338.
25. Kakinuma, T., 1956, *Proc. Res. Inst. Atmosph., Nagoya U.*, 4: 78.
26. Dodson, H. W., 1954, *Astrophys. J.*, 119: 564.
27. Covington, A. E., and Harvey, G. A., 1960, *Astrophys. J.*, 132: 435.
28. Christiansen, W. N., Mathewson, D. S., Pawsey, J. L., Smerd, S. F., Boischot, A., Denisse, J. F., Simon, P., Kakinuma, T., Dodson-Prince, H., and Firor, J., 1960, *Ann. d'Astrophys.*, 23: 75.
29. Christiansen, W. N., and Mathewson, D. S., 1959, *Paris Symp. on Radio Astronomy*, ed. R. N. Bracewell (Stanford, Calif.: Stanford University Press), 108.
30. Swarup, G., 1961, Scientific Rept. No. 13, Contract AF 18 (603)–53, Stanford Electronics Labs., Stanford, Calif.
31. Swarup, G., Kakinuma, T., Covington, A. E., Harvey, G. A., Mullaly, R. F., and Rome, J., 1963, *Astrophys. J.*, 137: 1251.
32. Covington, A. E., Harvey, G. A., and Dodson, H. W., 1962, *Astrophys. J.*, 135: 531.
33. Kundu, M. R., 1959. *Ann. d'Astrophys.*, 22: 1.
34. Ikhsanova, V. N., 1960, *Proc. Pulkova Obs.*, 21: 62.

35. HATANAKA, T., AKABANE, K., MORIYAMA, F., TANAKA, H., and KAKINUMA, T., 1955, *Astron. Soc. Japan Pubs.*, 7: 161.
36. TANAKA, H., and KAKINUMA, T., 1958, *Rept. Ionosphere Res. Japan*, 12: 273.
37. TANAKA, H., and KAKINUMA, T., 1958, *Proc. Res. Inst. Atmosph., Nagoya U.*, 5: 77.
38. TANAKA, H., and KAKINUMA, T., 1960, *Proc. Res. Inst. Atmosp., Nagoya U.*, 7: 79.
39. MOLCHANOV, 1962, *Astr. Zhurn.*, 38: 5; *Sov. Astron.—AJ*, 5: 651.
40. SMERD, S. F., 1963, Paper presented at the XIVth Gen. Assembly of URSI, Tokyo.
41. PICK, M., and STEINBERG, J. L., 1961, *Ann. d'Astrophys.*, 24:45.
42. VAUQUOIS, B., 1959, *Paris Symp. on Radio Astronomy*, ed. R. N. BRACEWELL (Stanford, Calif.: Stanford University Press), 143.
43. COVINGTON, A. E., 1949, *Proc. Inst. Radio Engrs.*, 37: 407.
44. KUNDU, M. R., 1959, *Paris Symp. on Radio Astronomy*, ed. R. N. BRACEWELL (Stanford, Calif.: Stanford University Press), 222.
45. TANAKA, H., 1961, *Proc. Res. Inst., Atmosph., Nagoya U.*, 8: 51.
46. KOROLKOV, D. V., SOBOLEVA, N. S., and GELFREIKH, G. B., 1960, *Proc. Pulkova Obs.*, 21: 81.
47. WALDMEIER, M., 1956, *Zs. f. Ap.*, 40: 221.
48. BABCOCK, H. W. and BABCOCK, H. D., 1953, *Ap. J.*, 121: 349.
49. DENISSE, J. F., and KUNDU, M. R., 1957, *Comptes Rendus*, 224: 45.
50. ALLEN, C. W., 1948, *Terr. Magn. Atmos. Elect.*, 53: 433.
51. BLAKE, R. L., CHUBB, T. A., FRIEDMAN, H., and UNZICKER, A. E., 1963, *Ap. J.*, 137: 1.
52. ZHELEZNYAKOV, V. V., 1962, *Astr. Zhurn.*, 39: 5 (*Sov. Astron.-AJ*, 6: 3).
53. GINZBURG, V. L., and ZHELEZNYAKOV, V. V., 1959, *Sov. Astron.*, 3: 236.
54. PAWSEY, J. L., and BRACEWELL, R. N., 1955, "Radio Astronomy," (Oxford: Oxford University Press), 83.
55. PIDDINGTON, J. H., 1951, *Mon. Not. Royal Astron. Soc.*, 111: 45.
56. SITENKO, A. G., and STEPANOV, K. N., 1957, *Soviet Physics*, JETP 4: 512.
57. WILD J. P., SMERD, S. F., and WEISS, A. A., 1963, *Annual Review of Astronomy and Astrophysics*, ed. L. Goldberg (Palo Alto, Calf.: Annual Reviews), 1: 291.
58. KUNDU, M. R., 1958, *Comptes Rendus*, 246: 2740.
59. PICK, M., 1961, *Ann. d'Astrophys.*, 24: 199.
60. LE SQUEREN, A. M., 1963, *these Proceedings*, paper no. 23.

DISCUSSION

Dr. Oster: Could you give a simple explanation for the fact that you get the strictly relativistic higher harmonics of the gyrofrequency at mean electron speeds of less than 1 percent of the speed of light?

Dr. Swarup: Yes. Even though most of the electrons have comparatively low speed compared with the velocity of light, still—since the electron density is very high, of the order of $10^9/cm^3$—the number of electrons exceeding several times the average value of 1 percent is appreciable. This gives rise to appreciable radiation at the first few harmonics.

Dr. Oster: You need particles of the order of ⅓ to 1/10; I would say ⅓ the speed of light. This is the extremely high energy tail of the distribution function.

Dr. Swarup: Yes. For example, in the case of microwave bursts, according to Takakura's theory, one does need velocities of the order you indicated; but the number of electrons required is very few—just a few per cubic centimeter.

I feel that even somewhat lower velocities than what you are indicating may be sufficient, but with a larger number of electrons.

Dr. Moore: On this point, I have a short paper tomorrow, in which I will show that there are ways of exciting these higher harmonics at the cyclotron frequencies other than by having relativistic electrons.

NW 30273 3

23 STUDY OF SOLAR NOISE STORMS AT 169 MC/S WITH THE AID OF THE NANCAY INTERFEROMETER*

A. M. Le Squeren
Observatoire de Paris, Section d'Astrophysique
Meudon (Seine et Oise), France

ABST 30273

The measurement of the positions of noise storm centers with the Nancay interferometer (References 1, 2, and 3), which is carried out with a precision of the order of the minute of arc, has permitted a more effective study of the connection between these storms and the centers of optical activity. In particular, we have emphasized the following points:

1. The relation between storm commencements and the chromospheric flares,
2. The connection between the sense of polarization of storms and the hemisphere in which the visible center associated with the coronal center is located,
3. The variation of the apparent position of the storms as a function of heliocentric longitude.

Author

RELATION BETWEEN STORM COMMENCEMENTS AND THE CHROMOSPHERIC FLARES

The interferometer allowed us to identify, often without too much ambiguity, the center of optical activity associated with the center of a storm that appears or undergoes an increase. Out of 109 commencements or increases of storm with flux densities exceeding 3×10^{-21} w m^{-2}(c/s)$^{-1}$, noted between 1958 and 1961, it is possible to associate with 85 percent of these cases a flare that has taken place within the 2 hours preceding the increase of flux at meter wavelengths. In most cases the flare is related to the center of activity which can be associated to the storm.

To check this association (which might be fortuitous because of the multiplicity of flares), we have used the method of superposed epochs. We have taken the time of the commencement of the storm as the zero hour, and we have counted the number of flares which started in the optical centers connected with the storms in the course of each of the 5 hours centered on the time zero. Figure 23–1 clearly shows that

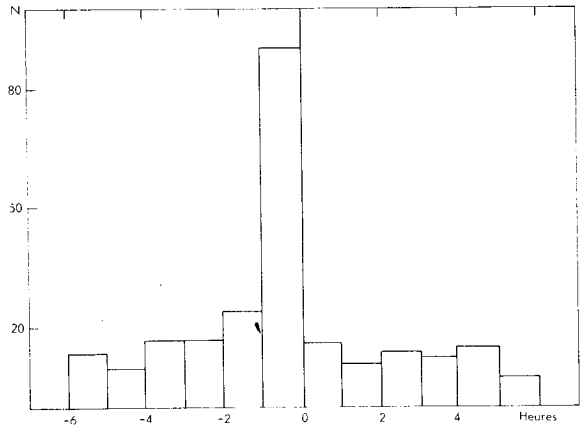

FIGURE 23–1.

the number of flares increases in the 2-hour interval preceding the radio event.

The storm centers for which the commencement or the augmentation is not connected with a flare are located in the eastern part of the disk in the majority of cases. Their appearance is naturally interpreted as due to the sun's rotation.

*Etude des orages radioélectriques solaires sur 169 MHz à l'aide de l'interféromètre de Nançay. This paper was given by Dr. André Boischot.

728–629 O—64——14

CONNECTION BETWEEN THE POLARIZATION DIRECTION AND THE HEMISPHERE OF THE ASSOCIATED OPTICAL CENTER

If one expresses (Figure 23–2) the sense of polarization of a continuum storm as a function of the latitude of the associated optical center, one sees that *there exists a preferred sense of polarization for each hemisphere.* If one supposes that the sense of the magnetic field in the corona at the level of the storms is determined by that of the leading spot, one deduces that the storm radiation corresponds to the ordinary mode of the magneto-ionic theory. Ten percent of the storm centers do not obey this law. In these cases, the associated optical centers have a complex structure in which the trailing spot sometimes has a stronger field than that of the leading spot.

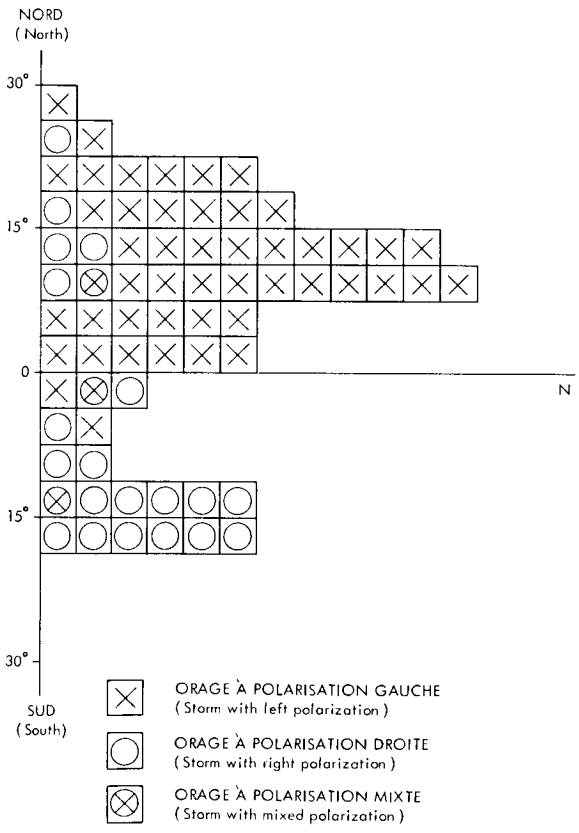

FIGURE 23–2.

THE VARIATION OF THE APPARENT POSITION OF THE STORMS AS A FUNCTION OF HELIOCENTRIC LONGITUDE

In the majority of cases the emission source occupies neither a radial nor a geometrical position that is well defined relative to associated optical centers, and it is impossible to measure for each case the altitude of the emission source. However, if the average is taken over a great number of cases, there appears a systematic altitude variation of the center of the storm as a function of its heliocentric longitude.

Curve C of Figure 23–3 represents the mean distance d of storm centers from the polar axis as a function of the distance δ of the associated optical spots from the same axis. The ratio d/δ measures the apparent altitude of storm centers. It may be seen that this altitude increases with the longitude: It varies from 0.15 $R_\odot$ above the photosphere for storms situated at the center of the disk to 0.5 $R_\odot$ for the storms situated at the limb.

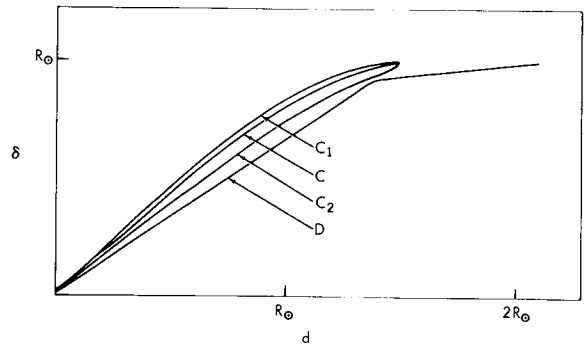

FIGURE 23–3.

It is possible to explain simultaneously the storm directivity, which is well known, and the altitude variation by assuming that statistically the intensity of storms decreases with increasing altitude. Indeed, as a result of the conditions of electromagnetic wave propagation in the corona, it is well known that there exists a cutoff level higher above the limb than at the center of the disk. If we admit that the decrease in storm intensity as a function of altitude is very rapid, we see that—on the

average—the altitude of storms for each longitude will be near the altitude of the point corresponding to the occultation surface and slightly above. Storms at lower altitudes will be occulted, and the contribution of storms of higher altitudes will be of little importance.

This interpretation allows the determination from the curve of directivity of the distribution of storm intensities with altitude. It can be verified in Figure 23–4 that this decrease is very rapid and that the emissivity of coronal regions is practically proportional to the electron density.

The knowledge of this emissivity and of the surface of occultation computed from the coronal densities, recently measured by Newkirk (Reference 4), has allowed us to compute the variation of the apparent altitude of the storms.

The curve C_1 of Figure 23–3 represents the altitude of the occultation surface and the curve C_2 that of the storms, calculated as indicated above.

We may notice that the proposed interpretation accounts very satisfactorily for the observations.

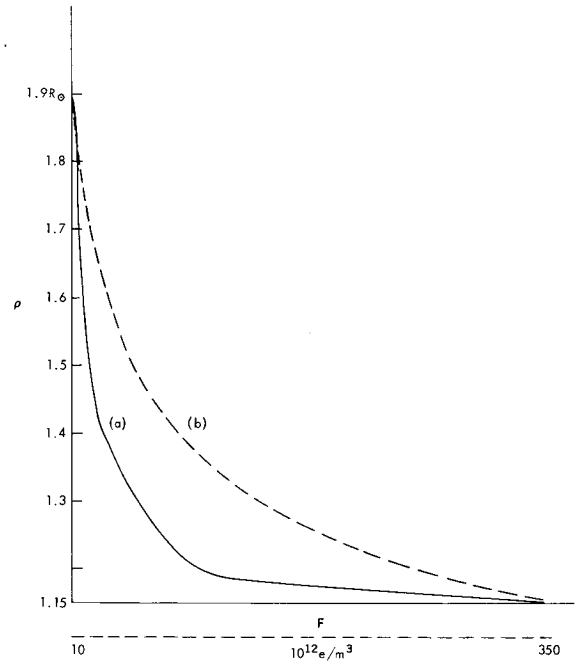

FIGURE 23–4.

REFERENCES

1. LESQUEREN, A. M., 1963, *Ann. Astrophys.*, 26(2): 1–56.
2. AVIGNON, V., BLUM, E. J., BOISCHOT, A., CHARVIN, R., GINAT, M., and SIMON, P., 1957, *C.R. Ac. Sc.*, 244: 1460.
3. BLUM, E. J., 1961, *Ann. Astrophys.*, 24(4): 359–366.
4. NEWKIRK, G. A., 1961, *Astrophys. J.*, 133: 983.

DISCUSSION

Dr. Oster: You showed polarization in the northern and southern hemispheres. Is that just reflecting the change in the normal sunspot cycle? Do you expect to find the reverse if you did the same graph in the next cycle?

Dr. Boischot: Yes. There have been observations during the previous cycle by Australian observers, and they did observe the inverse sense.

Mrs. Smith: I am curious about this correlation you find of noise storms with flares. What importance flares were these, and how do you decide when the next storm starts? It seems to me that the storms have many fluctuations up and down. What do you actually call the commencement of a noise storm?

Dr. Boischot: We retain as "commencement" or "enhancement" of noise storms the events which corresponded on 169 Mc to an increase of flux equal to, or greater than, 3×10^{-21} w m^{-2} (c/s)$^{-1}$ in a period of less than 1 hour. The associated flares were generally of Importance 1 and larger. Only in 10 percent of all cases do we have to associate a 1— flare.

Dr. Haddock: You don't predict flares from noise storms? The state of the corona after the flare in the noise storm study is important.

Dr. Boischot: We can't predict flares from noise storms because, in general, flares precede noise storms. Anyhow, the metric radio emission would be a bad indicator of visible activity because it is very directive.

Dr. Maxwell: In the case of a large sunspot, the noise storm radiation is quite variable and lasts for many days. Also, you may have flares being generated by the sunspot every 30 minutes or so. What is the probability of chance correlation between a flare and an apparent increase in the noise storm radiation? It must be very high.

Dr. Boischot: From Figure 23–1 we can see that the probability of having a flare within 2 hours before a radio event is about 6 times greater than the average probability.

N64-30215 4

24 STUDY OF THE SLOWLY VARYING COMPONENT AT 9400 MC/S AS A FUNCTION OF SOLAR ACTIVITY*

C. CAROUBALOS
Observatoire de Paris, Section d'Astrophysique
Meudon (Seine et Oise), France

The centers of solar activity are associated with continuous emission observed mainly at centimeter wavelengths and called radioelectrical condensations. These centers are sometimes the seat of chromospheric flares which give rise to various radioelectrical emissions. Among the latter, type IV radio bursts are particularly significant. Numerous authors have shown that they are particularly closely linked to solar cosmic rays produced at the moment of strongest flares, as well as to geomagnetic storms that follow several tens of hours later.

As was already established, certain centers associated with a strong condensation are "privileged" and give rise to several type IV radio bursts during their passage across the solar disk (Reference 1). We shall designate them as "repetition centers"; these are generally intense at 9400 Mc/s. To take this more precisely, we have characterized the centimetric condensations by their flux density measured at 9400 Mc/s and averaged over 3 days centered on the central meridian passage. We have designated by N_2 the number of type IV bursts originating in a total of N_1 condensations contained in a certain range of flux density. The diagram of Figure 24–1 shows for the years 1958, 1959, and 1960 the variation of the mean frequency of occurrence N_2/N_1 of type IV bursts as a function of the flux density of the associated centers. Only the most intense centers [$>50\times10^{-22}$ wm^{-2} (c/s)$^{-1}$] give rise to several type IV bursts.

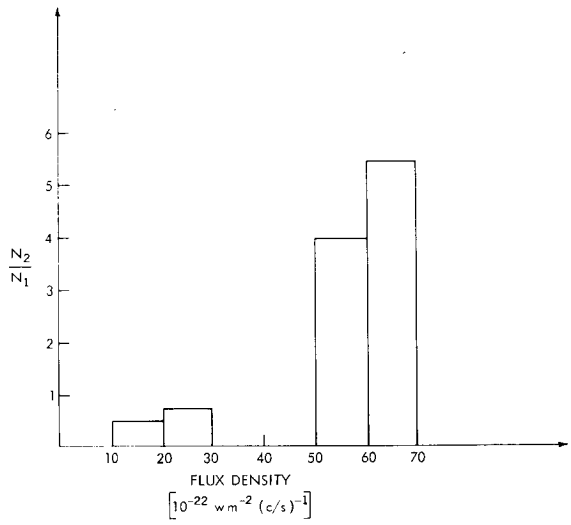

FIGURE 24–1.

Although they represent only 4 percent of the total, the latter are responsible for 40 percent of type IV bursts.

The study of these centers is particularly important for the forecasting of geomagnetic activity. For example, during the period 1958 to 1960 the centers which give at least two magnetic storms with SC, were responsible for more than 58 percent of SSC's, while they constituted 31 percent of all the geomagnetically active centers (Reference 2).

The most intense centers at 9400 Mc/s are thus very representative of the solar activity. Let us note that the emission at this frequency seems to provide a more significant criterion for the identification of repetition centers

*Etude de la composante lentement variable sur 9400 MHz en fonction de l'activité solaire. This paper was given by Dr. André Boischot.

than the emission at lower frequencies (Reference 2).

Elsewhere it has been shown that the flux density of centimetric condensations is very clearly dependent on the area of spots of the associated optical center. On the other hand, it has also been established that this correlation is better at 2800 and 1400 Mc/s than at 9400 Mc/s (Reference 3). It therefore appears that the spot area is not the only parameter intervening in the determination of the flux density of the sources at 9400 Mc/s.

We have reconsidered this study by selecting from all the centers associated with a detected centimetric condensation those that produced type IV bursts during their passage across the solar disk. The dependence of the flux density on the corresponding optical importance is plotted in Figure 24–2. This optical importance is the one indicated in the *Quarterly Bulletin on Solar Activity*. It is related approximately linearly to the spot area. The circles correspond to centers producing type IV bursts, and the dots to all the other centers. It can be seen

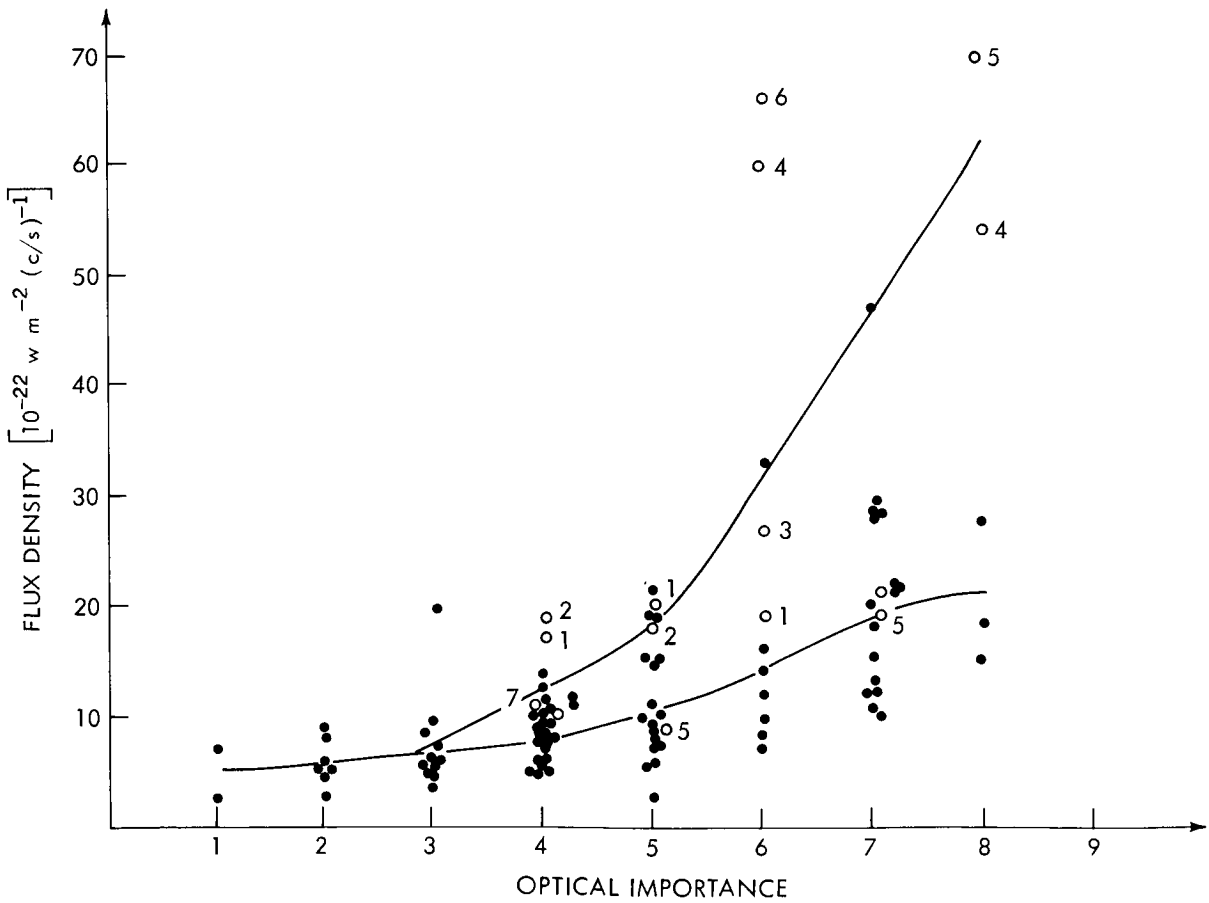

FIGURE 24–2.

that the mean curve obtained for the circles is situated higher than the other.

In conclusion, for an identical optical importance, only centers associated with the most intense centimetric condensations give rise to type IV bursts.

The efficiency of these repetition centers does not appear to be constant in the course of a solar activity cycle. We have computed the annual ratios r_1 of the total number of type IV bursts to the total number of associated centers, and r_2 of the number of type IV bursts stemming from repetition centers to the number of the latter. The graphs of Figure 24–3 show the respective variations of r_1 and r_2 in the course of the solar activity cycle since 1957: they show very clearly that the repetition character of these centers increase sensibly as the solar cycle decreases. The same effect recently has been reported elsewhere (Reference 4).

Finally, we know that the solar activity is localized in privileged regions of the solar disk (References 1 and 5). When one studies the distribution of repetition centers on the solar disk, it can be seen that they are situated mostly in these regions. These would thus be the consequence of these centers' activity and not that of accumulation of isolated cases.

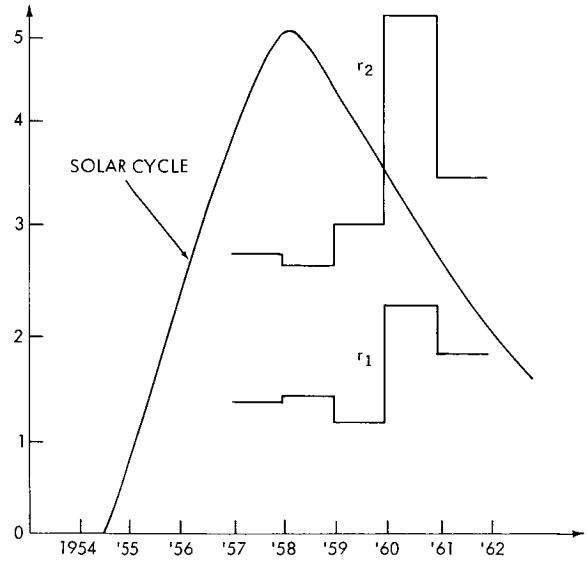

FIGURE 24–3.

REFERENCES

1. PICK, M., 1961, *Ann. d'Ap.*, 24(3): 183–210.
2. CAROUBALOS, C., 1963, *C.R. Ac. Sc.*, 256: 5062–65.
3. SWARUP, G., KAKINUMA, T., COVINGTON, A. E., HARVEY, G. A., MULLALY, R. F., and ROME, J., 1963, *Ap. J.*, 137(4): 1251–67.
4. FOKKER, A. D., 1963, *B.A.N.*, 1: 89–92.
5. NOYES, J. C., 1962, *J. Phys. Soc. Japan*, vol. 17, suppl. "International Conference on Cosmic Rays and the Earth Storm," A 11: 275–81.

N64 30275

25 ACTIVE DARK FILAMENTS AND TYPE III BURSTS*

TATSUO TAKAKURA and A. TLAMICHA†
Tokyo Astronomical Observatory
Mitaka, Tokyo, Japan

At the Ondrejov Observatory, simultaneous observations of a spectrohelioscope by L. Krivsky and radiometers at 231 and 260 Mc/s by A. Tlamicha were made, and showed a clear *time* coincidence between a type of group of bursts—even when the duration is short—and active dark filaments without flare in more than 15 cases during 1960 to 1962. This type of group of bursts, referred to as type N_A and N_B (Reference 1), is a group of short duration bursts without remarkable enhancement of base level. (More detail will be published elsewhere.)

To identify the spectral type of these bursts, the same type of groups of bursts recorded at the Tokyo Astronomical Observatory with a polarimeter at 200 Mc/s has been compared with the spectral data (15–210 Mc/s) obtained at Dapto Station, Sydney. The above type of bursts seems to be the group of type III bursts. Almost all the identifications were made by using a list of the spectral observations "Spectral Classification of Solar Activity, Dapto, Sydney"; but some were already identified with type III bursts by a direct comparison with the spectral records by the courtesy of the Sydney group. Also, these bursts are almost unpolarized as is usual with the type III bursts at 200 Mc/s.

To certify the correlation between the active dark filaments and type III bursts, active prominences and active filaments (without flare) observed in 1960 with a spectrohelioscope have been compared with radio activities observed with an interferometer and a polarimeter at 200 Mc/s at the Tokyo Astronomical Observatory. Even though the number of the optical observations is quite small, a good coincidence in *position* is found in 5 out of 6 cases between the active prominences (and active filaments) *without flare* and groups of type III bursts at 200 Mc/s occurring in the periods of the optical activities. The number of associations of the type III bursts with the optical activities is 8 out of 21, in spite of the fact that the high frequency cutoff for type III bursts sometimes may occur below 200 Mc/s and that the radio waves from the extreme limb may not be observed (Table 25–1).

TABLE 25–1

Active Prominences and Active Filaments		Type III Group at 200 Mc/s			
Type	No. of Events	No. of Associations	Coincidence in Position	No Observations in Position	No Coincidence in Position
Prominence	20	7	4	2	1
Filament	1	1	1	0	0
Total	21	8	5	2	1

During the periods of the active prominences and active filaments mentioned above, 27 cases out of 33 cases have type III groups given in the list of "Spectral Classification of Solar Activity, Dapto, Sydney," in some frequency ranges between 210 Mc/s and 15 Mc/s, although chance coincidences may be included; also, the sensitivity of the spectrometer is not enough to record weaker type III bursts.

*This paper was presented by Dr. Takakura.
†Visiting the Tokyo Astronomical Observatory from the Observatory of Ondrejov, Czechoslovakia.

These results may support a statistically significant, but small, correlation, which has been shown by Swarup, Stone, and Maxwell (Reference 2), between surges without flares and fast-drift bursts observed with spectrometers. The correlation probably would be better if more of the weaker type III bursts had been recorded. Warwick (Reference 3) has shown a good correlation between large ascending prominences and radio activities at 200 Mc/s. Wild and Zirin (Reference 4) have reported that, in some cases, limb surges were associated with groups of type I bursts. These groups of bursts shown in their paper, however, seem to us to be groups of type III bursts.

In order to derive a more definite conclusion, we should like to notice the importance of observations of active dark filaments and active prominences with a spectrohelioscope using a line shifter, taking a *direct* contact with radio observations with a interferometer, a more sensitive spectrometer, and a polarimeter. Both the starting and the location to be observed by the helioscope can be informed by the radio observations.

ACKNOWLEDGMENT

We wish to thank Mr. Kai for his help in the determination of radio positions.

REFERENCES

1. Tlamicha, A., Krivsky, I., and Olmr, J., 1963, Information Bulletin of Solar Radio Observatories, No. 14.
2. Swarup, G., Stone, P. H., and Maxwell, A., 1960, *Ap. J.*, 131: 725.
3. Warwick, C. S., 1954, *Ap. J.*, 120: 237.
4. Wild, J. P., and Zirin, H., 1956, *Aust. J. Phys.*, 9: 315.

N64-30276

26 THE ASSOCIATION OF BREMSSTRAHLUNG X RAYS WITH EXPLOSIVE FLARES

GAIL E. MORETON
Lockheed Solar Observatory
Burbank, Calif.

Measurements from balloons, rockets, and satellites suggest the classification of solar flare radiation into two general types: thermal, and nonthermal. The 2 to 8A x-ray flux (Reference 1) responsible for the sudden ionospheric disturbances commonly associated with flares may be attributed to a thermal or quasi-thermal source of temperature $\approx 10^6$ °K. On the other hand, the high-energy (>20 kev) x-ray "bursts" would seem to require some other explanation, since attribution to thermal processes would require unreasonably high (10^8–10^9 °K) source temperatures. The rapidity of rise of these bursts is also inconsistent with the concept of a thermal origin. Following Peterson and Winckler (Reference 2), Anderson and Winckler (Reference 3), and others, high energy x-ray bursts are now attributed to bremsstrahlung of suprathermal electrons. Kundu (Reference 4) has pointed out that these bremsstrahlung bursts are intimately associated with impulsive 10-cm radio bursts, and he suggests they have a common origin in the upper chromosphere. Not all Hα flares produce bremsstrahlung bursts; Pounds et al. (Reference 5), for example, have discussed three x-ray enhancements recorded in the 4 to 14A range detected by the satellite Ariel I (1962*o* 1). Two of these were slow enhancements, the spectrum of which can be satisfied by a thermalized plasma with temperature around 10^7 °K. The third event, however, consists of a "burst" superposed on a slow enhancement; the burst spectrum was attributed to a nonthermal source resulting in bremsstrahlung. Similarly, Neshpor (Reference 6), from analysis of ionospheric effects caused by flares, infers that some but not all flares may be characterized by a considerable increase in the high energy component of the x-ray spectrum.

The main purpose of this paper is to consider the optical properties of the flares associated with these bremsstrahlung bursts. Since 1958, some 15 such events have been recorded, including the most recent OSO satellite results reported by Frost (Reference 7). Hα filtergrams have been inspected for nine of these events, eight of which were recorded on good quality 10-sec-interval filtergrams of the Lockheed Solar Observatory (see Table 26–1).

All nine bremsstrahlung events shared a special optical characteristic: The flares are of the "explosive" type.

Explosive flares are exceptional events (Reference 8). In contrast to most flares that show continuous area and intensity development to maximum brightness, the explosive flare exhibits a distinct pre-maximum phase marked by an abrupt increase in the Hα flux. The principal factor in the sudden flux increase is the rapid expansion of the flare borders. Unlike common flares that usually have expansion rates of less than 10 km/sec, the explosive region appears to expand with a velocity of around 100 km/sec. The period of accelerated development—the explosive phase—can be as short as 10 seconds and is commonly less than 30 seconds, after which little or no further development may be evident. Other high energy phenomena suggest that the explosive phase, or what appears as a "burst" of Hα flux, is an optical characteristic of flares which have a localized high excitation region. In some cases fast-moving Hα disturbances are expelled during

TABLE 26–1

Times (UT) of Hα, Radio, and X-Ray Emission From Nine Events

Date	Hα Flare				10-cm Start	X-Ray Start	Reference
	Start	Explosive Phase	Max.	Imp.			
March 20, 1958	1259	1303	<1330	2	1304	1304. 4	2
Aug. 24, 1959	2233. 0	2234. 0	2239. 0	2+	2234. 5	*N.O.	9
Aug. 31, 1959	2235. 0	2249. 7	2252. 0	2+	*N.O.	*N.O.	9
Sept. 1, 1959	1656	1657	1707	2	1657. 5	*N.O.	9
Aug. 11, 1960	1916	1925. 5	1930. 0	2+	1925. 5	1926. 0	10
Oct. 12, 1960	1722	1727. 5	1728	1	1725	1730. 5	11
Oct. 12, 1960	1743. 5	1745. 3	1750. 0	1	1745. 7	1747	11
Sept. 28, 1961	2202. 0	2213. 0	2224	3	2214	2216. 3	3
Mar. 17, 1962	1936	1940. 2	1944	1	1939. 8	1939. 5	7

*No observation.

the explosive phase (Reference 12); viewed in movie projection, these disturbances appear as faint clouds or shock fronts moving with speeds of ≈1000 km/sec, and are probably the optical counterpart of the type II radio burst. In addition, explosive flares are more than twice as frequently associated with 10-cm impulsive radio bursts and type III emission as are common flares.

Temporal relations for the nine bremsstrahlung bursts caused by explosive flares are displayed in Figure 26–1. The Hα flare start and maximum time, and the start of the impulsive centimetric burst, are plotted relative to the initiation of the explosive phase. The initiation time of the x-ray burst is shown for six events where adequate time history of the x-ray flux was measured. Inspection of the figure shows the close association of the x-ray bursts and centimetric radiation, as already has been demonstrated for seven of these events by Kundu (Reference 4). Covington and Harvey (Reference 13) and Angle (Reference 14) have shown that the explosive phase is the relevant time for the production of centimetric bursts, and Figure 26–1 shows that this is also true for the bursts associated with x rays. Furthermore, it is also apparent that the explosive phase is closely related in *time* to the production of bremsstrahlung bursts; on the average, the burst follows the explosive phase by about 1.5 minutes.

The above provides limited but convincing evidence that the explosive effect in some flares is caused by a sudden nonthermal energy process occurring in a localized region of an otherwise normal flare. The normal flare produces low-velocity ejecta and a variety of slow emissions, such as the long-enduring centimetric burst and low energy x rays. Smerd (Reference 15) suggests these "glow-like" emissions are electromagnetic only and probably arise from thermal or quasi-thermal processes, such as compression of chromospheric regions by excess magnetic pressure. The explosive phase, on the other hand, is the relevant time for the acceleration of a burst of electrons to relativistic energies and the production of centimetric emission and hard x rays by synchrotron and bremsstrahlung processes.

REFERENCES

1. KREPLIN, R. W., CHUBB, T. A., and FRIEDMAN, H., 1962, *J. Geoph. Res.*, 67: 2231.
2. PETERSON, L. E., and WINCKLER, J. R., 1959, *J. Geophys. Res.*, 64: 697.
3. ANDERSON, K. A., and WINCKLER, J. R., 1962, *J. Geophys. Res.*, 67: 4103.
4. KUNDU, M. R., 1961, *J. Geophys. Res.*, 66: 4308.
5. POUNDS, K. A., WILLMORE, A. P., BOWEN, P. J., NORMAN, K., and SANFORD, P. W., 1963, *Proceedings of the Royal Society*, in press.

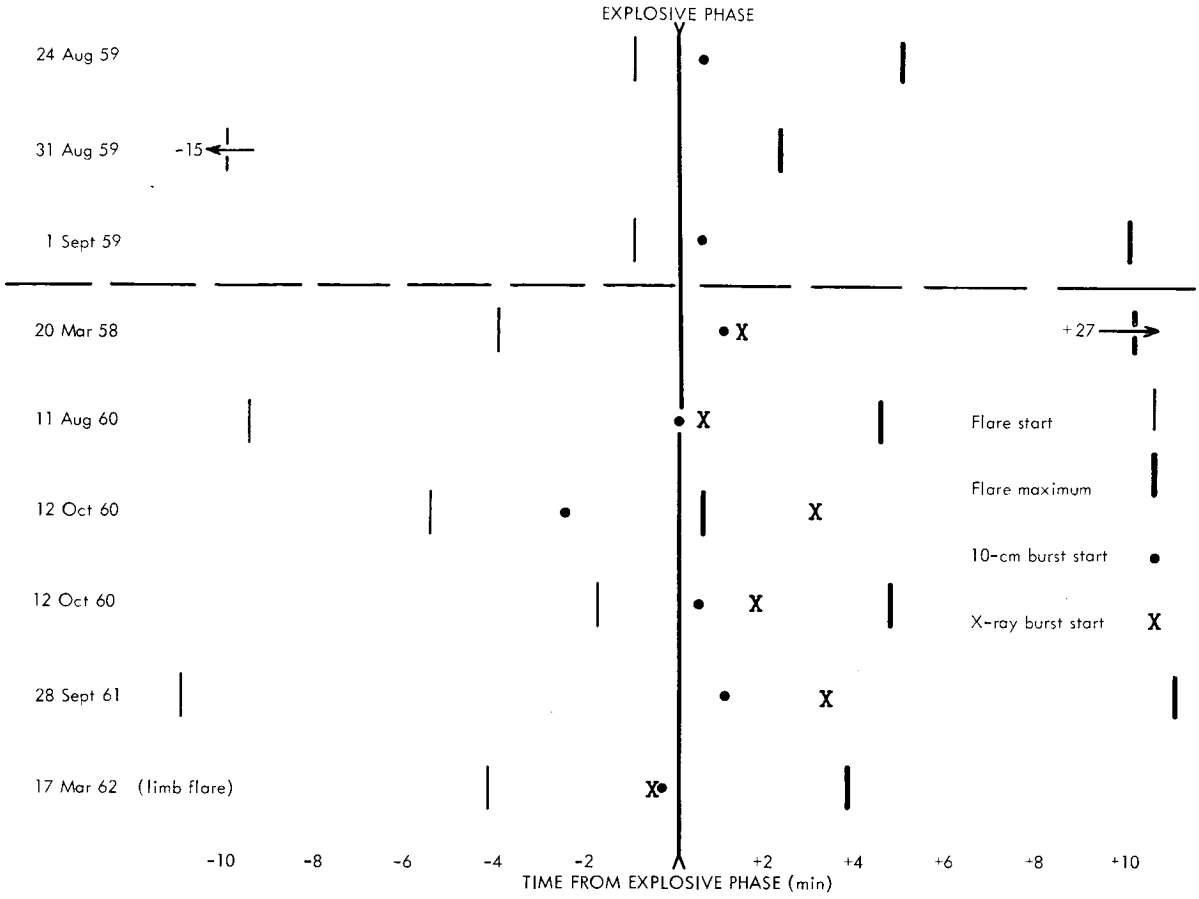

FIGURE 26–1. Start and maximum time of Hα flare, start of impulsive 10-cm burst, and start of x-ray burst; plotted relative to initiation time of the Hα explosive phase.

6. NESHPOR, Y. I., 1963, *Izv. Krim. Astrophys. Obs.*, 29: 152.
7. FROST, K. J., 1963, *these Proceedings*, paper no. 18.
8. ATHAY, R. G., and MORETON, G. E., 1961, *Ap. J.*, 133: 935.
9. CHUBB, T. A., FRIEDMAN, H., and KREPLIN, R. W., 1960, *J. Geophys. Res.*, 65: 1831
10. WINCKLER, J. R., MAY, T. C., and MASLEY, A. J., 1961, *J. Geophys. Res.*, 66: 316.
11. VETTE, J. I., and CASAL, F. G., 1961, *Phys. Rev. Letters*, 6: 334.
12. MORETON, G. E., 1961, *Sky and Telescope*, 21: 145.
13. COVINGTON, A. E., and HARVEY, G. A., 1961, *Nature*, 192: 152.
14. ANGLE, K., 1963, *A. J.*, 68: 533.
15. SMERD, S. F., 1963, "Solar Radio Emissions," to be published in the *Proceedings of the Symposium on Results of the IGY–IGC, University of Calif.*

DISCUSSION

Dr. Zirin: I am still a little confused as to whether the explosive phase is the phase at which the brightening spreads very rapidly, or the phase at which something is blown off.

Dr. Moreton: I have defined the explosive phase as the short period, commonly less than 30 seconds, during which time part or all of the flare borders undergo accelerated expansion. In explosive flares the borders often appear to expand at rates of several hundred kilometers per second. The time of initiation of the fast moving disturbances usually coincides with the explosive phase.

Dr. Zirin: One of the cases that comes to mind very clearly to me is the case of November 10, 1961, which was observed at Climax on the

limb very nicely, although I must admit not on the disk. In that case, I don't know whether any x rays were observed. There was a very nice microwave event, a pretty large PCA and proton event, and SCNA. Certainly there was a flash phase in the sense that the flare began very sharply, but all one saw was a small condensation of material boiling around above the limb. Would you call the flash phase the sudden brightening of that?

Dr. Moreton: There is not sufficient observational evidence to define an explosive flare as it appears at the limb, and we did not observe the November 10 event. The "spray" event defined by Warwick shares some characteristics of an explosive-type disk flare, that is, sudden expulsion of ejecta from a small region of a mound-shaped limb flare. Perhaps the explosive phase corresponds to the period of rapid vertical motion of a limb flare, or the time at which ejecta are expelled.

Dr. Zirin: The point was that nothing blew off on November 10.

Dr. Moreton: Then it is possible that the explosive phase cannot be identified optically.

I OBSERVATIONS ON FLARES

SESSION C

Chairman, Dr. Frank B. McDonald

N64-30278

27 A REVIEW OF SOLAR COSMIC RAY EVENTS

WILLIAM R. WEBBER
School of Physics, University of Minnesota
Minneapolis, Minn.

In this paper we shall review some of the more important properties of solar cosmic ray events. A great variety of information on solar cosmic rays has been obtained in the past few years with many different techniques. It is now worthwhile, as we approach sunspot minimum, to pause and attempt to assemble this information in a coherent manner.

We shall begin by rather arbitrarily defining a solar cosmic ray event as having occurred when a detectable intensity increase (above the nominal galactic cosmic ray background of 4 particles/cm^2-sec) of cosmic rays with energy $>$10 Mev is observed near the earth. Such a lower limit eliminates many interesting low energy events which are clearly of importance in our understanding of the production and propagation of energetic particles in the solar environment, but is necessitated by the wide scope of the material to be discussed.

By using the above criterion, during the sunspot cycle just being completed, approximately 80 cosmic ray events have been observed. The total integrated intensity of particles $>$10 Mev energy near the earth during this cycle is $\approx 10^{11}$/cm^2. The yearly frequency of events follows quite closely the average yearly sunspot number, as can be seen from Figure 27–1. The individual events are clearly related to solar flares occurring on the sun. Various optical and radio emissions from the flares are of importance in understanding the production of these cosmic rays; but, generally speaking, the more important the flare is optically or in the radio range, the more likely it is to produce cosmic rays. The closest association both in time and in intensity characteristics seems to be with the cm wave emission, as can be seen from Figure 27–2, which shows the correlation between the integrated radio emission at 10,000 Mc/s and the integrated cosmic ray intensity $>$10 Mev for various events.

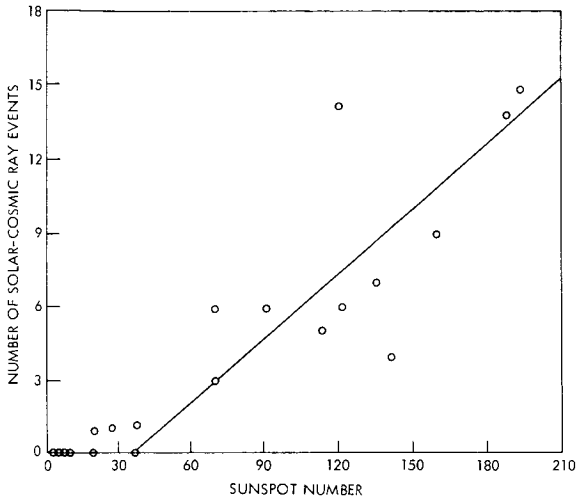

FIGURE 27–1. Yearly number of solar cosmic ray events observed as a function of yearly average sunspot number.

We shall not emphasize individual events in this review but shall attempt to study certain features common to all events. By a careful intercomparison of much data we shall attempt to define those features which will aid in our understanding of:

1. The method by which particles are accelerated to high energies in the vicinity of the solar flares,

2. The method by which these particles propagate outward from the flare region and through the inner solar system.

Before discussing the events themselves, we should at least mention briefly some of the methods used to detect the solar cosmic rays. It is the intercomparison of intensities measured

728-629 O—64——15

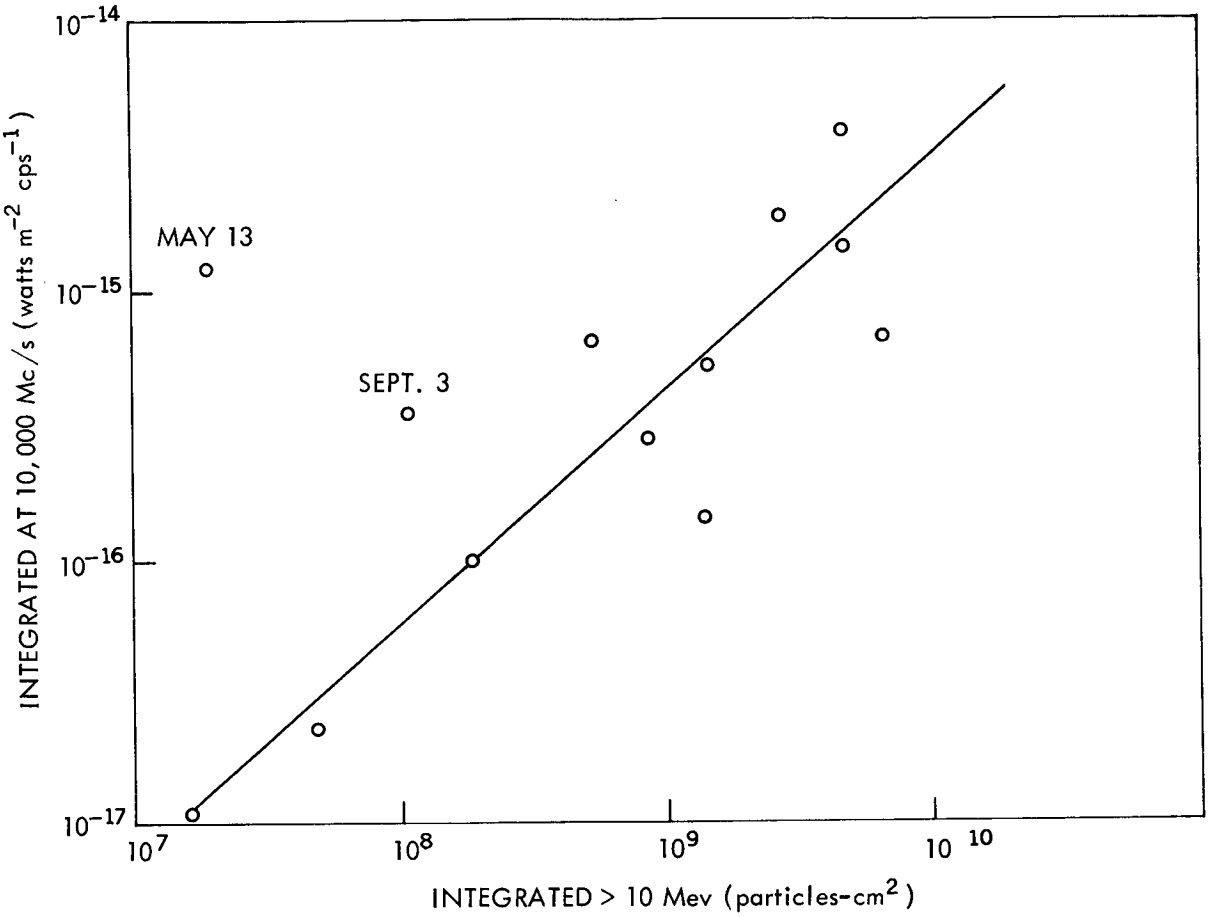

FIGURE 27-2. Integrated radio emission at 10,000 Mc/s versus integrated intensity of solar particles above 10 Mev at the earth for various events.

by using various techniques that has enabled us to construct energy spectra and intensity-time histories of the various events. Great strides have been made in the past few years in relating the intensities measured by different techniques of measurement, but significant improvements are still needed in certain areas.

The techniques used today include:

1. *The neutron monitor:* This device measures the secondary radiation near sea level and may be related to the solar cosmic rays at the top of the atmosphere by means of yield functions. It is relatively insensitive compared with the other techniques but has the advantage of giving a continuous time history of the event and, by utilizing the worldwide network of stations, of determining anisotropies in the solar particles.

2. *Geiger counters and ion chambers carried aloft in balloons:* These devices measure the integral intensity and ionization of the solar particles, respectively. The atmospheric depth versus excess particle intensity curves of these instruments are especially valuable for determining the spectra of the solar particles over the range 70 to 500 Mev.

3. *Emulsions and charge and energy discriminating counters carried aloft in balloons and rockets:* These devices may be used to obtain detailed spectra of the solar particles over the range 30 Mev (in rockets) to 500 Mev.

4. *Measurements of cosmic radio wave absorption in the ionosphere by riometers:* These instruments measure the total integrated ionization produced in the atmosphere by the solar

particles. This ionization is a complicated function of the spectrum and charge composition of the particles as well as the local geomagnetic cutoff. Use of measurements at a number of frequencies and at various latitudes enables some of these features to be separated. This method of detection has its maximum sensitivity to particles in the range 20 to 50 Mev and provides a continuous time history of particles in this range.

5. *Geiger counters, ion chambers, and scintillators carried on satellites and space probes:* These provide the same sort of information as is provided on balloons except they are now sensitive to much lower energies (10 to 30 Mev). They also provide a more or less continuous time history of the event.

6. *Charge and energy discriminating counters carried on satellites and space probes:* These devices provide the same sort of information as provided on balloons except they are now sensitive to much lower energies. They also provide a more or less continuous time history of the event.

A comparison of the relative sensitivity of the various instruments to different solar cosmic ray spectra is shown in Table 27–1.

The main features we wish to study in connection with the solar cosmic ray events are:

1. The onset characteristics of the particles including the relations with the main features of the flare,
2. The decay characteristics of the solar cosmic rays,
3. The charge composition of the flare particles,
4. The spectra of the solar cosmic rays.

To present these features intelligently, we must discuss in a preliminary way some of the main ideas concerning the propagation of the solar cosmic rays in the interplanetary medium. The first attempt to attack this problem in any detail was made by the workers at the University of Chicago (Reference 1). After a careful analysis of data obtained during the February 23, 1956, event they introduced a diffusion picture to account for the decay of particles in this event. A model in which the solar system inside ≈ 2 AU was essentially field-free or contained more or less regular radial magnetic fields while outside (from 2 to 6 AU) contained a region of disordered fields with a definite outer boundary was found compatible with the data obtained during this event.

Because of the lack of any definitive events, little was done to extend this approach until the period 1959, 1960, and 1961, when a large number of well-studied events provided new

TABLE 27–1

Comparison of Detection Capabilities for Solar Cosmic Ray Particles

Method	Minimum Observable Change	Corresponding J_0 (particles/cm²-sec)	
		P_0=50 Mv	P_0=100 Mv
Neutron monitor	±5%	--------	300, 000
f_{min}	±1Mc/s	480	120
Riometer (30 Mc)	±0.5 db	330	85
Integrated intensity:			
>100 Mev	±25%	75, 000	1, 000
>30 Mev	±25%	1, 500	140
>10 Mev	±25%	180	40
Differential intensity:			
100 Mev	±50%	3, 000	100
30 Mev	±50%	75	10

impetus for the study of solar flare particle propagation. As a result of detailed measurements of particles in the September 28, 1961, event over a wide range of energies by a scintillation counter telescope on Explorer XII (1961 υ 1) Bryant, Cline, Desai, and McDonald (Reference 2) suggested that a simple diffusion picture might explain the onset as well as the decay phase of this event. A similar conclusion was reached by Hofmann and Winckler (Reference 3) as a result of balloon measurements of both the onset and decay of particles of roughtly 200 Mev in at least six events. A detailed analysis by McCracken (Reference 4) of the anisotropies of particles ≈ 1 Bev energy, as revealed by neutron monitor intensities at various locations over the earth, also suggested that some form of scattering plays an important part in the propagation of the solar cosmic rays—even when a more or less regular interplanetary field configuration channels the particles to the earth. We shall discuss critically the features mentioned above after we have presented the data; but, meanwhile, to assist in organizing our ideas and the data in a coherent manner, let us recall certain features of the diffusion model for the propagation of the solar cosmic rays in the interplanetary fields as follows.

It is assumed that N particles of velocity v are released at time $t=0$ from a point 0 and diffuse through a homogeneous, isotropic three-dimensional medium. The appropriate diffusion equation is

$$\frac{\partial n}{\partial t}=\frac{1}{r^2}\frac{\partial}{\partial r}\left(r^2 D\frac{\partial n}{\partial r}\right),$$

where $D=D(v)$ is the diffusion coefficient which in this model is taken to be independent of r and t.

With the substitution $\Lambda=n/r$, the diffusion equation becomes $\partial\Lambda/\partial t=D(\partial^2\Lambda/\partial r^2)$.

In an unbounded medium the solution for the density (Green's function) is found to be

$$n(r,t,v)=\frac{N(v)}{[4\pi D]^{3/2}}\frac{e^{3t_m/2t}}{t^{3/2}},$$

where $t_m=r^2/6D$ is the time when n is a maximum at the point of observation and N is the total number of particles emitted.

Only if the particles are distributed isotropically in velocity space is the intensity $I\approx n$, and we arrive at the equation for the intensity

$$I(r,t,v)=\frac{N(v)v}{[4\pi D]^{3/2}t^{3/2}}e^{-3t_m/2t}.$$

Taking the $\ln$ of both sides, we see that a plot of $\ln I\,t^{3/2}$ versus $1/t$ is a straight line with slope s and an intercept t_0 ($I\,t^{3/2}=1$). The slope s is given by $s=3/2\,t_m$ from which $D=r^2/4s$. The measurement of s provides an important consistency check on the diffusion picture.

The total number of particles is given from the intercept t_0 as follows:

$$N=\frac{1}{v}\left[\frac{\pi r^2}{s}\right]^{3/2}e^{t_m/t_0}=\frac{1}{v}[4\pi D]^{3/2}e^{t_m/t_0}.$$

A necessary condition then for validity of the simple diffusion model is that, given the reference time $t=0$, a plot of $\ln t^{3/2}$ versus $1/t$ is a straight line. It is not true however that, if a value of the reference time can be found such that $\ln I\,t^{3/2}$ versus $1/t$ is a straight line, then the diffusion model is valid and this is the actual injection time. We must find some independent means for determining this time.

Now consider how this diffusion model is modified to account for the decay of the flare radiation. Meyer, Parker, and Simpson (Reference 1) first illustrated the characteristics of exponential decay and explained this in terms of a spherical absorbing boundary in the interplanetary medium. This picture has been followed by other workers, so let us examine some of the features of the introduction of such a boundary.

The solution of the diffusion equation gives

$$\bar{I}=\frac{6I_0}{\pi^2}e^{-t/t_D}\text{ at }t\geq\frac{r_0^2}{\pi^2 D}=t_E,$$

where r_0 is the boundary of the diffusing region and $t_D=r_0^2/\pi^2 D$.

Notice that exponential decay does not set in until the maximum in the diffusion wave reaches the outer boundary. Until this time the intensity is decreasing $\approx t^{-3/2}$. Note in particular that, if the mean free path $\lambda=$ constant and $D=\frac{1}{3}\lambda v$, then t_m, t_D, and t_E are

$\approx 1/v$. Also, for this model we have an important consistency check between the observed t_D and the time t_E at which exponential decay set in.

Now let us turn to the observational evidence on solar particle events, and we shall begin with a discussion of the onset phase.

ONSET PHASE

It is obvious from our previous discussion that, if we are going to establish the features on the onset phase of the cosmic ray events in a coherent manner, we must attempt to estimate accurately the time at which the cosmic rays are injected from the flare region into interplanetary space. This may not be the time at which the cosmic rays are accelerated.

A number of features of a solar flare are of interest in this connection. These include the Hα flash, the cm radio wave burst, the x-ray burst and emission of white light, and the flare nimbus. Not all of these features may occur in a single flare, since they may represent different manifestations of particle acceleration in the flare region. Most observers are in agreement however that, when a number of such indicators are present in a single event, they are very closely time-coincident—usually within 1 or 2 minutes. Furthermore, they occur soon after the flare is observed to start in Hα or from cm radio waves—usually within 10 minutes and in some cases only 2 to 3 minutes after the start.

The cm burst, the x-ray emission and the white light are presumably due to relativistic electrons; and it seems reasonable to believe the cosmic ray protons are accelerated by the same process. Also, since emissions which betray the presence of these electrons start during and only slightly before the Hα maximum, it seems highly reasonable that the protons are accelerated during this time also.

Granting that the protons are accelerated during this period of maximum emission, it is obvious that these particles cannot be injected before this time. To answer the question of when these particles are injected, data concerning direct cosmic radiation, which because of its high collimation is presumed to travel essentially without scattering along the field lines between the sun and the earth, are relevant. Such particles have been observed on at least nine occasions: six times by neutron monitors, and three times by balloons. Assuming that the spiral interplanetary field lines are inclined 55 degrees to the earth-sun line at 1 AU, one can calculate that the transit time for a "direct" 2 Bv proton should be ≈ 12 minutes. The results on the observed and calculated transit times for various events are shown in Table 27–2. Here the time of emission is assumed to be at the time of Hα max. or cm wave max., and the time of onset at the earth is obtained from stations nearest the correct viewing direction in space.

The difference between the calculated and observed transit times is never greater than 2 minutes. This suggests that we may assume the particles are indeed injected at this time and may use this accurately as time zero when

TABLE 27–2

Transit Times for Solar Flare Particles

Event	Times of Maximum				Cosmic Ray Onset			Transit Time (min)		
	H_α	Cm	W.L.	γ	$n(I)$	$n(0)$	B	Obs.	Calc.	Δt
Feb. 23, 1956	0340	0341	0340	----	0343	0348	----	12	12	0
Aug. 22, 1958	1456	1504	----	----	----------	------	1524	28	30	−2
May 4, 1960	1023	----	----	----	1027 (ch)	------	----	13	12	+1
Nov. 12, 1960	1329	1329	----	----	~1330	1348	----	10	12	−2
Nov. 15, 1960	0221	0227	0223	----	0227 (M)	0250	----	13	12	+1
July 18, 1961	1005	----	----	----	1010	~1030	1015 1026	14	12	+2
July 20, 1961	----	----	----	1553	----------	1605	1604	17	18	−1

discussing the propagation of these particles. It also suggests that the particles are not stored for an appreciable time in the flare region after acceleration, if we believe acceleration takes place at or near the time of maximum electromagnetic emissions.

Granting the previous arguments, then, we have established the injection time of the solar particles as a basis for studying the onset characteristics. To investigate how an uncertainty in this time might effect the results of a diffusion approach, we derive that $\Delta I/I \approx -3/2\ (t_m^{-1}/t^2)\Delta t_0$, where t_m and t are measured from t_0. Note that a small error in t_0 would have a negligible effect on I at sufficiently large times. Taking $t_m=2$ hours and $t=0.5$ hour with $\Delta t_0=2$ minutes gives $\Delta I/I \approx 15$ percent—a probably undetectable difference even at relatively early times.

Figure 27–3 shows the onset of particles of various energies as obtained by Bryant, Cline, Desai, and McDonald (Reference 2) during the September 28, 1961, event. In Figure 27–4 similar data obtained by the above workers are shown for the October 23, 1962, event. Figures 27–5, 27–6, 27–7, and 27–8 show the onset of particles as observed with balloons during the events of September 3, 1960; July 12 and 20, 1961; and September 28, 1961 (Reference 3). In addition, balloon data on the onset exist for the events of August 22, 1958; July 11 and 16, 1959; and July 18, 1961. Neutron monitor data exist for some nine events but have not been collected and presented in a systematic manner. The data presented in Figures 27–3 to 27–8 appear to fit a diffusion picture on four occasions. On September 28, 1961, the intensity appears to be too low at early times according to both balloon and satellite measurements.

In Figure 27–9 we have collected all the available data on the onset of solar flare particles, including that from neutron monitors. We have presented these data in a somewhat different fashion than in Figures 27–3 to 27–8, however. Here we plot $\ln I$ versus t/t_m. This makes use of the important consistency relation for t_m. The experimental points must not only lie along a straight line, but this line

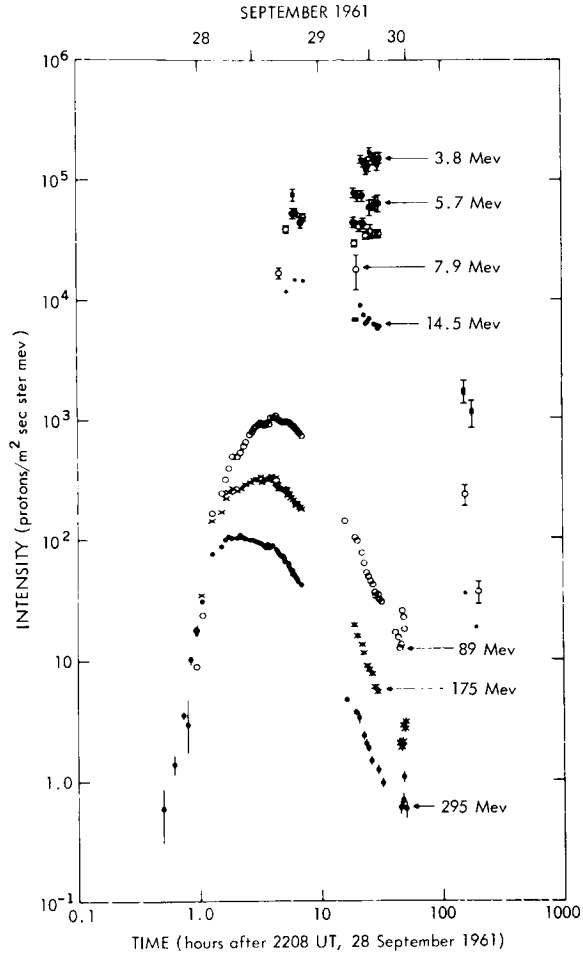

FIGURE 27–3. Intensity-time history of particles of various energies as observed during the September 28, 1961, event by Bryant, Cline, Desai, and McDonald. (Reference 2)

must have a particular slope of 3/2 if the diffusion approach is to be considered valid.

We immediately observe two types of curves—those in which $\ln I$ versus t/t_m is a straight line, and those where the intensity is less than expected for small times. In general, those curves corresponding to the latter group are from events in which the particles were observed to be direct as a result of neutron monitor observations. There are some notable exceptions, however. In the February 23, 1956, event even the indirect radiation, as observed at Ottawa (n), does not follow a straight line. In fact, it lies along the same curve as the direct radiation. In the November 15, 1960, event

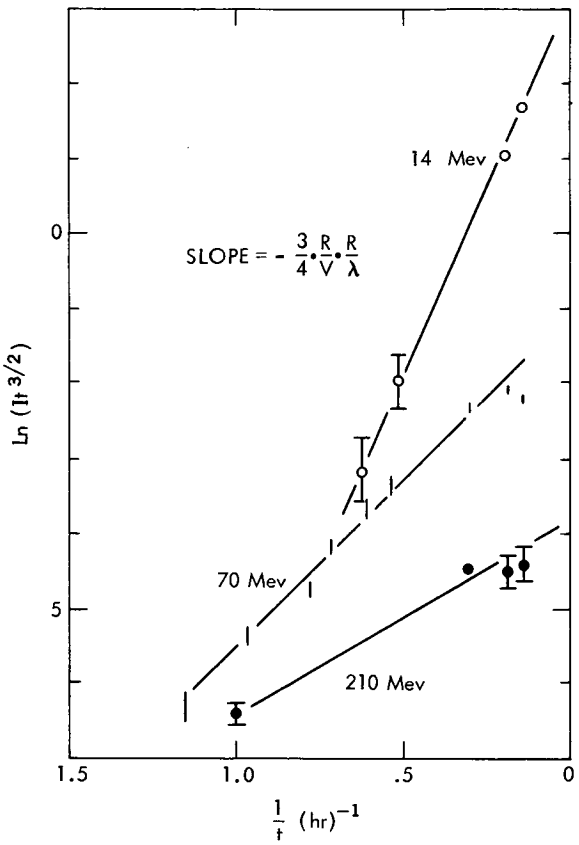

FIGURE 27–4. Onset characteristics for particles of various energies as observed during the October 23, 1961, event by Bryant, Cline, Desai, and McDonald. (Reference 2)

the indirect radiation as observed by neutron monitors is inconsistent with a straight line although lying along a different curve than the direct radiation. Neutron monitor data from other events do lie along a straight line. In fact this is the case for the July 18 and 20, 1961, events when anisotropies apparently existed in the incidence of particles. In these events, as well as those of July 16, 1959, and September 3, 1960, both balloon and neutron monitor data give a consistent picture for the propagation of particles, however.

We should note that the slope of the straight lines in Figure 27–8 is not generally 3/2, as would be expected from a diffusion picture, but tends to be slightly greater than this. The events which show a "diffusion-like" propagation over the time intervals considered (e.g., straight lines) occurred at 88° E, 30° W, and 120° W—and 90° W if we include the July 20, 1961, event. Those which deviate significantly from this mode of propagation occurred at 10° W, 33° W, 58° W, 82° W, and 90° W. The September 28, 1961, event, which is indecisive, occurred at 30° E. Thus, while all events which deviate from the diffusion-like mode of propagation occur in the western hemisphere of the visible sun, we do observe events occurring here which show a diffusion-like propagation. Remarkably, all of these events were the last to occur as the active region producing the cosmic rays approached the west limb (July 16, 1959; July 20, 1961; and November 20, 1960)'

Finally we recall, according to the diffusion picture, $t_m = r^2/6D$. If we take the diffusion coefficient $D = 1/3\ \lambda v$, where v is the average velocity of the particles and λ is the mean free path between collisions—and assume λ is independent of energy, then $t_m \approx 1/\bar{v}$. Figure 27–10 shows the behavior of t_m as a function of $\bar{v}$ for various events. Here we can identify two classes of variation of t_m with $\bar{v}$—one in which n, the slope of the curve, is ≈ -2.2 and another where the slope is ≈ -0.6. None of the values is consistent with the simple diffusion theory if λ is assumed independent of energy.

We shall return to a discussion of the onset characteristics after presenting data on other features of these events.

DECAY PHASE

We shall consider the decay phase of a solar cosmic ray event to be that period after t_m. A considerably larger body of data is available to cover this part of the event; however, the interpretation of these data is probably even less clear than in the case of the onset phase. Observations on the decay of particles of a given energy usually have been interpreted in terms of either a power law [e.g., $I \approx I_{max} (t-t_m)^{-n}$] or an exponential [e.g., $I \approx I_{max}\ exp\ (-t/t_D)$]. We see that from the point of view of the propagation of the particles this difference is a fundamental one. In the simple diffusion picture a power law decay with $n = 3/2$ implies propagation in an infinite medium; an expo-

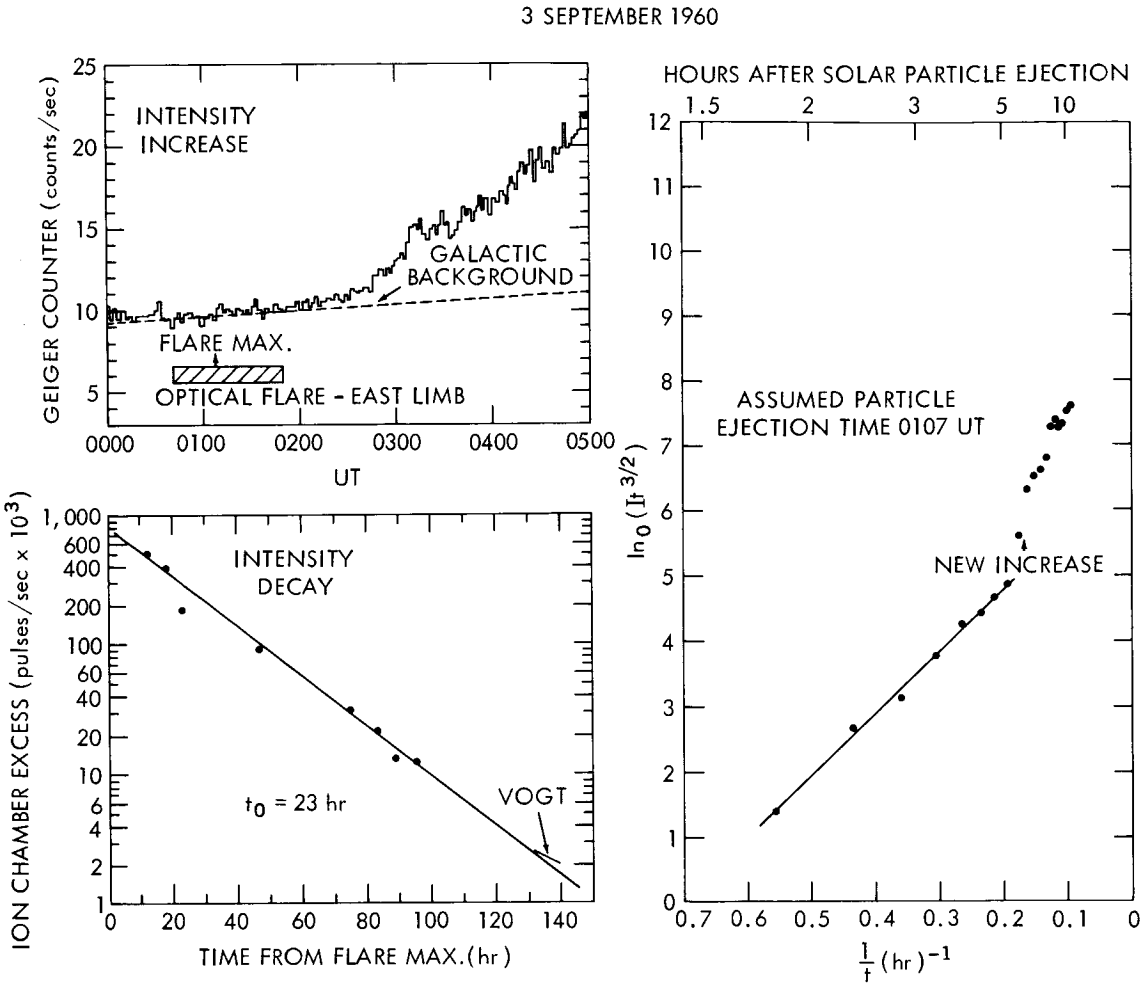

STATION	N $\left(\frac{\text{particles}}{\text{ster}}\right)$	Particle Energy (Mev)	L (AU)	t_m(calc.) (hr)	t_m(obs.) (hr)	r_0 (AU)
CHURCHILL	2.0×10^{30}	>120	0.019 ± .003	6	5	2.4

FIGURE 27-5. Onset and decay characteristics of solar particles observed by detectors on balloons during the September 3, 1960, event. (Hofmann and Winckler, Reference 3)

nential decay implies that the medium has a spherically symmetric absorbing boundary.

Most of the early attempts to express the decay of the solar particles were in terms of power laws, with values of n ranging from 1 to 3. The first attempt to fit an exponential to the decay of the solar particles was made by Meyer, Parker, and Simpson (Reference 1). A careful analysis of the decay of particles after the February 23, 1956, event revealed that the decay went from a power law to an exponential some 5 hours after the injection of particles, giving an outer boundary of ≈ 5 AU to the diffusing region surrounding the sun.

As observational techniques improved and, in particular, the length of time the decay could be monitored was substantially increased, it became apparent that the decay of particles in most events was more nearly exponential than a power law at all times after t_m. This is evident from observations on the decrease in radio wave absorption, which may continue for

12 JULY 1961

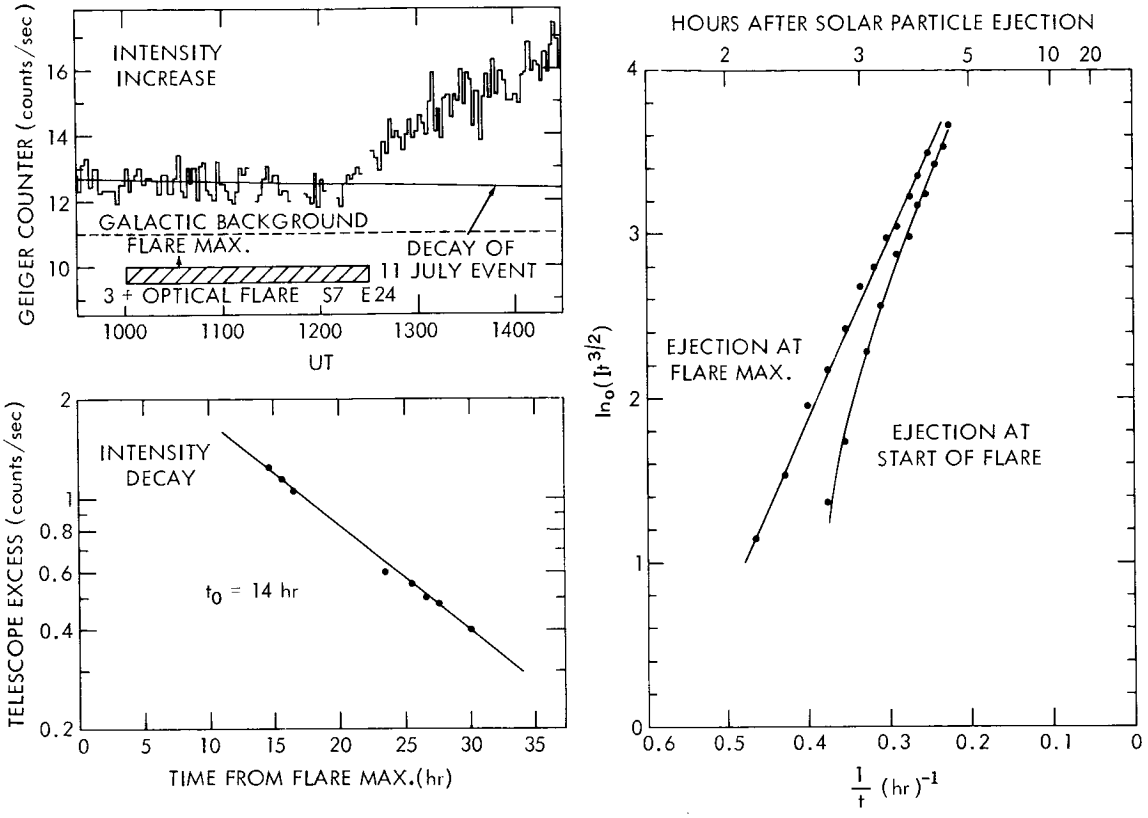

STATION	N $\left(\frac{\text{particles}}{\text{ster}}\right)$	Particle Energy (Mev)	L (AU)	t_m (calc.) (hr)	t_m (obs.) (hr)	r_0 (AU)
CHURCHILL	1.3×10^{30}	>95	0.016 ± .003	7.3	>4, <14	1.8

FIGURE 27–6. Onset and decay characteristics of solar particles observed by detectors on balloons during the July 12, 1961, event. (Hofmann and Winckler, Reference 3)

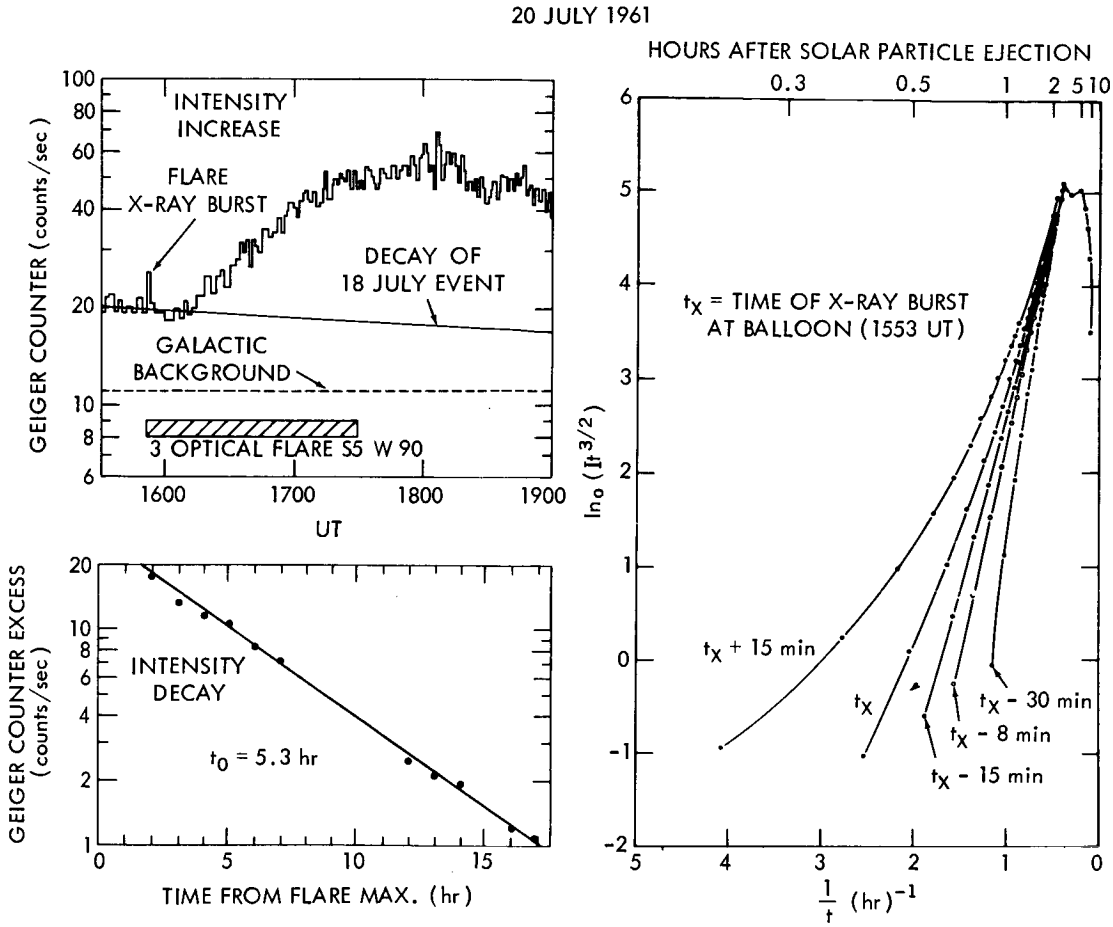

STATION	N $\left(\frac{\text{particles}}{\text{ster}}\right)$	Particle Energy (Mev)	L (AU)	t_m(calc.) (hr)	t_m(obs.) (hr)	r_0 (AU)
CHURCHILL	8.1×10^{30}	>95	0.040 ± .007	3.1	2.5	1.7

FIGURE 27–7. Onset and decay characteristics of solar particles observed by detectors on balloons during the July 20, 1961, event. (Hofmann and Winckler, Reference 3)

many days after an event, and from measurements on balloons and satellites as well as with neutron monitors. If we reexamine Figures 27–5 to 27–8, we see the decay of the integral intensity of particles >80 Mev as measured by balloons during a number of events (Reference 3). The values of t_D obtained in these measurements are typical of those for particles of this average velocity. The time decay of particles of various energies has been followed in detail with both balloons and satellites (Reference 2) for the September 28, 1961, event. This decay follows closely an exponential and is shown in Figure 27–11. Another comparison of the decay of different energies as measured with balloons and satellites (Reference 5) is available for the event of September 3, 1960 (Figure 27–12). In many events the decay of particles at the earth is interrupted by the arrival of plasma fronts (magnetic storms) which cause a discontinuous

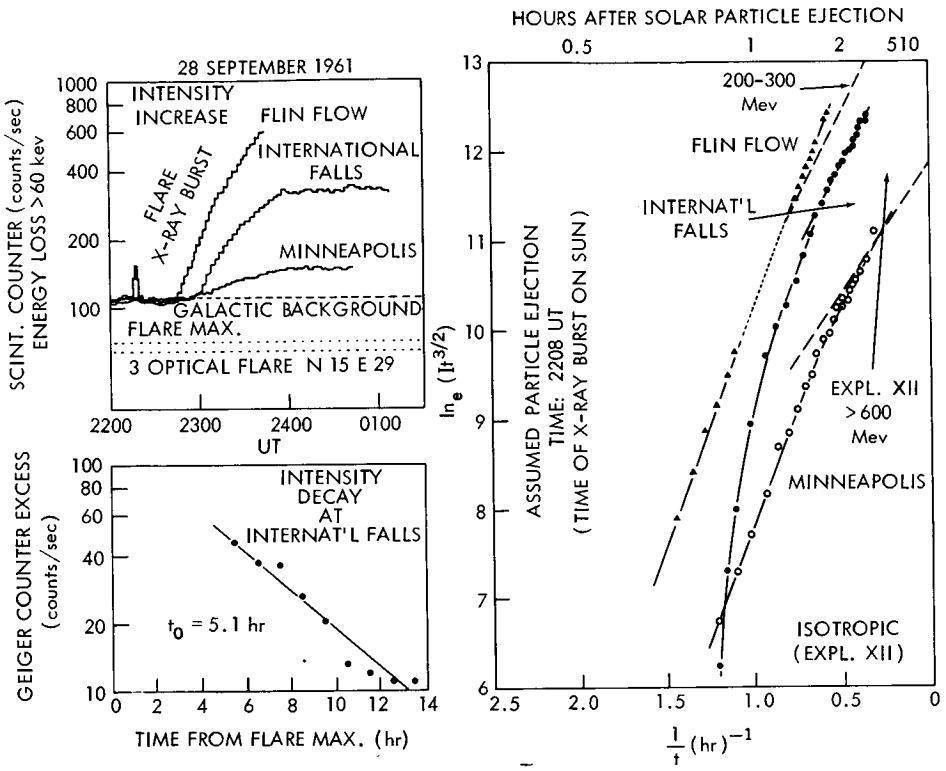

STATION	N $\left(\frac{\text{particles}}{\text{ster}}\right)$	Particle Energy (Mev)	L (AU)	t_m (calc.) (hr)	t_m (obs.) (hr)	r_0 (AU)
FLIN FLON	7.8×10^{30}	> 65	0.046 ± .006	3.33	> 1.75	———
INT. FALLS	1.9×10^{30}	> 220	0.042 ± .003	2.58	2.57	1.8
MINNEAPOLIS	3.8×10^{29}	> 400	0.038 ± .003	2.44	2.40	———
EXPL. XII (McDONALD et al)		> 200	0.04			2-3

FIGURE 27-8. Onset and decay characteristics of solar particles observed by detectors on balloons during the September 28, 1961, event. (Hofmann and Winckler, Reference 3)

change in particle intensity. This renders the interpretation of the decay of some events, such as November 12, 1960, extremely difficult. These effects are the most pronounced for the low energy particles.

A considerable amount of data is available on the decay phase of the solar cosmic ray events from neutron monitors. Data obtained at various cutoff rigidities during the February 23, 1956, event are shown in Figure 27-13. Note the onset of exponential decay for various rigidities at a time considerably in excess of t_m. Data obtained during the November 12, 15, and 20, 1960, and July 18, 1961, events are shown in Figures 27-14 and 27-15. Here the most conspicuous feature, outside of the striking exponential decay, is the fact that this decay sets in only a short time after t_m and no period of power law decay is evidenced. Furthermore, the time at which the exponential decay

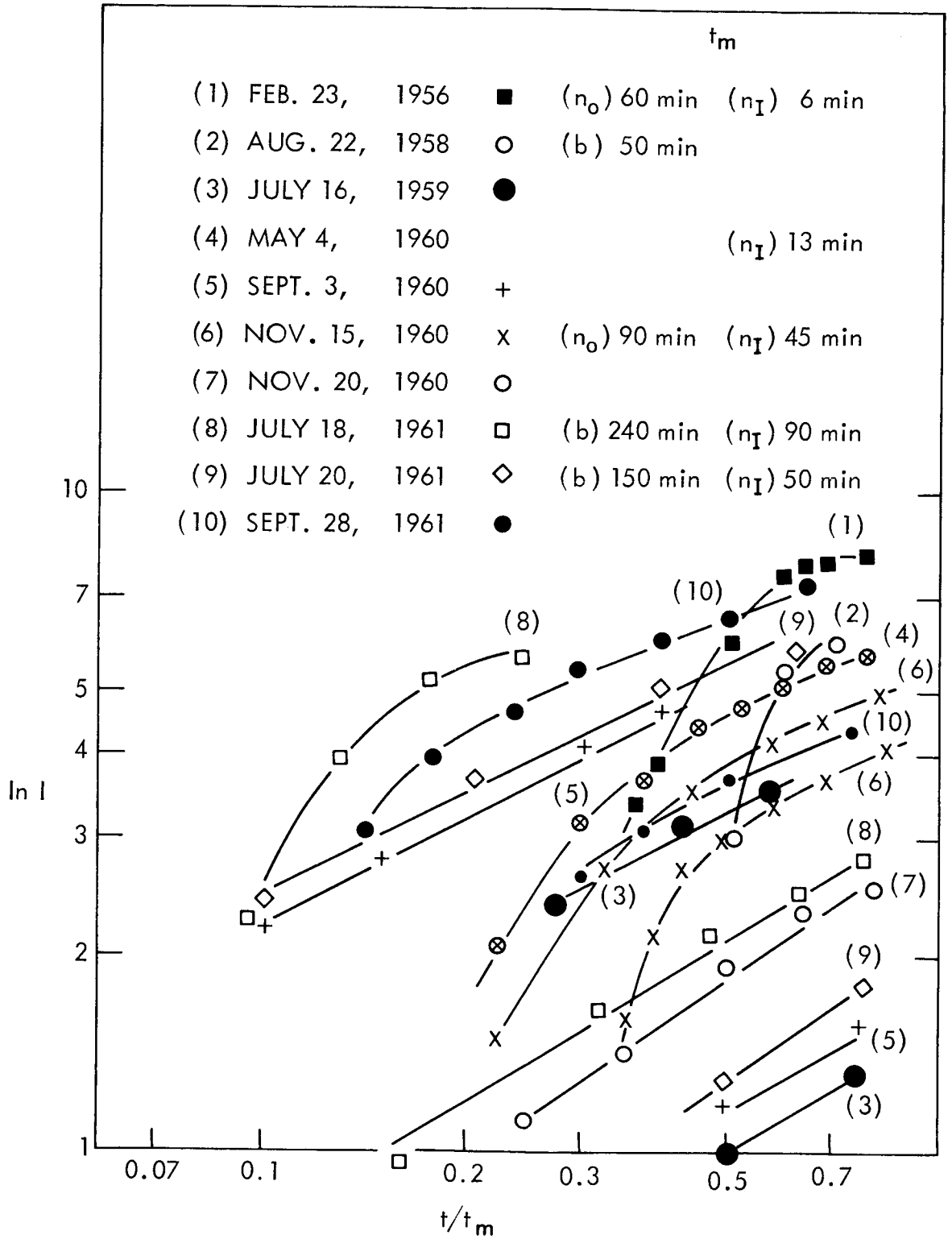

FIGURE 27–9. Compilation of onset characteristics observed from satellite, balloon, and neutron monitor data for various events.

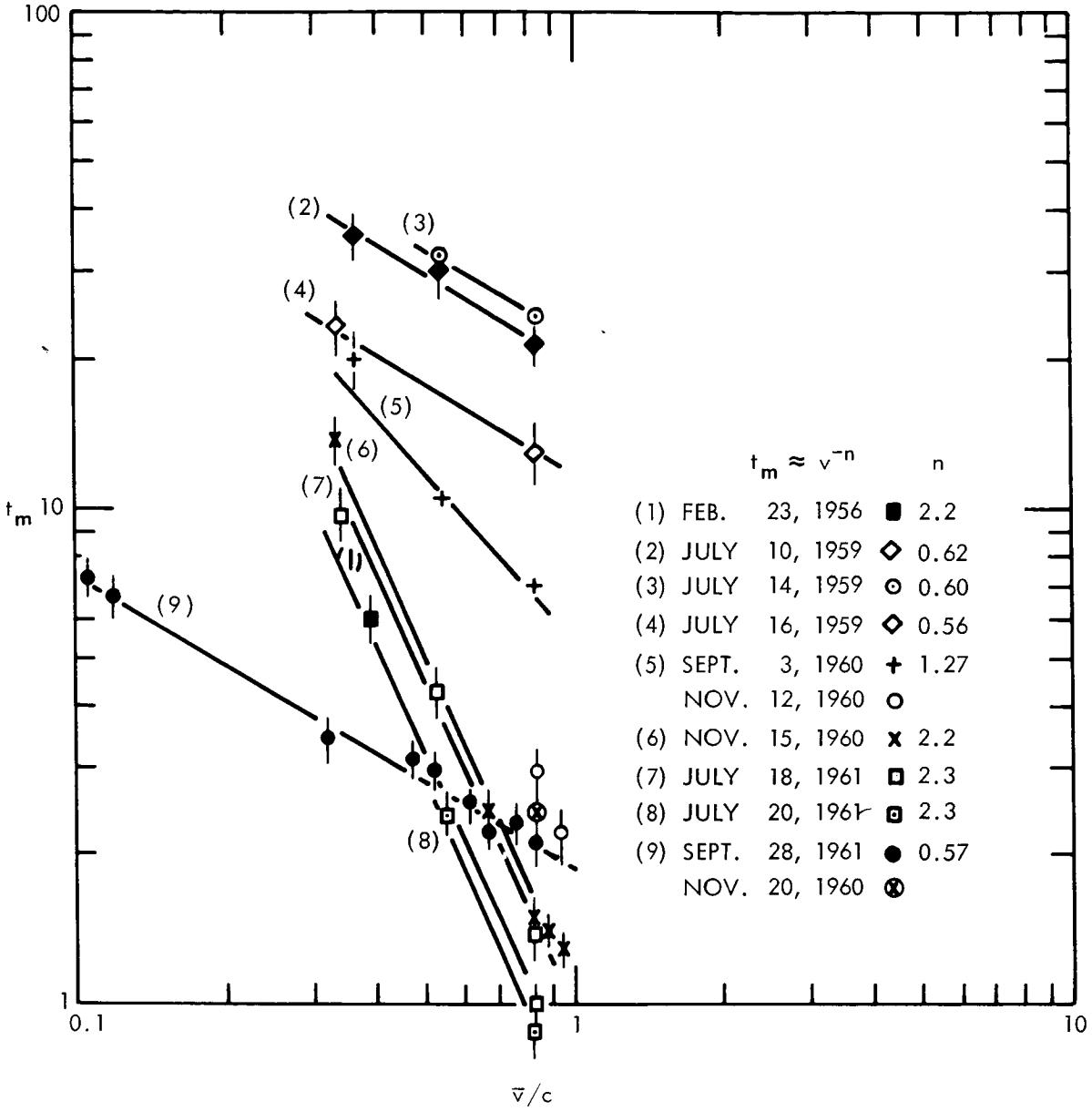

FIGURE 27–10. Variation of t_m with $\bar{v}$ (energy) for various events.

sets in is usually much less than t_D, a fact that is incompatible with the diffusion-absorbing boundary picture.

To examine the decay of the solar cosmic rays in a more general way, we show in Figure 27–16 a plot of t_D versus $\bar{v}$ for various events. According to the diffusion picture, if we assume the mean free path is not a function of energy, then $t_D \approx 1/\bar{v}$. This is clearly not the case for the data in Figure 27–14. Cases are observed where the exponent n is greater than 1 and less than 1. Events following one another seem to show the same type of velocity dependence, however (e.g., July 10 and 16, 1959; November 12 and 15, 1960).

Finally, we display in Figure 27–17 a plot of t_D/t_m versus $\bar{v}$. According to the diffusion-absorbing boundary picture, $t_D/t_m = 0.6\ (r_0/r)^2$;

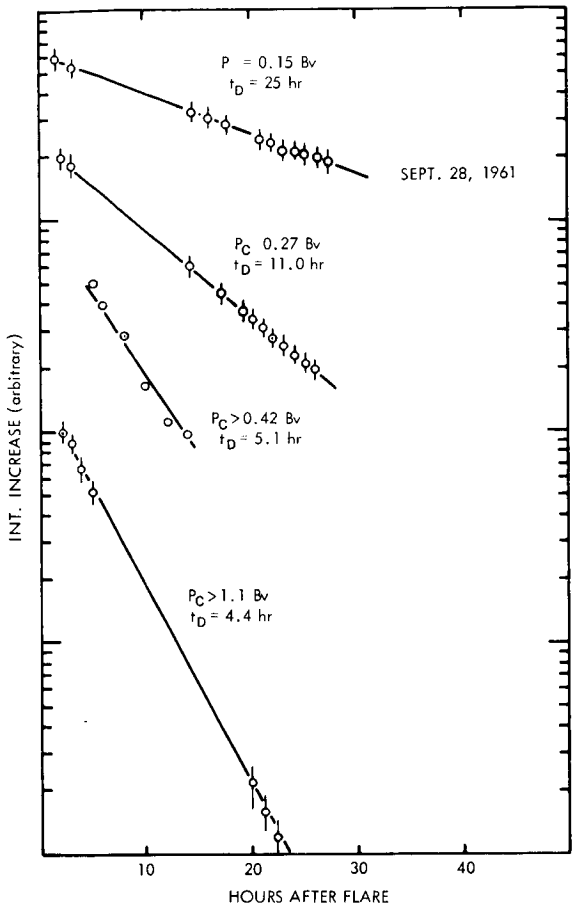

FIGURE 27–11. Decay of particles of different energies observed by both balloons and satellites during the September 28, 1961, event.

that is, this quantity should be a measure of the effective radius of the boundary for particles of different average v. For a reasonable picture of the scattering centers and how they decrease in strength with distance from the sun, we might expect this radius to increase with decreasing $\bar{v}$. This is, in fact, the case in only a few events. In most of the events, the tendency is the other way. Indeed, in a number of events, the effective radius of the absorbing boundary is $\lesssim 1$ AU for particles with certain $\bar{v}$. Yet these same particles show an exponential decay and onset characteristics not unlike those to be expected from a diffusion model.

At least one further comment concerning the decay of solar particles is appropriate here. This is related to the fact that in most instances we are measuring the decay of an integral intensity above a certain energy and attempting to deduce something about particles of some average energy $\bar{E}$ or velocity $\bar{v}$, since it is this quantity that is specified in the solution of the diffusion equations. In measurements made in balloons or by neutron monitors there are at least two reasons why the actual decay of particles of energy $\bar{E}$ will be different than that implied by the measured decay of the integral intensity. In the first place, the spectrum of solar cosmic rays is steepening during the decay phase of the event; thus, the conversion between a measured increase at balloon altitudes or for neutron monitors to an integral intensity at the top of the atmosphere will result in a relatively greater intensity at late times. Thus the actual decrease of integral intensity will be slower than exponential if the measured decrease is exponential. As a result of the steepening spectrum, the mean energy $\bar{E}$ or velocity $\bar{v}$ will become less with time, however. These two effects, which are important individually, tend to compensate one another; so that the statement of an exponential decay for the intensity measured by such instruments probably closely reflects an exponential decay of particles with a particular $\bar{v}$.

THE SPECTRUM OF THE SOLAR COSMIC RAYS

The determination of the spectral characteristics of the solar cosmic rays is one of the most difficult aspects relating to the study of these particles. This is so because of the wide range of particle energies. Each of the methods of detection may cover only a very narrow energy interval or, worse yet, it may be a single integral intensity measurement.

Thus one measurement or set of measurements is usually not enough to define a spectrum, and one must attempt to construct a spectrum from measurements made by a number of different detectors—perhaps with quite different types of responses. In addition, the intensity of the solar particles may be changing rapidly with time and space.

Usually it has been the practice to follow the spectrum of galactic cosmic rays and attempt

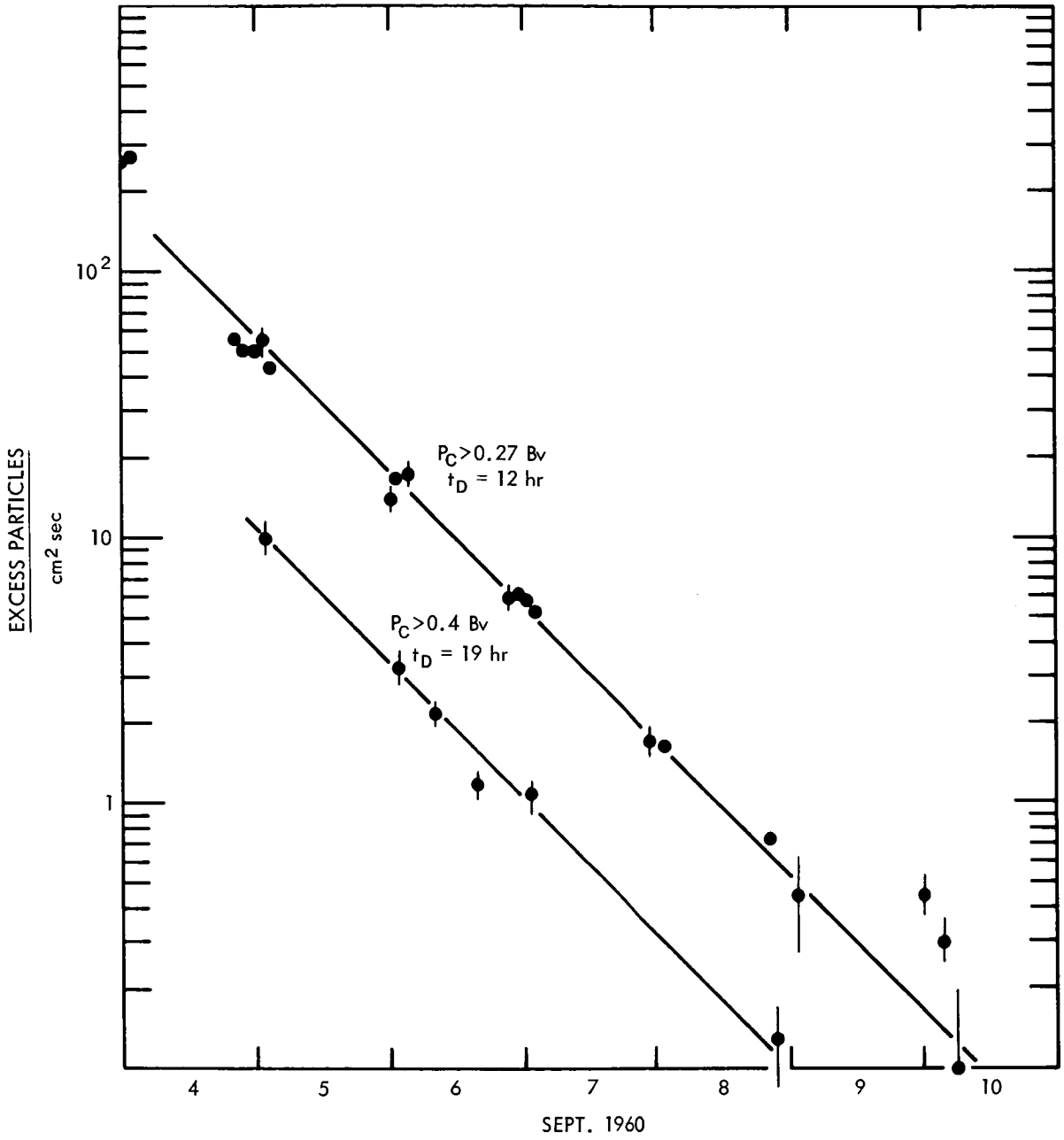

FIGURE 27–12. Decay of particles of different energies observed by both balloons and satellites during the September 3, 1960, event.

to represent the differential spectrum of solar particles by a form $dJ/dE = \text{const}/E^n$, where E=energy and n=constant range from 3 to 6. Such a spectrum, while compatible with individual observations over a rather narrow range, is totally inadequate to represent a large part of the spectrum of the solar particles. In particular, it is necessary to let n be a function of energy, decreasing as the energy decreases. Recently the application of other types of spectra to the solar cosmic rays has been investigated (Reference 6). As a result, a spectrum

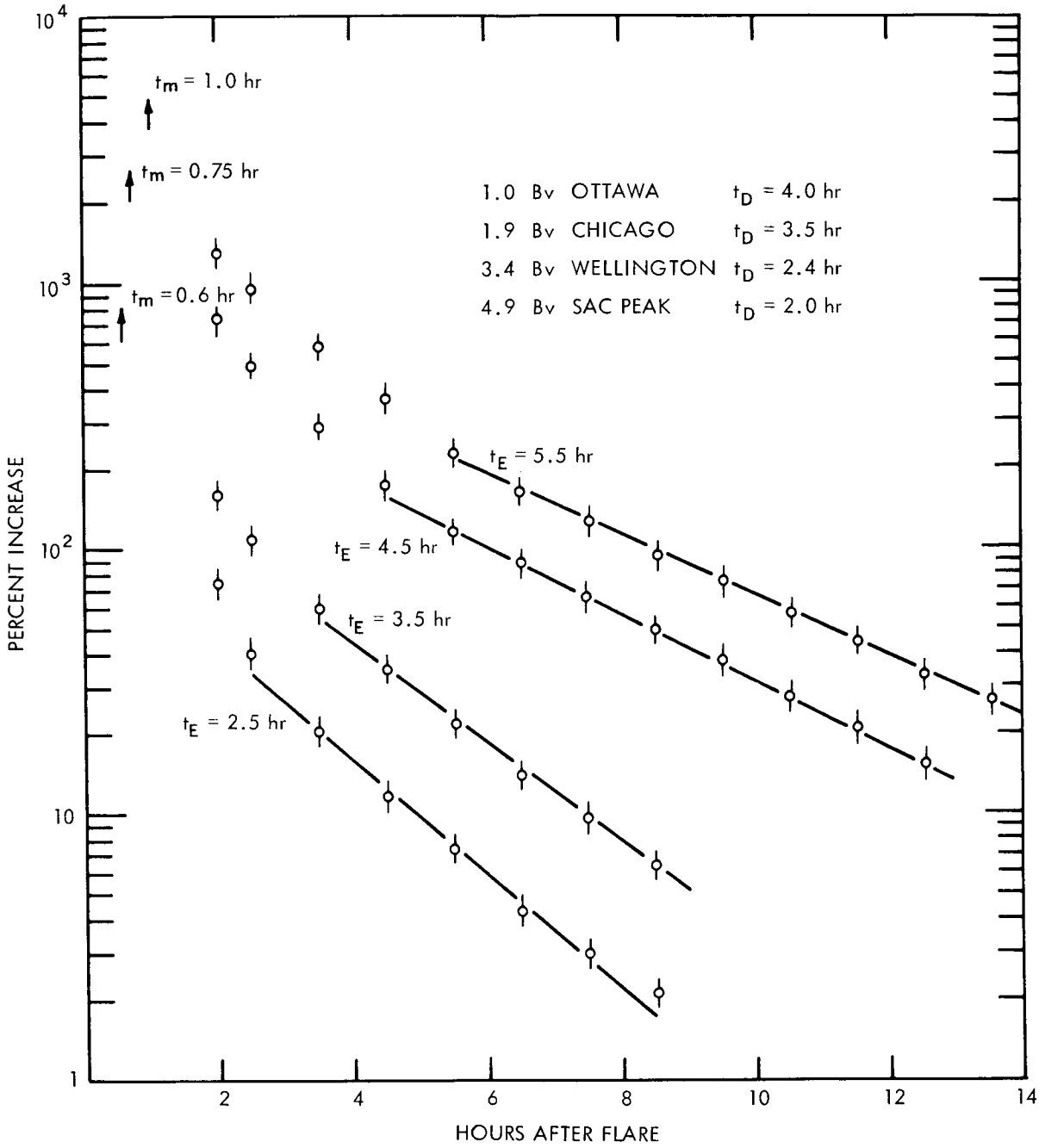

FIGURE 27–13. Decay of particles of different energies as observed by neutron monitors during the February 23, 1956, event.

of the form $dJ/dP = (dJ/dP)_0\,(t)\exp[-P/P_0(t)]$, which appears to have a very wide application to the decay phase of the solar cosmic ray events, was suggested. Here P_0 is a characteristic rigidity which is dependent on time and $(dJ/dP)_0$ also is a function of time. Perhaps the most significant feature of this spectrum is that it is a rigidity spectrum. This has impor-

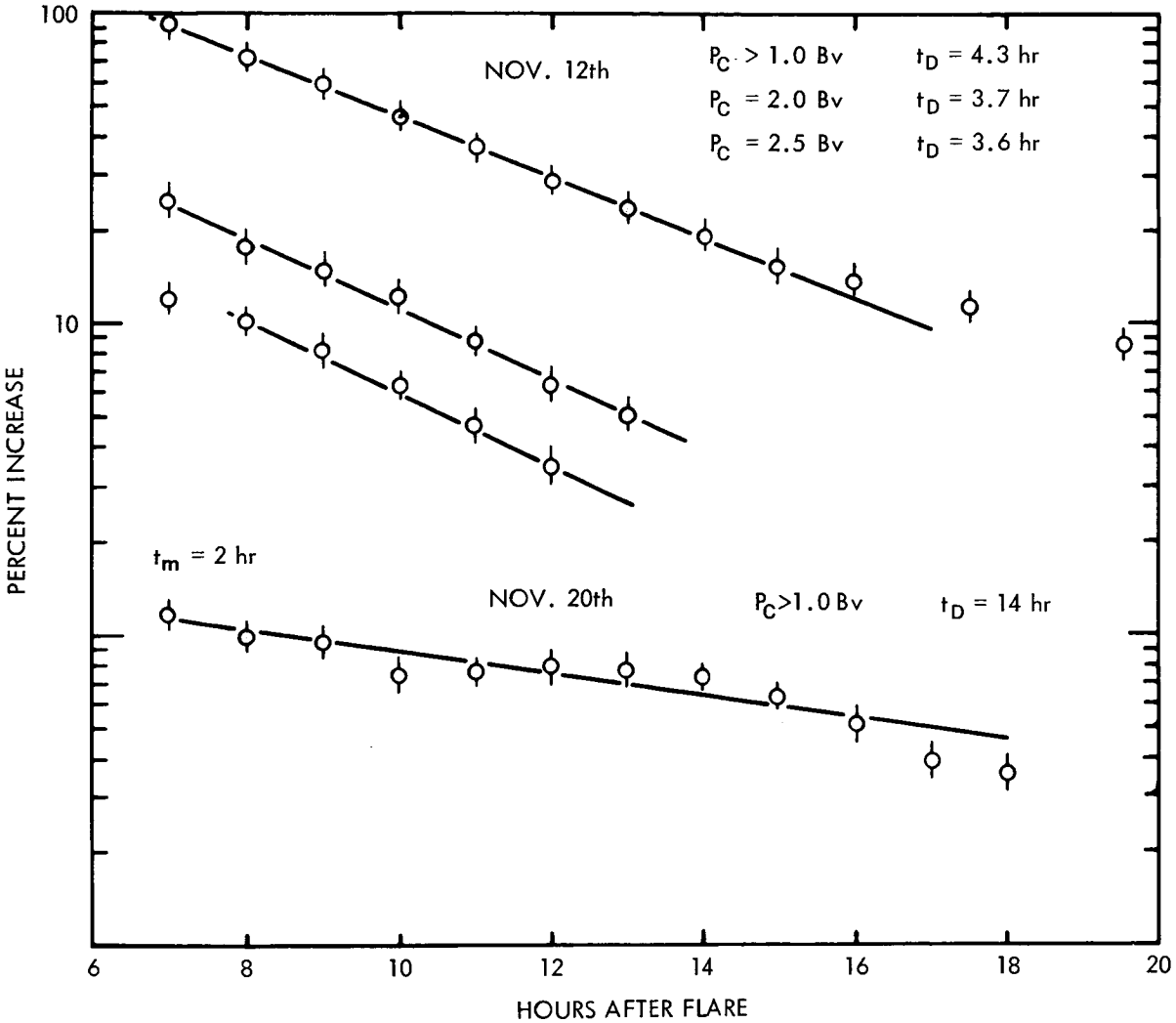

FIGURE 27–14. Decay of particles of different energies as observed by neutron monitors during the November 12, 1960, and November 20, 1960, events.

tant implications with regard to the charge composition of the radiation, as will be discussed in the next section.

One of the features of this spectrum is that it applies at all times during the decay phase of all of the events we have so far discussed, as well as others, as long as the energy of the particles is greater than about 20 to 30 Mev ($\approx$0.2 Bv rigidity). Some typical spectra for protons obtained at selected times in various events are shown in Figures 27–18 and 27–19.

It is important to realize that this spectrum does not apply during the onset phase of the solar cosmic ray events. Neither does it apply at the lower energies near the times of magnetic storms. At these times an excess of low energy particles appears. These low energy particles have a time behavior that is more closely related to the magnetic storm plasma than to the higher energy cosmic rays. It is possible that the behavior of these particles significantly influences the behavior of t_D at low energies ($\bar{v}/c<0.3$) presented in Figure 27–16. The behavior of these low energy particles can be studied in some detail during the events of November 12 and 15, 1960, and July 12, 18, 20, and 26, 1961. The most detailed results are available, however, from Explorer XII (Refer-

728–629 O—64——16

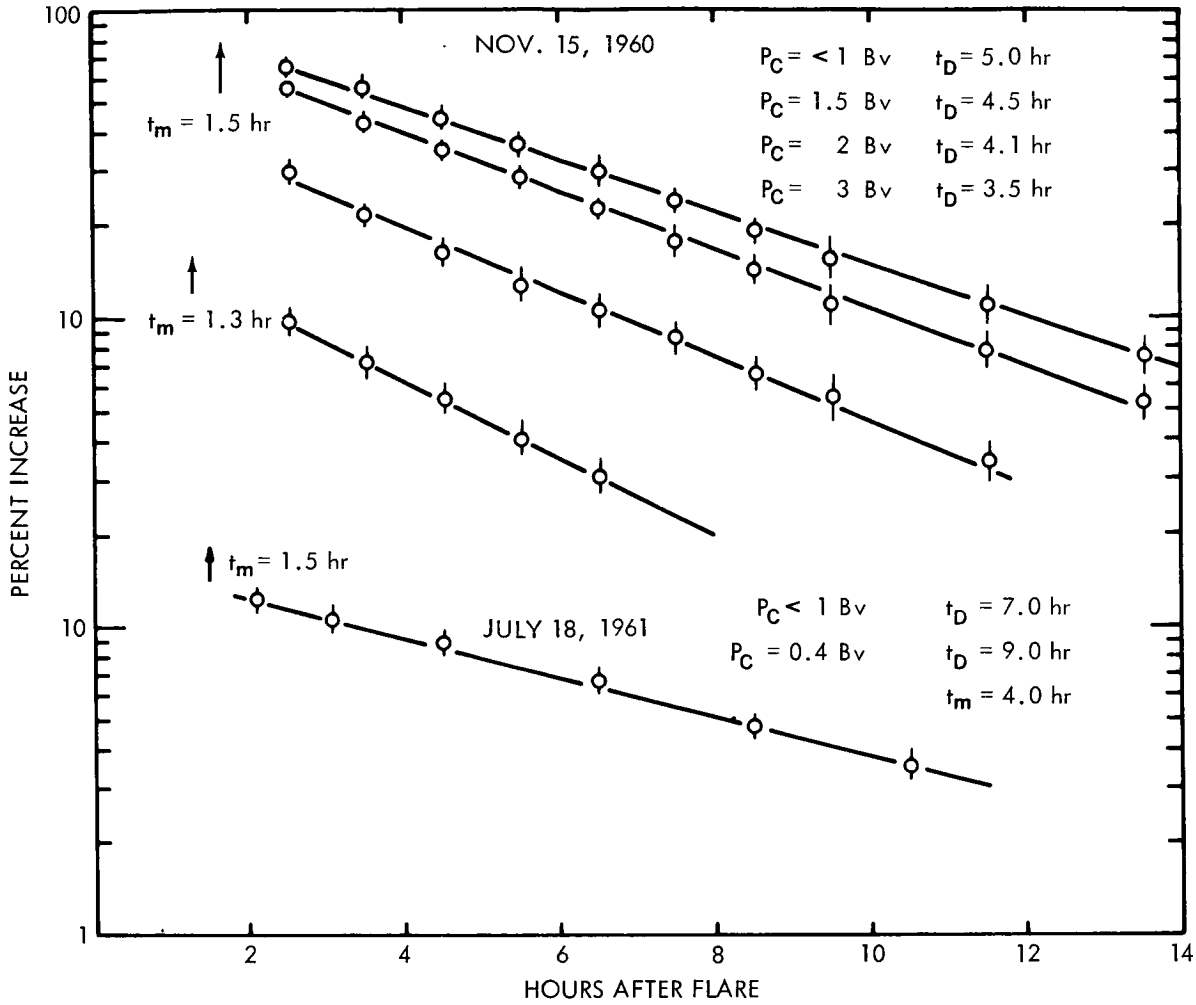

FIGURE 27–15. Decay of particles of different energies as observed by neutron monitors during the November 15, 1960, and July 18, 1961, events.

ence 2) for the event of September 28, 1961. The spectra as a function of time after t_m are presented in Figure 27–20, and clearly show the arrival of a greater and greater intensity of low energy particles although the high energy part of the spectrum is decreasing. This intensity reaches its peak value, as shown in Figure 27–21, precisely at the time of the magnetic storm. It appears that the low energy particles follow a spectrum similar to that of the high energy particles. The value of the characteristic rigidity P_0 is now much less, however.

Are we, in fact, dealing with two groups or populations of solar particles with different intensity-time characteristics and different spectra, or is the concept of an exponential spectrum simply breaking down and not a significant one in understanding the propagation and decay of the solar particles?

To investigate this question in more detail, we shall now use the parameters $(dJ/dP)_0$ and P_0 to study the decay of some solar cosmic ray events. In Figures 27–22 and 27–23 we show the time history of the July 1959 and November 1960 series of events expressed in terms of $(dJ/dP)_0$ and P_0. For the July 1959 events the similarity of the continuous-line values for $(dJ/dP)_0$ as determined by riometers and the open-circle determinations from balloon data suggests that the exponential rigidity spectrum

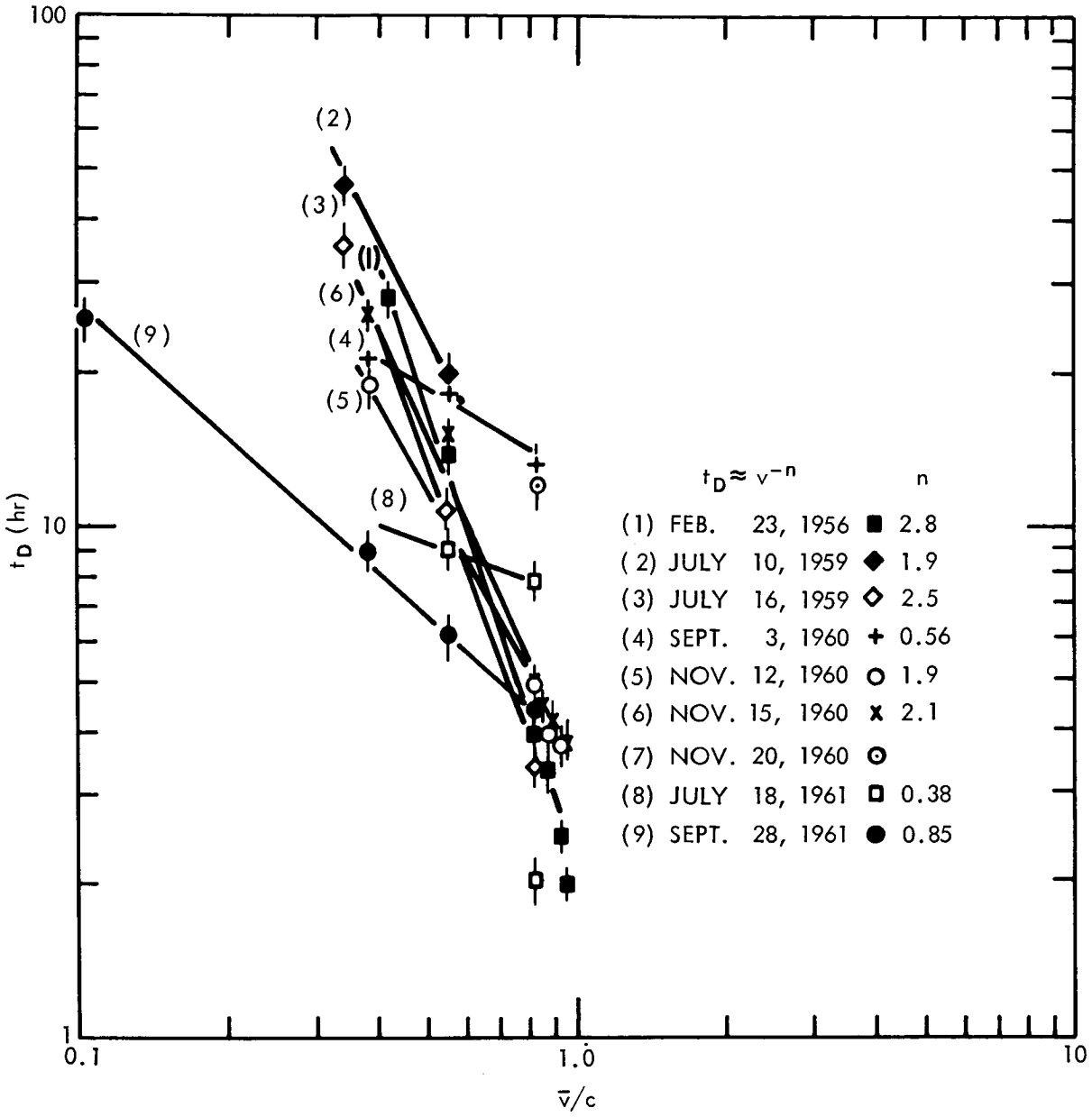

FIGURE 27–16. Variation of t_D with $\bar{v}$ (energy) for various events.

holds down to at least 30 Mev. Notice that P_0 decreases with increasing time and $(dJ/dP)_0$ also decreases after t_m. In this series of events the decay of the individual events is not simple. In fact, there is some indication of a superposition of the decays of the succeeding events.

For the November 1960 events, considerably more data are available. The exponential spectrum holds down to ≈30 Mev for all periods except those during which the continuous curve for $(dJ/dP)_0$ (riometer) and solid circles (satellites) are different from the continuous solid dots (neutron monitors) and open circles (balloons). The continuous decrease of P_0 can be observed with an apparently discontinuous change occurring during both events at the times of the magnetic storms. $(dJ/dP)_0$ also seems to behave in a continuous fashion at

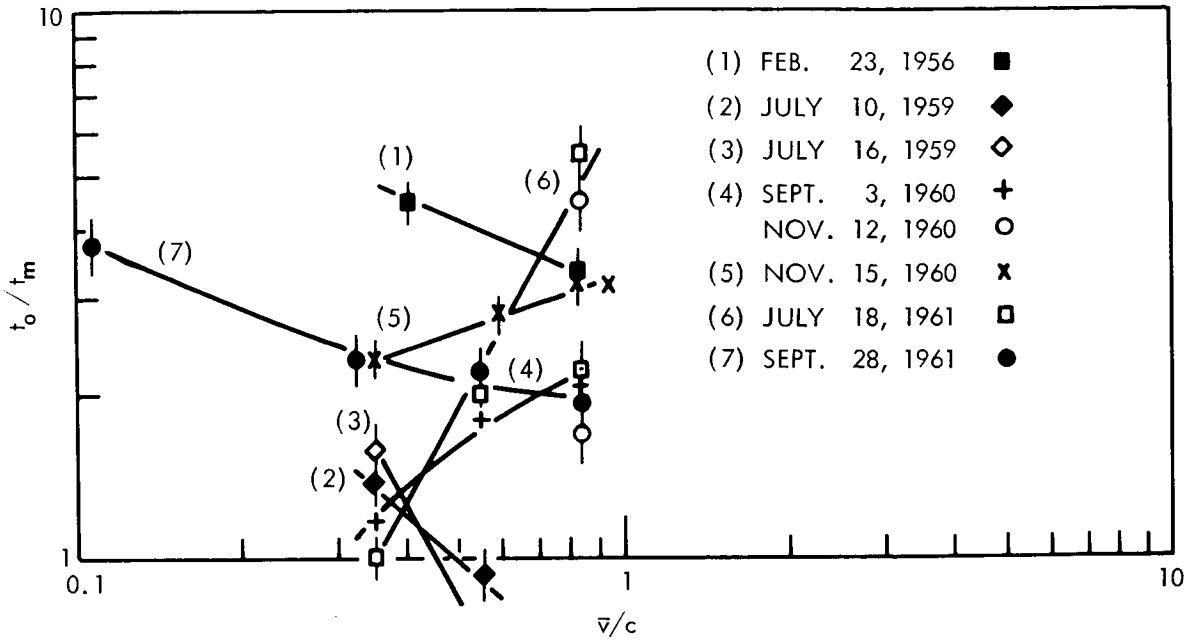

FIGURE 27–17. Variation of t_D/t_m versus $\bar{v}$ (energy) for various events.

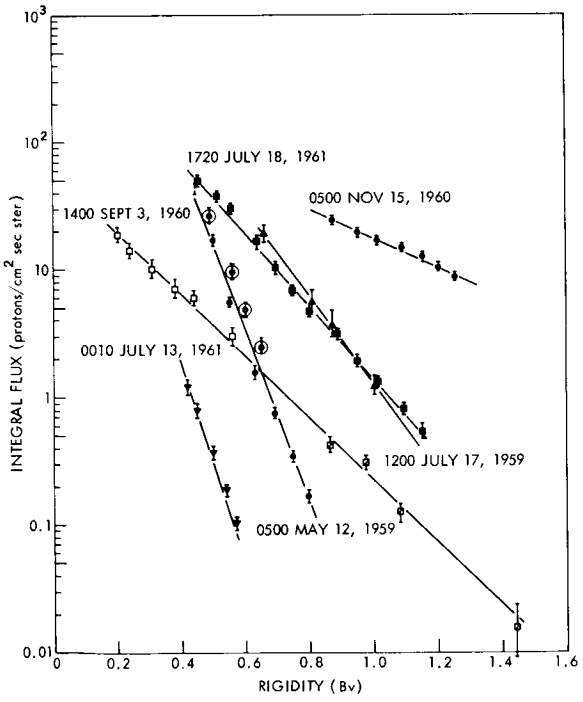

FIGURE 27–18. Exponential spectra for solar cosmic rays observed at selected times in different events.

late times in both events. This is particularly evident for the November 15 event, where a systematic decay continued for over 100 hours.

We realize that the actual observed (exponential) decay of particles of various energies must be compatible with that predicted from the variation of $(dJ/dP)_0$ and P_0 in the exponential spectrum. In other words,

$$\left(\frac{dJ}{dP}\right)_0 (t) e^{-P/P_0(t)} = \frac{6I_0}{\pi^2} e^{-t/t_D},$$

where t_D is the observed decay. Assuming $(dJ/dP)_0$ is slowly varying gives as a requirement that the decay for any energy be closely exponential, $P_0(t) = a/b + t$ where a and b are constants—with $b \approx t_D$. Thus $P_0(t)$ should have a time dependence $\approx 1/t^n$ where n increases with time, approaching 1 at late times. $(dJ/dP)_0$ does change however, and assuming an exponential time dependence for this variation gives an expression for $P_0(t)$ similar to the above except that now $b \approx t_D + t_j$, where t_j is the characteristic decay time for $(dJ/dP)_0$. If, however, $(dJ/dP)(t) \approx t^{-n}$, then $b \approx t_D$ becomes logarithmic in t. Thus, if we write the time dependence of $P_0(t) \approx 1/t^n$, n is still <1 but may appear to be more nearly a constant with time.

In Figure 27–24, we examine the time decay of P_0. One cannot distinguish a simple power

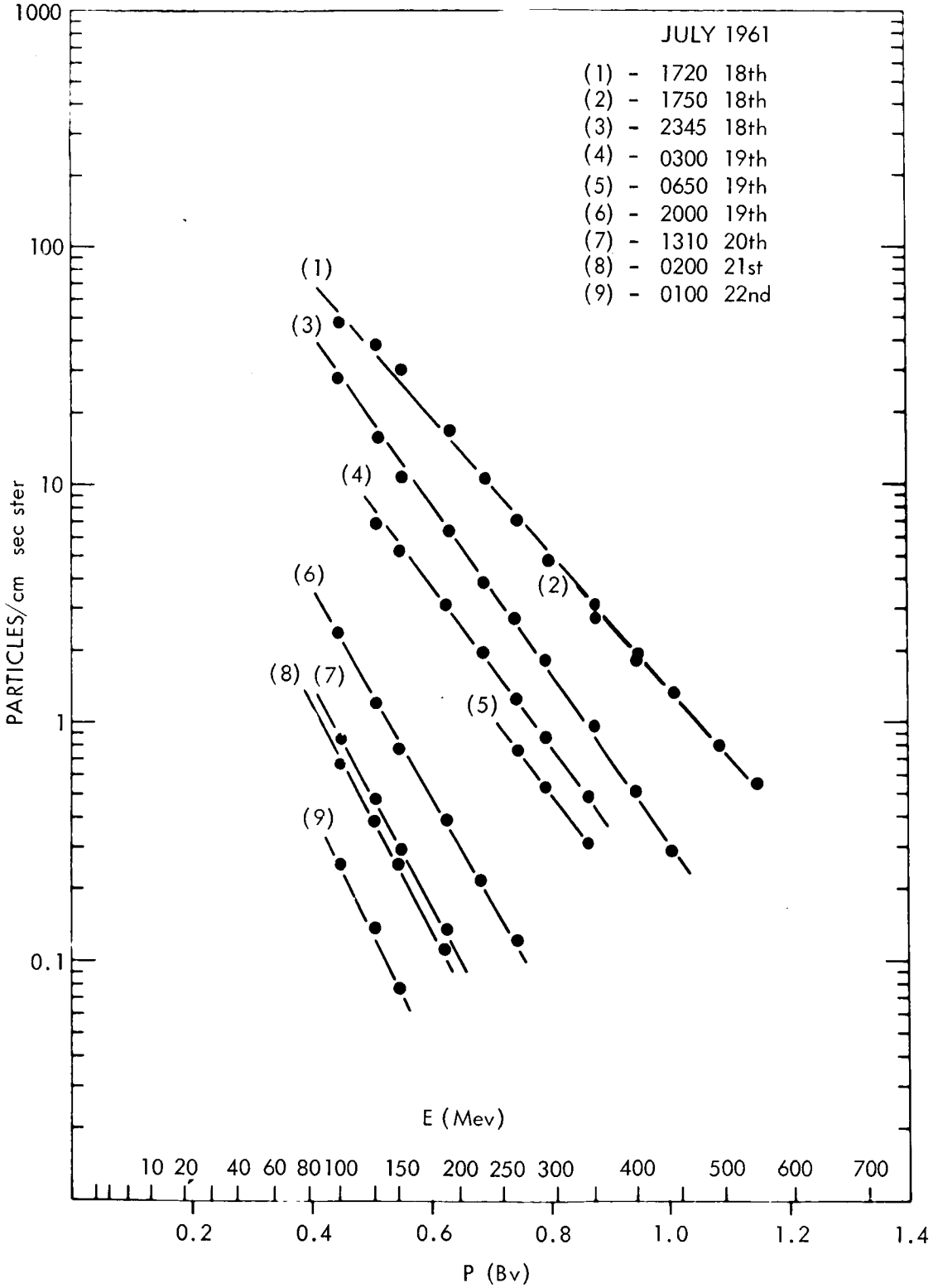

FIGURE 27–19. Exponential spectra for solar cosmic rays derived from balloon ascent data following the event of July 18, 1961.

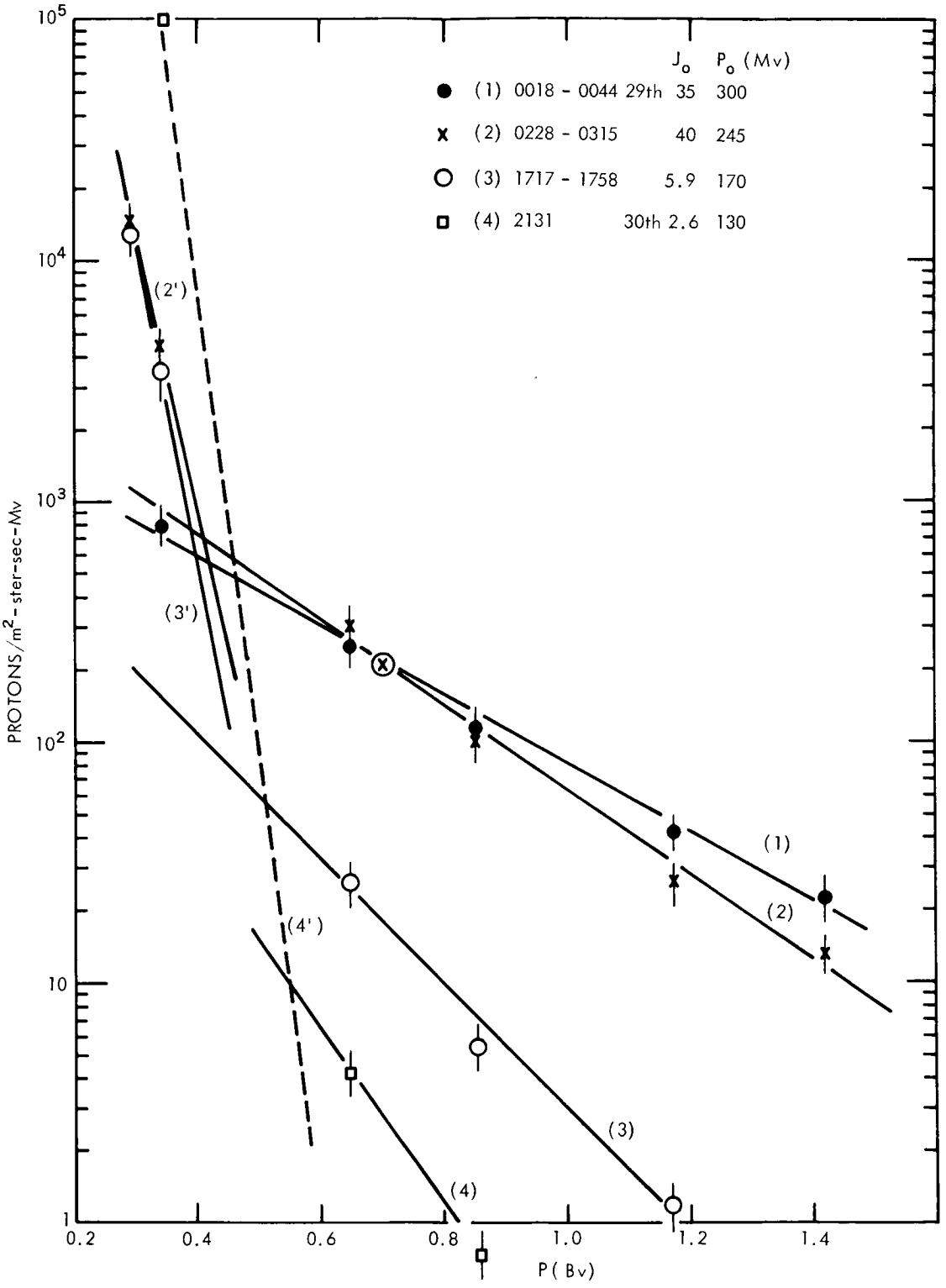

FIGURE 27–20. Spectra of solar cosmic rays at various times during the event of September 28, 1961. (Note the large excess of low energy particles.)

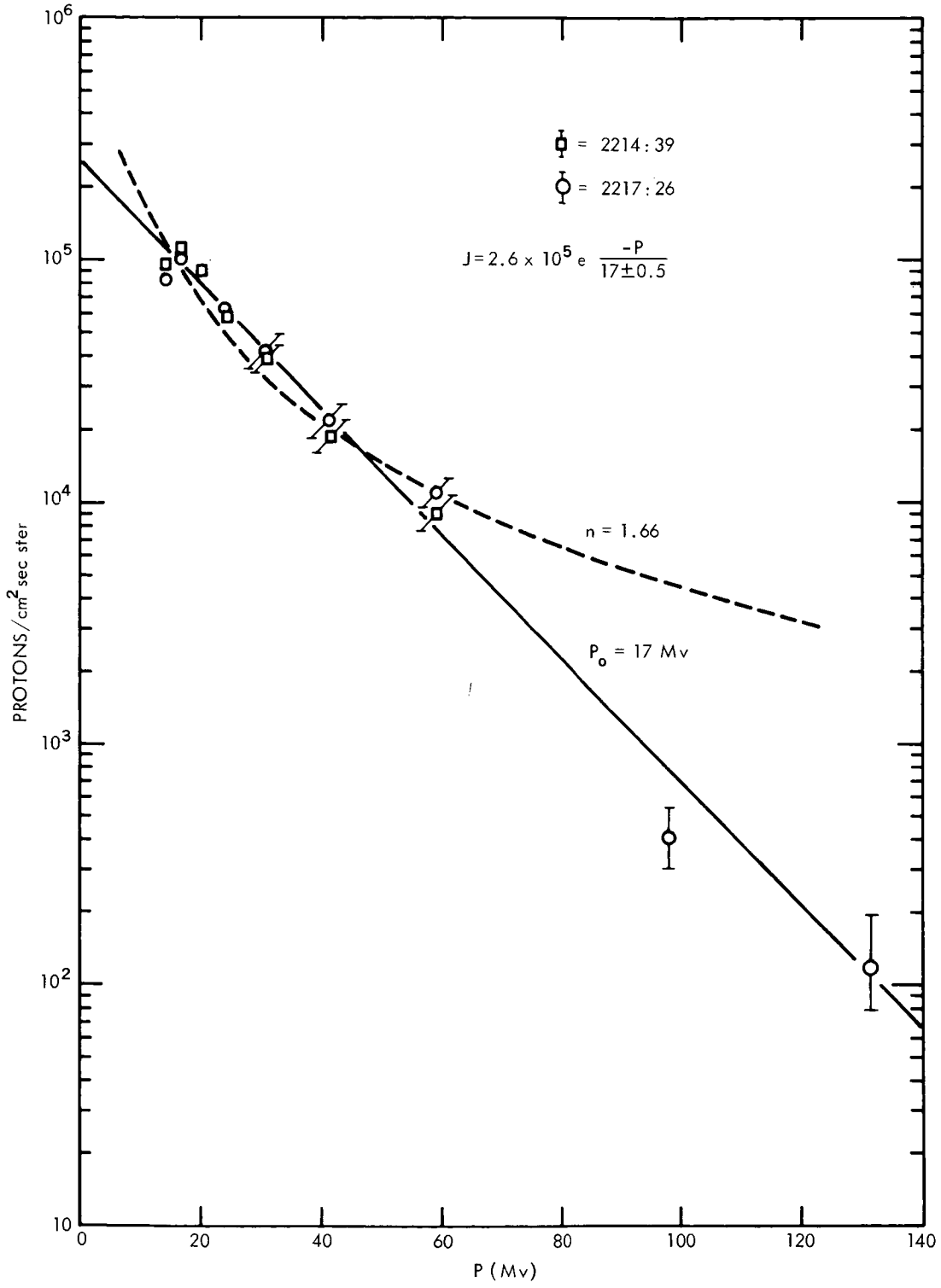

FIGURE 27–21. Spectrum of low energy solar cosmic rays at the time of the magnetic storm associated with the event of September 28, 1961. This spectrum appears to have a much smaller P_0 than the high energy particles present at this same time.

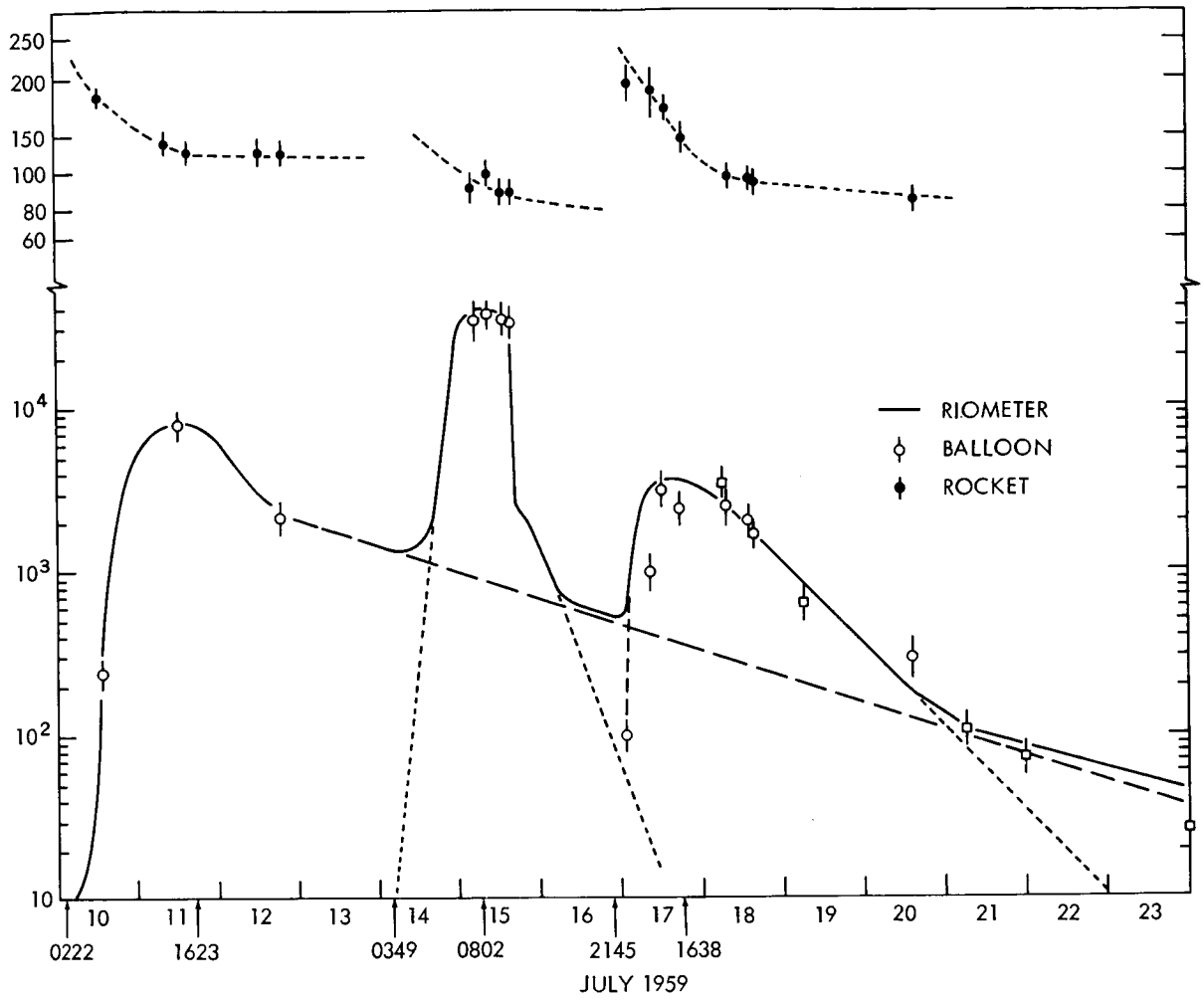

FIGURE 27–22. Time history of the intensity and spectrum of solar particles during the events of July 1959. The values of J_0 are determined by various techniques and include riometer and balloon.

law behavior from one in which n is varying, but, generally speaking, the average n is considerably less than 1. The two events with the lowest values of n (e.g., September 3, 1960, and July 18, 1961) are also those in which t_D showed a very weak velocity dependence and was quite long.

In Figure 27–25, we examine the time decay of $(dJ/dP)_0$. Here we have considered a power law type of decay purely for convenience. It appears that an exponential type decay might represent the data somewhat better. We note that events with a rapid decay of $(dJ/dP)_0$ have a slow decay of P_0, and vice versa.

All these characteristics of $P_0(t)$ and $(dJ/P)_0(t)$ are compatible with the exponential decay actually observed. What we have done essentially is to introduce two new parameters to describe this decay. The use of these parameters may be quite important in understanding the features of the decay. For example, $(dJ/dP)_0(t)$ represents an energy-independent part of the decay. This is compatible with the energy-independent form of the decay one would obtain for diffusion into an infinite medium, for example. The energy (or velocity)-dependent part of the decay is represented by $P_0(t)$. We shall discuss more fully the implication of these quantities in a later section.

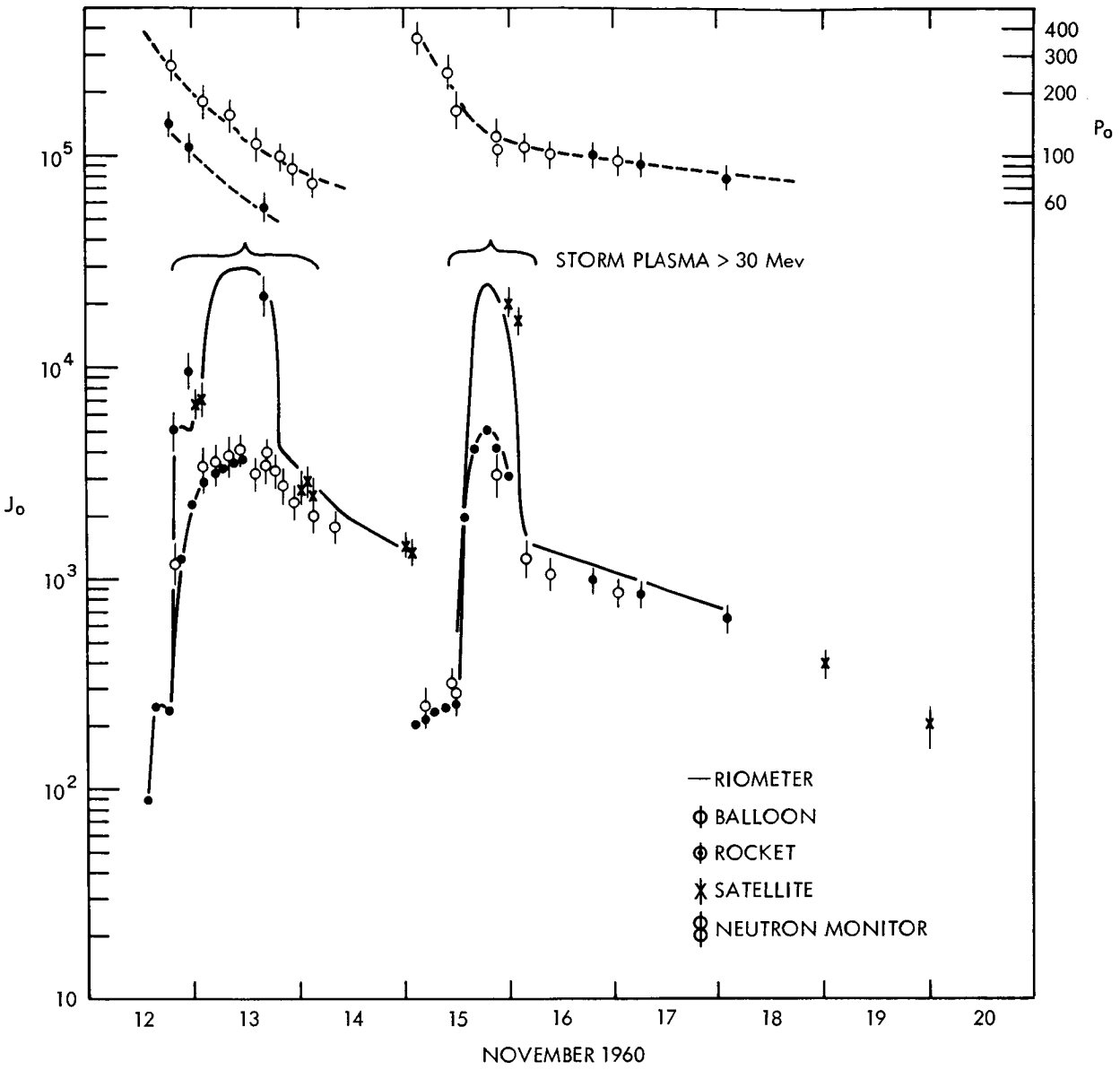

FIGURE 27–23. Time history of the intensity and spectrum of solar particles during the events of November 1960. The values of J_0 are determined by various techniques and include riometer, balloon, rocket, satellite, and neutron monitor.

CHARGE COMPOSITION

The discovery that particles heavier than protons are accelerated in solar flares is one of the leading achievements of the recent work on solar cosmic rays (Reference 7). To date, alpha particles have been observed in at least 10 events and heavier nuclei, principally CNO and Ne, in 2 events (Reference 8). The study of these heavier nuclei is important for at least two reasons. First of all, these particles are of extreme interest with regard to propagation conditions in the interplanetary medium, since they have a different P/v than protons. In this connection it is necessary to make a comparative study of the intensity-time characteristics of these particles and protons for various energies.

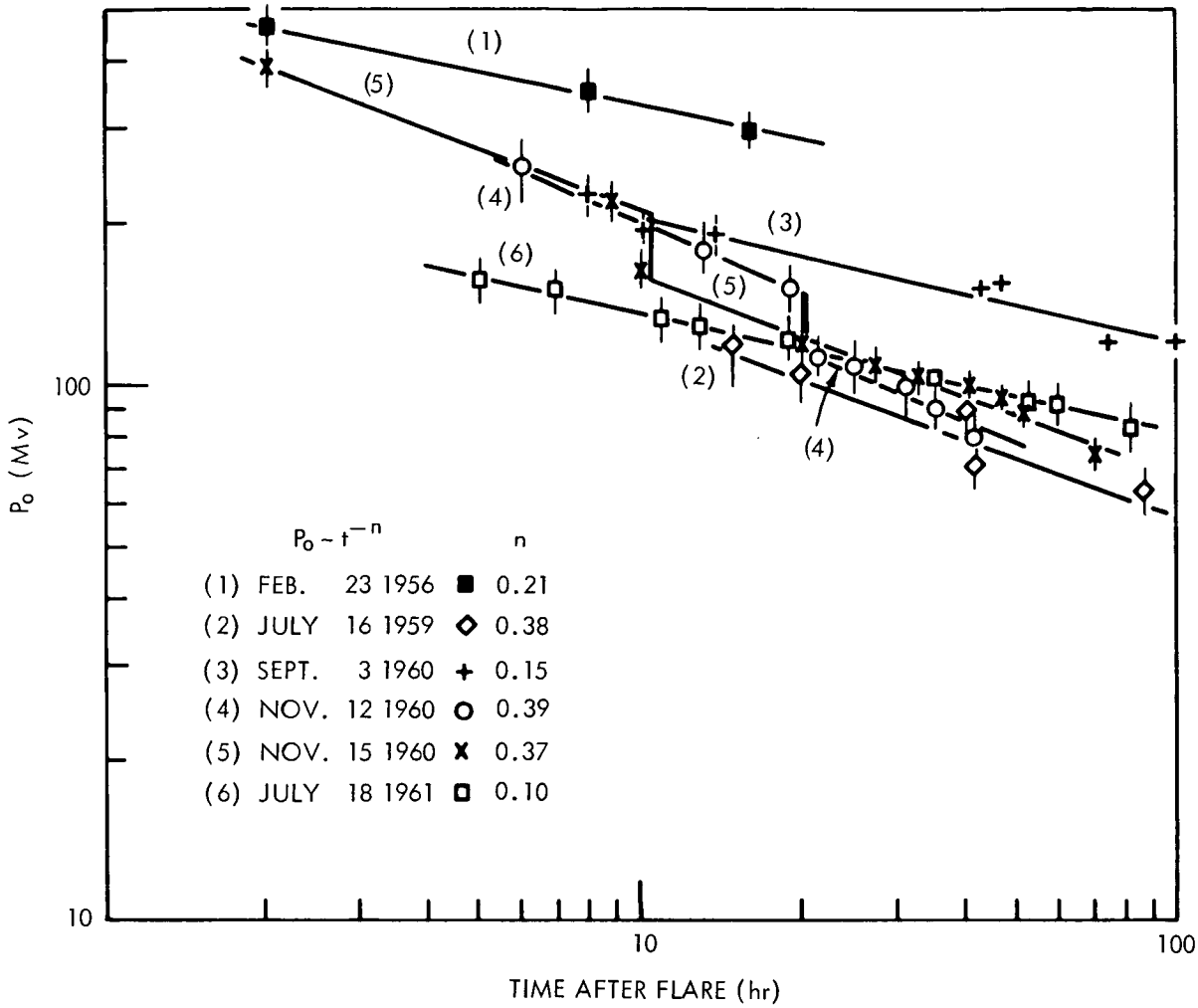

FIGURE 27–24. Variation with time of the characteristic rigidity P_0 describing the solar cosmic rays as observed in various events.

Second, a study of the comparative spectra of these particles, as well as the various abundance ratios such as proton/alpha, and of the individual heavier nuclei can give valuable information on the solar atmosphere and acceleration conditions in the flares. At the present time not enough measurements exist in any one event (a maximum of three were made during the November 15, 1960, event) on the heavier nuclei (principally alpha particles) to permit an investigation of the intensity-time characteristics of these particles. Considerable data exist on the spectra and abundance of these particles, particularly for alphas. It is in this connection that the exponential rigidity spectrum provides a means of systematizing the data. In all the observations to date, it is found that the alpha particles and heavier nuclei have the same type spectrum as the protons when the exponential rigidity spectrum is used. In fact the P_0 is nearly the same for these particles as it is for protons at the time the measurements are made. We can thus define a simple ratio of the various types of particles that is independent of energy. In particular here, we shall be interested in the proton/alpha ratio, since the alpha particles are overwhelmingly the most abundant of the heavier nuclei.

The fact that we can define a unique ratio for all energies at a given time would seem to be

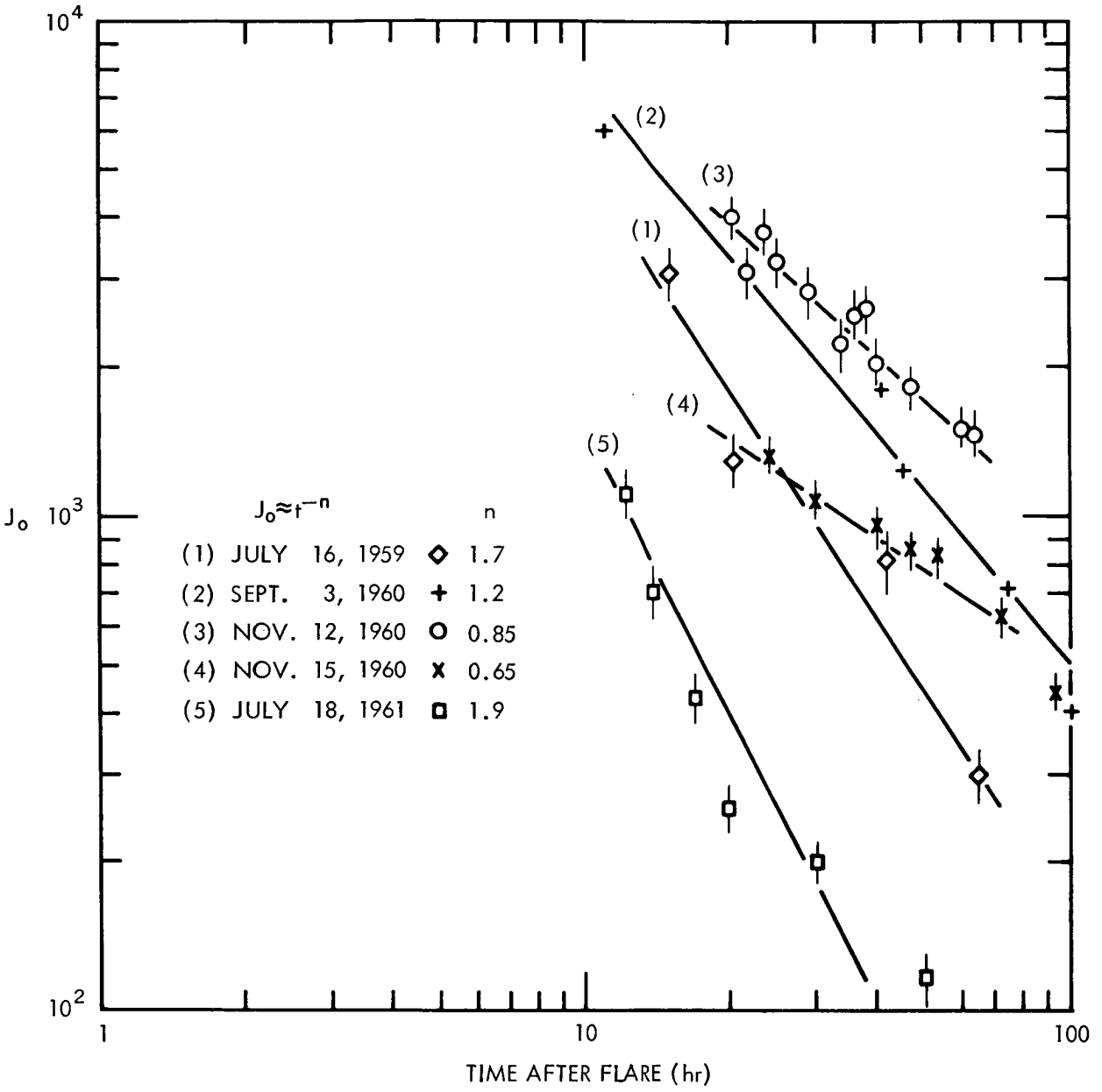

FIGURE 27–25. Variation with time of $(dJ/dP)_0$ as observed in various events.

of great significance. Just what this implies with regard to the acceleration and propagation conditions of these particles is not completely clear. The present approach to the problem is to assume that a particular P/α ratio is common to a particular event. With such a picture, the P/α ratio associated with different events ranges from 1 in a number of events to ≈ 50 in the May 4, 1960, event. It might then be tempting to associate a particular P/α ratio to the features of the accelerating region or method of acceleration of the solar cosmic rays. A more careful examination of the facts, however, suggests that this approach could be misleading. At present not enough measurements are available to determine whether or not this ratio is

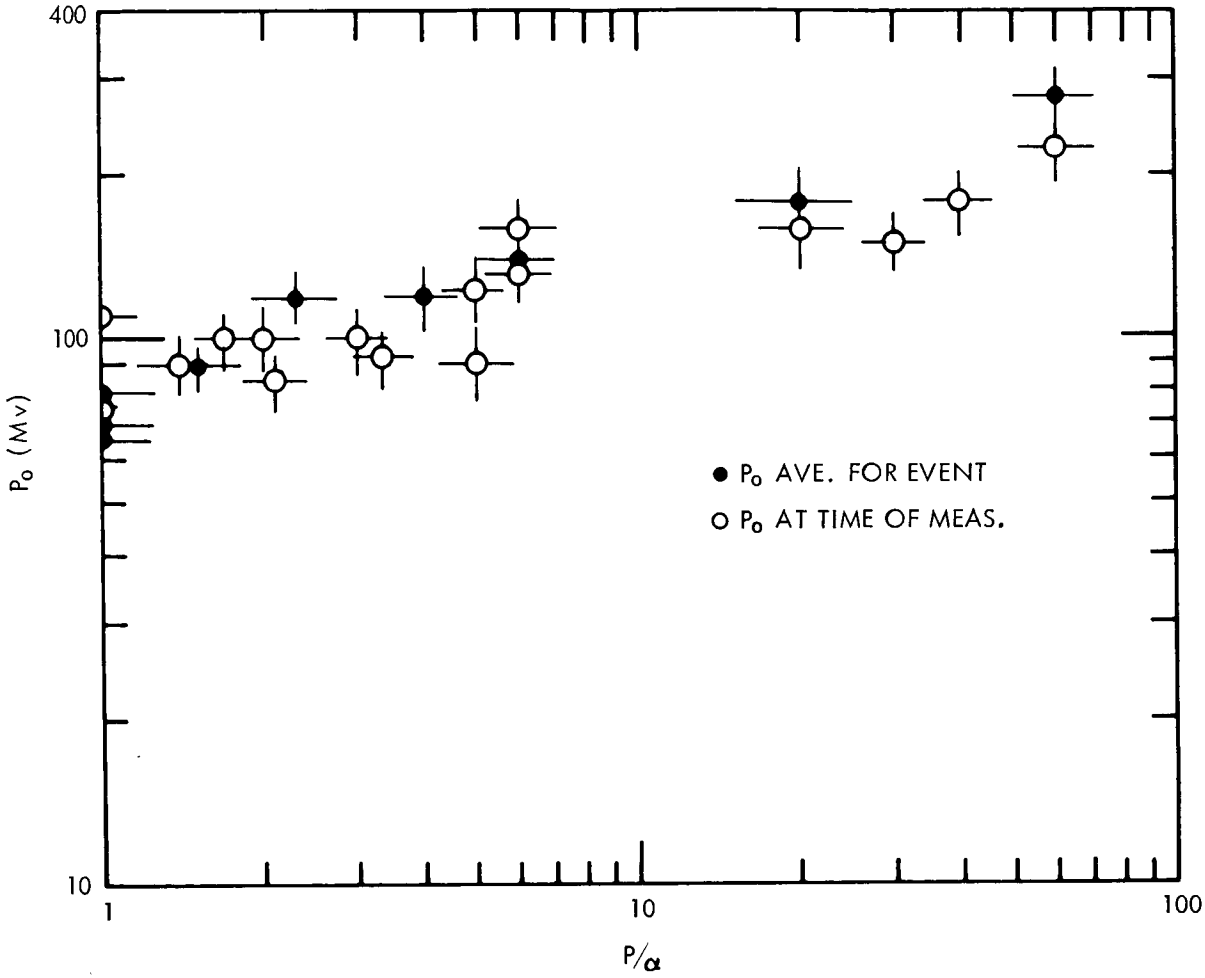

FIGURE 27–26. The proton/alpha ratio as a function of the characteristic P_0 of the spectrum for: (a) each individual event, associating an average P_0 for that event; (b) each individual measurement with its associated P_0.

a function of time in a single event. There is some evidence that it might increase with time in the July 10, 1959, and November 15, 1960, events (References 7 and 8). There is also some evidence that, in cases where the characteristic P_0 is large (e.g., September 3, 1960; May 4, 1960), the P/α ratio is also large.

Combining these two indications, we present in Figure 27–26 a graph of the P/α ratio versus P_0. The solid points, which refer to the P/α ratio as a function of the average P_0 associated with a single event, suggest that, in the manner an event can be characterized as having a flat or steep spectrum, those events with a flat spectrum are also characterized by a large P/α ratio. The open points, however, refer to all available measurements including a number of events in which several measurements have been made. If the P/α ratio were characteristic of an event and did not follow the variation of P_0 during the decay of the event, then the open points should lie to the right and below the closed ones, since the average P_0 relates to the time near t_m and most of the measurements were made at times after this. Note that there is some tendency for this to occur in the data, although the results are far from conclusive. If this were the case (e.g., that the P/α ratio is a characteristic

of the event and does not change with time during the decay phase), this would have an important implication, both with regard to the acceleration and the propagation of the particles. We shall discuss this point further in the following section.

SUMMARY OF SOLAR COSMIC RAY EVENTS

In the previous section we have attempted to present in as concise and coherent a manner as possible the present status of the study of solar cosmic ray events. We have presented these data within the framework of a simple diffusion picture for the propagation and decay of the particles, mainly because it contains many of the presently accepted ideas on this subject. It is, in fact, the only real "model" that has been advanced for the behavior of these particles. The data show, rather convincingly we believe, that this picture is inadequate. Some features of the onset in some of the events may be compatible with such a model, but many features of the onset and almost all the decay features are inconsistent with this picture.

Before we examine some of the features of a "model" suggested by the data, we should in fact summarize briefly what is actually known, by independent means, about the interplanetary medium. The only direct measurements of the magnetic fields and plasma available are those made on Pioneer (Reference 9) and Mariner (References 10 and 11). These measurements are consistent with the idea that the interplanetary medium is moving outward (expanding) with an expansion velocity compatible with other observations, that is, ≈ 500 km/sec at relatively quiet times.

The magnetic field direction lies primarily in the equatorial plane of the sun, although its exact character is unknown since the radial component has not been measured in detail. A comparison of the direct field measurement with the cosmic ray data relating to the onset of direct particles—which suggests that regions with rather regular radial fields, convected outward by the plasma, may be an important aspect of the azimuthal field distribution—is not possible. Some evidence exists in the direct magnetic field measurements for the idea that streaming motion, fairly narrowly collimated in angular extent, exists.

The in-situ measurements clearly show field and plasma variations of a character that could produce a randomizing of the motions of cosmic ray particles. The measurements are not detailed enough for us to estimate a spectrum of turbulence or an effective diffusion coefficient, however.

Measurements of radio wave scattering in the solar corona also suggest the importance of irregularities in the field and plasma distribution that would lead to a diffusion-like picture for the motion of the solar cosmic rays.

These observations, coupled with the remarkable degree of isotropy observed for the solar cosmic rays at times $\approx t_m$ and later suggest a picture in which the solar cosmic rays random-walk in some way through the interplanetary field, must play an important part in any model for the propagation of these particles. The breakdown of this approach during the onset of some events, and particularly during the decay, indicates that we must consider a more elaborate model, however—one in which other characteristics of the particle motion, such as the effects of convection and energy loss, must play an important role.

It seems reasonable to start with the simple diffusion model we have presented and see how it can be modified to explain the experimental data. We shall start with the onset phase.

EXPLANATION OF ONSET PHASE

The main observational feature of the onset phase that cannot be explained by simple diffusion theory is the fact that the intensity of particles at early times in some events is too small. These events are primarily those in which t_m is small, and the times therefore correspond to small absolute times as well. A number of effects might cause such onset characteristics. The most obvious are:

1. *A Finite Injection Interval:* In our simple approach we have assumed the injection time to be instantaneous. There is no direct experimental evidence concerning the injection interval of the solar cosmic rays. From our earlier discussion concerning the time of instantaneous

injection, and assuming that the particles are released only during the impulsive cm wave burst or explosive Hα phase, we may say that the injection interval Δt_i is probably not much greater than 2 minutes. On the other hand, if we say particles are released during the entirety of the Hα flash, then we must admit injection times as long as 30 minutes in some events for which we have direct observations—for example, July 18 and 20, 1961, and September 28, 1961.

Nagashima (Reference 12) has considered the effect of a finite injection interval on the $I(t)$ curve for diffusion from a step-function source in a homogeneous medium. He finds that the finite injection interval does have a significant effect during the early rise. We have obtained a solution to the diffusion equation for a finite impulse function of width Δt_i starting at t_0, which at late times—that is, when

$$\frac{2t_m \Delta t_i}{t(t-\Delta t_i)} << 1$$

—approaches that for an instantaneous source. At earlier times the intensity is less than that from an instantaneous source. If one finds that at times $>t'$ the data fit the simple diffusion picture, then roughly

$$\Delta t_i \lesssim \frac{0.2t'^2}{t_m}.$$

Consider some examples: On February 23, t_m for the indirect radiation was ≈ 60 min and t' appears to be $\approx 0.6\ t_m$; thus $\Delta t_i \leq 4$ min. The same limitations apply to the direct particles in this event. On November 15, 1960, t_m for indirect particles was ≈ 90 min, and t' appears to be $\approx 0.5\ t_m$; thus $\Delta t_i \lesssim 4.5$ min. For July 18, 1961, t_m for the particles measured in balloons was ≈ 240 min, and t' is $\approx 0.2\ t_m$; thus $\Delta t_i \lesssim 2$ min. For July 20, 1961, t_m for the particles measured in balloons was ≈ 150 min. In this case $t' < 0.1\ t_m$ from which we obtain $\Delta t_i \lesssim 0.3$ min. Finally, for the September 28, 1961, event, t_m for the high energy particles as measured in Explorer XII was ≈ 150 min; the corresponding t' is $\approx 0.25\ t_m$ so $\Delta t_i \lesssim 1.5$ min.

Thus we see that the cosmic ray data suggest the particles are not only emitted at a fairly definite time corresponding to the time of maximum electromagnetic emission but that this injection time must be short, probably less than 2 to 3 minutes in most cases. Furthermore, the above limits on the injection times should be regarded as upper limits since—as we shall presently show—there are other, perhaps more fundamental, effects that should cause the intensity at early times to be less than that predicted by simple diffusion theory.

2. *Validity of Diffusion Equation:* We recognize that the diffusion model must have limited validity, particularly during the onset phase, since it predicts that $n>0$ for all $t > t_0$ whereas actually $n(r, t)=0$ at times less than t_0+r/c, where c=velocity of light. It has been shown by Chandrasekar (Reference 13) that the diffusion equation is an approximation to the random walk of a (cosmic ray) particle. Viewing the motion of a cosmic ray particle as a "brownian" type of random walk, we may obtain the density of particles at r and t, $n'(r, t)$ under certain other restrictions which insure that $n=0$ for $t \lesssim r/c$. At sufficiently large times, n' reduces to n. At earlier times, n' is smaller than n by

$$\frac{n'}{n} \approx e^{-r^4/12v^2Dt^3}.$$

If, for example, a difference of $\lesssim 10$ percent could be detected, then at times less than γ_d, where

$$\tau_d \approx \frac{0.2}{\beta}\left[\frac{r^4\,\mathrm{AU}}{\lambda\,\mathrm{AU}}\right]^{1/3},$$

an observer would see a departure from diffusive propagation. We see that this is essentially the same sort of effect as is produced by a finite injection interval. This may also be regarded as the approximate time at which isotropy is observed. Notice that $\tau_d \approx 1/\beta$ when λ=constant, which implies that high energy particles become isotropic before low ones.

Let us examine the onset of the solar cosmic rays in the light of the above calculations. From the relation between t_m and D, we may write

$$\frac{r}{\lambda} = \frac{t_m\beta}{4.2},$$

where t_m is in minutes.

For February 23, 1956, we have for the indirect radiation for $\bar{\beta}=0.85$, $\lambda=0.081$, so that $\tau_d=0.46\ t_m$. For the direct particles for $\bar{\beta}=0.85$, $\lambda\approx0.6$ AU; thus $\tau_d\approx0.3\ t_m$. Actually the simple diffusion picture appears to hold after times $\approx0.6\ t_m$. Thus in this event we probably have both the finite onset time and the correction for the validity of the diffusion equation observable in the onset of the particles. The data are consistent in our extended picture with injection of particles at 0340 ± 1 min over an injection interval $\Delta t\lesssim1.5$ min.

In the event of August 22, 1958, for $\bar{\beta}=0.4$, $\lambda\approx0.2$ AU; thus $\tau_d\approx0.96t_m$. This is somewhat larger than the time $\approx0.8\ t_m$ at which the diffusion picture appears to apply. However, this time is not clearly established by the data. We may conclude that correcting for the validity of the diffusion equation accounts for all of the aspects of the onset in this event and that the injection occurred at 1504 ± 1 min over an interval $\Delta t_i\lesssim2$ min.

In the event of November 15, 1960, for $\bar{\beta}=0.85$, $\lambda\approx0.06$ AU for indirect particles; thus $\tau_d\approx0.6\ t_m$. Again, this is within experimental errors equal to the observed time when the diffusion picture applies, suggesting that the effect of the finite injection interval must be small. We conclude that injection occurred at 0226 ± 1 over an interval $\Delta t_i\leq2$ min.

For July 18, 1961, for $\bar{\beta}=0.4$, $\lambda\approx0.042$; thus $\tau_d\approx0.3\ t_m$—closely comparable with the observed time for diffusion to set in, $\approx0.2\ t_m$. Again it appears that the effect of a finite injection interval is masked, and we can conclude that injection occurred at 1003 ± 1 over an interval $\Delta t_i\lesssim1$ min.

On July 20, no difference from the diffusion picture is noted for $t/t_m>0.1$. λ is determined from t_m to be ≈0.06 AU for $\bar{\beta}=0.5$; thus $\tau_v\approx0.5\ t_m$. Thus, unless we have misidentified the injection by an unusually long time, this event appears inconsistent with our picture.

On September 28, 1961, very accurate measurements of the onset are available for a number of energies. Considering the high energy particles, $\bar{\beta}\approx0.7$, then $\lambda\approx0.04$ AU and $\tau_d\approx0.3\ t_m$. This is compatible with the observed time for diffusion to set in. Thus, injection occurred at 2217 ± 1 min with an injection interval $\Delta t_i\leq1$ min.

Finally, we may consider the September 3 event, which represents a diffusion picture with a large $t_m\approx18$ hours as observed in balloons. No deviation from this picture is noted for $t/t_m>0.1$. We obtain for $\bar{\beta}=0.5$, $\lambda\approx0.01$ AU from the long t_m, from which $\tau_v\approx0.1\ t_m$, in agreement with observations.

Thus, it appears that the onset characteristics of all events can be most simply explained by a simple correction to the diffusion equations at early times for the effects of finite travel time. No evidence can be seen for the effects of a finite injection interval. Careful examination of available data at early times may reveal such effects, but presently we must say that the onset data are compatible with injection at the time of the cm wave, x-ray burst ±1 min and over a very short time interval, probably less than 1 min.

One somewhat disturbing feature of the diffusion approach for the onset of cosmic ray particles is the great variability in the diffusion coefficient D calculated from t_m (or the slope s). This quantity ranges from $\approx2\times10^{20}$ cm^2/sec for the September 3, 1960, event to $\approx2\times10^{22}$ cm^2/sec for the August 22, 1958, event for the same energy particles. Now, it is unlikely that interplanetary conditions influencing diffusion vary by this much even over a whole sunspot cycle.

This variability in D is equivalent to the well-known fact that t_m for particles from west limb flares are significantly less than for east limb flares and that most major solar cosmic ray events are associated with west limb flares.

This suggests that some form of guiding occurs in the spiral interplanetary field (e.g., Reference 4). This cannot be explained by an isotropic diffusion picture, and suggests that it is more realistic to assume an anisotropic diffusing medium with diffusion coefficients applicable for motion along and perpendicular to the lines of force, differing in magnitude perhaps by a factor of 10 or 100.

We shall consider a system with radial symmetry which we shall assume has an axis of symmetry. The diffusing medium is both

inhomogeneous and anisotropic. We set $D_r = D_{\parallel} = D_{\parallel s}(r/r_s)^{\alpha}$ = const. and $D_\theta = D_{\perp s}(r/r_s)^{\alpha}$, where a=2.

Since the distance traversed by a diffusion wave in the direction normal to the field is $\approx\sqrt{D_\perp t}\approx r\sqrt{t}$, particles at different radial positions will diffuse through the same angular distance in a given time. We may use this fact to obtain a solution for the diffusion equation in a cylindrically symmetric medium, which applies during the onset phase of the cosmic ray events; for example,

$$n(r,t)\approx\text{const.}\times t^{-2}e^{-1/4t}\left[\frac{r^2}{D_\parallel}+\frac{r_s^2\theta^2}{D_{\perp s}}+\frac{(Z-Z_1)^2}{D_{Zs}}\right].$$

A plot of $\ln I\, t^2$ versus $1/t$ should give a straight line with slope

$$s=-\frac{1}{4}\left[\frac{r^2}{D_\parallel}+\frac{r_s^2\theta^2}{D_{\perp s}}+\frac{(Z-Z_1)^2}{D_{Zs}}\right].$$

For observations in the equatorial plane $Z=0$; thus

$$t_m=\frac{1}{8}\left[\frac{r^2}{D_\parallel}+\frac{r_s^2\theta^2}{D_{\perp s}}+\frac{Z_1^2}{D_{\perp s}}\right]$$

and $s=2t_m$. The parameter Z should reflect the features of a north–south asymmetry which has yet to be observed. For r we shall use the distance between the sun and the earth which, measured along the spiral field, is 1.3 AU. We shall measure θ from that point on the sun which is on the spiral magnetic field line that intersects the earth. For a uniform solar wind velocity v the longitude of this point is $\approx 2400/v$(km/sec) °W. This reference axis is thus variable, depending on the solar wind velocity at the time, but for a typical average velocity of 400 km/sec is at ≈ 60°W. The two unknowns $D_\parallel$ and $D_{\perp s}$ could, in principle, be determined by measuring s at two points in space. Alternatively we note that flares occurring at ≈ 60°W should have the smallest t_m. Generally $D_{\perp s} << r^2/D_\parallel$ so that, if we write $t_m = K\theta^2 + \tilde{t}$, where $K = r_s^2/8D_{\perp s}$ and $\tilde{t} = r^2/8D_\parallel$, and if $D_\parallel$ does not vary greatly from event to event, then we should find that a plot of t_m versus θ^2 for particles of a given $\bar{v}$ should be a straight line, the slope of which should give $D_{\perp s}$.

In Figure 27–27 we show two curves of t_m versus θ^2, one for particles with $\bar{v}/c\approx 0.85$, the other with $\bar{v}/c\approx 0.4$. We see that, although there is a great deal of scatter, the data are not inconsistent with a straight line. The scatter may be explained by the fact that both $D_{\perp s}$ and $D_\parallel$ may vary in the normal course of events by 20 to 50 percent, and the solar wind velocity also varies. For $\bar{v}/c\approx 0.85$ we find an average slope of 2500 sec, giving $D_{\perp s}\approx 5\times 10^{17}$ cm²/sec; and, for $\bar{v}/c\approx 0.4$, an average slope of 9000 sec, $D_{\perp s}\approx 1.4\times 10^{17}$ cm²/sec. The average perpendicular diffusion coefficient between the earth and sun is given by $\bar{D}_\perp = 1/3\ (1.3r_e/r_s)^2\ D_{\perp s}$; thus $\bar{D}_\perp = 1\times 10^{22}$ cm²/sec and 2.8×10^{21} cm²/sec, respectively. The parameter $D_\parallel$ may be obtained from the onset times for particles from events located at axis of symmetry. For the indirect particles, these times are typically ≈ 50 min, giving $D_\parallel\approx 1.5\times 10^{22}$ cm²/sec. For the anisotropic direct particles t_m is typically 10 min—given an effective $D_\parallel\approx 10^{23}$/sec. It does not appear that $D_\parallel$ is as strong a function of energy as $D_\perp$. Such a difference in energy dependence of these quantities might explain some of the features of the different t_m versus $\bar{v}$ curves shown in Figure 27–10.

Also note in Figure 27–27 that both the high and low energy data from July 1959 exhibit much greater t_m than the rest of the data (this is also evident from Figure 27–10). This was a period of exceptionally intense solar and interplanetary activity, and the modulation of galactic cosmic rays reached its highest level during this period. It is likely that the diffusion coefficients are different during this period. In fact, the data in Figure 27–27 suggest that a value of $D_{\perp s}\approx 1.5\times 10^{17}$ cm²/sec is more appropriate for the higher energy particles during this time. $D_\parallel$ may also be smaller at this time. A factor of 2 to 3 variation of these coefficients at extreme times is probably to be expected.

The result of the anisotropic diffusion picture is that inside the earth's orbit the radial field tends to provide a strong collimation of the solar cosmic rays. It is unnecessary to invoke diffusion coefficients varying by factors up to 100 during the course of a few months, but

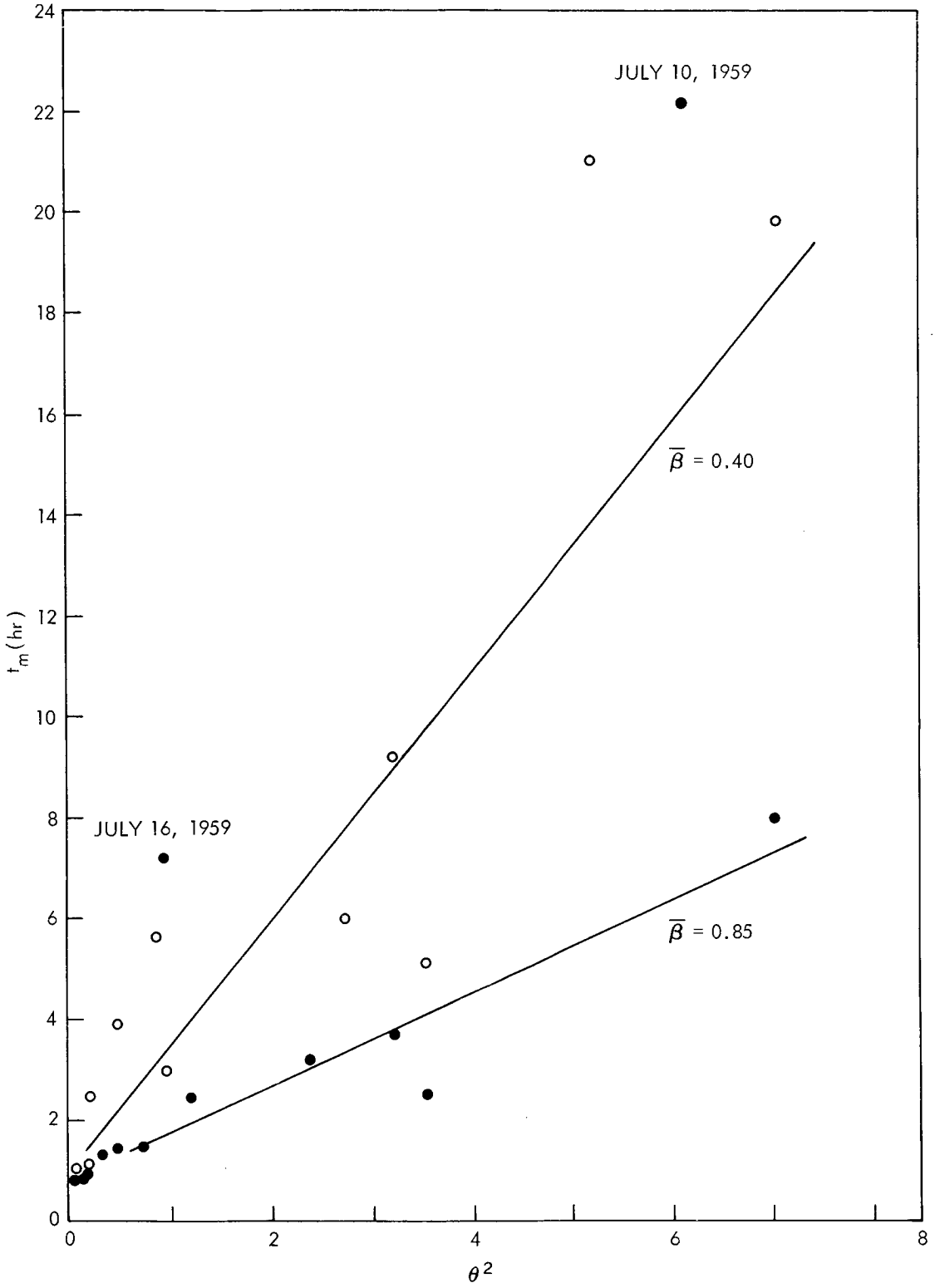

FIGURE 27–27. Dependence of t_m on θ^2 for particles of average velocities $\bar{v}/c=0.85$ and 0.40. (θ is the angle in radians from the reference location taken to be 60 to 70 degrees west of central meridian on the sun.)

728–629 O—64——17

instead we may consider that the diffusion coefficients do not change greatly with time and that the particles must diffuse across the lines of force. The energy dependences of $D_\perp$ and $D_\parallel$ may also differ.

The idea of anisotropic diffusion does not alter our previous discussions of the onset characteristics. It gives us a new insight into the anisotropies appearing during the onset phase of some events, however. We also note that outside of the earth's orbit at approximately 2 AU the two coefficients become comparable. In this region it may be more appropriate to consider the isotropic diffusion picture again.

DECAY PHASE

The most conspicuous experimental feature of the decay phase of the solar cosmic ray events is the exponential decay of particles of all energies when uninterrupted by plasma fronts moving through the interplanetary medium. Such a decay is most simply explained in the diffusion picture by the existence of an absorbing boundary and is clearly incompatible with diffusion in an infinite medium. A closer examination of the data reveals very serious problems in connection with the existence of such a boundary, however. In all events except one (February 23, 1956) the exponential decay has set in almost immediately after t_m, giving $t_E << t_D$ in disagreement with the consistency relation in a bounded medium, which requires that $t_E = t_D$. Also, a plot of the dimensionless quantity t_D/t_m should give a measure of the boundary of the diffusing medium. In more than half the cases the radius of this boundary is less for low energy particles than for high energy ones—a result difficult to interpret. Furthermore, in some events which apparently follow the diffusion picture during onset, this boundary is less than 1 AU—a very disturbing fact.

In view of these problems let us consider some alternative possibilities which explain these data but retain the diffusion picture:

1. *Solar Absorption:* In a diffusion picture, the adiabatic invariants are not conserved, and particles may be scattered into loss directions which carry them into the sun even though the magnetic field in the inner solar system is diverging. This kind of particle loss has been introduced by Elliot (Reference 14) in his model for galactic cosmic ray variations by including in his steady-state diffusion equation a general absorption term $N \times P(r)$, where $P(r)$ is a radially dependent (solar) absorption probability. Elliot estimates that $P(r) \approx r^{-2}$; we consider instead $P(r) = \text{constant}$ and obtain for the solution of the diffusion equation

$$\bar{n} = ne^{-t/t_d},$$

where n is the solution of the diffusion equation with an absorbing boundary and $t_D = 1/NP$. The significant feature of this result is that the exponential factor is present at all times after injection. This gives times for the onset of the exponential decay that are a factor of ≈ 2 to 3 smaller than those actually observed. Thus, while some features of this type of absorption may be important for the solar cosmic rays, a radially independent probability for solar absorption overcompensates for the early onset of exponential decay actually observed.

2. *Energy-Dependent Diffusion Coefficient:* The fact that the plot of the dimensionless quantity t_D/t_m versus $\bar{v}/c$ gives a series of improbable results suggests that simply allowing the diffusion coefficient to be energy-dependent cannot explain all the features of the decay. It is useful to inquire, however, whether this may explain certain features of the intensity-time behavior of the solar particles—in particular, the energy (velocity)-dependence of t_m and t_D. Recall that, if λ is energy-independent, t_m and t_D should be simply $\approx 1/\bar{v}$. The data in Figures 27–10 and 27–16 for both t_m and t_D show events with two types of $\bar{v}$ dependence. One group of events gives a dependence $\approx 1/v^n$, where $n \approx 0.5$, and the other where $n \approx 2.5$. There appears to be no consistent picture in a single event with regard to the energy dependence of t_m and t_D.

The energy variation of D will depend on the structure of the scattering centers—assumed to be magnetic irregularities—and on the ratio of the gyro-radius R_L to the scale of the magnetic irregularities L_i. The characteristics of the energy dependence of this diffusion coefficient have been discussed by Morrison (Reference 15)

and Parker (Reference 16). For our purposes we may describe the scattering centers as reflecting (hard) or transmitting (soft). If we find λ is constant with energy, we can conclude that hard scattering centers predominate. We can then identify λ with the mean free path and use the hard sphere analogy to write

$$\lambda_R = \frac{1}{\pi L_t^2 n_s}$$

where n_s is the density of scattering centers. In this case, $R_L < L_t$. When $R_L > L$, the change in the trajectory of a particle produced by a collision will be small; so the term "transmitting scattering center" is more appropriate. In this case the concept of a mean free path is ambiguous; however, Parker (Reference 16) identifies λ with the average distance a particle must travel to be deflected by 90 degrees and obtains

$$\lambda = \left[\frac{1}{\pi L_L^2 n_s}\left(\frac{\pi}{2}\frac{1}{L_L}\right)^2\right] R_L^2 \approx \beta P^2,$$

where P is the rigidity of the particle. Note that the mean free path rapidly increases with energy in this case, and the higher energy particles should propagate more rapidly than the low energies. The slope of the t_m or t_D versus $\bar{v}^n$ curves should thus increase from values of $n=1$ at lower energies to $n=4$ at higher energies. There is no evidence for this effect from the data as presented in Figures 27–10 and 27–16. However, a closer examination of the region of the graph where $\bar{v}/c \gtrsim 0.8$ for events in which high energy particles were observed at sea level gives definite evidence for this effect setting in at $\bar{v}/c \approx 0.85$, corresponding to a rigidity of ≈ 1.6 Bv. Particles with this rigidity must have a radius of curvature of $\approx 4 \times 10^{10}$ cm, or 0.003 AU in a magnetic field $= 10^{-4}$ gauss. Thus $L_t \approx 0.003$ AU. Taking a typical mean free path of 0.05 AU in conjunction with the above value gives for $n_s \approx 1/0.01$ AU.

In view of the difficulties in explaining the decay of the solar particles using a diffusion picture, it seems worthwhile to consider other characteristics of particle motion that might dominate over simple diffusion during this time. In this connection it may be useful to consider an approach based on the parameters J_0 and P_0 introduced earlier. Let us first consider the fact that alphas and protons appear to maintain the same P_0 during the decay phase of an event. Thus, $t_{\alpha D}(P) = t_{PD}(P)$, whereas according to diffusion theory $t_{\alpha D}(P)/v_\alpha(P) = t_{PD}(P)/v_P(P)$ (e.g., the decay time at the same rigidity P should be longer for alphas by a factor of 2 on low energies). Thus, we should find

$$\frac{\Delta P_0(\alpha)}{\Delta t} \approx \frac{(t_{PD}+t)^2}{(t_{\alpha D}+t)^2}\frac{\Delta P_0(P)}{\Delta t}.$$

At times $\approx t_D$, $P_0(\alpha)$ should change less rapidly than $P_0(P)$, although at later times the differences should be less marked. No such changes are observed, although it should be cautioned that most measurements have been made at times well after t_D when the changes may not be observable. It is also evident from the above relations that we may still retain a diffusion picture, and claim protons and alphas have and maintain the same P_0 if we claim that the time at which the measurements have been made is greater than t_{PD}. Then, of course, at early times the proton spectrum must be flatter than the alpha particle spectrum, and we would see a change in the characteristic rigidity for the spectra of the two components. The importance of measurements of alpha particles at early times in the solar cosmic ray events is emphasized by these arguments.

Let us now consider J_0 and P_0 and their dependence on time from another point of view. If a change in J_0 occurs, the intensity of particles of all energies is reduced by an equal amount—an energy-independent change. If a change in P_0 occurs, we have a rigidity-dependent change. This suggests that we should regard the decay of the solar cosmic rays as composed of an energy-independent part and a rigidity-dependent part. A natural explanation for such a spectral change would be if convection effects play an important part in the decay of the solar particles. Particle density would be reduced by expansion and betatron deceleration and inverse Fermi energy loss effects. The particle dilution as a result of expansion would be energy independ-

ent, and the same for protons and alphas. If we consider a radially expanding flow moving outward from the sun with velocity v, then at a distance $r \approx 1$ AU the particle dilution rate d is

$$d=\frac{\mathrm{d}n}{n}\,\mathrm{d}t\approx\frac{2v}{r}.$$

We may define a characteristic decay time

$$\tau=\frac{1}{d}\approx\frac{r}{2v}.$$

Taking $v\approx 700$ km/sec at times of solar activity gives $\tau\approx 30$ hours. The data on $J_0(t)$ contained in Figure 27–25 have been presented in power law form but, as pointed out earlier, may fit an exponential equally well. The characteristic times for the events in which we have data range from 12h to 50h. If this approach has any validity, we might expect some correlation between the characteristic times for the decay of $J_0(t)$ and the transit time for the arrival of the solar plasma to the earth. Reference to Table 27–3 shows that only a weak correlation exists between these quantities. It may be that we must consider the location of the flare on the sun and a more complex geometrical situation in order to relate the observed transit time to the effective outward propagation velocity resulting in the dilution of the cosmic ray intensity.

Turning now to the variation of $P_0(t)$, which represents an energy dependence of the decay process, let us associate this—in part—with the effects connected with the convection and expansion of material in the interplanetary medium. Specifically, let us consider betatron deceleration. A picture appropriate to the change of the spectrum of the solar flare cosmic rays due to this process has not been developed according to our knowledge. Laster, Lencheck, and Singer (Reference 17) have presented a model for Forbush decreases which invokes betatron deceleration. They assume that the characteristic diffusion times are short compared with the time scale of the expansion in obtaining a solution to the diffusion-energy loss problem. In the light of our earlier arguments, this appears inappropriate for the solar cosmic rays in some instances at least. However,

TABLE 27–3

Comparison of Transit Times for Solar Plasma to the Earth and the Characteristic Time Associated With Particle Dilution

Event	Transit Time (hr)	Characteristic Time (hr)
July 16, 1959	19	≈12
Sept. 3, 1960	46	≈18
Nov. 12, 1960	30	≈30
Nov. 15, 1960	?	≈50
July 18, 1961	38	≈12

consider the time rate of change of rigidity of a cosmic ray particle diffusing within an expanding spherical magnetic cloud. The betatron deceleration is given by

$$\left(\frac{\mathrm{d}P}{\mathrm{d}t}\right)_{Bet}=-\left(\frac{P_\perp}{2B}\right)\frac{\mathrm{d}B}{\mathrm{d}t}.$$

If we consider $BR^2=\text{constant}$ and $\mathrm{d}R/\mathrm{d}t=v$, we have

$$\left(\frac{\mathrm{d}P}{\mathrm{d}t}\right)_{Bet}=-\left(\frac{2v}{3R}\right)P;$$

R is the radius of the cloud or, since $R=vt$,

$$\left(\frac{\mathrm{d}P}{\mathrm{d}t}\right)_{Bet}\approx\frac{1}{t}=\frac{a}{t}.$$

If we consider a solar cosmic ray spectrum of the form $\mathrm{d}J/\mathrm{d}P=(\mathrm{d}J/\mathrm{d}P)\ \exp\ [-P/P]\ (t)]$, for the above variation of P we have $P_0\approx 1/t^a$. For the above special geometry, $a\approx 2/3$; whereas the observed values of a, as determined from Figure 27–24, range from 0.2 to 0.4—certainly not inconsistent with the idea that betatron deceleration plays an important role in the decay of the solar particles.

The previous discussions are intended only to point out some methods of approach to the problems of understanding the decay of the solar cosmic rays. It would seem that at the present time we do not have enough information to determine which features of particle motion dominate during this period and how we must modify the diffusion approach to fit the experimental data. We believe that convection and energy loss effect may be observable in some

events, probably masking the effects of diffusion and the boundary effects for the diffusing region.

CHARACTERISTICS OF SOLAR COSMIC RAYS AT INJECTION

One of the main objectives of our discussion of the propagation of the solar cosmic rays has been to help lay the groundwork for an evaluation of the intensity and spectrum of the solar cosmic rays at injection. We have already established the time of injection and the period during which injection occurs in a number of events. The determination of the intensity and spectrum of the particles at injection depends critically on the features of the model for the propagation of the solar particles to the earth. As we have pointed out, during the onset phase of the events, a suitably modified diffusion picture fits the cosmic ray data quite closely. Within this framework, then, we may attempt to determine the injection spectrum of the solar cosmic rays by two somewhat different methods:

1. Let us consider the onset of the indirect particles, those that seem to fit the simple diffusion picture quite well (ℓ n I versus t/t_m is a straight line in Figure 27–9). Here we have two methods of approach—both essentially the same, but one reflecting somewhat more accurate experimental data than the other. In the first instance we may determine the number of particles at injection from the relation

$$N(v)=v\left(\frac{\pi r^2}{s}\right)^{3/2} e\left(\frac{t_m}{t_0}\right),$$

where t_0 reflects the onset of the solar cosmic rays and is the time at which $It^{3/2}=1$ where I, the intensity, is measured in suitable units.

If onset data are available for particles of two or three velocities, it is possible to reconstruct the spectrum at the source. This method is relatively uncertain, however, since the intensities are usually small at times near t_0 and a small error in t_0 results in a large uncertainty in N.

In the second instance we may determine the number of particles at injection from the particle intensity at t_m from the relation

$$N(v)=\frac{10r^3 I(r,v,t_m)}{v}.$$

This corresponds to a spherical volume ≈ 1.3 AU surrounding the sun, filled to a density $n=I/v$ equal to that at the earth at t_m.

The relative numbers of particles of different velocities injected is then given by

$$\frac{N(v_1)}{N(v_2)}=\frac{v_2}{v_1}\frac{I(v_1 t_m)}{I(v_2 t_m)}.$$

Much more data are available at times near t_m, but here there is some evidence—as we have pointed out—that the diffusion picture is beginning to break down. Also, an anisotropic diffusion picture may be more appropriate to the solar particles, in which case a volume elongated in the radial direction may be thought of to contain the particles and $N(v)$ may be a more complicated function of $I(v)$ at t_m for various energies. Nevertheless, we show the injection spectra obtained in seven events in which data are available for at least three energies in Figure 27–28. We have restricted the data to the region where it is believed λ is independent of energy (e.g., less than ≈ 1.2 Bv rigidity). The total number of particles >10 Mev injected ranges from $\approx 10^{35}$ to $\approx 10^{32}$ in these events. We estimate that these numbers may be uncertain by a factor of ≈ 2 to 3. Present techniques allow us to observe events with as few as $\approx 10^{29}$ particles >10 Mev.

We have presented the injection spectra in Figure 27–28 in the form of exponential rigidity spectra. The data are more consistent with a "bowing" of the curves in this figure, suggesting that the spectrum may be more like a power law (in rigidity). In view of the uncertainties in the propagation picture, it does not seem possible at present to select between these or other possibilities for the injection spectra. Detailed measurements of the onset at a number of energies may make such a selection possible in the near future, however. The total energy carried by these particles ranges from $\approx 2\times 10^{31}$ ergs in the largest events down to $\approx 10^{24}$ ergs in the events that are just barely detectable. At the earth, the energy density of the solar cosmic rays >10 Mev may approach 10^{-9} erg/cm^3 in the largest events. It should be pointed out that this energy density is comparable with that residing in a 20γ magnetic field.

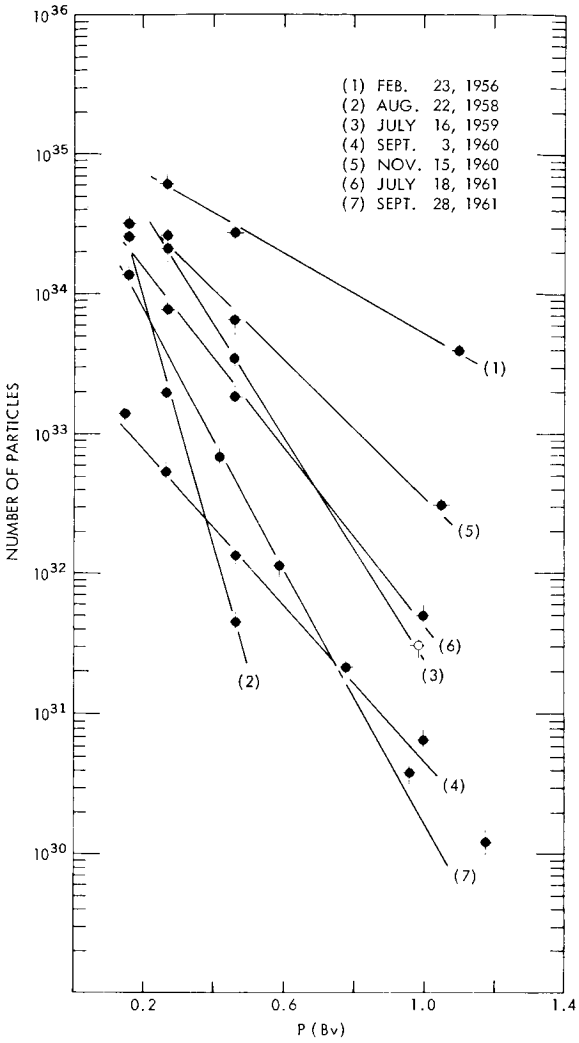

FIGURE 27–28. Intensities and spectra of solar cosmic rays at injection as determined in seven events.

2. Let us now consider the onset of the direct particles or those that propagate directly along the field lines without appreciable scattering. At present, all our definitive data on these particles come from neutron monitor observations and are thus restricted to high energies. Observations in which both the direct, and later the isotropic indirect, particles of the same energy can be observed should give a consistent picture for the intensity and spectrum of the injected particles, however.

Considering the simplest case possible—that is, the direct particles are emitted isotropically over a hemisphere and propagate rectilinearly to the earth (as optical or radio emission), we can estimate the total number of particles emitted by integrating the total number of particles observed in the direct particle pulse (intensity time profile) over a 4π solid angle. Application of this procedure to the direct particles observed during the February 23, 1956; May 4, 1960; and November 15, 1960, events gives a value of N for particles with $\bar{v}/c \approx 0.85$ compatible with a volume of radius ≈ 1–1.4 AU uniformly filled with cosmic rays at a density equal to that of the indirect particles at t_m. This corresponds to a value of N comparable with that determined by using the diffusion approach for the indirect particles in the same events.

Within the framework of simple rectilinear propagation of the direct particles, the intensity time profile should be a measure of the actual spectrum at injection. Consider the following particularly simple case: Suppose that N solar cosmic rays are injected parallel to the field lines (assumed to be uniform and non-diverging) with an exponential velocity spectrum $dN/dv = N/v_0 \exp(-v/v_0)$. During the interval Δt at time t, the particles which arrive at the earth are those with velocities in the interval $\Delta v \approx \Delta t/t^2$ centered at $v = r/t$. The observed flux of particles as a function of time would be given approximately by

$$I \approx \text{const.}\ \frac{N \exp[-r^2/4(rv_0/4)t]}{(rv_0/4)t^2}.$$

Thus, the intensity would appear to vary with time as though all particles were injected with the same velocity and propagated by diffusion through a medium with an effective diffusion coefficient $D_{eff} = rv_0/4$. Taking $v_0 = 6 \times 10^9$ cm/sec (corresponding to a $P_0 = 200$ Mv), which is typical of several solar events (Reference 6), we find that $D_{eff} \approx 2 \times 10^{22}$ cm^2/sec. Thus $t_m \approx 20$ min. Such times are certainly characteristic of the direct particles although we cannot take the above calculation seriously, since the essentially monoenergetic spectrum with the observed energy changing with time that it predicts at the earth is not compatible with the observations on the direct particles.

We recognize that the true picture for the propagation of the direct particles is more complicated than the simple ones we have outlined. In all likelihood, the interplanetary field is decreasing (diverging) from the vicinity of the sun to the earth. Some form of scattering probably exists for these particles as well (Reference 4), although it is questionable whether a diffusion picture is adequate to describe this scattering. It is now necessary to consider the angular distribution of the solar cosmic rays and how it changes with time in order to investigate the competing effects of a diverging field and scattering on an injection spectrum of cosmic rays. At present, very little work is available using this promising approach; but we may cite a number of very simplified pictures.

Considering a uniform field between the point of injection and the earth, the observed time of flight t for particles arriving with pitch angles θ is given by $t=R/v\times 1/\cos\theta$, where R is the distance along the field line. Thus, if monoenergetic particles were instantaneously injected isotropically at the source and no scattering were present, we should expect to see particles arriving from a fairly narrow angle in space—this angle increasing as time progresses. In a diverging field the passage between two points on the same field line takes a time (Reference 4)

$$\tau(\theta_1)=\frac{R}{v(\sqrt{B_0}-\sqrt{B_1})}\left[1\sqrt{B_0}\cos\theta_1 1 \pm (B_1-B_0\sin^2\theta_1)^{1/2}\right],$$

provided B_1+B_0; B_0 and B_1 are the magnetic field at the beginning and end of the interplanetary field lines, respectively. Thus again, if monoenergetic particles are instantaneously injected isotropically at the source and no scattering is present, we should expect to see particles arriving from a fairly narrow angle in space—this angle increasing as time progresses, only now slightly more slowly than in the case of a uniform field.

What is actually observed is radiation initially closely collimated about the field direction. As time progresses, this collimation becomes less and the angular distribution spreads out. The energy dependence of this radiation as a function of time has not been studied.

Two effects we have not considered could cause the observed effect. These are: (1) the spectrum of the radiation which can cause a superposition of many narrow angular distributions, gradually broadening out as time progresses (as we have noted previously); and (2) possible small angle scattering of the particles enroute to the earth. It is not immediately apparent which of these effects will dominate in determining the angular distribution of these particles at any one instant and how, also, this distribution varies with time. McCracken has argued qualitatively that scattering plays an important part. We have considered a specific case of small angle scattering. Then, for a monoenergetic injection spectrum with all particles moving parallel to a uniform field, we obtain an angular distribution (as a result of scattering) $I(\theta)\approx e^{-K\theta}$ essentially independent of time after the arrival of the particles. Here, K is a measure of the scattering constant.

It is clear that a complete treatment and study of the arrival of the direct particles can give valuable information on both the injection spectrum and characteristics of propagation of these particles.

REFERENCES

1. Meyer, P., Parker, E. N., and Simpson, J. A., 1956, *Phys. Rev.*, 104: 768.
2. Bryant, D. A., Cline, T. L., Desai, U. D., and McDonald, F. B., 1962, *J. Geophys. Res.*, 67: 4983.
3. Hofmann, D. J., and Winckler, J. R., 1963, *J. Geophys. Res.*, 68: 2067.
4. McCracken, K. G., 1962, *J. Geophys. Res.*, 67: 447.
5. Lin, W. C., and Van Allen, J. A., 1963, Univ. of Iowa Report No. 15.
6. Freier, P. S., and Webber, W. R., 1963, *J. Geophys. Res.*, 68: 1605.
7. Biswas, S., Fichtel, C. E., Guss, D. E., and Waddington, C. J., 1963, *J. Geophys. Res.*, 68: 3109.
8. Frier, P. S., 1963, *J. Geophys. Res.*, 68: 1805.

9. Coleman, P. J., Davis, L., and Sonett, C. P., 1960, *Phys. Rev. Letters*, 5: 43.
10. Neugebauer. M., and Synder, C. W., 1962, *Science*, 138: 1095.
11. Coleman, P. J., Davis, L., Smith, E. V., and Sonett, C. P., 1962, *Science*, 138: 1099.
12. Nagashima, K. J., 1962, *J. Phys. Soc. Japan*, 17, Suppl. A II: 575.
13. Chandrasekhar, S., 1943, *Ref. Mod. Phys.*, 15: 1.
14. Elliot, H., 1960, *Phil. Mag.*, 5: 601.
15. Morrison, P., 1956, *Phys. Rev.*, 101: 1392.
16. Parker, E. N., 1956, *Phys. Rev.*, 103: 1518.
17. Laster, H., Lencheck, A. M., and Singer, S. F., 1962, *J. Geophys. Res.*, 67: 2639.

DISCUSSION

Dr. Sturrock: Your estimate of the diffusion coefficient implies some assumption about the mean free path λ, since $D=\frac{1}{4}\lambda v$. What is this mean free path?

Dr. Webber: λ turns out to be about 0.03 or 0.04 astronomical units.

Dr. Sturrock: To what collision mechanism do you ascribe this estimate of the mean free path?

Dr. Webber: If I knew a little more about how the particles actually did diffuse in the interplanetary medium, I could say.

The ideas of this "random walk" process are not very developed. Presumably it is some sort of a characteristic angle that they are scattered through during this course of moving through the irregular interplanetary fields.

Dr. C. Warwick: There are a few observational facts that I would like to ask whether the diffusion model can explain. One is why the 10 Mev particles don't show the clear dependence on flare longitude that the Bev particles do.

Another is why we do not see a significant number of events that are associated with flares that are well beyond the west limb, that is, with no observed flare at all.

And, finally, can you explain—or have you wondered—why the travel time depends on the general level of solar activity?

Dr. Webber: To start from the last one first, at least, the general level of solar activity presumably determines the characteristic scattering or diffusion in the interplanetary medium. If the medium is very disturbed, then possibly, under some conditions, this diffusion coefficient could be small, meaning a lot of scattering, which would make the time long—the onset times and characteristic time of maximum long.

In the isotropic diffusion picture you can't explain anything with regard to the observed disk asymmetry of these solar particles. But in the anisotropic picture you can at least explain these in terms of a reference line which, let's say, they seem to propagate most directly at around 50 degrees west location, which would mean a more or less symmetrical distribution of characteristics about that line. I think this is not unlike what is seen.

An event occurring at 120 degrees west, November 20, 1960, for example—that propagation condition is not unlike something on central meridian or slightly east.

I don't know, as far as the first point, that we have very much in the way of observations on the anisotropic behavior of 10 Mev particles, so we really can't say much about what they are doing at all.

Dr. Giovanelli: Can you tell me whether any of this type of event has been observed without any visible occurrence on the surface of the sun? The point of this question is to find out whether any diffusion-type events occur in connection with things that might have occurred around the invisible side of the sun.

If there are no such events, then this must tell us something about the diffusion processes.

Dr. Webber: That is certainly correct. To my knowledge there have been no very well identified cosmic ray events that were not identified with events on the visible face of the sun. This is always a problem, whether in fact you are observing at the correct time, or something like that. But this, of course, would mean that an isotropic diffusion picture couldn't hold.

Otherwise, you would see events on the invisible side of the sun. So this is another

good argument for some sort of guiding and isotropy in the azimuthal propagation of the particles.

Dr. McDonald: There was one small solar event on September 7 that one keeps wondering about, just whether it did occur on the back side or not.

Jim Warwick and I discussed this at great length. It showed up as just a moderate size event with a very slow decay. I think the question is still unresolved, as to origin. There was obviously no solar flare connected with it. Whether it was connected with a radio noise storm without a flare is still an open question.

Dr. Wilcox: There is considerable discussion in the east-west effects. Do you ever make an attempt to look into latitude effects, and in particular any distinction between north and south latitude?

Dr. Webber: There have been some very feeble attempts, but not to the point where one can define any asymmetry or any line of symmetry in this direction.

Dr. Wilcox: Can such a thing be done? When you say feeble attempts——

Dr. Webber: There are not very many events. There may be a half-dozen different events. There are in fact five or six, I think, which appear to be north limb, in the Northern Hemisphere, and one or two in the Southern. But, then, three of these are related to the same active center. So, you can't really say very much.

Dr. Axford: With this more sophisticated diffusion model, can you get rid of the boundary which kept appearing at about 2 AU in earlier models? Have you ever seen any effects of the boundary which might appear at some 10's of astronomical units?

Dr. Webber: With this sophisticated approach we have worked it out only for an infinite medium. This is complicated enough with our present understanding. Therefore, we can't say anything about the boundary in this picture.

Dr. Oxford: You don't have to drag the boundary in, though, to explain anything, do you?

Dr. Webber: If we do have exponential decay, we may have to drag a boundary in if we want a diffusion-like approach. But my opinion is that exponential decay is sort of a by-product, maybe, of this picture and general expansion and betatron deceleration. Whether we actually can see the position of the boundary, which may be 5 or 10 AU, more or less, is questionable. I don't know whether the other terms ever get small enough to allow us to see this.

It may be the case in the September 28 event, when the diffusion picture appeared to be sensible, we were actually looking at a boundary between 2½ and 4 AU. I would not want to be sure of that.

N64-30278

28 THE ASSOCIATION OF ENERGETIC PARTICLES WITH SOLAR FLARES*

JOHN M. MALVILLE
Radio Astronomy Observatory, University of Michigan
Ann Arbor, Mich.

One of the more useful and accessible characteristics of flares associated with the generation of energetic particles in the solar atmosphere is the occurrence of type IV continuum emission. The relation between type IV radiation and energetic particles was first noted by Boischot and Denisse (Reference 1) and has been well documented by a number of subsequent investigations. Practically every proton event can be traced to a flare which produced a type IV burst.

A problem does arise, however, in the definition of a type IV burst. A number of different phenomena contribute to the total event, and at various times the radiation may be produced either by plasma oscillations or by the synchrotron process (Reference 2). Since the various components have different directivities, the event may have entirely different aspects depending on whether it occurs near the center of the disk or near the limb. As a working definition, the type IV burst may be regarded as long-duration continuum emission occurring in any portion of the radio spectrum following a flare. Physically, the appearance of the type IV radiation appears to signify the presence in the corona of a large collection of fast electrons with energies covering the range of a few kev to a few Mev. If proton acceleration accompanies the electron acceleration implied by the radio continuum, the observed association of type IV emission and energetic particles is reasonable.

However, many type IV events—in fact, the majority—are not associated with protons detected at the earth. The relation may improve as our ability to detect the very weak proton events improves. On the other hand, the many type IV events not followed by energetic particles may reflect a basic inadequacy in our definition of type IV radiation. There is undoubtedly need for more discrimination with regard to the energy spectra of the particles contributing to the type IV emission. Moreover, conditions in the interplanetary medium may on occasion be some of the dominant factors determining whether or not protons reach the earth following a flare.

There are certain characteristics of the type IV emission which seem to favor proton events. The probability that a proton event will be associated with a type IV burst increases with the intensity of the radio radiation, especially if the intensity is high over a broad wavelength range—from 3 to 30 cm, for instance (Reference 3). The time development of the burst appears also to be of significance. Dodson-Prince and Hedeman (Reference 4) find that if the 10 cm type IV emission reaches a maximum later than the optical flare maximum, there is an increased probability that protons will arrive at the earth.

It was first noted by Dodson-Prince and Hedeman (References 5 and 6) that the coverage of the umbrae of sunspots is a characteristic of flares associated with strong particle events. Investigations by Ellison et al. (References 7 and 8), Martres and Pick (Reference 9), and Malville and Smith (Reference 10) have all concluded that there is a relation, although not too well defined, between umbral obscuration and the generation of energetic particles. Many examples of flares covering portions of sunspot unbrae can be found for which no type IV radiation or energetic particles were detected. However, there does appear to be at

*This work was supported at the Univeristy of Michigan by NASA Contract NAS5-2051W.

least a statistical relation between umbral obscuration and particle acceleration. Figure 28–1 shows the variation of the percentage of flares associated with meter wave type IV bursts with the fractional coverage of the total umbral area of a spot group. Both this percentage and the intensity of cm wave type IV bursts increase with increasing coverage of the spot umbrae. Such a relation is undoubtedly a very indirect means of estimating the strength of the magnetic field in the flare region and certainly can be clarified by systematic field strength measures in umbrae and in flares.

Large flares frequently consist of parallel bright filaments lying on either side of the magnetic axis of the spot group. The bright flare filaments tend to drift apart with velocities of a few km/sec (References 11 and 12). Although the flare filaments may not originally cover any portion of a sunspot, the drift and expansion of the area of the filaments may result in the eventual obscuration of large umbrae. The greatest amount of obscuration frequently may occur not during the flash phase, but rather in the post-maximum phase. This delay between flare maximum and maximum obscuration of spots may be related to the delay between cm wave type IV maximum and optical maximum of the proton flares. There is a suggestion, in this evidence, that most of the acceleration to Mev and Bev energies occurs after flare maximum.

Individually, such characteristics of proton flares as discussed here have little significance. However, taken together, they may define a sufficient condition for the production of energetic particles. If, for instance, an Importance 3+ flare is observed which covers a large sunspot umbra and has intense type IV emission with a maximum of the cm wave component

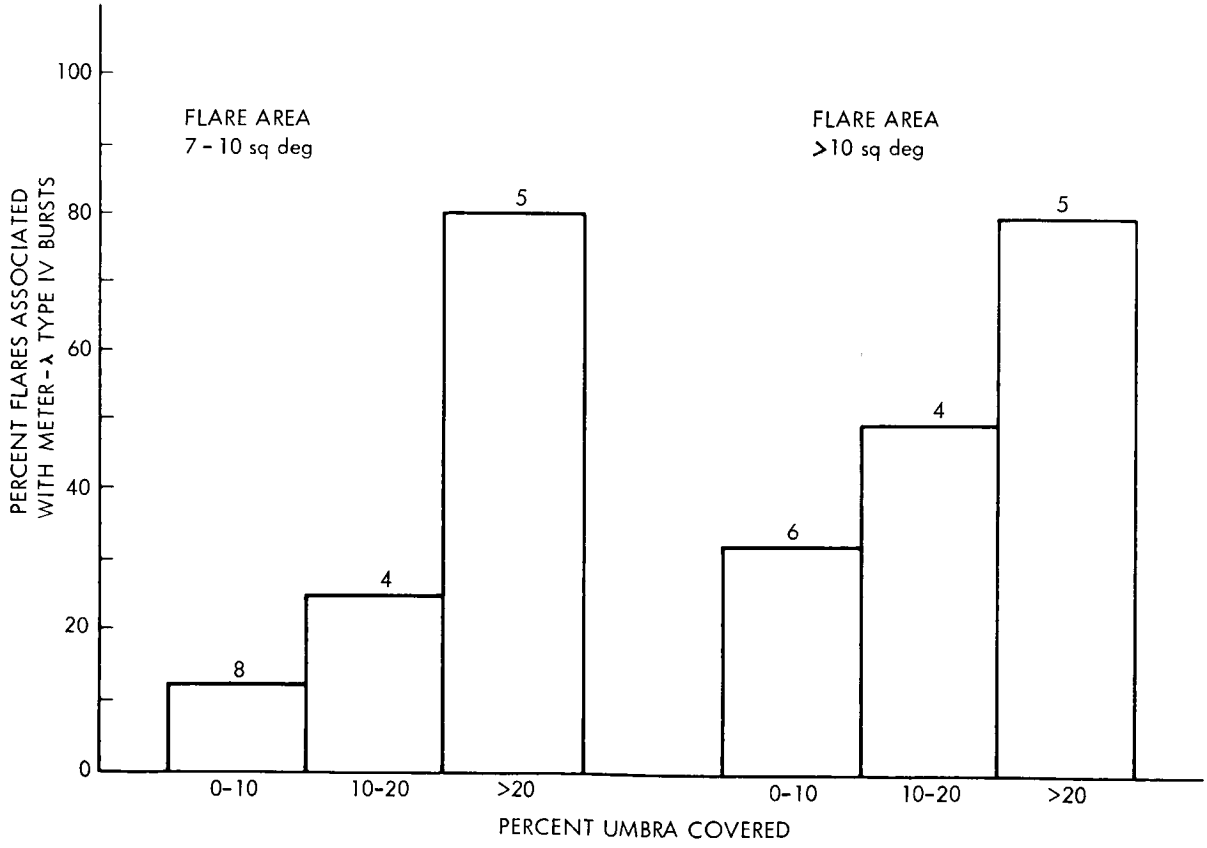

FIGURE 28–1. Percentage of flares associated with meter-λ type IV bursts as a function of the percent of the total umbral area of the spot group covered by flares in the group. (Reference 10)

lagging flare maximum, then one can be reasonably confident that energetic particles will ensue.

Brief mention should be made of type III radio bursts, x-ray bursts, and impulsive cm wave bursts. Each of these occurs primarily near the flash phase of the flare and indicates that acceleration of electrons to energies of 10 to 100 kev is occurring in a brief interval of a few minutes or less. Two independent accelerations may then take place in some flares: one occurring near the flash phase resulting in kev electrons, and the other proceeding more slowly in the post-maximum phase, producing the more energetic protons and electrons.

Extensive systems of loop prominences are occasionally seen following large proton flares (Reference 13). These loops are associated with coronal condensations and the yellow coronal line, [CaXV]λ5694. The presence of the yellow line indicates temperatures perhaps a factor of 2 or 3 greater than in the undisturbed corona. Zirin (Reference 14) has suggested that yellow line regions may be associated with the storage of energetic particles in the corona. Storage near the sun has been suggested by Gold (Reference 15) and others, and receives support from the strong anisotropies of solar protons during the first few hours of certain proton events (Reference 16).

The unusual state of ionization in the center of the condensations may be the direct consequence of storage of energetic particles in the corona. Such fast particles may either directly ionize calcium, or they may heat the gas as they are thermalized in the dense center of the condensation. We may estimate the density of such suprathermal electrons or protons needed to dominate the ionization equilibrium of calcium by using Seaton's (Reference 17) estimates of ionization and recombination cross sections. If the ionization is produced entirely by 5 kev electrons and recombination occurs at an electron temperature of 10^6 °K, in order that the ratio N(CaXV)/N(CaXIII)=1, the density of the suprathermal electrons must be approximately 1.3×10^{-2} that of the thermal electrons. A condensation with an electron density of $N_e=10^{10}$ cm^{-3} can radiate energy at the rate 1.7×10^{-3} erg cm^{-3} sec^{-1} (Reference 18), and in such a condensation the thermalization time of 5 kev electrons is of the order of 0.1 sec. Consequently the condensation would gain energy from the thermalized electrons at a rate several orders of magnitude faster than it can lose it by radiation, and would attain thereby an unacceptably high temperature. The same situation is true for ionization by protons of the same velocity, and we conclude that direct ionization by the suprathermal particles cannot be responsible for the state of ionization of the condensations.

On the other hand, a slow leakage of particles from the storage region into the condensation could supply energy at a rate sufficient to maintain the yellow line region at a temperature of approximately 2.5×10^6 °K, necessary for N(CaXV)≈N(CaXIII) (Reference 17). Heating due to thermalization of the stored particles implies a magnetic connection between the storage region and the tops of the loops. Such a magnetic configuration, which may follow a flare occurring along the magnetic axis of a spot group, is suggested in Figure 28–2. The storage region is formed by the outermost lines of force of the poloidal spot field. Stored particles with small pitch angles would be rapidly lost as they are scattered in the dense condensation. A continuing supply of particles with small pitch angles is probably assured because of time variations of the field. The dense portions of the condensation, that is, the regions with the shortest thermalization times, should receive most of the energy of the dumped particles. The corpuscular energy source would persist until the magnetic connection between the condensation and the storage region is broken or the supply of particles is exhausted through dumping, collisions in the storage region itself, or drift of the particles out of the region because of the gradient or time variations of the field. In order that the source of heating continue for 10^4 seconds, a typical lifetime of a yellow line region, the necessary energy in dumped particles is approximately 10^{30} ergs.

If the dumped particles are 10 to 100 kev electrons, they may be the source of the meter wave type IV continuum ascribed by Denisse (Reference 19) to Cerenkov radiation excited by downward traveling electrons. For in-

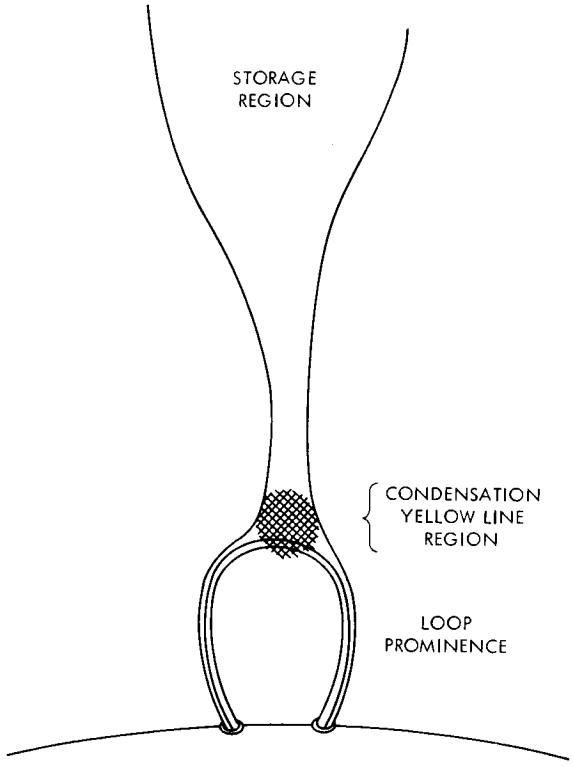

FIGURE 28–2. Storage region above a coronal condensation.

stance, the flux of 10 kev electrons necessary to maintain the enhanced ionization in the condensation is approximately 6×10^{13} cm^{-2} sec^{-1}. These electrons will lose energy through excitation of incoherent plasma waves at the rate given by Pines and Bohm (Reference 20):

$$\frac{dE}{dz}\approx\frac{\omega_p{}^2 m e^2}{4E_0}\,\ell n\left[1+\frac{E_0}{kT}\right].$$

Bunching of the electrons enhances the efficiency of the conversion of kinetic energy into energy of plasma oscillations, and the Pines and Bohm expression provides a lower limit to the energy of the excited plasma waves. At coronal temperatures and at a plasma frequency of 100 Mc/s the 10 kev electrons will lose energy at the rate of approximately 6×10^{-21} erg cm^{-1}. Over a length of 10^9 cm and an area of 10^{20} cm^2, the electrons will lose some 4×10^{22} ergs sec^{-1} into plasma waves. According to the suggestions of Denisse, the energy contained in these plasma waves traveling downward through the corona can be converted into energy of electromagnetic waves propagating into free space through reflection and mode coupling. If the efficiency of the conversion processes is 10^{-6}, for example, the radiation produced at the earth by the flux of electrons leaking out of the storage region would be approximately 10^{-21} wm^{-2} (c/s)$^{-1}$ over a bandwidth of 100 Mc/s. It is therefore conceivable that the same energetic electrons responsible for the ionization of the yellow line region also produce the type IV meter wave continuum as they pass from the storage region into the lower corona. Only a fraction of the stored particles should reach the condensation; if there is a difference of 10^3 in the field strength in the storage region and in the condensation, a total of 10^{33} ergs of trapped particles is required in the storage region. The striking relation occasionally found between the variations in the flux of solar protons detected at the earth and the variations in the intensity of meter and decimeter wave continuum such as that following the flare of August 22, 1958, (Reference 21) further supports the idea of a relation between coronal storage and low frequency continuum emission.

It appears that we may be able to distinguish three separate phases of a flare associated with the generation of energetic particles: (1) the brief acceleration of kev electrons during the flash phase as evidenced by type III bursts, x-ray bursts, and impulsive cm wave bursts; (2) acceleration of kev and Mev electrons and Mev and Bev protons during the post-maximum phase indicated by umbral obscuration and cm wave type IV radiation; and (3) storage of energetic particles in the corona perhaps resulting in the heating of a magnetically connected condensation, the generation of meter wave and decimeter wave continuum emission, and the eventual drift of particles onto lines of force connected with the earth's neighborhood.

REFERENCES

1. Boischot, A., and Denisse, J. F., 1957, *Comptes Rendues*, 245: 2149.
2. Wild, J. P., Smerd, S. F., and Weiss, A. A., 1963, "Solar Bursts," *Annual Review of Astronomy and Astrophysics*, 1: 291.
3. Kundu, M. R., and Haddock, F. T., 1960, *Nature*, 186: 610.
4. Dodson-Prince, H., and Hedeman, E. R., 1963, *A.J.*, 68: 290.
5. Dodson-Prince, H., and Hedeman, E. R., 1959, Paper presented at the Midwest Cosmic Ray Conference, Iowa City.
6. Dodson-Prince, H., and Hedeman, E. R., 1960, *A.J.*, 65: 51.
7. Ellison, M. A., McKenna, S. M. P., and Reid, J. H., 1961, *M.N.*, 122: 491.
8. Ellison, M. A., McKenna, S. M. P., and Reid, J. H., 1962, *M.N.*, 124: 263.
9. Martres, M., and Pick, M., 1962, *Ann. d'Astro.*, 25: 293.
10. Malville, J. M., and Smith, S. F., 1963, *J. Geophys. Res.*, 68: 3181.
11. Svestka, Z., 1962, *Bull. Astr. Inst. Czech.*, 13: 190.
12. Malville, J. M., and Moreton, G. E., 1963, *Pub. A.S.P.*, 75: 176.
13. Hansen, R. T., 1961, *Phys. Rev. Letters*, 6: 260.
14. Zirin, H., 1963, "The Solar Corona," ed. J. W. Evans, Academic Press, New York.
15. Gold, T., 1962, *J. Phys. Soc. Japan*, 17(A–11): 600.
16. McCracken, K. G., 1962, *J. Geophys. Res.*, 67: 423.
17. Seaton, M. J., 1962, *Observatory*, 82: 111.
18. Orrall, F. Q., and Zirker, J. P., 1961, *Ap. J.*, 134: 72.
19. Denisse, J. F., 1960, *Inform. Bull. S.R.W.E.*, No. 4: 3.
20. Pines, D., and Bohm, D., 1952, *Phys. Rev.*, 85: 338.
21. Boischot, A., and Warwick, J. W., 1959, *J. Geophys. Res.*, 64: 683.

DISCUSSION

Dr. Maxwell: I am unable to understand the physical reasons or the statistical basis for the proposition that the maximum intensity of type IV radiation in the microwave band should occur after the flare maximum if we are to have protons reaching the earth. I would give you the case of the September 28, 1961, burst which has been discussed several times during this meeting.

The flare started at 2202 UT. The x-ray burst and the maximum of microwave emission occurred at about 2216, and the optical maximum at 2224.

Dr. Malville: I have no comment on that. Maybe Mrs. Prince has.

Dr. Prince: I don't see why it should be. It just is that way. However, if you try to distinguish between the flares with great centimeter bursts that do produce protons and those that do not, it is very helpful to know whether the usual form of the 10 cm burst is maintained or an atypical one. The usual cm burst has its maximum while the Hα flare is rising to maximum intensity.

In the 5 years 1957–61 there were 74 flares with associated 10 cm flux $\geq 500 \times 10^{-22}$ w/m^2/(c/s) with known times of maximum for both Hα and the radio frequency event. For only 21 did the 10 cm maximum follow Hα maximum; and, of these, 19 were accompanied by Polar Cap Absorption. Fewer than ¼ of the remaining 53 cases were proton flares.

N64-30280
79

29 CHARGE COMPOSITION OF ENERGETIC SOLAR PARTICLES

CARL E. FICHTEL
Goddard Space Flight Center, NASA
Greenbelt, Md.

The problem of the composition of solar cosmic rays has been pursued with considerable success during the most recent solar maximum (approximately 1957 to 1962). Already many of the general features seem to be clear, and some detailed knowledge is beginning to emerge—although much is still to be learned. The energetic nuclei arriving at the earth from the sun are known to consist primarily of hydrogen nuclei when comparisons are made in the same velocity intervals; however, within the same rigidity intervals helium nuclei are sometimes as abundant as hydrogen nuclei (References 1 to 5). Smaller quantities of nuclei with higher charges also have been seen (References 4 to 10) in several events; and it seems likely that these heavier nuclei are always present, since they have been observed every time the intensity of the event was sufficiently great to expect to be able to detect them on the basis of their abundances in other events. Detailed charge composition studies (References 4, 5) seem to indicate that the multiply charged component (nuclear charge ≥ 2) has a composition similar to that of the sun and dissimilar to that of the galactic cosmic radiation. Electrons have been detected (Reference 11) in a solar cosmic ray event, although their intensity was very low compared with that of the protons.

The study of the various components of the solar particles provides information relating to several other astrophysical disciplines besides the study of the properties of solar particles themselves. After discussing the experimental observations on the composition of solar cosmic rays, an effort will be made to show how these data, when combined with other pertinent information, aid in the examination of two of the problems—namely, the dynamics of particle propagation in interplanetary space, and the solar composition. Although solar particle acceleration will not be discussed specifically here, the data naturally represent important conditions which any acceleration model must be able to explain.

EXPERIMENTAL OBSERVATIONS ON THE COMPOSITION OF SOLAR COSMIC RAYS

In recent years, many investigators have studied the solar hydrogen nuclei from a large number of solar events using a variety of particle detectors and vehicles, including balloons, sounding rockets, and satellites. Detailed information on the energy spectra and fluxes of these particles as a function of time in an event has already been presented by Dr. Webber; therefore, the discussion on these nuclei will be limited here to a presentation of the isotopic abundances and a comparison with other charge species.

Among the hydrogen nuclei, protons are by far the most abundant of the nuclear isotopes. Tritons have been detected (References 12 and 13) but in very small quantity. In the same velocity interval, tritons have a flux which is estimated to be of the order of $1/10$ to 1 percent of the proton flux. The uncertainty in the ratio is due both to the lack of exact information on the integral proton flux at the time the triton measurement was made and the lack of knowledge associated with some of the cross sections for helium production. Because deuterons cannot be detected by radio chemical means as the tritons can, at present only an upper limit to their abundance exists (Refer-

728-629 O - 64 - 18

ence 5). This limit, which is approximately 1 percent of the proton flux, is based on only one event and is consistent with the deuteron flux, being of the same order of magnitude as that of the tritons.

Among the multiply charged nuclei, helium particles are by far the most abundant, and measured energy spectra exist for several events. An examination of the particle spectra as a function of energy per nucleon has shown that the helium spectra have steeper slopes than those of the protons for the six instances in three events where the two could be measured in the same velocity region. Figures 29–1 and 29–2 show typical examples of this phenomenon. In general, then, the proton-to-helium ratio is not single-valued, but a function of velocity.

On the other hand, when the spectra are plotted in terms of rigidity, they are always found to be similar (References 2 to 5). A typical example of similar rigidity spectra (Reference 3) is shown in Figure 29–3. However, as Figure 29–4 indicates, spectral slopes are probably not exactly the same. In fact, an analysis (Reference 14) of the existing data shows that there is less than a 0.1 percent chance of the spectral slopes for protons and alphas being the same.

When proton-to-helium ratios are compared, however, it is found that, although the helium and hydrogen nuclei seem to have similar rigidity spectra, the ratio of the two components in the same rigidity interval varies greatly from one event to another and at different times in one event. For example, above approximately 0.8 Mv rigidity, the proton-to-helium ratio has varied from 50:1 to 1:1 with smaller ratios tending to be more common. Summary lists of some of the ratios that have been observed by experimentalists are given by Freier and Webber (Reference 3) for the rigidity range above approximately 0.8 Bv and by Biswas et al. (Reference 5) for the rigidity range from approximately 0.5 to 1.0 Bv.

Although the proton-to-helium ratio is not always the same in the same velocity interval, there is now some evidence to indicate that for a given velocity interval there is less variation than in the same rigidity interval. In considering comparisons in velocity, the interval must be specified, since the hydrogen-to-helium-nuclei ratio varies markedly with energy. The proton-to-helium ratios for several measurements are plotted as a function of energy per nucleon in Figure 29–5. Notice that there is a tendency for the proton-to-helium ratio to vary less with kinetic energy per nucleon late in an event.

Because of their short ranges, almost all of the information on energetic solar heavy nuclei has come from sounding rockets and satellites (References 4 to 10). In only two cases has it even been possible to detect them at balloon altitudes (References 2 and 15). Among the heavy nuclei, those with nuclear charge greater than 3, the medium nuclei ($6 \leq$ nuclear charge ≤ 9) are the most abundant (References 4 to 6). Present evidence indicates that the energy per nucleon spectra of the medium nuclei and the helium nuclei is the same (References 4 to 6). Further, since all of the medium nuclei which occur in detectable amounts have the same charge-to-mass ratio as He (Reference 4), the rigidity specta of these two nuclear species are also the same. These features are shown for typical cases in Figures 29–1, 29–2, 29–3, and 29–4. In addition to helium and medium nuclei having the same rigidity spectra, the relative abundances of these nuclei in the same rigidity intervals have been measured several times in three events (Reference 5) and were found to be the same within uncertainties. The relative abundances among those nuclei with charges of 10 or more for which measurements could be made in the same energy per nucleon intervals have also been found to be the same each time a measurement was made—namely, five times in two events. This result, of course, suggests that, if these heavier nuclei had been present in sufficient numbers to measure a rigidity spectrum, their rigidity spectrum would have been the same as the medium and helium nuclei.

The composition of the multiply charged nuclei in the same rigidity intervals as measured in the five flights mentioned above is presented in Table 29–1, with a base of 10 having been chosen for oxygen. From the table, it is seen that the relative abundances of the energetic solar particles are the same within un-

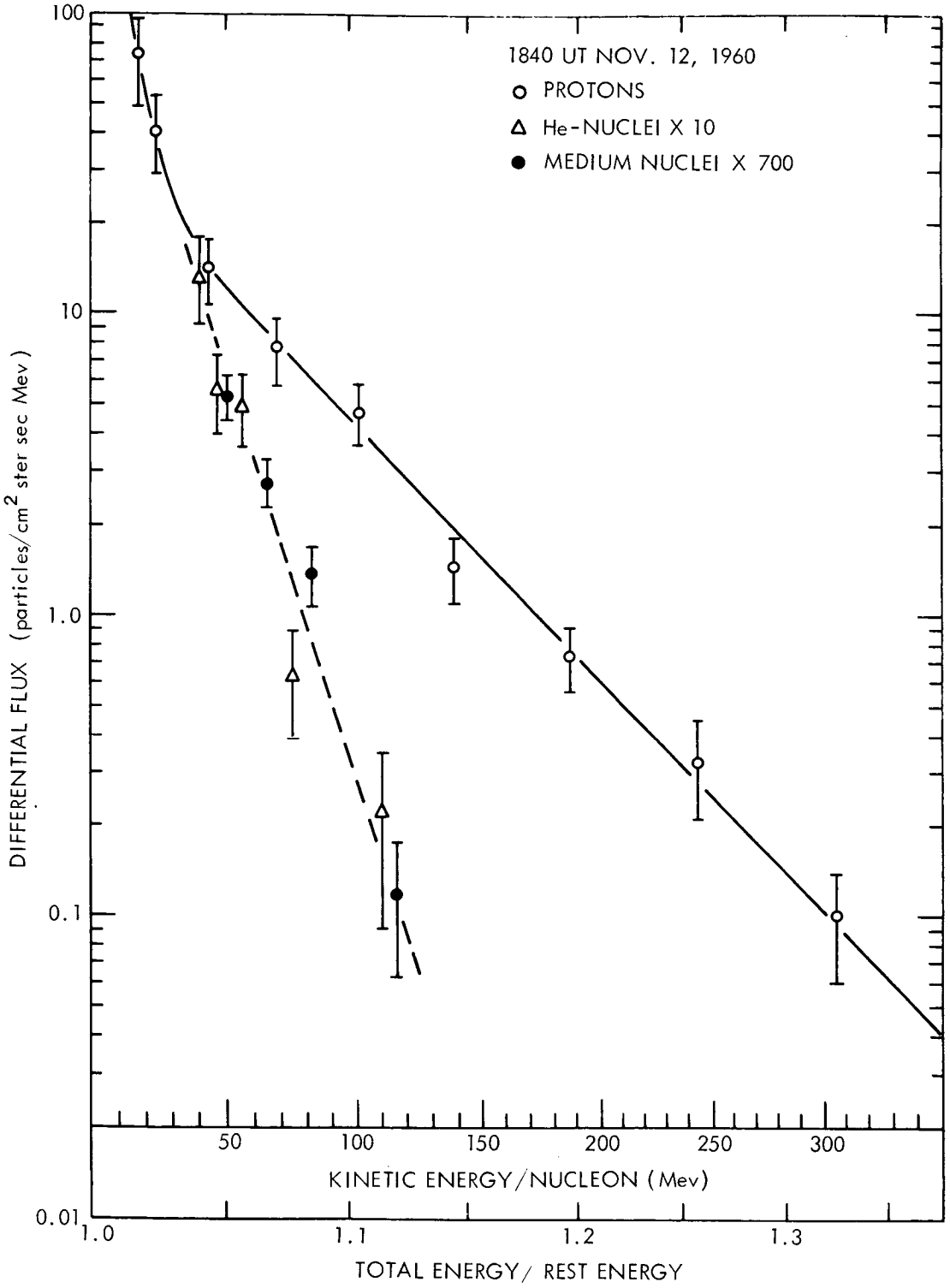

FIGURE 29–1. Differential spectra for protons, helium nuclei, and medium nuclei as a function of the total energy per nucleon in units of nucleon rest energy at 1840 UT, November 12, 1960. Note that the abscissa is an expanded logarithmic scale. (Reference 4)

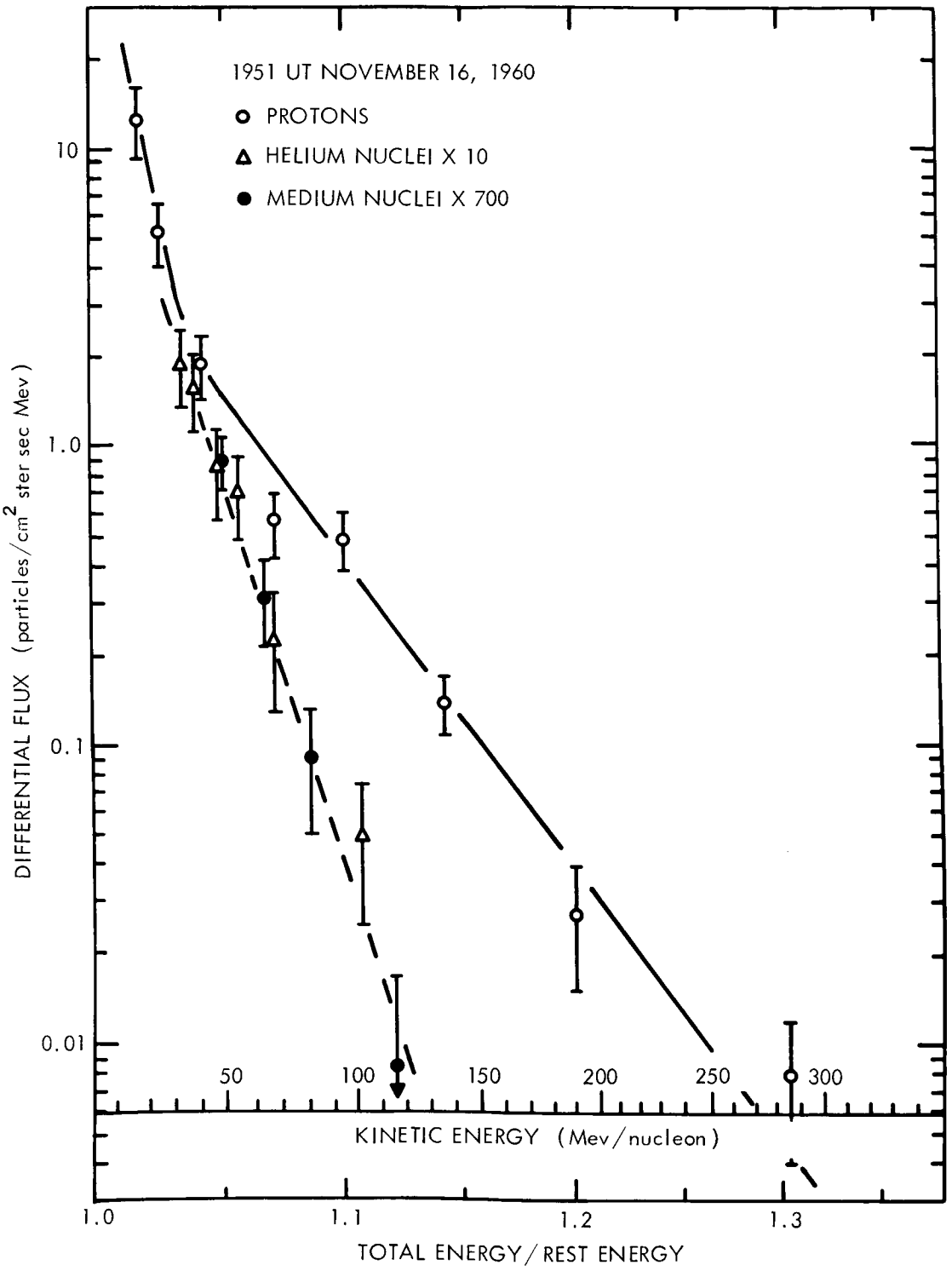

FIGURE 29–2. Differential spectra for protons, helium nuclei, and medium nuclei as a function of the total energy per nucleon in units of nucleon rest energy at 1951 UT, November 16, 1960. Note that the abscissa is an expanded logarithmic scale. (Reference 5)

TABLE 29–1

Relative Abundances of Nuclei in Solar Cosmic Rays, the Sun, and Galactic Cosmic Rays with a Base of 10 for Oxygen

Nuclei	He	Be, B	C	N	O	F	Ne	$_{11}Na$–$_{18}A$	$_{19}K$–$_{28}Ni$
Solar Cosmic Rays*	1100	<0.2	6	≲2	10	<0.3	1.3	1.3	≲0.2
Sun**	?	<0.01	6	1	10	<0.01	?	1	0.07
Galactic Cosmic Rays*	360	11	18	≲8	10	<1	2.9	7.3	3.6

*The uncertainty in the values in this line varies from 10 to about 30 percent.
**The uncertainty in the values in this line is of the order of a factor of 0.5 to 1.

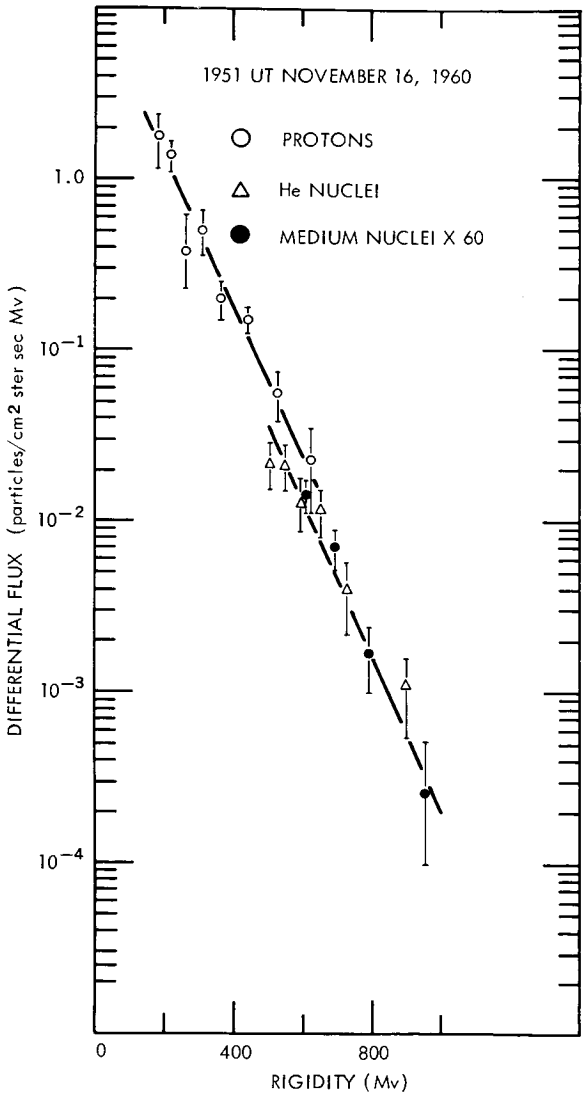

FIGURE 29–3. Differential spectra for protons, helium nuclei, and medium nuclei as a function of rigidity at 1951 UT, November 16, 1960. (Reference 5)

certainties as the solar abundances determined by spectroscopic means. Since the solar and universal abundances are similar, although not the same, the solar cosmic ray composition is also similar to the universal abundances. The solar cosmic rays are, however, markedly different in composition from the galactic cosmic rays, which are well known to be rich in the heavy elements. Table 29–2 shows these differences (Reference 14).

Kurnosova, Razorenov, and Fradkin (Reference 16) have reported a few increases of heavy nuclei above cosmic ray background in the relativistic region lasting for the order of 10 to 20 minutes and not associated with a solar particle event of the usual variety. Although other experiments which would have detected this type of increase have been flown by McDonald and Webber (Reference 17), no other increase of relativistic heavy nuclei has been reported. Since these events are apparently of a different nature from the low energy solar particle events being discussed here, they will not be treated further in this chapter.

The abundance of very energetic electrons is expected to be small because of the high rate of energy loss by synchrotron radiation at large relativistic energies; so, even if there were large numbers of these energetic electrons initially, they would soon lose their energy.

Although the flux of very energetic solar electrons is known to be relatively small, appreciably less than the proton component, positive evidence for electrons does exist for at least one event (Reference 11). In the July 18, 1960, event, a flux of electrons corresponding to a few percent of the proton flux in the same

TABLE 29–2

Solar Electron/Proton Ratios

Observer	Date of Measurement, 1960	Atm. Depth (gm/cm²)	Lower Limit for Integral Electron Flux (Bv)	Lower Limit for Integral Proton Flux (Bv)	Proton-to-Electron Ratio (Percent)
Earl	Sept. 4	10	0. 45	0. 45	<0. 25
Meyer & Vogt	Sept. 8	3	0. 1	0. 37	<4
Yates	Nov. 13	9	0. 4	0. 49	<0. 3
Ney & Stein	Nov. 15	6	0. 7	0. 7	<2
Meyer & Vogt	July 22	5	0. 49	0. 49	4. 6
			0. 7	0. 7	23

rigidity region was detected. In other events, September 3, 1960 (References 18 and 19), November 12, 1960 (Reference 20), and November 15, 1960 (Reference 2), upper limits to the electron flux have been determined which range from ¼ to 4 percent times the proton flux in the same rigidity interval. A summary of these results is given in Table 29–2.

In addition to the experiments related to direct measurements at the earth, Stein and Ney (Reference 21) have shown that the continuum electromagnetic radiation from large solar flares is consistent with the interpretation that this radiation is due to synchrotron radiation of electrons with an exponential rigidity spectrum of the type suggested by Freier and Webber (Reference 3). Their calculated values for the shape parameter of the spectrum are similar to the ones observed for protons in many large solar particle events. They have further shown that the number of electrons needed to produce the observed intensity is of the same order as the estimated number of protons accelerated in a large solar flare and that the necessary magnetic field is of the order of 500 gauss, which seems to be a conservative estimate of typical field strength. Therefore, present indications suggest that in fact the electrons are accelerated at the sun along with the protons, but lose their energy quickly by synchrotron radiation, so that only a relatively few high energy electrons ever reach the earth.

Relatively large fluxes of low energy electrons, kinetic energy <1 Mev, also have been seen on occasions. Hoffman et al. (Reference 8) saw 3×10^6 el/(cm² ster sec) between 10 and 35 kev for about 10 minutes on September 30, 1961, associated approximately with the arrival of the sudden commencement. Except for that period, the flux was less than the detectable limit of 2×10^5 el/(cm² ster sec).

RELATION OF THE COMPOSITION OF SOLAR COSMIC RAYS TO OTHER ASTROPHYSICAL PROBLEMS

Although the study of the composition of the solar cosmic rays is actually related to many astrophysical problems—such as the acceleration of solar particles, their propagation in interplanetary space, the composition of the sun, and the study of galactic cosmic rays—there is time now only to discuss the relation to two problems very briefly.

The first of these to be considered will be the propagation of particles from the sun to the earth. It is realized now that the propagation of solar particles is not a simple matter. The function which describes the rise and fall of particle intensity and the energy spectrum can in principle depend on both the particle velocity and rigidity. Since the multiply charged particles have a different charge-to-mass ratio from that of the protons by a factor of 2, they also have a very different rigidity from that of the protons for a given velocity. Thus, if the absolute differential energy spectra of both protons and helium nuclei, for example, could be measured throughout an event, very significant insight could be obtained into the propagation characteristics. Unfortunately, only isolated individual simultaneous measurements of the two spectra exist.

Even with these limited data, it seems possible to say that a purely rigidity-dependent

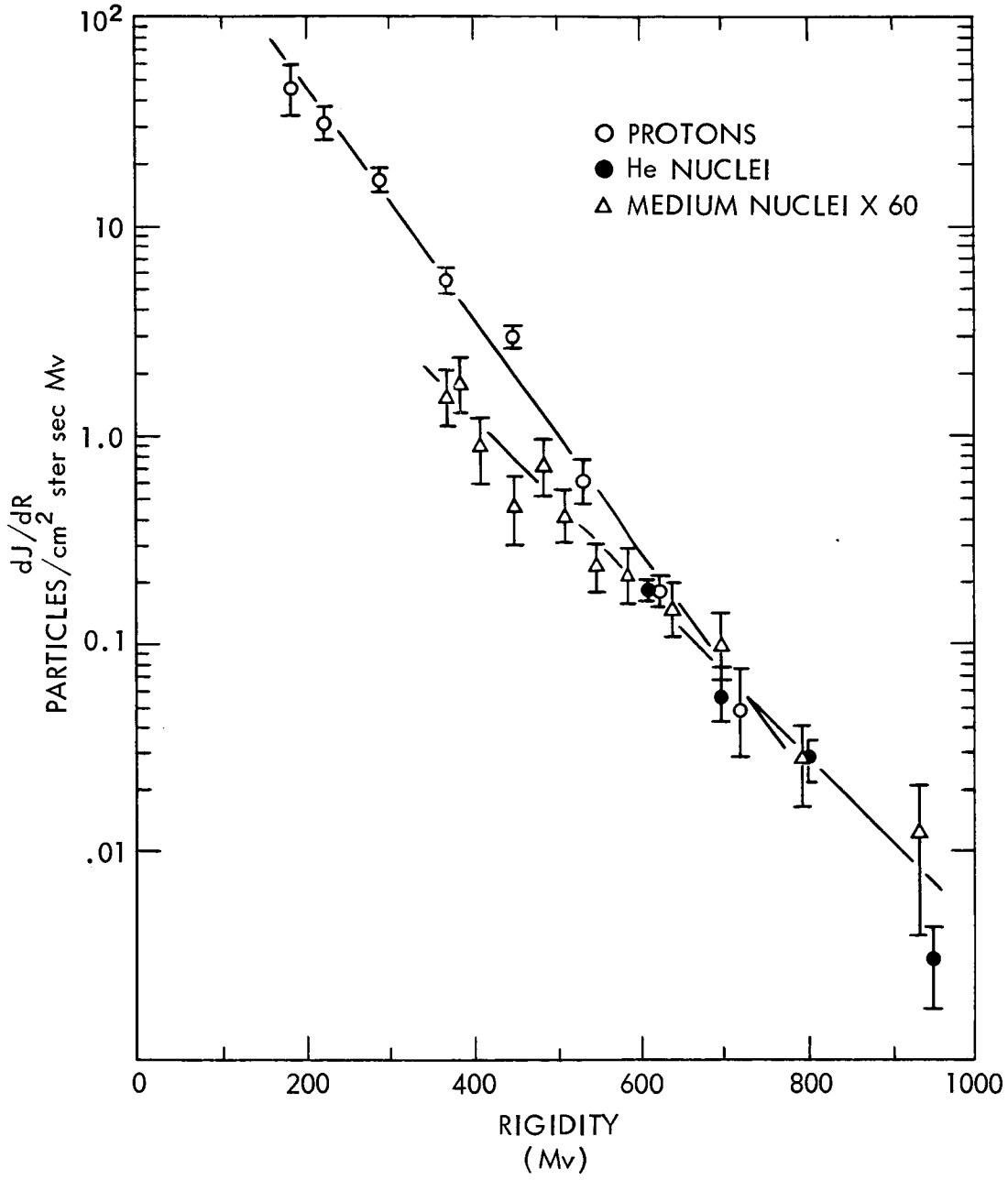

FIGURE 29–4. The differential rigidity spectra of hydrogen, helium, and medium nuclei at 1603 UT November 13, 1960. (Reference 14)

propagation can be excluded. As was shown earlier, the proton-to-helium ratio in the same rigidity intervals has been seen to vary appreciably from one time in a given event to another. Further, this ratio has varied very markedly from one event to another, while the helium-to-medium ratio has been the same in each of the three events it was measured. Therefore, other general classes of propagation besides the purely rigidity one must be examined. This problem cannot be examined in detail here; however, Biswas et al. (Reference 5) have

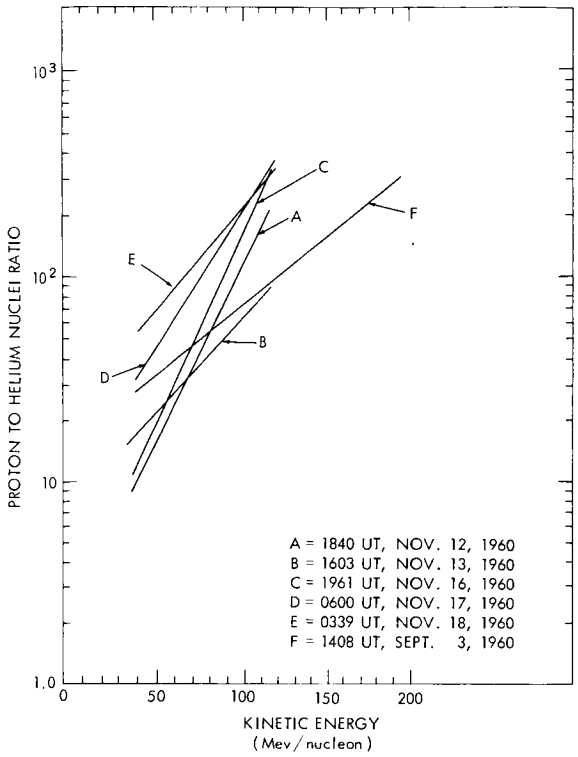

FIGURE 29–5. The proton-to-helium-nuclei ratio as a function of kinetic energy per nucleon at several different times. In each case, the line represents a best fitting straight line to the existing data. Uncertainties in the ratios range from 25 to 50 percent. (Reference 14, based on work from References 3, 4, 5, and 14)

already discussed the insight which can be obtained into particle propagation from the examination of existing data on particles with different charge-to-mass ratios.

The other problem which shall be treated here is the relation between the solar cosmic ray composition and that of the sun. There are a number of experimental facts which suggest that the relative abundances of the multiply charged nuclei (at least in the range $2 \leq Z \leq 20$) may reflect those of the sun.

Firstly, the multiply charged nuclei have had the same relative abundances in the same velocity intervals within uncertainties each time a measurement was made, whereas this has not been true for the protons and helium nuclei, which have different charge-to-mass ratios. Secondly, insofar as comparisons can be made, this composition reflects that of the sun. Thirdly, the helium and medium nuclei have had the same energy per nucleon spectrum in the two events where measurements could be made at the same time, whereas the proton and helium nuclei spectra in the same events were very different.

If the composition of the multiply charge nuclei is accepted as representative of the sun, the relative abundances given in Table 29–1 may be used to estimate the helium and medium nuclei abundances in the sun which cannot be determined easily by spectroscopic means. The average helium-to-oxygen ratio is 107 ± 14, and the average neon-to-oxygen ratio is 0.13 ± 0.02 (Reference 14). The neon-to-oxygen ratio is similar to the universal abundances estimated by Suess and Urey (Reference 22) and Cameron (Reference 23), although a bit on the low side. The helium-to-medium ratio is typical, but of course the more interesting ratio would be the proton-to-helium one. Because of the different energy spectra and charge-to-mass ratios, there is no simple reliable way to determine this ratio from solar cosmic rays alone. However, if the helium-to-medium ratio of 60 ± 7 is accepted as representative of the sun and the proton-to-medium value from spectroscopic data [namely, 650 (References 24, 25)] is used, a proton-to-helium ratio of 11 is obtained. The uncertainty in this number depends on the correctness of the assumption above and the uncertainty in the proton-to-medium ratio, which is probably good only to within a factor of 2.

REFERENCES

1. BISWAS, S., FREIER, P. S., and STEIN, W., 1962, *J. Geophys. Res.*, 67: 13.
2. NEY, E. P., and STEIN, W., 1962, *J. Geophys. Res.*, 67: 2087.
3. FREIER, P. S., and WEBBER, W. R., 1963, *J. Geophys. Res.*, 68: 1605.
4. BISWAS, S., FICHTEL, C. E., and GUSS, D. E., 1962, *Phys. Rev.*, 128: 2756.
5. BISWAS, S., FICHTEL, C. E., GUSS, D. E., and WADDINGTON, C. J., 1963, *J. Geophys. Res.*, 68: 3109.

6. FICHTEL, C. E., and GUSS, D. E., 1961, *Phys. Rev. Letters*, 6: 495.
7. POMERANTZ, M. A., and WITTEN, L., 1962, Paper presented at the Third International Space Science Syposium of COSPAR, Washington, D.C., May 1962.
8. YAGODA, FILZ, H. R., and FUKUI, K., 1961, *Phys. Rev. Letter*, 6: 626.
9. KURNOSOVA, L. V., RAZORENOV, L. A., and FRADKIN, M. I., 1962, *J. Phys. Soc. Japan*, 17, Suppl. A–11: 315.
10. KURNOSOVA, L. V., RAZORENOV, L. A., and FRADKIN, M. I., 1962, *Zemili*, No. 12: 31.
11. MEYER, P., and VOGT, R., 1962, *Phys. Rev. Letters*, 8: 387.
12. FIREMAN, E. L., DEFELICE, J., and TILLES, D., 1961, *Phys. Rev.*, 123: 1935.
13. TILLES, D., DEFELICE, J., and FIREMAN, E. L., 1962, "Measurements of Tritium in Satellite and Rocket Material, 1960–1961, "Smithsonian Institution Astrophysical Observatory Preprint.
14. BISWAS, S., and FICHTEL, C. E., 1964, *Ap. J.*, 139: 941.
15. BISWAS, S., FICHTEL, C. E., and GUSS, D. E., 1961, unpublished preliminary results of work on the July 18, 1961, event.
16. KURNOSOVA, L. V., RAZORENOV, L. A., and FRADKIN, M. I., 1961 and 1962, "Short-Term Increases of the Cosmic Ray Intensity Associated with the Solar Activity," *J. Phys. Soc. Japan*, 17 Suppl. A–11: 315–316 (1962); *Iskusstevenne Sputnik: Zemili*, No. 6: 132 (1961); *Iskusstvenne Sputnik: Zemili*, No. 12: 31 (1962).
17. MCDONALD F. B., 1963, private communications.
18. EARL, J. A., 1962, *J. Geophys. Res.*, 67:2107.
19. MEYER, P., and VOGT, R., 1961, *J. Geophys. Res.*, 66: 3950.
20. YATES, G. K., 1963, private communication of unpublished results.
21. STEIN, W. A., and NEY, E. P., 1963, *J. Geophys. Res.*, 68: 65.
22. SUESS, H. E., and UREY, H. C., 1956, *Rev. Mod. Phys.*, 28: 53.
23. CAMERON, A. G. W., 1959, *AP. J.*, 129: 676.
24. GOLDBERG, L. A., MÜLLER, E. A., and ALLER, L. H., 1960, *AP. J.*, Suppl. Vol. V, No. 45: 1–138.
25. ALLER, L. H., 1961, "The Abundance of the Elements," Interscience Publishers: New York.

DISCUSSION

Dr. Winckler: What is the current state of evidence about the degree of ionization of the heavier elements at the time they are produced, if there is any evidence on this?

Dr. Fichtel: This is an extremely hard problem to answer. One can begin with the charge distribution which is observed. A more detailed breakdown of the charge distribution (which I didn't show) indicates that, up to about charge 18, the nuclear composition seems to be a reflection of that of the sun. Therefore, there doesn't seem to be a bias against heavy elements.

But this result does not necessarily say anything about the degree of ionization during acceleration because it depends somewhat on the charge acceleration mechanism. If, for example, a pure Fermi mechanism is operative, the particles simply have to be ionized. It doesn't make any difference what degree of ionization. On the other hand, if an electric field is producing the acceleration, then the energy gain in terms of energy per nucleon depends on the ionized-charge-to-mass ratio, and a bias would be expected if particles were not fully ionized.

I think, therefore, that the type of acceleration mechanism determines whether or not partial ionization would lead to a biased composition. The experimental result is that one does not observe a biased composition for multiple charged nuclei; one seems to see a reflection of the composition of the sun.

N64-30280

30 MARINER SOLAR WIND MEASUREMENT

CONWAY W. SNYDER
Jet Propulsion Laboratory
Pasadena, Calif.

For a long time I have been intrigued by a remark once made by Robert Oppenheimer in characterizing his method of teaching, when he said that what we don't understand we explain to one another.

At times this might appear to be the motto of this conference. If not, at least it is a good description of what we are going to do here. We won't attempt at this time to summarize the Mariner II (1962 A–ρ1) data. Many, if not most, of you already have heard me talk about that. We will discuss briefly some aspects of the data, or our ideas about the data, which appear to be particularly pertinent to this conference.

If you have looked carefully at any of the commonly published data on geomagnetic indices (the Göttingen charts of Daily Geomagnetic character—Figures C9 in particular, or Bartels' "musical" K_p diagrams), you will be aware that the most striking thing shown on these plots during the past year is a series of recurrent geomagnetic disturbances occurring between approximately days 5 and 10 of each solar rotation. This was first observed in solar rotation number 1766, beginning in August 1962. It is still apparent during every solar rotation up to the latest data that I have seen, which is solar rotation 1778. Thus, it has persisted for at least 13 solar rotations.

It is of course customary to attribute phenomena like these to the presence of active regions on the sun that have a very long life, and there is indeed such an active region which began with McMath plage number 6504 that passed the central meridian on August 5, 1962.

Figure 30–1 shows a kind of a map of that region, similar to the one that Dr. Smith showed the other day except that this figure has a couple more things on it. It begins with rotation 1766 and is carried through 1774. This is not the end of the region's history, but we are not further interested in it because Mariner has ceased to function and also because, on subsequent rotations, it moves so far north that it gets off the top of the blackboard!

The data from which this diagram was constructed originated at the McMath-Hulbert Observatory and were published in the monthly *Compilations of Solar-Geophysical Data* (CRPL–F Part B). Each circle represents a calcium plage—its McMath number being given inside it and its time of central (relative to the earth) meridian passage (CMP), measured in days from the beginning of the solar rotation, being given just outside it. The lines connecting the circles represent the alleged "return" of old plages. For example, the original plage (6504) at 8° N solar latitude on rotation 1766 passed again at 10°, at 12°, at 15°, et cetera. The times of its first four passages were, respectively, 6.7, 7.0, 7.6, and 7.5 days.

The Mariner II data coincide with rotations 1767 to 1771. Note the structure of this region on the sun during these five rotations. In rotation 1767, the region contains two plages 0.6 day apart; these coalesce into one, which splits into two, 1.2 days apart, then 2.2 days apart; in the next pass, there are three plages spread over quite a distance.

The pertinent Mariner data are shown in Figure 30–2, which depicts the measured plasma velocity averaged over 1 day. There are 19 major peaks in the velocity-time graph. These peaks show a tendency to occur in groups with approximately 27-day spacing. The most conspicuous and persistent of these groups is the one marked "A," which appears from 7 to 10 days after the beginning of a solar rotation.

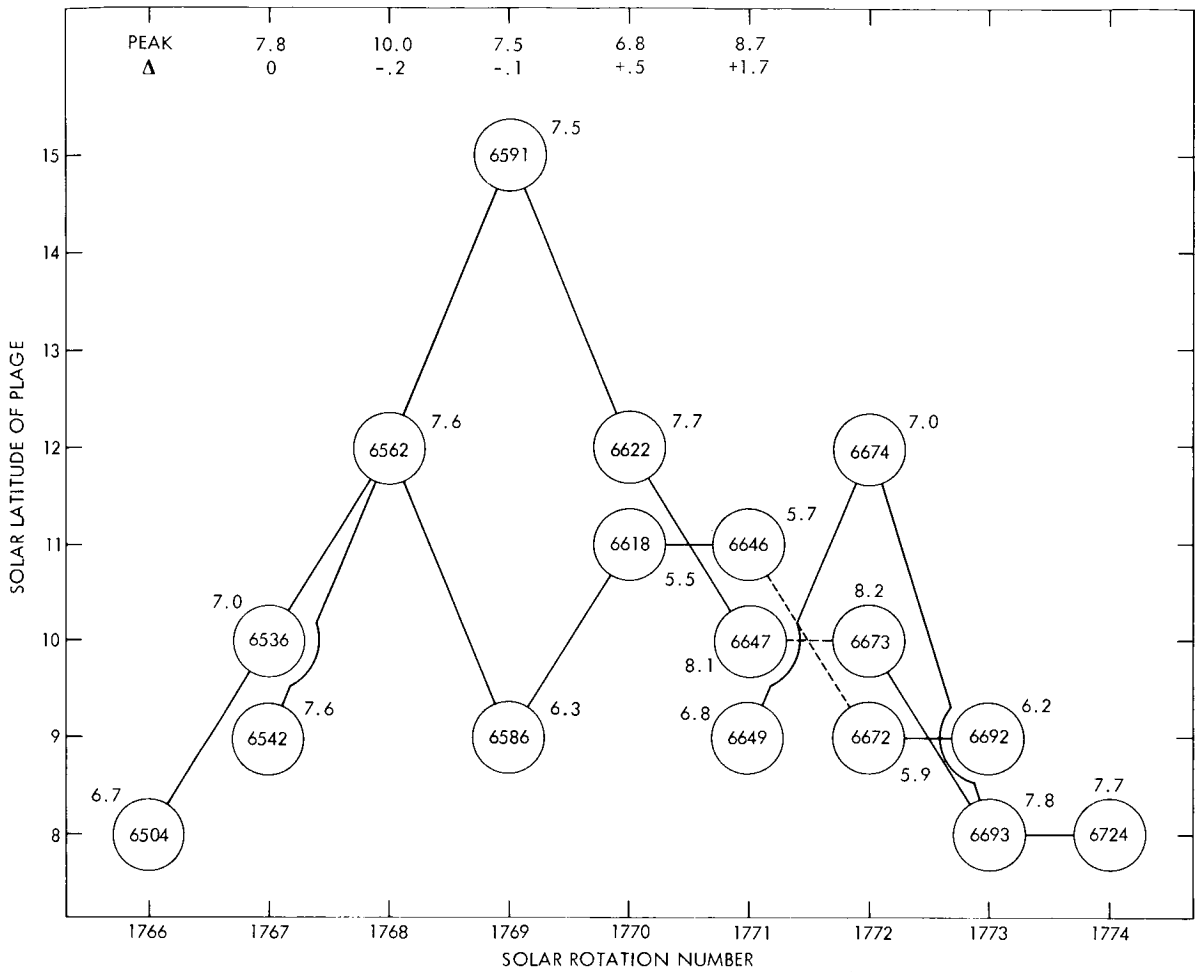

Figure 30–1.

We interpret these velocity peaks as streams of high-velocity plasma that are continuously ejected from particular regions on the sun, and it is natural to identify the source of the "A" stream with the active region that we have just been discussing. In addition to the persistence, the large size, and the approximate time of the stream, this identification appears to be supported by the detailed shape of its velocity profile. Thus, comparing Figures 30–1 and 30–2, note that:

In rotation 1767, there were two plages and a moderately broad peak

In rotation 1768, only a single plage remained, and the velocity peak was narrower

In rotation 1769, two plages again and a wider velocity peak

In rotation 1770, two plages passing more than 2 days apart, and the velocity peak was actually doubled

In rotation 1771, three plages and the largest peak of all

Qualitatively, the correspondence between the structure of the active region and that of the "A" series of plasma velocity peaks seems too close to be coincidental, but the quantitative aspects of the correspondence are disappointing.

Returning to the map of Figure 30–1, note the two rows of numbers at the top. The numbers labeled "PEAK" are the times of the observed peak velocities at the spacecraft. In some cases we do not know very accurately what time to choose, as the peak may be a couple of days in breadth. The numbers labeled "Δ"

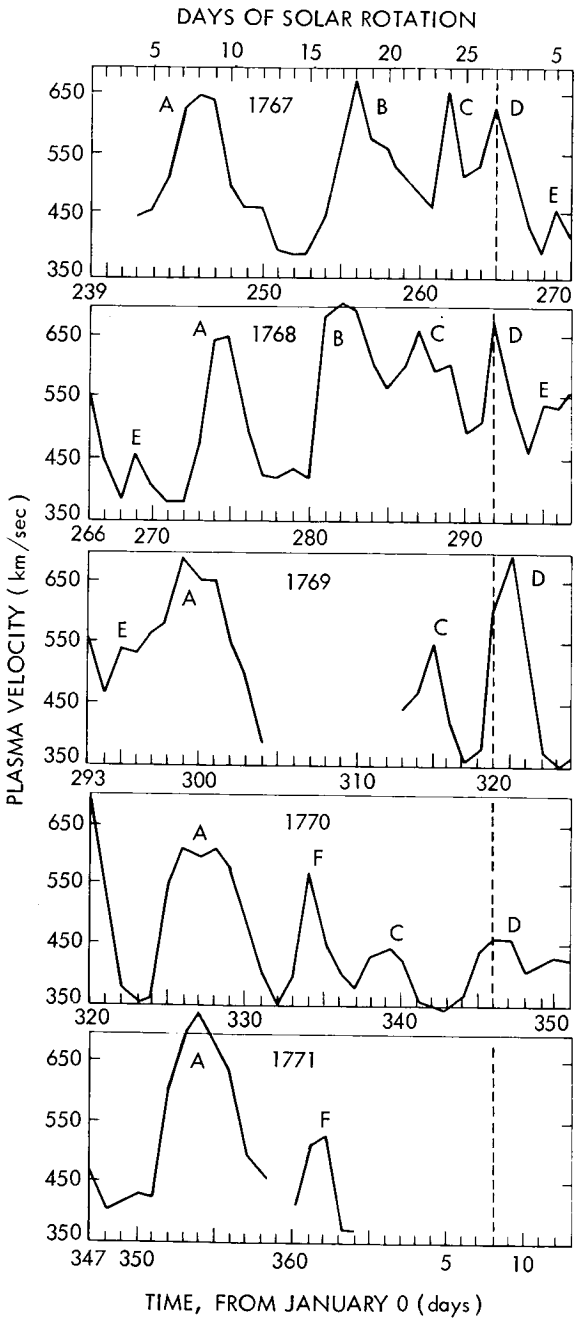

FIGURE 30–2.

are the corrections which must be added to the earth-related CMP times to obtain the Mariner CMP times. If we assume strictly radial flow and constant velocity for the plasma, then if the streams actually originate in the plages, the difference between the CMP time and the peak time should equal the ratio of the sun-probe distance to the peak velocity. For the second peak (rotation 1868) the agreement is fairly good, the transit time being about 2.5 days. In all other cases, the situation is confused by the presence of two or three plages; but all the observed transit times are less than 1.5 days, even for the westernmost plage. To travel from the sun to the earth in 1.5 days requires a velocity of 1150 km/sec, but sustained velocities exceeding 830 km/sec were never observed. I shall not speculate here on the meaning of this discrepancy.

It is customary to say that there are two kinds of geomagnetic events—sudden commencement storms, and recurrent storms—and that these are caused by streams of plasma that come, respectively, from solar flares and from M-regions that have nothing to do with flares. During the 4 months that we had good data from Mariner, there were 16 sudden commencements reported by one observer or another. Only 2 were reported by more than 40 observers, however: 51 observers reported the one at 20:26 on October 7 (day 280), which we saw as a B peak; and 42 observers reported the one at 03:34 on December 4 (day 338), which might be associated with a C peak, but not clearly. I conclude from this that most, if not all, of the high-velocity plasma streams observed by Mariner came from M-regions. The peak following day 280 may be an exception.

Let us consider one other set of peaks on Figure 30–2, the one marked "D." These peaks are attractive because they are rather isolated and they appear to correlate with a long-lived plage region which is rather isolated. The correspondence is shown in the following table:

Plage Number	Plage Latitude	CMP Earth	CMP Mariner	Peak Time	Transit Time
6563A	N 00	263. 6	263. 5	265. 6	2. 1
6581	N 03	291. 4	291. 3	292. 7	1. 4
6614	N 04	318. 0	318. 3	320. 0	1. 7
6644	N 02	344. 6	345. 8	346. 0	0. 2

This seemed fairly satisfactory when taking the information from the McMath-Hulbert tabulations, but then I looked up the solar

maps and discovered that plage No. 6563A did not even appear on the sun at all until day 267, being born at longitude 52° W. The tabulated CMP, of course, was the time that it would have passed if it had existed at the time. It seems difficult to believe that an active region on the sun could produce such a high-velocity plasma stream before it even becomes visible. And here again we have transit times that are too short.

In a flare conference, perhaps a little bit should be said about flares, so I will mention two other aspects of our data which may be interesting and suggestive.

During the first half of the mission, before the instrument was shut off on day 304, the solar latitude of Mariner was between 7° and 8° N. (Subsequently, it moved southward rapidly.) In this period, 25 class 2 flares and one class 2— flare were reported, none larger. Of these 26 flares, 9 occurred at least 12 degrees south of the latitude of Mariner; and one might think that they would be too far away to produce much effect on plasma that intercepted the spacecraft.

This leaves us 17 flares, all of which were within 8 degrees of the latitude of Mariner; and without exception every one of these occurred in a plage region which we associated with one of our velocity peaks on the basis of their time coincidence. Thus it may be that, although the observed plasma streams come not from flares but from plage regions, there is something about the flare-associated plages that causes them to produce especially high-velocity plasma streams.

In Figure 31–2, we have labeled 19 principal velocity peaks. Fifteen of these can be at least plausibly associated with particular long-lived calcium plages, and all such plages lie between the equator and 12° N. The four peaks for which no obvious source is seen include the two marked "E," which are rather insignificant. They include also the two marked "B," which are by no means insignificant. If may be that some of these four peaks represent plasma coming from a flare, but it does not appear possible to make a case for any particular flare.

The most interesting and most puzzling thing about the Mariner data at present is, I think, the apparently anomalously short transit times. We feel confident that our measurements of plasma velocity are correct to better than 10 percent, and the association of streams with plage regions seems to us very convincing. Among various suggested explanations for the descrepancy, I will mention only the one put forth by Dr. Leverett Davis of Cal Tech. His idea is that perhaps the magnetic field close to the sun is strong enough to carry the plasma around with it. In other words, the expanding corona co-rotates out to some reasonable distance, like one-third or one-half astronomical unit, and moves radially at larger distances where the field is too weak to continue to "funnel" the plasma.

DISCUSSION

Dr. Leverett Davis: Mr. Jokipii has pointed out that if one takes this evidence for varying velocity jets seriously and assumes that they come out from the sun all the time, then the plasma of a high-velocity jet will catch up with that of the preceding low-velocity jet and produce a shock wave.

If we ask where does this come with the kind of velocity patterns that are observed, we find it is apt to happen somewhere in the general order of 1 astronomical unit. This would lead one to think that in some cases, starting with a gradual rise of velocity at the sun, a shock wave would be observed near the earth, and in other cases the shock wave wouldn't start until farther out. The shock waves might look like sudden commencements on the earth, and indeed the mysterious B-peak, which has no source but which makes a sudden commencement, is a steeply rising one which would make its shock wave early. Thus, it could be just like the others and not have anything to do with a flare.

Dr. Howard: As I understand it, the geomagnetic storms have very precise 27-day periods. I don't understand how you can cor-

relate plages at low latitudes where the rotation period is not 27 days, but 25½ or 26 days, with the recurrent magnetic storms over any period of time. For a month or two it might be possible. Certainly not for 13 months where you would be 180 degrees out of phase.

Dr. Snyder: We don't have any correlation for 13 months. We have it only for less than 4 months. It is certainly quite good that long.

Dr. Axford: I don't understand Figure 30–1. Is this the same plage that comes back for 5 month at a period of 27 days?

Dr. Snyder: Let's have a look. All of these data were taken from CRPL–F, Part B. This is a particular plage (6536) which was alleged to the daughter of this one (6504) at the same spot; that is what the straight line connecting them means. 6542 is a new one. 6562, in the bulletin, is alleged to be the daughter of both 6536 and 6542.

I haven't attempted to make up my own mind by looking at the solar maps myself whether it is indeed true that this one comes from the coalescing of these two. I have taken that for granted from the published data.

Dr. Prince: Dr. Snyder, Dr. Howard, the regions you have listed on the board are perhaps "daughters" of the one at the head of the list, but I can assure you that Miss Hedeman and I are the "grandmothers" of them all! Each month we report on the age and identification of the plages, but we do this with uncertainty and hesitation. The associations between the regions represent only our best judgment in situations often far from clear. Miss Hedeman and I are familiar with the family of regions described by Dr. Snyder. Some are returns; some are new. They are all in the same general location on the sun. Perhaps Dr. Mustel should be looking at us and saying, "My, my, does it take the eyes of Mariner II to see what the rest of you could not join me in seeing over so many years—the association between certain plages and geomagnetic storms?" I wish Professor Mustel would tell us of his work.

Dr. Mustel: This problem requires a special investigation. It is necessary to point out that the curves showing the changes of plasma velocities (according to Mariner II data) and planetary geomagnetic indices K_p run more or less parallel one to another. Thus, for the solution of the problem of localization of the sources of corpuscular streams we may use only K_p indices. And it is quite evident that the interval studied by Dr. Snyder (September–December 1962) is too short for the solution of so complex a problem as the problem of localizing the sources of corpuscules creating M-disturbances. According to the analysis of M-disturbances, the mean delay time of these disturbances—to be more exact, the delay of the *onset* of disturbances—is equal to $+4^{d}_{,}5$. This value is in agreement with those magnitudes of plasma velocities, which according to the data of Mariner II also correspond to the *onset* of geomagnetic disturbances.

In connection with all this, the identifications proposed by Dr. Snyder are doubtful. For the solution of this problem it is necessary to take into account the fact that the sequence A_1, A_2, A_3, · · · of Dr. Snyder existed throughout 1963.

Dr. Prince: The reason we at the McMath-Hulbert Observatory have done nothing about the possible association between the recurrent series of plages described by Dr. Snyder and the sequence of recurrent storms is that there is a competitive sequence that fits almost as well. The choice between the two depends on the time interval that you prefer between central meridian passage of a possibly associated solar region and the start of geomagnetic disturbance.

Dr. Snyder: May I make two more comments?

One is that some of these plages are rather wide. They may well be 15 or 20 degrees wide. When you say some particular plage passed at day 7.0, it may be that the point on it which was putting out plasma went by a full day before that.

The other thing, with regard to Dr. Howard's objection that these things may not be too well established (and Mrs. Prince agrees to that), I would just point out that when I see plage 6562 at 12 degrees listed as the daughter of 6542 at 9 degrees, and the daughter of 6674 at 12 degrees being alleged to be 6693 at 8 degrees, I really wonder how that can be.

One other thing that has puzzled me is that Professor Mustel seems to find usually 3 to 7 days delay. I can never find anything like that in these data at all. It seems to be 2 days or less.

Dr. Mustel: In some places 3 days.

Dr. Snyder: But not consistently more than 2 days.

31 SOLAR SURFACE NUCLEAR REACTIONS

N64-30281

EDWARD L. FIREMAN
Astrophysical Observatory, Smithsonian Institution
Cambridge, Mass.

ABST

The high tritium and helium-3 content in Discoverer 17 (1960 o1) material indicates that nuclear reactions occurred on the solar surface during the November 12, 1960, flare. The ratio of helium-3 to tritium was approximately 70. If the tritium and the helium-3 are interpreted as the stripping of helium-4 flare particles in the solar atmosphere, the path length is at least 10 gm/cm². This lower limit on the path length is approximately the same as the upper limit, which is determined from the ratio of boron to carbon nuclei in the flare. The path length appears to be too restricted for the helium-3 and tritium to be produced solely by the stripping of helium-4 particles. It is more likely that the helium-3 and tritium are produced in a thermonuclear reaction, as Severny postulated.

Radiochemical studies on material recovered from Discoverer 17, which was launched at 20:42 UT on November 12, 1960—about 7 hours after the start of a +3 flare—and was flown in a polar orbit for 2 days, indicate that nuclear reactions occurred on the solar surface. Fireman, DeFelice, and Tilles (Reference 1) found that some of the material was exposed to an incident flux of tritons of approximately $5\times10^6/cm^2$. Schaeffer and Zähringer (Reference 2) found that some of the material was exposed to an incident flux of helium-3 of $4\times10^8/cm^2$, which is approximately 70 times the tritium flux. Measurements (References 3 to 7) of such other radioactive isotopes in the material as argon-37, xenon-127, and bismuth-205 show that these isotopes can be explained by the interaction of flare protons and Van Allen protons with the material. Measurements (References 8) of cobalt-57 indicate that the tritium cannot be explained by the stripping of flare alpha particles in the vehicle. The tritium content in Discoverer 17 material is approximately a factor of 100 and the helium-3 content approximately a factor of 10,000 too large to be explained by the action of flare protons and flare alpha particles on the material.

Additional tritium measurements (Reference 9) on other Discoverer satellites flown both before and after this particular flare indicated that some of the solar flare tritium was trapped in the inner radiation belt. This tritium disappeared with a mean lifetime of about two months. These additional measurements confirm that the November 12, 1960, energetic solar flare particles contained appreciable amounts of tritium. If the tritium and the helium-3 in the flare resulted from the stripping of helium-4 flare particles during their acceleration and storage in the solar atmosphere (References 10, 11), the path length in the solar atmosphere would have been at least 10 gm/cm².

Biswas, Fichtel, and Guss (Reference 12) studied nuclear emulsions flown on rockets launched from Fort Churchill, Canada, at 18:40 UT on November 12, 1960, 2 hours before the Discoverer 17 was launched. They found the heavy nuclei in the flare to be in approximately solar abundance. They found no tritons of 60 to 130 Mev energy and one deuteron of 50 to 95 Mev among 284 tracks of singly charged particles corresponding to protons of 40 to 56 Mev. This nuclear emulsion work does not overlap the tritium work sufficiently to serve as a check. The nuclear emulsion work sets upper limits on the abundance of Li, Be, and B nuclei in the flare. The limit of 0.05 for the ratio of the boron to carbon (Reference 12) sets an upper limit on the path length of approximately 10 gm/cm². This upper limit is approximately the same as the lower limit set by the ratio of helium-3 to tritium. The path length seems to be too restricted for the helium-3 and tritium to be produced solely by the stripping of alpha particles.

728-629 O—64——19

A rough estimate of approximately 10/cm^2 sec is given for the fast neutron and gamma ray flux that should be associated with a flare of the November 12, 1960, type. Although neutron and gamma ray measurements of the required sensitivity have not yet been made, such measurements are possible and would be desirable for future flares.

NUCLEAR REACTIONS

Table 31–1 gives the most probable nuclear reactions that may occur in the solar atmosphere during and after charged particle acceleration, if the solar deuterium abundance is much lower than 10^{-5}. Nuclear interactions between hydrogen and helium-4 predominate. Because most of the measurements correspond to flare particles of roughly 30 Mev/nucleon and because of the steep energy spectrum of the flare particles, we give the estimated cross sections values corresponding to 30 Mev protons. A more reliable calculation also would consider particles of other energies; however, the variations of the cross sections with energy are not well known. The energy history of the accelerated particles is also not known. Wickersham (Reference 13) measured the He^4 (p, 2p) He^3 and the He^4 (p, pn) He^3 cross sections to be 9 ± 1 mb and 5 ± 1 mb, respectively, for 28 Mev protons. Kim, Bunch, and Forster (Reference 14) measured the He^4 (p, d) He^3 cross section to be approximately 25 mb for 31 Mev protons. There are no measurements at other energies except for the total inelastic cross section of 95 Mev protons with helium-4 (Reference 15).

Nuclear reactions between protons and carbon and oxygen in the solar atmosphere are the next most likely reactions because of the solar abundances. The (p, pn) reactions on carbon and oxygen are a factor of 100 less probable that on helium-4. The values for the (p, pn) reaction cross sections on carbon and oxygen given in Table 31–1 are obtained from measurements on carbon (Reference 16). The threshold energy for nuclear reactions between protons and helium-4, carbon-12, and oxygen-16 are all in the neighborhood of 20 Mev. On the other hand, proton reactions with deuterium and tritium have a 2 Mev threshold and have very large cross sections (References 17 to 20). The values given in Table 31–1 for these cross sections for 25 Mev energy were estimated from measurements made at lower energies.

Since the cross section for a nuclear reaction depends only on the relative velocity of the particles, a heavy ion with 30 Mev/nucleon acts on chromospheric hydrogen with the same cross section as a 30 Mev proton acts on the heavy

TABLE 31–1

Nuclear Reactions on the Solar Surface

Reactions	Abundance	σ (30 Mev) (mb)
Primary Proton Reactions:		
$\vec{H} + He^4 \rightarrow H^3 + 2H$	$He^4/H = 0.1$	10
$\vec{H} + He^4 \rightarrow He^3 + D$	$He^4/H = 0.1$	25
$\vec{H} + He^4 \rightarrow He^3 + N + H$	$He^4/H = 0.1$	5
$\vec{H} + O^{16} \rightarrow O^{15} + N + H$	$O^{16}/H = 9.10^{-4}$	10
$\vec{H} + C^{12} \rightarrow C^{11} + N + H$	$C^{12}/H = 5.10^{-4}$	10
Proton Reactions With Secondaries:		
$\vec{H} + H^3 \rightarrow He^3 + N$		250
$\vec{H} + D \rightarrow 2H + N$		250
$\vec{H} + He^3 \rightarrow D + H + N$		10

ion in the chromosphere. Because of the conservation of momentum, protons produce less energetic reaction products than do heavy ions of the same energy per nucleon. Since accelerated heavy ions are present in approximately the solar abundance, the action of flare heavy ions on chromospheric hydrogen is more significant to the production of energetic secondaries than the action of flare protons on chromospheric heavy ions. Table 31–2 lists the most important nuclear reactions for the production of energetic secondary particles in the solar atmosphere during flares.

TABLE 31–2

Nuclear Interaction of 120 Mev Flare Helium-4 Particles on Chromospheric Hydrogen Producing Isotopes of ≈25 Mev/Nucleon	
I. $\vec{He}^4+H\rightarrow\vec{H}^3+2H$	$\sigma_1=10$ mb
II. $\vec{He}^4+H\rightarrow\vec{He}^3+H+N$	$\sigma_2=5$ mb
III. $He^4+H\rightarrow\vec{He}^3+\vec{D}$	$\sigma_3=25$ mb
Destruction of 25 Mev/Nucleon Isotopes on Chromospheric Hydrogen	
IV. $\vec{H}^3+H\rightarrow He^3+N$	$\sigma_4=250$ mb
V. $\vec{He}^3+H\rightarrow 3H+N$	$\sigma_5=10$ mb
VI. $\vec{D}+H\rightarrow 2H+N$	$\sigma_6=250$ mb

THE ABUNDANCE OF NUCLEAR REACTION PRODUCTS IN SOLAR FLARES

If thermonuclear processes play no role in flares, the abundance of the reaction products depends simply on the path length of the accelerated ions in the solar material during and after the acceleration process. To postulate that the flare particles encounter solar material during the acceleration process is more consistent with the heavy ion abundances in flares than to assume that the encounter took place after the acceleration process. Since the ionization loss of swift charged particles increases as the square of the atomic number, if heavy ions had a significant path length after their acceleration, there would be a significant reduction in the abundances of the heavy ions. The energy gain in the acceleration process exceeds the ionization loss over the total time of acceleration; however, the flare particles may often be in regions where the ionization loss exceeds the energy gain, since the scale height of the solar atmosphere (100 km) is small compared with the dimensions of the flare. To examine how the isotopic abundance of hydrogen and helium changes with path length, let us assume that the acceleration gain and the ionization loss balance. Under these conditions the following equations express the changes in the flux of H^3, He^3, and H^2 with path length that result from the action of helium-4 ions on chromospheric hydrogen:

$$\frac{dF(H^3)}{dx}=\sigma_1F(He^4)-\sigma_4F(H^3), \qquad (1)$$

$$\frac{dF(He^3)}{dx}=(\sigma_2+\sigma_3)F(He^4)+\sigma_4F(H^3)-\sigma_5F(He^3), \qquad (2)$$

$$\frac{dF(H^2)}{dx}=\sigma_3F(He^4)-\sigma_6F(H^2), \qquad (3)$$

where F is the flux and x is the path length which is the product of the hydrogen density and the distance. The cross sections are labeled in Table 31–2. The helium-4 flux, $F(He^4)$, equals $F_0\ell^{-\sigma_0 x}$, where F_0 is a constant and σ_0 is the total inelastic He^4 cross section, which is approximately $\sigma_1+\sigma_2+\sigma_3$. The solutions of Equations 1, 2, and 3 with the zero initial conditions are:

$$F(H^3)=\frac{\sigma_1F_0}{\sigma_4-\sigma_0}\left(\ell^{-\sigma_0 x}-\ell^{-\sigma_4 x}\right), \qquad (4)$$

$$F(He^3)=F_0\left\{\sigma_0\frac{\left(\ell^{-\sigma_0 x}-\ell^{-\sigma_5 x}\right)}{\sigma_5-\sigma_0}+\sigma_1\sigma_4\frac{\left(\ell^{-\sigma_5 x}-\ell^{-\sigma_4 x}\right)}{(\sigma_4-\sigma_0)(\sigma_5-\sigma_0)}\right\}, \qquad (5)$$

$$F(H^2)=\frac{\sigma_3F_0}{\sigma_6-\sigma_0}\left(\ell^{-\sigma_0 x}-\ell^{-\sigma_6 x}\right). \qquad (6)$$

The fluxes calculated for different path lengths are given in Table 31–3.

To explain the tritium in Discoverer 17, a path length of approximately 10^{24} atoms/cm^2 is required. To explain both the tritium and

TABLE 31–3

Flare Isotope Ratios Calculated for Different Path Length for Particles of 30 Mev/Nucleon

X (atoms/cm^2)	10^{23}	10^{24}	10^{25}	10^{26}
$F(H^3)/F_0$	0. 001	0. 01	0. 028	0. 001
$F(H^2)/F_0$	0. 0025	0. 02	0. 07	0. 002
$F(He^3)/F_0$	0. 003	0. 03	0. 33	0. 33
$F(He^4)/F_0$	0. 996	0. 96	0. 67	0. 018
$F(He^3)/F(H^3)$	3	3	12	330
$F(B^{11})/F(C^{12})$	0. 001	0. 01	0. 095	0. 67

the helium-3 requires a path length of 10^{25} atoms/cm^2.

The calculation of helium-4 stripping shows that the maximum deuterium and tritium abundances are only a few percent of the total helium flux. If the hydrogen-to-helium ratio is 10, then the maxium deuterium and tritium abundances in the flare are only a few tenths of 1 percent. Although this low abundance is difficult to measure in nuclear emulsions and it is difficult to distinguish He^3 and He^4 in nuclear emulsions, the nuclear emulsion measurements (Reference 12) of boron and carbon have a very important bearing on the path length. Accelerated C^{12} ions on passing through chromospheric hydrogen can be converted to C^{11}, which decays to B^{11} with a 20-minute half-life. The (p, pn) reaction on carbon-12 is similar to that on helium-4. The C^{12} (p, pn) C^{11} cross section is at least 10 mb. The threshold energy for the reaction on C^{12} and on He^4 is approximately the same. The nuclear emulsion studies of the November 12, 1960, flare set an upper limit of 5 percent of the boron-to-carbon ratio (Reference 12). The low boron-to-carbon ratio sets an upper limit of approximately 10 gm/cm^2 on the path length. This upper limit is the same as the lower limit set by the high helium-3 to tritium ratio. Although the limits on the path length are not inconsistent with one another, the path length seems to be too restricted for the helium-3 and tritium to be produced solely by the stripping of alpha particles.

If the energetic particles in flares were generated by the process described by Severny and Schabanskij (Reference 21), then the helium-3 and tritium could be produced without a long path length. According to the picture these authors postulate, the deuterium in the solar atmosphere is 10^{-5}. The contraction of the plasma and the increased temperature initiate a thermonuclear reaction. Suprathermal particles from this region are accelerated further by reflections from the magnetic fields converging on the region, that is the Fermi mechanism. Since the helium-3 and tritium produced from the deuterium-deuterium reactions are more energetic than the other ions, they will undergo more rapid acceleration by the Fermi mechanism. Until a deuterium abundance of 10^{-5} is measured, the mechanism should be regarded with some skepticism. The deuterium abundance of 10^{-5} must be the primordial deuterium abundance, since solar flares have a negligible effect on the isotopic abundance in the solar atomsphere.

Neutrons and gamma rays would arise from nuclear reactions on the solar surface. The neutron and gamma ray flux at the earth would be roughly 10/cm^2 sec from the November 12, 1960, flare. The neutron production in nuclear reactions approximately equals the helium-3 production. The neutron flux decreases with the distance from the sun according to the inverse square law. The area covered by the flare at 1 AU is not well known. We shall assume this area to be 1 percent of the hemisphere. Only about 1 percent of the fast neutrons survive radioactive decay in the time of travel to the earth. Under these approximations the total neutron flux is 10^{-4} of the total

helium-3 flux at the earth, or $4\times10^4/cm^2$ for the November 12, 1960, flare. The neutrons would continue to arrive at the earth for longer than 1 hour. The neutron flux at the earth would be approximately $10/cm^2$ sec.

Gamma rays could result from the capture of neutrons in solar material and from the decay of radioactive isotopes produced in nuclear reactions. Neutrons directed into the photosphere undergo more than 10 elastic scattering collisions before they have an appreciable probability for being captured. More than 99 percent of the neutrons are reflected back into space so that the capture gamma rays number less than 1 percent of the neutrons. The most probable radioactive isotopes produced by solar surface nuclear reactions are C^{11} and O^{15}. Since the production of these isotopes is less than 1 percent of the helium-3 production, the total gamma ray flux would be less than $4\times10^4/cm^2$ for the November 12, 1960, flare. If the gamma rays arrived at the earth for ½ hour, the gamma ray flux at the earth also might be $10/cm^2$ sec. Although neutron and gamma ray measurements of the required sensitivity have not been made during flares, such measurements would be highly desirable.

ACKNOWLEDGMENT

The author is grateful to Dr. D. Tilles for many helpful discussions.

REFERENCES

1. Fireman, E. L., DeFelice, J., and Tilles, D., 1961, *Phys. Rev.*, 123: 1935.
2. Schaeffer, O. A., and Zahringer, J., 1962, *Phys. Rev. Letters*, 8: 389.
3. Dodson, R. W., Friedlander, G., Hudis, J., and Schaeffer, O. A., 1961, *Bull. Amer. Phys. Soc.*, II, 6: 277.
4. Keith, J. E., and Turkevich, A. L., 1962, *J. Geophys. Res.*, 67: 4525.
5. Stoenner, R. W., and Davis, R., Jr., 1961, *Amer. Phys. Soc.*, II, 6: 277.
6. Fireman, E. L., DeFelice, J., and Tilles, D., 1963, *Radioactive Dating, IAEA*, 323.
7. Wasson, J. T., 1961, *J. Geophys. Res.*, 66: 2659.
8. Wasson, *J. Geophys. Res.*, 67: 3513.
9. Tilles, D., DeFelice, J., and Fireman, E. L., 1963, *Icarus*, 2: 258. (Also unpublished data.)
10. Tilles, D., DeFelice, J., and Fireman, E. L., 1962 (Abstract), *J. Geophys. Res.*, 67: 1660.
11. Flamm, E., Lingenfelter, R. E., MacDonald, G. J. F., and Libby, W. F., 1962, *Science*, 138: 48.
12. Biswas, S., Fichtel, C. E., and Guss, D. E., 1962, NASA Goddard Space Flight Center report X-611-62-27 (1962); also *Phys. Rev.*, 128: 2756.
13. Wickersham, A. F., Jr., 1957, *Phys. Rev.*, 107: 1050.
14. Kim, C. C., Bunch, S. M., and Forster, H. H., 1962, private communication and *Bull. Amer. Phys. Soc.*, 7: 434.
15. Selove, W., and Teem, J. M., 1958, *Phys. Rev.*, 112: 1658.
16. Crandell, W. E., Milburn, G. P., Pyle, R. V., and Birnbaum, W., 1960, *Phys. Rev.*, 101: 329.
17. Fowler, J. L., and Brolley, H. E., Jr., 1956, *Rev. Mod. Phys.*, 28: 103.
18. Deuchars, W., Perkin, J. L., and Batchelor, R., 1963, *Nuc. Inst. & Methods*, 23: 305.
19. Nisimura, K., 1961, *J. Phys. Soc. Japan*, 16: 2097.
20. Frank, R. M., and Gammel, J. L., 1954, *Phys. Rev.*, 93: 464.
21. Severny, A. B., and Schabanskij, V. P., 1960, *Astr. Zhurn.* 37: 609–615 (*Soviet Astron.-AJ*, 4: 583–589).

DISCUSSION

Dr. Teske: What concentration of deuterium would you expect relative to the protons in the flare?

Dr. Fireman: The ratio of heavy hydrogen isotopes to protons formed in the passage of flare helium-4 through the chromosphere is more uncertain than the ratio of the heavy hydrogen isotopes to helium-4. If, however, one assumes that the flare helium-4 to flare proton ratio is 1 to 10, then the ratio of flare deuterons to flare protons is 1 to 250 in the steady state limit.

Dr. Teske: The reason I asked: We were very fortunate to be able to get some spectra in the region of Hα in this flare. We see no evidence in the spectra for deuterium. We know fairly accurately where we were in the flare when the spectra were taken. I think, putting the results together, we could tell you at least where the deuterium was *not* being formed in the flare.

Dr. Fireman: The spectra that you observe do not arise from the particles accelerated to 30 Mev/nucleon. Our results apply only to 30 Mev/nucleon. These particles are probably not the ones that give the light in the region of Hα.

Dr. Wentzel: Concerning the particle acceleration, which methods of particle acceleration do you refer to? And why do you start with 30 Mev, which already requires some previous acceleration?

Dr. Fireman: In answer to your second question, we started with 30 Mev/nucleon particles because only particles of this energy and above are measured in the Discoverer satellites. Furthermore, only helium-4 particles with energies above 30 Mev/nucleon have an appreciable cross section for interacting with hydrogen.

Did you have another question? I don't remember your first question.

Dr. Wentzel: The other question was: Do you refer to Parker's paper concerning a great flare of 1956, in which he has a very inefficient acceleration mechanism, but at least he does have a way to inject particles into the mechanism?

Dr. Fireman: I should perhaps go into various theories and see which ones agree and which ones disagree with the radio-chemical studies made on the material which was exposed above the atmosphere during the November 12, 1960, flare.

N64-30283

32 SOME PROPERTIES OF CORPUSCULAR STREAMS FROM THE CHROMOSPHERIC FLARES*

E. R. Mustel and N. B. Egorova
Astronomical Council, U.S.S.R. Academy of Sciences
Moscow, U.S.S.R.

Very important information about the motion of gases ejected from chromospheric flares may be obtained from the analysis of sporadic geomagnetic disturbances. One of the principal properties of these disturbances is the presence of storm-time variation and of sudden commencement. It is clear that the above-mentioned analysis must be carried out only on the base of such a material when we have more or less reliable correspondence between sporadic disturbances and those chromospheric flares which created these disturbances. In the present work, we used two lists of chromospheric flares of importance greater than 2:

A. A list of chromospheric flares which have been observed during the period 1957 to 1960. This list was compiled on the basis of our previous article (Reference 1) and on its extension to the period 1959 to 1960. Moreover, we used data contained in References 2, 3 and in some other papers.

In the preparation of List A we tried to select only the most reliable cases. This is one of the most essential characteristics of our list. For example, the list contains only 60 identified geomagnetic sporadic disturbances, whereas a similar list published in Reference 3 contains 136 chromospheric flares.

B. This list is compiled on the base of a catalog of all chromospheric flares of Importance 2 and 3 recorded from 1859 up to 1956. This catalog, prepared by Fritzova, Kopecky, and Svestka (Reference 4), contains 438 chromospheric flares. We used mainly the period of 1924 to 1956. The authors of this catalog already have carried out a necessary identification of many chromospheric flares with the corresponding geomagnetic disturbances. We reconsidered these identifications carefully. For this purpose, we used magnetograms of the geomagnetic station in Tbilisi (Gorgia), because the recognition of the period of storm-time variation is the most reliable process for sufficiently southern geomagnetic latitudes. Besides, we used (beginning from 1932) planetary K_p indices according to the recent catalog of Bartels (Reference 5). The final version of List B contains 146 chromospheric flares, ⅓ of all chromospheric flares.

In the present communication we shall discuss only a very important problem: What information can we receive from the analysis of the longitudinal distribution of geomagnetically effective chromospheric flares on the visible disk of the sun?

Figure 32–1 gives a distribution of chromospheric flares (Lists A and B are combined) on the solar disk. This figure shows that the longitudinal distribution of the number of geomagnetically active chromospheric flares on the solar disk is practically uniform. However, Figure 32–1 does not give any idea about the intensity of those geomagnetic disturbances which are created by chromospheric flares at different longitudes. At the same time, this intensity must give very important information about the spatial distribution of gases ejected from the chromospheric flares.

To investigate these effects, the whole disk of the sun was divided into six zones: three to the west, and three to the east of the central meridian (see Figure 32–2). For flares entering each zone we applied a superposed epoch method; as a zero moment we used the moments of the appearance of the flares. The results

*Presented by Prof. Mustel.

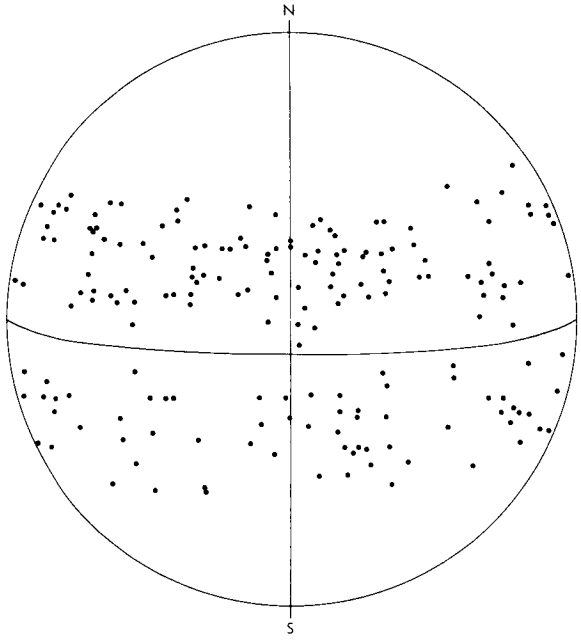

FIGURE 32–1.

of the computations are represented in Figure 32–2. According to this figure we may confirm the above-mentioned conclusion that the ejection of gases from a sufficiently intense chromospheric flare (of Importance 2 or 3) is practically uniform.

Since the gases which produce sporadic geomagnetic disturbances are generally the most dense component of gases ejected by a chromospheric flare, we cannot speak about the rise in the planetary space surrounding the sun of such regular radial formations as magnetic bottles, and so on. On the contrary there are reasons to think that high energy particles producing, for example, ground level effects in cosmic ray increases move from the flare along those relatively stationary magnetic tubes—coronal rays—which proceed from each active region in the form of strongly bent spirals (References 6 and 7).

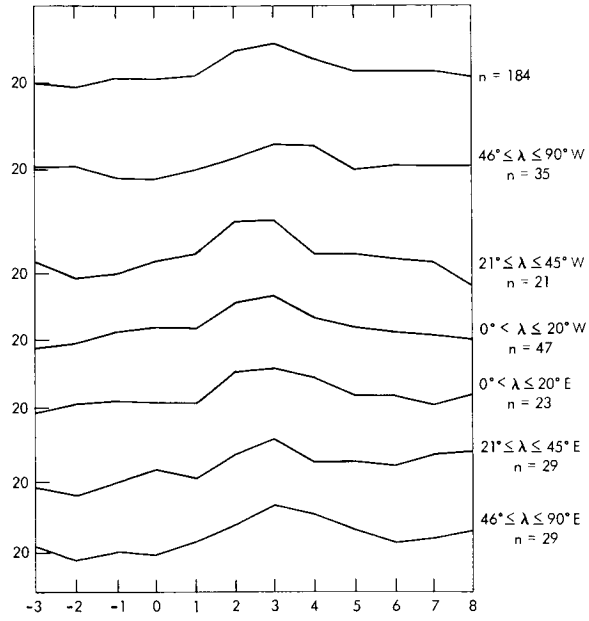

FIGURE 32–2.

REFERENCES

1. MUSTEL, E. R., and EGOROVA, N. B., 1961, "Results of Researches of the International Geophysical Year Program," series "Solar Activity," No. 1, p. 5, Moscow.
2. DODSON, H. W., and HEDEMAN, E. R., 1961 and 1962, IGY Solar Activity Reports No. 15 (1961) and 18 (1962), Boulder, Colorado.
3. MAEDA, H., SAKURAI, K., ONDOH, T., and YAMAMOTO, M., 1962, *Annales de Geophysique*, 18: 305.
4. FRITZOVA, L., KÔPECKY, M., and SVESTKA, Z., 1956, Astronomical Institute of the Czechoslovak Academy of Sciences, Publication No. 35, 99.
5. BARTELS, J. L., 1962, IAGA Bulletin No. 18.
6. MUSTEL, E. R., 1960, *Sov. Astronom. Jour.*, 37: 403.
7. MCCRACKEN, K., 1962, *Jour. Geophys. Res.*, 67: 447.

N64 30283

33 ON THE POSSIBLE ROLE OF FLARE-LIKE NONSTATIONARY PROCESSES IN THE ORIGIN OF SOLAR WIND

E. R. Mustel
Astronomical Council, U.S.S.R. Academy of Sciences
Moscow, U.S.S.R.

30283

Editor's Note: Prof. Mustel has requested that the text of the paper which he presented at the Symposium be replaced by the following paragraph:

The analysis of geomagnetic disturbances recorded at the polar caps of the earth gives reason to expect that the continuous outflow of gases from the undisturbed regions of the sun, the "solar wind," is produced at least partly by some nonstationary processes in the solar envelope and that these processes have some resemblance to chromospheric flares. The corresponding argument may be found in my article published in the Dutch magazine *Space Science Reviews*, 3: 2, 1964.

DISCUSSION FOLLOWING PROF. MUSTEL'S TALK

Dr. Axford: I would like to remark on the question of time delays mentioned by Dr. Snyder, and also by Dr. Mustel.

We should remember, of course, that it is a *disturbance* that is observed. Thus, we obtain only the time delay for a disturbance to propagate from the sun. This is not the time that it takes the individual particles to move from the sun to the earth. Consider, for example, the following two extreme cases: (a) If we have a very intense solar flare, then the associated sudden commencement at the earth might be observed 1½ days after the flare, corresponding to a "time delay" speed of 1000 km/sec. But, if you are out in space measuring the plasma velocity, you would observe something like 750 km/sec. This is because we observe initially the effects of a disturbance on the sun, and not particles which have been ejected from the sun. (b) If, instead of a flare, a very weak disturbance occurs—someone standing on the sun and shouting, say—then we would hear him after maybe 3 or 4 days if the solar wind is present and has a typical quiet-day velocity. We would, however, observe no permanent change in the plasma velocity at all, but just a sound wave coming from the sun at a speed equal to the sum of the solar wind and sound speeds.

To sum up, because we observe a disturbance with a certain time delay, we should not jump immediately to the conclusion that the gas is coming at that speed.

Dr. Mustel: Practically no space probes measured velocities for chromospheric flares. We don't know what the velocity is. But, from Pioneer V, it was concluded that the average velocity of propagation of gas from the sun is of the order of 800 km/sec.

Our figures, too, have shown that the average value of delay for chromospheric flares is of the order of 2½ days. Thus, we received practically the same figures.

Dr. Axford: Pioneer V observed the magnetic field changes which give only the propagation velocity of the disturbance, as also do your observations from earth-bound magnetometers. It is not surprising, then, that the results agree.

Only Mariner has been able to measure plasma velocities satisfactorily; and, as Dr. Snyder has pointed out, these do not agree with the disturbance velocity, which is actually somewhat higher.

Dr. Mustel: Yes, I know. It is very difficult to decide at the present how these velocities differ, the velocity of propagation and the velocity of plasma.

Nobody knows about that.

N64-30288

34 VELOCITY DEPENDENCE AND SOURCE SPECTRA OF SOLAR PROTON EVENTS*

D. A. Bryant†, T. L. Cline, U. D. Desai‡, and F. B. McDonald
Goddard Space Flight Center, NASA
Greenbelt, Maryland

It has become clear from recent satellite measurements (References 1 and 2) that solar protons can be transported from the sun to the earth in three distinct ways in addition to the direct way sometimes observed with cosmic-ray monitors at sea level (Reference 3). We will describe these four modes of propagation and then show how the velocity dependence of one of these modes makes it possible to determine the energy spectrum of the particles at the time of release from the sun.

Solar particle events consisting of radiation with energy above 1 Mev can be classified into four distinct classes. The distinction between the classes depends on the way in which the particles are transported from the sun to the region of the earth. The first two classes consist of particles that arrive at the earth in a manner determined by particle velocity; the first class consists of predominantly higher energy anisotropic particles that arrive after a nearly direct transit, and the second class consists of those that arrive after a diffusive propagation. The third class consists of those that arrive in a manner determined by the motion of enhanced solar plasma. The fourth class consists of those that depend on the rotation of the sun. Typical delays between the occurrence of a solar flare and the arrival at the earth of particles in these four classes are different. The delay of the first-class event is close to the rectilinear transit time for highly relativistic particles and is therefore only a few minutes. The arrival-time delay of the second class depends on the rate at which particles propagate through interplanetary space and so varies with energy up to a number of hours. The typical delay for particles in the third class is not a function of energy, since particles of all energies arrive with the enhanced solar plasma responsible for Forbush decreases and geomagnetic storms; it is the transit time of solar plasma across 1 astronomical unit, that is, about 2 days. The fourth-class event takes place near the time of central-meridian passage of a plage region responsible for a flare and solar particle events of the other classes during the previous solar rotation. This fourth class is closely associated with long-lived solar streams. The delay between the parent flare and the arrival of these particles is not a function of energy, since particles of all energy arrive with the plasma stream. The delay depends on the solar longitude of the parent flare and may therefore be as long as 1 solar rotation, or 27 days.

Figure 34–1 shows the times of occurrence of events of the latter three classes seen by Explorers XII (1961 ν1) and XIV (1962 B–γ1) during parts of 1961 and 1962. Four sequences of events are evident. No events of the first class were seen with sea-level monitors during these time intervals. Figure 34–2 shows the variation in intensity of interplanetary protons of energy greater than 3 Mev during a sequence involving all three classes of events seen. Superimposed on the intensity decay of the velocity-ordered event of September 28 is the plasma-associated event of September 30, fol-

*Presented by Dr. McDonald.
†Now at D.S.I.R. Radio Research Station, Slough, Bucks, England.
‡Now at Physical Research Laboratory, Navrangpura, Ahmedabad, India.

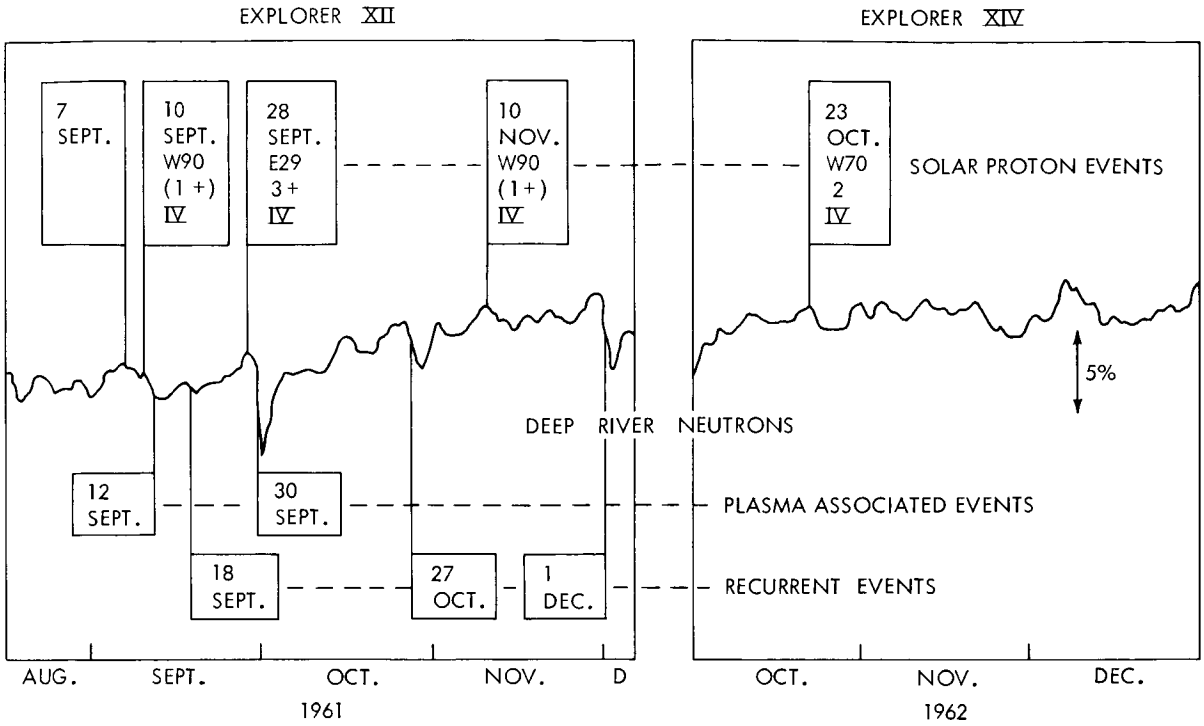

FIGURE 34–1.

lowed in turn after 27 event-free days by a recurrent event on October 27.

We now confine our attention to several velocity-ordered events observed on Explorers XII and XIV. We show how it has been possible in these events to determine separately the influence of the propagation medium and the form of the energy spectrum of particles released from the sun, that is, the source spectrum. These deductions were made possible by the fact that differential energy measurements could be made outside the magnetosphere with the equipment carried by these satellites.

A striking velocity dependence was shown by the solar proton event of September 28, 1961. This is shown by Figures 34–3 and 34–4. Figure 34–3 shows intensity versus time profiles for various differential energy components. The abscissa is in units of hours from the time of the flare. Figure 34–4 shows the behavior of the intensities of the same differential components of the event—but this time plotted not as a function of time but as a function of distance traveled. The distance traveled is simply the product of particle velocity and time from the flare. The intensity curves of the various components have been vertically scaled to give the best fit to a common curve. The physical meaning of this normalization will be examined further below. Note from Figure 34–4 that all components lie very closely on a common curve. We may interpret Figure 34–4 as a measure of the probability that a particle should travel a given distance before reaching the earth from the sun. The fact that there is essentially a common curve shows that particles of all energies traveled a given path length with equal probability. This is true for all path lengths to the extent that the various components of Figure 34–4 lie on a common curve. The statistical distribution of path length traveled is clearly a property of the propagation medium of interplanetary space. We note that the distance traveled by most particles is an order of magnitude larger than 1 astronomical unit. This indicates that propagation involved an important degree of scattering. Further, the degree of scattering is not a function of energy over the range examined. This suggests that the mode of propagation is a diffusion-like proc-

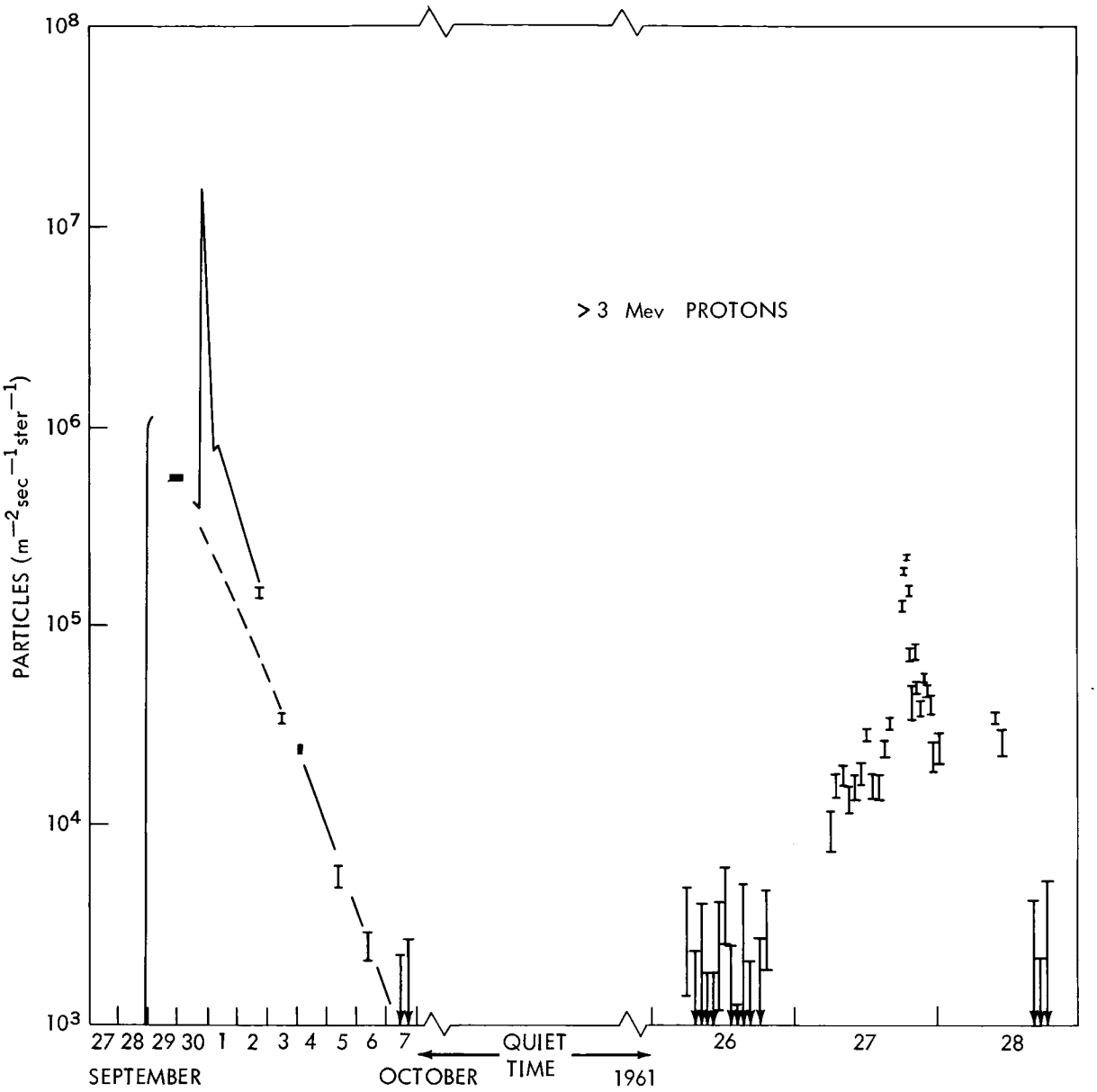

FIGURE 34–2.

ess and that energy-dependent processes, such as drift across magnetic field lines, do not play a dominant role. In fact, the equation for simple diffusion fits the propagation curve of this particular event through its maximum. It does not fit, though, at the beginning where anisotropy is dominant and at the end where boundary conditions must be taken into account.

Some of the other solar proton events we have observed with Explorers XII and XIV show the same degree of good fit to common, velocity-compensated, intensity versus distance curves; but a few contrast by not fitting at all. We believe that these exceptions do not weaken our argument for velocity dependence but strengthen it by illustrating that there are times when the properties of the propagation medium

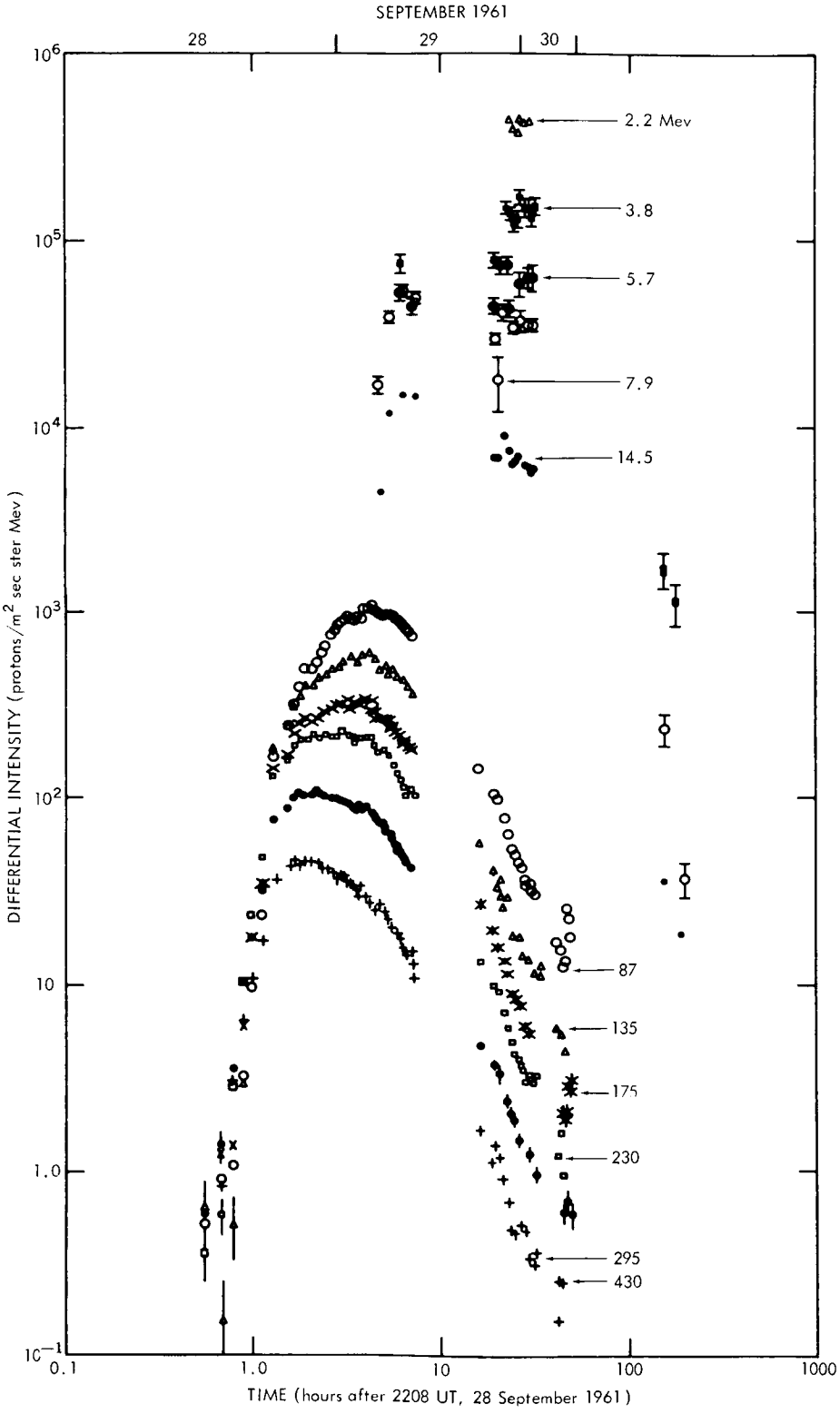
SEPTEMBER 1961
28
29
30
10^6
10^5
10^4
10^3
10^2
10
1.0
10^{-1}
DIFFERENTIAL INTENSITY (protons/m^2 sec ster Mev)
2.2 Mev
3.8
5.7
7.9
14.5
87
135
175
230
295
430
0.1
1.0
10
100
1000
TIME (hours after 2208 UT, 28 September 1961)

FIGURE 34–3.

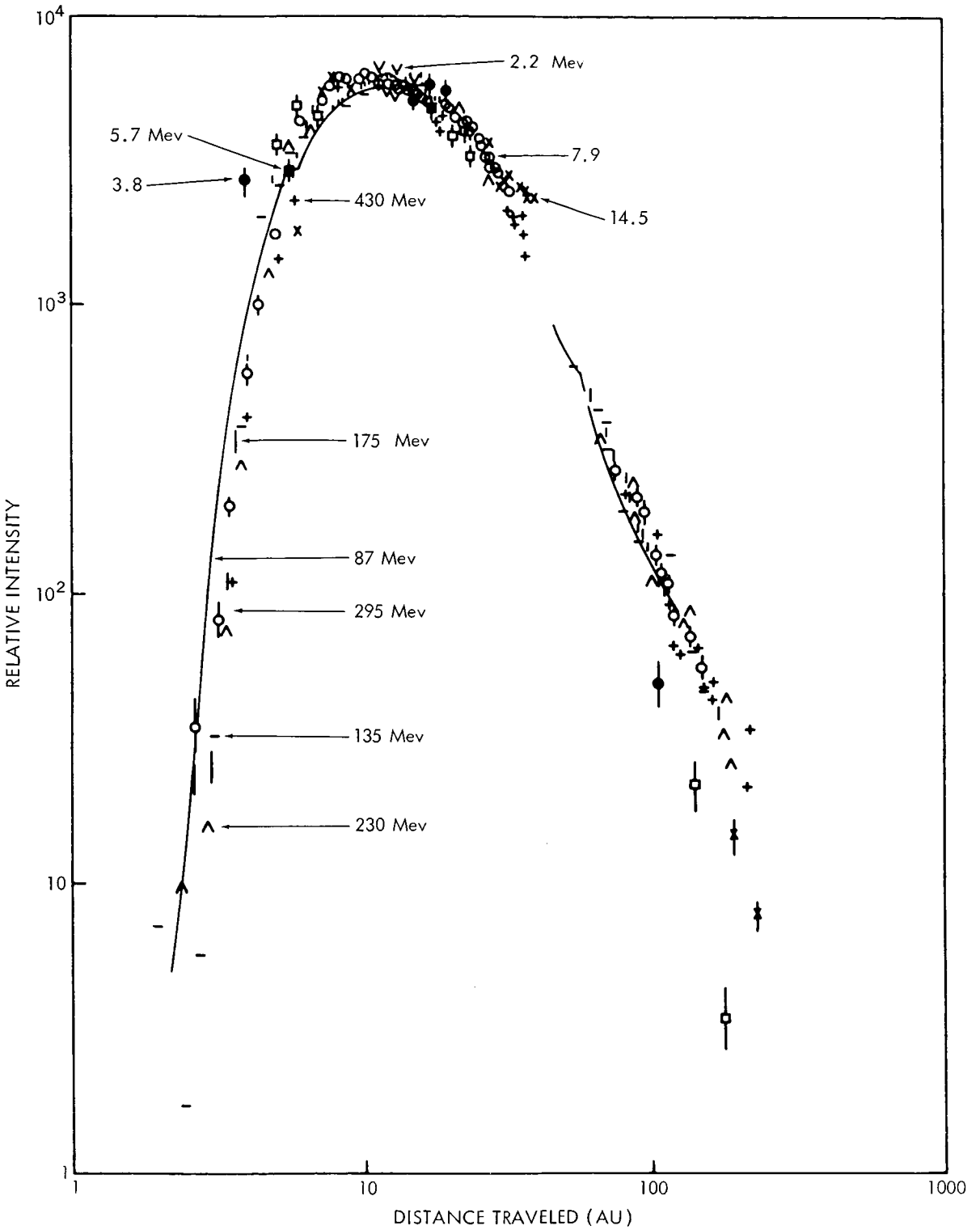
2.2 Mev
5.7 Mev
3.8
7.9
430 Mev
14.5
175 Mev
87 Mev
295 Mev
135 Mev
230 Mev
RELATIVE INTENSITY
DISTANCE TRAVELED (AU)
10^4
10^3
10^2
10
1
1
10
100
1000

FIGURE 34–4.

cannot, by this technique, be sorted from the source characteristics because, for example, the medium could be changing as the particles are propagating through it. In fact, some solar events may thereby be combinations of events of our first three categories. Although our observations indicate that solar proton intensities in some cases depend very closely on the first power of velocity, a choice between velocity and rigidity dependence cannot be made from these data alone. There are indications from earlier emulsion measurements of solar proton and alpha intensities (Reference 4), however, that velocity dependence is preferable.

We discuss now the physical meaning of the scaling factors used to construct Figure 34–4. Let us consider the relative intensity of two components of the event. We have recorded the intensities not as a function of time but as a function of distance traveled and found that the ratio of intensities is essentially constant over a range from 2 astronomical units to more than 100 astronomical units. There is nothing to suggest that an extrapolation back to zero distance is invalid. The ratio of the intensities of two components at zero distance is, by definition, a measure of the shape of the source spectrum. Figure 34–5 shows the source spectrum obtained directly from the scaling factors used to produce Figure 34–4. The source spectra of two other events analyzed in a similar way are also shown. The ordinate of Figure 34–5 is arbitrarily chosen to be the maximum intensity reached at the earth. The differential intensities shown are proportional to the absolute differential intensities of protons produced at the sun and retain, therefore, the same spectral form; but the constant of proportionality depends on the geometry of propagation, which is unknown. (For example, since simple diffusion theory fits this propagation curve through maximum intensity, the numerical solution it gives for the source intensity is of the same spectral form; but that solution is for diffusion in an infinite, isotropic sphere and is probably not a meaningful one.)

We note from Figure 34–5 that the source spectra are commonly very well represented by power laws in kinetic energy. This fact

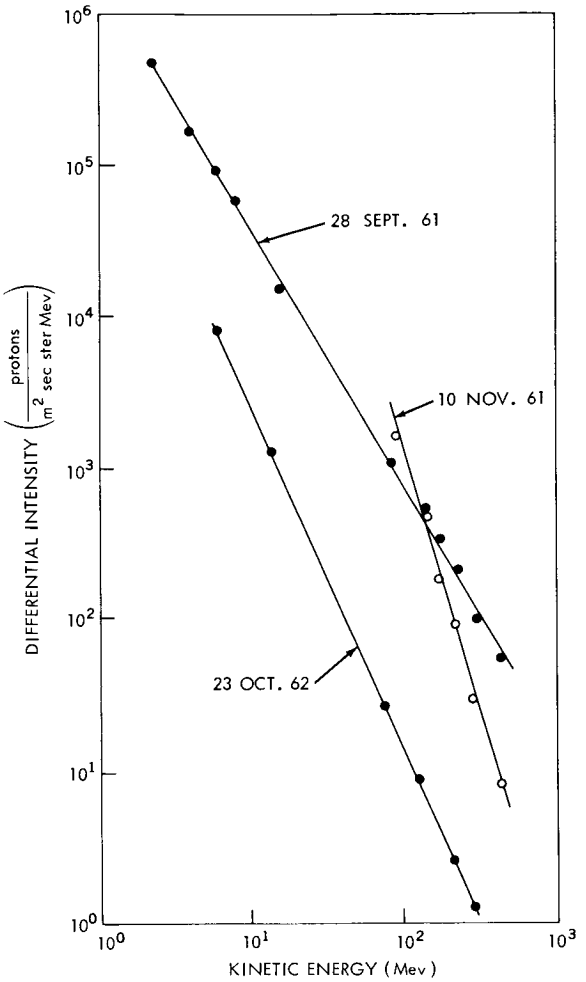

FIGURE 34–5.

prompts us to put forward the argument, based purely on aesthetic grounds, that the amount of matter traversed by the solar protons after acceleration was less than the range of 1 Mev proton—that is, about 1 mg cm^{-2}. It seems highly unlikely that an excess production of lower energy protons would so exactly compensate their absorption in an amount of material greater than their range such as to produce so simple a form of source spectrum.

An interesting feature of these events is the existence of small-scale deviations from a common curve. Superimposed on the generally velocity-dependent intensity-time profiles are fluctuations which are nearly periodic with the same frequency and phase over the entire

energy range studied. These fluctuations are evident in the velocity-ordered events discussed above but are more striking in the September 10, 1961, event which showed no velocity dependence and was no doubt influenced by greater interplanetary disorder. Figure 34–6 shows plots of some sample intensities and indicates the periodic fluctuations. In this event the period is about 1.5 hours; in other events the period is slightly different. Since the transit-time dispersion over the energy range studied is significant, the fact that—in any given event—the fluctuations have the same period and are in phase at all energies shows that their origin is local. We suggest, therefore, that they reflect the magnetic field structure in local interplanetary space, but we as yet have no explanation for their periodicity.

REFERENCES

1. Bryant, D. A., Cline, T. L., Desai, U. D., and McDonald, F. B., 1963, "New Evidence for Long-Lived Solar Streams in Interplanetary Space," *Phys. Rev. Letters*, 11(4): 144.
2. Bryant, D. A., Cline, T. L., Desai, U. D., and McDonald, F. B., 1962, "Explorer 12 Observations of Solar Cosmic Rays and Energetic Storm Particles after the Solar Flare of September 28, 1961," *J. Geophys. Res.*, 67(13): 4983.
3. Palmeira, R. A. R., and McCracken, K. G., 1960, "Observation of a Short-Lived Cosmic-Ray Solar Flare Increase with a High-Counting-Rate Meson Detector," *Phys. Rev. Letters*, 5(1): 15.
4. Biswas, S., Fichtel, C. E., Guss, D. E., and Waddington, C. J., 1963, "Hydrogen, Helium, and Heavy Nuclei from the Solar Event on November 15, 1960," *J. Geophys. Res.*, 68(10): 3109.

DISCUSSION

Mr. Hones: Did you say that in your three recurrent events you did see the discrete event or flare which caused the particles the first time you saw them?

Dr. McDonald: Yes, except the one on September 17. We ascribe this recurrence to a flare on the back side; although I would say that there are other views on that. In other words, there were several active regions right behind the east limb, and so we ascribe the event on September 17 to an active center immediately behind the east limb.

Dr. Winckler: In the case of the 27-day energetic particle observation, do you ascribe this to continued production or storage of these particles? I didn't get that.

Dr. McDonald: We ascribe this observation to the collection of solar or interplanetary particles by a plasma configuration in space. Of course, there could certainly be a PCA on the back side. I think there are particles that have been stored for at least a few days. We can't say there were no PCA's. There could have been additional events on the back side. What this primarily serves is, I think, to map out the effects of one of these streams.

Dr. Winckler: In that case, I think we have to put a new dimension into the decay characteristics of any solar cosmic ray event; namely, that the earth is moving out of a localized angular region in which the high-energy particles are predominantly moving. This sort of Lagrangian coordinate system will produce a sort of decay of the intensity just due to the relative motion which will have to be included in the description of the decay phenomena.

It occurred to me that it also could be used to account for your event behind the east limb which is approaching, and therefore tends to keep the intensity constant with time.

Dr. McDonald: Yes. On the other hand, we find in the event—regardless of latitude—the fact that one is able to get this simple velocity dependence which we think probably can be explained in terms of diffusion in an isotropic medium. This seems to fit regardless of whether you have these streams. We would say that these streams do not exert an undue influence because, for example, we must have

728-629 O—64——20

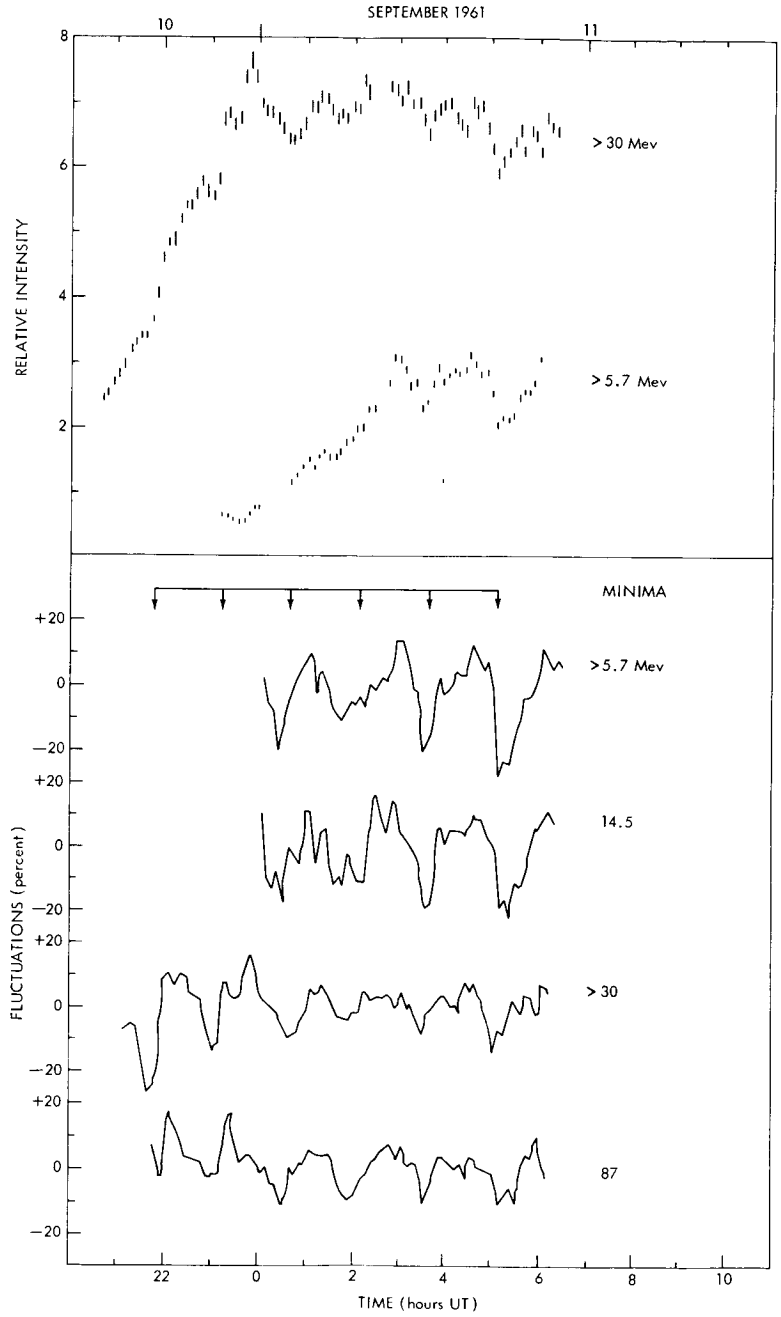
SEPTEMBER 1961
10
11
RELATIVE INTENSITY
8
6
4
2
> 30 Mev
> 5.7 Mev
MINIMA
FLUCTUATIONS (percent)
+20
0
−20
> 5.7 Mev
14.5
> 30
87
22
0
2
4
6
8
10
TIME (hours UT)

FIGURE 34–6.

intersected the stream that produced a very large magnetic storm on September 30. And so you are integrating over a much greater volume. This represents more or less a localized disturbance.

So I wouldn't ascribe too great an importance to it at the moment in looking at the decay of these events.

Dr. Cline: If I could elaborate with a brief comment about the separation that was illustrated between source and propagation of the solar cosmic rays, you might have noticed that the source spectrum of September 28, which was plotted, extends down to 2 Mev with the same unbroken slope on the kinetic energy plot as began at about 600 Mev. Since by definition this is a source spectrum in the sense that it is a spectrum of the particles after all acceleration has taken place, this would imply that—since the spectrum has not yet begun to curve over at 2 Mev—at the point of release of the particles from acceleration to the propagation medium, the protons probably have not gone through much absorber. Because this is a kinetic-energy power law fit and such a fit is extremely unlikely on a random basis, there must be physical significance to it. And, if there is physical significance, then one would expect that—since it does not deviate at very low energies—this means the amount of material the protons have gone through is certainly less than a few milligrams.

I OBSERVATIONS ON FLARES

SESSION D

Chairman, Dr. JOHN C. LINDSAY

Combinations of Observations

N64302865

35 CASE HISTORIES OF FLARES: THE LARGE FLARES OF JULY 11, 12, 18, and 20, 1961

ANTON BRUZEK
Fraunhofer Institut, Freiburg i. Br., West Germany, and Sacramento Peak Observatory, New Mex.

The preceding survey papers and communications have discussed individually the various aspects of the flare event, such as dynamic phenomena, the relation to magnetic fields, the various electromagnetic radiations, and particle emission. The present paper will try to combine and relate the different flare phenomena in order to present a rounded picture of a few particular flare events as a whole.

For this purpose, I have selected a series of large flares which occurred in July 1961 in one of the most active regions of the present declining solar cycle. The investigation of the visible phenomena is based on Hα photographs taken at the observing stations of the Fraunhofer Institute at Freiburg and Anacapri and on flare and prominence films of the Sacramento Peak Observatory, New Mexico, if not stated otherwise. Most of the other data is taken from the current publications quoted at the end of the paper.* Records of Hα linewidths and several radio bursts are from private communications.

THE EVOLUTION OF THE ACTIVE REGION

Before discussing the flares themselves, we have to know the associated active region with its spots and filaments. The spot group had a rather peculiar evolution with three distinct phases (Figure 35–1). On July 8 two tiny spots were discovered near the east limb of the sun within a few bright plage points. By July 9 there already was a penumbra with several umbrae which increased rapidly during the day. By the early hours of July 10 a large penumbra (area, 1286 millionths) had developed, which included a number of umbrae of both magnetic polarities with field strengths up to 2400 gauss. In the course of the day one of the umbrae of south polarity separated from the common penumbra, formed a single unipolar spot, and drifted westward with a velocity of about 1°/day, i.e., about 150 m/sec. This motion continued until July 12, when the spot group reached its maximum area of 1570 millionths. In the next phase, from July 13 to 15, the large penumbra stretched in the meridional direction and decreased slowly in size. On July 15 it divided into a northern and a southern part; the northern part contained northpolar umbrae only, and the southern one also included southpolar umbrae until July 16.

In the course of the next few days (July 16 to 18) the spot area continued to decrease while the two large penumbrae revolved around until, by July 18, the northpolar umbrae and the isolated southpolar spot lay roughly on a straight line. By July 18, moreover, the eastern penumbra was broken into several parts so that the group was made up now of three N-polar and one S-polar penumbral spots. There were no more changes until July 20, when the group reached the sun's limb, except the steady decrease in area due partly to foreshortening effect.

It should be mentioned here that the three other active regions of this solar cycle which produced a comparable number of large flares (June–July 1959, Reference 21; March–April–May 1960, Reference 33; Nov.–Dec. 1960) had about the same configuration as we find in this group after July 10—that is, a large penumbra with umbrae of opposite polarities and an ejected unipolar spot. Different authors (e.g., References 13,

*The Reference and Bibliography section is divided, for the reader's convenience, into three groups. Therefore, reference mention in this paper is not made in numerical order.

JULY 1961

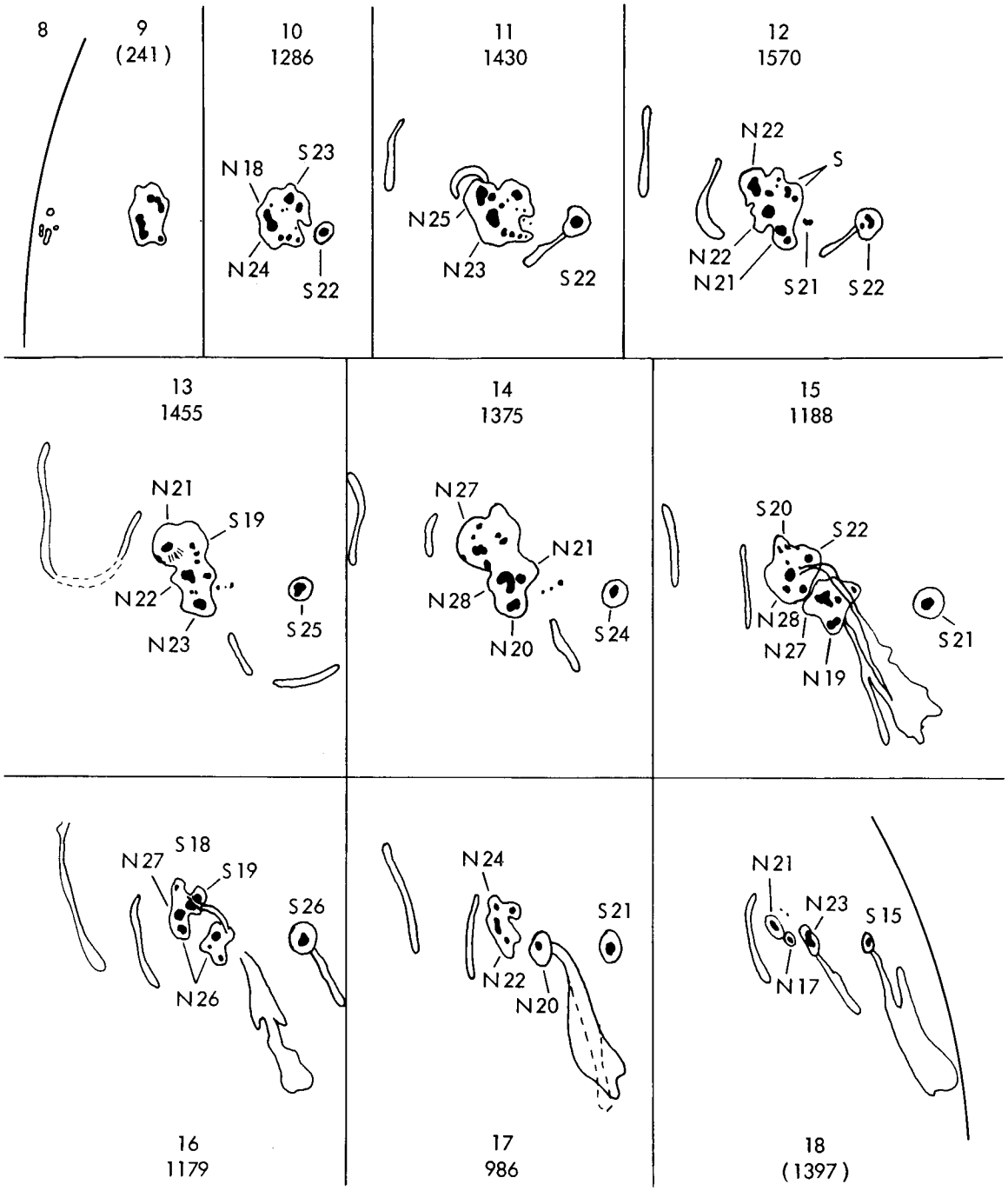

FIGURE 35-1. The evolution of the active region (spots and filaments) of July 1961. The numbers given on top or at the bottom of each frame are the date and the area of the whole spot group in millionths of the visible hemisphere. Numbers inside the frames are the magnetic field strength measured in the umbrae indicated (unit 100 gauss, S=southpolar field, N=northpolar field). Spot areas and field strengths are those given in Reference 3.

18, and 32) have found that large flares apparently prefer spot groups containing umbrae of opposite polarity in close proximity, mostly included in one big penumbra. From the results of the Crimean workers (Reference 26) it seems that steep gradients of field strength—as they exist in such spot configurations—are a necessary condition for the occurrence of large flares and that magnetic field gradients in spot groups are reduced sharply at the time of large flares.

There were obviously considerable changes in spot configuration and consequently also in the surrounding magnetic fields throughout the disk passage of the July 1961 group. It must be pointed out, however, that the gross changes of the configuration observed in this spot group went on more or less steadily. Thus it seems unlikely that they had any immediate bearing on the occurrence of the large flares. The same is true for the active spot groups of June–July 1959 (Reference 21) and March–April 1960. On the other hand, the gross configuration of the filaments associated with the active region did not change very much. The filament in the southeast of the spot group was present in slightly changing shapes, frequently activated from July 11 until the region reached the west limb. On July 11 and 12 only a rather weak filament originated from the isolated southpolar spot. On July 13 a new filament appeared, directed northwest (probably on the dividing line of polarities), which became highly active on and after July 15 and still existed when the spot group passed the west limb.

FLARES OF JULY 11 AND 12

After several flares of minor importance on July 10 and 11, the first major flare occurred on July 11 (Figure 35–2). At 1615 a few points brightened near the N- and S-polar umbrae. The flash phase, however, did not start until 1650, when a rapid brightening occurred in extended areas; the bright points merged rapidly to form two bright ropes bordering the "dividing line" of the magnetic polarities and overlying the two rows of umbrae of opposite polarity. Coincident with the optical flash an SSWF of Importance 3+ and an SCNA effect started, both ionospheric effects indicating the enhancement and hardening of x-ray radiation emitted from the flare region. Moreover, at the same time an impulsive radio outburst on 10.7 cm wavelength started, which was followed within a few minutes by strong bursts in the entire radio frequency (RF) range from 3 cm up to 3 m wavelength. Type II and Type IV bursts were also reported.

At about 1658 the arc-shaped filament was activated and disappeared while the southern flare rope extended, roughly bordering the former location of the filament and gaining maximum intensity and area at 1707. At the same time the maximum intensity of the 10 cm burst was recorded.

The filament reappeared, however, after about 15 minutes—obviously it had just slipped out of the filter pass band because of large Doppler shifts—and it proved to be one of the most persistent elements of this active region. The straight filament originating in the isolated S-polar spot disappeared rapidly after 1716. The flare itself ended some time after 2000 after a very slow fading, whereas the SSWF effect lasted until 2053.

The situation at July 12, 0745, is given by the first frame of Figure 35–3. The spot group had now attained maximum size with 1570 millionths of the sun's visible hemisphere. The general configuration and the field strengths had not changed appreciably; also the dark filaments were again the same as the day before. At 0904 the arc-shaped filament was distinctly active; it was rather diffuse and showed radial velocities, and from 0917 to 0933 a 1+ flare occurred. At 1000 the class 3 flare began with a line of bright points which appeared between the main umbrae and brightened slowly until 1019, when the flash phase started. The points merged and formed two very bright ropes which reached maximum intensity at 1030. By then, each of them covered almost completely all the umbrae of one polarity except the separated southpolar spot. Shape and position were quite similar to the flare of July 11—again, the two ropes bordering the dividing line. The intensity and area of this flare were, however, much higher than at the July 11 flare and the highest in this series of flares. The maximum measured line width of Hα was 9.4A (Reference

JULY 11, 1961

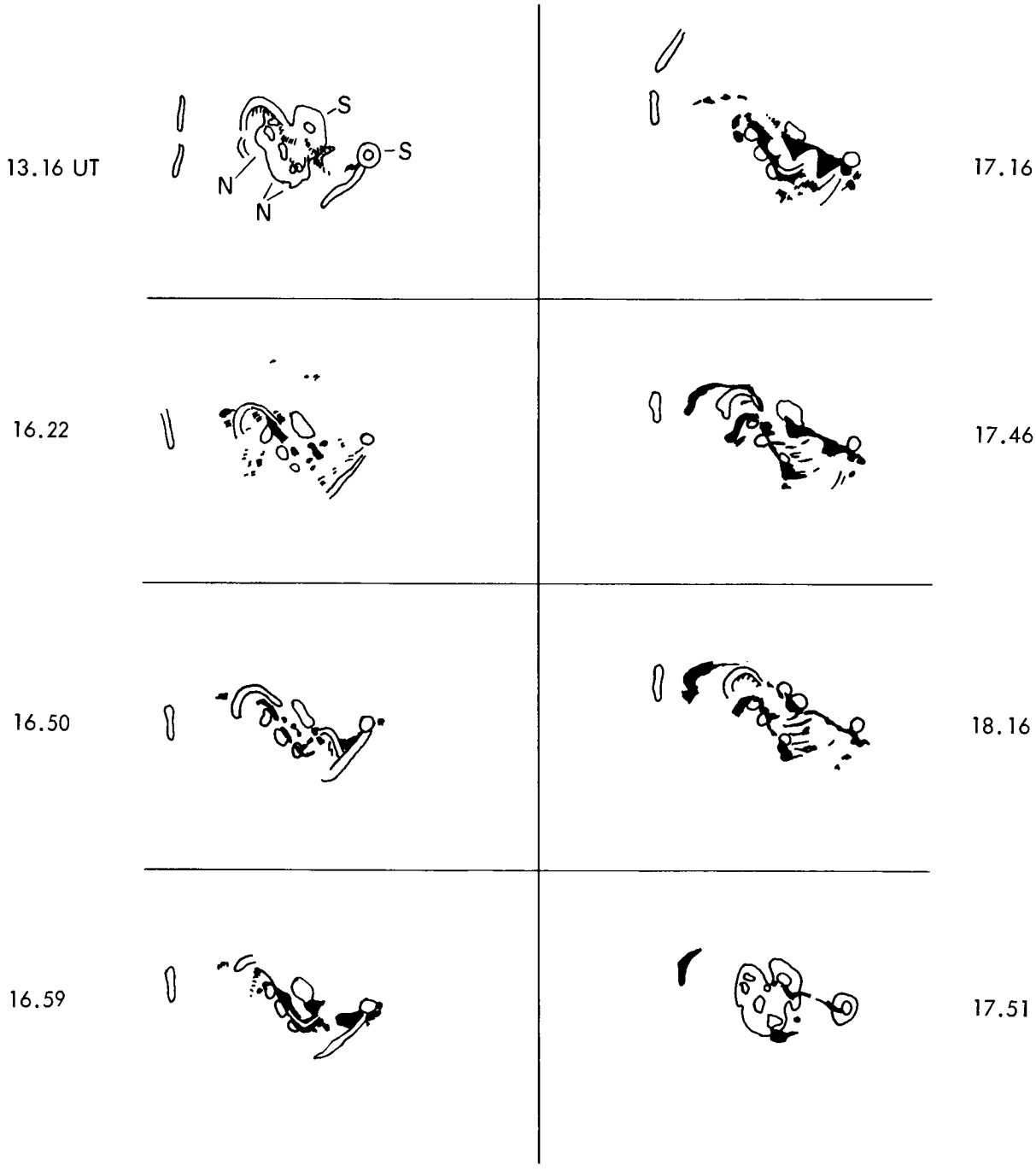

FIGURE 35–2. The evolution of the class 2+ flare July 11, 16.15–20.00, 7S–32E. Flare: full black or hatched; spot umbrae: full line; dark filaments: full line. In the first and last frame the penumbra also is outlined. (Drawings made from flare survey film, Sacramento Peak Observatory)

JULY 12, 1961

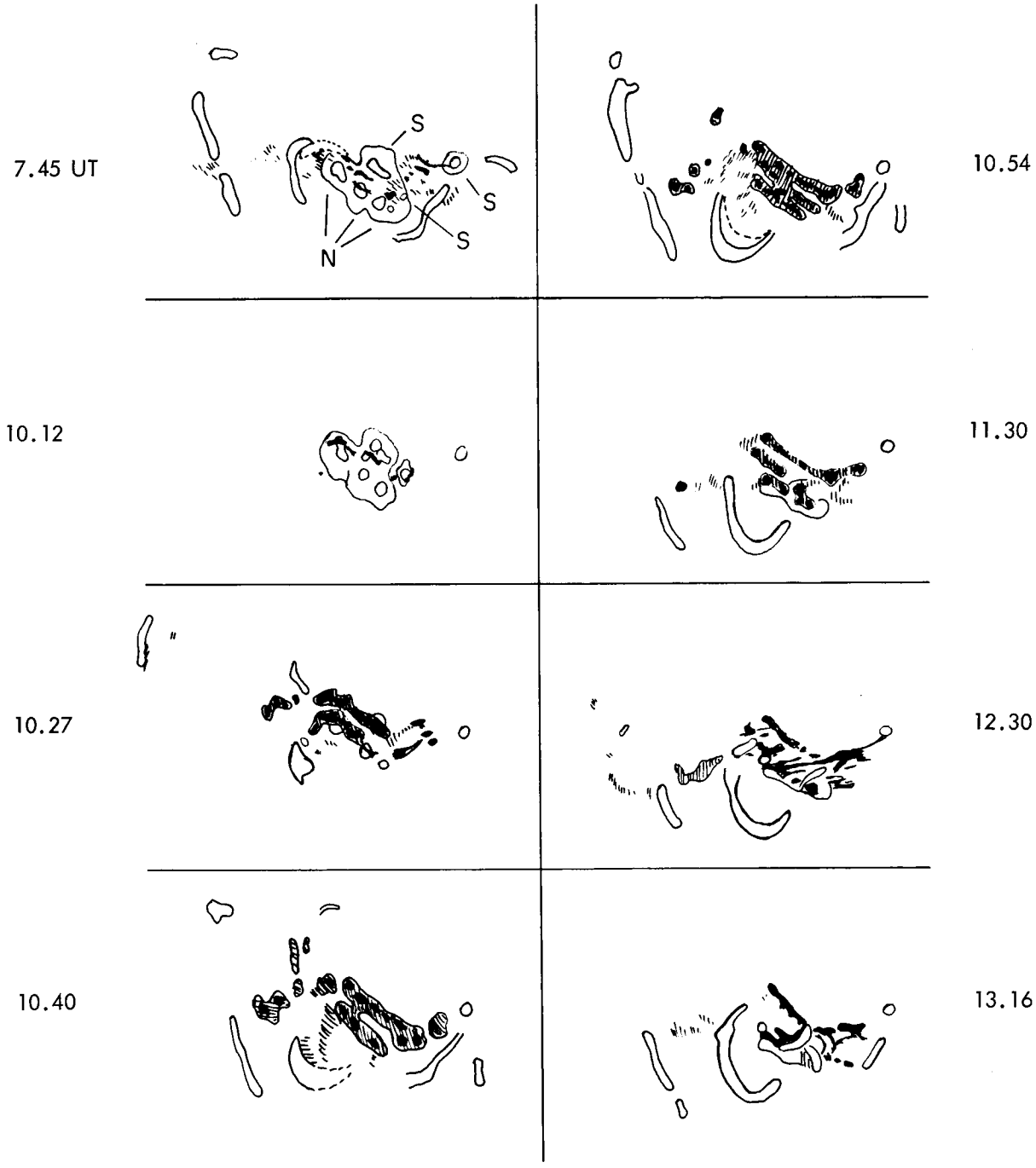

FIGURE 35–3. The class 3 flare July 12, 10.00–12.30, 7S–22E. First and second frames give also the outline of the penumbra; dashed parts of filament at 10.40 and 10.54 were visible in the blue wing only (active filaments). (Drawings made from filtergrams taken at the Fraunhofer Institute, Freiburg and Anacapri; flare in second frame taken from Reference 13)

1), the Hα intensity in units of the adjacent Hα background 2.5 (Reference 13).

Coincident again with the Hα flash started: an SCNA effect; a geomagnetic SFE; a C+ burst in the cm, dm, and m range; and, 3 minutes later, an SSWF 3+ (References 1, 2, and 4). A fadeout already had been reported from a European station beginning at 1003 (Reference 4) and an SPA at 1000. The maximum burst intensity again coincided with the maximum intensity of the Hα emission at 1030.

This close—if not exact—coincidence of the start of the optical flash, x-ray, and radio burst, as well as the coincidence of optical and RF intensity maximum, was obvious also at the flare of July 11 and was noticed at the flare of July 18, too. It is already known from a number of flares (References 13, 14, 24, and 28).

The arc-shaped filament, which had disappeared at the start of the flare, reappeared somewhat dislocated and with strong radial velocities at the time of the flare maximum. Gradually it became stable and partly reoccupied its former place. After 1040 the two flare ropes slowly faded and separated more and more with a velocity of about 2 km/sec (Reference 13).

During the last hour of the flare's lifetime and after its end at 1230, several short bright and one or two dark straight and curved filaments appeared and seemed to bridge the gap between the two flare ropes (Figure 35–3, frames 1230 and 1316). I will refer to these features which could be observed also during the last phases of the July 11 flare (Figure 35–2, frames 1746 and 1816) at the discussion of the flare of July 18.

There was another event apparently related to the July 12 flare. A large quiescent prominence at the east limb at position angle 110 degrees brightened at about 1300 UT and started rising slowly at 1317. At 1409 it was distinctly ascending and had partly disappeared at 1445, the remaining parts now ascending rapidly; by 1609 the prominence had disappeared completely. It is known that stationary filaments and prominences sometimes are activated or even destroyed by the action of large flares. Two types of disturbances originating in flares and affecting filaments have been found: (1) a fast one traveling with velocities around 1500 km/sec and revealing its existence and propagation by a "dark action" on the chromospheric structure, and generally causing a short-lived "winking" of the filaments hit by the disturbance (Reference 17); (2) a slow one traveling with velocities of about 60 km/sec, which was detected by its long-lasting activating (sometimes destructive) effects on distant stationary filaments (References 19 and 20). If such a disturbance started at about the start of the flash phase from the July 12 flares and activated the prominence at the east limb about 70 degrees away after a traveling time of about 3 hours, it would have had a velocity of about 80 km/sec. This is obviously the velocity of the second, slow type of flare disturbance. It is therefore highly probable that the sudden disappearence of the prominence was initiated by the distant flare.

Both flares of July 11 and 12 ejected high energy particles. As a first indication Type IV bursts occurred (Reference 1), which are known to be produced by relativistic electrons accelerated by the flare. There was no ground level increase in cosmic rays, but at 2400 UT on July 11 there occurred at PCA effect announcing the arrival of protons in the energy range 20 to 100 Mev emitted by the July 11 flare. After the July 12 flare the Injun satellite (1961o2) detected 1 to 15 Mev and >40 Mev protons as early as 1717 (Reference 10) and, at about 2000, a strong PCA effect started (References 6 and 7). Maximum flux in the 1 to 15 Mev range and for energies >0.5 Mev (Reference 11) were, however, not attained until July 13 after an SSC at 1113. The measured flux in the 1 to 15 Mev range then was 33,000 particles/cm^2 sec ster (Table 35–1).

On July 13 and 14 the configuration of the filaments did not change and only a few minor flares occurred. The next major flare, a class 2+, occurred in this active region on July 15 during a period of special activity of the large filament. Unfortunately, the flare coincided with another major flare in another active region. Thus it is not possible to decide which flare produced the observed strong SID effects, radio bursts, and high energy particle emission

TABLE 35–1

The Large Flare Events of July 1961 (References 1–9)

Phenomena	Details	July 1961 Date									
		11		12		18		20		21	
Optical Flare	Importance	2+		3		3+		2	2+	?	
	Position	7S–32E		7S–22E		6S–58W		6S–90W		4S>90W	
	Flare onset	1615UT		1000UT		0920UT		1524	1828	<1654UT	
	Flash start	1650		1019		0938		1552	——	(1716)*	
	Flare max	1707		1031		0959			1900	(1725)	
	Flare end	2000		1230		1400			1940	(1815)	
	Hα LW max	4.3A		9.4A		6.7A			6.7A		
	Area max	12 sq. deg.		17		26					
X Rays	SFE			1021–1052UT		0945UT		1552UT			
	SSWF	1648–2053	3+	1023–1230	3+	0940–1153		1550–2200	3+	1702–1815	2+
	SPA	1600–1930		1000–1300		0953–1036		1549–1615–1830		1702–1900	
	SPA max	1710		1040		1008		1557		1710	
	SCNA	1650–1750		1020–1133				1552–1240		1703	
	SCNA max	1704UT	76%	1035	43%				88%	1708	20%
Radio Bursts	2800 Mc/s	1650–1845		1018–1145		0938–1043		1552–2100		1655, 1701–1721	
	2800 Mc/s max	1705UT	1500†	1029UT	6000†	0958UT	2400†	1621UT	1800†	1703UT	59†
	200 Mc/s	1657–1847		1022–1142		0944–1044		1554–1613		1707–1710	
	200 Mc/s max		>900†	1031	22, 000†	0957	1000†	1600	4000†		36†
	Type II	1701[5]–1718						1554–1619		1704–1722	
	Type IV	1655–1845						1552–1629			
High Energy Particles.	Cosmic rays‡					1000	+12%	1610	+5%		
	PCA start	2400UT		2000UT		1145UT		(21.) 0300			
	PCA max		—1.5db	1400††	—20db	2100	—14db		—5db		
	Protons:										
	>0.5 Mev max.**			1546††	2×10^5						
	1–15 Mev start**			1717	410	1327	40				
	1–15 Mev max.**			1416UT††	33, 000	2232	1100	1921	570		
	>30 Mev†††	2×10^6		1.0×10^8		2.1×10^8		9×10^6			
	>100 Mev†††	3×10^5		1.6×10^6		4.8×10^7		1.2×10^6			

*Flare spray.
†Unit: 10^{-22} w/m² (c/s).
‡Ground level effect.

**Unit: Particles/cm² sec ster.
††July 13.
†††Unit: Integrated intensity particles/cm² sec.

(Table 35–1). July 16 was a quiet day. On July 17 a class 2 flare was observed from 0720 to 0910 which, however, did not produce strong bursts or SID effects. The large filament was very active throughout the whole day, showing considerable changes and internal motions.

THE FLARE OF JULY 18

In the early hours of July 18 the arrangement of the filaments had somewhat changed, compared with July 17 (Figure 35–4). A large active filament originated now at the isolated S-polar spot and extended north, and only a small filament was associated with the neighboring N-polar spot. The slightly curved filament in the east of the spot group still existed.

From 0754 to 0830 a flare of class 2 occurred in the spot group. There were again a few bright points visible near one of the larger northpolar umbrae between 0911 and 0916 until a new flare definitely started at 0920 with the brightening of several points. Within the next few minutes the thin dark filament became activated (as it was before), and the flaring points merged to form a bright filament which extended rapidly towards the newly activated filament. The flare brightened quickly after 0938 but did not yet grow much in area. When the flare had reached the active filaments, they disappeared rapidly between 0946 and 0947 from the on-band pictures (taken in the center of the Hα line) but were still visible off-band on the blue side until about 1000; apparently the filaments were ascending with velocities of about 50 to 100 km/sec. They reappeared on July 19, and one of them was blown off again on July 20 by a limb flare. At that time the entire eruptive event could be observed outside the sun's disk.

After the large filaments had disappeared, the flare expanded in all directions bordering the location of the recent active filaments as well as enclosing the curved dark filament in the east. The curved filament itself was not affected by the flare in any way.

This creeping of the flare along a filament—activating or destroying it or not—or along the location of a filament which has just disappeared is a rather common feature. It was also noted at the flares of July 11 and 12. This kind of expansion often is part of the flash phase and results in a prolonged flash and a considerable enlargement of the flare.

By 0955 (see Figure 35–5) there was an indication of splitting of the main flare rope and by 1002 actually two parallel ropes had formed, one of them completely covering one of the N-polar umbrae. The two parts separated gradually—each expanding itself—at an apparent velocity of about 3 km/sec. They connected or even covered all N-polar spots but did not reach the S-polar umbrae in any phase of the flare. Particular features of this flare were the thin bright loops which became visible after 1015 and obviously connected the two flare ropes. They expanded within the next hour at a rate of about 4 km/sec. They were well visible until 1117 and had disappeared by about 1200. These loops apparently were a system of loop prominences seen projected on the disk. Comparing them with the thin dark and bright threads connecting the flare ropes of July 11 and 12 (Figures 35–2 and 35–3), we may suppose that those less distinct features also were loop systems.

The splitting of flares and the apparent divergent motion of the two bright ropes is a feature common to many large flares, especially to cosmic ray flares and proton flares (References 14, 18, 20, and 22). It also could be noticed at the flares of July 11 and 12, which showed shapes and motions similar to those of the July 18 flare. In each case the splitting occurs along the dividing line of the magnetic polarities, and the two ropes move apart from this line (which may be marked by a thin dark filament) into regions of opposite polarity at velocities of a few km/sec. In many cases one rope connects or covers the umbrae of one polarity, and the other one connects the umbrae of opposite polarity. When the separation of the flare ropes had become rather conspicuous, loops or loop systems connecting the flare ropes became visible in a number of cases either in absorption (References 22 and 25) or, as on July 18, in emission. The loops seem to be rooted in the flare ropes and to increase at a speed of 5 to 10 km/sec as the flare ropes move apart. A large loop system related to the

JULY 18, 1961

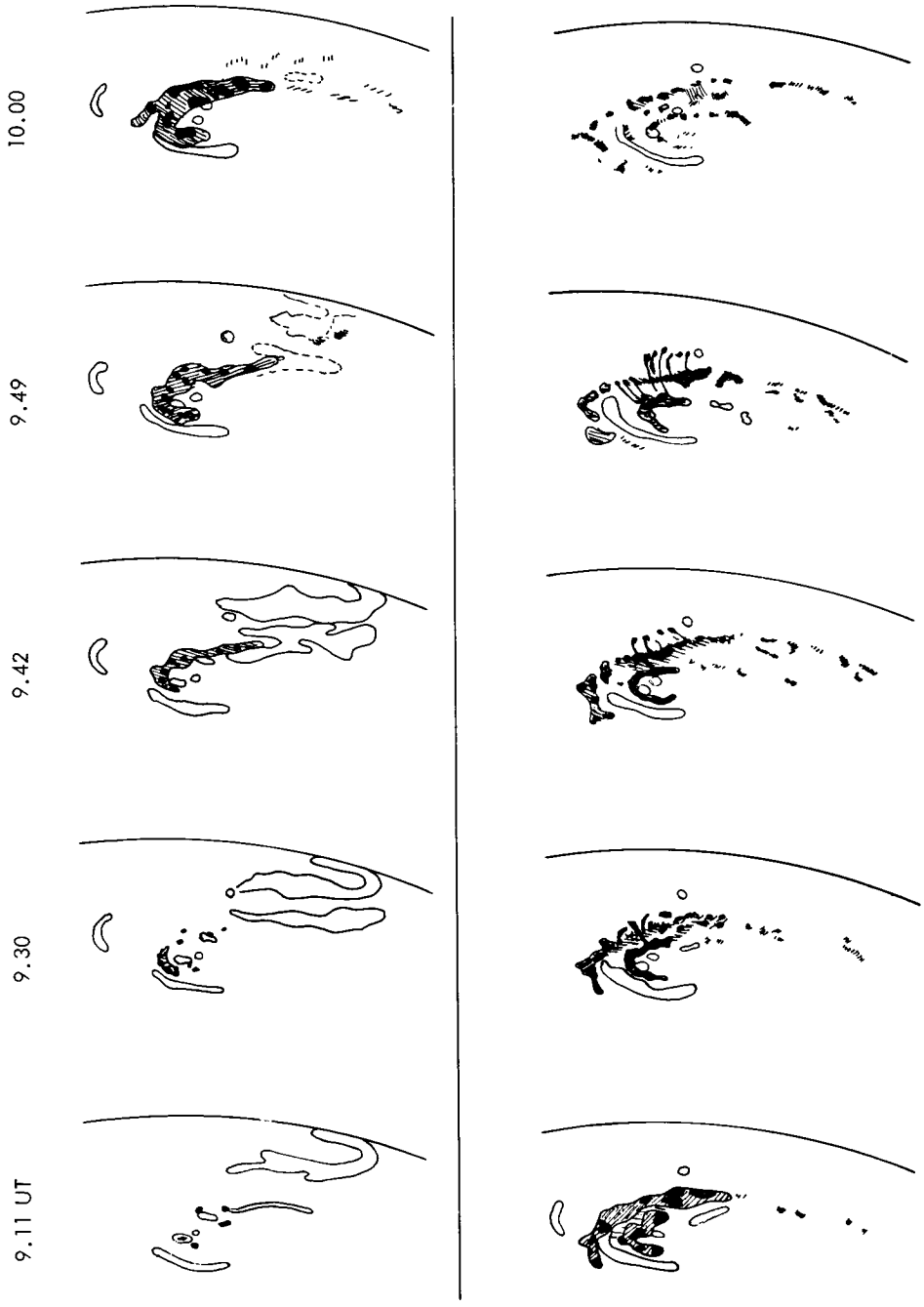

FIGURE 35–4. The class 3+ flare July 18, 09.20–14.00, 6S–58W. Flare: black or hatched; filaments and spot umbrae: full line; dashed filaments visible in the blue wing only, ascending (9.49, 10.00). (Drawings made from filtergrams taken at Fraunhofer Institute, Anacapri)

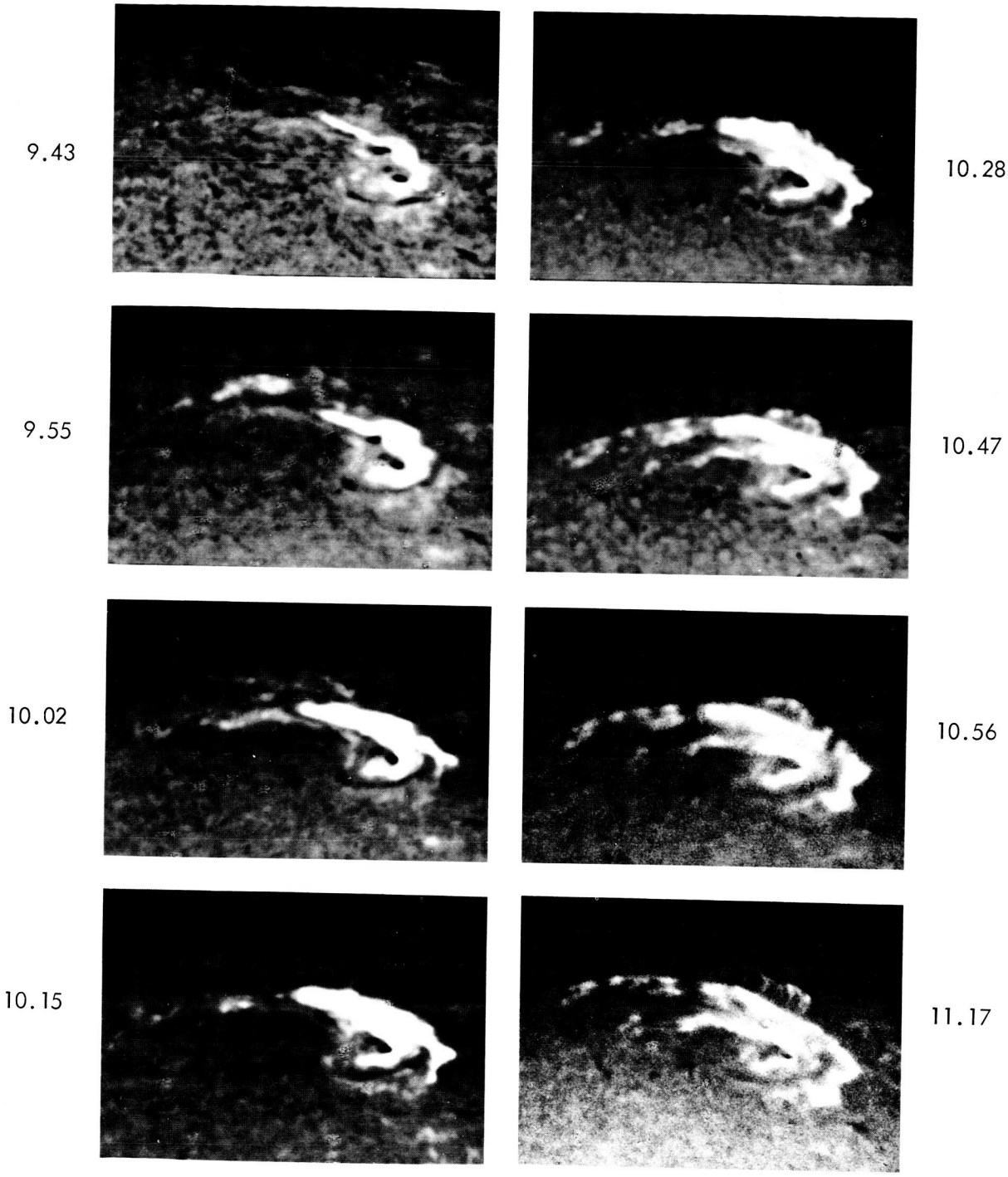

FIGURE 35–5. The flare of July 18, 1961. (Filtergrams at Fraunhofer Institute, Anacapri)

limb flare on July 20 occurring in the same active region will give us some evidence about the formation and growth of such loops. It appears that all typical large loop prominence systems are formed in association with large flares at about 1 hour after the flare flash (Reference 23).

The flare of July 18 had two distinct flash phases. From the Hα intensities plotted in Figure 35–6 (Reference 13) we find an optical

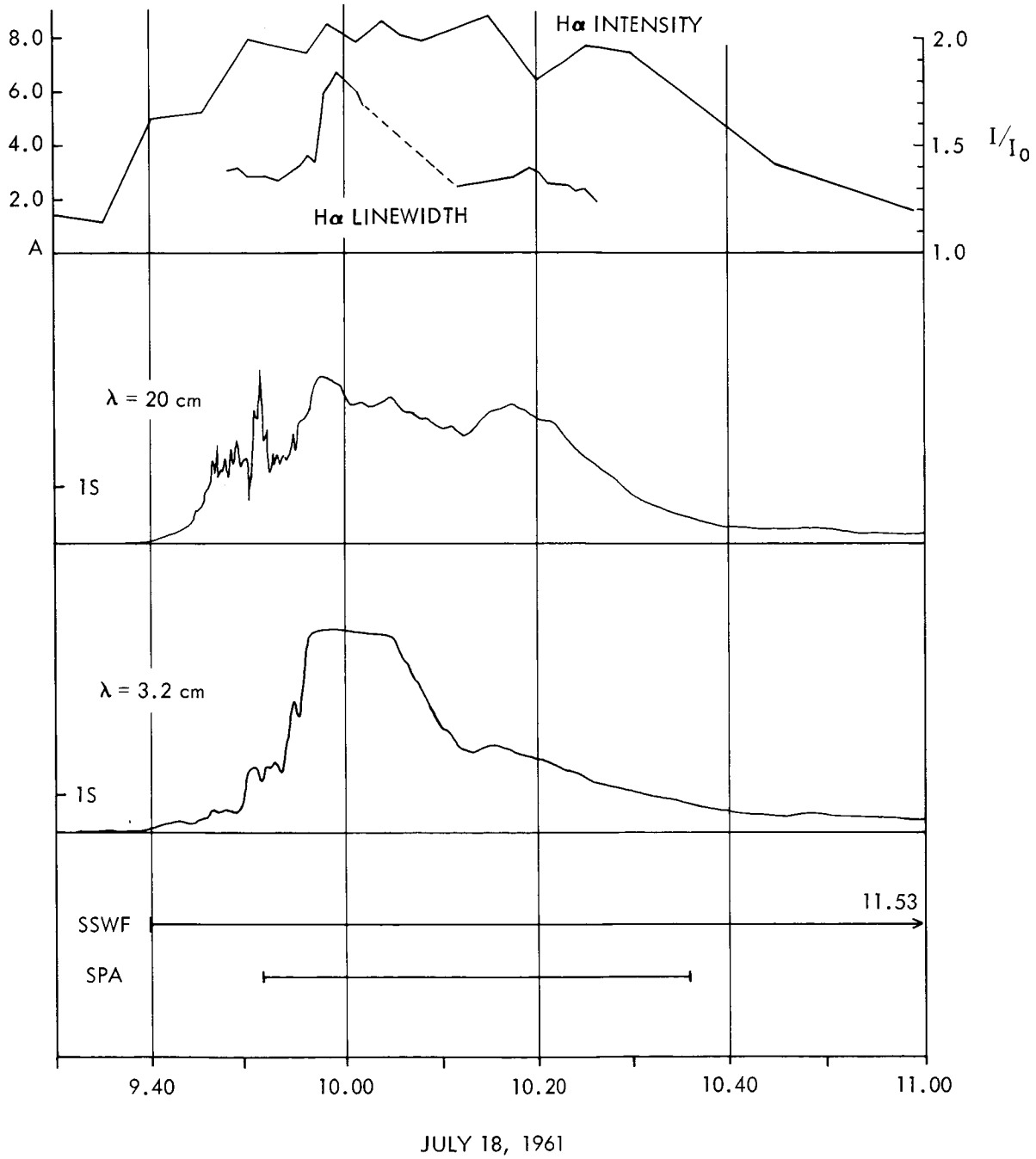

FIGURE 35–6. The time relation between optical, radio, and x-ray emission at the flare of July 18. Hα intensity M. A. Ellison (Reference 13); Hα linewidth: Observatory Ondrejov (courtesy Dr. Svestka); radio bursts: Heinrich Hertz Institut, Berlin (courtesy Dr. Mollwo); SID effects: Reference 2.

728-629 O—64——21

flash starting between 0935 and 0940 UT. The beginning of an SSWF effect was reported from European stations at 0940 (Reference 4), indicating enhanced emission of x radiation from the flare. And at 0938 and 0939 strong C+ outbursts started in the microwave region up to 20 cm. The graphs of Hα linewidth and burst intensities (Figure 35–6) indicate, however, the beginning of a second even more pronounced flash at 0952 to 0954; an SPA effect started at the same time. Notice that this flash coincided with the blowoff of the large active filaments and the following period of fast expansion of the flare. The maximum intensities were gained in the microwave range at 0957, 0958 (>2400 units) and in the *Hα* linewidth at 0959 [LW=6.7A (Reference 1)]. The Hα intensity reached maximum at about 1010. Intense bursts down to 15 Mc/s on m wavelengths started 0943 to 0946 and already had intensity peaks up to 3000 units between 0952 and 0957 (Reference 35). Thus this flare also showed the striking coincidence of beginning and maximum intensity of all observable electromagnetic radiations. It suggests that all these radiation bursts have some impulsive event as a common cause. The fact that the m wave bursts (Type IV burst), which are produced high in the solar corona by synchrotron radiation of trapped relativistic electrons, reach their maximum intensity during the flash means that the electrons have been accelerated and ejected at about the start of the flash. Thus it seems probable that the radiation bursts are related to the ejection of high energy particles. (It should be noticed that the Hα linewidth seems to be a better indicator of the flash phase than is the *Hα* intensity. I therefore want to suggest that these simple linewidth measurements should be continued on a regular basis.)

We may assume that the heavy particles (protons) are accelerated and ejected at the same time as the electrons, that is, during the flash. Actually, high energy particles had already arrived at the earth during the lifetime of the flare. At about 1000 UT—20 minutes after the start of the flare flash—the intensity of cosmic rays as measured by neutron monitors at ground level increased (Reference 2), indicating the arrival of >1 Bev protons. Their flux attained a maximum of about 12 percent above normal (galactic) intensity at 1145. At 1140 the Injun satellite detected solar protons of energies >40 Mev at a rate of 350 particles/cm^{2}sec (Reference 10), and at 1145 a PCA effect started (References 6 and 7). 1 to 15 Mev protons from the flare were first observed by Injun at 1327; their flux reached maximum at 2232 (1100 particles/cm^{2}sec ster) at about the maximum of the PCA effect (2100). It is remarkable that the energy spectrum of this particle event is much harder than that of the July 12 flare (Reference 11). The ratios of 1 to 15 Mev to >40 Mev maximum proton flux were 1650 and 1.2, respectively, for the two flares.

The July 12 flare produced no ground level increase of cosmic ray intensity, although its output of electromagnetic radiation was considerably higher on all wavelengths than that of the July 18 flare. Apparently the particle fluxes measured on and in the vicinity of the earth are highly dependent on the position of the flare on the sun and the magnetic conditions in interplanetary space and are not only determined by the flare itself (see References 13 and 37.)

FLARE EVENTS ON JULY 20 AND JULY 21.

From disk observations we get rather poor information on the extension in height and the spatial structure and motions of flares and related phenomena. This is true for instance for flare expansion, prominence activation, and surge and loop formation. We can have this information from observations at or near the limb provided we know how to identify corresponding limb and disk features.

The active region under consideration presented the rare opportunity to compare observations of corresponding limb and disk features, because it repeated a number of disk events when it was located on the limb on July 20. Comparing the configuration of filaments and spots on July 19 with the limb view of the active region on July 20 as given in the first two frames of Figure 35–7, we easily realize that the two prominences on the

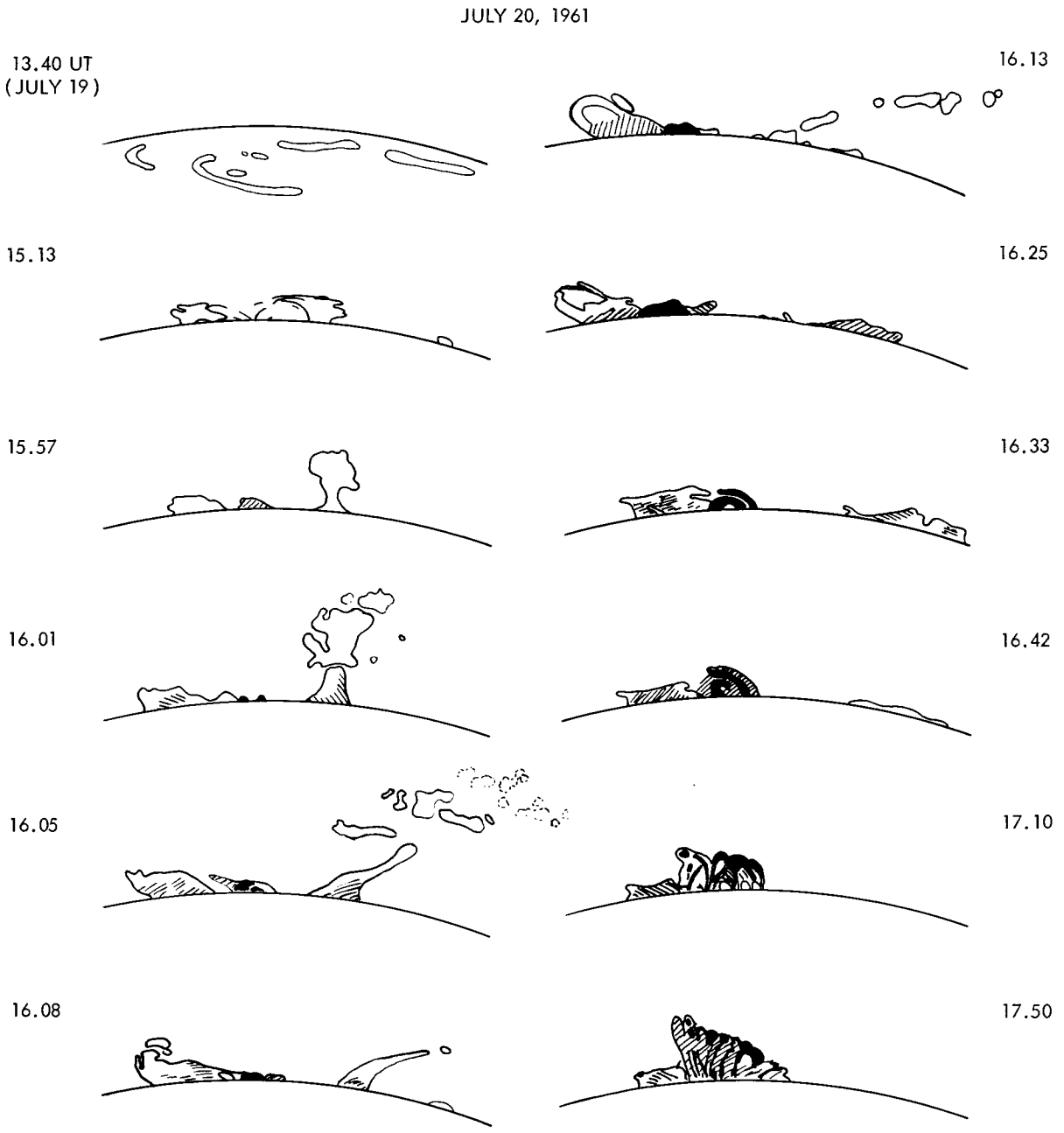

FIGURE 35–7. Flare and associated phenomena July 20, 1961, flare 15.52–1800, position angle 264 degrees. First frame: the active region on July 19; filaments and umbrae: full line. Limb phenomena are shaded according to brightness: Flares are full black; enhanced prominences and surges are hatched; prominences and surges of normal brightness are drawn in full line. The shading of the loops is made one grade darker. (Drawings of Figures 35–7 and 35–9 are made from flare survey and prominence films of Sacramento Peak Observatory.)

limb correspond to the curved filament and the straight filament, respectively, of July 19 and the preceding days. The small hump in the north obviously corresponds to the second, northern straight filament.

The two large prominences were active throughout July 20, being connected by thin streamers with the location of the spots. From 1524 to 1550 a small limb flare occurred approximately at the position of the spots (maximum intensity at 1535) without any effect on the prominences, which did not change during this period. At 1550, however, a remarkable sequence of flare events started, including a number of related prominence features.

By 1549 an SPA already had begun, and at 1550 a strong SSWF effect; and at 1552 an SEA, an SCNA, and a geomagnetic SFE started, all indicating the emission of enhanced x rays. Also, at 1552, an impulsive microwave burst started (References 2 and 5). It was already pointed out that these x ray and RF bursts are typical for the start of the explosive (optical flash) phase of a flare. Unfortunately, there was no optical observation between 1550 and 1553. An Hα filtergram of Ottawa, however, which was taken after a 2 minute gap in the Hα survey coverage showed (Reference 16) a bright small arch and a surge-like feature on the limb at 1553. This little ejection may be considered as an optical indication of the flash (explosion) of a flare mostly situated behind the limb. Within the next minutes this explosion revealed its existence, however, in a far more conspicuous way: At 1554 the northern prominence became strongly activated and straightened out from that arc inclined toward the flare (Reference 16). It increased rapidly, bent away from the flare, and finally was ejected into space at a speed of about 400 km/sec. The prominence was literally blown off by the action of the flare and had disappeared completely by 1620. You may remember that on July 18 the corresponding filament was also blown off rapidly after the flash phase of the flare had started. This was the first repetition of a disk event.

The visible flare proper consisted of only two small bright humps on the limb at 1601 and was growing only slowly during the next half hour. At 1602/1603 again a surge-like feature was ejected—now toward the southern prominence. The prominence started to increase and to brighten at about 1604 and became obviously more and more activated. During the maximum phase it developed a big arch which faded rapidly after 1625. The activation was only a transient one, after which the prominence immediately took its former shape at about 1640. It may be noticed that the curved filament to which this prominence corresponded has been activated many times by flares during its disk passage and that it had formed that conspicuous dark loop during the flare of July 12 (Figure 35–3). Now we realize—what was impossible from the disk observation—that this dark loop had been extending out into the solar corona. Such a loop was formed again 3 hours later during the next flare in this active region.

By about 1614 the little hump north of the active region, which was identified with the second straight filament, became conspicuous; it increased and brightened until about 1625. This was apparently another activation produced by the flare. The prominence faded and decreased again until 1650. Thus all three prominences in the vicinity of the flare—which we had seen as filaments on the disk—were affected. One was completely blown off within the first 30 minutes of the lifetime of the flare; later the other two were strongly enhanced and activated for about half an hour.

From the strong x-ray and RF bursts and the powerful actions on the surrounding prominences, we must conclude that the related flare was a large one despite the fact that it appeared as a rather small feature on the limb. Probably the main part was situated behind the limb and had no great extension in height. There was no part of the flare visible on the disk at any stage of evolution.

After 1630 the flare started to expand faster and to show distinctly internal structures as loops and arches. Within the next hour the typical knots and loops of a loop prominence system were gradually formed above the flare in increasing heights. The rate of growth of the system was about 8 km/sec until it reached

its maximum height and intensity at about 1800. The system of July 20 demonstrates how the loops are formed out and above the flare. It appears that there was not much real ascending or expanding motion except in the first phase (the transition between flare and loop system), when the flare itself seemed to expand. The whole loop system was enlarged as new knots and loops condensed out of the corona in gradually increasing heights, but the individual loops did not increase or expand very much (see also Reference 36).

The complexity of this flare event—as it was just depicted—is also found in surprising coincidences in the RF radiation and partly also in the x radiation. Figure 35–8 shows the records of the microwave bursts on 20, 15, and 3.2 cm from the Heinrich Hertz Institut, *Beobachtungsergebnisse* Juli 1961 (Reference 5), the SCNA record from Lake Angelus (microfilm), and the period of the SPA and SSWF effects. At the bottom of the figure, the important Hα events are marked by different signs. The coincidence of the starts of x-ray initiated effects and the RF bursts is obvious.

It can be noted, moreover, that the beginning of the three prominence activations apparently closely coincided with the beginnings of the individual microwave bursts at 1552, 1604, and 1612½. In the first two cases the activation was preceded by small surges. The radio burst probably was produced by the related flare impulse. The same may be true for the third activation. There seem also to be coincident enhancements of the SCNA (this relation, however, is not quite clear); and at 1614 a new SPA effect started.

Gaizauskas and Covington (Reference 16) had suggested that the post-burst microwave emission was associated with the prolonged activity of the loop prominence. Using the Ottawa Hα observations, they could not find a detailed relation between loop activity and the numerous post-burst maxima. From the Hα prominence film of the Sacramento Peak Observatory (SPO), I determined the times when a new prominence knot just became visible. These are marked in Figure 35–8 by vertical lines designated "knots." There are apparently a number of coincidences between knot formations and various peaks of microwave radiation. It was found that the onsets of microwave peaks occurred 55 sec before the knot formation and the intensity peaks 22 sec after the knot formation (mean values from nine cases). That means that the condensations started to emit microwaves about 1 min before the Hα emission began. This coincidence may, of course, be fortuitous because of the narrow sequence of emission peaks. The fact that the knot formations occurred at about the same intervals as the emission peaks seems to confirm, on the other hand, that there is a relation between the two phenomena. Kleczek and Krivsky (Reference 30) had observed three cases of sudden loop formation related to the flare of May 4, 1960, and found that they also were associated with distinct bursts on the wavelengths 37, 56, and 130 cm preceding the formation of the loops by 2 to 4 min. There also were unusual long SID effects after this flare; the SSWF effect lasted until 2200, and the SCNA until 2140. As there occurred no other phenomenon which could have been the source of the prolonged ionizing radiation, it seems highly probable that this x-ray emission also was associated with the loop prominence. The general intimate relation between x-ray and cm burst emission (References 27, 29, and 31) supports this assumption.

It should be mentioned here that Jefferies and Orrall (Reference 34) in spectra of loops have found very broad wings of the Hα line which give evidence to the existence of H atoms with energies in the kev range inside the knots.

This flare ejected high energy particles also which at 1610—20 minutes after the flash start—produced a ground level cosmic ray increase with a maximum of 5 percent at 1625 (Reference 2). At 0300, July 21, lower energy protons arrived, indicated by the start of a PCA effect with a maximum absorption of 5 db (Reference 7).

At 1828 a new flare brightened on the limb at about the same position as the first one in front of the large loop system (Figure 35–9). It expanded and spread out toward the prominence in the south. By 1853 that prominence gained flare brightness and became strongly

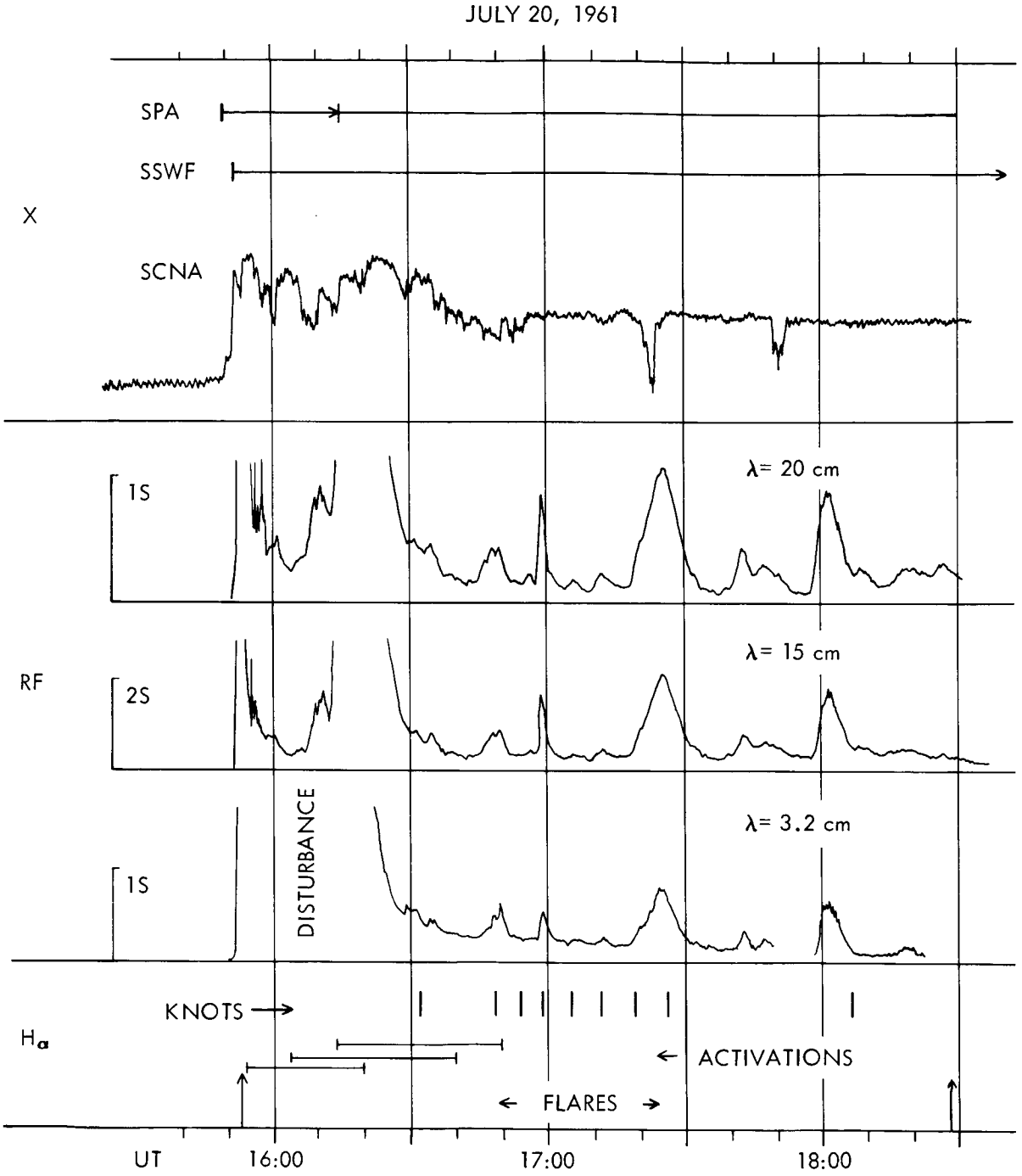

FIGURE 35–8. Coincidence of SID effects, radio bursts, and visible flare phenomena July 20. Radio bursts: Heinrich Hertz Institut, Berlin (courtesy Dr. Mollwo).

activated once more. It produced a large surge at about 1900 which formed a loop at 1930 very similar to that loop associated with the first flare of this day. At 1940 the flare had faded, at 1950 the loop had disappeared, and the prominence was still slightly active in the

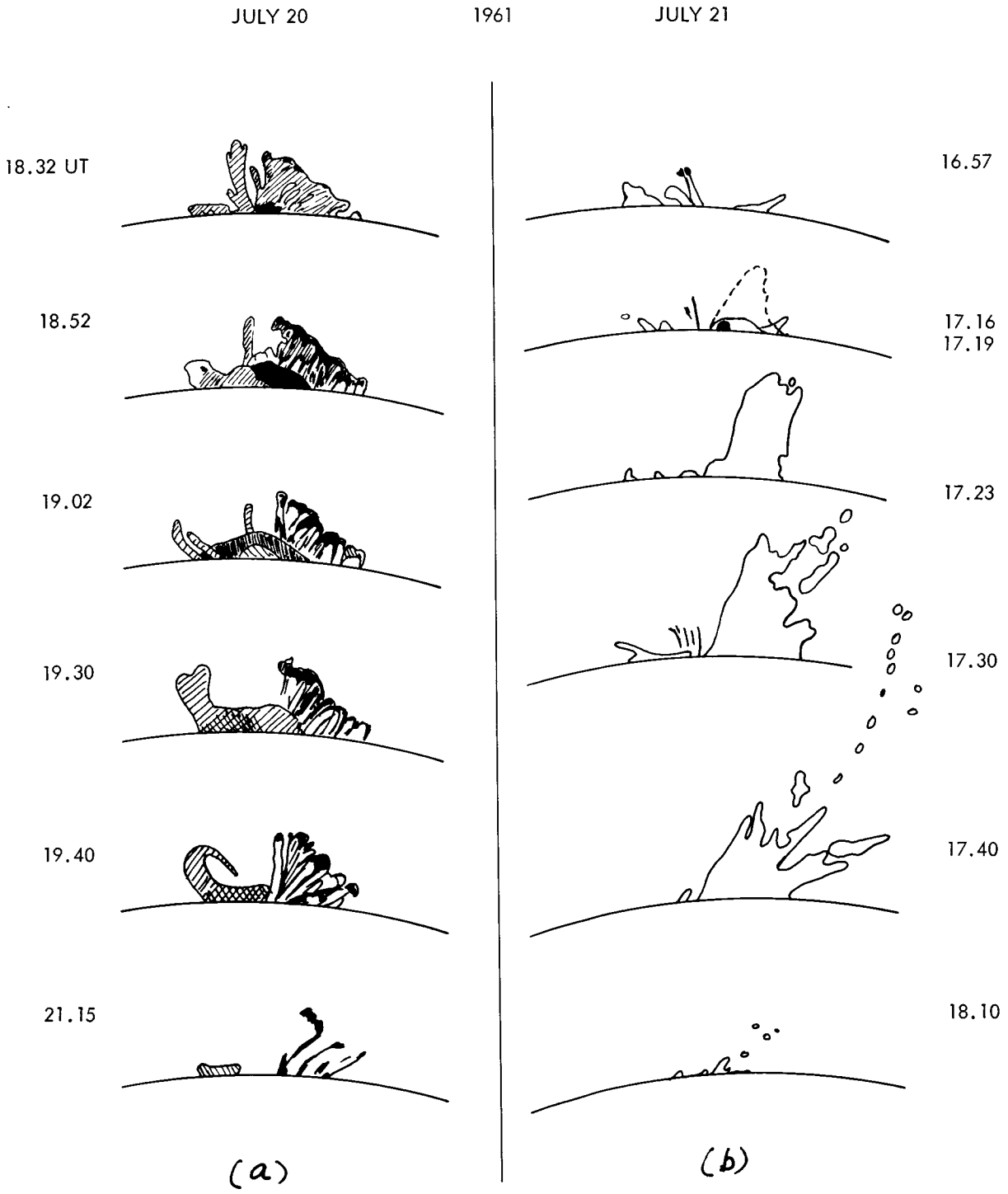

FIGURE 35–9. (a) The second flare of July 20, 18.28–19.40, position angle 264 degrees (explanation, see Figure 35–7). (b) The active region on July 21; loop prominence and giant spray 17.16–18.15, position angle 266 degrees.

course of the next hours. This flare produced no conspicuous RF or x-ray bursts. It is remarkable that the loop system was not effected by this flare. It kept slowly fading and decreasing until the end of observations at SPO at about 2330. There were a few bright knots and loops visible at the same position even the next day. Thus the lifetime of the system certainly exceeded 7 hours and probably was about 25 hours.

JULY 21

On limb photographs taken at 1654 and 1657 there was a bright hump made up of a few bright points in the latitude of our active region (Figure 35–9). It had not been visible at 1642, and decreased and faded until 1720. Because of its low brightness it was not rated as a flare. It might, however, have been related to a flare behind the limb because there were weak radio bursts on 2800 and 800 Mc/s at 1655 and 1656, respectively. At 1701 and 1702 bursts followed in the cm and dm range, at 1702 an SSWF 2+ and an SPA started, and at 1703 an SCNA effect began with 20 percent maximum absorption. The radio bursts had already attained maximum intensity at 1703½ (References 1 and 2).

All these events indicate, as we know, the flash phase of a flare, in this case obviously of a nonvisible flare. Fourteen minutes after the burst onset—at 1716—a bright point suddenly appeared on the limb, increased rapidly in height at a rate of more than 200 km/sec, forming a huge spray-type prominence (Figure 35–9). The main body reached maximum height at 1725 (h=100,000 km); the largest height reached by the ejection was 300,000 km at 1740. After 1735 the main body collapsed, and the entire spray had disappeared by 1815. At the same time the SSWF ended. This spray was rated by different observers as a flare of class 2 or 3 (Reference 1). The proper flare, however, was certainly hidden behind the limb; and its occurrence was indicated by the x-ray and radio bursts starting at 1702, as well as by the delayed visible spray. If indeed the flare occurred in our active region—and there is almost no doubt about that—it was situated about 13 degrees behind the limb. The x-ray and radio bursts related to the flare then were produced in levels at least 18,000 km above the chromosphere; otherwise we would not have observed these radiations. This case proves that we well may receive the x-ray and radio emissions of a flare without having any direct optical evidence of its occurrence.

This was the last eruptive event observed in this unusual series of large flares. When the related active region returned in the next solar rotation, it had faded to a dispersed plage region which contained no spot, only a few thin filaments, and produced no more flares.

THE FLARE EVENT: A SUMMARY

This series of large flares exhibited almost all the presently known flare phenomena. Combining and relating them, we get the following picture of a "complete" large flare event.

At first a few points brighten in the Hα plage—generally close to a spot or near the "dividing line" of the polarities, according to Severny in the neutral points of the magnetic field. The points merge to form one or two brightening and expanding ropes coincident with or bordering the dividing line of polarities. In this first, *pre-flash phase* of flare evolution the flare may already attain area and brightness of a class 1+ or even class 2 flare; sometimes, short radio bursts on discrete frequencies and some of the most sensitive SID effects (SPA, SEA) are detected. The pre-flash phase may be accompanied by the activation of a dark filament associated with the active region. About 1000 to 2000 sec after the onset of the flare the *explosive* or *flash phase* starts. Sometimes, however, the flash is preceded by an activated and growing filament only and no gradual pre-flash brightening occurs. If there is an active filament—with or without pre-flash brightening—it may be blown off at the beginning of the explosive phase and be rapidly replaced by the flare which is, in any case, now rapidly increasing and brightening.

Typical for the *flash phase* (Figure 35–10) is a very steep increase of the linewidth of Hα (strong broadening of the wings of the line) sometimes up to 15A and more, and coincident bursts of hard x rays ($<$2A, partly $<$0.1A)

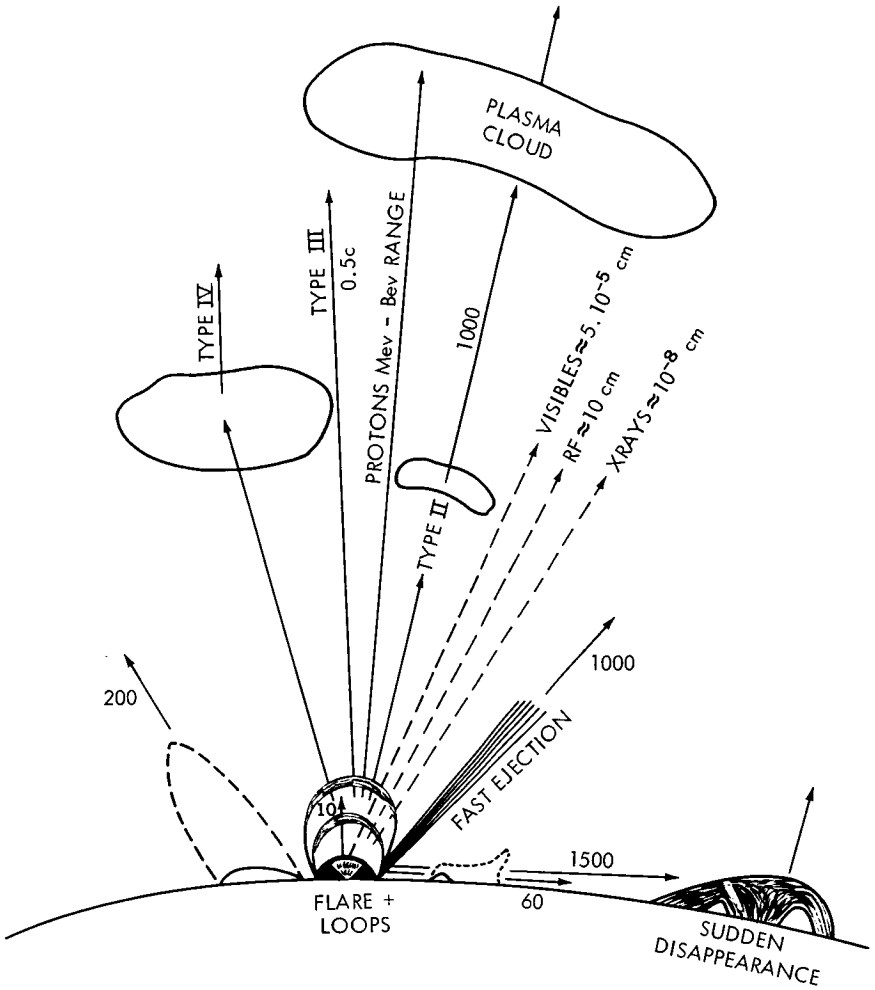

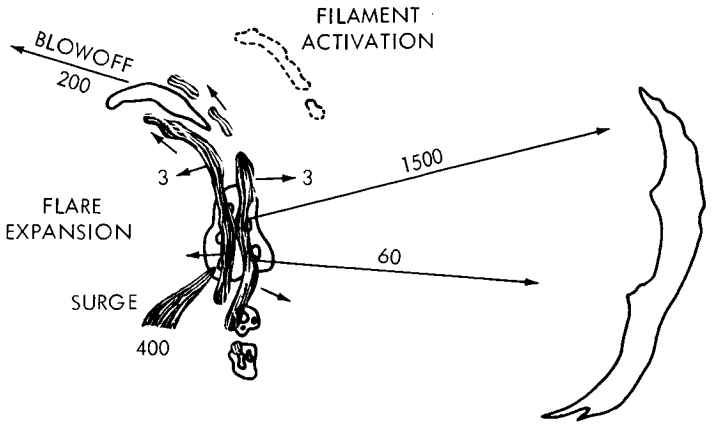

FIGURE 35–10. The phenomena of the flash and explosive phase of the flare (numbers are km/sec).

producing strong SID effects and strong bursts in the cm and dm range. After about 1000 sec, these three electromagnetic radiations attain maximum intensity almost simultaneously. The explosive character of this phase is revealed by a rich variety of visible dynamical effects. At the beginning of the flash sometimes the ejection of matter with velocities of about 1000 km/sec is observed (most cases of such high speed ejections will be missed because of the big Doppler shift). The flare expands, and surges (dark on the disk, bright on the limb) are emitted with velocities of the order of 100 km/sec; filaments in the vicinity of the flare are blown off or merely activated after the start of the flash. A fast dark action ($v \approx 1500$ km/sec) and/or a slow disturbance ($v \approx 60$ km/sec)—both probably of magnetohydrodynamic character—start from the flare and activate after some time even very distant filaments. On the other hand, there are the slow and the fast drifting m wave bursts and the radio continuum burst (Types II, III, and IV) which also start at or just a few minutes after the begin of the flash and indicate disturbances produced at the explosive phase and traveling through the solar corona at velocities of several 1000 km/sec and about 0.5 c, respectively, as well as the acceleration of electrons to relativistic energies which produce the Type IV synchrotron radiation. And it seems reasonable to assume that the high energy particles causing ground level increases of cosmic rays and proton events, as well as the cloud of lower energy plasma causing geomagnetic disturbances and Forbush effect, are accelerated and ejected also during the explosive phase. Unfortunately we have until now no optical evidence of the time and place of origin of the high energy particles.

Thus it seems that all the energy of the flare is released by the primary flare mechanism during the flash (explosive) phase in a huge blast (10^{32}–10^{33} ergs in 1000 sec or less, References 38 and 39). After the maximum of the electromagnetic radiations of the flare (which themselves are secondaries of the original energy output) there are only effects and processes of decline, diffusion, and redistribution of energy. The optical flare expands and fades, sometimes showing slow divergent motions (v=a few km/sec).

A somewhat puzzling and not yet understood phenomenon visible in the later stages of great flares are the loop prominence systems (flare loops). Their evolution seems to begin already at the flare maximum out of the expanding flare. Their expansion is rather slow ($v=10$ km/sec and less), and they reach maximum height and development a few hours after the flash and may outlive the flare by many hours. Their optical radiations (coronal lines, including the yellow line, extremely broad Hα wings) suggest a high energy phenomenon. They seem to be somehow a continuation of the flare in the solar corona.

The occurrence and shape of the flare depend obviously on the configuration of the magnetic fields. The shape of the flare apparently is related more to the dividing line and the configuration of the filaments than to the configuration of the spots. This may be the reason for the long known fact that large consecutive flares of one active region have very similar shape and development despite strong changes in the spot configuration.

ACKNOWLEDGMENT

The author is indebted to Prof. K. O. Kiepenheuer for the use of Hα filtergrams of the Anacapri Observatory of the Fraunhofer Institute, and to Dr. J. W. Evans for the use of flare and prominence films of the Sacramento Peak Observatory. My thanks are due to Dr. Mollwo, Heinrich-Hertz-Institut, Berlin-Adlershof, and Dr. Daene, Astrophysikalisches Observatorium Potsdam-Tremsdorf for records of radio bursts, and to Dr. Svestka, Astrophysical Observatory Ondrejov, for Hα linewidth data. Finally, I wish to thank Dr. Orrall for valuable advice on the presentation of this paper.

REFERENCES AND BIBLIOGRAPHY

Basic Data

1. *IAU Quarterly Bulletin*, 1961, No. 135, July–Sept. 1961, ed. Eidgen Sternwarte, Zurich.
2. "Solar-Geophysical Data," 1961, CRPL F 205, Sept. 1961, CRPL Boulder, Colorado.
3. *Solnetsnye Dannye*, 1961, Bull. No. 7, July 1961.
4. *Ionosphärenbericht*, 1961, 13 (21), Hamburg–Darmstadt.
5. *Beobachtungsergebnisse*, 1961, Heinrich Hertz Institut, Berlin–Adlershof, July 1961.
6. LINCOLN, J. V., 1962, "Geomagnetic and Solar Data," *J. Geophys. Res.*, 67: 2035.
7. WARWICK, C. S., and HAURWITZ, M. W., 1962, "A Study of Solar ActivityAssociated with Polar Cap Absorption," *J. Geophys. Res.*, 67: 1317.
8. MALITSON, H. H., 1963, "Table of Solar Proton Events," NASA TR R–169, 109.
9. MALITSON, H. H., and WEBBER, W. R., 1963, "A Summary of Solar Cosmic Ray Events," NASA TR R–169, 1.

Papers Describing Details of July 1961 Flares

10. PIEPER, G. T., et al., 1962, "Solar Protons and Magnetic Storms in July 1961," *J. Geophys. Res.*, 67: 4959.
11. MAEHLUM, B., and O'BRIEN, B. J., 1962, "Solar Cosmic Rays July 1961 and Their Ionospheric Effects," *J. Geophys. Res.*, 67: 3269.
12. FREDGA, K., 1962, "A Sunspot Group of High Activity in July 1961," *Arkiv f. Astronomi*, 3: 127.
13. ELLISON, M. A., et al., 1962, "Cosmic Ray Flares Associated with the 1961 July Event," *Monthly Not.*, 124: 263.
14. ELLISON, M. A., et al., 1961, "Cosmic Ray Flares," *Dunsink Obs. Publ.*, 1: 53.
15. FICHTEL, C. E., et al., 1963, "Details of Individual Solar Particle Events," NASA TR R–169, 19.
16. GAIZAUSKAS, V., and COVINGTON, A. E., 1962, "Radio and Corpuscular Emission Associated with the Flare Surge on the Western Limb of the Sun on July 20, 1961," *J. Geophys. Res.*, 67: 4119.

General References

17. ATHAY, R. G., and MORETON, G. E., 1961, "Impulsive Phenomena of the Solar Atmosphere; I. Some Optical Events Associated with Flares Showing Explosive Phase," *Ap. J.*, 133: 935.
18. AVIGNON, Y., et al., 1963, "Identification d'une classe d'eruptions chromospheriques responsables des absorptions ionospheriques polaires," *Comptes Rendues*, 256: 2112.
19. BRUZEK, A., 1952, "Die Ausbreitung von Eruptionsstörungen," *Z. Astroph.*, 31: 111.
20. BRUZEK, A., 1958, "Die Filamente und Eruptionen eines Aktivitätszentrums," *Z. Astroph.*, 44: 183.
21. BRUZEK, A., 1960, "Beobachtungen über die Beziehungen zwischen Eruptionen und Fleckenfeldern," *Z. Astroph*, 50: 110.
22. BRUZEK, A., 1962, "Über Fleckenprotuberanzen vor der Sonnenscheibe," *Z. Astroph.*, 54: 225.
23. BRUZEK, A., 1964, "On the Association Between Loop Prominences and Flares," *Ap. J.*, 140(2).
24. COVINGTON, A. E., and HARVEY, G. A., 1961, "Coincidence of the Explosive Phase of Solar Flares with 10.7 cm Noise Bursts," *Nature*, 192: 152.
25. DODSON, H. W., 1961, "Observations of Loop Type Prominences in Projection Against the Disk at the Time of Certain Flares," *Proc. Nat. Acad. Sci. USA*, 47: 901.
26. GOPASYUK, S. I., et al., 1963, "The Structure of Magnetic Fields and its Variations in Flare Regions," *Isv. KAO*, 29: 15.
27. HACHENBERG, O., and KRÜGER, A., 1959, "The Correlation of Bursts of Solar Radio Emission with Flares and SIDs," *J. Atm. Terr. Phys.*, 17: 20.
28. HANSEN, R. T., and KLECZEK, J., 1962, "Coincidence of Sudden Ionospheric Disturbance with the Explosive Phase of Solar Flares," *Nature*, 195: 1280.
29. KAWABATA, K., 1961, "Thermal Origin of the Post-Burst Increase of Solar Microwave Radiation," in: "The Solar Corona," *IAU Symp.* No. 16, Cloudcroft 1961, p. 143.

30. KLECZEK, J., and KRIVSKY, L., 1960, "Loop Prominences Accompanying Ionospheric Disturbances," *Bull. Astr. Inst. Czech.*, 11: 165.
31. KUNDU, M. R., 1961, "Bursts of Centimeter Wave Emission and the Region of Origin of X Rays from Solar Flares," *J. Geophys. Res.*, 66: 4308.
32. KUNZEL, H., 1960, "Die Flare-Häufigkeit in Fleckengruppen unterschiedlicher Klasse und Struktur, *Astr. Nachr.*, 285: 271.
33. WALDMEIER, M., 1961, "Die Entwicklung einer anomalen Fleckengruppe," *Z. Astroph.*, 52: 1.
34. JEFFERIES, J. T., and ORRALL, F. Q., 1963, Paper presented at the *Symposium on Solar Spectra*, Utrecht, August 1963.
35. DAENE, H., 1963, private communication.
36. KLECZEK, J., 1963, *these Proceedings*, paper no. 10.
37. MCCRACKEN, K. G., 1963, "Anisotropics in Cosmic Radiation of Solar Origin," NASA TR–R169, 57.
38. ELLISON, M. A., 1961, "Cosmic Rays from the Sun," *Proc. Royal Inst.*, 38(175); Dunsink Obs. Repr. No. 22.
39. SIMPSON, J. A., 1960, "Variations of Solar Origin in the Primary Cosmic Radiation," *Ap. J. Suppl.*, Ser. 4(4): 378.

DISCUSSION

Dr. Giovanelli: I wasn't sure, from your description, whether you observed the July 20 event to have flare brightness at the tops of the loops. On Figure 35–7 I think you showed these marked in black, and I didn't know whether that was merely to distinguish them or that they were much fainter than flares.

Dr. Bruzek: The loop prominences are shaded one grade darker than chromospheric phenomena of comparable brightness; the full black in loops corresponds to Hα plage brightness on the disk. Actually only a few knots of the July 20 loops had flare brightness.

NW4 3028B

36 AN ASSEMBLY OF FLARE OBSERVATIONS AS RELATED TO THEORY

K. O. Kiepenheuer
Fraunhofer Institut
Freiburg i. Br., West Germany

ABST

A short description of the observed macroscopic configurations of flares, spot groups, and dark filaments is given. The possible sub-telescopic structure of flares is discussed. It is shown that the high energy output of a flare (particle energies and radiation) must be produced in situ. The energy probably cannot be transferred to the flare's volume from the outside. To supply the energy, the assumption of the annihilation of a field of a few hundred gauss within the flare obviously cannot be avoided.

The close relation between flares and filaments, as well as the activation of the associated filaments (increase of density and of internal turbulence) well before the optical onset of the flare, suggests that this activation is already part of the flare phenomenon. One could say that a flare represents a more violent form of the densification of hot coronal material into a cool filament. While the formation of a dark filament (prominence) takes hours, the flare is condensed within a few minutes. The Schlüter-Kippenhahn model of prominences gives some indications for such a type of instability.

Flares occur in an almost unobservable level of the solar atmosphere somewhere between the uppermost chromosphere and the inner corona. As seen on the solar limb, the lower part of the flare is screened by the chromosphere of the foreground; on the disk it is very difficult to get an idea of the three-dimensional shape of a flare.

Flares come unexpectedly and deliver within seconds an enormous amount of information, possibly after a waiting time of weeks! It is quite unprobable that under such circumstances an optimal record will be obtained. A permanent recording of the sun, in order to be ready for every flare, on the other hand will be extremely expensive if spectral information is included and if high resolution (in the picture and in the spectrum) is wanted. But more and more it looks as if the basic processes in a flare occur in very small structures, which might even be sub-telescopic. Obviously an average picture or spectrum of a flare shows only a very diluted or smeared-out aspect of the physical process involved.

MACROSCOPIC STRUCTURE OF FLARES

It is quite difficult to say something reliable about the extension of a flare in height. Except for the rather rare events of white flares, the photosphere seems not to be involved in spite of the fact that we have been looking for it systematically for quite a number of cases. The chromosphere, however, is affected. On the limb the minimum height is given by the screening of the foreground chromosphere, while in projection on the disk it is observed that certain chromospheric structures typical for a center of activity are brightening—sometimes reaching full flare brightness (in general, without changing their shape and position)—and others are not affected at all.

I think that this can be understood by assuming that the main luminous volume of a flare reaches only into the higher parts of the chromosphere (where only its coarser elements—long threads, small filaments, etc.—are occurring), while the major part of the flare volume is probably seated in the very inner corona.

This means that a flare happens mostly in a coronal surrounding with $n \approx 10^{10} \cdots 2 \times 10^{10}$ cm^{-3} and $T > 10^6$ degree (permanent coronal condensation). It is important to notice that this surrounding is as dense as a prominence, but the temperature is some hundred times higher.

It is still doubtful whether there is a characteristic three-dimensional figure of a flare. As projected against the disk in Hα, the prime event of a flare appears in general as a bright thread or ribbon, somehow resembling in shape a dark filament. The structure itself sometimes seems to be built up by bright knots, sometimes by short pieces of threads, sometimes just like a continuous bright line (like a lightening stroke). On the limb the first onset of a flare has been observed as a little cone close to the limb, later on transforming itself into slowly rising loops. It must be emphasized, however, that the brightness fluctuations within a flare (in time and in space) are so strong that the shape of a flare might vary terribly with the isophotes selected.

The beautiful Sweet (Reference 1) model of a flare with two merging spot groups, which certainly does not give a representative picture of nature, has left the impression that many flares can be explained by the existence of neutral points in the chromosphere or in the corona, deduced from photospheric magnetograms and from sunspot configurations.

But there are by far not enough neutral points to explain the observed number and shapes of flares. It might be true that the onsets of flares occurring in or near a sunspot group coincide with neutral points of the magnetic field, but then obviously the phenomenon is propagating into regions with an undisturbed and continuous magnetic flux.

There are at least a few characteristic flare-spot configurations, which are shown in Figure 36–1 in a simplified form. From these configurations the following general rules can be deduced:

1. Flares in most cases coincide like dark filaments with the dividing line of magnetic polar-

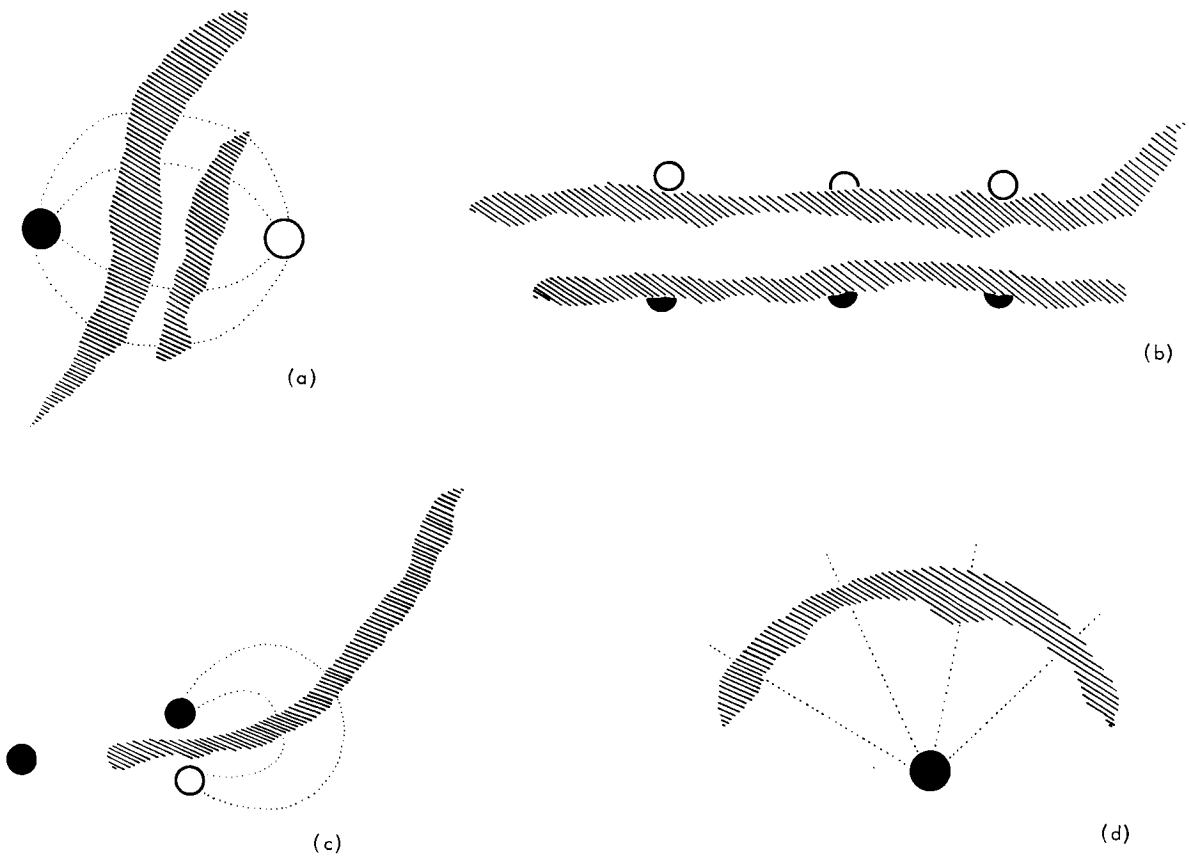

FIGURE 36–1. Four characteristic flare-spot configurations (magnetic field lines are indicated).

ities. Along this line the longitudinal component of the field disappears ($H_L=0$) and the gradient dH_L/dx is large.

2. Flares occur almost always in regions with horizontal field.

3. Flares *start* very often in regions with great dH_L/dx and where the photospheric field is changing.

4. The macroscopic structure of a flare extends across the magnetic field (like the macroscopic structure of filaments).

5. Flares often occur within a region of an obviously homogeneous magnetic flux and extend often into regions with small fields (<10 gauss).

Altogether, a typical magnetic configuration of a flare looks much more like the one given by Kippenhahn and Schlüter (Reference 2) for filaments [Figure 36–2(a)] than the one presented by Sweet (Reference 1) or by Gold and Hoyle (Reference 3), as shown in Figure 36–2(b).

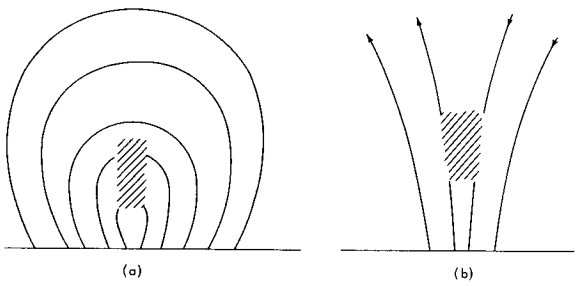

FIGURE 36–2. Magnetic field distributions around a flare.

6. There can be no doubt that flares occur within an extended center of activity or even in neighbouring CA's (distance up to several 100,000 km) almost simultaneously, such that a causal relation between the two must exist and that the velocity of the triggering agency must be of the order of 1500 km/sec (Reference 4). Triggered flares always seem to start in plage regions, which sometimes do not reach real flare brightness. This triggering effect makes it very unprobable that the energy of a flare is supplied from the outside of the flare volume.

7. Sometimes flares have the tendency to repeat themselves within hours, on the same place, showing the same time dependence of Hα, radio and x-ray emission (References 5 and 6) and mechanical output as the Moreton blast (References 7 and 8), and the flare surges. This obviously means that the magnetic field configuration responsible for the flare is very stable or is reinstalled again within an hour or so after the flare has occurred.

MAGNETIC FIELD CHANGES IN AND AROUND FLARES

There are no reliable field measurements available within the luminous volume of a flare; in almost all cases the field and the field variations with time at the locus of the flare have been estimated from magnetograms obtained in the underlying photospheric levels. The relation between photospheric, chromospheric, and coronal fields on the other hand is still quite a problem—especially in the active parts of the solar atmosphere.

There is no doubt that flares do begin preferably in regions with changing photospheric fields; however, this change is not indispensable. No change of field has yet been observed, which is as fast as the energy *output* of the flare. This probably means that the observed field changes around the flare might be characteristic for a region where flares can start but have no direct bearing on the flare mechanism as such. Unfortunately there is rather little hope to obtain reasonable field measurements within the very vicinity and inside a flare. But I will leave the discussion of this delicate problem to the experts in this domain.

RELATION BETWEEN FLARES AND FILAMENTS (PROMINENCES)

If there are filaments in a center of activity, then the flares occurring in this center are often associated with them. Sometimes a very fine, long filament—recognizable only in high resolution filtergrams—will act as a tracer for a violent big flare without suffering damage itself. This is the more astonishing, since both—flares and filaments—occupy the dividing line of polarities and the region of horizontal field.

There are different types of flare-filament associations:

1. The flare develops along an existing

filament in one or two parallel lanes [Figure 36–3(a)]. The two lanes show mostly (References 8 and 9) an expanding motion away from the filament, with velocities ranging from 2 to 20 km/sec. The motion comes eventually to a halt. It is astonishing that the same is true for the Disparitions Brusques (DB's) of quiescent filaments far away from centers of activity, which also show a two-lane brightening which is expanding the same way—and also a darkening of the involved filament, before it is lifted or raining down to the sun. Altogether one gets the impression that a DB is a "soft" version of a flare, which can teach us a lot about the flare mechanism!

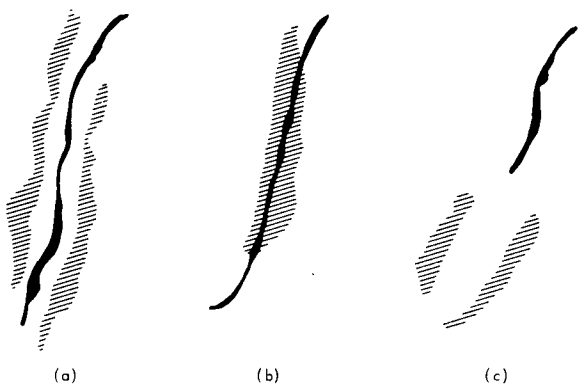

FIGURE 36–3. Characteristic flare-filament associations (flare regions are striped).

2. The flare coincides with a filament, which reaches flare brightness itself, but still the lower parts of it survive the flare unchanged [Figure 36–3(b)]. Sometimes the flare consists of preexisting chromospheric structures (threads) which stick a little higher into the inner corona.

3. There are flares without filaments, but even then the chromospheric fine structures underlying the flare often have the typical appearance observed in the prolongation of filaments. Sometimes the flare occurs in the prolongation of a filament [Figure 36–3(c)].

4. Quite often (Reference 9 and others) the flare filament becomes distinctly darker an hour or more before the onset of the flare. This can be observed best in the blue wing of Hα, less pronounced in the center of the line. This pre-flare activation of a filament means an increase of internal turbulence from 10 to ≈ 30 km/sec, a systematic upward motion of the whole filament, and possibly also an increase of the number of hydrogen atoms per cm^3 in the absorbing structures of the filament. The density of the coronal surrounding is already that of a quiet filament ($\gtrsim 10^{10}$cm^{-3}); its temperature, however, is 100 times higher. Assuming pressure equilibrium between filament and corona, a filament density of $\approx 10^{12}$ cm^{-3} is required. Still higher densities in certain parts of the filament are needed if Becker's (Reference 10) observations of structures of activated filaments in white light would be interpreted in terms of electron scattering or by H^- absorption.

5. There are a great number of flares which break out in the midst of an activated or rising filament. The change from Hα absorption to emission might take only a few minutes. The disappearance of the associated filament can occur in the form of ejection or by raining down into the chromosphere. Many striking examples of this type have been shown by G. Moreton with the 10-sec-Hα-Patrolfilms, obtained at Lockheed Solar Observatory, Los Angeles.

Summarizing this section, it must be said that the striking similarity of field configuration of flares and filaments, and still more the very close interplay of the time changes in filaments and flares, requires that these two phenomena should be treated together. Strongly exaggerating, one could say that filaments and flares represent the same phenomenon but with different time scales.

MICROSTRUCTURE OF FLARES

Extremely underexposed Hα filtergrams of flares which do not show any trace of the solar disk, obtained under good seeing conditions, sometimes show very fine, well-blackened points. This means that a flare—at least during the flash phase—shows a very strong fluctuation of brightness in dimensions which probably are sub-telescopic. In addition, one has visually the impression—similar with prominences and flare surges—that there is a hairy structure resolved only during short periods of excellent seeing. Quite a different

approach to the problem of the fine structure of a flare has been tried by Suemoto and Hiei (Reference 11) and others by discussing the flare spectrum. Assuming that the broadening of the high members of the Balmer lines observed in a flare is produced mostly by Stark effect, they come to the conclusion that the total emission comes out of a depth of only 10^6cm. The luminous part of a flare showing, however, dimensions of 10^8 to 5×10^8 cm, they conclude that the emission must occur in numerous fine structures distributed all over this volume, which are even much smaller than 10^6cm—perhaps only a few hundred meters. The hydrogen densities of these structures amount to about 10^{13}cm^{-3}.

In a different way the problem has been treated by Jefferies and Orrall (Reference 12). They develop a detailed theory of the Balmer decrement and the Balmer line profiles (using roughly the same widths as the Japanese workers). They ignore, however, the possible influence of the Stark effect (using only Doppler effects) and of small-scale density fluctuations within the flare. Keeping in mind that a density of $\approx10^{12}$ cm^{-3} gives already a mean disturbing field strength of 125 volt/cm (Reference 13) or a $\Delta\lambda_s\approx0.6$A, this looks a bit dangerous.

A complete spectroscopic discussion of the flare structures including Doppler and Stark broadening as well as possible density fluctuations has not yet been presented. From all we know, it would be strange—this is my personal impression—if flares do not possess sub-telescopic fine structures.

The shortness of the flash phase of a flare speaks very much in favor of small structures, assuming that the duration of this phase represents roughly the decay time σa^2 of a magnetic field in a conductor of dimension a; then dimensions of the order of a few kilometers are needed. Also, the rapid formation or densification of the pre-flare filament is very difficult to understand in terms of a structureless simultaneous increase of density all over a volume of more than 10,000 km extension. Even this process looks much more believable in the form of many small globules, condensed out of coronal material without need of supply of material outside the volume, occupied by the pre-flare filament.

ENERGY BALANCE OF A FLARE

The optical output of a flare lies mostly in an enhanced line emission and in a continuum of unknown intensity, which latter in the visible spectrum is for flare Importance ≤2 smaller than 1 percent of the photospheric radiation. Altogether the optical emission is certainly $\lesssim6\times10^8$ ergs/cm^2 sec, (the EUV-, x-, and visible line emission together still being smaller than this). Supposing that this emission occurs in a macroscopic depth of 5×10^8 cm and within 1000 seconds, about 1000 ergs/cm^3 will be needed. This leads for Importance 2 flares (10^{18} cm^2) to a total optical output of $\lesssim6\times10^{29}$ ergs and, for a 3+ flare (5×10^{19} cm^2), to $\gtrsim10^{32}$ ergs.

The "mechanical" energy output of a flare is supplied in the form of surges ($v\approx100$ km/sec), sudden expulsion of material during the explosive flare phase ($v\approx1000$ km/sec), and the ejection of a proton cloud, producing terrestrial PCA's ($v\approx10^{10}$ cm/sec):

Flare Surges—Their volume amounts roughly to $\lesssim10^{27}$ cm^3; their velocity $\approx10^7$ cm/sec; their density might be of the order 10^{11} cm^{-3}, which gives for their kinetic energy something like 10^{28} ergs. The mass of the surge is equivalent to that of a small prominence ($\approx10^{14}$ grams).

Solar Blast—Discovered by Moreton (Reference 8), propagating over the solar disk with a velocity of 1000 to 2500 km/sec. It looks, when observed in the wing of Hα, like an almost transparent cloud, being shot out by the flare in certain directions. It affects filaments and other chromospheric structures up to distances of a solar radius. It is difficult to estimate the mass of this cloud. Probably it is also of the order of 10^{14} grams; this would correspond to a kinetic energy of $>10^{30}$ ergs.

Interplanetary Blast—Producing one or two days later a geomagnetic storm. Assuming (Reference 14) a particle density of ≈30 atoms/cm^3 in the earth' orbit, and occupying there a volume of 0.1 AU in diameter with a velocity of 1500 km/sec, a total mass of $\approx2\times10^{15}$ grams

728-629 O—64——22

(mass of a medium-sized prominence) and a total kinetic energy of $>2\times10^{32}$ ergs result. The work to bring this mass out of the sun's gravitation is already $\approx10^{30}$ ergs.

It can be assumed with some confidence that this interplanetary blast is the same as observed by Moreton propagating over the sun's surface—the major part of the blast going into space.

Proton Event—Or acceleration of protons into interplanetary space, energy 30 Mev, $v\approx0.7\times10^{10}$ cm/sec, flux (Parker, Reference 14) 10^4 protons/cm^2/sec within a volume of 1 AU diameter contain an energy of $\approx10^{30}$ ergs. The cloud contains a total of $\approx10^{10}$ grams of protons.

In general, therefore, the flare's output of "mechanical" energy seems to surpass the optical energy by a factor of 5 or even 10 (Reference 14). This is especially true for the bigger flares.

MASS BALANCE

Most of the energy and the mass seem to be contained in the particle cloud ejected by the flare into space. If this mass were supplied from the corona surrounding the flare's volume, then the total of the permanent coronal condensation would have to fly away. This contradicts observations which show that certain structures in a coronal condensation seem to survive a flare. It must be mentioned, however, that only very few and uncomplete observations of this kind are available. The problem of mass supply also should be discussed in connection with the results presented by Jefferies and Orrall in this symposium for the mass transport in the loop structures following the flare.

The fact that the ejected mass ($\approx2\times10^{15}$ grams) is probably larger than the total mass contained in the luminous volume of the flare ($\approx10^{14}$ grams) makes it almost impossible to think that the mass is supplied by the flare itself. Far more chromospheric and coronal observations are needed to obtain reliable information about the origin of this mass.

ORIGIN OF ENERGY

An important question is whether the flare's energy is developed in situ—in the Hα volume of the flare or in the surrounding corona—or whether the energy is being delivered to the flare from the outside?

A strong argument against energy supply from the underlying photosphere as suggested by Warwick (Reference 15) is that the needed energy flow through the chromosphere (which certainly is much denser than the blast observed by Moreton sweeping over the chromosphere) should leave well observable traces. If only 1 percent of the momentum of the particle flow would be transferred to the chromosphere, the latter would be carried away.

Also, the fact that flares can be triggered by other flares far away—the triggering agency obviously traveling through the corona—makes it very difficult to believe that the energy is supplied from the photosphere. It suggests strongly that the energy is originating within the volume occupied by the flare, ready to be released within a few hundred seconds.

FLARE MODEL, BASED ON ASSOCIATION WITH FILAMENTS

No doubt there is a very close geometrical and physical relation between flares and close-by filaments. Therefore, it seems reasonable to suspect that the physics of a filament—as developed by Schlüter and Kippenhahn (Reference 2)—has some bearing on the physics of a flare and that the instabilities observed in filaments (activations, Disparitions Brusques) represent perhaps the same phenomena as a flare, only in a less violent form.

In the Kippenhahn-Schlüter model of filaments, the filaments' material hangs like laundry in the horizontal sections of the lines of force. In a quiet filament within a BM region without sunspots, the field distribution might look as indicated in Figure 36–2(a). As soon as the filament becomes activated for some reason, an additional deformation of the field probably will set in because of the increase of the filaments' density and kinetic energy

(internal turbulence). For a turbulence of 3×10^6 cm/sec and a density of 3×10^{11} cm^{-3}, $E_{kin}=E_{magn}$ is reached already for 10 gauss, with 10^{13} cm^{-3} for 50 gauss.

As a consequence of the growing disorder of the field configuration within and around the activated filament, produced by the increase of turbulence and of density, the field will become more and more twisted, probably on a sub-telescopic scale. There also will occur collisions between regions of different field strength and field directions. While encounters of antiparallel fields will be favored because of attraction between the associated electric currents, encounters of regions with parallel fields will be hindered because of repulsion.

This kind of interaction between turbulence and magnetic field will become a sufficient energy source for a flare only if the above collisions end up in a kind of pinch effect, such that a considerable fraction of the magnetic field in the flare's volume is annihilated and the field energy transformed into Joule heat and kinetic energy of ejected particles. It can be also assumed that on a sub-telescopic scale a great number of processes occur, similar to the macroscopic flare mechanism described by Dungey and Sweet (Reference 1) and Gold and Hoyle (Reference 3). Those who have seen in an accelerated movie the brightening of a flare out of a dark filament, and the almost chaotic interaction of bright and dark structures, will not doubt the existence of a causal relation between the activation of a dark filament and the formation of a flare. It would be worthwhile therefore that these micro-instabilities in a condensing coronal plasma would be studied by the specialists in this field.

On the observational side, more information about the pre-flare situation in the ambient chromosphere and corona is urgently needed. Sequences of highly resolved Hα pictures and spectra of activated filaments in active regions should be obtained from sites which guarantee good seeing over periods of reasonable length.

CONCLUSIONS

1. The occurrence of a flare as such, its shape, its program of emission (x-radiation, EUV, visible, radio, particle emission) depends strikingly upon the configuration of the underlying photospheric magnetic field and of the associated filaments.

2. The flare is macroscopically located in a horizontal magnetic field, mostly in places where no neutral points are to be expected. The flare extends and propagates across the magnetic field and reaches very often into regions with very small fields.

3. The energy of a flare should be supplied inside the flare's volume and not from the photosphere or chromosphere below it.

4. The interpretation of a flare as a purely macroscopic explosion or collapse phenomenon is in contradiction with observation and with mechanical or hydromagnetic models. The possibility of sub-telescopic processes (densifications, collapses, pinches) cannot yet be excluded.

5. The close relation of flares and filaments—they both have the same magnetic field configuration—lets us expect that the formation of a dark filament and the formation of a flare represent probably the same phenomenon in different time scales. The great similarity between Disparitions Brusques and flares points in the same direction.

ACKNOWLEDGMENT

I wish to express my sincere thanks to Dr. Bruzek, who assisted me greatly in discussing the great variety of observational aspects of flares.

REFERENCES AND BIBLIOGRAPHY

1. Sweet, P. A., 1956, *I.A.U. Symposium*, No. 6, Paper 14 (Stockholm).
2. Kippenhahn, R., and Schlüter, A., 1957, *Z. Astrophysik*, 43: 36.
3. Gold, T., and Hoyle, F., 1960, *M.N.*, 120: 89.
4. Becker, U., 1958, *Z. Astrophysik*, 44: 243.
5. Fortini, T., 1963, *Ap. J.*, 138: 278.
6. Fokker, A. D., 1963, *Space Science Rev.*, 2: 88.

7. Athay, R. G., and Moreton, G. E., 1961, *Ap. J.*, 133: 935.
8. Moreton, G., and Malville, J. M., 1963, *PASP*, 443: 176.
9. Bruzek, A., 1957, *Z. Astrophysik*, 42: 76.
10. Becker, U., 1959, *Z. Astrophysik*, 48: 189.
11. Suemoto, Z., and Hiei, E., 1959, *Publ. Astr. Soc. Japan*, 185: 11.
12. Jefferies, J. T., and Orrall, F. O., 1961, *Ap. J.*, 133: 963.
13. Unsöld, A., 1955, *Physik der Sternatmosphären*, 323 (Berlin).
14. Parker, N. E., 1963, *Ap. J. Suppl.*, Vol. VII; 177.
15. Warwick, J., 1962, *PASP*, 34: 302.
16. Bruzek, A., 1958, *Z. Astrophysik*, 44: 183.
17. Bumba, V., 1958, *Publ. Crim. Obs.*, 19: 105.
18. Martes-Tropé, M. J., and Pick-Gutman, M., 1962, *C.R.*, 254: 3975.

DISCUSSION

Dr. Gold: I would like Dr. Kiepenheuer to amplify his statement about the geometry of flares which argued for some points of view and against others. As you were talking, I sat there complacently saying to myself how wonderfully well all the details that you are giving fits the Gold and Hoyle model of the flare. Namely, horizontal filaments with opposing horizontal fields meet where the area of contact is the area giving rise to energy dissipation. Then, in the same phrase, you say that this doesn't work!

Dr. Kiepenheuer: Altogether, I have to apologize. There is indeed no macroscopic twist observed in filaments of the amount needed to explain a flare. Also, no macroscopic encounters of filaments are observed, to which you refer in your flare theory. However, there can be no doubt that there will occur all kinds of "microtwists" in filaments.

Dr. Gold: In general, the filaments will have twist in them unless somebody has taken them and combed them out.

Dr. Kiepenheuer: I agree completely with that.

Dr. Gold: I challenge that you can see whether a filament on this small scale on which flares occur is twisted or not twisted. What you can see is, in general, some elongation of objects giving a rough idea of which way the lines of force run. But whether those in turn have a twist on them or not, I don't think it is possible to see.

Dr. Elste: I would like to ask:

Are these bright dots along the filaments observed in white light?

Dr. Kiepenheuer: They are observed in white light. They do not show any color. They come and go, and they appear much more often than people think. You can see them almost in active periods of the sun. You can see them almost every day. But you need good eyes, good seeing, and good contrast.

Dr. Elste: Do these dots resemble the well-known bright facular granules?

Dr. Kiepenheuer: They have no relation at all with structures observed in the photosphere. So we are reasonably sure that they are above the photosphere, something in the chromosphere, maybe in the corona. We do not know the height. They have nothing to do with the observations made by Loughhead and Bray, for instance, of certain structures which also look like threads in the photosphere, which seem to be arrangements of granules.

Dr. Dungey: On the question of twisted fields, I did my homework and read Severny's paper. By the way, he mentions that usually the lines of the horizontal field—or transverse, if you like; but it is easier to think about them as horizontal—run around in loops. This, I think, means the field is twisted.

Dr. Kiepenheuer: I beg your pardon. I did not understand: The field runs along in loops.

Dr. Dungey: We are talking about the horizontal component of the field in the photosphere?

Dr. Kiepenheuer: Yes.

Dr. Dungey: If the horizontal component runs around in a circle, now you add a vertical component which, let us say, has the same polarity over the region we are talking about; then the total field is twisted?

Dr. Kiepenheuer: Yes, this might be true.

Dr. Schmidt: For circular loops, this point

is certainly correct. I would like to draw attention to the fact that the observed figures are large-scale whirls with strong radial components. They might produce field configurations similar to the original Gold-Hoyle model. Such large-scale whirls as Prof. Kiepenheuer emphasized are not easily made consistent with the geometrical feature of flares. But, on the other hand, they might produce the buoyancy for the rising prominences. I doubt that use can be made of these observed gross structures in explaining flares at all.

Dr. Dungey: Would you explain why they cannot be used?

Dr. Schmidt: If this large-scale order in the field would be important, it should be resembled in the flare structure. I am just repeating the statement by Prof. Kiepenheuer. Furthermore, I want to emphasize that the observed large-scale whirls in the transverse of the horizontal field* are relatively weak. In many cases, it is even hard to prove that a net rotation (i.e., a twist) exists. This implies that the energy stored in the large-scale twist probably will not be comparable with the total energy content of the field. Therefore, it should be too small to account for the flare losses.

*J. L. Leroy, 1962, Theses presentees a la Faculte des Sciences de l'Univ. de Paris.

A. B. Severny, 1962, *Astron. Zh.*, 39: 961.

V. E. Stepanov and A. B. Severny, 1962, *I.K.A.O.*, 28: 166.

V. E. Stepanov and S. I. Gopasyak, 1962, *I.K.A.O.*, 28: 194.

II THEORY OF FLARES

SESSION A

Chairman, Prof. WILLIAM C. ERICKSON

N64-30287

37 A SURVEY OF THE INTERPRETATIONS OF RADIO AND X-RAY BURSTS

MUKUL R. KUNDU
Astronomy Department, Cornell University
Ithaca, N.Y.

With regard to the radio and x-ray emissions from solar flares, we are principally concerned with the following mechanisms of generation:

1. *Bremsstrahlung from ionized solar plasma:* Thermal bremsstrahlung, that is, when the electrons are nonrelativistic, is responsible for the quiet sun and slowly varying component of radio and x-ray emission and possibly also some cm-λ and x-ray bursts. Nonthermal bremsstrahlung is responsible for certain cm-λ bursts and high energy x-ray bursts during solar flares.

2. *Gyro and synchrotron radiation from electrons in the presence of a magnetic field:* The gyro radiation (low-order harmonics of the gyro frequency) from electrons in the sunspot magnetic field is responsible for a part of the slowly varying component on short centimeter wavelengths and possibly also noise storm radiation on meter wavelengths. The synchrotron radiation appears responsible for type IV continuum bursts.

3. *Radiation from plasma waves excited in the solar atmosphere by corpuscular streams ejected from solar flares:* The corresponding excitation of a longitudinal plasma wave by a single or incoherently acting electron seems to be the plasma wave analogue of Cerenkov radiation. Such plasma radiation can account for type II and type III bursts on meter waves.

CENTIMETER WAVE AND X-RAY BURSTS

We know that for a cloud of isothermal gas of temperature T and total optical thickness τ in free space, the brightness temperature is given by

$$T_b = T(1-e^{-\tau})$$

where $\tau = \int_l^\infty \chi \, dl$ is the optical depth. The absorption coefficient χ for free-free emission is proportional to $N^2T^{-3/2}$ (N is the electron density). If the cloud is a uniform slab of thickness l, then substituting the exact expression for absorption coefficient as given by the theory of thermal bremsstrahlung gives

$$T_b = T\{1-e^{-aT^{-3/2}l}\},$$

where a is a constant.

The optical depth of the solar atmosphere between the observer and plasma level is typically of order unity for radio frequencies whose plasma levels lie in the corona, that is, for meter and decimeter wavelengths. For very high frequencies—centimeter wavelengths—the plasma levels lie in the cooler and denser chromosphere. Consequently, the optical depth increases sharply with increasing frequency with the result that the radiation originating at the plasma levels of cm-λ frequencies is strongly attenuated. However, at times of flares, the cm-λ plasma levels lie in hotter regions, the optical depth decreases, and attenuated cm-λ burst emissions may be observed originating from near their plasma levels. This is probably the reason why one observes only rarely drifting bursts on centimeter waves. Now, if there is a sudden localized heating of the plasma, then—referring to the expression for T_b—we find that, if the optical depth is large as for cm waves in the solar atmosphere, T_b increases linearly with T. On the other hand, if the optical depth is small, $T_b \approx aT^{-1/2}l$ with the result that heating causes a decrease in

brightness temperature, as occurs in the corona where the meter waves originate. Consequently, bremsstrahlung bursts cannot occur in the corona. The flux densities in the two regions ($\tau >> 1$ and $\tau << 1$) can be expressed (Reference 1) as

$$\frac{S_f}{f^2} = 2\times 10^{-44} T \frac{F}{F_0} \quad \mathrm{wm^{-2}(c/s)^{-1}}$$

and

$$S_a = 2\times 10^{-45} T^{-1/2} \int N^2 \, \mathrm{d}\ell \, \frac{F}{F_0} \quad \mathrm{wm^{-2}(c/s)^{-1}},$$

where T=electron temperature, N=electron density, F=source area, F_0=area of solar disk.

The above conclusions apply equally to nonthermal bremsstrahlung, where we have a non-Maxwellian distribution of electrons, provided we replace T by T_r (radiation temperature) and a by a different constant characteristic of the type of energy distribution (Reference 2).

The cm-λ bursts of type "gradual rise and fall," as well as weak impulsive bursts (not associated with concomitant emission on meter waves), have a power spectrum decreasing sharply around 1000 Mc/s. Thus, these bursts originate in a hot plasma with chromospheric density, which is optically thick at low frequencies and optically thin or thick at higher frequencies in the cm-λ region. These bursts, which begin early in the life of the Hα flare, appear to have a thermal origin and are due to local heating of the dense chromospheric plasma to temperatures of about 10^6 °K. Even for intense cm-λ bursts one obtains similar spectra for the post-burst monotonic decay, where one obtains from the optically thick part of the spectrum electron temperatures around 10^7 °K (Reference 1). The impulsive burst maxima whose spectra are different from that of a hot and dense plasma often have brightness temperatures exceeding 10^7 °K and are probably due to nonthermal bremsstrahlung or synchrotron radiation in a magnetic field of 100 to 1000 gauss due to superthermal electrons produced and accelerated during the flare. The extremely rapid rise of the cm-λ impulsive burst is quite consistent with nonthermal bremsstrahlung which appears capable of reproducing the rapid variations characteristic of a nonthermal source.

The x-ray bursts appear to be satisfactorily explained by bremsstrahlung. The low energy x-ray bursts in the 1–10A range can be explained by thermal bremsstrahlung, whereas the high energy (>20 kev) x-ray bursts are produced by nonthermal bremsstrahlung. In the same x-ray bursts both thermal and nonthermal bremmstrahlung could be operative: Pre-heating of the solar plasma immediately before the flare explosion could result in the "gradual" cm-λ bursts as well as the emission of low energy x-rays by thermal bremsstrahlung; at the explosive phase, superthermal electrons are ejected or electrons rapidly attain superthermal energies by means of Fermi-type acceleration and produce high energy x-ray bursts by nonthermal bremsstrahlung, and impulsive cm-λ bursts by nonthermal bremsstrahlung or synchrotron mechanism. The extremely close correlation between the cm-λ and x-ray bursts, both in their frequency of occurrence and in their intensity variation with time, suggests that probably the same electrons produce x-ray and cm-λ bursts. The electrons gradually lose their energy by collisions and approach their thermal velocities, and so the x-ray spectrum undergoes a softening. This is quite consistent with the observed decrease of intensity and increase of angular size with consequent decrease of brightness temperature during the cm-λ post-burst decay, which is thermal in nature. For this reason, intensity variation of a cm-λ burst in its post-burst phase may not correspond closely with that of an x-ray burst, if we consider only high energy x rays (say, >20 kev). In this phase, the intensity variation of a cm-λ burst should correlate better with that of the associated x-ray burst in the low-energy (say, 1–10A) region.

It appears that a total of about 10^{33} fast electrons (energy >20 kev) can account for the observed intensity of some x-ray bursts—say, that of September 28, 1961 (Reference 3). If we consider that the x-ray burst has the same source-size as the cm-λ burst, that is, 2′ arc diameter or a volume of about

10^{30} cm^3, there should be about 10^3 electrons of >20 kev/cm^3. This number is higher by about one order of magnitude than the number of electrons of several hundred kev's required to produce the cm-λ burst by synchrotron radiation. This is not surprising, since electrons with small pitch angles do not contribute to synchrotron radiation but do produce bremsstrahlung bursts.

TYPE IV AND STORM RADIATION

The first two phases of type IV radiation—type IVA and type IVB—appear to be satisfactorily explained by synchrotron radiation of high energy electrons. Using approximate formulas given by Schwinger (Reference 4), Boischot and Denisse (Reference 5) showed that a total of 4×10^{32} electrons of 3 Mev energy (or 100 electrons/cm^3) in a magnetic field of 1 gauss could account for the observed intensity of type IVB burst on 169 Mc/s. Using exact formulas for the synchrotron radiation of electrons in both quasi-circular and helical orbits, Takakura (Reference 6) showed that electrons of a few hundred kev's gyrating in a magnetic field of ≈1000 and ≈50 gauss could account for the observed properties of type IVA and type IVB bursts, respectively. According to Takakura and Kai (Reference 7), the brightness temperatures of 10^8–10^6 °K for type IVA can be accounted for by electrons of density about 10^2 to 1/cm^3 and of mean energy about 4×10^5 ev, by assuming that self-absorption for synchrotron radiation is small or negative in this frequency range.

The type IVA burst in the dm-λ region shows a reversal of the sense of polarization—ordinary mode, as compared with the extraordinary mode in the cm-λ region. Assuming that the dm-λ emission originates from the same source as the cm-λ emission, the reversal of the sense of polarization can be explained either as a propagation phenomenon due to magneto-ionic mode coupling in a quasi-transverse region (Reference 8) or as due to differential absorption of synchrotron radiation near the gyro frequency of ambient thermal electrons (Reference 6). However, the existence of a distinct maximum in the type IV power spectrum in the dm-λ region (Reference 9) appears to argue for a separate source in this wavelength region.

The third phase of the type IV radiation, type IVC, has not yet been satisfactorily explained. Attempts have been made to explain the type IVC as well as storm radiation on meter waves in at least three different ways—involving gyro, synchrotron, and plasma radiations—as discussed below.

One can show (Reference 2) that, unlike the case of bremsstrahlung, the absorption coefficient in gyro radiation increases with temperature as $T^{s-3/2}$ $(s\geq2)$. This means that, if the absorption is mainly due to gyro radiation, then even an optically thin slab of hot plasma can have a high brightness temperature. This gyro radiation is of great importance in the generation of the slowly varying component on centimeter wavelengths and possibly also storm radiation on meter wavelengths. For an isothermal layer of magneto-active plasma, the brightness temperature T_b, radiation intensity I, and degree of polarization P are given by

$$T_b=\frac{T}{2}\left[(1-e^{-\tau_o})+(1-e^{-\tau_e})\right],$$

$$I_\omega=\frac{\omega^2kT_b}{4\pi^3c^2},$$

$$P=(e^{-\tau_e}-e^{-\tau_o})/(1-e^{-\tau_e}+1-e^{-\tau_o}),$$

where τ_e and τ_o are the optical thickness of the layer for extraordinary and ordinary waves. It is obvious that $T_b<<T$ when $\tau_{e,o}<<1$, and $T_b\approx T$ when $\tau_{e,o}\gtrsim1$. In the corona and chromosphere, $\tau_{e,o}$ is due to absorption by electron-proton collisions, as well as to resonance absorption occurring in layers $\omega=\omega_H$, $2\omega_H$, $3\omega_H$, etc. According to Ginzburg and Zheleznyakov (Reference 10), $\tau_{e,o}^{res}\propto NT^{s-1}$ $(s\geq2)$ and $\tau_{e,o}^{res}\propto NT$ $(s=1)$ where s is the order of the harmonic. In the corona ($T\approx10^6$ °K and $N\approx3\times10^8$ cm^{-3}), τ^{res} for $\omega=\omega_H$, $2\omega_H$ (ordinary wave) and $\omega=2\omega_H$, $3\omega_H$ (extraordinary wave; ω_H of extraordinary mode cannot escape from the solar atmosphere) is usually comparable with or even larger than unity.

The increase in resonance absorption or emission along with an increase in the kinetic temperature of the solar plasma led Ginzburg and

Zheleznyakov (Reference 10) to suggest an explanation of the noise storm radiation on meter wavelengths in terms of gyro radiation. They considered a subsystem of weakly relativistic electrons, whose velocity is $v \approx 0.3c$; if the temperature T_p and density N_p of the system is such that $\tau_p \approx 1$, then one can explain effective temperatures $T_b \lesssim T_p$. It turns out for $T_p = 2.5 \times 10^8$ °K ($T_b \lesssim 2.5 \times 10^8$ °K) and the scale of the magnetic field, $L_H \approx 2.10^{10}$ cm, the optical depth τ at 100 Mc/s ($\omega \approx 2\omega_H$) is of the order of N_p. Thus, T_b of emission for the subsystem heated to $T_p \approx 2.5 \times 10^8$ °K attains the same value if $\tau \approx N_p \approx 1$ electron/cm^3. Ginzburg and Zheleznyakov (Reference 10) related the polarization of the storm radiation to the distribution of fast electrons with height. Thus, the polarization will be ordinary if the fast electrons with $v \approx 0.3c$ are situated below the level $\omega \approx 2\omega_H$; that is, they radiate in a layer with frequency $\omega \approx \omega_H$, which allows only the ordinary wave to escape from the corona. When fast electrons are located mostly above the ω_H level, the extraordinary-mode polarization should be observed, since the emission from the ω_H level is small and, in $2\omega_H$ and $3\omega_H$ levels, $\tau_e > \tau_o$. If the density of fast electrons high in the corona is high and in the $2\omega_H$ level, the optical thickness of the subsystem $\tau_{e,o} > 1$, the degree of polarization should be reduced. Since the distribution of fast electrons with height depends on specific conditions above a sunspot active region (on the nature of acceleration of particles, magnetic field configuration, etc.), one should expect irregular sense of polarization, which is not observed. Indeed, the sense of polarization which is ordinary does not seem to depend in any significant manner on the altitude of emission. It should be pointed out, however, that the degree of polarization decreases with increased height of emission, as observed near the limb.

The directivity of storm radiation on meter waves can be due partly to refraction in the corona and partly to the fact that in the region of emission, the refractive index $n \approx 1$. Thus, for propagation at large angles to the magnetic field, ordinary and extraordinary waves originating from the ω_H and $2\omega_H$ levels will be strongly absorbed in the $2\omega_H$ and $3\omega_H$ levels, respectively. The resulting degree of directivity will depend on the magnetic field structure and on the height distribution of fast electrons.

If $T_b > 10^9$ °K, then the energy of the radiating electrons should be 10^5–10^6 ev, and, also, N_p should be greater than 1. The electrons are probably accelerated high in the corona by some mechanism, not clearly understood. It is likely that the electrons are carried into the corona by means of shock waves. Further, there may be migration of fast electrons from lower to higher levels in the corona.

The storm radiation on meter waves also has been explained as due to synchrotron radiation by Takakura (Reference 6), who showed that electrons of Mev energy spiraling in helical orbits with steep pitch angles can emit synchrotron radiation of ordinary mode with narrow bandwith and high brightness temperature. Probably the most plausible explanation of storm radiation, as far as its polarization and directivity are concerned, was given by Denisse (Reference 11) in terms of radiation from plasma waves. According to Denisse, the low energy electrons trapped in magnetic configurations associated probably with coronal streamers slowly diffuse towards regions of higher electron density and excite Cerenkov plasma oscillations. These longitudinal plasma waves are transformed into electromagnetic (EM) waves of ordinary mode, when the dispersion curves of the P and EM waves come close to each other; this coupling occurs in regions of $\omega \approx \omega_o$ and is caused by large-scale variations of density or magnetic field in an inhomogeneous plasma. The corresponding coupling coefficient is $Q \lesssim 10^{-6}$.

TYPE III AND TYPE II BURSTS ON METER WAVES

A detailed theory of the generation of type III bursts has been worked out by Ginzburg and Zheleznyakov (Reference 12). According to this theory, coherent plasma waves are excited by Cerenkov mechanism, that is, by the passage of a stream of electrons traveling at a velocity V greater than the phase velocity V_ϕ of the wave. The frequency spectrum of

the plasma wave is sharply peaked around the plasma frequency ω_o because of the high value of refractive index near $\omega \approx \omega_o$ in the range of velocities $V >> V_T$ (V_T = rms thermal velocity of electrons) and also because of Landau damping. The longitudinal plasma waves are coupled to the transverse EM waves by scattering on small-scale fluctuations of plasma density. Both the ions and the electrons in a thermal plasma contribute to the fluctuations. The fluctuation spectrum for $Kh << 1$ (K is the wave number and h is the Debye length), calculated by Salpeter (Reference 13), is shown schematically (Reference 14) in Figure 37–1. The frequency ($\omega_i \approx Kv_i$, where v_i is the rms ion velocity) is due to Doppler shift from fluctuations controlled by the ions. The "plasma line" at ω' is at the frequency given by K and the dispersion relation for electron plasma waves: $\omega'^2 = \omega_o^2 + K^2 V_T^2 >> \omega_i^2$.

When $\left(\frac{KV_T}{\omega_o}\right)^2 = 3(Kh)^2 << 1$, as occurs in many applications, then $\omega' \approx \omega_o$. When a plasma wave with wave vector K and frequency ω is incident on a scattering volume, the amount of scattered signal is determined by the spectrum of the fluctuations. The spectrum of the scattered signal is obtained by the convolution of the incident spectrum with its fluctuation spectrum. The result of this convolution is that we get EM waves of frequencies $\omega = \omega_o \pm \omega_{ih}$. Since the variation of plasma density occurs rather slowly, scattering due to the ion component does not result in any significant change in the wave frequency ($\omega = \omega_o \pm \omega_i \approx \omega_o$, since $\omega_i << \omega_o$) so that the EM waves formed because of this scattering have the same frequency as the incident plasma wave. This scattering is called *Rayleigh scattering*. The radiation in this case is emitted incoherently and mainly in the forward direction, and the transformation coefficient in the typical solar corona is $Q' \approx 3 \times 10^{-6}$.

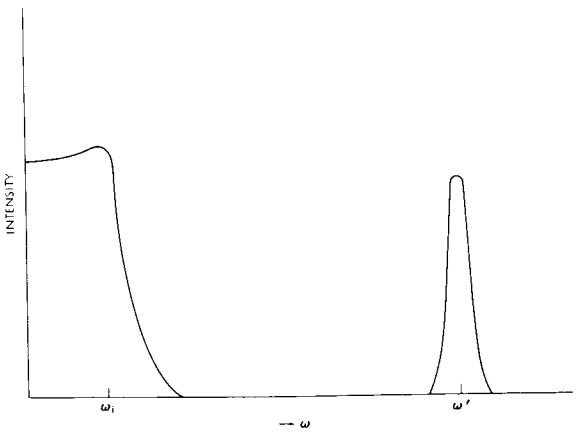

FIGURE 37–1.

The scattering due to the electron component results in a wave of frequency $\omega = \omega + \omega' \approx 2\omega_o$, which satisfies the usual dispersion relation; this is *combination scattering*. There is another combination frequency $\omega - \omega' \approx 0$, for which $n^2 < 0$, with the result that combination emission occurs only at $\omega \approx 2\omega_o$. Ginsburg and Zheleznyakov proposed combination scattering to explain the harmonics of type II and type III bursts, the fundamentals being attributed to Rayleigh scattering. According to combination scattering there should be no third or higher harmonics, as is observed in type II and type III bursts. This, however, does not explain why one sometimes observes a third harmonic of U-type bursts which are supposed to be generated in the same way as the type III bursts. The radiation from combination scattering is emitted mainly in the backward direction, so that it is reflected at its proper plasma level before it is observed. As a result, the second harmonic should be below the fundamental. This has, indeed, been confirmed by the observations of Smerd, Wild, and Sheridan (Reference 15). Ginzburg and Zheleznyakov (Reference 12), as well as Wild, Smerd, and Weiss (Reference 2), showed that the intensities of the fundamental and the harmonic of type III bursts calculated on the above hypothesis agreed roughly with observations.

It is obvious that one cannot easily make similar calculations for type II bursts, since they cannot be generated by the initiating particle stream whose velocity $V_0 < V_T$. However, it has been suggested that type II bursts continuously eject streams of fast electrons which excite the plasma waves. This hypothesis is supported in some, but not all, type II bursts showing fine structure bursts (e.g., her-

ringbone structure) emanating from the main drifting band. An alternative hypothesis has been proposed by Tidman (Reference 16) in that the fast electrons contained in an outward moving shock front directly generates transverse EM waves which we observe as type II bursts. The generation of type II bursts is, indeed, complex; it is possible that the smooth background of type II bursts is somehow generated by the shock wave and the sharp superimposed structure is produced by particles accelerated by the shock.

DRIFTING BURSTS ON DECIMETER WAVES

The drifting bursts—intermediate-drift and fast-drift bursts—on decimeter waves are not amenable to an easy explanation. The intermediate-drift bursts are of short duration (0.2–0.6 sec) at one frequency and have typical drift rates between approximately 10 and 50 Mc/s per second. Assuming that they are due to plasma oscillations excited in the corona by outward moving disturbances and assuming a standard model of coronal electron density distribution, the inferred speeds of the exciting disturbances are found to lie between approximately 50 and 200 km/sec. If the disturbances travel along coronal streamers, the speeds will be about twice these values. The wide range of values here reflects both the wide range of observed drift rates as well as the rapidly changing gradient in the assumed electron density model. These apparent low velocities of the bursts are less than the mean thermal electron velocity of about 7000 km/sec in a 10^6 °K corona, and hence Cerenkov electron plasma waves cannot be excited. The simplicity of these bursts indicates that they are probably not generated in the same manner as type II bursts, that is, by turbulent fast electrons in an outward moving shock front. It should be noted, however, that the velocity inferred from drift rates depends critically on the assumed electron density gradient in the corona. A small density gradient could result in a considerable decrease in the drift rate for a disturbance of a given velocity. Further, a low gradient increases the effects of group retardation, which in turn tends to reduce the drift rate. In the extreme case of a suitably small density gradient in the lower corona, particle streams may appear to have drift rates 10 to 100 times less than those anticipated from standard models. However, the existence of fast-drift bursts on decimeter wavelengths indicates a real difference in velocities between the fast-drift and intermediate-drift bursts.

If the dm-λ fast-drift bursts (in the 500–1000 Mc/s range) are due to plasma oscillations as in the case of meter wave type III bursts, then a disturbance traveling outward along a coronal streamer (with 10 times the electron density given by a standard model) with a velocity of $\approx 0.5c$ would pass from the 1000 Mc/s plasma level to the 500 Mc/s level in less than 0.1 sec. These delays are too short to be detected with the present spectrum analyzers and are much less than the delays usually observed in events resembling meter-λ type III bursts. This discrepancy possibly may be due to the group delay whose effects are important at the fundamental frequency of the plasma oscillations. If there is a difference in electron density gradient between two plasma levels, then the effect of group delay increases the delay between the arrival of the two plasma frequencies at the earth. It appears that a delay of several tenths of a second (which is sometimes observed) can arise if the gradient at the 1000 Mc/s plasma level is similar to that of the chromosphere, while at the 500 Mc/s level resembles that of the corona (Reference 17). For reverse-drift bursts, the plasma hypothesis implies a motion toward higher electron densities, which may be due to an inward motion of the exciting disturbance or to a reversal in the atmospheric gradient. The former situation would arise if the flare explosion takes place in the region of origin of the decimeter waves, so that the electrons which are ejected travel into different directions both into the chromosphere and into the corona. This appears to be the case since on decimeter waves one occasionally observes type II-like bursts, but drifting in the reverse direction—that is, from lower to higher frequencies (Reference 18).

The fast-drift bursts or other variabilities occur for a considerable period (several tens of minutes) after the start of the associated flare. They are not associated with any visible erup-

tions or new brightenings of the flare region. On the plasma hypothesis, the continued occurrence of dm-λ fast-drift bursts for a considerable period after the flare start indicates the occurrence of similarly repeated electron jets. Theories of the origin of solar flares predict that electrons are liberated only during the explosive phase of the Hα flare. The electron jets responsible for the continuously occurring fast-drift bursts on decimeter waves must then be related to some kind of plasma instability, whose effects can be traced only through a limited range of plasma levels in the solar atmosphere. Present observations do not permit us to decide whether the repeated instabilities occur in the region of the original explosion or in the region of acceleration where the trapped electrons produce type IVA radiation through the synchrotron mechanism. High resolution directional observations certainly will contribute considerably toward a better understanding of the fast phenomena in the decimeter wave region. It appears that an angular resolution of several seconds of arc will be necessary to determine any possible source movement in the 500–1000 Mc/s range. Such a determination seems extremely important to substantiate the plasma hypothesis and, if possible, to determine the structure of the decimeter wave emissive regions, which may be closely related to the seat of the flare explosion.

REFERENCES

1. Hachenberg, O., and Wallis, G., 1961, *Zeit fur Astrophys.*, 52: 42.
2. Wild, J. P., Smerd, S. F., and Weiss, A. A., 1963, *Annual Review of Astronomy and Astrophysics*, 1: 291.
3. Anderson, K. A., and Winckler, J. R., 1962, *J. Geophys. Res.*, 67: 4103.
4. Schwinger, J., 1949, *Phys. Rev.*, 75: 1912.
5. Boischot, A., and Denisse, J. F., 1957, *C.R.A.S.*, 245: 2194.
6. Takakura, T., 1960, *Pub. Astr. Soc. Japan*, 12: 325 and 352.
7. Takakura, T., and Kai, K., 1961, *Pub. Astr. Soc. Japan*, 13: 94.
8. Cohen, M. H., 1961, *Ap. J.*, 133: 978.
9. Takakura, T., 1963, *Pub. Astr. Soc. Japan*, 15: 327.
10. Ginzburg, V. L., and Zheleznyakov, V. V., 1961, *Soviet Astronomy-AJ*, 5: 1.
11. Denisse, J. F., 1960, XII General Assembly, URSI, London.
12. Ginzburg, V. L., and Zheleznyakov, V. V., 1958, *Sovier Astronomy-AJ*, 2: 653.
13. Salpeter, E. E., 1960, *Phys. Rev.*, 120: 1528.
14. Cohen, M. H., 1962, *J. Geophys. Res.*, 67: 2729.
15. Smerd, S. F., Wild, J. P., and Sheridan, K. V., 1962, *Aust. J. Phys*, 15: 180.
16. Tidman, D. A., 1962, *Phys. Fluids*, 5: 1104.
17. Young, C. W., Spencer, C. L., Moreton, G. E., and Roberts, J. A., 1961, *Ap. J.*, 133: 243.
18. Kundu, M. R., and Spencer, C. L., 1963, *Ap. J.*, 137: 572.

DISCUSSION

Dr. Takakura: One point is that the origins of decimeter and microwave components may be different. Even the continuum has two maxima in intensity corresponding to microwave-IV and decimeter-IV. The observed heights are different; the height for microwave-IV is about 0.05 solar radius, and the height of decimeter-IV measured at 200 Mc is 0.3 solar radius above the photosphere.

The second point: If the reversal of sense of circular polarization *with frequency* is due to the coupling suggested by Dr. Cohen, we may expect longitudinal dependence, because the sense reversal with frequency may occur only in some restricted regions in the longitude. But we don't have any such evidence. Furthermore, the chance that the sense reversal *with frequency* would occur is small for any configuration of magnetic field. However, the sense reversal occurs for about 70 percent of impulsive bursts at a frequency somewhere between 9000 and 1000 Mc.

The third point concerns the type IV–c. We can't find any difference between type IV–c and type I storms. There is no difference in their heights and no difference in the sense of

polarization; and, also, the directivity is similar, both having sharp directivity. Furthermore, Dr. Boischot showed that at the beginnings of type I storms there are some flares. Therefore, what is the difference between type I and type IV–c storms?

Dr. Kundu: I think that the polarization question should be addressed to the French. It is mainly their results on polarization which distinguish types IV–b and IV–c.

On the first question, I think 200 Mc, we consider as meter waves. Do you consider it as decimeter?

Dr. Takakura: Yes.

Dr. Kundu: There is a difference in height between 200 and, say, 1000 Mc. That, I include in my type IV–b. I didn't consider that as decimeter.

Dr. Takakura: A histogram of center frequencies of type IV bursts shows that the bursts at 200 Mc are generally included in a group of decimeter type IV.

Dr. Kundu: It is 1.5 meters. How can it be decimeters?

Dr. Takakura: The name of the category is rather confusing. I would say that the histogram showing the number of bursts plotted against center frequency indicates three groups in frequency range: One group, which I called dm–IV, is ranging from 1000 Mc to 200 Mc; the other is 140 to 50 Mc; and another is 2000 to 10,000 Mc.

Dr. Kundu: That is a good point. I saw that yesterday. But that is the only point.

Dr. Cohen: I think it is going to take a number of us to comment on all of that story from Dr. Takakura. I will just speak to the one point about the change of polarization.

You would expect a longitude dependence only if you expected the fields to be regular; but, if you expected the field to be rather erratic and twisted, one wouldn't expect a longitude dependence, at least not much. If it comes from absorption, as you suggest, you need more than 1000 gauss in the source region. I think that is an objection to your theory.

Dr. Boischot: The two main differences between continuum storm and ordinary noise storm are the following:

1. The center of emission of the continuum storm stands lower in the corona than the center of the noise storm.

2. The size of the former is, on the average, much smaller than for a noise storm.

After a few hours, type I bursts may appear; the continuum storm degenerates into a normal noise storm.

Dr. Takakura: What are the heights for continuum storms?

Dr. Boischot: Less than 0.1.

Dr. Takakura: Less than 0.1?

Dr. Boischot: Yes. Certainly much lower than the average height of noise storms.

Dr. Oster: I missed one point. What was the reason that beams cannot excite plasma radiation in the decimeter range?

Dr. Kundu: I think the Cerenkov plasma radiation mechanism, which Dr. Smerd will speak about later, requires that the velocities of the exciting electron streams must be higher than the rms thermal electron velocity in the corona. The velocity deduced from the drift rate of intermediate-drift bursts is less than this velocity.

Dr. Smerd: I think Dr. Wild pointed out yesterday that there were two quite distinct phases in the meter wavelength type IV burst. One of these is the moving type IV, and the other is the stationary type IV. In the moving type IV, the movement certainly has never been observed above 200 Mc. It might be that phase of an outburst which Dr. Takakura refers to when he calls any simultaneous 200 Mc radiation part of a decimeter wave component.

But I think, in the stationary meter wave IV, the 200 Mc radiation is well within the spectrum which sometimes seems to extend up to 2000 Mc. I think that is the sort of picture which Dr. Kundu had in mind when he referred to his type IV–c and said that 200 Mc belongs to the meter wavelength IV.

One other point: Dr. Kundu seems to associate all the drifting bursts in the decimeter waves with plasma waves. That is at present a hypothesis, and I think the test of that hypothesis by direct observations—which means that one has to observe where the radiation comes from over a range of decimeter wavelengths—is going to be one of the greatest challenges to the observers in this coming solar cycle.

N64-30288

38 ON THE GENERATION OF SOLAR RADIO BURSTS

S. F. Smerd
Radiophysics Laboratory,
CSIRO, Sydney, Australia

The sources of solar radio bursts have been identified with fast electrons and shock fronts streaming through the background plasma of the sun's atmosphere. Their movements and the accelerations of the source electrons are presumably governed by the complex magnetic fields in the active solar regions. It is in terms of the radio emissions from such sources that the observed burst spectra have to be interpreted. 30288

In the present survey we will discuss briefly the following properties of waves, plasmas, and their interactions which are needed in such work:

(1) The wave modes at which radio waves can be excited and propagate in the solar plasma,

(2) Some general requirements on source electrons and generating mechanisms to account for the observed high brightness temperatures,

(3) Some characteristics of the radiations emitted by three known emitting mechanisms.

This review is a short and slightly revised form of the material presented in Section 4 of "Solar Bursts," by Wild, Smerd, and Weiss (Reference 1). Only those references which are not included in the above review article are listed here.

RADIO WAVES IN A PLASMA

The Wave Modes

Four wave modes can exist in a plasma; we will refer to these as the *ordinary* and *extraordinary* waves, and the *electron* and *ion* waves. Without the coupling provided by a transverse magnetic field the former two waves are purely transverse electromagnetic waves and the latter two are longitudinal plasma waves. For electromagnetic waves the plasma merely acts as a dielectric medium; for longitudinal waves the plasma is essential because it takes part in the wave motion. The organizing force which makes plasma waves possible is the smeared-out, long-range electrostatic force due to many ions; it is effective only at wavelengths greater than the Debye length. At shorter distances the electrostatic force of individual ions dominates; this makes short wavelength plasma waves impossible.

The Dispersion Equations

The frequencies ω and propagation constants k of the waves are related through dispersion equations. The equations quoted here are derived from a macroscopic transport-equation treatment and with the neglect of the electron-ion mass ratio compared with unity (which dispenses with the ion mode altogether). The wave is described by the refractive index (real part) $\mu=c/v_{ph}$, where the phase velocity $v_{ph}=\omega/k$ and the corresponding group velocity $v_g=d\omega/dk$. The plasma is specified by the critical, or plasma, frequency ω_0 where

$$f_0=\omega_0/2\pi=(e^2N/\pi m)^{1/2}=9\times10^{-3}N^{1/2}_{(\mathrm{cm}^{-3})} \quad \mathrm{Mc/s}, \tag{1}$$

N being the electron density by ω_H, the electron gyro-frequency, where

$$f_H=\omega_H/2\pi=eH/2\pi mc=2.8H_{(gauss)} \ \mathrm{Mc/s} \tag{2}$$

and the root-mean-square (rms) velocity of thermal electrons

$$v_{th}=(3KT/m)^{1/2}=6.7\,T^{1/2}{}_{(^\circ\mathrm{K})} \ \mathrm{km/sec},$$

where K is Boltzmann's constant.

728-629 O—64——23

For *longitudinal propagation*, when the angle between the directions of propagation and the external magnetic field $\Theta=0$, the three remaining modes retain their identity and are given by

$$\mu^2=1-\omega_0^2[\omega(\omega\pm\omega_H)]^{-1}, \qquad (3)$$

$$\mu^2=(c/v_{th})^2(1-\omega_0^2/\omega^2); \qquad (4)$$

they are plotted for the case $\omega_H/\omega=\frac{1}{2}$ and $T=10^6$ °K as full lines in Figure 38–1. The two modes of Equation 3 are the *ordinary* (+ sign) and *extraordinary* (− sign) modes of the magneto-ionic theory; the remaining mode (Equation 4) is the *electron* mode, designated p=mode.

For *transverse propagation* ($\Theta=\pi/2$), only the ordinary mode

$$\mu^2=1-\omega_0^2/\omega^2$$

retains its identity. However in this, as in the general case, mode separation is possible through asymptotic approximations which have a large range of validity, provided $v_{th}^2<<c^2$ (for a million-degree corona $v_{th}^2/c^2\approx5\times10^{-4}$).

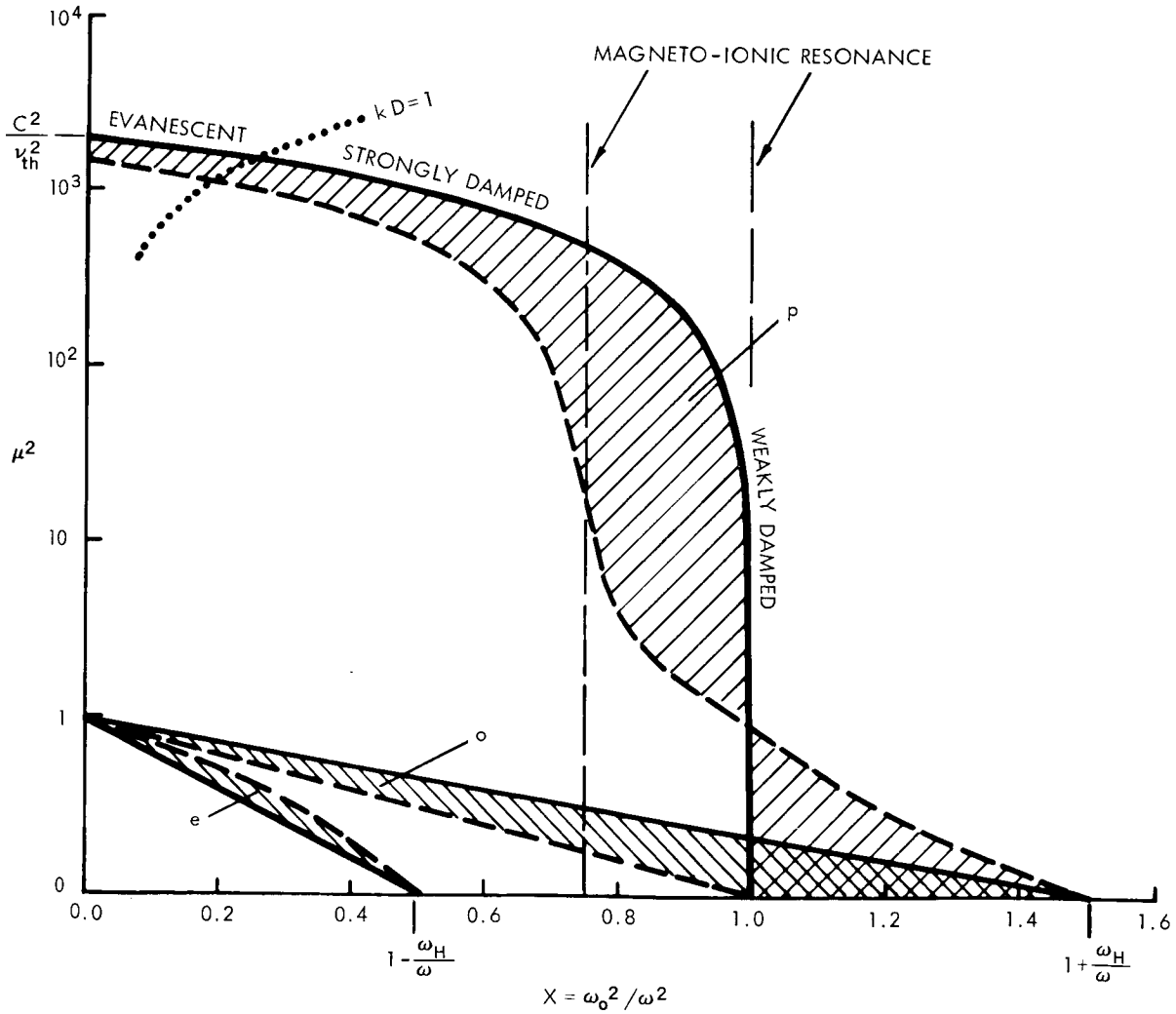

FIGURE 38–1. The dispersion curves for the ordinary o, extraordinary e, and electron p modes in a hot plasma; they are drawn for $T=10^6$ °K and $\omega_H/\omega=\frac{1}{2}$. Longitudinal propagation is shown thus ———, transverse propagation thus — — — —. For propagation at intermediate angles to the magnetic field the curves lie in the hatched areas. At $kD>1$, the wavelength becomes less than the Debye length and plasma waves become evanescent. (Reference 1)

For $\mu^2 \lesssim 1$, the approximate general solutions are identical with the equations defining the electromagnetic o and e modes of the magneto-ionic theory for a cold plasma. For $\mu^2 >> 1$, the electron mode is a plasma wave and is described by

$$\mu^2 \approx (c/v_{th})^2[1-(\omega_0/\omega)^2-\omega_H^2 \sin^2\Theta/(\omega^2-\omega_H^2\cos^2\Theta)].$$

The dispersion curves for transverse propagation are shown as broken lines in Figure 38–1. To complete the picture as it emerges from a macroscopic representation of the plasma, we reproduce as Figure 38–2 a sketch by Denisse and Delcroix (1961) of all four wave modes for an intermediate value of Θ and over a wider range of frequencies. Three modes (not the

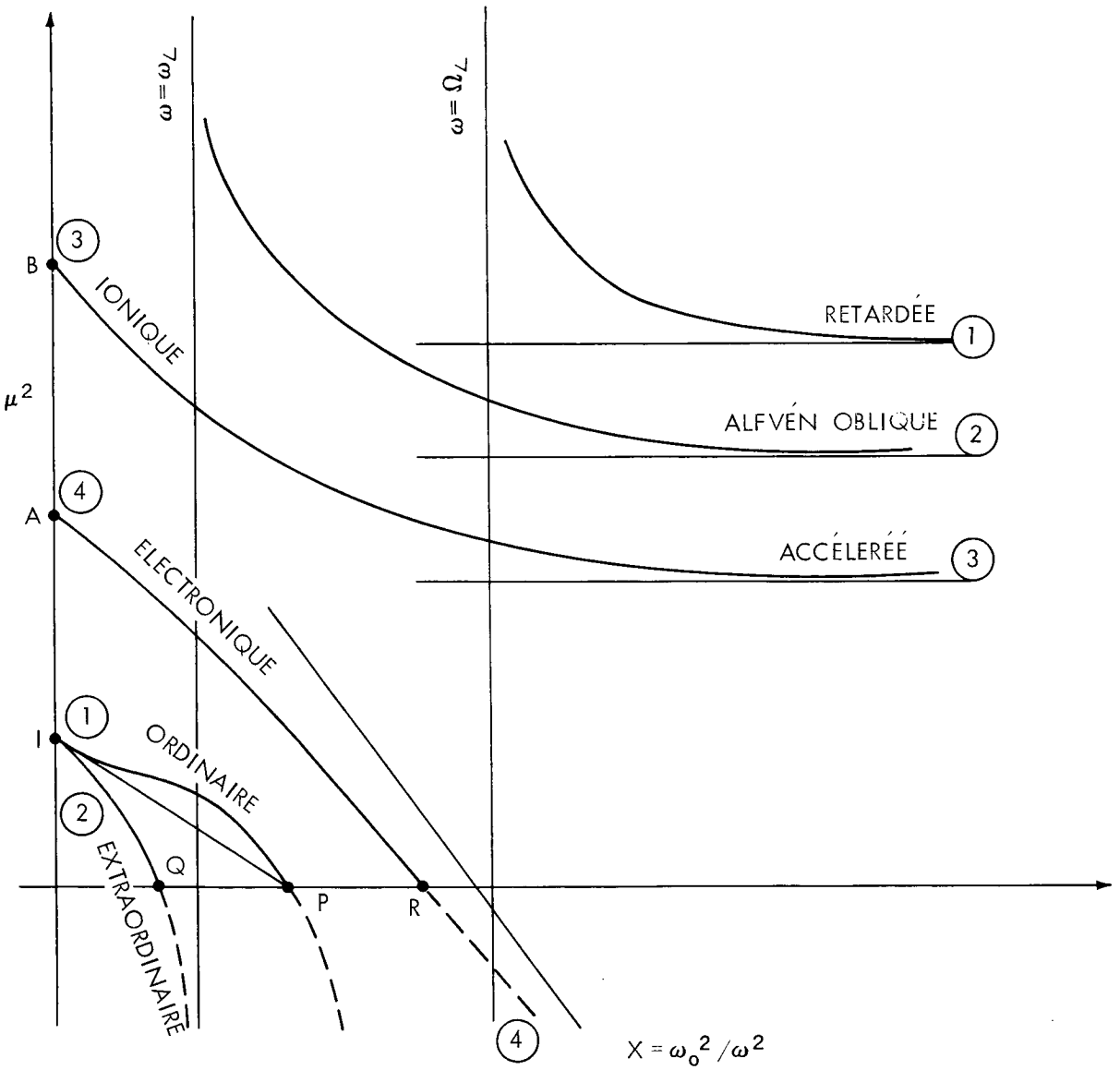

FIGURE 38–2. The dispersion curves for the four wave modes (ordinary, extraordinary, electron, and ion) in a hot plasma for propagation obliquely to the magnetic field. The points P, Q, and R correspond to the critical frequencies (Equation 5). The three, asymptotic low-frequency branches belong to the nondispersive magnetohydrodynamic waves. (Denisse and Delcroix, 1961)

electron mode) asymptotically approach horizontal tangents; in the nondispersive region these low-frequency (low compared with ω_0, ω_H) waves are collectively called magneto-hydrodynamic waves.

The results obtained from a macroscopic representation of the plasma are probably substantially correct, at least at wavelengths greater than the Debye length. However, they are incomplete. So, for instance, Gross (Reference 2) from a microscopic representation of the plasma finds gaps in the spectrum of the dispersion relations for transverse propagation at the harmonics of the electron gyro frequency; the width of the gaps is proportional to the plasma temperature. The significance of this result will become clearer when we discuss noncollisional wave damping.

Characteristic Frequencies

The wave modes of the dispersion equations have two characteristic frequencies associated with them. They are: the *critical frequencies* at which the refractive index vanishes, and the *resonance frequencies* at which the refractive index becomes infinite.

Physically, a critical frequency is the lowest frequency at which a wave mode can propagate. We find, thus, that the electromagnetic modes can propagate above the following frequencies:

$$\left.\begin{array}{l} \omega=(\omega_0^2+\omega_H^2/4)^{\frac{1}{2}}\mp\omega_H/2\,(-o+e); \\ \qquad\qquad\qquad\qquad \text{longitudinal propagation,} \\ \left.\begin{array}{ll} \omega=\omega_0 & (o) \\ \omega=(\omega_0^2+\omega_H^2/4)^{\frac{1}{2}}+\omega_H/2 & (e) \end{array}\right\}\text{transverse propagation.} \end{array}\right\} \quad (5)$$

It is clear from Figures 38–1 and 38–2 that there are no resonances for the electron and ion waves and that the electromagnetic waves in a hot plasma do not show their cold-plasma resonance, whose frequencies are given by

$$\omega^2=\tfrac{1}{2}\{(\omega_0^2+\omega_H^2)\pm[(\omega_0^2+\omega_H^2)^2-4\omega_0^2\omega_H^2\cos^2\theta]^{1/2}\}; \quad (6)$$

that is, in the high-frequency range ω_0 (longitudinal) to $\sqrt{\omega_0^2+\omega_H^2}$ (transverse) and the low-frequency range ω_H (longitudinal) down to 0 (transverse). It is at these resonance frequencies that the hot-plasma dispersion curves of the electron and ion waves have their steepest gradient, called *pseudo-resonance* (see, for instance, Figure 38–1 for the pseudo-resonance of the electron wave). The pseudo-resonance of the electron wave occurs at the high resonance frequency, that of the ion wave at the low resonance frequency.

Physically, the cold-plasma resonance separates the fast-wave region ($\mu^2 \lesssim 1$) when the electron wave is essentially electromagnetic and of the e mode from the slow-wave region ($\mu^2 >> 1$) where the electron wave is essentially a plasma wave; coupling between the two waves is strong at the cold-plasma resonance (Reference 3).

Because of the previously mentioned restriction to wavelengths longer than the Debye length, plasma waves can only exist for about one octave above the cold-plasma resonance frequency, as given by Equation 6.

Collision Damping

So far we have dealt only with real frequencies and propagation constants; we have not considered wave attenuation or growth. When collisions of frequency ν between electrons and ions are taken into account, they characteristically introduce an imaginary term in the dispersion equations. This leads to collision damping in the form exp $(-\nu t)$ for the intensity of plasma waves; such damping has been invoked to explain an observed exponential decay in type III bursts. In a million-degree corona the collision frequency is about 1 at the 40 Mc/s plasma level and varies as the square of the plasma frequency.

Again, for field-free propagation in the z-direction collisions lead to damping of electromagnetic waves as exp $(-\kappa z)$ when the absorption coefficient

$$\kappa=\nu\omega_0^2/\omega^2\mu c. \quad (7)$$

The attenuation along the path s between source and observer is usually expressed by the optical depth $\tau=\int\kappa ds$, the attenuation factor being exp $(-\tau)$. In the quiescent corona the optical depth to the plasma level decreases from

about 1 at 1 meter toward the longer wavelengths. At the microwaves, whose plasma levels normally lie in the cooler gas below the corona, the optical depth increases rapidly and may prevent us from seeing bursts at the plasma level. However, heating or compression of plasma levels during a flare may make such bursts observable.

Each absorption process must correspond to an emission process. Collision absorption corresponds to bremsstrahlung emission; it is the only absorption process in a macroscopic plasma treatment. Other emission processes are known to be effective in a plasma so that the absorption coefficient will, in general, be of the form

$$\kappa=\kappa_1+\kappa_2+\kappa_3+\cdots.$$

We will investigate non-collisional absorption in connection with the corresponding emission processes.

NONTHERMAL SOURCES AND WAVE AMPLIFICATION

Bailey (Reference 4) first suggested the possibility of amplification and instability from electrons streaming in a plasma; his conclusions were based on his interpretation of complex propagation constants and frequencies in the appropriate dispersion equations, again derived for a macroscopically specified plasma. Twiss (Reference 5) pointed out that such general conclusions from the dispersion equations could be misleading; for instance, it may not be possible to distinguish an apparent wave growth in one direction from an actual damping of the reflected wave in the opposite direction without introducing the appropriate initial and boundary conditions.

Twiss (1958) later pioneered what seems a more satisfactory way of finding the conditions under which wave amplification is possible. Amplification is there linked with negative absorption; the conditions for this are given in terms of energy distribution of the nonthermal source electrons and the electron emissivity for the effective radiating mechanism.

The possibility of wave amplification is clearly of interest in our search for an explanation of the high intensities of solar bursts.

Positive and Negative Absorption

We start with the quantum formulation for the macroscopic radio absorption coefficient—that is, the difference between all stimulated absorptions and all stimulated emissions. It should be noted that stimulated processes are vastly more likely and important at the low radio frequencies than they are at the higher optical frequencies. The reason for using quantum formulation in a classical problem is one of convenience. Correspondence between classical and quantum theory is established by identifying the electron emissivity $Q_f(\epsilon)$ with spontaneous emission.

This allows us to write for the volume emissivity,

$$\eta_f=\int_0^\infty Q_f(\epsilon)n(\epsilon)\mathrm{d}\epsilon, \tag{8}$$

where $n(\epsilon)\mathrm{d}\epsilon$ is the number density of electrons with energy in the range ϵ to $\epsilon+\mathrm{d}\epsilon$. We relate the Einstein transition coefficients in the usual way; the statistical weight, $g(\epsilon)\mathrm{d}\epsilon$, in these relations and for continuous energy levels is defined by

$$NF(\epsilon)g(\epsilon)=n(\epsilon), \tag{9}$$

where N is the number density of electrons and $F(\epsilon)$ their energy distribution in momentum space. From Liouville's theorem the statistical weight is that volume in momentum space which corresponds to the energy interval ϵ to $\epsilon+\mathrm{d}\epsilon$ of the radiating electrons. For isotropic momenta p,

$$g(\epsilon)\mathrm{d}\epsilon=4\pi p^2\mathrm{d}p. \tag{10}$$

In the non-relativistic case ($\epsilon<<m_0c^2$),

$$g(\epsilon)=4\pi(2m_0^3)^{1/2}\epsilon^{1/2}; \tag{11}$$

in the highly relativistic case ($\epsilon>>m_0c^2$),

$$g(\epsilon)=(4\pi/c^3)\epsilon^2. \tag{12}$$

With the well-justified assumption that $hf<<\epsilon$ we finally obtain for the absorption coefficient,

$$\kappa=\frac{-c^2N}{\mu^2f^2}\int_0^\infty \frac{\mathrm{d}F}{\mathrm{d}\epsilon}Q_f(\epsilon)g(\epsilon)\mathrm{d}\epsilon. \tag{13}$$

If Q and F are well behaved functions, integration by parts yields an alternative form

$$\kappa=\frac{c^2N}{\mu^2f^2}\int_0^\infty F(\epsilon)\frac{\mathrm{d}}{\mathrm{d}\epsilon}[Q_f(\epsilon)g(\epsilon)]\mathrm{d}\epsilon. \quad (14)$$

In most natural circumstances the absorption coefficient is positive; in that case we can specify a radiation temperature T_r, which from Equations 8, 9, 13, 14 and the Rayleigh-Jeans radiation law is given by

$$KT_r=-\frac{\int_0^\infty F(\epsilon)Q_f(\epsilon)g(\epsilon)\mathrm{d}\epsilon}{\int_0^\infty \frac{\mathrm{d}F}{\mathrm{d}\epsilon}Q_f(\epsilon)g(\epsilon)\mathrm{d}\epsilon}$$

$$=\frac{\int_0^\infty F(\epsilon)Q_f(\epsilon)g(\epsilon)\mathrm{d}\epsilon}{\int_0^\infty F(\epsilon)\frac{\mathrm{d}}{\mathrm{d}\epsilon}\{Q_f(\epsilon)g(\epsilon)\}\mathrm{d}\epsilon}. \quad (15)$$

For a thermal source of Maxwellian velocity distribution,
when

$$F(\epsilon)=(2\pi m_0KT)^{-3/2}\exp(-\epsilon/KT),$$

the radiation temperature is identical with the electron temperature.

In the case of a nonthermal source, but still with positive absorption, the radiation temperature is again determined by Equation 15, which essentially gives $KT_r=\bar{\epsilon}$, a weighted mean energy of the radiating electrons. Such radiation from nonthermal source electrons may be called temperature-limited.

Twiss (1958) pointed out that under certain conditions the absorption coefficient becomes negative. It is clear from Equation 13 that (a) *A positive gradient in the electron energy distribution is a necessary condition for negative absorption.* This is the continuous energy-distribution equivalent of the quantum-theory requirement for overpopulation of the high-energy states.

It is furthermore clear from Equation 14 that (b) *A negative gradient in the product of statistical weight and electron emissivity is needed in addition to condition (a) for negative absorption.*

Four cases of different conditions leading to positive and negative absorption are illustrated in Figure 38–3.

Electron streams through the solar background plasma are likely to meet one requirement for negative absorption, namely, a positive gradient in the energy distribution. Whether amplication actually will occur has to be investigated for each particular emission mechanism. First, however, we have to determine the effect of anisotropy.

In the presence of a magnetic field, emission is directional. The fundamental gyro frequency is emitted in a wide cone around the direction of the magnetic field; with increasing harmonic number the emission is more and more confined to the direction of the instantaneous electron velocity. We allow for this anisotropy by specifying the directional electron emissivity $Q_f(\epsilon, \theta-\phi)$, where θ and ϕ are the angles between the magnetic field and the directions of emission and electron velocity, respectively.

We then obtain for the volume emissivity and the absorption coefficient:

$$\eta_f(\theta)=N\int_0^\infty\int_0^{2\pi}F(\epsilon,\phi)Q_f(\epsilon,\theta-\phi)g(\epsilon,\phi)\mathrm{d}\epsilon\mathrm{d}\phi$$

and

$$\kappa(\theta)=-\frac{c^2N}{\mu^2f^2}\int_0^\infty\int_0^{2\pi}\left[\left(\frac{\partial}{\partial\epsilon}+\frac{\Delta\phi}{hf}\frac{\partial}{\partial\phi}\right)F(\epsilon,\phi)\right]Q_f(\epsilon,\theta-\phi)g(\epsilon,\phi)\mathrm{d}\epsilon\mathrm{d}\phi,$$

respectively, where $\Delta\phi$ is the change in the direction of electron motion due to emission or absorption of a photon. The statistical weight is now that annular volume in phase space which contains electron energies in the range ϵ to $\epsilon+\mathrm{d}\epsilon$ and the corresponding electron velocities in the direction ϕ to $\phi+\mathrm{d}\phi$; this gives

$$g(\epsilon,\phi)\mathrm{d}\epsilon\mathrm{d}\phi=2\pi p^2\sin\phi\mathrm{d}p\mathrm{d}\phi=\tfrac{1}{2}g(\epsilon)\sin\phi\mathrm{d}\epsilon\mathrm{d}\phi,$$

where $g(\epsilon)$ is defined by Equation 10 and given by Equations 11 and 12 for non-relativistic and highly relativistic electrons, respectively. The conditions for negative absorption remain unchanged if we replace

$$\frac{\mathrm{d}}{\mathrm{d}\epsilon}\text{ by }\left(\frac{\partial}{\partial\epsilon}+\frac{\Delta\phi}{hf}\frac{\partial}{\partial\phi}\right).$$

RADIATION PROCESSES

Bremsstrahlung

The first radiating process we consider is bremsstrahlung—that is, electromagnetic radiation from electrons which are deflected by

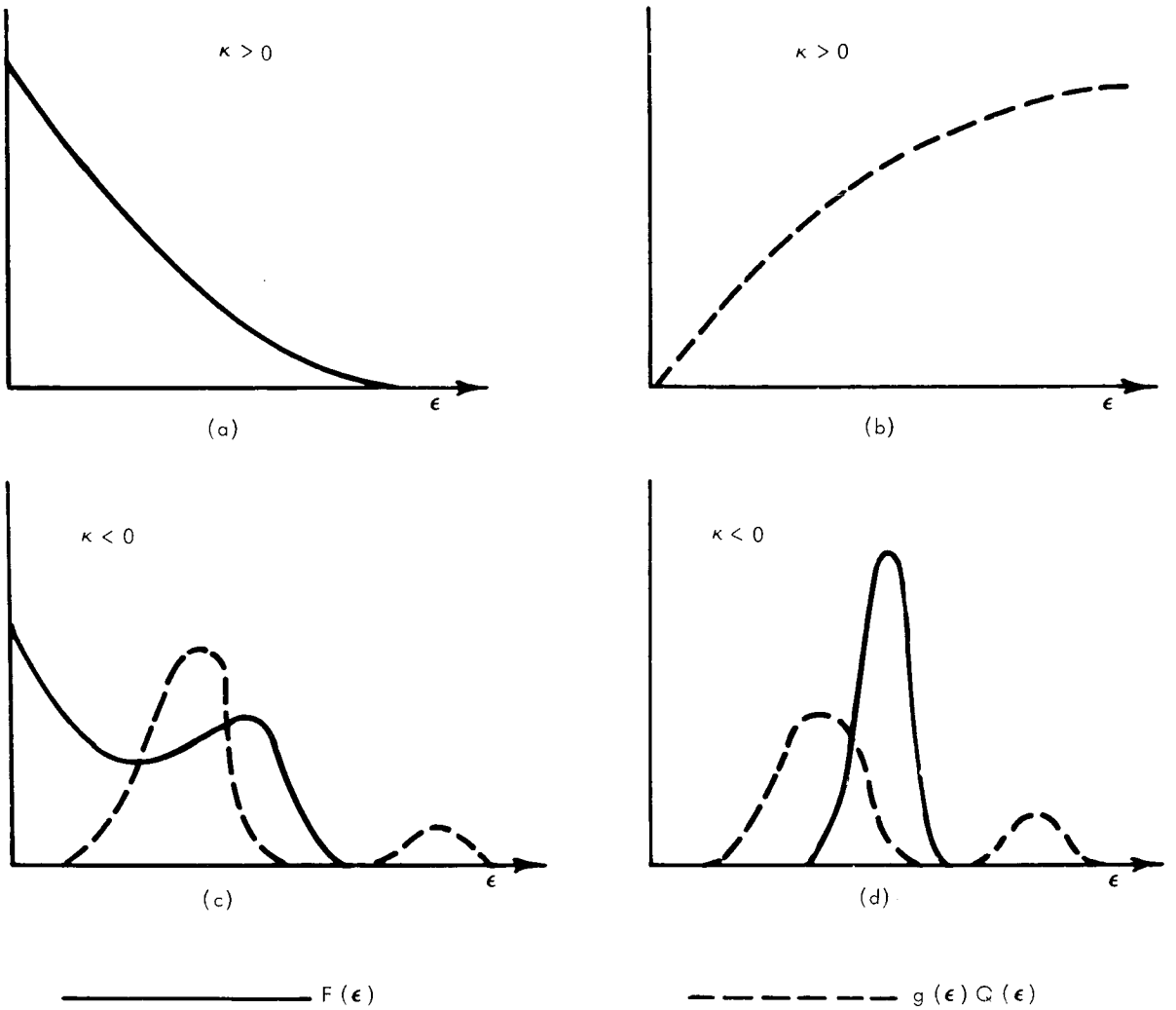

FIGURE 38–3. Examples of electron energy distributions $F(\epsilon)$, the product of statistical weight $g(\epsilon)$, and electron emissivity, $Q_f(\epsilon)$, which lead to positive and negative absorption. (a) Positive absorption when $dF/d\epsilon$ is negative; a thermal source of radiation is an example. (b) Positive absorption when $(d/d\epsilon)\ [g(\epsilon)\ Q_f(\epsilon)]$ is positive; bremsstrahlung is an example. (c) and (d) Two situations which lead to negative absorption where $dF/d\epsilon$ is positive and $(d/d\epsilon)\ [g(\epsilon)\ Q_f(\epsilon)]$ is negative as in conditions (a) and (b); this can apply to gyro-radiation. (Reference 1)

ions. Both close—or binary—encounters, and distant—or multiple—encounters, are effective. Scheuer (1960) points out that the ions in a distant encounter interact with an electron as in a binary encounter, so that the total emission is that of binary encounters out to an *effective* maximum collision distance. The same result seems implied by Oster (Reference 6), who has shown that—contrary to earlier opinion (for instance, Smerd and Westfold, 1949)—the emission can be integrated over all collision distances, provided one allows for a finite collision interval at large collision distances. The effective maximum collision distance is reached when this radiation pulse becomes too long to contain appreciable Fourier components at the frequency considered.

Averaging over the collision distances, we find the mean emissivity of non-relativistic electrons

$$Q_f(\epsilon) \propto \xi(\epsilon)/\epsilon^{1/2},$$

where

$$\xi(\epsilon)=\ln (2\epsilon)^{3/2}+\text{const.}$$

From this and Equation 11 we see that $(d/d\epsilon)[Q_f(\epsilon)g(\epsilon)]$ is always positive, and we conclude therefore that such *bremsstrahlung cannot be amplified.*

The characteristics of temperature-limited bremsstrahlung from nonthermal source electrons is well exemplified by the thermal case. The brightness temperature cannot exceed the electron temperature (or, in the nonthermal case, the radiation temperature given by $KT_r \approx \bar{\epsilon}$); it will reach this limit only if the source is optically thick. The opacity depends on the electron temperature—or on the mean energy of nonthermal electrons—characteristically as $T^{-3/2}$. This means that, as the energy of the source electrons increases, the resulting changes in brightness temperature depend on the opposing trends of an increasing radiation temperature and a decreasing opacity; the brightness of an optically thin source will decrease, and so will the opacity of an originally optically thick source.

We found earlier that at meter and longer wavelengths the opacity through a 10^6 °K corona was about unity or less. An increase in temperature will soon decrease the brightness; bremsstrahlung bursts are therefore not likely at the meter and longer wavelengths.

Again we found earlier that the optical depth of the solar atmosphere below the corona becomes large at the microwaves. Typically, the brightness temperature may rise to about 10^8 °K before further heating (>10 kev) will no longer increase the brightness of microwave emission.

Thus microwave bursts, even with rapid intensity fluctuations, of not more than about 10^8 °K brightness temperature could be due to bremsstrahlung from fast nonthermal electrons.

Gyro-Synchrotron Radiation

The terms *gyro* and *synchrotron* radiation are used for the electromagnetic radiations from electrons gyrating in a magnetic field.

If an electron gyrates at an angle ϕ to the magnetic field, it will be observed to emit harmonics $s=1,2,3, \cdots$ of the Doppler-shifted gyro frequency. For observation at an angle Θ to the magnetic field, the observed gyro frequency is given by

$$f_H(\beta,\phi,\theta)=f_H(1-\beta^2)^{1/2}/(1-\mu\beta \cos\phi \cos\theta),$$

where βc is the electron velocity and where we denote the non-relativistic gyro frequency by $f_H\ (0,\phi,\theta)\equiv f_H$, as in Equation 2.

Takakura (1960) has derived an expression for the energy $Q_s\ (\beta,\phi,\theta)$ emitted in vacuo ($\mu=1$) by an electron per unit solid angle and unit time in the s th harmonic.

The electron emissivity is then obtained by summing over all harmonics which contribute to a given frequency; thus,

$$Q_f=\sum_{s=1}^{\infty} Q_s(\beta,\phi,\theta)\delta[f-sf_H(\beta,\phi,\theta)],$$

where $\delta(x)$ denotes the Dirac delta function. This then enables us to evaluate the absorption coefficient as outlined in the previous section, "Nonthermal Sources and Wave Amplification." Such calculations have not been done analytically. Takakura (1960) and Takakura and Kai (1961) worked out numerical solutions to interpret the observed characteristics of microwave impulsive bursts and several phases of type IV emission in terms of gyro-synchrotron radiation from intermediate energy electrons (10^4–10^6 ev) in a magnetic field of 10–10^3 gauss. These authors precluded any possible amplification by considering electron energy distributions which, though nonthermal, decrease continously with increasing energy. This leads to difficulties in explaining the high intensity, long duration, relatively narrow bandwidth of a type IV continuum at the decimeter wavelengths, which is treated as separate from the adjoining centimeter and meter wave continua.

A further generalization and degree of complexity was introduced by Eidman (References 7 and 8), who derived an expression for the emissivity of gyrating electrons in a medium of refractive index μ. A departure from unit refractive index is more likely in sources of low-harmonic gyro radiation ($\omega_H \lesssim \omega$). In particular it appears that such radiation is emitted most strongly in directions given by

$\mu\beta \sin\phi \sin\theta = 1$. The consequences of this so far have not been applied to solar burst interpretations; the medium has been taken into account only in determining the frequencies (see Equation 5) at which the predominantly e-mode, gyro radiation can escape the sun.

Again, for emission in vacuo the two limiting cases $\epsilon \lesseqgtr m_0c^2$ can be treated analytically by Schwinger's (1949) approximations.

Gyro Radiation ($\epsilon << m_0c^2$)—The emission from such mildly relativistic electrons decreases rapidly over the first few harmonics of the gyro frequency. First, we determine the gyro resonance absorption coefficient in the case of a continuously decreasing electron energy distribution as exemplified by the Maxwellian distribution; this is a case of a non-collisional absorption as mentioned in the section on "Collision Damping" (page 346). We find* that gyro resonance absorption, unlike the collision absorption of bremsstrahlung increases with temperature as $T^{1/2}$ ($s=1$) and $T^{s-3/2}$ ($s \geq 2$). For transverse propagation the harmonics of the gyro frequency cannot propagate at all (Reference 9); these are the "stop gaps" in the dispersion curves previously noted by Gross (Reference 2) (see section on "Dispersion Equations," page 343). Gyro resonance absorption at meter wavelength in coronal sources is probably more important than collision absorption; this provides a means of achieving substantial optical depths at the first few harmonics of the gyro frequency in coronal hot spots. Ginzburg and Zheleznyakov (1961) used this idea to explain broad continuum emission at meter waves as well as the peak in the slowly varying component spectra at the microwaves.

Next we explore the possibility of amplification of gyro radiation in the presence of electron streams. Twiss (1958) suggested that, similarly to the discrete set of harmonic frequencies radiated by an electron of given energy, there should be a discrete set of energies corresponding to the emission or absorption at given frequency. We find (Reference 1) these energies to be given by

$$\epsilon_s = m_0c^2[s(f_H'/f) - 1],$$

where f_H' is the Doppler-shifted value of the non-relativistic f_H. Thus, if we neglect line broadening, $Q_f(\epsilon)$ has a discrete energy spectrum with the lines separated by

$$\epsilon_s - \epsilon_{s-1} = m_0c^2(f_H'/f).$$

From the criteria derived in the last section, we conclude that *negative absorption and hence amplification at the sth harmonics are possible, provided* $(dF/d\epsilon)_{\epsilon_s} > 0$ *and* $F(\epsilon)$ *does not spread across more than one line.*

In the presence of Doppler and magnetic line broadening, amplification is still possible as long as the lines do not overlap. The requirements (Reference 1)

$$s < c/\Delta v \text{ and } s < H/\Delta H$$

restrict such "resonance" amplification to the lower harmonics.

Synchrotron Radiation ($\epsilon >> m_0c^2$)—In this case emission occurs over a wide range of high harmonics of the relativistic gyro frequency; the lines lose their separate identity, and the radiation can be treated as a continuum. Synchrotron radiation from 3 Mev electrons gyrating in fields of about 1 gauss was proposed by Boischot and Denisse to account for the moving type IV burst at the meter waves.

Synchrotron radiation is highly directional; it occurs within the angle $\Delta\theta \approx m_0c^2/\epsilon$ around the direction of the electron velocity. For this anisotropic radiation we have to determine the sign of

$$\left(\frac{\partial}{\partial\epsilon} + \frac{\Delta\phi}{hf}\frac{\partial}{\partial\phi}\right) g(\epsilon,\phi) Q_f(\epsilon,\phi,\theta)$$

in order to determine the possibility of amplification. Wild, Smerd, and Weiss (Reference 1) find that gradient to be invariably positive and conclude, contrary to Twiss's (1958) result, that *synchrotron radiation cannot be amplified.*

*The absorption coefficient derived (Reference 1) for $\mu=1$ by the method of the previous section, "Nonthermal Sources and Wave Amplification," is found to agree with that derived by Stepanov (1958). The latter is determined for an imaginary frequency in a kinetic theory (microscopic) treatment of the dispersion of waves in a plasma by Sitenko and Stepanov (Reference 9).

PLASMA WAVES

The third mechanism which may lead to radio emission from the solar plasma is an indirect one; the primary wave excited by the streaming electrons is a longitudinal plasma wave. It is only after partial conversion of the plasma wave into electromagnetic waves that observable radio emission can escape the sun.

We found in the section on "Radio Waves in a Plasma" that the electron waves are plasma waves at frequencies above the cold-plasma resonance frequency. Such plasma waves existing in the region $\mu > 1$ can be excited analogously to Cerenkov radiation in a neutral medium by the streaming through the plasma of electrons at speeds greater than their phase velocity. This excitation can occur incoherently by a single electron or a loosely knit group of electrons in which each particle emits independently. Ginzburg and Zheleznyakov (1961) have pointed out that the smallest electron density needed in a burst source to explain the observed burst intensities is far too high for incoherent emission.

Coherent plasma waves have been investigated by Bohm and Gross (1949). These authors have shown that those electrons whose velocities are not too different from the phase velocity of the plasma wave remain "trapped" in a potential trough of the wave sufficiently long to allow strong interaction between wave and particles. Those electrons which are slightly faster than the wave supply energy for the wave to grow; the slower particles lead to damping. This damping, referred to as Landau damping, is another form of noncollisional damping which does not emerge from a macroscopic representation of the plasma as in the above mentioned section. The existence of Landau damping has been questioned [e.g., Bernstein, Greene, and Kruskal (1957), Denisse (1961)] because of its derivation from linearized Boltzmann (or Vlasov) equations. However, a numerical treatment (Reference 10) of a simple application of the nonlinear Vlasov equation shows that, in the case considered, Landau damping as given by the linear theory does occur and for much longer than one would expect from an estimate of the validity of linear theory; nonlinear effects manifest themselves in the appearance of harmonic radiation.

The condition for wave growth, similarly to that for resonance amplification, is given by

$$\left(\frac{\partial F_s}{\partial v}\right) v = v_{ph} > 0,$$

where F_s is the velocity distribution in the electron stream. This Bohm and Gross criterion for "two-stream instability" has been generalized by Sturrock (Reference 11).

In the case of a growing plasma wave—but also in all other cases of wave growth—the final wave amplitude, or intensity, has to be calculated by equalizing the energy supply to and the energy losses from the wave. This was done by Bohm and Gross for a coherent electron plasma wave by allowing for energy dissipation through collisions. The amplified wave is thought to exist mainly at the plasma frequency f_0 (see Equation 1). Terashima (private communication) estimates the bandwidth as less than $10^{-3} f_0$.

Ginzburg and Zheleznyakov (1958) have estimated stream velocities and densities to account for the observed characteristics of type III bursts. In this they used Bohm and Gross's value for the amplitude of the amplified plasma wave and expressions for the conversion efficiency from plasma to electromagnetic waves. The conversion mechanism is thought to be the scattering of the plasma wave on thermal fluctuation of the background plasma. The random fluctuations of the ions lead to electromagnetic radiation at unchanged frequency and mostly in the direction of the incident plasma wave through Rayleigh scattering. The electron density fluctuation, themselves plasma ripples in all directions, lead to electromagnetic radiation at about twice the plasma frequency; the scattered radiation intensity from such "combination scattering" peaks approximately at right angles to the incident plasma wave.

Similar calculations have been carried out by Wild, Smerd, and Weiss (Reference 1) on the basis of later observational results; these calculations suggest that one can explain a brightness temperature of 10^{11} °K from streams of velocity $v_0 \approx c/3$ and stream densities N_s of

about 1 percent the background density N. The very strong instability inherent in such streams is highlighted by the high-powered functional dependence of the calculated brightness temperature (Reference 1) of the fundamental radiation after conversion through scattering, namely,

$$T_b' \approx 10^{16} \ (N_s N)^8 (v_0/\Delta v)^9 {}^\circ\mathrm{K},$$

where Δv is the velocity spread in the stream. Similar calculations for the brightness temperature of the second harmonic suggest that the observed intensities and structure of fundamental and harmonic bands in type III bursts can probably be explained in terms of coherent plasma waves excited by an electron stream and scattered on the thermal fluctuations of the solar plasma. Terashima and Yajima (Reference 12) find an additional factor $(v_0/c)^2$ in the conversion efficiency through combination scattering. With $v_o/c \approx 1/3$, this would not substantially alter the conclusions of the above numerical examples.

A similar interpretation of the slow-drift type II burst is linked with the assumption that the slow type II source carries and at times ejects electrons of approximately type III velocities. This assumption was already made [Smerd, Wild, and Sheridan (1962)] in an attempt to explain the "switched" relative positions of the fundamental and harmonic sources in type II bursts. Recent observational evidence and Weiss's interpretation as reported by Wild (Reference 13) in an earlier session make it clear that there are still inconsistencies in the current ideas on the origin of type II burst radiation. Progress in the interpretation of these bursts probably will come with a better understanding of radiations from a shock front traversing a plasma obliquely to a magnetic field.

In the absence of a magnetic field, Larenz (Reference 14) and coworkers have proposed an interpretation of type II and type III bursts in terms of plasma waves excited by the runaway electrons from a plasma shock moving at Mach numbers of at least 6.5 through the solar background plasma. It is pointed out, as previously had been done by Sturrock (Reference 11), that the group velocity of the plasma waves should be the same as the source velocity, since otherwise the plasma waves would soon move out of the excitation region. A difficulty noted, but not yet overcome, by Larenz is the great depth of the shock front which in the field-free case is linked with the very large mean free path in the tenuous corona. The presence of a magnetic field may help there, since the depth of the shock front is then related to the much smaller Larmor radius.

A different mechanism for converting from plasma to electromagnetic waves was invoked by Denisse (1960) in an interpretation of type I storms. The conversion is there attributed to mode coupling between the electron plasma and ordinary waves in the region where $\omega \approx \omega_0$. This requires down-streaming electrons exciting plasma waves moving toward the denser regions of the sun's atmosphere and thereby toward the coupling region. There exists the possibility that such traveling plasma waves would lose an appreciable fraction of their intensity through scattering before reaching the mode-coupling region.

Another theory to account for the type I burst was recently presented by Takakura (Reference 15). Again, the burst radiation is thought to be scattered radiation from coherent plasma waves. An interesting feature is the relatively low velocity, about 2 to 3 times v_{th}, assigned to the electron streams which are invoked to excite the plasma waves; the low velocity is necessitated by the short duration of type I bursts. The small amount of electron acceleration needed is attributed to oppositely moving Alfvén waves in the source region.

From the observations (Reference 13) it would seem that whatever interpretation is thought to explain the type I continuum should also be able to account for the stationary type IV emission at the meter wavelengths. On present evidence both these continua, as well as the drifting bursts of types II and III, are probably radiations from coherent plasma waves. This same indirect mechanism of generating solar radio bursts also may play an important part in explaining some of the drift-

ing bursts, striated and continuum emissions in the—at present—least understood part of the burst spectra, that is, at the decimeter wavelengths.

REFERENCES

1. WILD, J. P., SMERD, S. F., and WEISS, A. A., 1963, *Annual Review of Astronomy and Astrophysics*, 1: 291.
2. GROSS, E. P., 1951, *Phys. Rev.*, 82: 232.
3. ALLIS, W. P., and BUCHSBAUM, S. J., 1962, *Nuclear Fusion*, 2: 49.
4. BAILEY, V. A., 1948, *J. and Proc. Roy. Soc. N.S.W.*, 82: 107.
5. TWISS, R. Q., 1952, *Phys. Rev.* 88: 1392.
6. OSTER L., 1961, *Rev. of Modern Phys.*, 33: 525.
7. EIDMAN, V.Ia., 1958, *J. Exptl. Theoret. Phys. U.S.S.R.*, 34: 131; Engl. Transl.: *Soviet Physics JETP*, 7: 91.
8. EIDMAN, V.Ia., 1959, *J. Exptl. Theoret. Phys. U.S.S.R.*, 36: 1335; Engl. Transl.: *Soviet Physics JETP*, 9: 947.
9. SITENKO, A. G., and STEPANOV, K. N., 1956, *J. Exptl. Theoret. Phys. U.S.S.R.*, 31: 642; Engl. Transl. (1957): *Soviet Physics JETP*, 4: 512.
10. KNORR, G., 1961, *Z.f. Naturforschung*, 16a: 1320.
11. STURROCK, P. A., 1962, *J. Res. N.B.S.*, 66D: 153.
12. TERASHIMA, Y., and YAJIMA, N., 1963, Research Report of Inst. of Plasma Physics, Nagoya University *IPPJ*, 9.
13. WILD, J. P., *these Proceedings*, paper no. 21.
14. LARENZ, R. W., 1963, XIVth General Assembly, URSI, Tokyo.
15. TAKAKURA, T., 1963, XIVth General Assembly, URSI, Tokyo.

DISCUSSION

Dr. Maxwell: Do you envisage any conditions in the solar plasma under which Cerenkov plasma waves could couple energy into gyro frequency modes, or harmonics thereof, in any substantial quantities?

Dr. Smerd: I don't know whether it can occur in the sun. There is a very interesting laboratory experiment which was first carried out by Landauer of the Max Planck Institute and has since been repeated by Bekefi and other people at MIT, and by Terashima and other people at Nagoya Plasma Physics Institute. They find that in a slow discharge, quite a cool discharge, they observe up to about 40 harmonics of the gyro frequency. This cannot be explained as emission from highly relativistic particles because they simply are not highly relativistic.

The only suggestion I have heard put forward so far is that there is a resonance at the electron gyro frequency. That is, there is a peak—it doesn't have to be an infinity, but a very high value of the refractive index—at the gyro frequency. A relatively slow particle or stream of particles will thus have a chance to excite the gyro resonance analogously to Cerenkov radiation. I gather this is one of the interpretations which has been put forward to explain this laboratory experiment. I do not know whether this would apply to the sun.

Dr. Maxwell: One further question, if I may: In view of your concluding remarks, do you believe that the microwave bursts are amplified bremsstrahlung rather than synchrotron?

Dr. Smerd: I can't say what portion of microwave bursts is likely to be bremsstrahlung. However, I said earlier bursts could not be amplified bremsstrahlung. As long as they are not too bright—up to about 10^8 °K which is quite substantial, but not 10^{10} °K or so, brightness temperature—they could be nonthermal bremsstrahlung.

Dr. Sturrock: An important aspect of the last experiments which you quoted, those by Landauer and by Bekefi, is that these are carried out in a positive column discharge in which there is necessarily a sheath. There are high electric fields and high gradients of electric field in a sheath, so that in this region electrons do not move in circles but in cycloids or similar complicated paths. This is considered to be one likely explanation of the observed harmonic.

I also wish to refer back to your statement that Twiss has asserted one cannot distinguish between amplifying and decaying waves by looking at the dispersion relation alone. This statement is incorrect.

Dr. Smerd: I believe one of the Nagoya people, Takayama, produced this multiple gyro effect in a very pure plasma. He had specially shaped anodes and cathodes to prevent the striation sheath.

Regarding the other point, that you can tell about the amplification: Surely, unless you specify the boundary conditions of your system, where the injection takes place, this would be extremely difficult to do.

Dr. Sturrock: My paper in *Physical Review*, Vol. 122, page 1488 (1958) explains how it is possible to distinguish amplifying from evanescent waves by investigation of the dispersion relation.

N64-30289

39 TYPE III SOLAR RADIO BURSTS*

PETER A. STURROCK
Institute for Plasma Research, Stanford University
Stanford, Calif.

The observational characteristics of type III solar radio bursts have already been reviewed by Dr. Wild (Reference 1). A more complete discussion has been given by Wild, Smerd, and Weiss (Reference 2), which also gives an extensive list of references to other work on this subject. The theoretical interpretation of type III bursts, which was given by Wild, was based on the theory of Ginzburg and Zhelezniakov (Reference 3). The theory briefly presented here differs significantly from that of Ginzburg and Zhelezniakov in ways which will be pointed out subsequently.

The observed frequency range of type III emissions is from about 600 Mc down to about 5 Mc for the fundamental, the time duration being about 10 seconds. It appears that type III bursts are related to the flash phase of chromospheric flares, although the event giving rise to a type III burst is frequently too weak to be observed optically. The accepted sequence of physical mechanisms giving rise to this radiation is the following.

The solar flare produces a stream of high-energy electrons; this electron stream travels out through the corona, necessarily following any magnetic field which may be in existence, and excites plasma oscillations in the ambient coronal plasma; the plasma oscillations are coupled in some way to electromagnetic waves, so that radiation appears at the plasma frequency and also at twice the plasma frequency. Comparison of the frequency drift rates with interferometric measurements indicates that the exciting source (electron beam) has a velocity in the range 0.2c to 0.8c and that the beam is traveling along a coronal streamer in which the density is about 10 times the normal coronal density.

To test our proposed chain of physical mechanisms and to distinguish among alternative mechanisms where these exist, we consider the following four questions:

1. Can we explain the frequency at which a burst is first observed?
2. Can we explain why the electron stream has such a well-defined velocity?
3. Can we explain why the beam is not significantly decelerated?
4. Can we explain why radiation is observed at the fundamental (ω_p) and at the second harmonic ($2\omega_p$) and at no other harmonics?

We now consider these questions in order.

1. *What determines the time of commencement of observed radiation?*

If all type III bursts are first observed at frequencies in a well-defined range (a few hundred megacycles), it must follow either that the event which leads to the phenomenon takes place at a well-defined height in the solar atmosphere, or that the event begins at a lower height but is observable only when it has reached a certain well-defined height. The first of these alternatives is not attractive, especially when one notes that a plasma frequency of $10^{8.8}$ sec^{-1} corresponds to a plasma density of $10^{9.6}$ cm^{-3} which is to be found at heights of 7000 km in the normal atmosphere or at 15,000 km if the density is ten times normal. Chromospheric flares, which are often associated with type III bursts, frequently occur much lower in the solar atmosphere.

We should therefore consider the second possibility: that the observed onset is due to observational requirements. An electromagnetic wave propagating through the solar atmos-

*This study was supported by the Air Force Office of Scientific Research under Grant No. AF-AFOSR-62-326.

phere is damped because of collisions of electrons with other particles. A rough estimate of the spatial damping rate (which ignores dispersion) is

$$\kappa \approx \nu/c, \tag{1}$$

where (Reference 4)

$$\nu \approx 10^{1.8} n T^{-3/2} \tag{2}$$

(n is the electron density and T is the temperature in degrees). Hence the attenuation is given by

$$A = \int \kappa \, ds \approx \frac{1}{c} \int \nu \, ds \approx 10^{-18} \int_h^\infty n \, ds \tag{3}$$

if we take $T \approx 10^6$ degrees.

If, at the height of origin, the density is approximately exponential with scale height H, then

$$A \approx 10^{-18} H(h) n(h). \tag{4}$$

Since the frequency of onset corresponds to $n(h) \approx 10^{9.6}$ cm^{-3}, this frequency is explained by absorption if H (the scale height) is, in fact, of the order 2500 km or more at heights of 10,000 km or more. It appears, therefore, that consideration of the absorption of electromagnetic waves can account satisfactorily for the observed frequency of onset of type III bursts.

2. *Why is the source velocity well defined and in the range 0.2c to 0.8c?*

One possible explanation is that the electron beam is produced by an accelerating mechanism which yields a well-defined velocity. This, however, leaves us with the problem of explaining why the source velocity varies little from flare to flare; that is, we must explain why the "acceleration potential" does not vary greatly from one flare to the next. It is difficult enough to find any acceleration mechanism, and the prospect of finding an acceleration mechanism which meets this stringent requirement seems remote.

However, a second possibility is that the electron beam is produced with varying characteristics in the chromosphere and that the properties of the emerging beam are determined by the passage of the electron stream through the solar atmosphere.

If the electron stream is produced at the flare with an energy distribution $n_f(E)$, so that the number of electrons in the range dE is $n_f(E)dE$, then the corresponding energy density in the corona will be $n_c(E)$, where

$$n_c(E) = T(E) n_f(E). \tag{5}$$

$T(E)$ is a "transmission factor," which is the probability that an electron of energy E, produced at the flare, will emerge into the corona. It will be given by

$$T(E) = \exp\left[-\int \lambda^{-1} \, ds\right], \tag{6}$$

where λ is the mean free path for coulomb collisions. Since, approximately,

$$\lambda \approx 10^{22.8} (v/c)^4 n^{-1}, \tag{7}$$

T may be written as

$$T \approx \exp\left[-(E/E_c)^2\right], \tag{8}$$

where the "cutoff energy" in kev is given by

$$E_c \approx 10^{-9} \int_h^\infty n \, ds. \tag{9}$$

We now see from Equation 8 that T rises sharply from $T \approx 0$ to $T \approx 1$ in the neighborhood of $E = E_c$. Hence no matter what the form of $n_f(E)$, provided it has a rapidly decreasing density (a "tail") beyond E_c, the density $n_c(E)$ will be sharply peaked near the energy E_c. This is shown schematically in Figure 39–1.

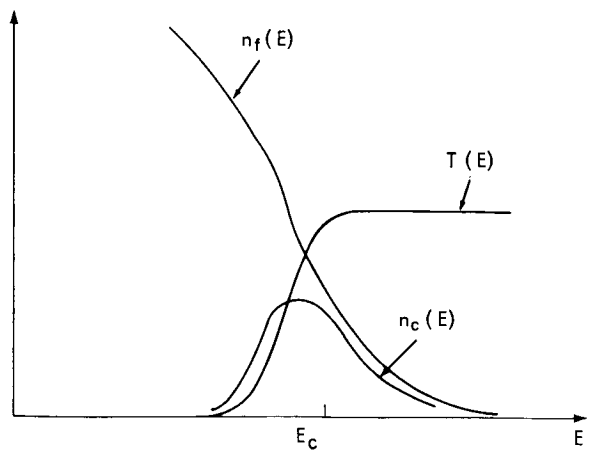

FIGURE 39–1.

Equation 9 gives us a numerical check of this hypothesis, since it enables us to determine the height at which the electron beam is produced as a function of the energy of the electron beam. We find that it is necessary to include the effect of collisions of electrons with neutral atoms in the chromosphere, so that the coulomb-scattering formula, Equation 7, is strictly invalid. However, we may obtain an approximate check on our theory by using the coulomb-scattering formula, including in n the density of free electrons and ions, and also the density of electrons and ions which are bound in the form of neutral hydrogen atoms. The hypothesis underlying this approximation is that the collision of a near-relativistic electron with a proton or electron in a bound state is not very different from that of a collision with a free proton or electron, since the energies involved are very much greater than the binding energy. If we adopt this hypothesis, we obtain the following relation between the estimated height of production of the electron stream with the final velocity of the stream:

v/c	Height of Flare (km)
0. 03	10, 000
0. 10	5, 000
0. 25	2, 000
0. 35	1, 000

This calculation certainly needs refinement, but it indicates that our hypothesis is correct and that the observation of streams of electrons of well-defined energies, in the range mentioned, is to be attributed to the transmission properties of the chromosphere.

3. *Why is the electron beam not decelerated by two-stream instability?*

It is known that a velocity distribution function for electrons, of the type shown in Figure 39–2, leads to two-stream instability (Reference 5). The spatial growth rate is given approximately by

$$k_i \approx \frac{n_b v_b^3 \omega_p}{n_p (\Delta v_p)^2 (\Delta v_b)^2}, \qquad (10)$$

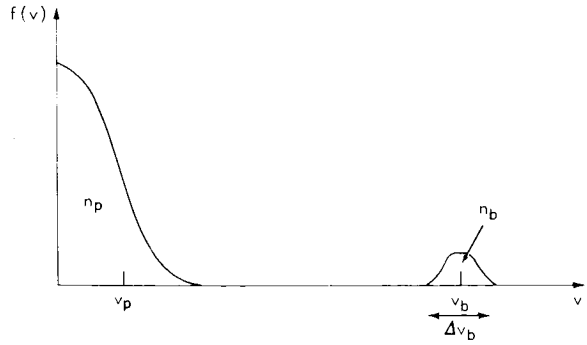

FIGURE 39–2.

where Δv_p, Δv_b are the widths in velocity of the plasma peak and the beam peak, respectively. Figures appropriate to the low corona are

$$n_p = 10^8 \text{ cm}^{-3},\ \omega_p = 10^9 \text{ sec}^{-1},\ \Delta v_p = 10^{8.8} \text{ cm sec}^{-1}.$$

Observations indicate that $v_b \approx 10^{10}$ cm sec^{-1}, $\Delta v_b \approx 10^9$ cm sec^{-1}, $n_b \approx 10^4$ cm^{-3}. Hence the length for amplification by 1 neper (about 8 db) is $k_i^{-1} \approx 3$ cm. This indicates that two-stream instability, if it occurs, will produce tremendous beam deceleration in only a few meters. The growth rate in time may be estimated from $(\Delta v_p)^2 v_b^{-1} k_i$ to be about 10^7 sec^{-1}, whereas the electron collision frequency is only 10^2 sec^{-1} or less, so that collision damping is not nearly strong enough to inhibit the instability.

It seems to the author that one must conclude from this argument that two-stream instability does not take place. It will be necessary to explain this fact. It seems to the author that the most likely possibility is that the simple theory for a homogeneous plasma is invalid and that the instability is inhibited by scattering of plasma waves by inhomogeneities. A theory of this effect which should make it possible to test this hypothesis quantitatively is being developed.

The fact that two-stream instability does not take place means that plasma oscillations are excited only by the comparatively weak Cerenkov mechanism. The assertion that the relevant mechanism for plasma oscillations in the corona is the Cerenkov mechanism rather than two-stream instability represents one important difference between the present theory and that of Ginzburg and Zhelezniakov.

728–629 O—64——24

4. *Why do we observe emission at ω_p and $2\omega_p$ and at no other harmonics?*

As has already been indicated, it is necessary to consider mechanisms for coupling the electrostatic plasma waves (plasma oscillations) with the transverse electromagnetic waves which propagate the observed radio noise out of the solar atmosphere.

It is convenient to begin by discussing the second harmonic, since in this case one can demonstrate by a simple argument that the mechanism now proposed is more effective than that adopted by Ginzburg and Zhelezniakov. We suppose that, in the quiescent coronal plasma (unexcited by the electron stream), there is an energy density of plasma oscillations E_q. In the presence of an electron stream there is a further excitation of plasma oscillations, the energy density of which will be written as E_e. Ginzburg and Zhelezniakov observe that one would expect radiation at frequency $2\omega_p$ due to the scattering of the excited plasma waves by the quiescent plasma waves, which they identify with those to be found in a plasma in thermal equilibrium. The emissivity due to this mechanism may be written as s_{qe}, and it is clear that

$$s_{qe}=AE_qE_e. \tag{11}$$

However, it is also clear that waves of the excited spectrum may scatter with each other, to produce radiation by the intrinsic nonlinearity of equations governing the wave mechanisms (Reference 6). The corresponding emissivity may be written as

$$s_{ee}=BE_e^2. \tag{12}$$

It is convenient to add to these equations a formula for the corresponding emissivity of a quiescent plasma,

$$s_{qq}=CE_q^2. \tag{13}$$

The coefficients A, B, C will of course depend on the distribution of wave energy in wave-vector space. Unless the spectra are so different that the coefficients A, B, C differ by very large coefficients, it is clear that the ratio of s_{ee} to s_{qe} will be similar to the ratio of s_{qe} to s_{qq}. Hence, if the mechanism proposed by Ginsburg and Zhelezniakov leads to radiation in excess of that of the quiet sun, then radiation by nonlinear coupling would be more important than that proposed by Ginzburg and Zhelezniakov. This argument can be made more precise, since one can prove a theorem of the form of Schwarz's lemma, demonstrating that

$$s_{qe}^2 \leq s_{ee}s_{qq}. \tag{14}$$

Since the volume of plasma excited by the electron stream is very large compared with the wavelength of the plasma waves, it is appropriate to consider the volume emissivity of plasma oscillations which are described only in a statistical way. A recent calculation by Ball and Sturrock (Reference 7) has developed such a theory. If one makes the simple assumption that the energy density spectrum is isotropic and of "width" k_s, which is large compared with k_0 where

$$k_0=3^{\frac{1}{2}}\omega_p c^{-1}, \tag{15}$$

the volume emissivity is given approximately by

$$s\approx 0.05\frac{\omega_p}{nmc^2}\left(\frac{k_0}{k_s}\right)^3 E_e^2 \tag{16}$$

where m is the electron mass. We might note at this point that the earlier assumption concerning the scattering of plasma oscillations by inhomogeneities would tend to isotropize the wave spectrum which, when excited by the electron stream, would be anisotropic.

Observations on earth indicate that the total power emitted in a type III burst is typically $10^{12.4}$ watts or $10^{19.4}$ erg sec^{-1}. If the dimensions of the emitting region are taken to be about 10^9 cm (it cannot be much greater in view of the sharpness of the observed spectrum), the volume emissivity must be about $10^{\bar{8}.4}$ watt ($=10^{-8}\times 10^{0.4}$ watt). If the wave number k_s is estimated to be ω_p/v_b, Equation 16 leads to the estimate

$$E_e\approx 10^{\bar{5}.2}\ \text{erg cm}^{-3} \tag{17}$$

for the energy density of excited plasma oscillations. We note that the time constant for

radiation damping is $10^{2.8}$ sec. Since the electron collision rate is about 10 sec^{-1} where the plasma frequency is about 100 Mc/s, we may infer that the efficiency of conversion of plasma-oscillation energy into electromagnetic energy is about 1 percent. The total energy in plasma oscillations, in a region which is emitting at any one instant, is about 10^{22} ergs, so that the total energy extracted from the electron stream and converted into plasma oscillations (from the time the burst becomes visible) is about 10^{23} ergs.

If one refers to the theory of the Cerenkov excitation of plasma oscillations by fast electrons, one finds that the stream must contain about 10^{31} electrons, which therefore have a volume density of about 10^4 cm^{-3}. Comparison of the total energy in the electron stream with the energy given up to plasma oscillations indicates that the total efficiency is a few percent. This high efficiency indicates that it would be an embarrassment, rather than an asset, to have the plasma oscillations excited by two-stream instability rather than the Cerenkov mechanism, since the former is greatly more efficient than the latter.

Radiation at the fundamental is attributed to the scattering of plasma oscillations from density fluctuations, or from current fluctuations in the coronal plasma. Ginzburg and Zhelezniakov considered scattering from density fluctuations but identified those fluctuations with those to be found in a thermal plasma. In discussing the inhibition of two-stream instability, and radiation at $2\omega_p$, we have already supposed that there are weak density fluctuations in the coronal plasma with wavelengths of order v_b/f_p, that is, wavelengths of the order of 1 meter. A theory recently has been developed by Baldwin and Sturrock (Reference 8) for the volume emissivity of a random spectrum of plasma oscillations in the presence of random density homogeneities and random currents.

If we accept the above estimate of the plasma-oscillation energy density, we may obtain estimates of the density fluctuations and current fluctuations necessary to explain radiation at the fundamental. We find that, if one were to select out fluctuations with wavelengths of the order of 1 meter, the density fluctuation $\Delta n/n$ must be of the order 10^{-5}. If the radiation is to be explained by scattering from current fluctuations, it is necessary that the magnetic field in the corona should have a component, with wavelengths in the neighborhood of 1 meter, of the order 10^{-3} gauss. These estimates do not seem unreasonable but are very much higher than would be obtained from thermal fluctuations alone. The reason that our calculations have led us to higher fluctuation amplitudes than those postulated by Ginzburg and Zhelezniakov is that the nonlinear mechanism for radiation at $2\omega_p$, being more efficient, led us to lower estimates of the plasma-oscillation energy density.

REFERENCES

1. Wild, J. P., 1963, *these Proceedings*, paper no. 21.
2. Wild, J. P., Smerd, J. F., and Weiss, A. A., 1963, *Annual Review of Astronomy and Astrophysics*, 1: 291.
3. Ginzburg, V. L., and Zhelezniakov, V. V., 1958, *Astron. Zh.*, 35: 694 (Eng. transl., *Soviet Astron.-AJ.*, 2: 653).
4. Spitzer, L., 1956, "Physics of Fully Ionized Gases," Interscience, p. 80.
5. Stix, T. H., 1962, "The Theory of Plasma Waves," McGraw-Hill, p. 147.
6. Sturrock, P. A., 1961, *J. Nucl. En.*, Part C: "Plasma Physics," 2: 158.
7. Ball, R., and Sturrock, P. A., 1963, to be published.
8. Baldwin, D., and Sturrock, P. A., 1963, to be published.

DISCUSSION

Dr. Cohen: I would like to make a general remark. You base much of this on the second harmonic, but in fact many type III bursts do not have second harmonics. That is a general objection. And I have a specific remark, also.

You can avoid two-stream instability by using Cerenkov effect, but then you get 1000 particles/cm^3; I think that was your number.

So, the inter-particle distance is quite small, very much less than the Debye length. The collective effects between the stream particles must have some effect, and it will reduce the necessary number of particles.

There is no doubt that the general two-stream mechanism can't be used because it will damp out the whole motion very quickly, as you pointed out. I think what is needed is a theory of how a few particles will interact, something between the individual particle Cerenkov effect and the general two-stream instability. I don't think the theory of that has, in fact, been worked out.

Dr. Sturrock: As has been pointed out by Wild, Murray, and Rowe (*Australian Journal of Physics*, 1954, 7: 439), it is more difficult to distinguish harmonic structure in the study of type III bursts than in the study of type II bursts, because of the wide bandwidth and the rapid frequency drift. After considering these facts, and considering the sub-class of type III bursts which exhibit a "tail," Wild and his colleagues have concluded that the proportion of bursts in which fundamental and harmonic are both of detectable magnitude may exceed 50 percent.

It is my impression that the number density of the stream responsible for type III bursts is sufficiently high for the Vlasov equation to be applicable, since there are about 10^3 or more electrons in a Debye sphere. My present view is that the absence of two-stream instability is to be attributed to macroscopic density fluctuations.

Dr. Meyer: I have a question concerning the magnetic field fluctuations. The magnitude of these field fluctuations probably depends on how they are made. They should be correlated to density fluctuations if they are not pure Alfven waves because of the pressure equilibrium.

It seems to me that the order of magnitude of the magnetic field fluctuations in general should correspond to that of density fluctuations.

I wonder what number you would forecast for the magnetic field fluctuations?

Dr. Sturrock: My estimate of the magnetic field fluctuations is 10^{-3} gauss. Since I can alternatively explain radiation by density fluctuations of order $\Delta n/n = 10^{-5}$, one should, I think, conclude that scattering by density fluctuations is more important than scattering by magnetic field fluctuation, unless the strength of the magnetic field should exceed 10^2 gauss in the case which I computed. This seems unlikely.

Dr. Meyer: If I understand correctly, these are the field fluctuations of the scale of your wavelength again?

Dr. Sturrock: Yes.

Dr. Wild: I would like to comment on this distinction between plasma waves interacting on themselves and plasma waves interacting on thermal plasma waves. The Russian theory of combination scattering, which appears in various forms—in fact, there is a paper by Sturrock on this question—shows that, when a plasma wave interacts with another plasma wave, the resultant intensity is proportional to the product of the two intensities times the sine of the angle between them This means that, if a wave interacts with itself, the emission is zero.

Dr. Sturrock: Let me be quite clear. One plane electrostatic wave (plasma oscillation) will not interact with itself to produce radiation. I am dividing up the *spectrum* of fluctuation into two categories: One is that due to thermal excitation; and the other is that due to excitation by a electron beam, either by the Cerenkov effect or by the two-stream mechanism.

Each spectrum of oscillations contains an infinite number of plane waves. I am referring to an interaction among beam-excited waves, or to the interaction of excited waves with thermal waves.

Dr. Bailey: I have what I suppose is an incredibly naive question, being unfamiliar with the raw material for these studies. I want to know whether or not people working on these theories can be sure that what they are calling a fundamental *is* a fundamental, and whether they have correctly identified the harmonics. This surely must be very important in some of the conclusions that are being drawn.

Dr. Wild: The evidence for harmonics is much stronger in the case of type II bursts where the ratios are not exactly 2 to 1 but typically about 1.95 or 1.96. This can readily be explained in terms of absorption near

the plasma frequency, this small difference. In fact, I think it is greater evidence of fundamental and second harmonics than if the ratio had been exactly 2 to 1, in which case one might have been dealing with the second and fourth harmonics.

Type III's rely on rather less evidence. It is often very difficult to see them. They may often be there when you don't see them because they overlap so much. But in many striking cases, especially when the type III takes the form of an inverted "U," the ratios between the turnover points are again about 1.9, often lower.

EDITOR'S NOTE IN PROOF:

The following list of references belongs to paper No. 40 by G. Elwert, but was submitted too late to include at the end of the paper.

REFERENCES

1. CHUBB, T. A., FRIEDMAN, H., and KREPLIN, R. W., 1960, Paper presented at the First COSPAR Symposium, Nice.
2. KAWABATA, K., Preprint of High Altitude Observatory, Boulder, Colo.
3. WALDMEIER, M., 1963, *Z. Astrophys.*, 56: 291.
4. NEWKIRK, G., 1959, *Paris Symposium on Radio Astronomy*, ed. R. N. Bracecock, Stanford, p. 149.
5. SCHMIDT, M., 1953, *Bull. Astr. Inst. Neth.*, 12: 61.
6. DE JAGER, C., *Mem. Soc. Roy. Sci. Liège*, cinq. série, tome IV, 635.
7. DORMAN, L. F., 1960, *Proc. Moscow Cosmic Ray Conf. IV*, 134.

NUH-30290

40 SOME NOTES ON THE RELATIONS OF X-RAY, PARTICLE, AND RADIO EMISSION OF THE SUN DURING FLARES

GERHARD ELWERT
Astronomisches Institut der Universität Tübingen
Tübingen, West Germany

These few remarks are meant to point out some relations which seem to exist in the x-ray radiation, the particle emission, and certain types of radio emission.

The starting point of our study is the x-ray radiation of the sun. In the case of the undisturbed corona it is approximately in the wavelength interval between 40 and 100A, the total flux at earth distance being some tenths erg/cm² sec. In undisturbed conditions the flux in the short wave tail below 20A is about 10^{-4} erg/cm² sec, but during flares it may rise approximately four orders of magnitude. We are now going to examine measurements of x-ray emission made by Friedman (Reference 1) during a flare of class 2+, that is, a flare of medium intensity. Figure 40–1 shows the time of the beginning and the maximum in Hα as well as the development of the radio-emission at 2 wavelengths in the cm region according to measurements in Toyokawa (Reference 2). About $2\frac{1}{2}$ minutes and 5 minutes after the maximum intensity in Hα, the x-ray emission was measured in the wavelength ranges between 0.2 and 0.6, 2 and 8, as well as 8 and 20A.

In the short wavelength range between 0.2 and 0.6A, which corresponds to energies of the quanta between 60 and 20 kev, a spectrum was taken with a scintillation counter. It shows, according to Figure 40–2, an exponential decrease of the number of quantae as a function of the energy of the photons. This spectrum may be interpreted as brems-

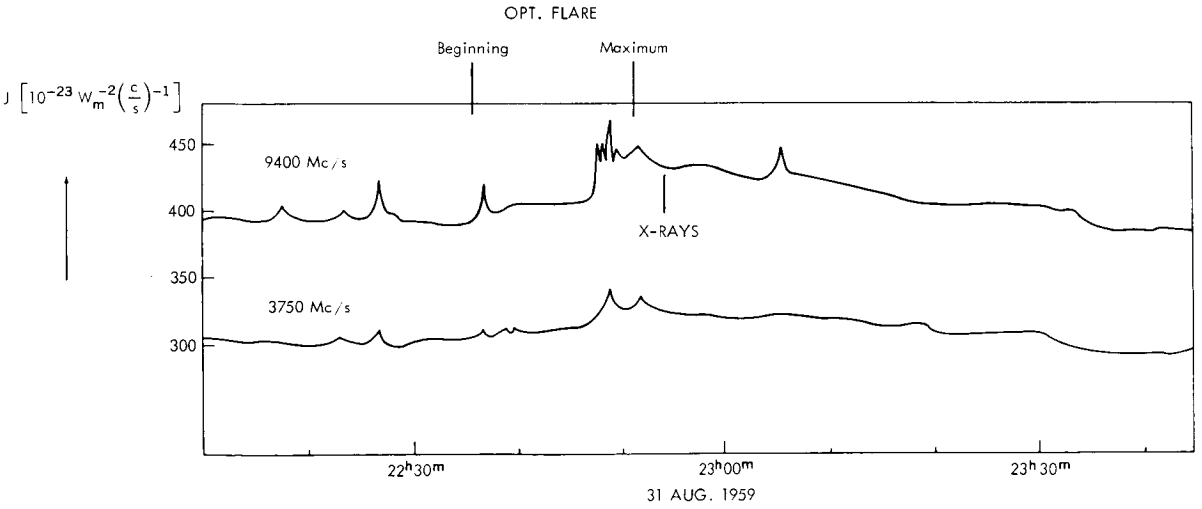

FIGURE 40–1. Development of x-ray and radio emission during the flare observed August 31, 1959.

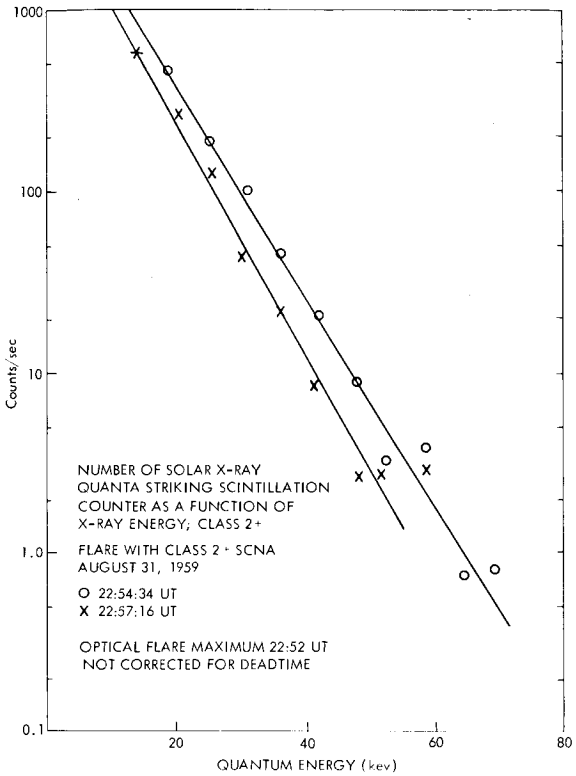

FIGURE 40–2. X-ray quantum flux as measured by Friedman.

strahlung of electrons of a hot gas with a Maxwellian velocity distribution.

According to the equation in Figure 40–3 the flux then is proportional to $e-(h\nu/kT)$ and the integral of the square of electron density taken over the radiating volume. In order to receive the measured slope, one has to set $T=10^8$ °K, as has been pointed out by Friedman. From the absolute value of the flux being 4×10^{-5} erg/cm² sec in earth distance, we can determine $\int n_e^2 dV=4\times10^{46}$ cm^{-3}. We are now going to replace this integral by the product of the square of a medium particle density and the radiating volume n_e^2V.

Moreover, in the range between 2 and 8A a total flux of at least 0.2 erg/cm² sec, and between 8 and 20A a minimum of 0.5 erg/cm² sec, was measured. As these data are lower limits, the actual fluxes may be even larger. The corresponding minimum fluxes are also shown in Figure 40–3 by horizontal lines. The spectrum of the hot region at 10^8 °K falls off rapidly above 1A. It is therefore inadequate to explain the radiation between 2 and 20A. For this a region of lower temperature and larger n_e^2V is required. Indeed, it cannot to be assumed that a region with a temperature of 10^8 °K is located in the surrounding corona without any transition of temperature. Nor is it to be assumed that the velocity distribution of the electrons is at all strictly Maxwellian. From the measurements we can probably merely infer that the spectrum in this range can be approximated by a Maxwellian one with 10^8 °K, while the total distribution can be represented by the superposition of several Maxwellian distributions. As already pointed out by Kawabata a distribution of about $T=2\times10^7$ °K is required to represent the measurements between 2 and 8A (curve II in Figure 40–3). As it has decreased considerably between 8 and 20A, it can not reproduce the observations in this range. Though it may be that the higher fluxes in this wavelength range arise from line emission, we have nevertheless drawn in an additional curve III in Figure 40–3 in consideration of the fact that the measured fluxes are lower limits; the addition to curve II results in the fully drawn curve II+III.

It seems remarkable that this spectrum can represent not only the measured flux between 2 and 20A but also the radio emission at 3 and 8 cm (Reference 2) indicated by crosses in Figure 40–4 belonging to a range which differs from that of the x-rays by about eight orders of magnitude. Therefore not only the x-ray emission but also the radio emission of the cm range can be interpreted as a thermal one. This was also pointed out by Kawabata. The transition of the emission in an optically thin layer to one in a thick layer takes place at cm wavelengths.

By the absolute value of the fluxes the product n_e^2V is determined again. It is also noted for the curves II and III of Figure 40–3.

It is to be assumed that the spectrum in the transition region between 0.6 and 2A can be represented by a smooth curve. This is indicated by the broken line. Unfortunately, up to now no measurements have been taken in this region.

From n_e^2V we may obtain the total number of electrons n_eV if we know the particle density

$$J_\lambda = 2,2\cdot 10^{-50}\cdot \int n_e^2 dV\cdot \left(\frac{10^6}{T}\right)^{1/2} e^{-\frac{h\nu}{kt}}\, g\, \frac{d\lambda[A]}{\lambda^2[A]}$$

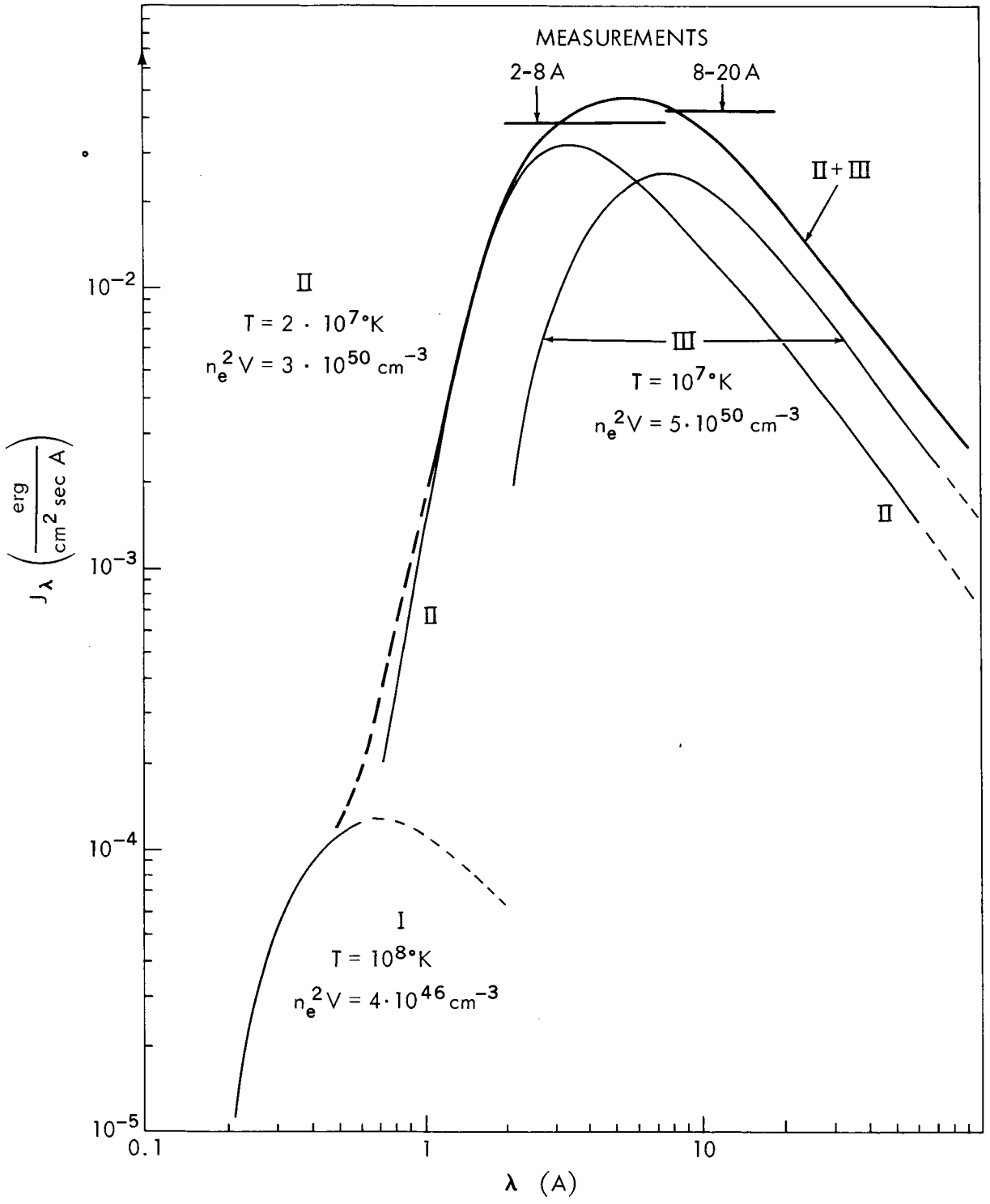

FIGURE 40–3. Spectral curves approximating the measurements.

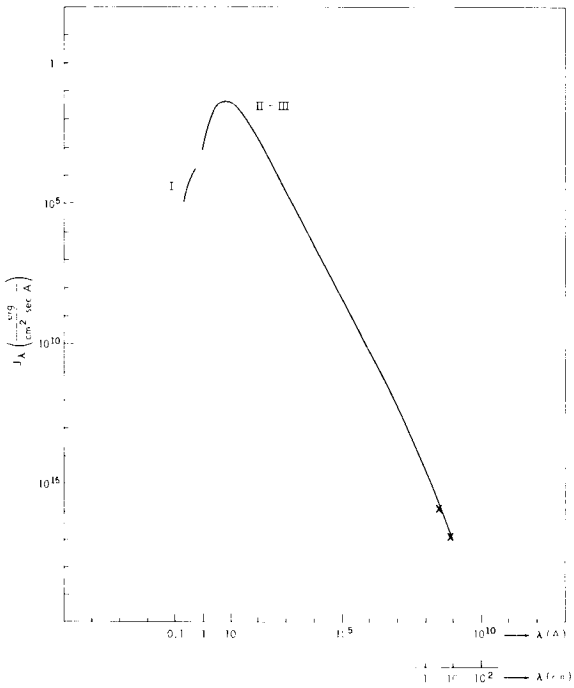

FIGURE 40–4. Theoretical x-ray spectra used for radio frequency and compared with radio measurements.

of the electrons. This may be done approximately by an easily made estimate of the radiating volume. First, it seems reasonable to assume for the area F of the hot region at 10^8 °K the order of magnitude of the area of the optically visible flare. For a flare of class 2+ it is ½ percent of the area of the solar disk, that is, 10^{19} cm^2. Assuming the height of this region to be of the order of some 10,000 km, V turns out to be of the order of 10^{28} cm^3; from this we obtain a particle density of the electrons and protons of some 10^9 cm^{-3} and a total number of the fast electrons and protons of some 10^{37}. If we interpret the curves II and III as contributions of cooler surrounding regions, we obtain the same order of electron density of some 10^9, assuming a volume of 10^{31} cm^3, which means a linear extension of 2×10^{10} cm. This dimension, as well as electron density, corresponds nearly to the estimations of a coronal condensation observed by Waldmeier (Reference 3) during the solar eclipse of February 5, 1962. These electron densities of some 10^9 also agree with the densities which could be deduced, according to Newkirk (Reference 4) and Schmidt, (Reference 5) from observations of the brightness of the corona above flares. As a total number we find nearly 10^{41} fast particles. As Figure 40–5 shows, we obtain a distribution function $Ff(E)=\mathrm{d}N/\mathrm{d}E$, which can be represented by superposition of three Maxwellian distributions; the corresponding temperatures and total numbers of electrons are indicated in this figure. Function III, corresponding to the lowest temperature of 10^7 °K, must naturally not be considered at high energies. This model may be called *model A*.

Another contrary possibility would be to assume for the cooler regions the same volume as for the hot region of 10^8 °K. This model we shall call *model B*. We then obtain electron densities of the order 10^{11} cm^{-3}. They correspond to the transition region from the chromosphere to the corona; in this case we would have to imagine the cooler regions to be below the hotter ones. Or assuming a uniform region with a non-Maxwellian velocity distribution then the heating takes place mainly in this transition region. The total number of fast electrons is then one order of magnitude smaller than in model A. The respective distribution functions II′ and III′ are shown as broken curves.

What conclusions may be drawn from these distribution functions? The velocities of the electrons v_E and of the protons v_P corresponding to the energies E are drawn in on two additional scales of Figure 40–5, assuming that by the mechanism of acceleration not only the electrons but also the protons are accelerated at the same, or nearly the same, energies. The velocities of the electrons are small fractions of the velocity of light; the mean velocity corresponding to a temperature of 10^8 °K being ⅕c. As a result of this high velocity the electrons will leave the corona, provided they are not prevented from escape by magnetic fields or by collisions with the particles of the surrounding undisturbed corona. If one calculates the mean free path, the result is—according to de Jager (Reference 6)—that electrons with velocities about ⅕c can escape into space. Passing through the corona, these electrons might produce the type III bursts by

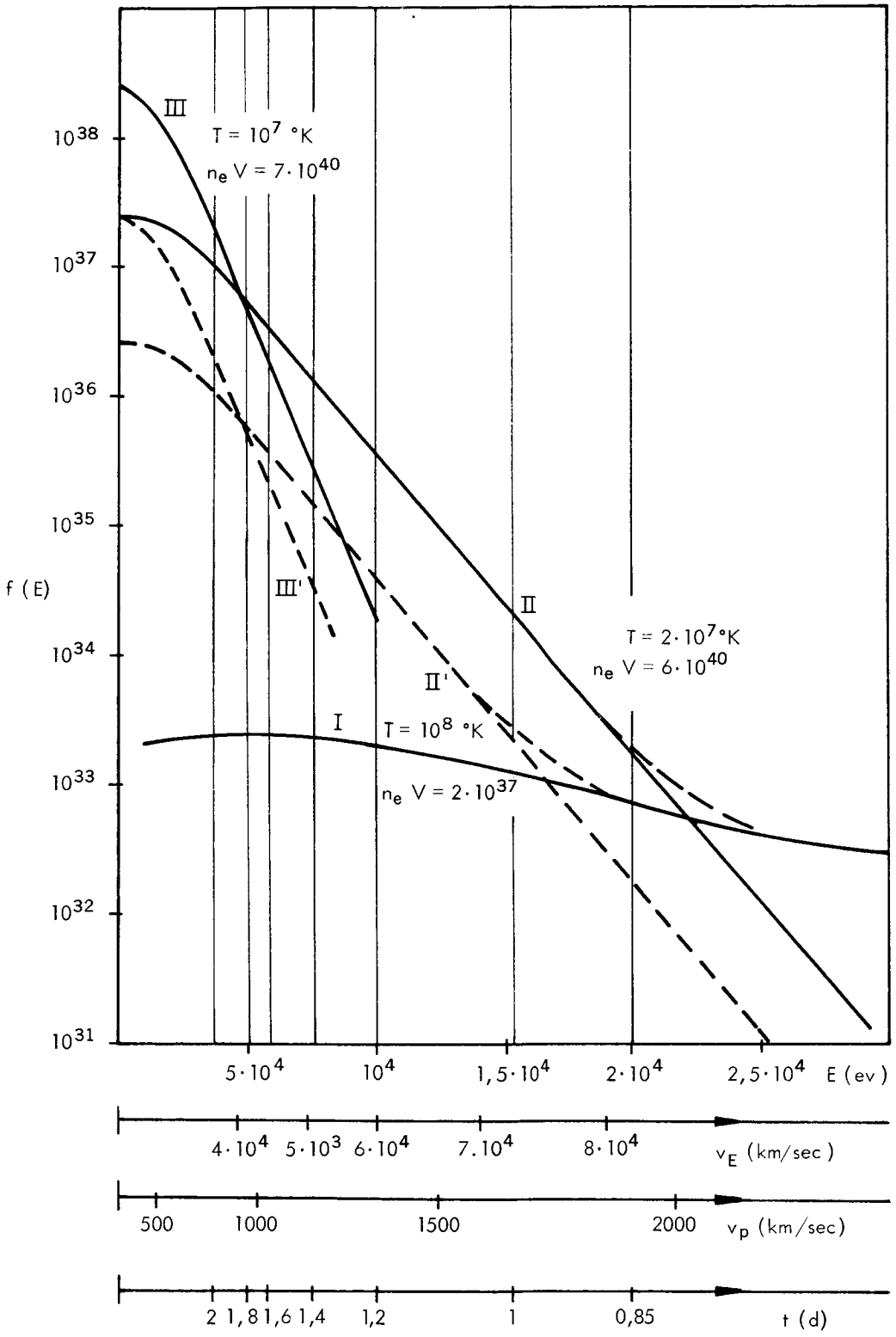

FIGURE 40–5. Total number of fast particles as calculated by the x-ray measurements.

excitation of plasma waves. On the other hand, protons of the same mean energy have a velocity of about 1500 km/sec. This is, firstly, the velocity of the regions from which the type II bursts arise. They seem, therefore, to be induced by streams of protons. Secondly, this is the velocity which is necessary for a plasma stream to reach the earth approximately 1 day later. The flight times corresponding to the energies and velocities are indicated in a further scale in Figure 40–5.

$$\bar{\rho} = \frac{\bar{j}}{v} = \frac{1}{F\,v}\,\frac{dN}{dt} = \frac{0.35}{F_{cm^2} \cdot v_{cm/sec} \cdot t_d}\,\frac{dN}{dt}$$

$\Omega = 0.1$

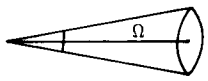

$F = 2 \times 10^{25}\ cm^2$

t_d	1.2	1.4	1.6	1.8	2
$\bar{\rho}$	50	150	400	600	1200 Model A
$\bar{\rho}$			40	60	120 Model B

FIGURE 40–6. Particle densities in earth distance after the investigated flare as calculated from the x-ray observations.

The question now arises as to whether, from these considerations, we obtain sufficient fast particles. At first, instead of the energy interval dE, the velocity interval dv can be introduced: $dE = mv\ dv$. If we use the equation for uniform motion, a velocity interval dv corresponds with a constant distance s to a time interval: $dt = (s/t^2)\ dt$. In this time interval dt the number of particles dN traverses the distance s from the sun to the earth. Consequently the number of particles $dN = f(E)\ dE$ in the energy interval dE passing through a surface at earth distance in the time interval dt can be given by

$$dN = f(E)\,dE = f(E)\,mv\,dv = f(E)\,\frac{ms^2}{t^3}\,dt.$$

The current at earth distance dN/dt is after $t/_d$ days thus given numerically as

$$\frac{dN}{dt} = f(E)6 \times 10^{-11}\,\frac{1}{t_d^3}.$$

In order to make any statements about the current density and the particle density, one must estimate the area of the surface through which this current passes. According to Dorman (Reference 7) the solid angle Ω into which the fast particles are emitted can be estimated between 0.01 and 1. Using the medium value of 0.1 corresponding to an opening angle of about 10 degrees one obtains $F = 2 \times 10^{25}$ cm^2. From this, the mean current density $\bar{j} = (dN/dt)F$ and the mean particle density $\rho = \bar{j}/v$ can be calculated (Figure 40–6). Thus we obtain in model A a particle density at earth distance of about 50 after 1^d,2, of 150 after 1^d,4, of 300 after 1^d,6, of 600 after 1^d,8, and of about 1000 after 2^d. In the case of model B, densities of the order of 100 will be reached only after about 2 days. It is well known that particle densities of some 100 cm^{-3} at earth distance may exist during magnetic storms. These densities result immediately in model A; they may, however, also be obtained in the center of the current in model B, since there even larger densities could be expected.

In addition we have to take into account that the x-ray fluxes between 2 and 20A, which were the basis for our conclusions, are lower limits. Further, we have to consider that the measurements were taken about 2½ minutes after the maximum of the visible flare so that it may be assumed that the x-ray flux, and also the number of fast particles, has already decreased at the time of observation. This decrease in time is also confirmed, as two spectra have been taken in the region between 0.2 and 0.6A (Reference 1); they show a decrease of about a factor of 3 within 2½ minutes. Finally, we have to take into account that the flare we have considered was one of medium importance. In any case it would seem useful to investigate further the relations we have indicated. For this purpose it would be necessary, above all, to take further spectra during flares at different stages of development in the total wavelength range between 0.1 and 1A.

W64-30291

41 RADIOFREQUENCY RADIATION AND PARTICLE ACCELERATION FROM SOLAR FLARE FILAMENTS DUE TO COLLECTIVE MOTION AT MULTIPLES OF THE CYCLOTRON FREQUENCY*

RICHARD L. MOORE and J. R. JOHNSTON
Aircraft Division, Douglas Aircraft Company, Inc.
Long Beach, Calif.

Abst

30291

A mechanism is proposed through which the turbulent energy of a plasma is converted into induction and traveling RF fields. The mechanism is the rotational collective motion of an ion or electron gas in a magnetic field at both the plasma frequency and multiples of the cyclotron frequency.

A cylindrical ring of the gas involved is assumed to have its macroscopic angular velocity equal to the cyclotron frequency. Coupling between the convective terms of the acceleration field and the electromagnetic potentials results in waves rotating around the axis whose intensity is given by the turbulence intensity. These current waves emit RF radiation which, as it travels outward, also travels around the axis at angular rates which are (1) integral fractions of the plasma frequency, or (2) the cyclotron frequency. Combined with the magnetic field external to the filament, the waves can accelerate particles to high energy. Properties that the filament must have and a preliminary comparison with experiment are given.

Author

This paper presents an hypothesis (Reference 1) concerning a means by which the kinetic energy of turbulence in a single source region can be converted into much of the phenomena observed in connection with solar flares. The means for doing this is through the local induction or radiation fields associated with a particular frequency, or frequencies, arising from collective motion of either the ions or the electrons of the source region.

The model of the collective motion presented herein is in qualitative agreement with recent laboratory experiments such as the emission of RF radiation at high harmonics of the ion (Reference 2) or electron (Reference 3) cyclotron frequency. Complete test of the theory by experiment is expected to be complex, from the very nature of the theory itself, so that confirmation of the theory has not yet been achieved.

Figure 41–1 shows the assumed geometry of a plasma wave associated with a small filament. For simplicity, the particles are

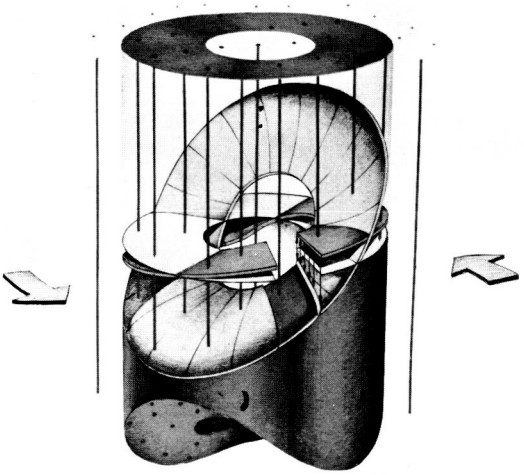

FIGURE 41–1. Notes on figure: The vertical lines represent the B_z field. The particles occupy the cylindrical ring. The cutaway shows the rotating velocity field and the rotating electric field. The unshaded plane is the reference z equal to zero plane. The difference between the dark surface and the reference plane gives the velocity vector at that point in space. The difference between the reference plane and the curved, lightly shaded surface is the electric field at that point in space.

*Presented by Dr. Moore.

assumed confined to a cylindrical ring of inner radius R_1 and outer radius R_2. The chief assumption is that the macroscopic (or average) angular velocity equals the angular velocity of an individual particle located in the region; that is, the angular velocity equals the cyclotron frequency. At the same time, superimposed on this uniform angular motion and uniform magnetic field are both a macroscopic fluctuating velocity field and macroscopic fluctuating electric and magnetic fields, which travel around the axis. Figure 41–1 shows the rotating velocity and electric fields.

The essence of the theory is given in Equations 1 through 4:

$$\rho \frac{d\mathbf{V}}{dt}=nq(\mathbf{V}\times\mathbf{B}+E_{zm}\mathbf{k}), \tag{1}$$

$$\frac{\partial V_r}{\partial t}+\omega \frac{\partial V_r}{\partial \theta}=0;\ V_\theta=r\omega, \tag{2}$$

$$\frac{\partial V_z}{\partial t}+\omega \frac{\partial V_z}{\partial \theta}=\frac{q}{M}(E_{zm}-r\omega B_r), \tag{3}$$

$$V_z=V_{zm}\sin(\omega_m t+m\theta). \tag{4}$$

If there is a wave in the z direction, which travels around the axis, it is assumed to have the time and angular dependence given by Equation 4.

The general macroscopic momentum equation is given by Equation 1, and two of its components by 2 and 3, where the hydrodynamic operator d/dt has been expanded as appropriate to the conditions assumed.

The left sides of both Equations 2 and 3 will vanish if the form of Equation 4 is substituted in them, and if ω equals ω_c and ω_m equals $-m\omega_c$.

This example shows that the way that the cyclotron frequency becomes related to the vibration frequency is through the angular variation in the velocity field. It may also be shown that the right side of Equation 3 will vanish, thus satisfying the equation; however, the derivation becomes complex when we combine Maxwell's equations with the momentum equation, so that we will pursue a slightly different method of derivation in general.

The assumptions made for the general derivation are the following:

n_0, $\mathbf{B}_0$ are uniform and steady,

$$\mathbf{V}=r\omega 1_\theta+\nabla\psi+\mathbf{V}_t,$$

$$\omega=-qB_0/M,$$

$$\mathbf{B}=\mathbf{B}_0+\mathbf{B}_a+\mathbf{B}_t,$$

$$\mathbf{A}=\mathbf{A}_0+\mathbf{A}_a+\mathbf{A}_t,$$

$$\mathbf{E}=-\mu\frac{\partial \mathbf{A}_t}{\partial t}-\nabla\phi.$$

For a cylindrical ring of particles, these assumptions are believed to be reasonable. The velocity field has three components: a steady term, and small periodic solenoidal and potential terms. The magnetic flux density **B** has three components whose vector potentials are given by the corresponding components of **A**. The electric field has no steady component but is composed of both a solenoidal term $[-\mu(\partial\mathbf{A}/\partial t)]$ and a potential term $-\nabla\phi$.

The basic equations assumed are these:

$$\mu^{-1}\nabla\times\mathbf{B}=n_0q\mathbf{V}-\frac{1}{c^2}\frac{\partial^2\mathbf{A}_t}{\partial t^2}-\epsilon\nabla\frac{\partial\phi}{\partial t}, \tag{5}$$

$$\frac{\partial\phi}{\partial t}=\frac{n_0q}{\epsilon}\psi, \tag{6}$$

$$\frac{d\mathbf{V}}{dt}=\frac{q}{M}(\mathbf{V}\times\mathbf{B}+\mathbf{E}), \tag{7}$$

$$=\frac{\partial\mathbf{V}}{\partial t}+\nabla\frac{V^2}{2}-\mathbf{V}\times\nabla\times\mathbf{V}. \tag{8}$$

Equations 5 and 6 come from Maxwell's equations. Equation 7 is the equation of momentum. Equation 5 comes from substituting the assumptions about **E** into the Maxwell equation relating the curl of the magnetic field and the convection and displacement currents. Equation 6 comes from the continuity of matter and Equation 5. Equation 8 represents an expansion of the left side of Equation 7 in a more convenient form. The utility of this expansion, together with the assumptions made about **V**, **B**, and **E**, is evident from Equation 9, where the substitutions have been made in Equation 7, and the result written as Equation 9:

$$\nabla\left(\frac{\partial\psi}{\partial t}+r\omega_c V_{t_\theta}+\frac{q\phi}{M}\right)=(\mathbf{V}_t+\nabla\psi)\times\omega_c\mathbf{k}+\mathbf{V}\times\nabla$$

$$\times(\mathbf{V}_t+\mu q\mathbf{A}_t/M)-\frac{\partial}{\partial t}(\mathbf{V}_t+\mu q\mathbf{A}_t/M), \quad (9)$$

and

$$\left(\nabla^2-\frac{1}{c^2}\frac{\partial^2}{\partial t^2}\right)\mathbf{A}_t=-n_0 q\mathbf{V}_t. \quad (10)$$

Let

$$\mathbf{V}_t=-\mu q\mathbf{A}_t/M. \quad (11)$$

Equation 10 follows from the substitutions for **B, V,** and Equation 6 in Equation 5. From the forms of Equations 9 and 10 it is obvious that, if Equation 11 were true, both the former equations would be greatly simplified. This assumption may be shown to be equivalent to assuming that the electric and magnetic energy associated with the vibrational motion is all potential energy and that this potential energy is equal in magnitude to the kinetic energy of the vibrating current. Making this assumption, the momentum equation reduces to Equation 12, and the equation for the vector potential becomes Equation 13:

$$\nabla(i\alpha\psi+rV_{t_\theta})=(\mathbf{V}_t+\nabla\psi)\times\mathbf{k}, \quad (12)$$

and

$$(\nabla^2+K^2)\mathbf{V}_t=0, \quad (13)$$

$$\alpha=\frac{\omega_m^2-\omega_p^2+m\omega_m\omega_c}{\omega_m\omega_c}, \quad (14)$$

$$K^2=(\omega_m^2-\omega_p^2)/c^2, \quad (15)$$

$$\mathbf{V}_t \text{ and } \psi\propto \exp[i(m\theta+\omega_m t)]. \quad (16)$$

Equations 14 and 15 give definitions of the parameters α and K. Equation 13 is seen to be a vector Helmholtz equation, but Equation 12 is not easily characterized. Equations 12 and 13, plus the condition that the divergence of $\mathbf{V}_t$ is zero, gives us seven equations in four unknowns to be simultaneously satisfied.

The solutions found may be shown to be unique, and depend on the values of the parameters K^2 and α^2. We have found solutions under the following conditions:

1. $K=0$ (this implies that α equals m, and m is not equal to ± 1)
2. $K\neq 0$; $\alpha^2=1$.

Equations 17 through 20 give the set of solutions when K is zero:

$$K=0,\ \omega_m=\pm\omega_p, \quad (17)$$

$$\xi_{i\pm}=[A_i r^m\pm B_i r^{-m}]\exp[i(m\theta\pm\omega_m t)], \quad (18)$$

$$\psi=(1+\beta z)\xi_{1+}, \quad (19)$$

$$\mathbf{V}_t=\nabla\times[(1+\beta z)i\xi_{i-}\mathbf{k}]+\xi_2\mathbf{k}. \quad (20)$$

A_i, B_i, and β are arbitrary constants, and velocity is null in the r and θ directions. ξ_1 is a function as defined by Equation 18, which occurs in the solution for both ψ and V_t. A_i, B_i, and β are constants of integration. The velocity $\nabla\psi+\mathbf{V}_t$ is zero in the r and θ directions, because the components of $\nabla\psi$ and $\mathbf{V}_t$ are equal and opposite in these directions. The frequency of vibration is the plasma frequency, which was a result not unexpected. The motion corresponds to a special case of the plasma oscillations.

Equations 21 through 26 show the second class of solutions obtained for the systems 12 and 13.

$$K\neq 0, \quad (21)$$

$$\alpha^2-1=0,\ \alpha=\pm 1, \quad (22)$$

$$\psi_m=[A_{m1}r^m+A_{m2}r^{-m}]\exp[i(m\theta+\omega_m t)], \quad (23)$$

$$\mathbf{V}_{t_m}=\mathbf{k}[B_{m1}J_m(Kr)$$
$$+B_{m2}N_m(Kr)]\exp[i(m\theta+\omega_m t)], \quad (24)$$

$$\frac{\omega_m}{\omega_c}=-\frac{m\mp 1}{2}\left[1\pm\left(1+\left[\frac{2\omega_p/\omega_c}{m\mp 1}\right]^2\right)^{1/2}\right], \quad (25)$$

$$\approx-(m\mp 1)\left[1+\frac{\omega_p^2/\omega_c^2}{(m\mp 1)^2}\right]. \quad (26)$$

If K is not zero, α must equal ± 1 to satisfy the system. The frequency of vibration ω_m is given by Equation 25 and is approximated by 26 if $[\omega_p/\omega_c(m\mp 1)]^2$ is small compared to unity. In this case we find motion at frequencies* near integral multiples of the cyclotron frequency. Again we have the arbitrary constants A_{mi}, B_{mi}, which are determined by the *initial conditions* (in the solar flare, this is the kinetic energy of turbulence at the frequency corresponding to the mth mode); $J_m(Kr)$ and $N_m(Kr)$ are the Bessel and Neumann functions as

*We suggest the name *hypergyromagnetic* frequency.

usually defined. It is appropriate to note that in work in progress, in which nonuniform density and acoustic waves are permitted by assumption, we find simpler results in that the vibration frequency is a simple integral multiple of the cyclotron frequency.

Having this type of vibrational motion in either the ion component or the electron component of the gas, we consider the electric field radiated and some of its properties.

A simple answer to the general solution has not been obtained, nor is it expected. However, by assuming a current similar to that of Equation 24, namely, $qn_0V_{zm}\exp i(m\theta+\omega_m t)$, where V_{zm} is *not* a function of the radius but is an arbitrary constant determined by the initial conditions, it is possible to give some relatively simple results. Since B_{m1} and B_{m2} could be adjusted so that the z component of V_{tm} is approximately uniform in a thin ring of inner radius R_1 and outer radius R_2, we may take the above assumption of constant V_{zm} as a good approximation for such a case.

Equations 27 through 29 show the electric field at large distances from a source of length L as given in a spherical coordinate system (r, θ, ϕ) with the origin on the axis of the source and $\theta=0$ corresponding to the z-axis of the cylindrical coordinate system.

$$\mathbf{E}_1=\sqrt{\frac{\mu_0}{\epsilon_0}}\frac{qnV_{z1}L}{24kr}[(kR_2)^3-(kR_1)^3]\times\left[\mathbf{1}_\theta\cos\left(kr+\phi-\omega_c t-\frac{\pi}{2}\right)-\mathbf{1}_\phi\cos\theta\sin\left(kr+\phi-\omega_c t-\frac{\pi}{2}\right)\right], \tag{27}$$

$$\mathbf{E}_2=\sqrt{\frac{\mu_0}{\epsilon_0}}\frac{qnV_{z2}L}{96kr}[(kR_2)^4-(kR_1)^4]\sin\theta \times[\mathbf{1}_\theta\cos(kr+2(\phi-\omega_c t)-\pi)-\mathbf{1}_\phi\cos\theta \sin(kr+2(\phi-\omega_c t)-\pi)], \tag{28}$$

$$\mathbf{E}_3=\sqrt{\frac{\mu_0}{\epsilon_0}}\frac{qnV_{z3}L}{640kr}[(kR_2)^5-(kR_1)^5]\sin^2\theta \cdot \times\left[\mathbf{1}_\theta\cos\left(kr+3(\phi-\omega_c t)-\frac{3\pi}{2}\right)-\mathbf{1}_\phi\cos\theta\sin\left(kr+3(\phi-\omega_c t)-\frac{3\pi}{2}\right)\right]. \tag{29}$$

Equations 27, 28, and 29 correspond to motion at the fundamental of the cyclotron frequency and the first two harmonics. The physical facts of interest are that the field is proportional to the following: the amplitude of vibration V_{zi}, the length of the source, the number density, and the difference of high powers of the inner and outer radii. Even far from the axis, it is a wave which rotates around the axis while traveling outward. The waves are left-hand circularly polarized at the $\theta=0$ direction, and linearly polarized when θ is $\pi/2$.

Figure 41–2 shows the distribution of the power emitted where the power for $m=1$ is normalized at unity, and for $m=2$ and 3 is normalized at one-half. If m is unity, the power is largest along the axis. For higher harmonics the power is concentrated along the equatorial plane. These properties are in qualitative agreement with observation so far as they can be checked. The calculation of the total power emitted will be deferred until after a discussion of the mechanism proposed for particle acceleration.

Figure 41–3 shows schematically the situation which may occur. First, a rotating, outward traveling wave is emitted from a long thin filament. Outside, but near to the filament, are rotating induction fields; and we assume that a magnetic field of approximately the same strength (this is not necessary, but will be as-

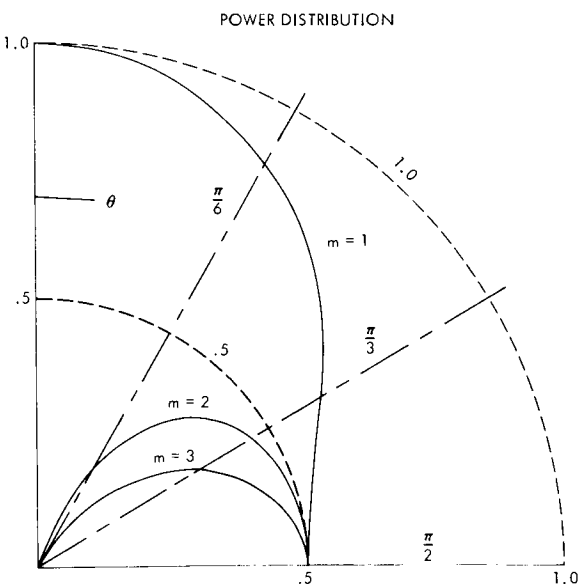

FIGURE 41–2.

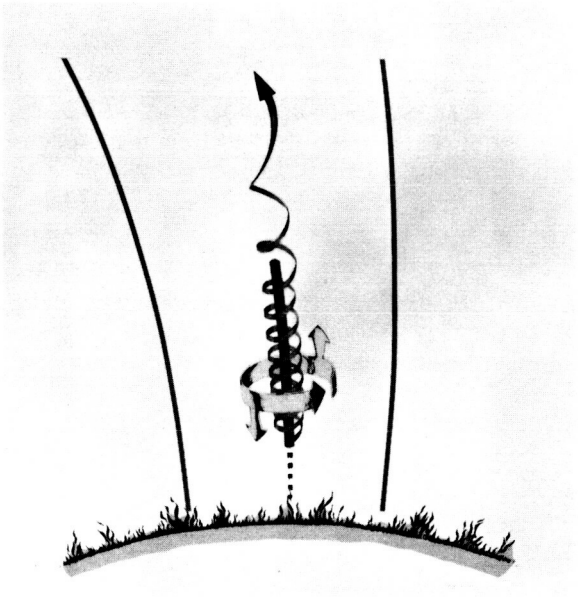

FIGURE 41–3.

sumed for illustrative purposes) occupies the space of *relative vacuum* outside the filament. A particle introduced with sufficient transverse energy to remain at the same Larmor radius will rotate with the same angular frequency as the wave, and will be accelerated along the vertical axis as long as it continues to rotate in phase with the electromagnetic wave. This is a simple case of the acceleration of particle. It is not to be inferred that this is the only case. The existence of one case is sufficient to illustrate the premise of this paper, namely, that the RF radiation does not necessarily come from synchrotron radiation of relativistic particles but that the RF radiation may indicate the presence of outward traveling waves from a coherent source, and the waves in conjunction with an appropriate steady magnetic field form a mechanism by which particles may be accelerated to high energy.

To become more quantitative in order to check the feasibility of the theory, we may calculate back from the power W, received at the earth's surface, to obtain information about the source. Thus let r_o be the radius of the earth's orbit about the sun, W the power density at the peak of the received angular frequency ω, χ the width of the line, and G the gain of the emitted power density in a given direction. The left side of the following equation gives the parameters of the source, and the right side the observed parameters:

$$2\pi nqV_{zm}L\,\frac{[R_2^{m+2}-R_1^{m+2}]}{m+2} = \frac{r_o}{k^{m+1}}\left[\frac{(2m+2)!(8\pi)^{1/2}\omega WGc\chi}{2m}\right]^{1/2}. \quad (30)$$

From this expression, we note that the product $nV_{zm}L$ is one important term and, assuming m is 1, the expression $R_2^3-R_1^3$ becomes approximately R_2^3 if R_1^3 is small compared with R_2^3. None of these four parameters can be estimated with confidence.

However, n probably varies between 10^8 to 10^{12} cm^{-3}, and possibly might be as high as 10^{15} cm^{-3}. The lower limit of L may safely be taken as 1 km (10^5 cm). V_{zm} may range upwards to 10^7 cm/sec, judging from typical velocities observed, although we would happily accept a lower value. This leaves R_2 to be calculated from the right side of Equation 30 as observed, and the typical numbers inserted on the left side. The outer radius is particularly important, since it is a direct measure of the Larmor radius of the most energetic particle in the source region. Putting the numbers in Equation 30 as shown in Expression 31, we may compute the outside radius and the energy of a particle corresponding to that Larmor radius in the magnetic field estimated by taking the cyclotron frequency equal to the emitted frequency.

$$\left.\begin{aligned} &L=10^5\text{ cm},\ f=70\text{ Mc},\\ &\qquad\qquad 10\%\text{ linewidth},\ G=1,\\ &V_{z1}=10^7\text{ cm/sec},\\ &W=10^{-16}\text{ watts}/(m^2hz). \end{aligned}\right\} \quad (31)$$

Table 41–1 shows the result of the computation of R_2, plus the energy of a particle having the particular Larmor radius. A number density of 10^{12}, a ring radius of 60 cm, and an electron energy of 2 kev would be the most plausible case to choose of those computed in

728-629 O—64——25

TABLE 41–1

n (cm^{-3})	R_2(cm)	Electron Energy (kev)	Proton Energy (Mev)
10^8	1300	900	1600
10^{12}	60	2	3

this table. An even more plausible case would be one in which the number density is higher, say 10^{15}; the value of turbulence $(V)_{zm}$ is lower, say 10^5 cm/sec; the source region is slightly longer and the radius somewhat reduced, but the electron energy is appreciably reduced. This would not require the electrons to have unreasonably high initial energy.

In summary, we have presented a model in which the major event occurring in a flare is the emission of radio frequency radiation by a turbulent ring of particles in a magnetic field. This emission of RF radiation is accompanied by the simultaneous acceleration of particles to high energy by traveling waves rotating at the cyclotron frequency.

REFERENCES

1. MOORE, R. L., 1963, *Bull. Am. Phys. Soc.*, Ser II, 8: 442. This was a preliminary version of this paper. Previous but different work on the same problem was summarized by R. L. Moore, *Ibid* 7: 132 (1962).
2. DUNLAP, J. L., BARNETT, C. F., DANDL, R. A., POSTMA, H., 1962, *Nuclear Fusion*, Supplement Part 1, p. 233.
3. BEKEFI, G., et al., 1962, *Phys. Rev. Letters*, 9: 6. We are also indebted to Prof. D. Smerd for information on the work of G. R. Landauer, as in paper F–2, 1963 meeting of Plasma Physics Division, *Bull. Am. Phys. Soc.* (to be published).

N64-30292

42 ELECTROMAGNETIC RADIATION FROM PLASMA OSCILLATIONS*

LUDWIG OSTER and M. ALTSCHULER
Yale University Observatory
New Haven, Conn.

30292

The general nature of a mechanism that would be able to produce electromagnetic radiation of the kind observed in type III bursts is determined. This mechanism is shown to be a generalized bremsstrahlung mechanism whose spectral features are computed numerically in the single-particle limit. Refinements that permit relating the remaining observational details to the particulars of the exciting stream are described.

There appears to be a consensus that some of the nonthermal radio emissions observed on the sun are caused by "plasma oscillations"; that is, that they are connected in some way or other with the collective behavior of plasma electrons which manifests itself in the existence of a resonance frequency, the so-called *plasma frequency*. In fact, one of the strongest arguments in favor of this hypothesis is the narrow bandwidth of these nonthermal emissions and their occurrence at radio frequencies consistent with their identification as local plasma frequencies of the coronal electrons. The bursts which fall clearly into this category are the type II and III bursts, whereas in the case of type I bursts the alternate explanation in terms of synchrotron radiation must at present be considered as a distinct possibility. Hence, type I bursts will not be studied in this communication.

There also is a consensus that type III bursts with their fast moving source are most likely excited by a stream of fast moving *particles*. The case of type II bursts in this respect is more complex, since at the inferred speeds the most probable source is a shock front rather than a cloud of particles; although the microstructure of the emission as it is occasionally observed raises the suspicion that the type II bursts might be nothing but a fast succession of a large number of type III bursts (Reference 1). In this latter case, the radiation problem would be reduced to explaining the type III emission, whereas the physically significant question would be the generation of fast particles from the shock wave. Otherwise, a mechanism of generating electromagnetic radiation by the shock front proper has to be devised. The theoretical dicussion to be presented in the following sections is not suitable for this purpose.

We shall for this reason concentrate on type III bursts. After evaluating—from the viewpoint of the theorist—the available evidence, we will review briefly a set of theoretical deductions conventionally identified with the generation of plasma oscillations. The relation of the electric field distributions predicted on this basis with the emission of electromagnetic radiation is derived, and the characteristic features of the radiation spectrum are discussed. Numerical results for a specific case (single-particle limit) are included.

THEORETICAL EVALUATION OF OBSERVATIONAL EVIDENCE ON TYPE III BURSTS

Type III bursts consist typically of a narrow banded emission (bandwidth of the same order as, or less than, center frequency) centered around frequencies corresponding to meter wavelengths and thus to plasma frequencies for electron densities of the order present in the lower corona. As a function of time, the center frequency moves rapidly from higher to lower values. If one identifies the in-

*Presented by Dr. Oster. This work was supported by the National Aeronautics and Space Administration under Grant NsG 176-61.

stantaneous center frequency with the local plasma frequency of a suitable corona model, speeds of order 0.1c and higher result. Commonly, a simultaneous emission centered at approximately twice the basic frequency is observed. The energies emitted per unit bandwidth exceed greatly the values expected in thermodynamic equilibrium at temperatures of the order 10^6 °.

From this evidence, three basic points can be extracted:

1. The emission has the character of a broad spectral line produced by the coronal electrons which are in turn excited by fast moving agents such as a particle stream,
2. There commonly exists a second harmonic,
3. The radiating electrons are not in thermal equilibrium with the undisturbed corona.

The question then arises as to what general class of mechanisms fits these postulates.

First, if one adopts a cloud of particles with a common velocity not much below the speed of light as exciting agent, one looks for a mechanism which converts part of the cloud's kinetic energy into radiation. One then would expect the coronal electrons to pick up energies comparable with the cloud's kinetic energy and thus to be in a position to produce radiative spectra with intensities far in excess of the emission at the initial thermal energy level. Hence, point no. 3 would have to follow immediately from any mechanism involving fast particles. It is, for instance, unnecessary to postulate Maser-type amplification of an initial small resonance (Reference 2).

Second, once a resonance emission is established at the plasma frequency, the appearance of a second harmonic (and, for that matter, the absence of higher harmonics) can be understood subsequently by combining the basic mechanism with a process of the type suggested by Ginzburg and Zheleznyakov (Reference 3) or Sturrock (Reference 4). In either case, the question of harmonics can be left unanswered for the time being. Admittedly, this procedure may lead in a wrong direction since it is conceivable that the correct mechanism simultaneously* produces first and second harmonics. In that sense, our procedure ought to be considered as only one—though rather plausible—possibility.

The fundamental problem, then, is to derive a mechanism which leads to the emission by a group of electrons of a "spectral line" at, or close to, the local plasma frequency. This mechanism should be a logical consequence of the appearance of the resonance frequency—that is, the plasma frequency—for any ensemble of free electrons and not require any additional assumptions, such as large-scale inhomogeneities or the presence of magnetic fields (References 3 and 5). The plasma frequency is present for transverse oscillations—which after all represent in the classical picture electromagnetic radiation—as well as for longitudinal waves and should therefore show up directly in the radiation spectrum as a resonance.

The fact that the plasma frequency is independent of the electron ensemble's kinetic energy and can be derived from a macroscopic theory strongly suggests a macroscopic theory to be as well sufficient to predict the resonance mechanism. In other words, it should be unnecessary to involve kinetic theory, or the electron ensemble's energy distribution function, the Boltzmann equation, etc. This point has indeed been proven explicitly (cf. the section "The Field Surrounding a Plasma Particle").

BREMSSTRAHLUNG AND PLASMA RESONANCE

In the light of the foregoing discussion it appears clear that whatever mechanism is responsible for the type III emission should be based solely on interactions between charged particles in a plasma—in particular, between electrons and either ions or other electrons. The radiation obtained from any such interaction is basically a "bremsstrahlung" event. This label is conventionally attached to a

*The term "simultaneous" should be understood in a conceptual sense; a spectroscopic doublet is a necessary consequence of the basic structure of the atomic levels. The Zeeman splitting of a spectral line, on the other hand, can be treated after the existence of this line has been proven. Complications would arise only in a hypothetical case in which the magnetic field itself produces the original spectral line.

restricted system which is obtained by assuming that any electron interacts with one specific ion and that the actual simultaneous occurrence of many such interactions can be split into a sum of unrelated events.

The concept ceases to be a reasonable approximation for the spectrum at low frequencies, since it leads to a logarithmic divergence at zero frequency (Reference 6). One might attempt to save this concept by introducing the Debye potential for the ions—a procedure which leads to the correct dc limit (Reference 7), predicts the onset of departures from the normal bremsstrahlung coefficients at the plasma frequency where one would expect it, and moreover can be justified on the basis of kinetic theory (Reference 8) which leads exactly to the same results. No resonance however, appears at the plasma frequency.

What one effectively does in this approximation is to introduce *a priori* a field distribution for the plasma ions (Debye potential) which corresponds to an oversimplified case and, as it happens, suppresses the resonance terms at the plasma frequency. We might conclude that the correct solution can be obtained by simply turning to a more accurate description of the field of an ion as seen by a plasma electron.

Such a "more accurate" description is available and indeed leads to the desired resonance behavior (next section). In that sense, then, the radiation encountered in type III bursts could legitimately be called bremsstrahlung or, more precisely, the resonance line part of the general bremsstrahlung continuum.

THE FIELD SURROUNDING A PLASMA PARTICLE

In this section, we derive expressions for the electric field surrounding a plasma particle of charge q which we shall call "test particle." Such field expressions were first described by Pines and Bohm (Reference 9) on the basis of kinetic theory and later, using fluid dynamics methods, independently by Majumdar (Reference 10) and Cohen (Reference 11). Following Majumdar, we envisage a charged particle, moving with speed u along the x-axis through a plasma whose electrons have a mean therma speed v. The test particle induces a space and time varying electric field $\vec{E}=-\nabla\phi$, with

$$\Phi(\vec{r},t)=q\cdot\frac{v^2-u^2}{v^2}\frac{\left[R_x^2+\frac{v^2-u^2}{v^2}\cdot R_\rho^2\right]^{1/2}}{R_x^2+\left(\frac{v^2-u^2}{v^2}\right)^2R_\rho^2}\times\exp\left\{-\frac{\omega_p}{(v^2-u^2)^{1/2}}\left[R_x^2+\frac{v^2-u^2}{v^2}\cdot R_\rho^2\right]^{1/2}\right\},\quad u<v,\quad (1a)$$

$$\Phi(\vec{r},t)=-q\cdot\frac{u^2-v^2}{v^2}\frac{\left[R_x^2-\frac{u^2-v^2}{v^2}R_\rho^2\right]^{1/2}}{R_x^2+\left(\frac{u^2-v^2}{v^2}\right)^2R_\rho^2}\times\exp\left\{\frac{i\omega_p}{(u^2-v^2)^{1/2}}\left[R_x^2-\frac{u^2-v^2}{v^2}\cdot R_\rho^2\right]^{1/2}\right\},\quad u>v,\quad (1b)$$

where $\vec{R}=\vec{r}-\vec{u}t$, $R^2=R_x^2+R_y^2+R_z^2=R_x^2+R_\rho^2$.

Equations 1a and 1b give correct expressions for the field surrounding a charged particle in a plasma and take the place of the oversimplified form derived from a pure Debye potential which, as already mentioned, does not lead to the expected plasma resonance. The charge distribution corresponding to 1a and 1b has the form of ellipsoids for particle speeds u less than the thermal speed v of the plasma electrons, and goes over to Mach-type cones for speeds $u>v$. The Debye distribution is recovered by going to the limit $u\rightarrow 0$, which is obviously not a suitable description of an actual situation in a plasma.

Any charged *field particle* subject to the electric field derived from 1a and 1b will be accelerated and will thus emit electromagnetic radiation. In fact, the appearance of radiation due to this "mechanism" is unavoidable.

From 1a and 1b we find the Fourier transforms

$$E_x=-\left(\frac{2}{\pi}\right)^{1/2}\frac{qi\omega}{u^2(\omega^2-\omega_p^2)}\left[\omega^2K_0\left(\frac{b\omega}{u}\right)-\omega_p^2K_0(bS)\right],\quad (2a)$$

$$E_\rho=\left(\frac{2}{\pi}\right)^{1/2}\frac{q}{u(\omega^2-\omega_p^2)}\left[\frac{\omega^3}{u}K_1\left(\frac{b\omega}{u}\right)-\omega_p^2\cdot S\cdot K_1(bS)\right], \quad (2b)$$

where

$$S\equiv\left[\frac{\omega_p^2}{v^2}+\omega^2\left(\frac{1}{u^2}-\frac{1}{v^2}\right)\right]^{1/2}$$

and b is the radial distance from the path of the test particle ("impact parameter"), ω_p the plasma frequency, K_0 and K_1 the Bessel functions of the third kind.

Describing the space and time distribution of the (radiating) field "particles" of mass M by a charge distribution $Q(b,t)$, we obtain from the Fourier transforms of the acceleration:

$$\vec{a}(\omega)=\frac{Q}{M}\vec{E}(\omega) \quad (3)$$

the spectrum

$$\pi Q_\omega=\frac{2Q^2}{3c^3}[a(\omega)]^2. \quad (4)$$

SINGLE PARTICLE APPROXIMATION

To illustrate the spectral behavior, we consider the case of a single field particle subject to the fields 1a and 1b, due to a positive test particle; that is, we set $q=+e$, $Q=-e$. The resulting spectrum

$$\pi Q_\omega=P\left\{\frac{\Omega^2}{\eta^2}\left[\Omega^2K_0\left(\frac{\lambda\Omega}{\eta}\right)-K_0(\lambda F)\right]^2+\left[\frac{\Omega^3}{\eta}K_1\left(\frac{\lambda\Omega}{\eta}\right)-F\cdot K_1(\lambda F)\right]^2\right\},$$
$$\Omega^2\left(1-\frac{1}{\eta^2}\right)\leq 1, \quad (5a)$$

$$\pi Q_\omega=P\left\{\frac{\pi^2}{4}\frac{\Omega^2}{\eta^2}[J_0(\lambda G)]^2+\frac{\Omega^2}{\eta^2}\left[\Omega^2K_0\left(\frac{\Omega\lambda}{\eta}\right)+\frac{\pi}{2}Y_0(\lambda G)\right]^2+\left[\frac{\Omega^3}{\eta}K_1\left(\frac{\Omega\lambda}{\eta}\right)+\frac{\pi}{2}G\,Y_{11}(\lambda G)\right]^2+\frac{\pi^2}{4}[G\cdot Y_1(\lambda G)]^2\right\},\quad \Omega^2\left(1-\frac{1}{\eta^2}\right)\geq 1 \quad (5b)$$

(where

$$P=\frac{2e^2}{3c^3}\left(\frac{e^2}{M}\right)^2\frac{4}{\pi}\eta^{-2}(\Omega^2-1)^{-2},$$

$$F=\left[1+\Omega^2\left(\frac{1}{\eta^2}-1\right)\right]^{1/2},$$

$$G=\left[\Omega^2\left(1-\frac{1}{\eta^2}\right)-1\right]^{1/2}$$

and J_i, Y_i, and K_i are Bessel functions of first, second, and third kind) has been computed numerically as a function of angular frequency Ω (in units of the plasma frequency) for various parameter values of the Mach number η (where $\eta=1$ is the thermal electron speed) and the impact parameter λ (in units of the Debye distance). A few typical curves are shown in Figures 42–1 and 42–2. The results verify perfectly the expectation that the spectrum consists of the "normal" bremsstrahlung con-

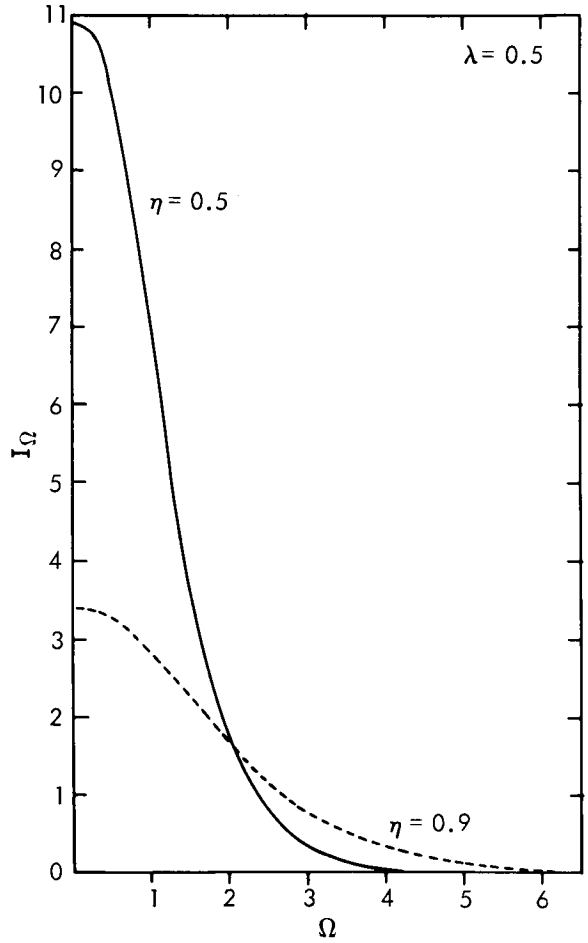

FIGURE 42–1. Bremsstrahlung emission by plasma electrons due to the charge distribution induced by a single positive test particle. [Plotted as specific intensity in arbitrary units vs. frequency in units of the plasma frequency. Collision parameter equals half the Debye distance. Test particle speed below thermal speed of plasma ($u<v$).]

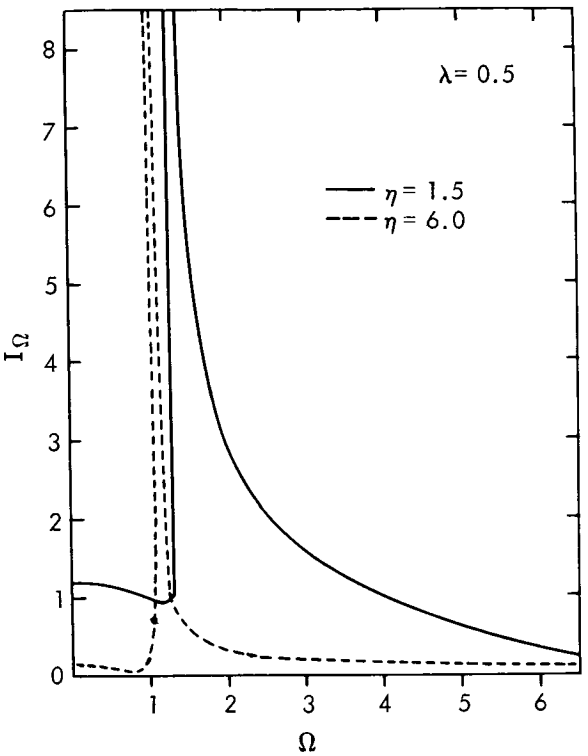

FIGURE 42-2. Same as Figure 42-1, but test particle speed above thermal speed of plasma ($u>v$).

tinuum on which a resonance line is superimposed, however, only if $u>v$, again according to expectation. It can be shown by applying appropriate limiting expressions for the Bessel functions that, for $\omega>>\omega_p$, the well-known bremsstrahlung spectrum is recovered and moreover that, for $u<v$ and $\omega\rightarrow 0$, the correct dc limit (Reference 7) results.

The neglect of damping terms in the basic equations makes the amplitude of the resonance emission infinite, corresponding to the infinite charge density on the Mach cone, predicted in the framework of this simple theory. The inclusion of damping terms easily remedies this deficiency, although the computations become rather lengthy. Their review is beyond the scope of this communication.

APPLICATION TO TYPE III BURSTS

On the basis of these results it is possible to predict what kind of physical system is required to represent the observed characteristics of type III bursts. The following points are of particular interest:

First, the resonance occurs at the plasma frequency of the surrounding corona ("field particles").

Second, the spectral features do not depend on the sign of the charges that constitute the exciting agent ("test particle"). Hence, protons as well as electrons can be responsible.

Third, it is generally expected that the exciting particle stream consists of a concentrated cloud of N charges. The spectrum intensity thus becomes N^2 times the single particle case and can easily exceed thermal values of the order 10^6 °K.

Finally, since in addition to the resonance line at the plasma frequency a continuum occurs which—in the case of electrons with speed 0.1c corresponding to an energy of 50 kev—will extend all the way down to the x-ray region, it is suggestive to identify some of the observed high energy emissions—in particular, the x rays (Reference 12)—with this continuum.

REFERENCES

1. WILD, J. P., 1963, *these Proceedings*, paper no. 21.
2. WILD, J. P., SMERD, S. F., and WEISS, A. A., 1963, *Annual Review of Astronomy and Astrophysics*, 1: 291.
3. GINZBURG, V. L., and ZHELEZNYAKOV, V. V., 1958, *Astron. J. USSR*, 35: 694; *Sov. Astronomy* 2: 653.
4. STURROCK, P. A., 1961, *Nature*, 192: 58.
5. DENISSE, J. F., 1960, *Inform. Bull. S.R.O.E.*, No. 4: 3.
6. OSTER, L., 1961, *Rev. Mod. Phys.*, 33: 525.
7. OSTER, L., 1964, *Phys. Fluids*, 7: 263.
8. DAWSON, J., and OBERMAN, C., 1962, *Phys. Fluids*, 5: 517.
9. PINES, D., and BOHM, D., 1952, *Phys. Rev.*, 85: 338.
10. MAJUMDAR, S. K., 1960, *Proc. Phys. Soc.*, 75: 657.
11. COHEN, M. H., 1961, *Phys. Rev.*, 123: 711.
12. FRIEDMAN, H., 1963, *Annual Review of Astronomy and Astrophysics*, 1: 59.

N64-30294 3

43 TYPE II BURSTS AND THE MAGNETIC FIELD IN THE CORONA

TATSUO TAKAKURA
Tokyo Astronomical Observatory
Mitaka, Tokyo, Japan

VELOCITY OF ELECTRONS THAT EXCITE PLASMA WAVES

Smerd et al. (Reference 1) have suggested that a type II burst is a continuous succession of fast-drift bursts. The slow disturbance of the order of 10^3 km/sec seems to be a seat of continuous ejections of high-energy electrons which excite plasma waves. Larentz (Reference 2) reported that runaway electrons from a shock front may excite coherent plasma waves. If we take this reasonable hypothesis, the bandwidth of type II bursts may correspond to a mean free path Δh of the runaway electrons,

$$\Delta h \approx v_0 \tau(v_0), \qquad (1)$$

where v_0 indicates the velocity of the runaway electrons and $\tau(v_0)$ indicates their lifetime, which is a function of v_0.

The observed bandwidths of type II bursts around 100 Mc/s ranges from a few Mc/s to 50 Mc/s. If we take the distribution of electrons in the corona to be 10 times the Baumbach-Allen model, the observed bandwidths correspond to the widths of layers Δh of 10^4 km to 1.5×10^5 km in the plasma layer for 100 Mc/s.

The shortest lifetime for the runaway electrons has been shown (Reference 3) to be the deflection time given by

$$t_D \approx 3.0\times10^{-28} v_0^3 \quad \text{(in cgs units)}$$

at $N=10^8$ cm^{-3}, $T\approx2\times10^6$ °K, and at $v_0>2v_T$, where v_T indicates the most probable speed of thermal electrons. Putting $\tau=t_D$ into Equation 1, we obtain

$$\Delta h \approx 3.0\times10^{-28} v_0^4 \quad \text{(in cgs units).}$$

Thus, we have

$v_0\approx1.4\times10^4$ km/sec for the narrow-band type II bursts

and

$v_0\approx2.7\times10^4$ km/sec for the wide-band type II bursts.

These values show the velocity range of runaway electrons which excite coherent plasma waves. Radio waves are caused by the scattering of the plasma waves due to thermal fluctuations (Reference 4).

UNPOLARIZED NATURE OF TYPE II BURSTS

The condition for the radio waves caused by Rayleigh scattering of the plasma waves to be unpolarized is

$$Y<1-X,$$

where $Y=\omega_H/\omega$ and $X=(\omega_P/\omega)^2$. The dispersion equation for the plasma waves in the quasi-longitudinal case is

$$\omega^2=\omega_P^2+\left(\frac{3\kappa T}{m}\right)k^2.$$

Putting $k\approx\omega/v_0$ and $\kappa T/m=\frac{1}{2}v_T^2$, one obtains

$$X=1-\tfrac{3}{2}(v_T/v_0)^2.$$

Equation 2 reduces to

$$Y<\tfrac{3}{2}(v_T/v_0)^2.$$

Putting $v_T=7.75\times10^3$ km/sec($T=2\times10^6$ °K)

and $v_0 \approx 2.7 \times 10^4$ km/sec, mentioned above, into Equation 3, we obtain

$$Y < 0.12 \text{ or } H < 4.5 \text{ gauss}$$

at 100 Mc/s for the condition to be unpolarized.

If we further take the same procedure for a type II burst at 50 Mc/s, we obtain $v_0 = 2.2 \times 10^4$ km/sec from the bandwidth of 30 Mc/s, and hence

$$Y < 0.19 \text{ or } H < 3.4 \text{ gauss at 50 Mc/s.}$$

These upper limit values of the magnetic field strength are shown as IIa in Figure 43–1. In this diagram, the other estimates using several types of bursts are also given (the detail will be published elsewhere). Differences between the field strengths estimated by using different types of bursts may not be so serious because of the differences in position and in time of occurrence for different types of bursts.

BAND SPLITTING

Band splitting of type II bursts was analyzed by Roberts (Reference 5). He suggested that the splitting was magnetic splitting. However, observed lack of polarization of the split band was hard to explain. Sturrock (Reference 6) has proposed another splitting mechanism due to the magnetic field in cold plasma, but his conclusion is not valid for hot plasma.

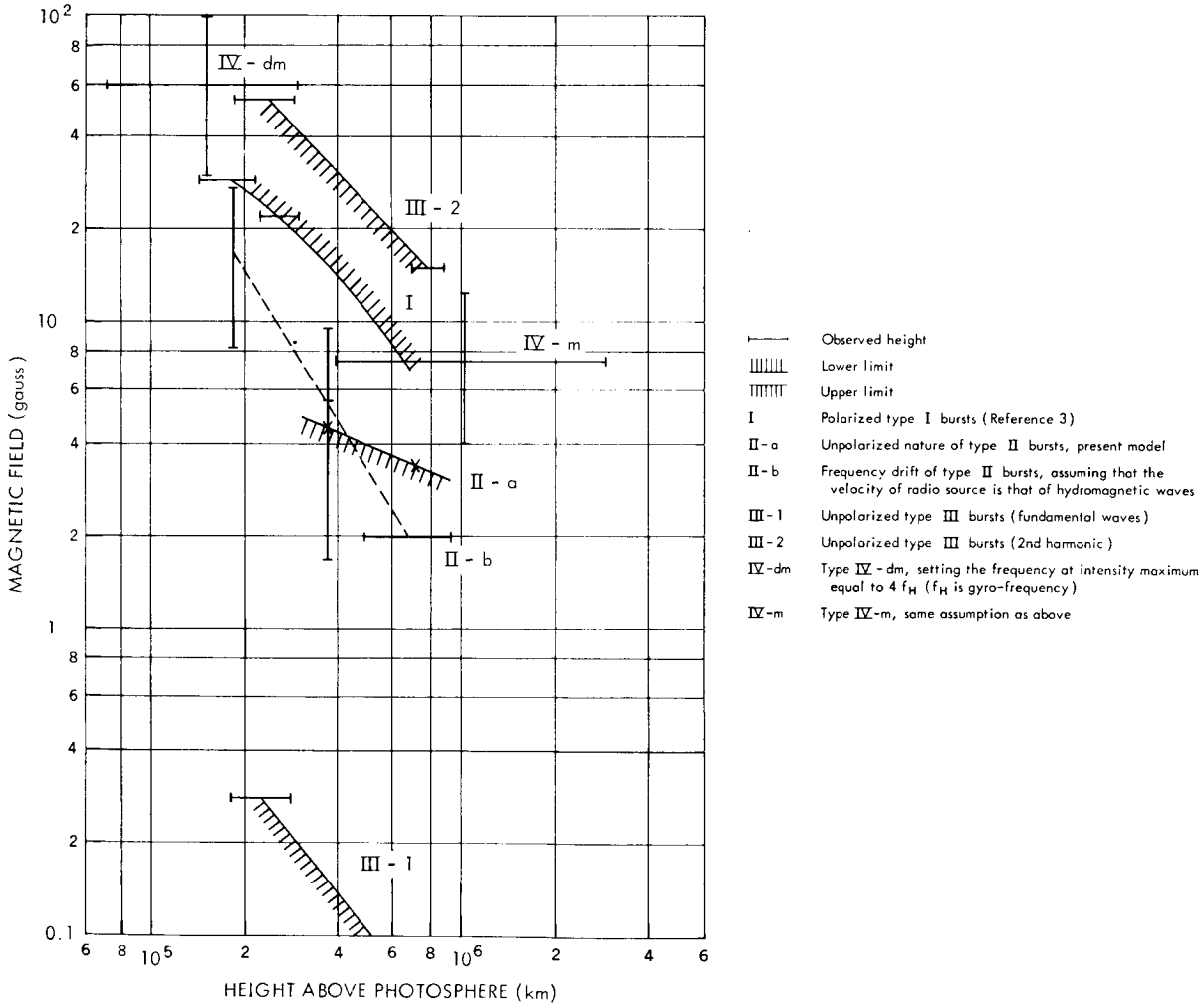

FIGURE 43–1. Distribution of magnetic field strengths estimated from several types of bursts. Corona density is assumed to be 10 times greater than that given by Baumbach and Allen.

Taking the thermal motion into account, Sitenko and Stepanov (Reference 7) have obtained the dispersion relation for the plasma waves,

$$\omega^2=\omega_P^2+\omega_H^2\sin^2\theta+\left(\frac{3\kappa T}{m}\right)k^2\ ,\omega_H<<\omega_P,$$

which reduces to

$$\omega^2=\frac{\omega_P{}^2+\omega_H{}^2\sin^2\theta}{1-3/2(v_T/v_\varphi)^2}, \qquad (4)$$

where v_φ indicates phase velocity of the plasma waves and where θ is an angle between the magnetic field and the propagating direction of the plasma waves. One mode may be obtained by putting $\theta\approx 0$ and $v_\varphi\approx v_0$; the waves propagate along the magnetic field. In this case, we have

$$\omega_1{}^2=\omega_P{}^2[1-3/2(v_T/v_0)^2].$$

This mode has already been discussed above. The frequency ω_1 of this mode is minimum, since $\theta=0$ and v_φ is maximum; $v_\varphi\leq v_0$ in order to satisfy the condition for the excitation of coherent plasma waves.

Another mode proposed by Sturrock (Reference 6) for the cold plasma, $v_T=0$, is $\theta=\pi/2$, for which $\partial\omega/\partial k$ and $\partial\omega/\partial\theta=0$. However, if we take into account the thermal motion, the plasma waves have the phase velocity, and hence the plasma waves for $\theta=\pi/2$ cannot propagate along with the beam of electrons, since the electrons drift along the magnetic field in helical orbits. Therefore, coherent plasma waves cannot be excited in the direction perpendicular to the magnetic field.

Another mode which is favorable for excitation by a beam of electrons in a hot plasma with magnetic field is not clear because of a lack of knowledge on the excitation of coherent plasma waves due to electrons in helical orbits. In any case, if another mode exists under a favorable combination of θ and v_φ, the frequency ω_2 of this mode is always higher than ω_1, since ω_1 is minimum as mentioned above. Therefore, if the radio waves emitted by the Rayleigh scattering of the plasma waves at ω_1 are unpolarized as mentioned previously, another band at ω_2 is also unpolarized even if the band splitting is due to the magnetic field.

REFERENCES

1. Smerd, S. F., Wild, J. P., and Sheridan, K. V., 1960, *Aust. J. Phys.*, 15: 180.
2. Larentz, R. W., 1963, URSI Meeting, Tokyo, September 1963. (Welly, J. D., Technical Report, Contract NR.AF. 61(052)-161, 1963).
3. Takakura, T., 1963, *Publ. Astr. Soc. Japan, 15*: 462.
4. Ginzburg, V. L., and Zheleznıakov, V. V., 1958 and 1959, "Paris Symposium on Radio Astronomy," Stanford University Press, 1959, p. 574; *Soviet Astronomy, A.J.* ,2: 653 (1958).
5. Roberts, J. A., 1959, *Aust. J. Phys.*, 12: 327.
6. Sturrock, P. A., 1961, *Nature*, 192: 58.
7. Sitenko, A. G., and Stepanov, K. N., 1957, *Soviet Phys. J.E.T.P.*, 4: 512.

DISCUSSION

Dr. Smerd: Did you carry out similar calculations for narrow bandwidth type II bursts?

Dr. Takakura: Yes.

Dr. Smerd: What did you get out of that?

Dr. Takakura: If we take a few megacycles for the bandwidth, v_0 becomes 1.4×10^4 km/sec. Since Δh is proportional to the fourth power of v_0, the value of v_0 is very insensitive to the bandwidth, which corresponds to Δh.

II THEORY OF FLARES

SESSION B

Chairman, Prof. Leo Goldberg

N64 30295

44 MAGNETIC ENERGY SHEDDING IN THE SOLAR ATMOSPHERE

THOMAS GOLD
Center for Radiophysics and Space Research
Cornell University, Ithaca, N.Y.

We will discuss the manner in which the dissipation of magnetic energy can occur in the solar atmosphere, both in the steady condition of plages and in the sudden events of flares.

The Hoyle-Gold theory of flares was a discussion of one such dissipation mechanism, as it would occur with one particular geometrical configuration. This served to demonstrate a possibility; but, since the actual field configurations in the solar atmosphere tend to be of high complexity, it is certain that any single geometrical model will not ever be really representative.

Let us first discuss some examples of magnetic dissipation. As the *first case*, we will consider a medium which has the properties of being a perfect conductor below a certain plane and which changes its state in such a way as to become a perfect insulator above it (Figure 44–1). Suppose further that the gas pressure is high compared with the energy density of the magnetic field everywhere and that turbulent motions exchange material freely across the dividing plane. The magnetic field below will be of a general kind, free from any particular restrictions, with gas pressure and accelerations accounting for any stresses that are unbalanced in the electromagnetic stress pattern. Above the dividing plane, since there can be no currents there, the field must be curl-free—that is,

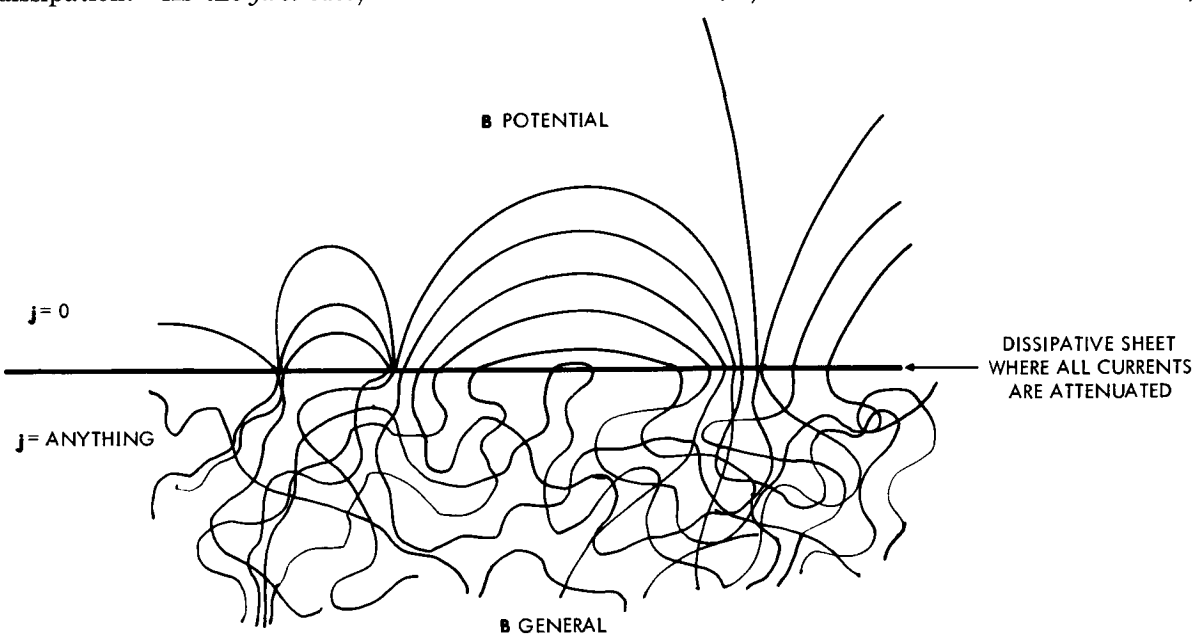

FIGURE 44–1. Magnetic field in the condition of a turbulent conducting medium below a plane and an insulating medium above. The fluid pressure is assumed large compared with magnetic forces.

the potential one—defined fully at any instant by the distribution of the normal component across that plane, a component which I shall call the *feet of the lines of force.*

As the motion proceeds, a readjustment must take place, according to which all fields convected to the upper space lose all but the potential, current-free components. Since the potential field is the one of least energy compatible with the *feet,* it is clear that this readjustment involves the loss of energy.

Where does this energy disappear? It would seem at first that in a medium which is either a perfect insulator or a perfect conductor there is no place for dissipation. This, however, is not correct. Here, as in many other electromagnetic problems, there is no physically meaningful way of changing over from perfect conductivity to perfect insulation except with a region, however narrow, which is of finite conductivity. It is in this region, in a zone arbitrarily close to the dividing plane, that the dissipation must be taking place. As the turbulence below keeps twisting and tangling the field, so the convection to the upper space continues to simplify it again, making for a continuous supply of heat in that dividing plane.

The *second example,* which is a little more closely related to the conditions on the solar surface, is again one where a horizontal dividing plane separates two conditions of the material: below, a general turbulent medium in which again the gas pressure is large compared with the magnetic energy and where there are therefore no restrictions on the magnetic field configurations that may occur; and the space above the plane, where the gas pressure is negligibly small but where the medium continues to be a conductor (Figure 44–2). In this case, as the convection of fields proceeds across the dividing plane, all fields in the upper space are not now required to be potential fields; but they

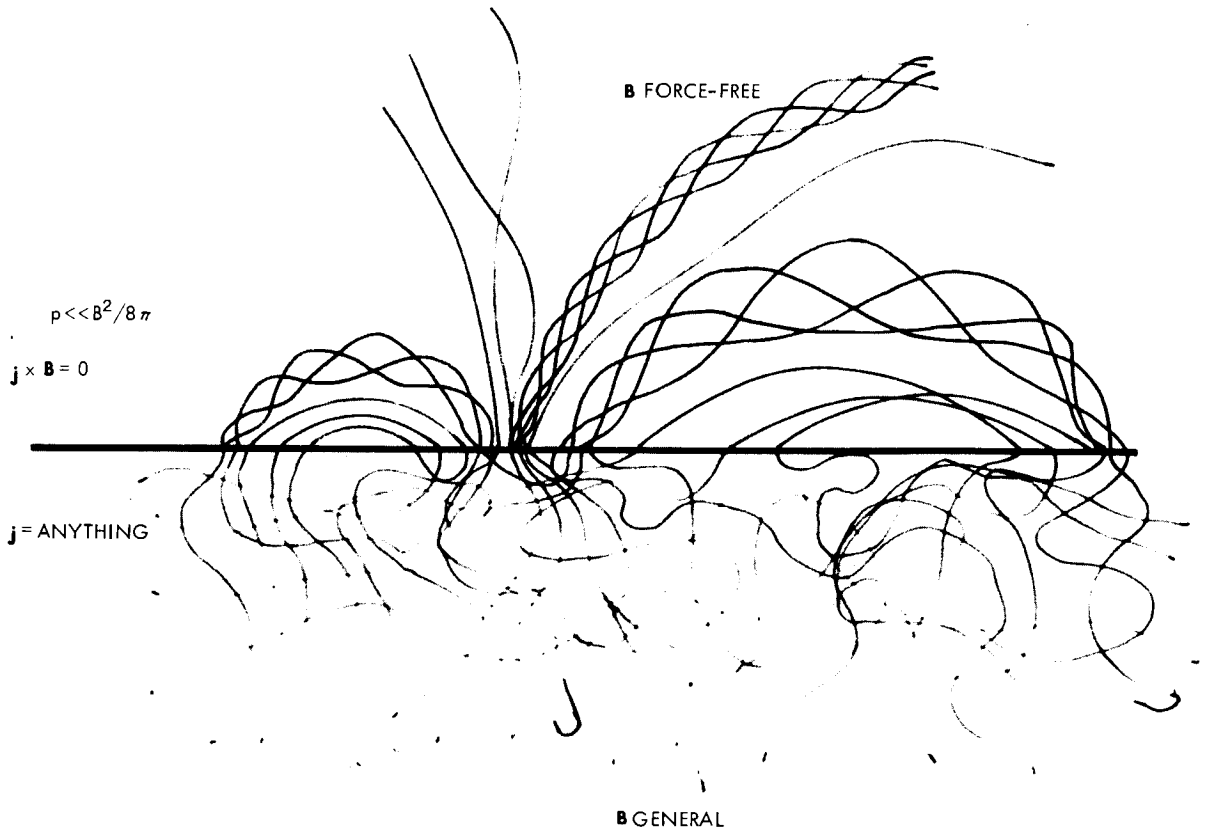

FIGURE 44–2. Magnetic field in a turbulent conducting medium. The fluid pressure is assumed large compared with magnetic forces below the dividing plane and small above it.

can, on the other hand, not be the general fields as exist below the surface. The fields above must belong to the class that are force-free in the upper space and must, of course, match up again with the normal components supplied at the dividing plane. This is to say that currents can now flow but they must always flow only along lines of force. This has a tendency to make helical shapes in the field.

In this example, as the motion proceeds, some destruction of magnetic energy must be taking place; but this is not now confined or even concentrated to the dividing plane. It is in the entire upper space that stresses in the field cannot be maintained; but they can, of course, be produced by a motion of the *feet*. Therefore, processes to shed the stressed components must be taking place in the entire upper space.

It is important to note that in this case the field in the upper space is by no means uniquely defined by the normal component over the entire dividing plane. By contrast with the potential field situation, it is now not only the instantaneous distribution of the feet which determines the field above the plane but also the entire history of fields and motion. (Even the specification over the surface of both the normal component of the magnetic field and of the current is insufficient to define the entire upper field.)

What can be the nature of these processes that dissipate magnetic energy? As the motion proceeds, there has to be a shedding of energy associated with the maintenance of force-free fields in spite of the fact that stressed fields will be constantly generated by the turbulent motion below. The magnetic energy content of the upper space is now not clearly defined, as it was in the previous case, by the distribution of the feet. All that one can say with generality is that this energy content cannot be less than that which the potential field would possess, standing on the same feet, for of course the potential field is the one of minimum energy; and it cannot be more than some level at which the forces exerted on the feet would exceed those that can be exerted by the turbulent motion below, the fully wound-up condition. (We have no proof that this condition defines a finite energy content but believe that it either does or would do with some additional physically reasonable conditions.)

Figure 44–3 represents the situation schematically. The actual energy content (level B) has to be between the fully wound-up level A and the level of the potential field standing on the same feet (level C).

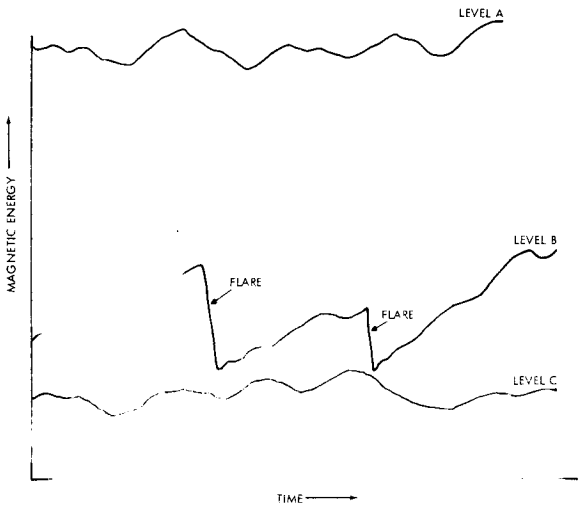

FIGURE 44–3. Schematic diagram to represent the possible course of events regarding the magnetic energy storage in the region of force-free fields. Level A refers to the energy stored at which stresses are so great as to interfere with the motion in the underlying region (the fully wound-up condition); level B represents the actual energy content, with a tendency to rise towards level A—the rise towards equipartition of energy with the turbulence, and occasionally depleted by instabilities; this depletion could not go below level C, the energy content of the curl-free field with the same lower boundary.

One can distinguish three types of processes that can occur in the upper space as the motion below causes the feet to move: First, there can be the strictly adiabatic motion where the field remains force-free and where the changes in the energy content are just given by the work done in the motion of the feet. Second, there can be the type of motion which is non-adiabatic because a certain motion of the feet implies a much higher speed of motion of a part of the gas in the upper space—so high a speed that the kinetic energy content of the gas is no longer negligible. Viscosity, heat conduction, and finite conductivity will then in practice

728-629 O—64——26

come into play and dissipate out motions caused in that way.

The third possibility is that unstable configurations are set up. In the adiabatic motions each slight change in the position of the feet must result in a slight change in the field configuration, moving it to a neighboring force-free shape. Not all force-free configurations are stable, and the system may hence be taken to a boundary of a stable regime. While in the stable regime, the actual configuration was one of minimum energy relative to all infinitesimal distortions; in an unstable regime, there exist nearby configurations of lower energy. If the system reaches such a boundary, it will begin to move and the motion will not result in reaching an adjacent force-free shape. Such an instability will then cause magnetic energy to be converted into energy of motion or compression of the gas, and the process will be arrested if eventually another stable force-free configuration—necessarily of lower energy content—is reached. This could of course be the configuration of the potential field; and in that case the instability would have led to the dissipation of all the available energy, since no field of lower energy content can be set up in the upper space. Also it is possible that the motion can be arrested by running into a stable configuration which is not curl-free and which represents therefore a greater energy content than the potential field.

How far does a configuration have to be deformed before it is likely to reach an unstable form? This is the central question in the attempt to understand the behavior of our model and, I believe, of the solar atmosphere in magnetic regions. One can give examples of configurations in our model which are certainly stable and which certainly have a set of adjacent stable shapes. One can also give examples of unstable configurations and even of transition from stable to unstable situations. The phenomena that we have discussed can certainly take place. But, given the speeds of the turbulent motion and the characteristic scale of the turbulence and fields, can we make any estimate of the frequency and violence of instabilities?

We may put the question in another way. In a representation of the configurations as points in a multidimensional space, we would like to have an idea of the size of domains that represent stability. This would enable us to estimate the distance that a random walk through this space would have to proceed on an average to reach instability. But, however subtle and sophisticated the manner in which we can ask the question, we cannot at the present time give any answer.

The model we have been discussing is in fact a good representation of the circumstances in the solar atmosphere above magnetic regions. The atmospheric scale height at the top of the photosphere is a great deal less than the separation of magnetic poles at that level, and for this reason the rate of fall-off of gas pressure with height is much faster than of the magnetic field. The hydromagnetic regime thus changes over in a comparatively small interval of height from one where the gas pressure dominates to one where the magnetic field dominates. Our model with an abrupt changeover probably contains the essential features. Whatever continuous shedding of energy occurs, associated (as we have discussed) with the maintenance of force-free shapes, may then represent the constant appearance of extra heat above magnetic regions, the so-called plages. The instabilities, of course, are the flares.

This discussion should help to put a theory of flares into perspective. The actual shapes of fields are very complex and would completely defy an analysis for stability. Only grossly simplified configurations can be discussed in detail. Such discussions should therefore not be taken to imply more than a demonstration of the possibility of instabilities. The purpose of the Hoyle-Gold model of solar flares (Figure 44–4) was just that, and therefore the assumed geometrical detail should not be taken as too meaningful. In that model the geometry was chosen so as to demonstrate a sudden transition from stability to instability and to maximize the available energy to be dissipated. A great variety of other shapes also will do, although they will be a little less efficient.

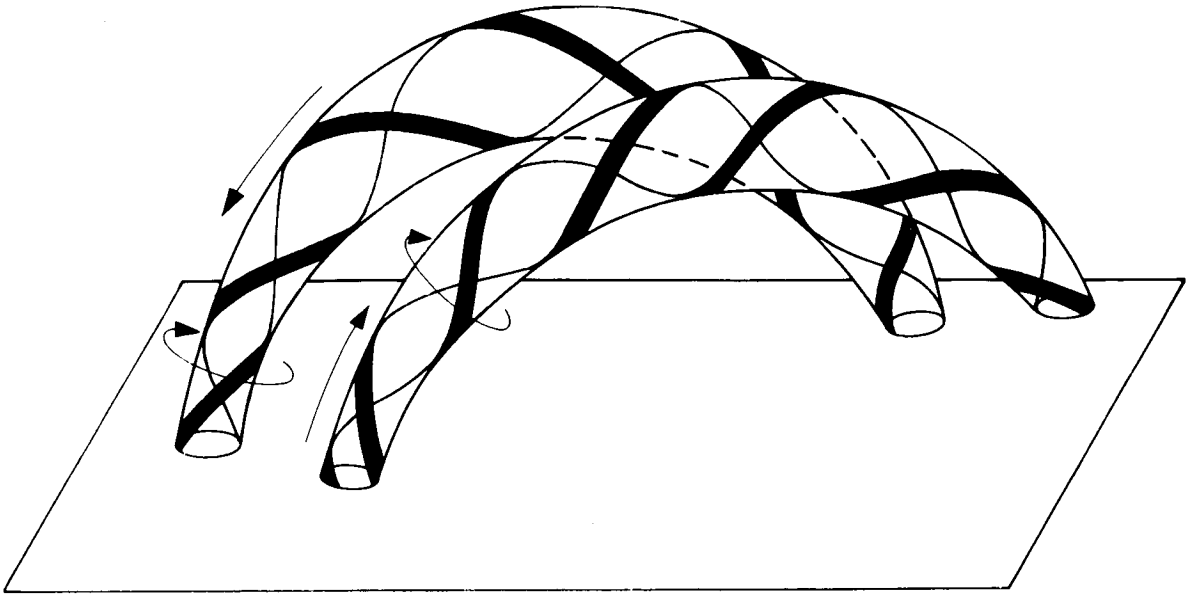

FIGURE 44–4. The particular geometrical configuration assumed in the Hoyle-Gold theory of flares. Arrows indicate the sense of the components of the magnetic field, which represents two oppositely directed twisted bundles, with opposite hand of twist. Instability is reached when such a pair comes into contact, and the excess energy over the potential field can be released.

Let me say a few words about the degree of twist to be expected in chromospheric fields. The question is sometimes raised whether enough circulating motions occur on the solar surface to make all the twists that some discussions presuppose. I think this is quite the wrong question. In the presence of a good conductivity of the medium there is no reason to expect an absence of twists. If we were brought up in a conducting medium instead of an insulator, we would be familiar with twisted fields and would regard these as the normal, and the untwisted ones, like potential fields, as very special ones. This is the appropriate outlook for the solar photospheric fields, generated in turbulence. In the region of the chromosphere and corona above a strong field zone in the photosphere there is the requirement to reduce the general field to a force-free one and, while this must imply the removal of very tight twists which cannot be force-free, it does not imply anything about the steeper pitched twists. (For a long and thin bundle the division would come at a pitch angle of 45 degrees.)

Flares appear to have a tendency to trigger other flares. Also, individual flares are often so much larger than any estimate of the characteristic scale of the magnetic fields that it is hard to understand how all the region reached instability at once. Even in what appears as a single flare we may have to invoke triggering, or a process akin to an explosion wave setting off more and more of the region. Can this be understood in the framework of the present discussion?

The motion of the turbulent photosphere may drag the feet of a chromospheric field to an instability. When this has happened, the neighboring chromospheric fields are all shaken up by the violent waves that are generated; and this may be a deformation of a magnitude that has a high probability of taking a region to the edge of instability. In this way flares can beget flares, small instabilities can cause larger ones to arise, and the general positive feedback implied can be held responsible for the occasional great extent and magnitude of the phenomenon.

Lastly, a word about the speed of progression of the instabilities: It has been pointed out that dissipative processes which are expected would seem to be too slow by a factor of 10 or so to

account for what actually seems to take place, and this discrepancy has been taken to cast doubt on the entire identification of flares as hydromagnetic instabilities. It is, of course, always the fastest growing effect in an instability that dominates; and, wherever a theoretical discussion has failed to single out that particular effect for analysis, the answer will be one of too slow a course of events. This, in the presence of the great complexity of the actual situation and the great analytical difficulties in pursuing the course of an instability, implies that the analysis must indeed be expected to err on the slow side.

DISCUSSION

Dr. Sturrock: Dr. Gold has proposed that the field-plasma configuration becomes unstable as a consequence of the motion of the "feet" of the magnetic field in the photosphere. It seems to me that the type of instability which would be required here is different from that which is normally met and discussed in plasma theory.

In plasma theory, one says that a configuration is unstable if some small-amplitude perturbation grows exponentially in time. This type of instability cannot explain the sudden and catastrophic transformation of energy which constitutes a chromospheric flare. If changes in the parameters of the system take it from a stable regime to an unstable regime, the changeover occurs when the system becomes neutrally stable. This means that, when the instability takes place, it is necessarily a weak instability.

What one needs is a different type of instability. In order for the change of configuration to be sudden and catastrophic, it appears to me to be necessary that the pre-flare configuration should be one which is stable against small-amplitude perturbations, but unstable against large-amplitude perturbations. In other words, the pre-flare configuration should be metastable. This interpretation of the pre-flare requirements explains why it is possible to trigger flares by propagating disturbances.

Dr. Gold: I am not quite sure whether I am to take the amplitude of the perturbation as a separate thing or whether I am not just discussing the indefinitely large amplitude of perturbation; namely, as one moves around in a stable regime by moving the feet around, one moves into all the possible perturbed states from a given stable configuration. It is a large amplitude perturbation that I am discussing to get to an unstable configuration. But, of course, one could move slowly as close to the instability as one wants.

Dr. Schmidt: I have a related question: that the boundary conditions for the force-free field just are fixed already, as you said, by the motions of the field lines.

I will put it this way: Given the distribution of flux and given the current density for half the flux (e.g., where the field lines come out), the field would be fixed completely. This should give you a unique solution. For this reason I don't understand how you expect to have regions of approximately force-free fields which are unstable.

Dr. Gold: B_z and j_z over the surface do not specify the field above uniquely.

Dr. Schmidt: Do you claim that the unstable fields are not completely force-free fields so that there might be a release of energy due to violation of conservation of flux? Otherwise I don't understand why there could be unstable regions, why there could be regions of unstable field configurations.

Dr. Gold: What I am saying is that you certainly have many possible stable field configurations. I will take up this point about how to define them on another occasion with you. You can have many stable field configurations that are compatible with the same feet. All that I am saying is that usually, as you move the feet, you will make nearly an adiabatic motion of all the upper material and its field lines to a neighboring, still stable, force-free configuration. What we do not know is whether, in making such adiabatic motions in the upper space, we will always have the possibility of moving to yet a further adjacent, stable, and force-free configuration.

It is possible that we come to geometrical situations where the arbitrarily small forces needed to move this material up there to the adjacent configuration are not annihilated by that small motion, so that they do not allow an adiabatic change to a neighboring configuration. But where instead the motions as they occur result in a larger force up there. That is what would be an unstable regime.

I certainly can give you examples of unstable regimes in the upper space—configurations which have the property of being at one instant force-free, but where a limitingly small force will take it to another configuration in which the same force has gotten larger.

Dr. Schmidt: I resented slightly the term "dissipation" in the pictures you draw. I guess you would agree that there need not be any dissipation for these kinds of transitions from a case where the pressure or the motion of the material overran the magnetic field to the case where you have a force-free field. Both could still be ideal conductors and would behave accordingly.

Dr. Gold: What I mean to say is that energy is lost if you were to move the medium down below. It is not quite right to think of it as dissipation. In the first place, it will set up kinetic energy; it will shake the system about. And then, of course, in practice there will always be ways of getting rid of all the kinetic and wave energy due to viscosity, heat conduction, electrical finite conductivity. It is that kind of dissipation which has to occur all the time as turbulent motion takes place down below. I believe that is the origin of the plages.

N64-30295

45 THE ORIGIN OF SOLAR FLARES AND THE ACCELERATION OF CHARGED PARTICLES

DONAT G. WENTZEL*
University of Michigan Observatory
Ann Arbor, Mich.

THE ORIGIN OF OPTICAL SOLAR FLARES

Theories concerning flares have been guided by two major considerations. First, the energy radiated by a large flare has led to postulating a supply of magnetic energy. One must then explain how the required magnetic fields are created, how they are stored in the chromosphere, and how the magnetic energy may suddenly be released at the time of a flare. This release might be in the form of a breakdown when the stored energy exceeds some critical value. Alternatively, it follows the creation of a magnetically neutral point or surface, where the field strength vanishes. The cause of a flare is then assigned essentially to a pinch effect. But, even given an unstable situation, a second major consideration has been the rapidity with which the magnetic energy is converted to radiation. So far, no theory naturally explains the duration of the flare and much less the shape of the light curve.

Storage of Magnetic Fields, Formation of Neutral Points

Most theories have been concerned with the very large flares and have, therefore, been based on estimates of the emitted optical energy for such flares. Both Parker (Reference 1, 1957a) and Ellison (Reference 2) allowed for white light and have estimated the total optical emission of very large flares to be 10^{32} ergs. This value exceeds by at least two orders of magnitude the thermal energy stored in the flare region and is, in fact, of the order of magnitude of the total heat content of the chromosphere and corona. Conceivably, the energy may arrive in the form of hydromagnetic waves or fast particles from the photosphere, as has been suggested by Piddington (Reference 3) and Warwick (Reference 4), respectively. But, aside from some problems in details, it seems difficult to understand the lack of changes in the photosphere due to such a sudden upward surge of so much energy. Therefore, the more common belief is that magnetic energy must have been stored in and near the flare. The required field strengths depend on the assumed volume of storage and the degree to which the fields are dissipated.

De Jager (Reference 5) emphasizes the observation by Suemoto, Hiei, and Hirayama (Reference 6) that an Hα flare must consist of a great many small threads with a total volume of only 10^{18} cm^3 and that 10^{32} ergs of magnetic energy cannot be stored in this small volume. As an opposite extreme, suppose that the dissipated fields are stored in a volume of area 10^{20} cm^2 and depth 10^9 cm. Then 10^3 ergs/cm^3 (a value plausible also for smaller flares) can be obtained by a complete dissipation of 150 gauss or, more likely, by the reduction of stronger fields, such as from 500 to 475 gauss. (Thus, changes in fields and their gradients are not limited by energy considerations.) Similar estimates have been made by Parker (Reference 1, 1957a), Gold and Hoyle (Reference 7), and Ellison (Reference 2).

Few estimates have been made for smaller flares. Because of their smaller volumes, the required fields are not greatly reduced. However, it is possible that the required energy can

* Alfred P. Sloan Research Fellow.

be supplied, instead, by influx either from above or below the flare.

The storage of the magnetic fields in the chromosphere presumably requires times of the order of days. During this time, the forces exerted on the chromospheric gas must be very nearly in equilibrium. This can occur only if the magnetic fields are nearly force-free; that is, if the fields **H** and their associated currents $\mathbf{j} = \text{curl } \mathbf{H}/4\pi$ are nearly parallel to each other. But force-free fields can never exist in isolation. The chromospheric fields must have their roots in the photosphere or below, where the magnetic forces can be fully exerted and where there is also plenty of energy available to actually generate the whole magnetic configuration. Two processes for generating the flare fields have been suggested.

Sunspots—Since flares occur near sunspots, their fields may be extensions of the strong sunspot fields. On this view, the occurrence of flares favors complex spot groups because this complexity leads very naturally to the formation of magnetically neutral points. Figure 45–1 shows a very simple situation in which the opposing fields between two aligned spot pairs form one neutral point (Reference 8, 1958a).

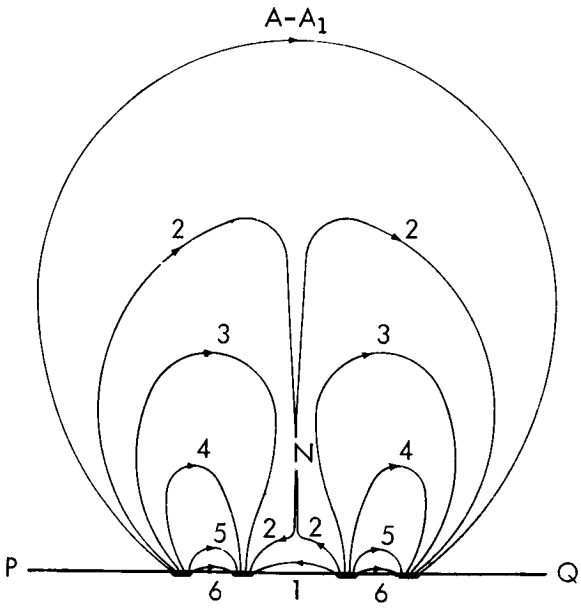

FIGURE 45–1. Lines of force of two aligned, bipolar spot pairs. (Reference 8, 1958a)

Sweet (Reference 8, 1958b) has shown that a more general arrangement of two spot pairs involves two neutral points which lie on the same line of force. Some other arrangements have been considered by Severny (Reference 9, 1958a).

The influence of external fields in causing a flare near a neutral surface has been investigated by Severny (Reference 9: 1961, 1962a, 1962b). He shows that even a relatively slow variation of sunspot fields can lead to a rapid and considerable compression of the plasma near a neutral surface, in a time which is comparable with the time of formation of flares. In this model, the energy which is dissipated in the flare is replaced at the expense of the magnetic energy of the sunspot configuration. Gopasyuk (Reference 10: 1961, 1962) has estimated that field changes of the required magnitude are in accord with observations. An alternative cause of a flare through external influence, suggested by Shabanskii (Reference 11), is a sudden change in the photospheric magnetic field which may be propagated into the chromosphere and there initiate a flare at a neutral point.

Severny (Reference 9: 1958a, 1958b, 1962b) has also investigated the breakdown of an initial equilibrium if the magnetic field strength increases until thermal pressure gradients can no longer balance the magnetic forces. The boundary conditions which should be applied to this stability problem have been the subject of some argument between Syrovatskii (Reference 12) and Severny (Reference 9, 1962a).

Filaments—Gold and Hoyle (Reference 7) have emphasized the close relation between flares and chromospheric filamentary structures. They suggest that filaments are magnetic tubes of force which are anchored in the photosphere. It seems possible that such a tube is twisted by photospheric convection cells and that the twist, applied at the feet of a tube, is distributed evenly along the whole tube. The fields within the tube are thereby strengthened and must be force-free, aside from the small twisting forces. If such twisted flux tubes can migrate, they may occasionally meet each other. If oppositely directed fields come into contact,

they will form a neutral point (Figure 45–2). Moreover, the motion of the tubes presses the fields toward the neutral point, so that an instability and a flare develop rapidly. The solution of the force-free field presented by Gold and Hoyle is a very special solution, but the physical picture of a chance meeting of oppositely directed fields seems very plausible, in view of the many types of chromospheric motions which have been observed. In fact, I think it must occur very frequently if one wants to explain in this manner the high frequency of small flares.

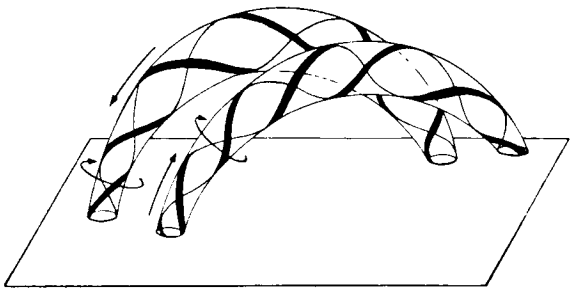

FIGURE 45–2. Two bundles of lines of force, both twisted up. The arrows indicate the components of the fields. (Reference 7)

Dissipation Mechanisms

Let me denote the scale of the flare by L and the scale of the magnetic field by ℓ. The field scale is the smaller of the distances over which either the strength or the direction of the field changes appreciably. The current density $\mathbf{j}=\text{curl } \mathbf{H}/4\pi$ will be assumed to have a magnitude $H/4\pi\ell$. The electrical conductivity σ is assumed to be scalar and is evaluated for an ionized gas at an electron temperature of the order of $T=10^4$ °K, $4\pi\sigma=2\times10^{-7}$ sec cm^{-2} (emu). This value may be lowered by ambipolar diffusion, that is, by dissipation through friction between the ionized and neutral components of the gas. From the structure of the hydromagnetic differential equations one deduces that a time

$$t_{dis}=4\pi\sigma\ell^2$$

is needed to dissipate a magnetic field. With some care, one may speak of the gas and the magnetic lines of force drifting relative to each other at the rate

$$v_d=\ell/t_{dis}=(4\pi\sigma\ell)^{-1}.$$

The dissipation time has frequently been identified with the rise time of the flare, which lasts at most a few minutes. I think this is rather incorrect, since it assumes that all the magnetic energy has been dissipated into heat shortly after flare maximum and that all subsequent radiation is at the expense of thermal energy. If this were true, flares would be exceedingly hot at times near flare maximum. On the contrary, electron temperatures are observed to be surprisingly constant. A more appropriate decay time may therefore be the total flare duration, of the order of 1 hour. One may then suppose that the heat generated by dissipation is radiated by the dense gas in the flare as quickly as it is produced. This point of view makes the light curve proportional to the rate of magnetic dissipation. If we now blithely set $\ell=L=10^4$ km, we obtain $t_{dis}\approx6\times10^3$ years, rather than 1 hour. Flares occurring at magnetically neutral points offer the possibility of greatly reducing the scale of the fields which are to be dissipated. Theories on the motions which may occur at neutral points have been restricted to two types: The first is concerned with a two-dimensional flow which is assumed to be stationary; the second treats the development with time of a one-dimensional collapse toward a neutral surface.

Sweet's Mechanism—Mathematically, the most relevant type of neutral point is what has been called x-type, as shown in Figure 45–3. Suppose that such a neutral point and the corresponding uniform current have somehow been formed. If there is any deviation from the ideal situation, the singularity of the kinked lines of force at the neutral point is quickly removed by ohmic dissipation; and the acting magnetic forces cause the gas and the embedded lines of force to move in a manner such that the lines of force become more parallel to each other. For this reason, the physical condition which has been assumed in many papers is a region in which two anti-parallel magnetic fields meet in a neutral surface, as

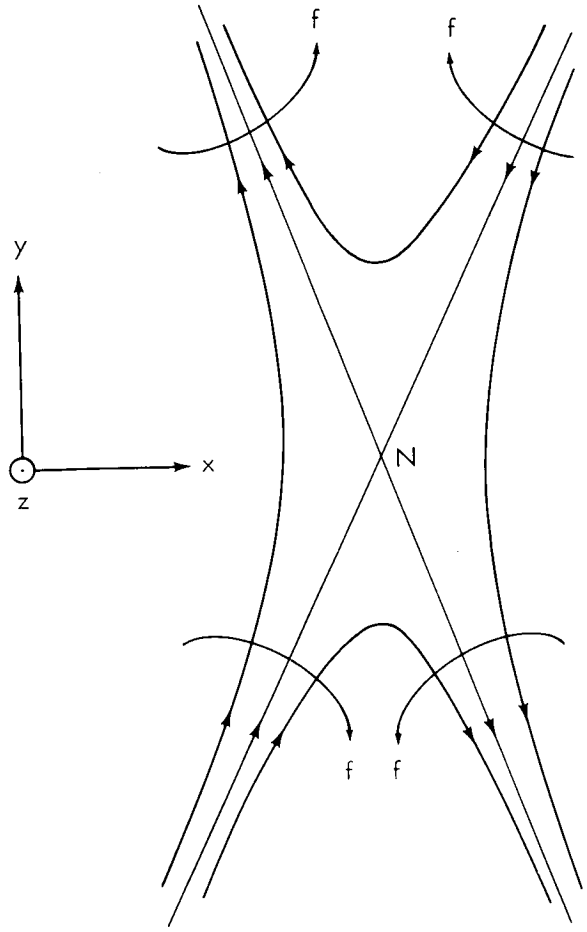

FIGURE 45–3. The direction of the magnetic force, $\mathbf{f}=\mathbf{j}\times\mathbf{H}$, near an x-type neutral point. (Reference 13)

shown in Figure 45–4. The magnetic pressure gradients cause the gas to approach the neutral surface until the scale of the fields at this surface is so small that dissipation may not be neglected. A stationary state may then be established in which gas and embedded magnetic field flow toward the neutral surface at such a rate that it is possible both to dissipate the field and also to squeeze the gas out of the ends of the configuration. The region where the fields are being dissipated we shall call the *gap*. Sweet first discussed the stationary state in 1956, using the analog of hydrodynamical flow between two rigid parallel plates which approach each other (Reference 8, 1958a). Subsequently, Parker (Reference 1, 1957a) obtained some semi-quantitative hydromagnetic solutions.

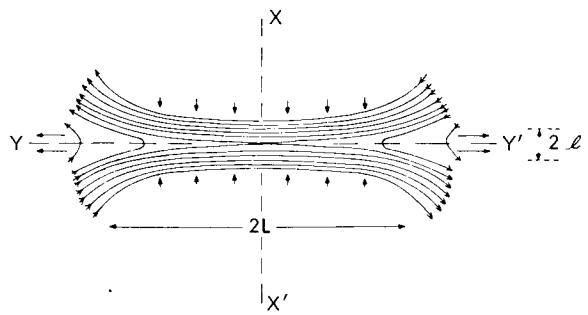

FIGURE 45–4. Schematic representation of the magnetic lines of force of two antiparallel regions of magnetic field pressed firmly together, with the fluid caught between free to escape out the ends Y and Y'. (Reference 1, 1963a)

A detailed investigation for compressible flow has been presented by Parker very recently (Reference 1, 1963a). One can obtain rough estimates of the rate of collapse toward the gap from a few physical principles. For a compressible fluid, the assumption of a stationary state is permitted only if the thermal pressure of the compressed gas in the gap can balance the external magnetic pressure. Unless the temperature varies excessively, the density in the gap n_g must greatly exceed the external density n_o. In turn, the high pressure in the gap causes the gas to flow out of the ends of the gap. This flow takes place at approximately the speed of sound v_s and is essentially parallel to the lines of force. The equations for the rate of dissipation, for momentum balance, and for the conservation of mass and of energy suffice to derive the rate of flow toward the gap v_d and the total dissipation time T:

$$v_d=\frac{l}{t_{dis}}=\left(\frac{v_s n_g}{4\pi\sigma L n_o}\right)^{1/2}, \quad T=\frac{L}{v_d}=\left(\frac{4\pi\sigma L^3 n_o}{v_s n_g}\right)^{1/2}.$$

If we now substitute $L=10^4$ km, $n_o=10^{11}$ cm^{-3}, temperature$=10^4$ °K, and an external magnetic pressure corresponding to $H=150$ gauss, we obtain $n_g=7\times10^{14}$ cm^{-3} and $T=40$ hours. Parker's analysis, therefore, leads to two main conclusions. First, it is difficult to obtain a sufficiently short total dissipation time for this model of a stationary flow (even if Parker's more favorable values are used). Second, in the gap the required high gas pres-

sures imply densities of the order of 10^{15} atoms cm^{-3}. This is rather larger than indicated by observations. Parker shows also that T is significantly increased if the merging fields are not very nearly anti-parallel.

Within the framework of the assumed stationary state there are several possibilities for reducing the dissipation time. First, perhaps solutions exist in which the gas pressure is less important. The fields could then approach each other more closely, and they would be dissipated more rapidly. Second, the effective value of σ might be reduced by ambipolar diffusion. However, in a stationary state the invoked friction between ionized and neutral gases requires that the pressure of the neutral gas balances the external magnetic pressure. Parker (Reference 1, 1963a) shows that the needed high density of neutral gas in the gap causes such a large friction that little differential motion occurs and, therefore, that the conductivity is not significantly reduced. Third, n_o/n_g might be decreased. Here n_o is determined by the location of the flare and may well be lower than 10^{11} cm^{-3} if the flare occurs very near the corona, but not so near that the temperature and σ are significantly increased. An increase in n_g implies a greater external magnetic pressure. Certainly fields are available to provide larger pressures, but such pressures also imply a noticeable reaction force somewhere in the vicinity of the flare. Perhaps the solar wind and/or the rising cloud of plasma which produces type IV radio bursts should be considered as evidence for such a reaction force. Fourth, L might be reduced. But if we subdivide the flare into smaller regions, the flow out of the ends of the gaps is soon inhibited and the computations fail. Instead, Parker (Reference 1, 1963a) has investigated the effect of a corrugation in the neutral surface. If the amplitude of such a corrugation is sufficiently large, it effectively reduces the field scale l in the gap.

Before turning to other theories, I want to mention two observations which particularly concern the two-dimensional aspects of flare theory. First, Ellison (Reference 2) and others have emphasized the existence of homologous flares, which repeat themselves after a time interval of the order of 1 day. This seems to imply little change in the topology of the field from one flare to the next. But in the two-dimensional flow pattern the lines of force are reconnected across the neutral surface (Figure 45–4), so that the field topology does change appreciably. Second, Severny (Reference 9: 1961, 1962b) has reported that the shape of spectral lines emitted by a laboratory plasma jet depends on the direction of view. If the jet flowing out of the gap in a flare is analogous, perhaps the uncertainties in the assignment of either Doppler or Stark broadening to the emission lines may be resolved by taking into account the direction of view of the jet.

One-Dimensional Time-Dependent Models—Both Dungey (Reference 13) and Severny (Reference 9: 1958a, b) have contended that the collapse toward a neutral surface does not necessarily lead to pressure equilibrium and a stationary state. As the density increases during a collapse, there results a race between the magnetic and the thermal forces to build up fastest; and it is not obvious which force wins. Let me summarize some of the theoretical aspects of a nonstationary one-dimensional collapse toward a neutral surface. The initial magnetic field may be given by $\mathbf{H}=H_o h(x/L)\hat{z}$; H_o=constant, and the simplest choice of the function h is $h=x/L$ for small x.

1. The rise time of a flare is comparable to the time needed by a hydromagnetic wave to traverse the flare. Therefore, Severny has identified the rise time of the flare with the time needed for the collapse to the neutral surface, since this collapse is likely to proceed at roughly the hydromagnetic velocity. Severny (Reference 9: 1958a,b) and Severny and Shabanskii (Reference 14) have investigated three stages of a collapse toward a neutral surface. First occurs an adiabatic contraction of the whole region. For this stage, some special solutions have been derived by Severny (Reference 9, 1962b). Later a shock forms on each side of the neutral surface. Finally, the reverse pressure gradients behind the shocks cause the surrounding plasma to expand, while the shocks themselves collide. In this model, the magnetic energy is first converted to kinetic energy of motion toward the neutral surface, and then

the resulting shocks convert the kinetic energy into heat and radiation. Temperatures in excess of 10^6 °K are produced in a layer which is of the order of 10 km thick. Perhaps such conditions are applicable to the moustaches which are the subject of some of these investigations, but it seems difficult to account for normal flares on this basis.

2. Gold and Hoyle (Reference 7) explain the short rise time of the flare on the basis of ambipolar diffusion. When two twisted magnetic filaments first meet, the gas densities are low and ambipolar diffusion may indeed be important. In this case, the effective conductivity and the time scale of dissipation are proportional to H^{-2}. The dissipation time at first is long, since the fields on the outside of the filaments are weak. But, when these are dissipated, stronger fields are pushed together by the motion of the filaments; these dissipate more rapidly, and thus a vicious circle ensues. The rapid increase in the rate of dissipation causes a very sudden brightening of the flare. This process depends on a continued low degree of ionization, since otherwise ambipolar diffusion ceases to be dominant. Furthermore, at large densities the dissipation decreases with the decreasing relative motion of neutral and ionized gas (Reference 1, 1963a).

In the same paper Gold and Hoyle also suggest that the two touching filaments may be magnetically connected to each other during the flare, so that the lines of force can quickly unravel. This would make more magnetic energy available for dissipation.

3. Recently I looked into some of the effects of invoking turbulence in a flare (Reference 15, 1963b). Perhaps most important is an adequate rate of dissipation for plausible sizes of the turbulent eddies. Differing magnetic fields must frequently meet at eddy boundaries. If the eddies have a scale D and typical velocities v_t, then the boundaries are in contact only for a time D/v_t. This limits dissipation to a skin depth ℓ given by $D/v_t = t_{dts} = 4\pi\sigma\ell^2$. A local, but high, rate of dissipation is thereby assured. The total dissipation time is t_{dts} multiplied by the number of boundary skin layers that fit into an eddy:

$$T = \frac{D}{v_t}\frac{D}{\ell} = \left(\frac{4\pi\sigma D^3}{v_t}\right)^{1/2}.$$

All the field can be dissipated in about 1 hour if the eddies have scales $D = 100$ km and turbulent speeds $v_t = 200$ km/sec, which seems plausible. There is, however, no theoretical reason for choosing such a D. With these values the width of the current systems is about $\ell = 17$ meters. If these eddy boundaries are sufficiently dense that they can immediately radiate away the generated heat, then the flare emission should come from roughly 1 km of the total flare depth. The corresponding depth deduced observationally by Hirayama (Reference 16) and Suemoto et al. (Reference 6) is about 10 km.

Turbulent dissipation and flaring cannot occur until kinetic energy is available to twist the magnetic fields; that is, until the velocity of collapse has reached some appreciable fraction of the hydromagnetic velocity. The rise time of the flare may then be identified with the time interval needed to start turbulence in most of the collapsing gas. The collapse and the increase in density must begin some time before they become visible. In this turbulence model, the magnetic energy of initially large-scale fields is rapidly transformed into magnetic and kinetic turbulent energy during the collapse and is then stored in this form for gradual dissipation throughout the flare duration.

4. The magnetic fields need not be exactly anti-parallel. Parker (Reference 1: 1957b, 1963a) has considered configurations such as shown in Figure 45-5. The field direction changes gradually across a surface where the magnetic pressure attains a finite minimum. A simple representation of a similar field is $\mathbf{H} = H_o h(x/L)\hat{z} + \text{constant} \times \hat{y}$. If a collapse occurs with such a configuration, new magnetic pressure gradients are set up near $x = 0$ which counteract and stop the collapse. The violence attained during the collapse depends on the value of the initial pressure minimum. I hope to report on my computations concerning such a collapse later in this session.

Until now I have emphasized problems related to the energy supply and to the rate of

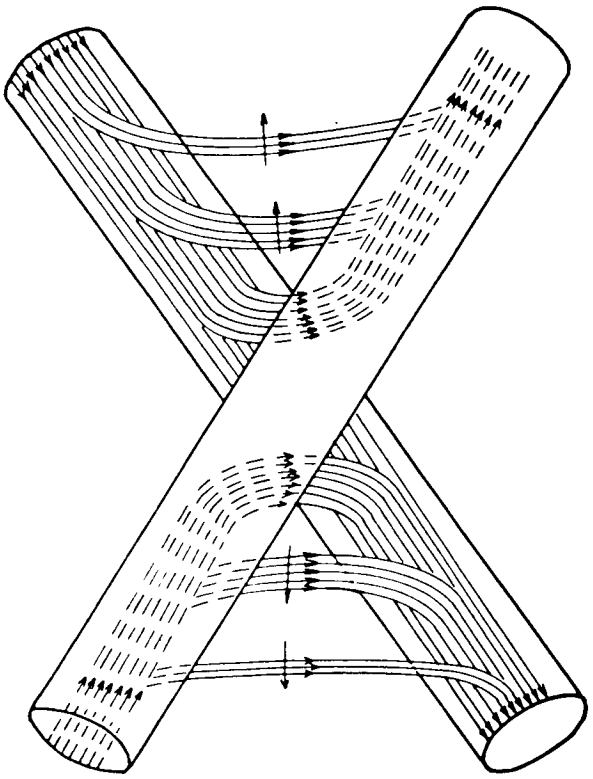

FIGURE 45–5. Schematic drawing of the merging of two perpendicular flux tubes by Sweet's mechanism. (Reference 1, 1957b)

dissipation. Let me briefly mention a few other features of flares which should be explainable within the framework of hydromagnetics. *First*, the relative frequency of flares of different importance should follow from theory. What happens in the case of the thousands of small flares? *Second*, why does the density in a flare exceed that in the surrounding chromosphere? De Jager (Reference 5) considers the suddenly acquired density as the essential feature of a flare. *Third*, what clues can we derive from flares which occur in the form of two parallel filaments and from others which start in many points and then coalesce? *Fourth*, we have not exhausted the possible magnetic geometries that can lead to instabilities. Ultimately the magnetic configurations should, of course, correspond to the maps of the observed magnetic fields and of their changes during a flare.

ACCELERATION OF CHARGED PARTICLES

The observed phenomena which are associated with optical flares force us to ask the question: Is the optical flare the major phenomenon, and must we search for the cause of shocks and fast charged particles in the optical flare? Or are the flare and the associated phenomena together evidence of a much more extensive event than the optical flare indicates? All the theories that I have treated so far have been restricted to explaining just the optical flare. But in recent years many phenomena have been observed which are very difficult to reconcile with the dominance of the optical event. Perhaps the strongest arguments rest on energy considerations, which have been reviewed by Warwick (Reference 4), De Jager (Reference 5), and Parker (Reference 1, 1963a). These indicate that the flare-associated phenomena, such as the enhanced solar wind, involve more energy than the optical emission. A plausible picture which de-emphasizes the optical flare has been presented by Wild (Reference 17). He considers a neutral point between two spot pairs as the source of all the phenomena. The instability first causes the ejection of fast electrons. This is followed by shock waves, which accelerate other particles, and by the generation of the optical flare in a lower and denser region. My own impression is that the collapse toward a neutral surface between spot pairs may involve regions of greatly differing heights and densities. Where the collapse increases the density above some critical value, radiative losses cool the gas and an optical flare arises; where this critical density is not reached, the collapse causes strong heating, particle acceleration, and radio events.

These arguments show primarily that the location of particle acceleration is still quite unknown. Many physical conditions suitable for acceleration have been and may be invoked. A check on theories must concentrate on the deduced energy ranges, on the time scales and, if the theory provides it, on the intensities and spectra of the particles which are produced. The observed intensities and spectra also depend on the manner of propagation in interplanetary space.

A crucial parameter for any theory of particle acceleration is the injection energy. The faster the particle when it is first accelerated, the smaller are its energy losses by coulomb collisions. Suprathermal particles may be produced by plasma phenomena, by shock waves, or possibly by thermonuclear reactions; but the quantities of the particles so produced are practically unknown. Let me simply assume that collisional losses of energy are negligible, and summarize the methods of acceleration which have been suggested.

Electric Fields

The original discharge theory of flares ascribed the heating of the flare region to electrons which had been accelerated in electric fields. Normally, such high electric fields cannot be built up in ionized gases. But they may be byproducts of a flare which is started by other causes. The observed extremely short time scales of some of the phenomena and the periodic repetition of bursts in some groups of radio bursts certainly make an electric discharge seem very plausible. However, it is also possible that the particles are continuously accelerated and then pulsed by some sort of instability.

If an observer sees a conducting fluid move with velocity $\mathbf{v}_f$, then he sees an induced electric field $\mathbf{E}_i = -\mathbf{v}_f \times \mathbf{H}$, as well as the electric field $\mathbf{E}_d$ which is due to dissipative processes. Let me suppose first that $\mathbf{E}_d = 0$, in the limit of infinite conductivity. The particle velocity $\mathbf{v}_p$ consists of the Larmor motion $\mathbf{v}_L$ and any drifts $\mathbf{u}$, $\mathbf{v}_p = \mathbf{u} + \mathbf{v}_L$. The total force on the particle is $q(\mathbf{E}_i + \mathbf{v}_p \times \mathbf{H})$. The electric drift is $\mathbf{u} = \mathbf{E}_i \times \mathbf{H}/H^2$, so that $\mathbf{u} = \mathbf{v}_f$ and $\mathbf{E}_i + \mathbf{u} \times \mathbf{H} = 0$. The particle simply moves with the fluid and the induced electric field is ineffective in accelerating the particle (compare Reference 1, 1963b, p. 7), except indirectly. The total force exerted on the particle is just $q\mathbf{v}_L \times \mathbf{H}$, and the energy gained is $\mathbf{u} \cdot (\mathbf{q}\mathbf{v}_L \times \mathbf{H}) = q\mathbf{v}_L \cdot (-\mathbf{v}_f \times \mathbf{H})$, which represents betatron acceleration and is treated separately below.

Let me now neglect any induced fields $\mathbf{E}_i$ and consider only the electric field $\mathbf{E}_d = \mathbf{j}/\sigma$. Any component of $\mathbf{E}_d$ which is perpendicular to $\mathbf{H}$ causes a drift velocity $\mathbf{E}_d \times \mathbf{H}/H^2$, which is generally of the order of $v_d = (4\pi\sigma l)^{-1} = 5 \times 10^{12} / T^{3/2} l$ cm/sec. This motion is generally subsonic and is simply the drift velocity of the magnetic lines of force, with which the charged particle moves, relative to the gas. Much higher drift velocities occur at neutral points, where $\mathbf{E}_d$ may be finite while $\mathbf{H}$ becomes vanishingly small. Until the particle reaches these high drift velocities, or until it leaves the neutral region, the acceleration takes place as if there were no magnetic field. The same is true for any component of $\mathbf{E}_d$ which is parallel to $\mathbf{H}$. Where the electric field thus accelerates the particle as if $\mathbf{H}$ were absent, the gain of energy is of the order of

$$1.6 \times 10^{-20} \; H v_d \text{ erg/cm} \approx 0.05 \; H/l \text{ ev/cm} \quad (\text{for } T = 10^4 \text{ °K});$$

note that the drift velocity $v_d = l/t_{dts}$ enters, but not the fluid velocity. The current density has again been assumed to be $H/4\pi l$, where H now is the field strength external to the neutral region. Effective acceleration requires very narrow current systems. With $H = 1000$ gauss and $l = 1$ km, a distance of 20,000 km is needed to obtain 1 Mev. To find l of the order of meters, we must look for effective accelerating fields in more complicated situations, including turbulence, shocks, and plasma phenomena. Since the electric fields under such conditions are not likely to act over large distances, we should ask, following de Jager (Reference 5), for the probability that a given particle sees sufficiently many accelerating electric fields in order to attain high energy, within the time allowed by the observations. Sweet (Reference 8: 1958a, b), Dungey (Reference 13), and de Jager (Reference 5) have deduced electric fields of the order of 1 ev/cm for several situations. It seems probable that in each case only a small fraction of these fields is really effective in accelerating particles.

Betatron Acceleration

An increase in field strength increases the kinetic energy of Larmor gyration of a charged particle proportionately. As an upper limit to the increase in energy which can be obtained in this way, suppose that the magnetic field strength is proportional to the gas density. Then the

increase in particle energy due to the collapse of flare material is at most about three orders of magnitude, and most probably it is smaller. De Jager (Reference 5) has proposed acceleration of protons to cosmic ray energies by what amounts to betatron acceleration. He has estimated the induced electric field from the rate of change of magnetic flux through a surface fixed in space. But charged particles travel with the field lines, which in turn travel with the gas; and hence the appropriate surface to integrate over is one fixed in the fluid. The magnetic flux is then found to be constant, and only the normal betatron acceleration occurs. Dissipation and $\mathbf{E}_d$ are zero in the limit of infinite conductivity, which is an excellent approximation in the situation envisaged by de Jager.

Fermi Acceleration

On the basis of the guiding-center approximation, a particle which enters a sufficiently strong magnetic field is reflected by this field. If the magnetic "wall" moves with speed w, then the particle energy and its speed v are increased or decreased by a fraction of the order of w/v, depending on whether the collision is a head-on or an overtaking collision (Reference 18). Normally one assumes $w \ll v$, but in general only $w \lesssim 0.5v$ is required (Reference 15, 1963a). Two important conditions must be satisfied for successful acceleration of particles by this mechanism.

Realignment of Pitch Angles—Reflection by any given magnetic inhomogeneity requires that the pitch angle (angle between **v** and **H**) exceed some critical value before the reflection occurs. But the Fermi acceleration decreases this angle and, therefore, tends to be self-defeating. To obtain repeated Fermi acceleration, it is necessary that the pitch angle is repeatedly increased, without an associated deceleration. For this purpose Davis (Reference 19) proposed betatron acceleration between hydromagnetic waves which cross each other. More usually it has been assumed that pitch angles are redistributed through violations of the guiding-center approximation. Takakura (Reference 20: 1961, 1962) pointed out that a fast electron may be appreciably deflected by coulomb collisions without losing appreciable energy and that this mechanism may be effective for acceleration in the upper chromosphere. Alternatively, one may suppose that a particle crosses a hydromagnetic shock front which is thinner than the Larmor radius of the particle. The resulting distribution of pitch angles has been assumed to be random (Reference 1: 1958, 1963b; Reference 15: 1963a), but this is certainly not exact.

Accelerations Must Outnumber Decelerations—If regions of acceleration and of deceleration occur in equal numbers, then the net efficiency of Fermi acceleration is small. Parker (Reference 1, 1958) showed that hydromagnetic shocks which cross each other can provide very efficient acceleration (Figure 45–6). Particles are swept ahead of the shocks, so that the density of particles being accelerated is generally greater than the density of particles being decelerated. Moreover, the length of the accelerating trap shrinks to zero, so that all particles in the trap must necessarily be accelerated up to their escape energy. In contrast, particles which have crossed a shock find themselves in a decelerating trap whose length is increasing, so that decelerations become progressively less frequent. Finally, the shocks cross each other and all particles again are in an accelerating trap. I have extended Parker's analysis (Reference 15, 1963a) and have shown that a net acceleration occurs even if the shocks are very weak. A shocklike structure is then needed only for the scattering of the pitch angles. In the same paper I also showed that acceleration in nonuniform fields can be very efficient. If a shock moving into stronger fields becomes

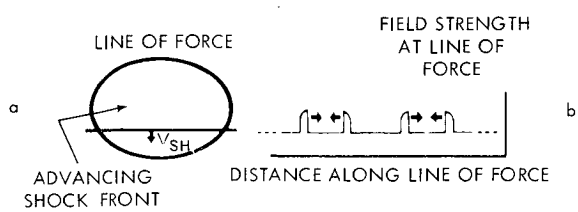

FIGURE 45–6. Field strength measured along a line of force with two pairs of interpenetrating shocks (right), and the equivalent situation of a shock crossing a closed line of force. (Reference 15, 1963a)

stronger with time, then the shock simply pushes the particle ahead of it and acceleration is greatly prolonged. A similar shock moving into weaker fields yields no corresponding deceleration.

Let me emphasize that Fermi acceleration can provide energy for both protons and electrons. A given magnetic trap multiplies the particle energy by a given fraction, independent of particle mass. If protons and electrons are injected with the same velocity and different energies, then indeed the protons gain much more energy than the electrons; but, if they are injected with the same energy, both gain the same amount of energy.

It is usually stated that Fermi acceleration produces an energy spectrum. Even this need not always be the case. The Fermi acceleration depends on the reflection of a particle by a strong magnetic field. If this field is a shock, then the efficiency of reflection may depend on the ratio of the Larmor radius of the particle to the thickness of the shock front. The guiding-center approximation strictly requires that this ratio be small. The opposite extreme, the transmission of particles across a sharp magnetic discontinuity, has been considered by Parker (Reference 1, 1963b, p. 166–170). His results depend on the assumption that an isotropic velocity distribution is maintained as the particles cross the discontinuity.

The conclusion from these arguments is that we cannot yet predict what types of charged particles can or cannot be produced by Fermi acceleration. I am sure that we have not yet imagined all possible efficient field configurations. The energies achieved depend on the injection energies; and, if acceleration occurs by hydromagnetic shock, the spectra may depend also on the particle rigidity.

Finally, let us summarize the specific situations that have been proposed for specific types of charged particles. Most of these proposals have been limited to stating that the conditions are favorable for some one accelerating process. Only a few detailed analyses have been made. Parker (Reference 1, 1957a) proposed that cosmic ray protons from the flare of February 23, 1956, were accelerated by a Fermi mechanism within the region of the optical flare. He assumed injection of protons at hydromagnetic velocities and obtained a reasonable energy spectrum. He had to postulate somewhat extreme parameters, but these might be made more plausible by invoking a more efficient Fermi acceleration. Severny and Shabanskii (Reference 14: 1960, 1961) and Shabanskii (Reference 11) have proposed the Fermi acceleration of protons between two magnetic walls which are collapsing toward each other during a flare. Thermonuclear reactions in the center of the collapsing region may serve as particle injectors. Takakura (Reference 20, 1962) has suggested that fast electrons are accelerated by hydromagnetic waves over sunspots. There the waves are so fast that just a few accelerations suffice to achieve the desired energies, and no great efficiency of acceleration is needed. It seems probable to me that such acceleration becomes much less efficient when the electron Larmor radii become greater than the thickness of hydromagnetic shocks, which is presumably a few Larmor radii of thermal protons. In regions with temperatures between 5×10^4 and 2×10^6 °K, one would then expect electrons in the energy range from 10 to 500 kev, which corresponds well to the energies required by x-ray and radio observations (Reference 15, 1963a). The flaw in all of these specific theories is that each explains only one type of particle. It seems to me that no theory can be convincing unless it includes as an essential ingredient the explanation of at least several of the many phenomena that are associated with a flare.

REFERENCES

1. Parker, E. N., 1957a, *Phys. Rev.*, 107: 830–836; 1957b, *J. Geophys. Res.*, 62: 509–520; 1958, *Phys. Rev.*, 109: 1328–1344; 1963a, *Astrophys. J. Suppl.*, 8: 177–212 (no. 77); 1963b, "*Interplanetary Dynamical Processes*," Interscience Publ., New York.
2. Ellison, M. A., 1963, *Quart. J. Roy. Astr. Soc.*, 4: 62–73.

3. PIDDINGTON, J. H., 1958, in "*Electromagnetic Phenomena in Cosmical Physics,*" B. Lehnert, ed., Cambridge Univ. Press, p. 141–149.
4. WARWICK, J. W., 1962, *Publ. Astr. Soc. Pacific*, 74: 302–307.
5. DE JAGER, C., 1960, in "Space Research," Vol. 1 (H. Kallmann Bijl, ed., North-Holland Publ. Co., Amsterdam) p. 628–636; 1963, *Space Science Reviews*, 1: 487–521.
6. SUEMOTO, Z., HIEI, E., and HIRAYAMA, T., 1962, *J. Phys. Soc. Japan*, 17, Suppl. A–II: 231–233 (Kyoto Conf. on Cosmic Rays and the Earth Storm).
7. GOLD, T., and HOYLE, F., 1960, *Mon. Not. Roy. Astr. Soc.*, 120: 89–105.
8. SWEET, P. A., 1958a, in "*Electromagnetic Phenomena in Cosmical Physics,*" B. Lehnert, ed., Cambridge Univ. Press, p. 123–134; 1958b, *Nuovo Cimento*, 8, Ser. X, Suppl.: 188–196.
9. SEVERNY, A. B., 1958a, *Izv. Krim. Astrophys. Obs.*, 20: 22–51 (Transl. for Geophysics Research Directorate, AF Cambridge Research Center, by the Am. Met. Soc.); 1958b, *Astr. Zhurn.*, 35: 335–350 (*Soviet AJ*, 2: 310–325); 1961, *Astr. Zhurn.*, 38: 402–408 (*Soviet AJ*, 5: 299–303); 1962a *Astr. Zhurn.*, 39: 990–995 (*Societ AJ*, 6: 770–773); 1962b, *Izv. Krim. Astrophys. Obs.*, 27: 71–108 (Transl. Sac. Peak Obs. Solar Res. Note no. 38).
10. GOPASYUK, S. I., 1961, *Astr. Zhurn.*, 38: 209–217 (*Soviet AJ*, 5: 158–164); 1962, *Izv. Krim. Astrophys. Obs.*, 27: 110–119 (Transl. Sac. Peak Obs. Solar Res. Note no. 24).
11. SHABANSKII, V. P., 1961, *Astr. Zhurn.*, 38: 844–848 (*Soviet AJ*, 5: 647–650).
12. SYROVATSKII, S. I., 1962, *Astr. Zhurn.*, 39: 987–989 (*Soviet AJ*, 6: 768–769).
13. DUNGEY, J. W., 1958, in "*Electromagnetic Phenomena in Cosmical Physics,*" B. Lehnert, ed., Cambridge Univ. Press, p. 135–140.
14. SEVERNY, A. B., and SHABANSKII, V. P., 1960, *Astr. Zhurn.*, 37: 609–615 (*Soviet AJ*, 4: 583–589); 1961, *Izv. Krim. Astrophys. Obs.*, 25: 88–113 (Transl. Sac. Peak Obs. Solar Res. Note no. 40).
15. WENTZEL, D. G., 1963a, *Astrophys. J.*, 137: 135–146; 1963b, *Astr. J.*, 68: 299 (Abstract).
16. HIRAYAMA, T., 1961, *Publ. Astr. Soc. Japan*, 13: 152–165.
17. WILD, J. P., 1962, *J. Phys. Soc. Japan*, 17, Suppl. A–II: 249–258 (Kyoto Conf. on Cosmic Rays and the Earth Storm).
18. FERMI, E., 1949, *Phys. Rev.*, 75: 1169–1174.
19. DAVIS, L., Jr., 1956, *Phys. Rev.*, 101: 351–358.
20. TAKAKURA, T., 1961, *Publ. Astr. Soc. Japan*, 13: 166–172; 1962, *J. Phys. Soc. Japan*, 17, Suppl. A–II: 243–249 (Kyoto Conf. on Cosmic Rays and the Earth Storm).

DISCUSSION

Dr. Moore: I believe the discussion that you gave concerning the acceleration by electric fields was based on quite a special set of assumptions in that you assumed the acceleration took place in the same fluid which was generating the electric fields.

Dr. Wentzel: Yes.

Dr. Moore: The mechanism that I proposed this morning is different. The electric fields that accelerate the particles were generated in a central region, and the acceleration of the particles takes place outside the source region in the traveling waves emitted by the source.

Dr. Axford: I do not understand the turbulent dissipation you have described. It seems to me that you should expect turbulence only where the gas pressure is large compared with the magnetic pressure, and in such regions there is not much field to dissipate anyway.

Dr. Wentzel: The place where I invoked the turbulence is where the kinetic energy density of the collapsing motion is comparable with the magnetic energy density. In other words, one needs speeds of collapse comparable with Alfven speeds to obtain turbulence.

728–629 O—64——27

N64-30296

46 INSTABILITY PROBLEMS IN THE ORIGIN OF SOLAR FLARES

PETER A. SWEET
The University Observatory
Glasgow, Scotland

30296

The types of hydromagnetic instability which could account for the sudden onset of flares are discussed. Emphasis is laid on the possibility of a large-scale resistive instability. An outline is given of a method by which the existence of such a mode could be established theoretically.

It is clear from the observations that the dissipation of energy occurs in small regions of the upper chromosphere or corona. It is not certain, however, whether these regions also are the seat of the controlling mechanism. This mechanism, if assumed to be an instability of some kind, could not operate below a height at which an Alfvén wave would travel across the flare during the development of the flash phase. On the basis of a buildup time of 10^2 seconds, a flare diameter of 10^9 cm, and a magnetic intensity of 500 gauss, the maximum gas density is of the order 2.10^{-10} gm/cm^3. This is the mean density at a height 700 km above the photosphere. The important point is that the gas pressure at such a height is negligible compared with the magnetic stress, and the field is therefore force-free. It is certainly possible to describe force-free fields that are in unstable equilibrium. To achieve them in practice, they must be established in times less than the time of development of the instability they are to exhibit. While this can be done in the laboratory, it is irrelevant for the solar flare, since it would merely introduce a faster mechanism to account for. In the pre-flare condition the equilibrium configuration is changing far more slowly than the instability time. What is required for a solar flare is a system which passes from stable to unstable equilibrium as some configuration parameter passes through a critical value.

THE STABILITY OF A FORCE-FREE TWISTED FLUX TUBE

The problem of finding a true dynamic instability of the type just mentioned can be illustrated by considering the simplest force-free system, namely, a twisted flux tube. Voslamber and Callebaut (Reference 1) have considered a flux tube within a rigid cylindrical boundary and carried by a compressible perfectly conducting fluid. The parameter in the force-free condition curl $\mathbf{B}=\alpha\mathbf{B}$ is taken to be uniform and is a configuration parameter giving a measure of the twist.

When $0<\alpha<\alpha_{crit}$, the tube is stable in all normal modes. Instability sets in first at a finite wavelength in the $m=1$ mode at $\alpha=\alpha_{crit}$. As α is increased beyond this value, the range of unstable wavelengths increases. As mentioned previously, if α is increased more slowly than the buildup time of the instability, the flux tube can never get into the unstable configurations examined by the stability theory. It will automatically proceed in an adjacent stable configuration. Since the instability sets in at the $m=1$ mode, it seems reasonable to suppose that in the new stable configurations, the axis of the flux tube no longer coincides with the axis of the cylinder but describes a spiral encircling it—the wavelength of the spiral being initially the wavelength of the marginal stability.

The behavior of the tube, energy-wise, is described diagrammatically in Figure 46–1; W is the mean energy per unit length of the cylinder in excess of that of the untwisted tube, p is the perturbation amplitude in the $m=1$ mode, and the curves are curves of constant α.

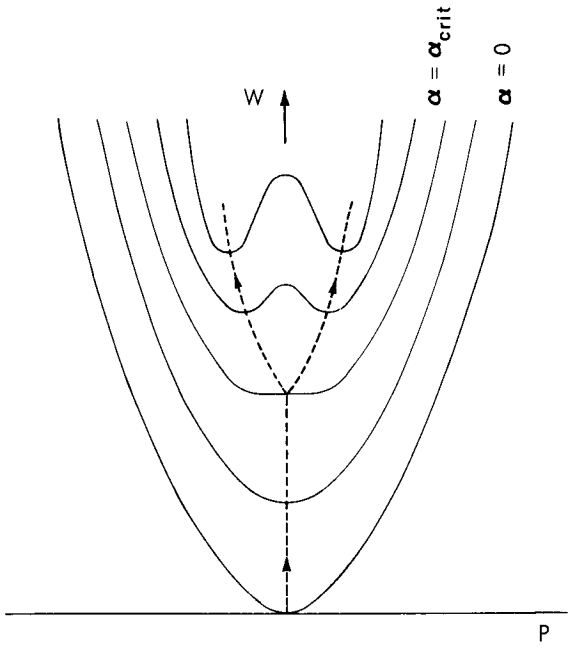

FIGURE 46–1. Stability diagram for a force-free twisted flux tube.

As α increases from zero, the configuration sits at the bottom of its curve and is increased in energy, performing the trajectory indicated. As α increases beyond α_{crit}, the curves develop a hump, the trajectory bifurcates, and the system must proceed as indicated in one or other of the adjacent hollows, and no decrease of energy occurs.

As α increases still further, a similar situation will occur each time a stable mode develops an instability. A dynamical instability of the type required for a solar flare demands a more complex type of energy curve. Such a curve will be discussed in the next section.

AN EXAMPLE OF DYNAMICAL INSTABILITY

It is necessary that, when the first mode to do so develops an instability, no adjacent stable modes should be present. The sequence of configuration curves in the neighborhood of equilibrium must therefore be of the type shown in Figure 46–2. In any bounded system the energy curve must eventually turn upward for sufficiently large perturbation amplitudes, not shown in the figure. The energy curves are therefore more complex than those depicted in Figure 46–1.

This type of curve is to be found in a cylindrical system in which gas is confined to a cylindrical region containing the axis, by a magnetic field surrounding it. On increasing the twist of this field, the Suydam criterion for stability in the transition region between gas and field can eventually be violated. The instability is manifested in this case by the intrusion of the field into the gas. With certain special distributions of twist, it is possible for helical flux strands to detach themselves from the field and contract as a whole into the gas. In this way the energy of the system can be lowered to below the level in the equilibrium system before the onset of instability. This effects a turndown in the curve, of the type shown in Figure 46–2.

It is to be remembered, however, that the Suydam instability essentially requires gas pressures of the same order of magnitude as the magnetic stresses. For the reasons given in the introductory paragraph, this precludes such systems from the flare phenomenon.

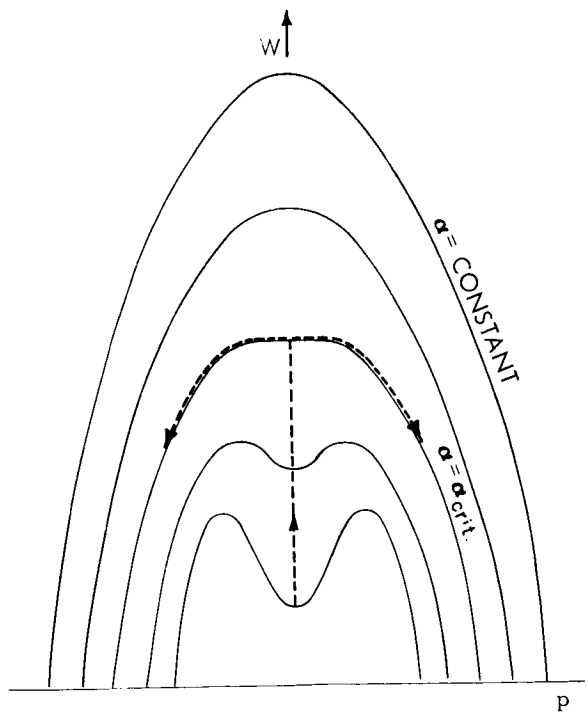

FIGURE 46–2. Stability diagram for a twisted flux tube with gas pressure.

THE PRODUCTION OF CURRENT SHEETS

It has been shown by the author (Reference 2) that magnetic fields in fluids with formally infinite electrical conductivity, and comprising more than one topologically distinct flux system, are prone to develop sheet currents. These sheets can occur only along the lines of intersection of the magnetic surfaces which separate the flux systems mentioned. These lines may be appropriately termed *asymptotic lines*. Typical fields with asymptotic lines, which could occur in the solar atmosphere, are shown in Figures 46–3 and 46–4. The first was proposed by the author (Reference 2), and the second by Gold and Hoyle (Reference 3). The Gold and Hoyle model is more amenable to analysis, since it is essentially a two-dimensional field. In a rectangular coordinate system (x,y,z), the field can be taken to be independent of z.

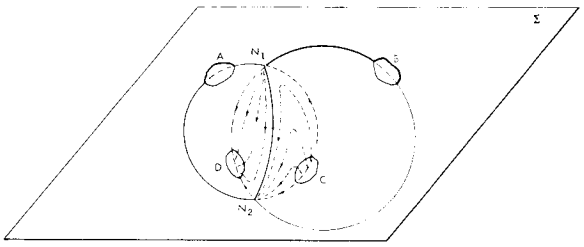

FIGURE 46–3. Topology of a complete field above a complex spot group.

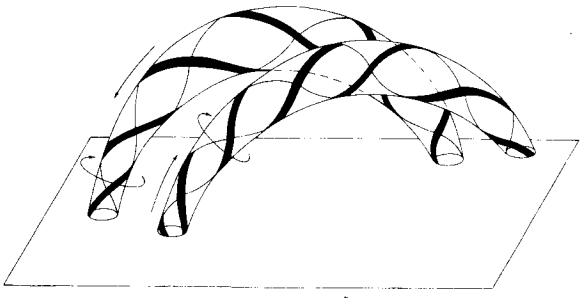

FIGURE 46–4. The Gold and Hoyle double flux tube system.

The xy-component has the topological form shown in Figure 46–5. The total field has a z-component perpendicular to the plane of the figure. The points A and B represent the axes of the flux tubes. The curves through O represent magnetic surfaces separating the three flux

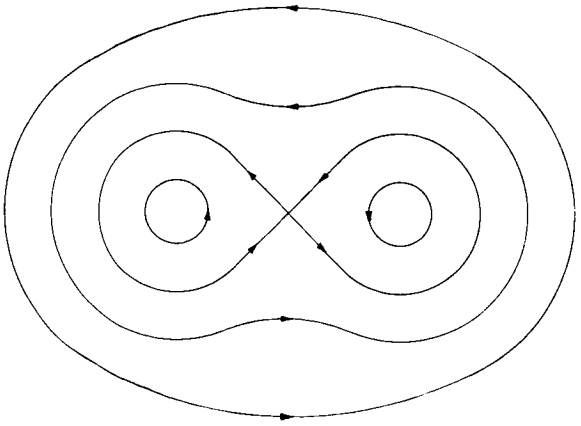

FIGURE 46–5. The xy field of a double twisted flux tube without a current sheet.

systems involved; O represents the asymptotic line of force referred to above. The configuration in Figure 46–5 does not necessarily represent an equilibrium system. It can be shown that, when the system is allowed to come into equilibrium, a current sheet will be formed if the xy-field is sufficiently strong compared with the combined effects of the gas pressure and the z-field. The gas pressure is neglected in the present case. The criterion for the occurrence of a current sheet therefore concerns only the relative strengths of the xy-field and the z-field. A typical current sheet configuration is shown in Figure 46–6, in which the current sheet is represented by the line LM.

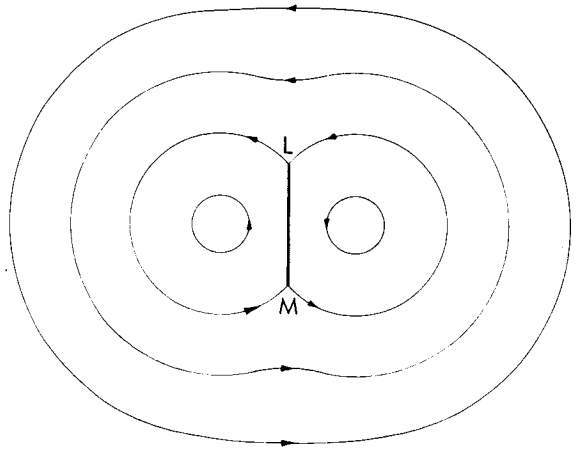

FIGURE 46–6. The xy-field of a double twisted flux tube with a current sheet.

THE STABILITY OF FIELDS WITH ASYMPTOTIC LINES

The stability of the system just described can be discussed in terms of energy surfaces as in previous sections. In the present case the occurrence of current sheets makes it relevant to introduce a second configuration parameter to describe changes due to ohmic dissipation. Ohmic dissipation has two general effects: (1) to reduce the total fluxes of the xy-field in the three systems, and (2) to transfer flux from the two inner systems to the outer enveloping one. Process (1) occurs whether there is a current sheet or not, and proceeds only negligibly slowly. Process (2) also occurs in both cases, but when a current sheet is present the rate is very much higher. The mechanism proposed recently by Petschek (Reference 4) can proceed at a rate high enough to account for the flare phenomenon. The ohmic dissipation parameter is denoted by β in Figure 46–7. A precise definition is not required for present purposes, since Figure 46–7 is intended only as a conjectural representation. A possible definition could be $\beta=1-F/F_0$, where F is the flux in one of the inner systems after dissipation has occurred, and F_0 is the flux present if the xy-field had been set up by twisting without dissipation.

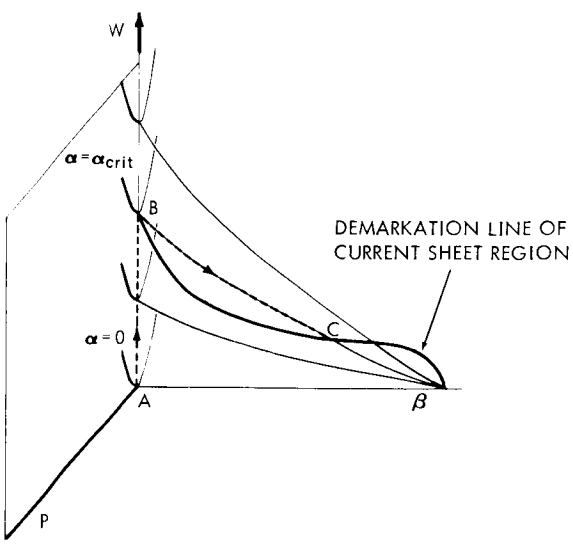

FIGURE 46–7. Energy diagram for a double flux tube illustrating resistive instability.

The other configuration parameter α is analogous to that of the previous sections, namely, a measure of the twist imposed on the flux tubes by photospheric motions. The relative energy W and the perturbation amplitude are also defined as in the previous sections.

In the plane $\beta=0$, the situation is similar to that for a twisted flux tube as shown in Figure 46–1, where the field was frozen in the medium. When for any given twist α dissipation occurs, the energy decreases and vanishes when the flux has completely disappeared. Thus $W=0$ when $\beta=1$ for all values of α, as shown in Figure 46–7. When $\alpha=0$, there is no xy-field and hence no current sheet. As α increases, in the absence of dissipation, the xy-field strengthens and eventually becomes large enough for the production of a current sheet. The value of α_{crit} will be modified by dissipation, that is, will depend on β and will also depend on the perturbation amplitude. Thus there will be a critical surface, given by $\alpha=\alpha_{crit}(\beta,p)$ in the space of Figure 46–7, above which the system contains a current sheet. The intersection of this surface with the plane $p=0$ is indicated by the thickened curve in Figure 46–7.

The behavior of the system depends on whether this critical curve initially dips below the α-curves. The effect of transferring flux from the inner systems to the outer one is to bring the inner layers of each flux tube successively into proximity to the asymptotic line. If for each α the xy-field increases sufficiently steeply toward the axes, then, after transferring flux, the current sheet would set in at a lower value of α. In such a case the critical curve would initially fall more steeply than the α-curves in the p-plane as β increased. Such a situation is represented in Figure 46–7.

The behavior of the system as the flux tubes are increasingly twisted is indicated in Figure 46–7. Starting with an untwisted field at A, there will be effectively no dissipation since there is initially no current sheet; β therefore remains zero, and the system follows the broken line to the point B. At B a current sheet sets in which allows rapid dissipation and consequent increase in β. During this time α, which is changing much more slowly, effectively

remains constant. The system will therefore proceed to the right in Figure 46–7 on a surface of constant α. Neglecting inertia effects, the system would keep to the bottom of the potential well and would proceed in the plane $p=0$ along the broken line indicated.

Now, whatever the distribution of twist with axial distance, for a given α, the xy-field vanishes on the axes of the tubes while the z-field does not. As the inner layers of each tube approach the current sheet during dissipation, a point will therefore be reached when a current sheet is no longer possible. Thus, the system can never discharge itself to zero relative energy. Point C in Figure 46–7 denotes the end of the discharge. The energy released during the dissipation is $W_B - W_C$.

The geometry of the process is illustrated in Figure 46–8.

CONCLUSIONS

In a simple force-free magnetic system such as a twisted flux tube, the instability properties usually considered are not relevant to the problem of solar flares. If a dynamical instability of the type required exists, then a more complex system must be involved.

To establish the existence of an instability of the type shown in Figure 46–4, it would be necessary to show that, at $\alpha=\alpha_{crit}, \partial^4 W/\partial p^4 < 0$.

There is a prima facie case for the existence of a different process which has the character of a macroscopic resistive instability rather than a dynamic instability. One of the essential features—namely, the existence of current sheets—has been established with certainty. The other feature—namely, the slope of the critical curve as compared with the slope of the curve $\alpha=$constant—has not been established with certainty and requires further work.

REFERENCES

1. Voslamber, B., and Callebaut, D. K., 1962, *Phys. Rev.*, 128: 2016.
2. Sweet, P. A., 1958, *Nuovo Cimento*, Supp. 8, Ser. 10: 188.
3. Gold, T., and Hoyle, F., 1960, *M.N.*, 120: 89.
4. Petschek, H., 1963, *these Proceedings*, paper no. 50.

DISCUSSION

Question: I am concerned about the energy diagram that you showed on the second figure (Figure 46–2), because it seemed to me that they have bad features along the lines of those I think discussed by Professor Sturrock earlier today; namely, that a situation was stable until you reached a certain point and then it became unstable only marginally, so that the growth times corresponding to that were large.

On the other hand, I may have missed something; because the last figure (Figure 46–8) seemed to me to indicate a mechanism which was rather weakly unstable most of the time but eventually had a much quicker rate. The second figure didn't coincide with the last one.

Dr. Sweet: The second mechanism is not a dynamical instability at all. It is a resistive instability.

The second figure I showed was a way in which one could get dynamic instability if there were an appreciable gas pressure. Of course, the growth rate for that is zero at that point. The growth rate for the resistive instability as shown in the last figure is not. That starts off with a finite growth rate, which is often possible when one is allowed to alter the topology of the field by resistive dissipation. This does not involve passage through a marginally stable condition. It is the same sort of instability that Furth, Killeen, and Rosenbluth talk about in a very thin current sheet.

Dr. Prince: If it is not inappropriate, could an observer perhaps help a theoretician? Do not cast aside computations that yield flares just because they involve relative magnetic and gas pressures different from those determined for certain great flares. Some flares do form where the magnetic fields are very strong, but I believe most flares do not. The magnetic

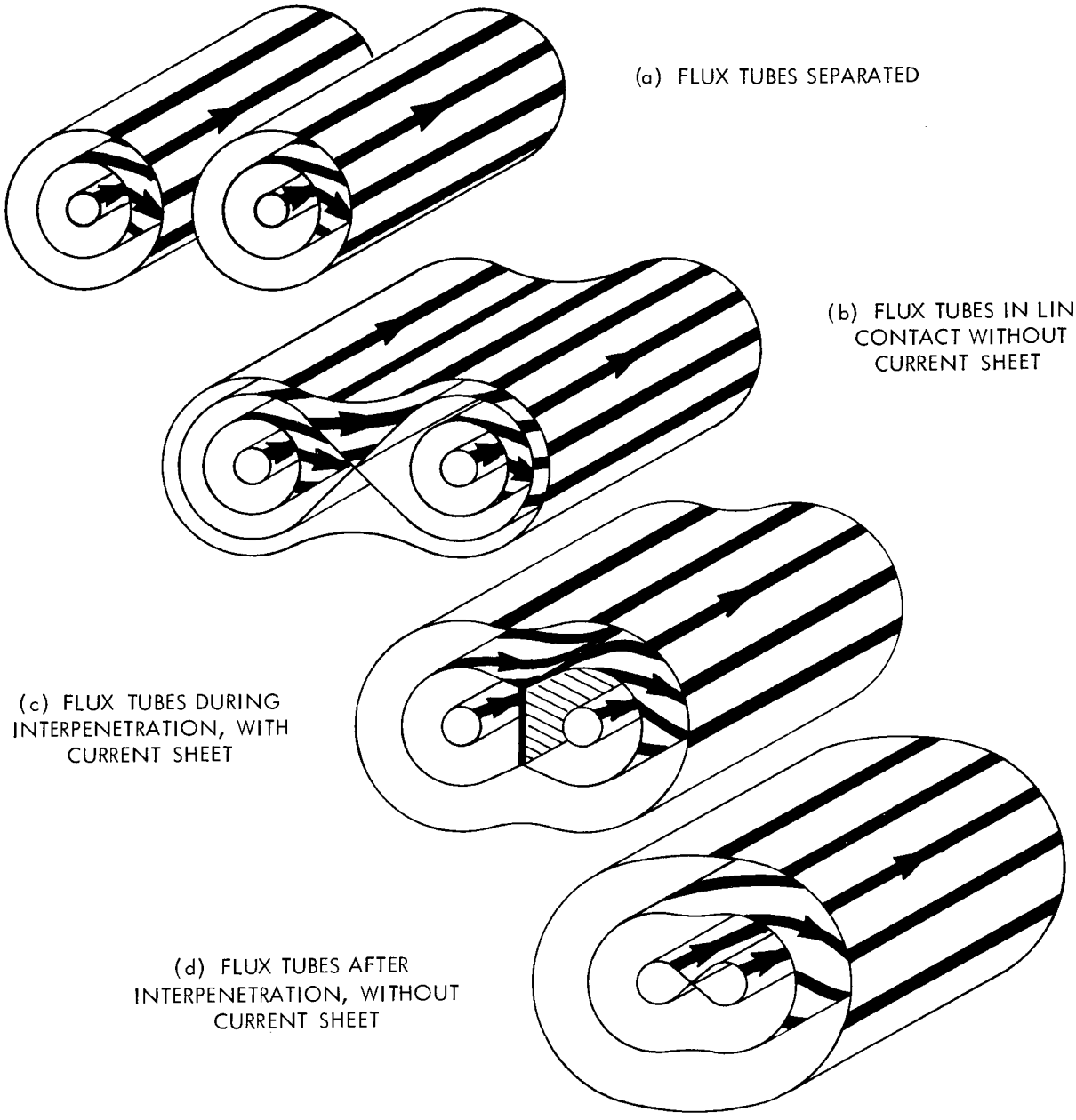

FIGURE 46-8. Geometry of the interpenetration of a double flux tube.

fields are relatively weak where many flares take place.

Dr. Sweet: That is a question you would have to answer by further investigations and models. There is nothing that would stop this sort of thing occurring with weak fields.

N64 30297

47 REMARKS ON THE DISCHARGE THEORY OF FLARES

JAMES W. DUNGEY
Imperial College
London, England

Petschek (Reference 1) has demonstrated that the discharge mechanism (References 2 and 3) is not seriously impeded by the pressure of the plasma as suggested by Sweet (Reference 4) and Parker (Reference 5). Here, three remarks are made in relation to observations of flares.

THE GROWTH RATE

The growth of flares is much faster than the growth of sunspots, and this cannot be easily accounted for by a linear theory of instability. If the instantaneous growth rate given by linear theory itself varies with a time scale corresponding to spots, the instability will grow appreciably when the growth rate is not much greater than that of spots; and the flare cannot wait for the growth rate to become much larger. The earlier treatment (References 2 and 3) is not linear, however. The equations for the rates of change of the gradient tensors of magnetic field and velocity, $B_{ij}=\partial B_i/\partial x_j$, $u_{ij}=\partial u_i/\partial x_j$, are

$$\partial B_{ij}/\partial t=-u_{kj}B_{ik}+B_{kj}u_{ik}-B_{ij}u_{kk}$$

and

$$\partial u_{ij}/\partial t=-u_{kj}u_{ik}+(B_{ik}-B_{ki})B_{kj}/4\pi\rho,$$

which are bilinear. If an instantaneous growth rate can be defined from these equations, this growth rate will itself grow in a similar way to all the other quantities, such as the current density at the neutral point, the electric field, and the velocity. It seems likely that only the later stage of the growth phase is observed—in Hα, say, and that by this time the growth rate has already grown by a large factor. The theory predicts that at earlier times the rate of growth would be smaller; at time t before the flare the growth rate should be $\approx t^{-1}$. It may be possible to detect x rays from satellites some time before flares, and the variation in the spectrum would be of great interest. The interpretation involves the production of energetic particles, which is the subject of my second remark.

ACCELERATION OF PARTICLES

If the magnetic field reverses at a current sheet and there is an electric field in the direction of the current, particles of either sign will gain energy. Their motion may be affected by oscillations and waves, although a static corrugation of the current sheet should not be important. The spectrum of the particles emitted should have a characteristic energy comparable with the voltage of the discharge, and this can be estimated independently. The total current in the discharge must be $\oint \mathbf{B}\cdot d\mathbf{s}/4\pi$ taken round a curve which links the current sheet. If the width of the sheet is $\approx 10^4$ km, the current is $\approx 10^9\ B$ amp. Now the energy dissipated in a large flare may be 10^{30} ergs and the time taken 10^3 sec, giving an average power of 10^{20} watts. Then the voltage required is $\approx 10^{11}\ B^{-1}$ volts. The voltage is likely to vary through the course of the flare more than the current, but it is in reasonable agreement with the characteristic energy of the particles observed. The production of energetic particles is therefore inherent in the mechanism, and the kind of spectrum observed is reasonable. The number of particles accelerated cannot be predicted for any other mechanism (Reference 6), but in the discharge this can also be estimated

roughly from the current. It is observed that the energy dissipated is divided not very unequally between particle energy and energy of fluid flow. This seems plausible for a discharge, but needs further study—using Petschek's model, say. The total rate of dissipation per unit volume is $\mathbf{Ej}$, while that going into fluid flow is $-(\mathbf{u}\times\mathbf{B}).\mathbf{j}/c$. The electric field $\mathbf{E}$ is approximately uniform and $-(\mathbf{u}\times\mathbf{B})/c$ is nearly equal to $\mathbf{E}$ outside the discharge but is reduced inside, where j is large.

Observations of x rays may provide quantities characterizing the energetic particles. The characteristic energy and total energy flux may be converted to a voltage and a wattage, which should be more significant for the comparison of flares than the present measures of magnitude. One may hope that these quantities can be compared with measurements of magnetic field to see whether the variation of voltage and current between large and small flares agrees with theory. Observations of x rays may also yield information concerning energetic particles which may be trapped in the field above sunspots.

TOPOLOGY OF FIELDS WITH NEUTRAL POINTS AND PROTON EVENTS

The topology of the field near a neutral point is such that either two lines go in and an infinity of lines come out covering a surface, or vice versa. Computations by D. Fairfield at Penn State show that most of the accelerated particles come out near this surface of lines which connect to the neutral point. The flare in Hα should then occur where this surface intersects the chromosphere. The polarity of the region depends on whether the lines point into or out from the neutral point, being north or south respectively; and the flare should lie wholly inside a region of one polarity.

Now Ellison and McKenna (Reference 7) have found an association between proton events and those flares which have two bright filaments lying on regions of opposite polarity. This suggests that the two parts of the flare come from different neutral points—one with a surface of lines coming in, the other with a surface of lines going out. The flare at one neutral point can trigger the other. In fact, there must always be more than one neutral point simply because the infinity of lines coming out from one neutral point have to go into another. One of the neutral points could be below the photosphere, in which case none of the accelerated particles might go far from the sun. When there are two neutral points above the chromosphere, Ellison-McKenna flares are possible. For the purpose of predicting proton events, it then seems that the topology of the magnetic field is important. This adds to the case for measuring the transverse component of the magnetic field.

REFERENCES

1. Petschek, H. E., 1963, *these Proceedings*, paper no. 50.
2. Dungey, J. W., 1953, *Phil. Mag.*, 44: 725.
3. Dungey, J. W., 1958, "Cosmic Electrodymamics," 6.4, Cambridge University Press.
4. Sweet, P. A., 1958, *I.A.V. Symposium on Electromagnetic Phenomena in Cosmical Physics*, p. 123.
5. Parker, E. N., 1963, *Astrophysical Journal Supplement.*
6. Wentzel, D., 1963, *these Proceedings*, paper no. 45.
7. Ellison and McKenna, 1963; from, say, Kiepenheuer's paper (*these Proceedings*, paper no. 36).

N64-30299
98

48 COMMENTS ON UNDERSTANDING THE SOLAR FLARE

EUGENE N. PARKER
Enrico Fermi Institute for Nuclear Studies and Department of Physics
University of Chicago, Chicago, Ill.

These remarks will be confined to general impressions on the nature of the problem of understanding the solar flare. Recently I have published the results of an extended quantitative study of current ideas on the origin of the solar flare (Reference 1), some of which has been reviewed here today; so there is no need to go into those details.

The solar flare phenomenon is a transient effect on the sun, which the best observational estimates show to be principally an outburst of solar corpuscular radiation or solar wind. To a lesser extent the flare is an outburst of energetic particles and electromagnetic radiation. The visible portion of the flare above the photosphere has typical maximum dimensions of a few times 10^4 km in all three directions. Thus, the visible flare is a phenomenon which occurs in the lower corona. We believe that the outburst of solar corpuscular radiation comes from the solar corona, too, as the result of the enhanced temperatures observed there in association with the flare (Reference 2). Thus, altogether, the flare seems to be a coronal phenomenon.

We usually assume that the visible flare marks the seat of the general flare disturbance, although the visible flare is probably much smaller than the region involved in the whole flare disturbance.

The visible portion of a flare occurs always in association with sunspots, so that thoughts on the nature of flares naturally have involved magnetic fields in a leading role. The only plausible energy source for the general flare disturbance seems, at the present, to be magnetic fields; and of course strong magnetic fields are a part of ideas concerning particle acceleration and some of the radio emission. One feels, too, that magnetic fields must play a role in the tendency for successive flares in a given site to repeat the same form in time and space.

On the other hand, it has proved extremely difficult to progress from the general association of flares and magnetic fields to specific processes by which the field actually produces flares. At least on our scratch pads the magnetic field stubbornly refuses to dissipate on command. There are two obvious directions in which to search for dissipation of fields. One is that the magnetic fields in active regions on the sun may be a tissue of small-scale twisted ropes of flux, whose average we mistake for a large-scale amorphous field. I have in mind something like the picture of Gold and Hoyle (Reference 3), but a much greater number of such tubes, each of which is much smaller than they consider. The other is a plasma instability of some kind which enhances the dissipation. There are evidently such processes which occur "unwanted" in laboratory plasma experiments. Jaggi (Reference 4) recently suggested one such instability which may be of interest in the flare. Unfortunately the nature of the enhanced dissipation caused by any given instability is extremely difficult to analyze by theoretical calculation because the dissipation occurs in the nonlinear regime.

We place great hopes on the steady improvement in the observation of the longitudinal Zeeman effect with high resolution at various heights in the solar atmosphere, and on the possibility of the observation of the transverse Zeeman effect. It is to be hoped that detailed observation of these kinds over both the site

of the visible flare and elsewhere may provide further clues as to what is happening.

We should be aware, however, that we are observing an extremely complex phenomenon. There is always the chance—which we don't want to think about yet—that we will not succeed in unraveling the basic nature of the flare process. At present, all we can do is try very hard and be sure that we do not settle for some easy, but incorrect, explanation.

Recently, there has been considerable interest in prediction of the occurrence of flares, with particular importance for the man in space. To put forecasting in the proper perspective, we should remember that the flare is a complicated solar meteorological phenomenon and is subject to the same general kind of predictability as terrestrial meteorology. There are two types of forecasting that may be developed. On the one hand, with improvement of high resolution magnetic observations of active regions on the sun, it may become possible to anticipate flares by an hour or so. If there is anything at all to the idea of the magnetic origin of flares, one may expect that the fields may become increasingly strained just before the outburst begins. On the other hand, with the present monitoring of active regions on the visible disk of the sun, it is possible—as studies have shown—to anticipate the passage of active regions into the central and western portions of the disk, where their flares may be expected to send energetic particles to the earth. In this way a period of increased likelihood for flare particles at the earth can be forecast. These are the two types of flare prediction that are tractable. Until we have mastered such simple phenomena as terrestrial meteorology, we will not do more with the complications of solar meteorology.

REFERENCES

1. Parker, E. N., 1963, *Astrophys. J. Suppl.*, 8: 177.
2. Parker, E. N., 1961, *Astrophys. J.*, 133: 1014.
3. Gold, T., and Hoyle, F., 1960, *Mon. Not. Roy. Astron. Soc.*, 120: 89.
4. Jaggi, R. K., 1963, *J. Geophys. Res.*, 68: 4429.

DISCUSSION

Dr. Krook: In view of the various professions of faith that have been made, this is something of hearsay.

Is there any cast-iron argument which rules out the possibility that energy for the flare event is stored in superthermal particles?

I can see some arguments against it. But are there any cast-iron ones that you could produce?

Dr. Parker: To give you a facetious reply, I would say that storing the energy for flares in superthermal particles has in common with the magnetic field theory the fact that you can observe neither. I just don't know.

I think we ought really to investigate all the possibilities. There is this idea that the energy of the flare comes from beneath the photosphere. This has been rejected repeatedly. I have argued against it, too, on the ground that you should see something happening in the photosphere when there is a flare. And yet, if you remember that the 10^{32} ergs—not 10^{30} ergs of visible light but 10^{32} ergs that goes into the whole flare phenomenon—may come from a very broad region of the sun, you can dilute this energy flux due to the photosphere to where you can't see it.

So I really think that we ought seriously to consider something besides annihilating and dissipating magnetic fields in the corona. There are many ways to turn; that is why I haven't bothered to enumerate them. Your superthermal particles are certainly one of them.

N64 30279

49 A MECHANISM FOR THE DISSIPATION OF THE MAGNETIC FIELD IN SOLAR FLARES

RADHE K. JAGGI
Goddard Space Flight Center, NASA
Greenbelt, Md.

Solar flares are extremely complicated structures and involve diverse physical phenomena. In this paper, we shall concentrate on only one feature of a flare: namely, a mechanism by which energy is released in the chromosphere, leading to the initial production of the flare. This energy release must take place in an extremely small time scale, of the order of 10^3 seconds.

From a comparison of the energy available in different forms (thermal, kinetic, and magnetic) above the photosphere, it appears that the magnetic field is the only sufficient source of energy. The magnetic energy density exceeds either the thermal or the kinetic by several orders of magnitude. The basic problem thus becomes one of finding a mechanism by which the magnetic field energy can be dissipated over a large volume in the short time of $\approx 10^3$ seconds. I have studied the role that plasma instabilities may play in initiating a flare. In particular, Sweet's model, for the field geometry (Figure 49–1), was examined (Reference 1).

It is interesting to note that, if each pair of sunspots is regarded as a small dipole, the height of the neutral point N in Figure 49–1 is $d/\sqrt{2}$, where d is the distance between the dipoles. This points toward the importance of the magnetic neutral point in a flare theory because observations show that the flare usually is observed to be at a height of a few thousand kilometers. A reasonable value of d is 10^9 cm; that is, $d/\sqrt{2} \approx$ a few thousand kilometers.

Chapman and Kendall (Reference 2) have considered the problem of the instability of hydromagnetic flow in an X-type neutral point

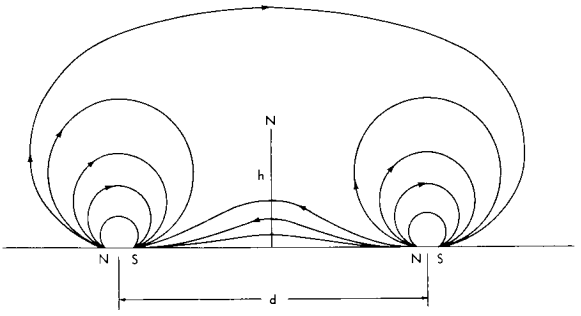

FIGURE 49–1. Magnetic field configuration for four sunspots located on a straight line.

and have shown the existence of an instability with a growth time of the order of the time required for an Alfvén wave to cross the system.

The difficulty with an instability, which exists in an X-type neutral point, is that such an instability may be able to produce dissipation only in a small region in the neighborhood of a neutral point while energy considerations require much larger dimensions to be involved in the process.

In what follows, we shall make somewhat different assumptions, following Sweet (Reference 1), which help to produce thermalization of the magnetic field and the plasma in large dimensions. We assume that the ionized atmospheres situated in the magnetic fields of two pairs of sunspots shown in Figure 49–1 approach each other with a velocity of approximately a few kilometers per second. The fluid squeezes out from between two oppositely directed magnetic fields, and a steady state is reached in this way with the fields moving slowly together with a region of relatively intense dissipation between. Such a steady state is shown in Figure 49–2.

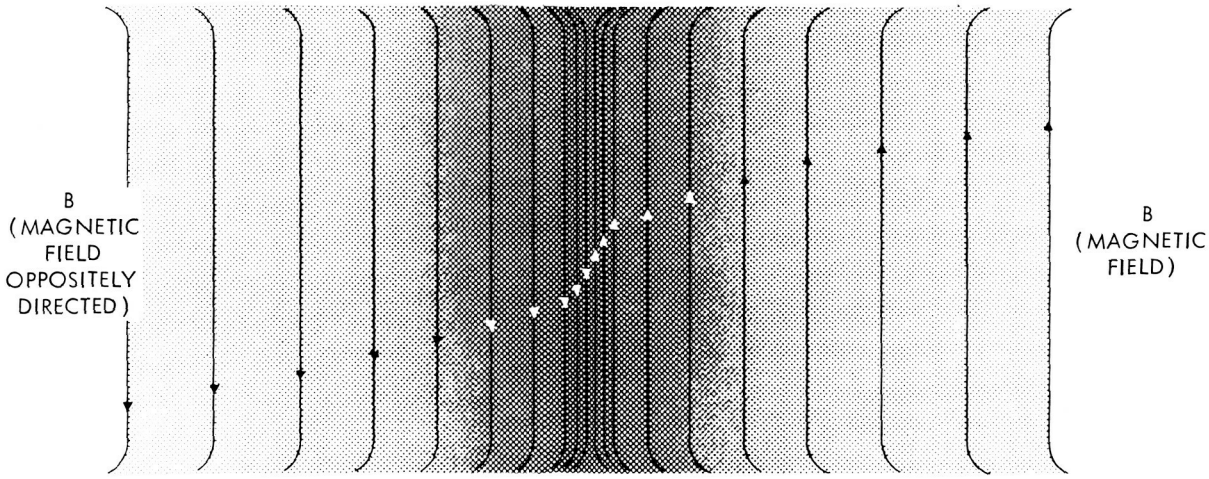

FIGURE 49–2. Formation of the current sheath during the approach of two dipole fields.

Stability problems connected with this process have been studied in papers by Syrovatskiy (Reference 3), Severny (Reference 4), and Jaggi (Reference 5). Syrovatskiy has shown that, in the limit of infinite conductivity, a layer of plasma in hydrostatic equilibrium between two oppositely directed magnetic fields is stable. In the same issue, Severny's paper follows that of Syrovatskiy. Severny has shown that a plasma layer of finite conductivity situated between the planes $x=\pm x_0$ with magnetic field $\mathbf{B}=(0,B_0(x/x_0),0)$ is in unstable equilibrium.

In Reference 5, we have examined three different stability problems:

1. The stability of a magnetohydrostatic equilibrium which may arise when two opposing fields are impressed upon each other. The plasma conductivity is assumed to be infinite. It is proved that such a magnetohydrostatic equilibrium is stable.

2. Some instabilities due to the gradients of the magnetic field discussed by Krall and Rosenbluth (Reference 6). It was found that these instabilities are very slow.

3. Some instabilities due to the finite conductivity of the plasma. These were found to be applicable to the present problem and are discussed below.

The physical mechanism for the dissipation of a magnetic field considered here occurs in three stages. First, the two dipole magnetic fields situated in the solar atmosphere approach each other and "squash" together, changing the nearly curl-free magnetic field into a magnetic field which has a curl. We assume that this stage takes a time equal to that given by the flare dimensions ($\approx 3\cdot 10^8$ cm) divided by a typical fluid velocity for the chromospheric plasma ($3\cdot 10^5$ cm sec^{-1}), that is, of the order of 1000 seconds. This is apparently an upper limit to the time required to change the magnetic field configuration in the central region, close to the neutral point of the magnetic field.

The second stage consists of the occurrence of finite conductivity instabilities. The time of onset of these instabilities is estimated below.

We shall now consider further some instabilities due to finite conductivity recently discussed in Reference 7 by Furth, Killeen, and Rosenbluth (FKR). Of the three instabilities discussed by FKR, the tearing mode instability is found to be applicable to the present case, and it corresponds to the breakup of the layer along current flow lines. In Figure 49–2 the current flow direction is perpendicular to the plane of the paper. The expression for the growth rate of instability ω is given by:

$$\omega=\frac{\alpha^{-2/5}S^{-2/5}}{4\pi\sigma a^2}, \tag{1}$$

where $\alpha=ka$ (k is the wave number of a perturbation, a the thickness of the current sheath), $S=3\times 10^{-9}aT^2/\sqrt{\beta}$ (T is measured in degrees K,

$\beta=4\pi P/B^2$, P is the kinetic pressure, and B the magnetic field). The condition under which the instability applies is $S^{-\frac{1}{2}}<\alpha<1$. The growth rate ω has a maximum and a minimum value corresponding to these two limits of α. The value of the growth rate depends on the three parameters: T, β, a. It is required to estimate a value of a in order to determine a value of ω. The temperature range of interest to us is $T=10^4$ °K to 10^7 °K. We are using high values for T, particularly because the compression of the two magnetic fields will possibly raise the temperature of the plasma.

In Figure 49–3, we give a plot of the time of instability versus a for $T=10^4$ to 10^7 °K and $\beta=0.1$, 1, 10. The dashed line in the figure gives log t_{assembly} vs. log a (t_{assembly} denotes the time required to change the magnetic field configuration). The figure clearly shows that the appropriate times for the growth of instabilities is of the order of 10^{-3} sec and is achieved for values of $a\lesssim 10^2$ cm. This thickness of the current sheath is somewhat higher than the 1–10 cm values required by Sweet (Reference 8).

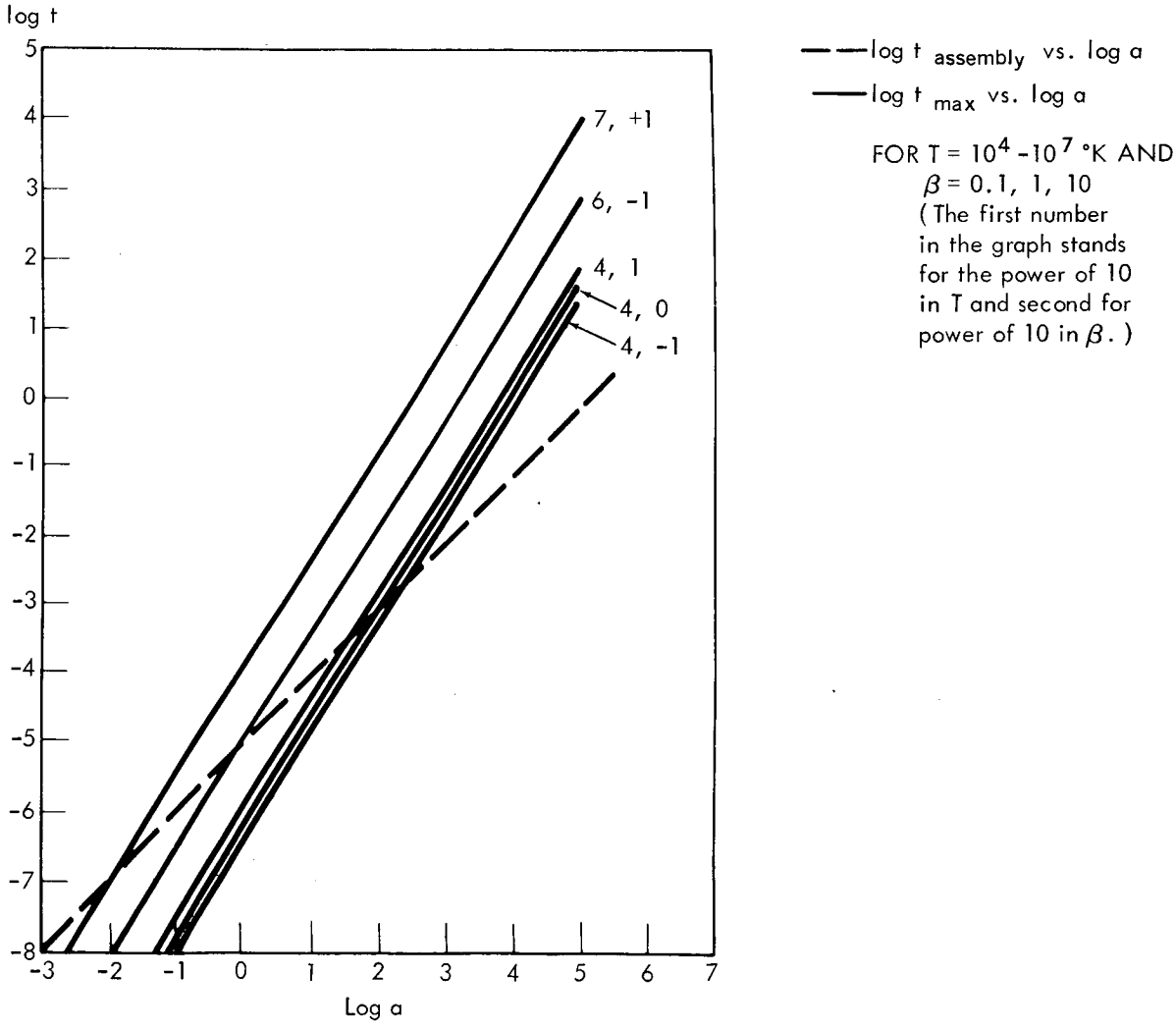

FIGURE 49–3. For $T=10^4$ to 10^7 °K and $\beta=0.1$, 1, and 10.

TABLE 49–1

Values of $S^{-\frac{1}{2}}$ for Different Values of T and β

T(°K)	β		
	10^{-1}	1	10
10^4	0. 37	0. 50	0. 66
10^5	0. 11	0. 16	0. 21
10^6	0. 037	0. 050	0. 066
10^7	0. 011	0. 016	0. 021

TABLE 49–2

Maximum and Minimum Values of the Growth Rate $\omega \times 10^{-5}$ for $T=10^4$ °K to 10^7 °K and $\beta=10^{-1}$, 1, 10^1

T(°K)	β		
	10^{-1}	1	10
10^4	0. 142 0. 044	0. 089 0. 025	0. 056 0. 014
10^5	0. 028 0. 014	0. 018 0. 0079	0. 011 0. 0044
10^6	0. 0056 0. 0044	0. 0036 0. 0025	0. 0022 0. 0014
10^7	0. 0011 0. 0014	0. 00069 0. 00075	0. 00044 0. 00043

In Tables 49–1 and 49–2 we have tabulated the values of $S^{-\frac{1}{2}}$ and ω for the above-mentioned values of T and β. Throughout the tables the value of a used was 10^2 cm. The lower values in each column of Table 49–2 are the minimum values of ω determined from the inequality satisfied by α. From this table we find that the maximum e-folding time, which is inverse of the growth rate, is $\leq 10^{-3}$ sec. It is worth mentioning that in the theoretical work of FKR employed here it is assumed that the conductivity of the region surrounding the current sheath is zero. We justify this assumption by the reason that the compression accompanying stage 1 can raise the temperature of the central region, and thus raise the conductivity of the current-carrying region.

The amount of magnetic energy dissipated by the instability taking place in a sheath 10^2 cm thick (in a 10^{19} cm^2 area) is $10^{19} \times 10^2 \times 10^4 = 10^{25}$ ergs, where the strength of the magnetic field is assumed to be 500 gauss. To get a total output of energy $= 10^{31}$ ergs required by observation, the process must continue for some time with a fresh magnetic field being brought close to the neutral point and repeating the instability.

The third stage, that is, the dissipation of the disordered magnetic field in the central region, follows the second stage.

Figure 49–4 shows the magnetic field lines after the instability. Clearly, the scale of the magnetic field in the central region is reduced to the scale of the wavelength of instabilities.

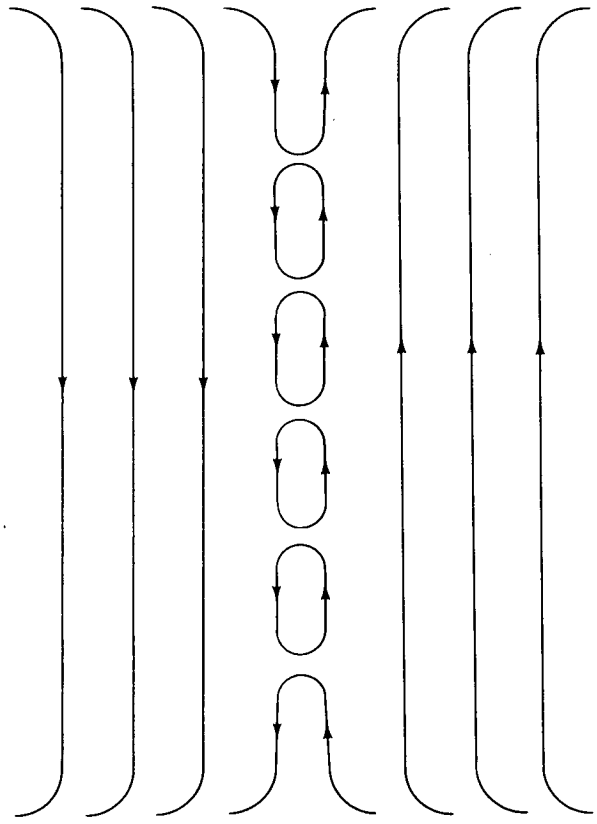

FIGURE 49–4. Formation of small-scale magnetic fields by finite conductivity instabilities.

The dissipation time of a magnetic field of scale L is given by

$$\tau = 4\pi\sigma L^2, \tag{2}$$

where σ is the conductivity of the medium in emu. For $T=10^4$ °K and $L=10^2$ cm, τ=a few milliseconds.

The compression accompanying stage 1 can raise the temperature of the current-carrying region. Now, a raise in the temperature corresponds to raising the conductivity and therefore the dissipation time of the magnetic field. At the same time, Figure 49–3 shows that the thickness of the current sheath in which the instability takes place is much less for high temperature curves. This reduces the value of L and therefore τ in Equation 2.

In conclusion, we see that finite conductivity instabilities may play an important role in the dissipation of magnetic fields in sufficiently short times so as to produce a solar flare. However, several problems remain; and we must understand how magnetic flux is continuously carried into the central region in order to continue this process and thus release sufficient energy.

ACKNOWLEDGMENT

I would like to thank Dr. W. N. Hess for suggesting this investigation and for his helpful discussions.

REFERENCES

1. Sweet, P. A., 1958, *Proceedings of the International Union Symposium on Electromagnetic Phenomena in Cosmical Physics*, No. 6 (Stockholm 1956), p. 123.
2. Chapman, S., and Kendall, P. C., 1963, "Liquid Instability and Energy Transformation Near a Magnetic Neutral Line, a Soluble Non-Linear Problem," *Proc. Roy. Soc.*, 271: 435.
3. Syrovatskiy, S. I., 1963, "The Stability of a Plasma in a Non-Uniform Magnetic Field and On the Mechanism of Solar Flares," *Soviet Astronomy*, 6: 768.
4. Severny, A. B., 1963, "On Plasma Layer Instability with the Neutral Point of a Magnetic Field," *Soviet Astronomy*, 6: 770.
5. Jaggi, R. K., 1963, "The Role of Plasma Instabilities in the Origin of Solar Flares," *J. Geophys. Res.*, 68: 4429.
6. Krall, N., and Rosenbluth, M. N., 1962, "Trapping Instabilities in a Slightly Inhomogeneous Plasma," *Phys. Fluids*, 5: 1435.
7. Furth, H. P., Killeen, J., and Rosenbluth, M. N., 1963, "Finite-Resistivity Instabilities of a Sheet Pinch," *Phys. Fluids*, 6: 459.
8. Sweet, P. A. (Rottach Egern 1963) Paper presented at the *IAU Symposium No. 22 on Solar and Stellar Magnetic Fields.*

DISCUSSION

Dr. Wentzel: Do I understand that the little loops you were forming have essentially the same dimension in the two directions perpendicular to the gap and along the gap?

Dr. Jaggi: There is a range of wavelength which is a little higher than the thickness of the current sheath, so that the instability occurs for wavelengths between the thickness of the current sheath and some, say, 10 times the thickness of the current sheath. So, one can differ by about 10. That is given in Table 49–2.

I can't go into further details. But it isn't much different.

Dr. Wentzel: The reason I asked is these eddies are essentially round—and I see no great difference between this and the mechanism which Parker treated in his supplement, except that you have divided the scale by 2, something like this, which doesn't do much.

Dr. Parker: What you are saying is that you get an instability in the transition region between the oppositely directed fields. This instability grows exponentially with time, and who knows what happens thereafter. I think this is really the essence of the argument.

Dr. Jaggi: This is what I think can happen after the instability; that is, the instability corresponds to breakup of the magnetic field lines.

Evidently, if you break, the only possibility is that the magnetic field lines will get connected with their nearest neighbor and form loops.

728–629 O—64——28

50 MAGNETIC FIELD ANNIHILATION*

HARRY E. PETSCHEK
Avco-Everett Research Laboratory
Everett, Mass.

Sweet's mechanism for the rate of annihilation of the magnetic field at the boundary between two regions of plasma containing oppositely directed field lines is re-examined. It is pointed out that previous analyses overlooked standing magneto-hydrodynamic waves as a possible mechanism for converting magnetic energy to plasma energy. An estimate of the annihilation rate including such waves is made. Using this rate, it is found that the energy required for a flare can be released in 10^2 sec. This time is short enough to account for the observed solar flare times if the source of the flare energy is stored magnetic energy.

One of the principal objections which has been raised to the suggestion that solar flares result from the rapid release of magnetically stored energy has been that the rate at which magnetic energy can be released is too slow. The model of the boundary between regions in which oppositely directed field lines exist, which was originally suggested by Sweet (References 1 and 2) and evaluated quantitatively by Parker (Reference 3), leads to times for the release of energy which are too large by a factor of 10 to 100. This is true even when it is assumed that the gas remains partially ionized and the resulting decrease in the effective conductivity due to ambipolar diffusion is included. It has been pointed out by Jaggi (Reference 4) that on the basis of the resistive instability analysis of Furth, Killeen, and Rosenbluth (Reference 5) the boundary in the Parker-Sweet model would be unstable. It is thus clear that the Parker-Sweet annihilation rates underestimate the actual rate of magnetic field annihilation. However, the linearized instability analysis does not lead immediately to an estimate of what the actual rate would be.

The existence of this instability leads to the suggestion that the flow becomes turbulent and that the increased annihilation rate results from the increased dissipation due to turbulence (References 6 and 7). The purpose of the present paper is to point to another possibility. This alternate possibility is based on the fact that Parker's analysis has overlooked a significant mechanism for the dissipation of magnetic field energy. If this mechanism is also included, it is possible to construct a steady flow configuration with much faster annihilation rates. Parker's solution should be regarded as a special case in a series of possible solutions. The existence of the instability of this particular solution should probably be considered largely as an indication that the particular solution underestimates the actual rate at which annihilation will occur.

To illustrate the mechanisms by which magnetic energy can be converted into plasma energy, let us consider for the moment a completely one-dimensional time-dependent situation in an incompressible fluid in which two regions with oppositely directed magnetic field lines are placed in contact at zero time (the actual situation to be discussed in the body of this paper will not be one-dimensional or time-dependent). In the present case, two mechanisms exist for the annihilation of magnetic field energy: (1) dissipation due to to the finite conductivity of the plasma which may be regarded as diffusion of the magnetic field, and (2) annihilation of the magnetic energy by the propagation of an Alfvén wave.

Figure 50–1(a) illustrates the diffusion case. The thickness of the region of reduced magnetic field is given by the ordinary skin depth formula. If, on the other hand, there is a component of magnetic field normal to the boundary, waves will travel outward in both directions and give

*This work was sponsored by the Department of the Navy, Office of Naval Research, under contract No. Nonr-2524(00).

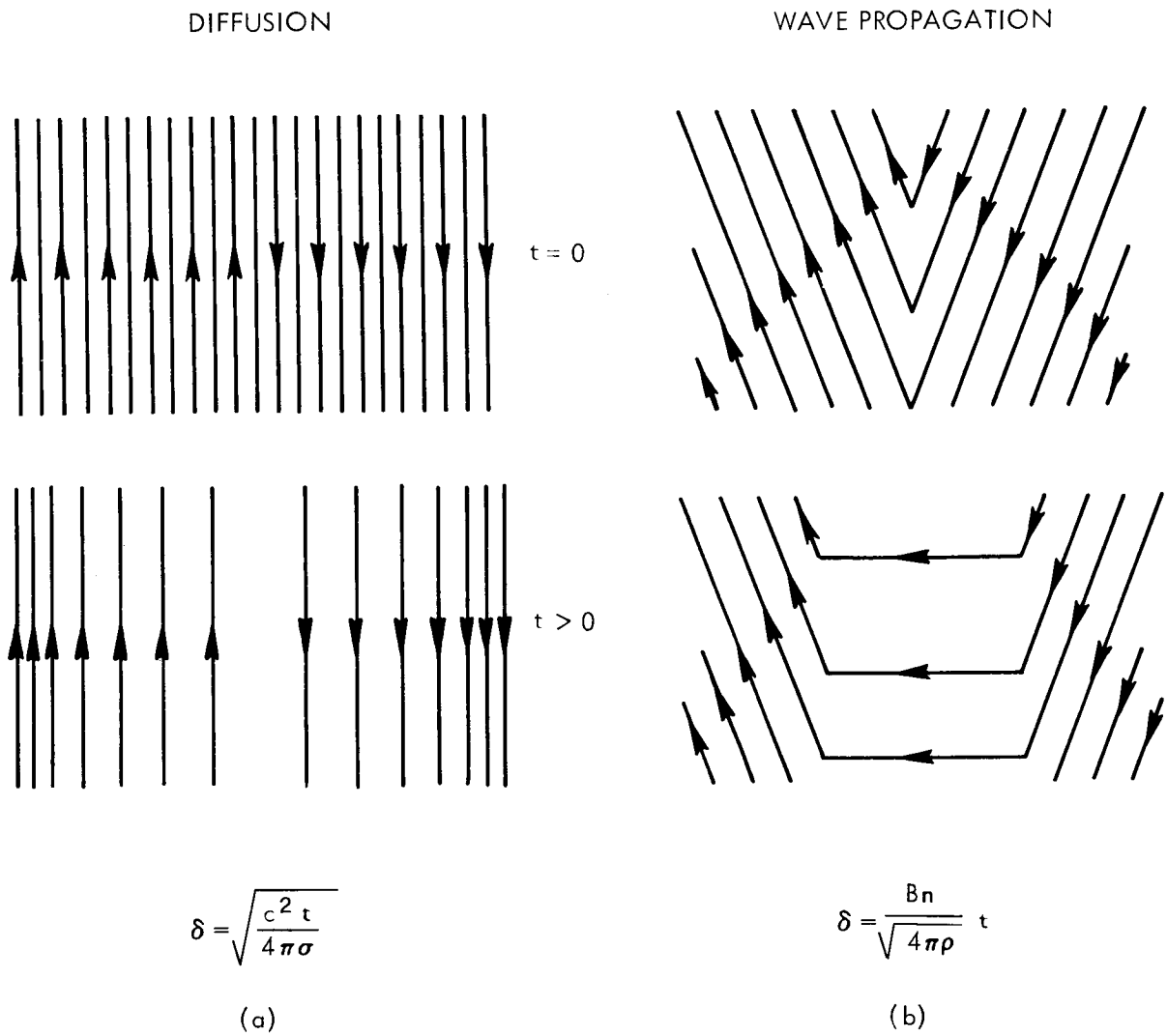

FIGURE 50–1. Illustration of the conversion of magnetic to plasma energy by: (a) diffusion, and (b) wave propagation. The initial magnetic field configuration and the configuration at a later time are sketched for a hypothetical one-dimensional time-dependent situation.

rise to a magnetic field configuration as shown in Fig. 50–1(b). The waves, or bends in the magnetic field lines, propagate at a constant velocity equal to the Alfvén speed. It is apparent from the spacing between field lines that the magnetic energy is considerably reduced between the waves. This energy has been converted into directed kinetic energy of the plasma which is moving upward. Since the Alfvén speed is independent of conductivity, the rate at which magnetic energy is converted to plasma energy is in this case independent of the conductivity. Since the diffusion rate decreases with increasing conductivity, we may expect the wave propagation mechanism to be important at high conductivities. We may also note that, since the diffusion velocity due to finite conductivity decreases as the square root of time, diffusion would be the faster and therefore the dominant effect at early times. However, at later times the wave propagation velocity will be faster, and therefore this effect should predominate. In this paper we will show that, in the steady flow situation, both

the diffusion and the wave propagation mechanism are important and that this leads to a much more rapid rate of annihilation and reconnection of field lines in a high conductivity medium than is obtained when the wave propagation mechanism is overlooked.

Since the analysis to be given in this paper is in many respects similar to Parker's, we will review his analysis briefly in the next section for the case of incompressible flow. In the section titled "Incompressible" we will present the analysis including the effects of wave propagation again for the incompressible case. Since incompressible corresponds to high gas pressure as compared with magnetic pressure, the compressible case is of more interest for solar flares. Thus, in the section "Compressible" the analysis will be extended to the case of a compressible fluid. In the last section, "Application to Solar Flares," we will discuss briefly the application of this analysis to solar flares.

DIFFUSION MODEL

It was recognized by Sweet that the strictly one-dimensional situation illustrated in Figure 50–1(a) is not applicable, since the fluid will be ejected outward along the boundary. The region in which the magnetic field goes through zero must have a higher pressure than the surrounding medium by an amount equal to the magnetic pressure. If we imagine that the boundary has a finite length determined by the general dimensions of the flow field which is being considered and that beyond this length the pressure is reduced to the ambient pressure, then the pressure gradient along the boundary will accelerate fluid outward. As this fluid moves outward, the distance between oppositely directed field lines decreases and thus a more rapid rate of dissipation is obtained than in the purely one-dimensional time-dependent case.

Parker recognized that this effect could lead to the steady flow situation sketched in Figure 50–2. The fluid moves toward the boundary from both sides and is ejected along the boundary. The magnetic field lines are brought toward the boundary by the fluid. Within the boundary an x-type neutral point exists at

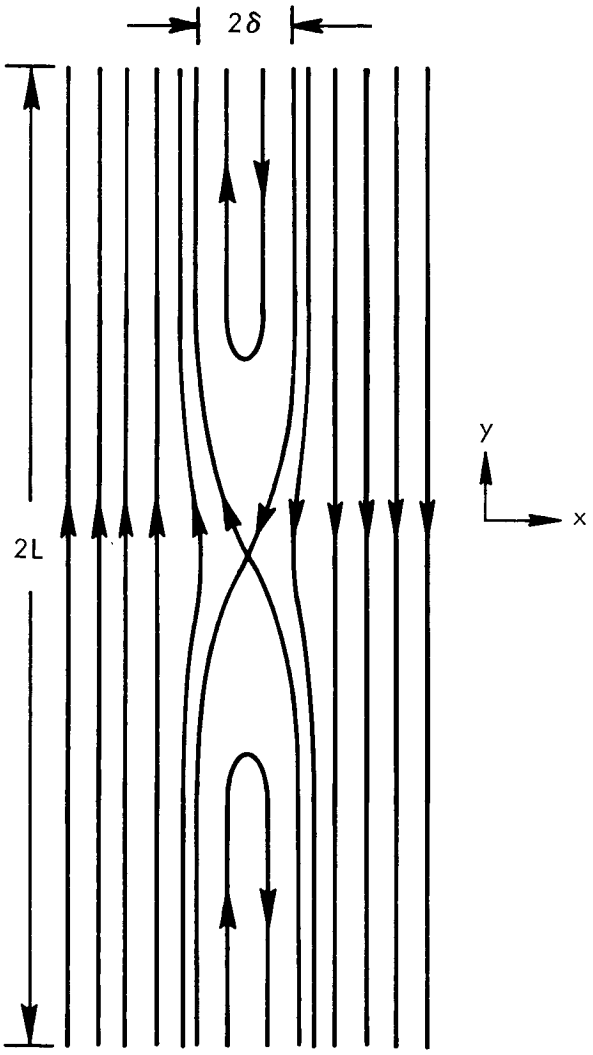

FIGURE 50–2. Magnetic field configuration for Parker's analysis of the Sweet mechanism. The fluid moves toward the boundary from both sides and is ejected along it.

which the field lines are reconnected by finite conductivity and the magnetic energy is dissipated.

For a steady flow, the rate at which fluid moves into the boundary is balanced by the rate at which fluid is expelled along the boundary. Thus,

$$u_{xo}L=v\delta, \tag{1}$$

where u_{xo} is the velocity of the fluid toward the boundary, v is the flow velocity along the boundary, and $2L$ and 2δ are respectively the length and thickness of the boundary. The

velocity along the boundary was obtained from Bernoulli's law:

$$\frac{\rho v^2}{2}=p-p_0, \tag{2}$$

where ρ is the density, p is the pressure in the middle of the boundary, and p_o is the gas pressure at large distances from the boundary. We may note that this relation neglects the magnetic forces which, as can be seen from the sketch of the magnetic field pattern, also tend to pull the fluid out along the boundary. Actually, the magnetic and pressure forces are comparable, so that there is an error of the order of a factor of 2 in v^2. The pressure balance across the boundary is essentially a hydrostatic condition, since the flow velocity into the boundary is expected to be very small. Thus,

$$p-p_0=\frac{B_{yo}^2}{8\pi}, \tag{3}$$

where B_{yo} is the field outside of the boundary.

Since both the magnetic field and the velocity are small in the neighborhood of the neutral point, Ohm's law may be written as

$$j_z=\sigma E_z, \tag{4}$$

where j_z and E_z are the current density and electric field and σ is the electrical conductivity assumed to be a scalar. For a steady flow $\nabla\times E=0$, and therefore E_z is a constant throughout the flow field. The constant may be evaluated from the fact that outside the boundary layer the current density is zero, and therefore

$$E_z=-\frac{u_{xo}B_{yo}}{c}. \tag{5}$$

Since the change in magnetic field across the boundary must be equal to $2B_{yo}$, the total current in the boundary layer is specified; and

$$\frac{4\pi j_z}{c}(2\delta)=2B_{yo}. \tag{6}$$

Equations 4 through 6 may be combined in the form

$$u_{xo}=\frac{c^2}{4\pi\sigma\delta}. \tag{7}$$

For future reference we may note that in this form the equation can be interpreted as the statement that the flow velocity into the boundary layer u_{xo} must be equal to the diffusion velocity of the magnetic field relative to the fluid as given by the right-hand side. In other words, in order to maintain a steady state, the rate at which the magnetic field diffuses relative to the fluid must just equal the rate at which it is blown back by the fluid velocity.

We may now combine Equations 1 through 3 and 7 to obtain a complete description of the basic parameters of the flow configuration. In particular, if we solve for the velocity u_{xo} at which the fluid and magnetic field lines approach the boundary, we obtain

$$u_{xo}=\left(\frac{B_{yo}}{\sqrt{4\pi\rho}}\frac{c^2}{4\pi\sigma L}\right)^{1/2}. \tag{8}$$

If we define the Alfvén speed in terms of the magnitude of the field away from the boundary,

$$V_A=\frac{B_{yo}}{\sqrt{4\pi\rho}}, \tag{9}$$

and introduce the nondimensional flow velocity

$$M_o=\frac{u_{xo}}{V_A} \tag{10}$$

and also a magnetic Reynolds number based on Alfvén speed as

$$R_m=\frac{4\pi\sigma V_A L}{c^2}, \tag{11}$$

Equation 8 may be rewritten as

$$M_o=R_m^{-1/2}, \tag{12}$$

which expresses the rate of annihilation in nondimensional terms. We may note that, since in most astronomical applications the magnetic Reynolds number is very large, the above relation leads to a very slow rate at which field lines approach each other and annihilate.

INCOMPRESSIBLE

If we now modify the picture to take into account the effects of wave propagation, we expect a magnetic field pattern as shown in Figure 50–3. The general topology of this field

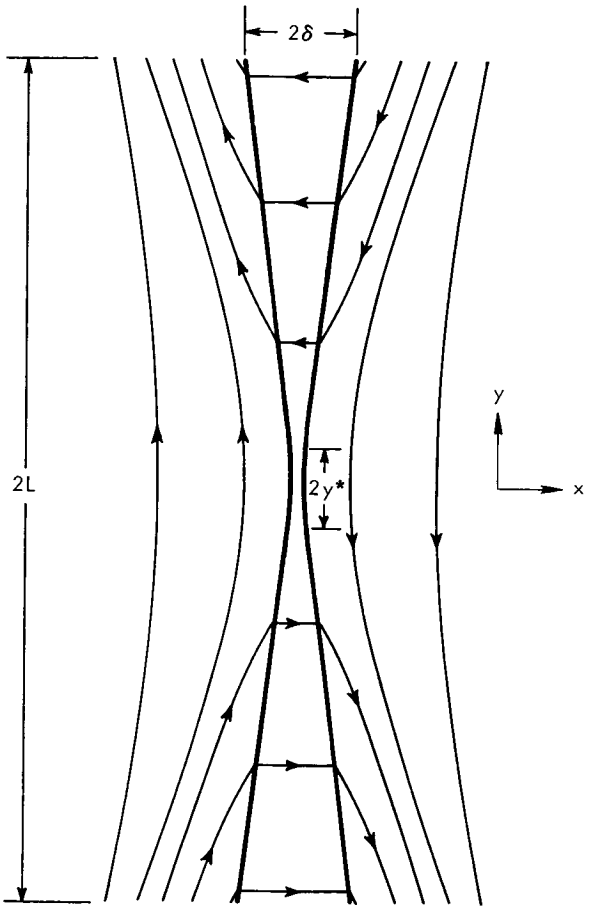

FIGURE 50–3. Flow configuration including standing waves. The magnetic field is indicated by light lines. The heavy lines indicate the edge of the boundary layer. For $y > y^*$, the edge of the boundary layer is determined by magneto-hydrodynamic waves and is therefore rather sharply defined. The fluid again moves toward the boundary and is ejected along it.

configuration is the same as in the previous section in that it is consistent with an x-type neutral point. In the neighborhood of the origin, the normal component of magnetic field must be zero by the symmetry of the problem. Since the propagation speed of waves is proportional to the normal component of magnetic field, the wave propagation speed must vanish in this neighborhood. Locally, the flow is therefore controlled by diffusion and will be quite similar to the flow discussed in the previous section. However, at some distance from the neutral point the normal component of magnetic field can be large enough so that wave propagation becomes faster than diffusion. At large distances from neutral point, we therefore expect that waves will be predominant. In this region the field lines bend sharply at the wave as opposed to turning gradually throughout the boundary layer.

It will be convenient to subdivide the flow into two regions which we will refer to as the *boundary layer* and the *external flow*. The *boundary layer* may be defined as the region near the boundary in which the magnetic field has an appreciably different magnitude than it has far from the boundary. Within the boundary layer the flow velocities will be high, of the order of V_A. In the *external flow* the changes in magnetic field are by definition small. Condiditions are, however, not completely uniform in this region. As is illustrated in Figure 50–3, the presence of a normal component of the magnetic field at the boundary requires the magnetic field lines in the external flow to be bowed toward the boundary. The external flow may be regarded as being distorted because the plasma is pushed out along the boundary. In the analysis which follows, we will find it necessary to consider both the external flow field and the boundary layer. In fact, we will see that the distortion of the external flow by the boundary layer will ultimately limit the rate of field annihilation.

Before proceeding with the analysis, we may point out that—whereas the analysis in the previous section yielded only a single value for the rate of approach of the field lines—in the present analysis we will find that consistent solutions exist for a range of values. This would seem to be more reasonable, since one can imagine that the rate of flow could be controlled by a throttle placed elsewhere in the flow field (for example, motions of the *feet* of the magnetic field lines in the solar surface). Thus, all flow velocities up to a maximum one, allowed by the rate of field cutting, should be possible. In proceeding with the analysis, we will therefore assume that the flow velocity at infinity has a predetermined value which will appear as a parameter when describing the flow field. The actual value of this flow veloc-

ity which would occur in situations where the flow rate is controlled only by the allowed rate of field cutting will then be the maximum value of the parameter for which a consistent solution can be obtained.

In view of the above discussion, we may subdivide the analysis into three parts: (1) the boundary layer, (2) the external flow field, and (3) the evaluation of the maximum flow velocity for which a consistent flow pattern exists.

Boundary Layer

Since in the limit of infinite conductivity the boundary layer reduces to a single line, we would expect that for large conductivities the boundary layer will still be thin. In the analysis that follows, we will assume this to be the case.

It was pointed out just above that the external flow field will be slightly distorted. In considering the boundary layer itself, we will assume that to lowest order the flow at the edge of the boundary layer is the same as the flow at infinity. The validity of this assumption can be checked after we have examined the external flow field.

Within the above approximations, the requirement of conservation of mass leads to the relation

$$u_{xo}y = v\delta, \tag{13}$$

where both the flow velocity along the boundary layer v and the boundary layer thickness δ are functions of y.

The momentum equation in the y-direction may be written as

$$\frac{\mathrm{d}}{\mathrm{d}y}(\rho v^2\delta) = -\frac{B_{yo}B_x}{4\pi}, \tag{14}$$

where B_x is the x-component of the magnetic field within the boundary layer and is also a function of y. The above equation has equated the rate of change of momentum flux within the boundary layer to the magnetic forces. The pressure gradient in the y-direction has been neglected. This would correspond to a situation in which the pressure is maintained constant along the boundary and all of the pressure drop which was used in discussing the diffusion model occurs at the end of the boundary. Actually the pressure gradient is probably a linear function of y whose magnitude becomes comparable to the magnetic force near the end of the boundary, $y \approx L$. It is therefore reasonably small for small values of y, and the net effect of the pressure gradient is probably to reduce the effective length of the boundary. Since the annihilation rate is insensitive to the length of the boundary, the error introduced is quite small. It is convenient to combine Equations 13 and 14 in the form

$$M_o^2 \frac{\mathrm{d}}{\mathrm{d}y}\left(\frac{y^2}{\delta}\right) = -b_x, \tag{15}$$

where we have introduced some of the notations from the previous section and where $b_x = B_x/B_{yo}$.

At appreciable distances from the neutral point we expect wave propagation to be important. To maintain a steady flow, the speed at which the wave propagates relative to the fluid must equal the rate at which it is blown back by the flow. Equating the flow velocity into the boundary layer with the wave propagation speed yields

$$M_o = |b_x|. \tag{16}$$

It is important to remember that the wave propagation speed depends only on the normal component of magnetic field and not on its magnitude. The absolute value of b_x is required in the above equation, since a wave can propagate in either direction along the magnetic field. This equation requires that, within the approximation of only small distortions of the external flow, the absolute value of b_x be a constant along the boundary layer. Substituting this result into Equation 15 gives

$$\delta = M_o|y|, \tag{17}$$

or the thickness of the boundary increases linearly with y.

Since the x-type neutral point requires that b_x be an odd function of y, the constancy of the absolute value of b_x implies a discontinuous jump of b_x at the neutral point. This is, of course, unreasonable and indicates that near the neutral point diffusion—and not wave propagation—must be considered.

For the immediate vicinity of the neutral point we will therefore return to essentially the same situation as discussed in the previous section. Equating the flow velocity with the diffusion velocity, we obtain

$$M_o=\frac{c^2}{4\pi\sigma V_A\delta}, \tag{18}$$

which replaces Equation 16 for the neighborhood of the neutral point and may be regarded as specifying the thickness of the boundary layer at the origin.* From the symmetry of the flow pattern, the boundary layer thickness must be an even function of y and therefore constant in the neighborhood of the origin, thus substituting the above value of δ into Equation 15. We obtain

$$b_x=-\frac{M_o^3 8\pi\sigma V_A}{c^2}y, \tag{19}$$

which states that the neighborhood of the neutral point b_x varies linearly with y.

To estimate the extent of the diffusion region, we may ask when the value of b_x, as obtained from its linear slope at the origin, becomes equal to the value required in the wave-dominated region. The length of the diffusion region is therefore given by

$$y^*=\frac{c^2}{8\pi\sigma V_A M_o^2}. \tag{20}$$

Roughly speaking, the boundary is diffusion-dominated for $y<y^*$ and Equations 18 and 19 apply; and it is wave-dominated for $y>y^*$ and Equations 16 and 17 apply. We may note that in terms of the length y^* the flow in the diffusion region is quite similar to the flow calculated in the previous section; that is, apart from a factor of 2, Equations 20 and 12 are identical if y^* and L are interchanged. (This difference is probably related to the use of the magnetic force rather than the pressure gradient.)

The principal effect of including the wave propagation mechanism is to reduce the length over which the diffusion mechanism must operate. Therefore, if the flow velocity is higher than the value given by Equation 12, based on the length of the entire boundary, wave propagation becomes important and the length of the diffusion region is reduced to the value required to accommodate this much flow.

External Flow Field

To analyze the external flow field quantitatively, we will first show that both the magnetic field and the flow field can be solutions of Laplace's equation in this region—in other words, that the flow is irrotational and the magnetic field is current-free. Since we are dealing with a high conductivity medium and are outside of the region of high current concentration (boundary layer), we may neglect j/σ in Ohm's law and obtain the usual frozen flux relation:

$$\mathbf{E}+\frac{\mathbf{u}\times\mathbf{B}}{c}=0. \tag{21}$$

As was mentioned earlier we will make the assumption, to be checked *a posteriori*, that the flow in this region departs only slightly from a uniform flow. Thus we may write

$$\begin{aligned}\mathbf{u}&=u_{xo}(\mathbf{i}+\mathbf{u}'),\\ \mathbf{B}&=B_{yo}(\mathbf{j}+\mathbf{B}'),\end{aligned} \tag{22}$$

where $\mathbf{i}$ and $\mathbf{j}$ are unit vectors in the x and y directions and $\mathbf{u}'$ and $\mathbf{B}'$ are small compared with unity. If we now take the curl of Equation 21 twice, remembering that $\nabla\times E=0$ and using Equation 22 to first order in the primed quantities, we obtain

$$\frac{\partial}{\partial x}(\nabla\times\mathbf{B}')=-\frac{\partial}{\partial y}(\nabla\times\mathbf{u}'). \tag{23}$$

This particular equation is obviously satisfied if both $\mathbf{B}'$ and $\mathbf{u}'$ are curl-free. We must still show that this is consistent with the remaining magnetohydrodynamic equations. For

*We have tacitly assumed that the only dissipation mechanism present is due to finite electrical conductivity. Actually, other mechanisms such as viscosity may also be present. If the kinematic viscosity is larger than $\frac{c^2}{4\pi\sigma}$ viscosity would be the controlling diffusion mechanism at the origin and $\frac{c^2}{4\pi\sigma}$ should be replaced by the kinematic viscosity. The formulas in the remainder of the paper may be regarded as applying directly if the electrical conductivity gives rise to the fastest diffusion. In other cases, the formulas can probably also be applied if $\frac{c^2}{4\pi\sigma}$ is reinterpreted as the appropriate diffusion coefficient.

$\nabla \times \mathbf{B}'=0$ there are no magnetic forces; and therefore the fluid flow equations and the magnetic field equations are decoupled. For the ordinary fluid equations in an incompressible, inviscid two-dimensional flow it is well known that vorticity ($\nabla \times \mathbf{u}'$) is conserved. Therefore, since the vorticity is zero at infinity, it will remain zero throughout the flow field external to the boundary layer. It is therefore consistent with the complete set of equations to assume that both $\mathbf{B}'$ and $\mathbf{u}'$ are curl-free.

If we returned to Equation 21, we would find that this specifies a relation between the potential for $\mathbf{B}'$ and the one for $\mathbf{u}'$. In the present discussion we will consider only the calculation of $\mathbf{B}'$. In the boundary layer analysis Equations 16 and 19 specified the x-component of magnetic field along the y-axis in terms of conditions far from the boundary. This in turn determines $\mathbf{B}'$ in the external flow. Alternatively we may say that, since there are no currents in the external flow, $\mathbf{B}'$ must be related to a change in the current distribution in the boundary. Instead of a boundary layer current per unit length which is independent of y, the boundary layer current will be somewhat reduced near $y=0$ to produce the required x-component of magnetic field at larger values of y. This change in boundary layer current will be small in the same sense that $\mathbf{B}'$ is small. (In order to satisfy the velocity potential required by Equation 21, the boundary layer thickness and velocity would have to depart slightly from the values calculated in the discussion titled "Boundary Layer.")

Since we consider the boundary layer to be thin, we may regard the boundary layer analysis as specifying B_x' along the y-axis. Since $\mathbf{B}'$ satisfies Laplace's equation, this is sufficient to determine B′ everywhere. In order to determine B_x' immediately outside the boundary layer, we note that across the edge of the boundary layer the normal component of magnetic field is conserved; therefore,

$$B_x'+\frac{\mathrm{d}\delta}{\mathrm{d}y}=b_x. \tag{24}$$

The term $\mathrm{d}\delta/\mathrm{d}y$ arises from the fact that the zero order magnetic field has a component normal to the edge of the boundary layer unless $\mathrm{d}\delta/\mathrm{d}y=0$. In the wave-dominated region ($y>y^*$) Equations 16 and 17 specify b_x and $\mathrm{d}\delta/\mathrm{d}y$ as having equal magnitudes M_o; and we obtain

$$B_x'=-2M_o\frac{y}{|y|}, \qquad \text{for } y>y^*. \tag{25}$$

In the diffusion-dominated region b_x varies linearly with y. Although $\mathrm{d}\delta/\mathrm{d}y$ was not specified in this region, it goes from zero at $y=0$ to a value equal to b_x at $y=y^*$. Therefore, it cannot produce a serious error to take $\mathrm{d}\delta/\mathrm{d}y$ as equal to b_x within the diffusion region also. Therefore,

$$B_x'=-2M_o\frac{y}{y^*}, \qquad \text{for } y<y^*. \tag{26}$$

To determine $\mathbf{B}'$, we may now regard the B_x' as specifying a distribution of magnetic sources along the y-axis; and therefore

$$\mathbf{B}'(\mathbf{r})=\frac{1}{\pi}\int_{-L}^{L}\frac{B_x'(\eta)(\mathbf{r}-\boldsymbol{\eta})}{|\mathbf{r}-\boldsymbol{\eta}|^2}\,\mathrm{d}\eta, \tag{27}$$

where $\mathbf{B}_x'$ is given by Equations 25 and 26, $\mathbf{r}$ is the position vector, and η is a dummy integration variable along the boundary. (This formula gives rise to logarithmically divergent values of $\mathbf{B}'$ in the vicinity of the boundary for $r=L$. This is probably not significant, since L is intended only as a measure of the scale of the overall flow field. A more detailed consideration of the flow at very large distances would presumably eliminate this singularity.)

Equation 27 specifies completely the magnetic field in the external flow in terms of the flow velocity at infinity M_o. Coupled with the relations of the discussion titled "Boundary Layer," which define the boundary layer, we therefore have a complete description of the flow in terms of M_o.

In carrying out the analysis, we linearized the external flow. The justification of this assumption depends on $\mathbf{B}'$ being small compared with unity. The largest value of $\mathbf{B}'$ occurs just outside the boundary layer at the origin. Using Equations 25 and 26 to evaluate the integral in Equation 27 at this point, we obtain

$$B_y'(0)=-\frac{2M_0}{\pi}\,\ell\mathrm{n}\left(\frac{L}{y^*}\right), \tag{28}$$

where we have assumed that the logarithm is large compared with unity. The linearization is therefore valid for M_0 sufficiently small.

Maximum Annihilation Rate

The results of "Boundary Layer" and "External Flow Field" state that a consistent solution of the flow field can be obtained for all values of M_0, provided that $B'(0)$ as given by Equation 28 remains small compared with unity. It remains to be seen whether or not larger flow velocities are possible if nonlinear terms in the external flow field are considered. This has not been done in any rigorous sense; however, a rough argument can be given to show that these nonlinear terms would not allow larger flow velocities.

Let us first recapitulate the procedure we have followed thus far. The boundary layer was analyzed assuming that the external flow was completely uniform. This analysis showed that, for large enough flow velocities (such that $y^*<L$), an appreciable x-component of magnetic field was required at the boundary at some distance away from the neutral point. To produce this field, the current in the boundary layer (and what is equivalent, the y-component of magnetic field just outside the boundary layer) had to be reduced at small values of y.

To estimate the effect of the nonlinear terms, we will examine the changes in the boundary layer properties required by the nonuniformity of the external flow. We will find that these changes in turn tend to increase rather than decrease the required nonuniformity.

In the wave-dominated region the decrease in B_y at the edge of the boundary layer leads to a decrease in the flow velocity v along the boundary. The continuity equation therefore leads to a larger value of δ than is given by Equation 17. From Equation 24 this implies that B_x' must be larger than previously and hence that the decrease in boundary layer current near the origin must be larger. On the other hand, since at $y=0$ the flow velocity has increased and the magnetic field has decreased, the length of the diffusion region y^* must decrease. The change in current in the boundary layer therefore tends to be confined to a smaller region. These two facts combine to make the magnetic field just outside boundary layer go to zero more rapidly with increasing M_0 than the linear analysis would indicate.

An absolute limit exists when this field goes to zero, since at this point the boundary layer itself would vanish. The situation may therefore be summarized as follows: (1) solutions exist for $B_y'(0)\ll -1$; (2) $B_y'(0)$ approaches -1 more rapidly than the linear analysis would indicate; and (3) $B_y'(0)$ cannot exceed -1. To determine the maximum allowed flow velocity, we must estimate the largest magnitude of $B_y'(0)$ possible within the above restrictions. We will choose this value somewhat arbitrarily as corresponding to the case in which the linear analysis gives

$$B_y'(0)=-1/2. \tag{29}$$

Substituting this estimate in Equation 28 gives as the limiting flow velocity

$$M_{0_{\max}}=\frac{\pi}{4\,\ell n\left(\frac{L}{y^*}\right)}. \tag{30}$$

It should be pointed out that the uncertainty in $M_{o_{max}}$ is directly proportional to the uncertainty in the estimate used to obtain Equation 29. Equation 30 is, therefore, probably good to a factor of 2 but not much better.

Using Equation 20, we may rewrite Equation 30 in the form

$$\begin{aligned} M_{o_{max}} &= \frac{\pi}{4\,\ell n\left(\frac{8\pi\sigma V_A L}{c^2} M_{o\,max}^2\right)} \\ &= \frac{\pi}{4\,\ell n\,(2M_{o\,max}^2 R_m)}. \end{aligned} \tag{31}$$

This equation gives an explicit relation which determines the maximum flow velocity in terms of the macroscopic flow parameters. It is a fortunate circumstance that this answer depends only logarithmically on the magnetic Reynold's number and is therefore rather insensitive to our ignorance of the effective conductivity of the plasma.

We note by comparing this result with Equation 12 that at large Reynolds numbers the al-

lowed flow velocity is appreciably larger than is obtained from the diffusion analysis. Furthermore, since the allowed flow velocity or annihilation rate decreases only logarithmically with Reynolds numbers, rapid annihilation can be achieved even for extreme conductivities and length scale.

COMPRESSIBLE

The incompressible case discussed in the previous section corresponds to the situation in which the gas pressure is large compared with the magnetic pressure. The case which is of most interest for solar flares is one in which the gas pressure is small compared with the magnetic pressure. In this section we will describe the flow for arbitrary values of this pressure ratio.

Neither the general flow configuration nor the annihilation rate change appreciably as compressibility is considered. The compressible case, however, involves waves with whose properties the reader is probably less familiar. A relatively brief but fairly complete discussion of both small amplitude waves and shock waves in a compressible medium in the presence of a magnetic field has been given by Shercliff (Refence 8). For the present discussion, we will simply notice that the magnetic field configuration shown in Figure 51–3 corresponds to the waves being *switch-off* shock waves. A switch-off shock wave is defined as a shock wave behind which the magnetic field is normal to the wave front (the tangential component is switched off across the shock). From symmetry considerations the magnetic field must be purely in the x-direction between the waves. Since the waves make only a small angle with the y-axis, it is clear that this field configuration corresponds to a shock wave which is almost a switch-off shock.

Switch-off shock waves have the special property that they propagate at a speed equal to the Alfvén speed based on the normal component of the magnetic field. The propagation speed of these shocks is thus the same as it was for the Alfvén wave in the incompressible case. This fact is to a large extent responsible for the rates of annihilation being quite similar throughout the whole region of compressible cases.

The principal difference which does arise is that the density increases across a switch-off shock, and thus the density within the boundary layer, is larger than the density in the external flow. The switch-off shock wave also requires dissipation within the shock front; thus the temperature of the gas within the boundary layer, is also increased. The analysis of the compressible case requires keeping track of density changes, which necessitates including both the energy equation and the x-component of the pressure balance. Neither of these equations was required in our analysis of the incompressible case. A rough consideration of these equations will show that the density may be assumed constant inside the boundary layer, unless radiative cooling is important and occurs in a time scale comparable to the flow time along the boundary.

Since B_y just outside the boundary layer is constant to zero order, the pressure within the boundary layer is constant to the same order. The energy dissipated per unit mass is essentially the magnetic energy per unit mass outside the boundary layer and is therefore also independent of position along the boundary layer. If energy is conserved, this implies a constant temperature and, therefore, density along the boundary layer. If radiative cooling is important, the density would be further increased. If the cooling is such that the gas is cooled to a fixed temperature in a time short compared with the flow time, the density would again be constant. In the more general case, density variations would have to be taken into account.

For the present analysis we will assume a constant density in the boundary layer and define the density ratio α by

$$\alpha = \frac{\rho_0}{\rho_{bl}} \tag{32}$$

where ρ_0 is the density far from the boundary layer and ρ_{bl} is the density within the boundary layer. In the incompressible limit α is, of course, equal to unity. As the ratio of gas to magnetic pressure decreases, α is always less than unity. For a perfect monatomic gas in the limit of zero pressure ahead of the wave,

$\alpha=2/5$ if energy is conserved. For either more internal degrees of freedom or radiative cooling, α would be smaller.

If we assume that α is a known quantity, only minor modifications of the incompressible analysis are required. In what follows we will indicate the required changes. Corresponding equations will be given the same numbers primed.

Modifying the continuity and y-momentum equation to take into account the difference in density inside and outside the boundary layer, we obtain

$$\alpha u_{xo} y = v\delta, \tag{13'}$$

$$\frac{d}{dy}(\rho_o v^2 \delta) = -\alpha \frac{B_{yo} B_x}{4\pi}. \tag{14'}$$

Since the propagation speed of the switch-off shock wave is the Alfvén speed based on the normal component of magnetic field, Equation 16 is unchanged; however Equation 17 is modified to

$$\delta = \alpha M_o |y|. \tag{17'}$$

In the vicinity of the neutral point where diffusion is important, the diffusion velocity of the magnetic field depends on the actual thickness of the boundary layer and therefore Equation 18 is unchanged for the compressible case. However, the modifications of the continuity and momentum equations change Equation 19 to the form

$$b_x = -\alpha \frac{M_o^3 8\pi\sigma V_A}{c^2} y. \tag{19'}$$

Since b_x increases more slowly with y but must reach the same value at large distances from the neutral point, the length of the diffusion region is somewhat increased:

$$y^* = \frac{1}{\alpha} \frac{c^2}{8\pi\sigma V_A M_o^2}. \tag{20'}$$

In the discussion of the external flow in the incompressible case, we first showed that the magnetic field in this region was current-free and was therefore a solution of Laplace's equation. This conclusion is still valid in the compressible case.

If the ratio of gas pressure to magnetic pressure is of the order of unity or greater, the arguments given in the discussion "External Flow Field" apply directly—since the flow velocities described are then small compared with the ordinary sound speed in the gas, and the flow in this region is then essentially incompressible. If the gas pressure is very small compared with the magnetic pressure, the current must again be small since the gas has no inertia. From Equation 21 it follows that along the stagnation streamline the ratio of the change in dynamic pressure to the change in magnetic pressure is of the order of M_o^2. The change in magnetic pressure must therefore occur without forces, and hence the field is current-free to this order. We have thus shown that the magnetic field satisfies Laplace's equation at low gas pressures as well as at intermediate and high gas pressures. We will assume that it does so through the range of gas pressures. The quantitative evaluation of the external flow again follows straightforwardly; Equation 24 is unchanged except for the fact that δ has been changed. Because of this change in δ, Equations 25 and 26 become

$$B_x' = -(1+\alpha) M_o \frac{y}{|y|}, \text{ for } y > y^*, \tag{25'}$$

$$B_x' = -(1+\alpha) M_o \frac{y}{y^*}, \text{ for } y < y^*. \tag{26'}$$

Equation 27, which defines the magnetic field everywhere in the external flow, is unchanged except for the fact that B_x' has been modified. This modification leads to Equation 28 taking the form

$$B_y'(0) = -\frac{(1+\alpha) M_o}{\pi} \ln\left(\frac{L}{y^*}\right). \tag{28'}$$

The estimate of the maximum annihilation rate is still based on the same arguments: namely, that, if the change in magnetic field outside of the boundary layer but near the origin becomes too large, the rate of annihilation in the neighborhood of the neutral point will tend to limit itself. Using the same choice of the limiting values of change of magnetic field as given in Equation 29, we find that the

maximum annihilation rate is defined by

$$M_{o_{\max}}=\frac{\pi}{2(1+\alpha)\,\ln\left(\frac{8\pi\sigma V_A L}{c^2}M_{o_{max}}^2\alpha\right)}$$

$$=\frac{\pi}{2(1+\alpha)\,\ln\,(2M_{o_{max}}^2\alpha R_m)}. \qquad (31')$$

We may note that Equations 31 and 31′ differ only slightly. The predominant change is in the factor outside of the logarithm. Since the density ratio α is necessarily between 0 and 1, the difference over the whole range of compressibility is less than a factor of 2. In view of the accuracy of our estimate of the limiting velocity, this difference probably is not very significant.

APPLICATION TO SOLAR FLARES

The rate of annihilation of magnetic energy calculated in the previous section will now be applied to the conditions presumed to exist in solar flares. Parker has estimated that typical conditions might be a magnetic field strength of 500 gauss over a volume corresponding to a length scale of 10^4 km in a region in which the density is roughly 2×10^{11} particles/cm^3. To account for the energy for a flare, all of the magnetic energy within this volume must be converted to plasma energy in a time of the order of 10^2 to 10^3 seconds. From the rate at which field lines approach the boundary, the time to convert all of this energy can be estimated roughly as L/u_{xo}. In Table 50–1, Parker's results are compared with the results obtained from the present calculation using the above plasma conditions.

TABLE 50–1

Results From:	Conductivity Corresponding to:	Annihilation Time (sec)
Parker	$T=10^4$ °K	5×10^4
	Ambipolar diffusion	6×10^3
Present Observations	$T=10^6$ °K	10^2
		10^2–10^3

The conductivity to be used in estimating these times is somewhat ambiguous. Parker has given cases corresponding to conductivity of a fully ionized plasma at 10^4 °K, as well as an estimate which he considers somewhat dubious in which the conductivity is reduced by ambipolar diffusion under the assumption that the gas is partially ionized. It will be seen that neither of these times is sufficiently rapid to account for the observations. The estimate using the present calculation has been based on a conductivity corresponding to a fully ionized gas at 10^6 °K. This is an overestimate of the actual conductivity and was done merely to illustrate that the annihilation rate is very insensitive to the conductivity and that times which are short enough to account for the observations can be achieved even with extreme assumptions about the electrical conductivity.

The fact that this conductivity is too high is illustrated by the fact that the thickness of the boundary layer in the vicinity of the neutral point as given by Equation 18 for the above conditions is 10^{-4} cm. This is unreasonable, since it is impossible to carry the required current in less than an electron gyro-radius. The electron gyro-radius for an electron having an energy equal to the magnetic energy per particle is about 1 cm. The finiteness of the electron gyro-radius would then decrease the effective electrical conductivity to the point where the boundary layer thickness at the neutral point is at least 1 cm. From Equation 18 this corresponds to a reduction by a factor of 10^4 in the conductivity. The corresponding reduction in annihilation time is only 30 percent. There are probably other effects which reduce the effective conductivity further. However, in view of the insensitivity of the annihilation time to the conductivity, it does not seem fruitful to pursue the subject further in this paper.

A more serious uncertainty in the annihilation time is probably caused by uncertainties in our knowledge of the magnetic field strength density and length scale of the region involved. No attempt will be made to evaluate the accuracy of these estimates. However, it is worth noticing from Equation 31′ that the annihilation time varies directly as the length

scale involved, as the square root of the density, and inversely as the first power of the magnetic field.

In this paper, we have considered only the case in which the magnetic field directions on the two sides of a boundary differ by 180 degrees. This is, of course, a rather special condition which one would not expect to have satisfied in general. There is, however, nothing in the theory which would suggest that the result is particularly sensitive to the angle between the fields. Let us consider briefly the special case in which a magnetic field, perpendicular to the plane of the flow and of equal magnitude on both sides of the boundary, is added. For the case of incompressible flow, the analysis remains completely unchanged and the perpendicular component is uniform throughout the whole flow field. The annihilation rate in that case is therefore unaltered by the addition of this field. It should be remembered, however, that the magnetic energy associated with this field is, of course, not released and that throughout the paper we have used quantities defined in terms of the magnetic field in the plane of the flow. For the compressible case, the perpendicular component of magnetic field would tend to be increased within the boundary layer, thus effectively reducing the compressibility. However, since our result was relatively independent of compressibility, the addition of this magnetic field will probably not have a significant effect in the compressible case either.

In conclusion, the results of this analysis indicate that the rate at which magnetic energy can be converted into plasma energy is sufficiently rapid to account for the observed times in solar flares. The rate at which energy can be released is therefore not a valid criticism of the suggestion that solar flares result from the release of magnetically stored energy.

ACKNOWLEDGMENT

The author is indebted to A. R. Kantrowitz for the initial suggestion that waves might be important in this problem. He also wishes to acknowledge helpful discussions with T. Gold, R. H. Levy, S. Olbert, and G. L. Siscoe.

REFERENCES

1. Sweet, P. A., 1958, *Proceedings of the International Astronomical Union Symposium on Electromagnetic Phenomena in Cosmical Physics*, No. 6 (Stockholm, 1956), p. 123.
2. Sweet, P. A., 1958, *Nuovo Cimento, Suppl.*, 8, Ser. X, 188.
3. Parker, E. N., 1963, *Astrophys. Journal, Suppl.*, Ser. 77, 8: 177.
4. Jaggi, R. K., 1963, *J. Geophys. Res.*, 68: 4429.
5. Furth, H. P., Killeen, J., Rosenbluth, M. N., 1963, *Phys. of Fluids*, 6: 459.
6. Jaggi, R. K., 1963, *these Proceedings*, paper no. 49.
7. Wentzel, D. G., 1963, *these Proceedings*, paper no. 45.
8. Shercliff, J. A., 1960, *J. Fluid Mech.*, 9: 481.

DISCUSSION

Dr. Parker: This is a very interesting idea that Petschek has expressed. By introducing the magnetic field ejecting the fluid, this permits him to confine the diffusion to a very narrow strip about the neutral point. And this is—as I see it, at least—the reduction of the width of that diffusion strip which then gives the enormously enhanced diffusion rates, is that right?

Dr. Petschek: It is the reduction of the width and the reduction of the length which goes with it which allows the fields to go through faster there. But I think the important point is not that the magnetic field ejects the fluid but that, instead of having the change in the magnetic field diffuse into the fluid, it propagates as a wave whose propagation velocity is not limited by the conductivity of the medium.

Dr. Parker: The reason I put it the way I did, still, even in this model, is that the rate at which the fields come together is limited by the diffusion at the neutral point, and you have greatly enhanced that diffusion. The

other way of looking at it is true, too. I am just trying to contrast what has been said before and what you are saying today.

Dr. Petschek: It is limited by the diffusion. However, the wave mechanism allows you to shrink the diffusion region; and, as the conductivity increases, that region shrinks farther and farther. So that the final answer does depend on conductivity, but only logarithmically. The annihilation rate is, therefore, very insensitive to conductivity.

Dr. Meyer: I must confess that I don't quite understand the difference between your picture and the general picture which Sweet and Parker have discussed.

It seems to me that, in the configuration which you draw, the waves do not travel outward but would travel inward until they are curved in such a way that they are just able to do what has been suggested earlier, namely, to pull the fluid out in the direction of the gap with Alfvén velocity.

This, of course, because of the large extension along the gap, limits the velocity of the flow approaching from the sides to a much slower value; and thereby, it seems to me, one comes back to the old picture.

I don't see how your waves travel outward with the Alfvén velocity, which is the point where your picture differs from the old one. It seems to me that, if you start with a configuration as you draw it, they travel inward; and the field assumes a curvature in the stationary case which accelerates the material from the gap outward until it flows with Alfvén velocity.

Dr. Petschek: The fluid inside the boundary is escaping along the boundary at the Alfvén velocity. I don't see at all why you expect the waves to propagate inward. One can set up a steady configuration where they are propagating outward relative to the fluid but are blown back at an equal velocity by the flow so that they stand still.

In the first example I gave, the time-dependent case, you start with a corner in the magnetic field and waves do travel outward from it.

Dr. Meyer: It seems to me the field configuration will have not as sharp a boundary but will be generally curved, and that was the reason I thought the kink has to wander inward One would have not a sharp kink but just a continuous curve.

Dr. Petschek: In drawing the sharp kink, I really put in some ideas from the compressible case. The wave corresponds to compression of the gas, as the density is higher inside the layer than outside. Therefore, the wave corresponds to a shock wave. It is what is called a slow shock in terms of magnetohydrodynamics. These shock waves do steepen to form a discontinuity, so that it would be a sharp edge in that case. The incompressible case is intended as a limit of the compressible case.

Dr. Sweet: I would like to make two points:

One is that I am in favor of your theory, which I thoroughly approve. Dr. Parker and I have been living with this problem for several years and have got the feel of it. Your solution struck me at once as the solution for which we have been seeking.

Secondly, in actual application, a B_z field would be present. It is, therefore, important to know what effect this would have on the rate.

Dr. Petschek: Yes, as far as the B_z field goes, I haven't looked at it in detail, except for one special case mentioned in the written manuscript. In general, I don't see anything in the theory which would make it very sensitive to field orientation.

It was observed by Parker that in the diffusion case you get an appreciably faster rate for compressible, as opposed to incompressible, flow. However, the B_z field tends to make the flow less compressible, so that you lose the gain you had achieved by considering the compressible case. In the present analysis, however, there is not much difference between the compressible and incompressible cases. So that this effect would not be important.

Dr. Wentzel: Most stationary flow theories provide only one time scale, whereas a flare has a rise time and a decay time. It seems to me your model could be well modified to give a rise time equal to the time which it takes to set up your pattern of flow. This time is determined essentially by the hydromagnetic velocity and the size of the region.

Dr. Petschek: I haven't looked at the time it takes to set up this flow. I would imagine that as in most flows it would take a time to establish, which is the time it takes to flow through. In this case, I would take it as the time it takes to go along the boundary layer which, as you said, is essentially the length of the system divided by the Alfvén speed.

Dr. Wentzel: Secondly, I am surprised that the observational people here have not complained of flares which are 100 cm wide theoretically. Somehow one has to adjust a single dissipating plane to the observed, rather than large, flare volume.

Dr. Petschek: This fluid is ejected along the boundary, and where it goes from there I think is completely open. I would expect the gas to spread out and to see luminosity from a much larger region than the boundary. Incidentally, the boundary is only narrow near the neutral point. The standing waves spread at an angle of about one-tenth of a radian, so that the boundary thickness is quite large at the ends of the region.

728-629 O—64——29

N64-30300

51 STABILITY OF THE SOLAR MAGNETIC FIELD IN THE REGION OF FLARES

JAMES W. WARWICK
High Altitude Observatory
Boulder, Colo.

In the past three days we have seen striking evidence for the origin of flares in magnetic fields generated entirely by current systems buried in the photosphere, that is, the potential fields that we heard of earlier from Prof. Gold. The annihilation of magnetic fields in the chromosphere and corona may well be irrelevant to the flare mechanism.

We have heard several times during the meeting about observations of changes in magnetic fields observed on the day of, and the day after, major flares. For example, Hermann Schmidt described his attempt to evaluate the energy changes in the flare region of the solar atmosphere from the magnetic potential energy, and how the time variations of this energy before and after a flare were essentially identical with the time variations of total field energy density, if it is represented by $H^2/8\pi$.

Schmidt argued that his result, which was that the methods gave identical complicated time variations, must mean that the fields didn't vary at all during the particular event, the flare of July 16, 1959.

In regard to this same flare Dr. Howard pointed out that at the 40 gauss level, in the weaker fields of the region, changes were less than the observing limits. On the other hand, Severny and Howard identified changes—that is to say, a weakening of the strong fields in the region—from the day of the flare to the next day.

It is clear that any changes of the strong fields of this region may be easily interpreted in terms of the ordinary variations in spot strengths and field configurations, a phenomenon that has been known for many years.

Mrs. Dodson-Prince showed the complex post-flare loops in the same flaring region. They appeared in absorption against the disk of the sun and were remarkably similar in position and distribution to the filamentary bright structures of the preceding flare.

It would seem as though, in this event, the loops define at their highest point the locus along which lies the bright emission of the flare itself. Each loop has an apparently poloidal shape, if we can infer that they are the same as post-flare loops seen in other events at the limb.

I do not regard this as a structural relation which appears in many flares, but rather as evidence for the stable configuration of the magnetic field shapes from flare to post-flare conditions.

The conclusion to be drawn is that we have negative evidence for changes in field strength or configuration during a major flare.

One further connection with Severny's ideas seems immediate. At the tops of loops, at what apparently is the locus of the bright emission regions of this flare (and of others if we note Prof. Kiepenheuer's talk earlier today), the field is very likely transverse to the line of sight.

If a magnetometer measurement is made at that point, even where the sight line strikes the photosphere, the field is probably transverse. In other words, in this geometry the field will go from positive through zero to negative across the locus of the flare. In fact, this is precisely the region along which flares have been believed to occur, as we heard from Dr. Howard on Monday.

It also may explain Severny's neutral point observations, at least in his earlier papers.

Unlike his conclusions, it seems clear that the field is merely transverse at these points. Furthermore, flares do have bright regions seen occasionally in projection against the umbrae of sunspots so that some, or even large, departures from a simple interpretation of a neutral point configuration are possible in many cases.

We will make only two additional points to this observational conclusion on the constancy of the coronal field before, during, and after flares. Of course, I don't speak to the possibility of a change from 500 gauss to 470 gauss as we heard a few moments ago, nor to the possibility of very small changes. In fact, these would not be detected in the type of observational evidence to which we have just referred.

Concerning the fast particle production during a flare, we know of these particles from their geophysical effects and from the solar radio emission, the latter very difficult to interpret in quantitative terms as far as particle fluxes are concerned. I regard the total production of particles by the flare—as inferred from the terrestrial observations of these particles—as equally difficult to evaluate for many reasons, although we have heard estimates given in the meetings.

From earth-based or even satellite observations of particle fluxes at the distance of the earth we observe only, of necessity, the particles which have escaped from the sun.

Given the apparent complexity and stability of coronal magnetic fields during flares, we should ask how particles escape the sun. It appears very likely that only a small fraction of the total protons produced during a given event actually escapes from the sun. The very large estimate of total flare particle energy made on the basis of earth-based detectors therefore needs to be multiplied by an unknown, but large, factor to account for trapping near the sun. And these regions of trapping, if we may believe the very high association of optical flares with PCA's, are small compared with the radius of the sun.

Furthermore, in the nature of things, we must suppose that the particle losses in these trapping regions occur not only from diffusion out of the trapping region and escape to the earth and interplanetary space, but also from diffusion downward into the solar atmosphere.

It seems to me that we should contemplate the role these fast particles play in the optical phenomena of flares.

What is the role played by the optical phenomena of ejections, sprays, or rising prominences observed in connection with flares? If we assume that a catastrophic process is involved from the point of view of destruction or realignment of magnetic fields, then we can estimate field energy densities from kinetic considerations. An estimate made in this way of the field energy density is not very successful, except for the most violent flare sprays, and is perhaps unrealistic even for them. We remember that loop configurations often persist in the visible structures of these most violent events

It seems to me that a self-consistent role for the eruptive prominences observed during and after flares lies in the readjustment of coronal magnetic fields to fit changes in photospheric current distributions. This readjustment cannot occur impulsively in the coronal plasma but rather in a way dictated by propagation conditions of hydromagnetic shocks or waves.

These move in complex patterns, following the structural complexity of coronal magnetic fields. We can explain the often seemingly "chancy" way in which prominences move and are chosen to move from this point of view.

The escape of particles to the earth does not then relate to the momentary existence of an "open" channel to the earth but to other characteristics of particle motions—for example, their diffusion outward from trapping regions near the sun.

52 SOLAR MAGNETIC FIELDS AND SPACECRAFT OBSERVATIONS*

LEVERETT DAVIS, Jr.
California Institute of Technology
Pasadena, Calif.

The observations of the solar magnetic fields discussed earlier in this meeting were all made in, or near, the photosphere. However, it is the fields at higher elevations, in the chromosphere and corona, that are directly involved in flares. And it is the fields above the flares that govern the escape of energetic particles from the sun and are so important in influencing the radio noise emitted in conjunction with flares. Unfortunately, no direct observations of these magnetic fields have been made, and we must seize upon any indirect clues available. Thus, although the observations made by Mariner II (1962 A–ρ1) between the orbits of the earth and Venus have much less bearing on fields in flares than do observations in the photosphere, I feel that this source of information should not be disregarded completely. It tells us a good deal about the outer boundary conditions for the solar corona at one stage of the solar cycle; and we cannot understand the corona, or phenomena that occur within it, unless we take account of these boundary conditions.

In my own view, the most important observation made by Mariner II was the confirmation by Snyder and Neugebauer that, at this phase of the solar cycle at least, the solar wind blows all the time with a velocity that is usually between 350 and 750 km/sec. It is a universal phenomenon, not merely an intermittent product of disturbances.

Let me describe a tentative model that may explain several features of the Mariner II observations of the solar wind. It will be very surprising if this model turns out to be really correct, but it is the best that I can suggest now; and perhaps consideration of it will guide us to the correct model.

Near the orbit of the earth, the momentum flux of the solar wind is so much greater than the magnetic stresses that the wind dominates the field, blowing where it will and sweeping any field imbedded in it along. But, as one goes in toward the sun, it is easily seen that the magnetic stresses grow more rapidly than does the momentum flux. Somewhere within about 10 or 20 solar radii, the magnetic field comes to dominate the situation. In the lower corona, the gas cannot rise up uniformly to provide the source of the solar wind. Over most of the surface of the sun the gas must be partially held down by being confined within tubes of force, both of whose ends are attached to the sun. Only where the field is relatively regular, fairly weak, and nearly vertical can the gas rise up easily to higher elevations and eventually pull the field lines out. Thus it appears that, as the solar wind carries away the outer corona, the gas which replenishes it may well up from the photosphere over only a few areas and may spread out at higher elevations to fill the upper corona. It would then follow that the magnetic field in the outer corona, which is swept out to interstellar space by the solar wind, would come up through the photosphere in these few areas. The radial component of the solar magnetic field in the solar wind should remain of the same sign over much larger areas of the sun than does the field observed in the photosphere. This model was originally suggested by the Mariner II magnetometer observations, which give some support for this feature of the coronal field. However, alternative interpretations that do not require it are possible.

*This work was supported in part by NASA Grant NsG-426.

At intermediate distances from the sun, the magnetic fields and the momentum of the gas become of comparable importance in determining the motion. The gas sweeps the field lines, but they are still able to influence the gas motions. In this region the tubes of force should resemble nozzles that direct the gas flow. The gas flow in such a nozzle is affected both by its shape and, on Parker's theory of the solar wind, by the temperature distribution along its axis. The temperature distribution is presumably determined by adiabatic expansion, by energy derived from damped waves, and by thermal conductivity which should be mainly along the field lines. Since the temperature distribution resulting from conductivity will be a function of the dependence of the cross section of the tube of force on distance from the sun, nozzles of different shapes should produce solar wind streams of different velocities and densities. Thus the high velocity streams which Snyder and Neugebauer find recurring at 27-day intervals over the same area of the sun may be due to a persistence in the magnetic field configuration. The relatively narrow angular width of these streams seems to require ejection from some kind of nozzle rather than an origin in a local hot spot from which the gas would stream forth in a wide cone with both high velocity and high density.

Finally, this model may provide an explanation of the fact that there is a delay of only about 1 day between the central meridian passage of a plage region and the arrival at the earth of the high velocity jet of solar wind that Dr. Snyder associated with it. From the velocity alone, one would expect a delay of more than 2 days. As Dr. Snyder pointed out in his paper yesterday, co-rotation out to about ½ AU would explain the effect. Indeed, if one allows for the facts that disturbances should propagate outward with the sum of the wind and hydromagnetic wave velocities and that, even beyond the point where there is co-rotation, there is some further motion in longitude because the wind tends to conserve angular momentum, one finds that co-rotation is necessary out to only about ¼ AU. I believe that co-rotation is unlikely to extend this far out. However, if the lines of force are systematically inclined forward near the sun, rather than backward as one might at first expect, it becomes very easy to explain the short delay. An investigation, still in its preliminary stages, of the interaction between the field swept out by the wind and the rotation of the wind about the sun gives some support for the possibility that the lines may be inclined forward. Alternatively, it could be argued that the high velocity gas comes systematically from the leading part of the plage area.

N64 30307

53 PRODUCTION OF GAMMA RAYS AND NEUTRONS IN SOLAR FLARE REGIONS

E. L. Chupp
Department of Physics, University of New Hampshire
Durham, N.H.

An understanding of the processes by which the sun accelerates protons, alphas particles, and other solar constituents has been of considerable interest to cosmic ray physicists and astrophysicists since the first solar cosmic ray event was observed in 1941. Many attempts have been made to extrapolate observations of charged particle fluxes at the earth back to the sun but, since any charged particles accelerated at or near the sun follow tortuous paths in the magnetic fields between the sun and the earth, it is not a straightforward matter to deduce direct information on the source of particles at the sun. It seems clear that it is necessary to first understand the propagation of the charged particles in the interplanetary magnetic fields. In view of this it seems wise to seek other ways to probe conditions at the sun during or shortly after the acceleration process. It is expected that the accelerated protons and other solar constituents will initiate nuclear reactions in the flare region and that neutrons and gamma rays will be byproducts.

Balloon, satellite, and neutron monitors have given a fairly complete picture of the energy spectrum and composition of charged particles emitted by the sun following certain solar flares, and indicate that the energetic particles seen near the earth's orbit are present on some occasions in approximately the same relative abundance ratios as the same species in the solar atmosphere (Reference 1). On the basis of the observations of solar high-energy particles it is also inferred that anywhere from 1 to 50 percent of the flare energy is present in the form of accelerated particles at the sun, or 10^{30} ergs to 5×10^{31} ergs for a flare of total energy 10^{32} ergs. This, in turn, suggests inquiry into the question of the nuclear reactions induced by these accelerated particles in the solar atmosphere during or after the time they were accelerated. Indeed, there is possible direct evidence for the occurrence of nuclear reactions in the solar atmosphere based on the observation of He^3 and tritium in recovered satellite casings (References 2 and 3).

In this note, however, we are interested in estimating the production of neutrons and gamma rays by nuclear reactions at the sun. At the present time there is no experimental evidence for neutron or nuclear gamma ray bursts associated with solar flares, but adequate experiments have not yet been performed. It is expected that these will be accomplished during the coming solar maximum. At the present time, though, it is important to consider the question of the production and detection of the radiations in question so that optimum experiments can be designed. If either are produced in sufficient quantity during a flare to be detected in space satellites or balloons, then we will have new information on processes taking place in a solar flare. Combined with a laboratory knowledge of nuclear reaction yields and solar observation in the visible, ultraviolet, x-ray, and radio frequency ranges, it may be possible to determine the total energy in accelerated particles at the sun. In general, the neutrons and gamma rays will propagate directly from their point of origin. (If the medium is sufficiently dense, the neutrons may scatter somewhat before leaving the solar atmosphere.) In addition, successful detection of either of these neutral radiations would allow accurate determination of the initiation time and duration time for the nuclear processes.

TABLE 53–1

Upper Limit Fluxes for Solar Neutrons and Gamma Rays

Neutrons and Gamma Rays	Flux	Remarks
Neutrons	<0.02 neutron/cm² sec (R. Haymes, *JGR*, 69: 853, 1964).	Balloon flight, quiet solar conditions. Assuming solar neutron spectrum similar to earth's albedo.
Gamma Rays:		
0.51 Mev	<0.6±0.2 photon/cm² sec (K. Frost et al.; *Bulletin AGU*).	OSO I (1962 ζ1) results, quiet solar conditions.
0.51 Mev	<0.1 photon/cm² sec (L. Peterson, *JGR*, 68: 979, 1963).	Balloon flight, quiet solar conditions.
0.51 Mev	0.01 photon/cm² sec	Ranger III (1962 α1), quiet solar conditions.
2.23 Mev	0.03 photon/cm² sec (J. Arnold et al.; *JGR*, 67: 4878, 1962).	
>2.1 Mev	Ranger III flux anomalously high (Ibid.)	

Table 53–1 summarizes the present knowledge on the upper limits for the neutron and gamma ray fluxes. It should be emphasized that we are considering here only the photons of distinct nuclear origin and thus confine ourselves to quantum energies greater than 0.5 Mev— that is, the radiation from β^+–β^- annihilation and nuclear energy levels. Also, the energetic gamma rays from π^0 meson emission are not considered since we feel that the lower energy nuclear gamma rays (0.5 Mev–15 Mev) will be more copious because of the steep flare spectra giving relatively fewer nucleons capable of producing π^0 mesons.

NEUTRON AND GAMMA RAY PRODUCTION

During the time of particle acceleration, our knowledge of the prevailing conditions in the solar atmosphere is very incomplete. For example, it is not now possible to state with certainty the extent of the region where particles are accelerated, the time scale of the process, the injection energies required for acceleration, or even the exact acceleration mechanism. Thus, in order to make any estimates of neutron or gamma ray production, it is necessary to assume some reasonable model for the process.

As mentioned earlier, there is experimental evidence suggesting that all nuclear species present in the solar atmosphere are accelerated. We will assume, for the present, that all species are present after acceleration, in proportion to their normal solar surface abundances. The type of accelerating mechanism generally considered to be operative under the dynamic conditions existing in solar flare regions is the Fermi mechanism (Reference 4). To a first approximation, then, all charged particles will have the same final velocity, independent of their mass and charge; and thus it is expected that all particles would achieve the same final energy per nucleon. A power law energy spectrum follows naturally for this mechanism and gives all charged particles the same energy per nucleon. With these assumptions, an estimate of the relative reaction rates can be made for the accelerated solar constituents bombarding the ambient solar atmosphere. The fraction of solar surface constituents accelerated in a given volume is likely 10^{-7} to 10^{-4}.

Let us denote a process producing a number x gamma rays (or neutrons) by $X\ (a,\ xb)$, where a is any one of the accelerated ions, X is any one of the ambient atoms or ions, and b is either a neutron or gamma ray. If we consider some volume of the solar atmosphere containing the accelerated and unaccelerated species, the average reaction rate for the two species will be

$$\overline{R}=\eta_a\eta_X\sigma[X(a,xb)]\overline{v}_{aX}\ \frac{\text{reactions}}{\text{cm}^3\text{sec}},$$

where η_a=density of accelerated ions a (cm^{-3}),
η_X=density of ambient ions or atoms X (cm^{-3}),
$\sigma[X(a, xb)]$=cross section for the process of interest (cm^2),
v_{aX}=average velocity for a approaching X.

An estimate to the relative reaction rate per unit volume can be made by taking the average energy per nucleon as 100 Mev for a and using the geometric cross section for the total reaction cross section. This procedure gives a simple way of estimating the relative importance of the various reactions giving neutrons and gamma rays. Table 53–2 shows a comparison of the more interesting reactions. η_a and η_X were taken as proportional to their corresponding relative solar surface abundance.

TABLE 53–2

Bombarding Particles (a)	Target Nucleus (X)	Relative Abundances* for X (Si=10^6)	Reaction Weighting Factor	Principal Neutral Emission
P (Abundance 3.2×10^{10}) (Si=10^6)	He^4	3.2×10^9	1	n
	C	1.7×10^7	8×10^{-3}	n, γ
	N	3×10^6	2×10^{-3}	n, γ
	O	2.9×10^7	2×10^{-2}	n, γ
α (Abundance 3.2×10^9) (Si=10^6)	H^1	3.2×10^{10}	1	n
	He^4	3.2×10^9	1×10^{-1}	n
	C	1.7×10^7	1×10^{-3}	n, γ
	N	3×10^6	2×10^{-4}	n, γ
	O	2.9×10^7	2×10^{-3}	n, γ

*Abundances from Fowler et al., *Geophysics Journal*, 6: 148 (1962).

Neutron Production

Consideration of the energetic processes giving rise to neutron production during a solar flare indicates that the processes He^4 (P, xn) and H^1 (α, xn) are most probable. To estimate the absolute yield of neutrons during a flare, we assume that the particles have been accelerated in the region of the flare and then released over 4π steradians. Assuming that one-half of these protons pass into the denser solar atmosphere beneath the flare, the downward flux of protons can be expressed as:

$$F_p=\frac{1}{2}\frac{\sum_a}{\bar{\epsilon}_a}\times\frac{\bar{v}_a}{V_f}\text{ protons/cm}^2\text{-sec},$$

where Σ_a, $\bar{\epsilon}_a$ and v_a are, respectively, the total energy in energetic particles, the average energy of species a, and its mean velocity. V_f is the volume of the flare region occupied by energetic particles. The total neutron production is then $N_T=F_pN_X\sigma dA_fT_b$ neutrons, where d is the effective path length in the solar atmosphere, A_f is the area of the flare region, and T_b is the bombardment time of the dense medium. Using the following values:*

$$\Sigma_a=10^{30}\text{ ergs},\ \bar{\epsilon}_a=100\text{ Mev},\ V_f=6\times10^{28}\text{ cm}^3,$$
$$N_X=10^{11}/\text{cm}^3,$$
$$\sigma=10^{-25}\text{cm}^2, d=2.5\times10^9\text{cm}, A_f=2.5\times10^{19}\text{cm}^2$$

gives $N_T=5\times10^{29}$ T_b neutrons.

The average flux of Mev energy neutrons at the earth is then

$$F_n=f\frac{N_T}{4\pi(R_{AU})^2}\times\frac{1}{\Delta T}$$
$$=f\frac{5\times10^{29}}{4\pi(R_{AU})^2}\frac{T_b}{\Delta T}\text{ neutrons/cm}^2\text{-sec},$$

where f is the fraction surviving due to decay loss and ΔT is a factor of about 10^4 seconds

*These values correspond to a flare similar to that of Feb. 23, 1956, and assume 1 percent of the total energy in fast-charged particles. N_X is based on assuming a total average flare density of $10^{12}/cm^3$ with 10 percent He^4.

corresponding to the spread in time of arrival at the earth for neutrons of energy between 1 and 10 Mev. Using $f=10^{-2}$ gives $F_n=1.8\times10^{-4}\ T_b$; and, comparing with the total equatorial albedo neutron flux (Reference 5) of 0.1 neutron/cm^2-sec, it is seen that T_b must be of the order of 1000 seconds for the solar neutron flux to be comparable with background for the flare conditions cited. It is interesting to note that a solar neutron event at the earth actually may be spread over a time interval long compared with the production time interval at the sun because of the neutron time of flight. This is important in designing an experiment to search for the neutrons and also in interpreting a flare neutron event in the light of conditions at the sun.

Gamma Ray Production

An estimate of the solar flare nuclear gamma ray yield can be made in a manner similar to that for the neutrons. In this case protons bombarding carbon, nitrogen, and oxygen are expected to give the major flare gamma ray source. Taking an average cross section $\sigma_\gamma=1$ barn for 100 Mev protons and an abundance ratio of 3×10^{-3} for gamma-producing nuclei to neutron-producing nuclei gives a flare gamma ray production of $2\times10^{28}\gamma$'s/sec. At the earth this corresponds to ≈5 photons/cm^2-sec. This estimate is for large flares (total energy 10^{32} ergs) which are relatively rare. It is difficult to say just when to expect a flare gamma ray event and it may occur before, during, or after the time of optical maximum. Also, the peak gamma ray intensity may be high in some flares; but the event may be of short duration and thereby give a small total number of gamma rays per cm^2 at the earth.

DETECTION CONSIDERATIONS

To optimize the detection of a neutron or gamma ray flare event, it is necessary to have the sensitivity of detection as high as possible. In addition, the signal-to-noise ratio S/N must be maximized.

The signal certainly can be increased by going closer to the sun. It is not clear, however, what will happen to the noise. One can guess that the sun only puts out neutrons during extreme active periods; and, since the neutron half-life of 11.7 min essentially prevents their coming from anywhere but our sun, the neutrons should be reduced if one is away from planetary atmospheres. Local neutron production from low-energy charged flare particles present when flare neutrons are expected is possible, and this causes an increase in noise which would negate the above statement. This might happen for west limb flares but not for east limb flares, presumably.

Gamma rays, on the other hand, can come from anywhere in the universe; and it is not clear that the gamma ray background can be sufficiently reduced by going into a deep space orbit.

Another important consideration in detector design to optimize the detectability of an event concerns the total number of signal counts—that is, an event cannot be considered statistically significant unless the detector gives sufficient counts over background from a flare event. This, of course, depends on whether the event puts out enough flux; but it can be increased for a given flux by choosing a detector of highest absolute efficiency and largest area.

It also may be possible to infer the rate of emission of gamma rays and neutrons during an event. If this is possible, then in the case of gamma rays the rate and duration time of an event would correspond to the production rate and total time of production at the sun. Because of the time of flight of different energy neutrons, this would not be the case for neutrons. Unless the neutron detector is capable of distinguishing energy, one may not be able to be as specific as in the case of gamma rays.

In summary, the nuclear gamma rays and neutrons are expected to be produced in similar processes and at the same time. It is therefore important to attempt detection of both radiations simultaneously, since there should be a definite time relation between events detected at some distance from the sun.

REFERENCES

1. FICHTEL, C. E., and GUSS, D. E., 1962, NASA, Goddard Space Flight Center Report X-611-62-27.
2. SHAEFFER, O. A., and ZAHRINGER, J., 1962, *Phys. Rev. Letters*, 8: 389.
3. FIREMAN, E. L., et al., 1961, *Phys. Rev.*, 123: 1935.
4. PARKER, E. N., 1957, *Phys. Rev.*, 107: 830.
5. TRAINOR, J., and LOCKWOOD, J. A., 1963, private communications.

Note Added in Proof:

Fireman [Cosmic Ray Conference, Jaipur, India (1963)] suggests that the observed He^3 and T abundance ratios observed in Discoverer satellite casings require that some He^3 be produced in D–D reactions and would, therefore, provide a source of 3 Mev neutrons. Because of the very uncertain abundance of deuterium in the solar atmosphere (if any at all) this possible source is not considered too likely, compared with the reactions discussed here.

N64-30308

54 A PROCESS FOR FLARES*

HUGH CARMICHAEL
Deep River Laboratory, Atomic Energy of Canada, Limited
Chalk River, Ontario

A concept of the solar flare process which I have had in mind for some time (Reference 1) has been considerably strengthened and extended while listening to the papers given at this Symposium and while watching the photographic slides and movies. On the observational side, not many phenomena were noted that could not readily be provided with a plausible explanation in terms of the concept. Indeed, most of the well-known effects—the occurrence of homologous flares, the sudden movements of filaments at the time of a flare, the triggering of other flares by flares, the intimate association of the flare with its "own" filament, the rich variety of flares, the characteristic appearance of the great flares when they start and while they are growing and dying away—seem to fall into place in a very obvious and convincing manner. The concept also permits, as is observed, the occurrence of flares associated with plages of very simple magnetic structure. It may be worthwhile, therefore, to describe the concept to find out whether others consider it a useful hypothesis.

On the theoretical side, it is gratifying to note the progress that has been made in solving the problem of cutting magnetic lines of force in a plasma and allowing them to rejoin into a new pattern to permit the rapid release of the energy associated with a magnetic field. The possibility of an effect of this kind is an essential requirement for the concept about to be described; and the particular variation discussed by Petscheck seems to be very close to what is needed.

An important feature of the concept is that the primary energy involved in flares is the mechanical energy of the solar wind—the magnetic field acts only as a temporary store for this energy. If these ideas are correct, there is no longer any need to postulate esoteric energy sources such as, for example, explosive nuclear processes at the site of the flare; nor is it necessary to destroy or alter the strong chromospheric magnetic field of the sunspot group to provide a source of energy for flares. The magnetic field concerned is being *manufactured* in a continuous manner by the action of the solar wind high above the active region; and from time to time some of it collapses, producing flares and the numerous manifestations that accompany them.

Another feature of the concept is that the energy of the magnetic field, when a collapse occurs, is first utilized in the direct acceleration of particles to rather high energies. The optical flare results from the descent of most of these high energy particles into the chromosphere. High energy particles also may find their way outward or be separately accelerated outward into planetary space. *All* flares are considered to be produced in this manner as a result of the acceleration of particles in the corona and their absorption in the chromosphere.

Further, it is considered that the same primary source of mechanical energy, the solar wind, is itself the agent which propels disturbances from the sun to the earth. These disturbances cause sudden commencement magnetic storms and cosmic ray sudden decreases and may be thought of as expanding balloon-like structures of plasma, containing magnetic fields the large-scale pattern of which is rather well ordered. The condition of the corona in the sector above an active region is probably such that the normal outward streaming of the solar wind is impeded by the magnetic field.

*A contribution offered near the end of the Symposium on the Physics of Solar Flares but not delivered because of lack of time.

A condensation forms in which the coronal temperature becomes enhanced and hence the force tending to expand that sector of the corona becomes very strong.

It follows, then, that the energy associated with a flare is principally the energy initially transferred from the magnetic field to the accelerated particles. The x-ray, optical, radio, and thermal energies in the flare must not be included because they derive from these particles; neither has mechanical energy associated with a plasma disturbance traveling to the earth to be provided—such a disturbance is to be thought of as being *released* at the time of the flare rather than propelled by the flare. On its way to the earth the front of this disturbance, because of the postulated rapid expansion of its balloon-like structure, probably moves faster than the ambient solar wind and so may be expected to generate the relatively weak, and often quite thin, shock needed for the sudden commencement. A rapid expansion of the disturbance is necessary to provide the very wide angle of emission from the active center characteristic of these disturbances.

All this, it must be acknowledged, is only conjecture; and no calculations have been made. Nevertheless, a more precise description of this concept of the flare process now will be given in the hope that some of the main features at least may prove to be correct.

ENERGY FROM THE SOLAR WIND

Let us assume that the energy in flares is derived from the solar wind coming from the region of the plage. Parker gives the power of the quiet sun solar wind in the lower corona as 1.36×10^{28} ergs/sec. The area of an average size plage is $\approx 10^{-3}$ of the solar surface; therefore, above such a plage we have available $\approx 10^{25}$ ergs/sec. Hence, per day ($\approx 10^5$ sec) we have available above the plage an outward mechanical force doing work at the rate of $\approx 10^{30}$ ergs/day. If this energy were accumulated and some of it occasionally released, it would appear to be about enough to maintain the sequences of solar flares that are observed. Furthermore, in plages the outflow of mechanical energy may be greater than that of the quiet sun by a factor of 10 or more, and the area of a large plage may be more than five times what we have assumed. Hence, ample energy would appear to be available from this source for the production of flares.

MAGNETIC STORAGE OF ENERGY

We now note that the solar wind begins rather slowly at the base of the corona and blows outward with increasing velocity as we move upward in the corona. We also note that new plages are bipolar or multipolar magnetic areas above which, in the chromosphere, an arched magnetic field connects between the regions of opposite polarity. We postulate that the relatively weak, high, outermost loops of this magnetic field get caught by the solar wind and are extended up into the corona so that the magnetic system of the plage separates into two parts, as shown in Figure 54–1. The inner part remains unchanged and forms a strong arch between the regions of opposite polarity. The outer part, with the ends of its lines of force anchored in the outer regions of the plage area, forms a sort of mushroom or balloon-like structure, the head of which gradually expands and moves outward from the sun. The structure has two stalks of oppositely directed magnetic field. These stalks lengthen by stretching, but the total magnetic flux through any cross section of a stalk remains constant.

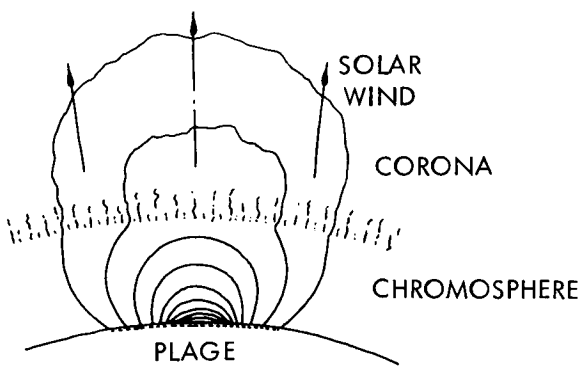

FIGURE 54–1.

Hence there must be creation of a *new magnetic field*. The new field is created and sustained by electric currents induced *locally* in the

coronal plasma. This effect is well known in astrophysics and, in a turbulent plasma, is sometimes called the "spaghetti" process; it is a conversion of kinetic energy into magnetic energy. So, as shown in Figure 54–2, we get two solenoidal currents enclosing newly created, vertical magnetic fields.

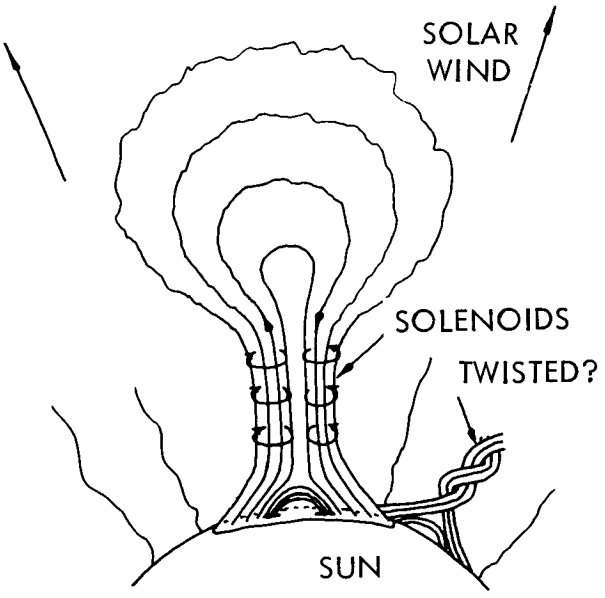

FIGURE 54–2.

ACCELERATION OF PARTICLES

Now, we require only that the above two solenoids be pressed together by twisting or by the surrounding corona (they do not attract each other), and the conditions are provided for a release of some magnetic energy. This release proceeds, as indicated in Figure 54–3, by the shortening of newly joined magnetic field lines from adjacent parts of the two solenoids. It is postulated that this process accelerates particles, or releases particles already accelerated, which then produce the flare. Clearly, energy discharges of different size will occur and the smaller sizes will be much more frequent, as is observed. Also, above magnetically complicated plage regions there may be a long, wandering, laminar interface between the solenoids conducive to more frequent and more energetic flares.

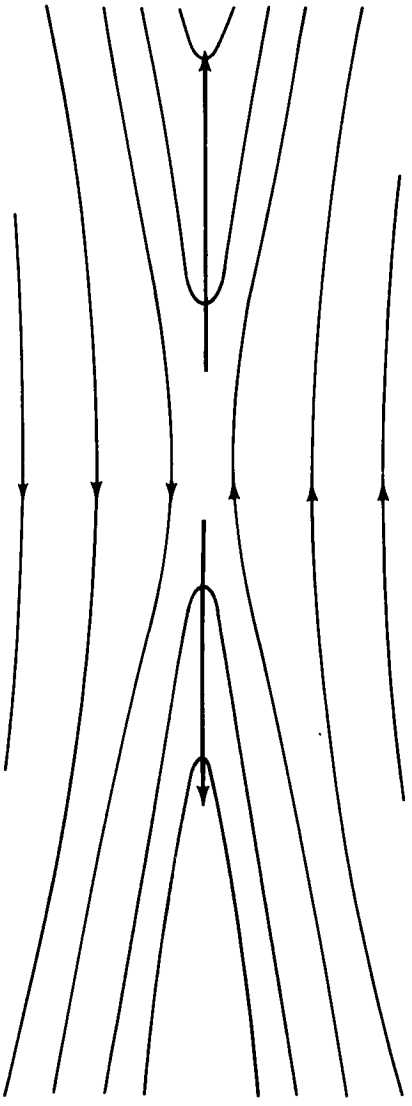

FIGURE 54–3.

The mushroom-like magnetic structure is thought of as having a head, perhaps comparable in size to the size of the sun; and the stalks are thought of as perhaps 10^5 km in diameter and of the order of a solar diameter ($\approx 2\times10^6$ km) in height.

The process by which the particles are accelerated does not have to be identified—all we need say is that the observations seem to require such acceleration. Nevertheless, it is perhaps worth noting that Wild mentioned 10^{35} as the number of electrons needed for the

type III radio bursts. Presumably a comparable number of protons are accelerated. These numbers represent just about all the available charged particles in the volume in which we envisage the acceleration to be taking place, which is quite high up in the corona. Hence the process may be a rather simple electromagnetic process involving a demand for an electric current approaching the saturation value of Swann (Reference 2), $n_o c\ e$, where n_o is the number of ion pairs per cm^3. In this case the particles will be already accelerated before the collapse takes place. In this connection a remark of Nye in the discussion of Wild's paper is suggestive. He said, "The electrons must be monoenergetic; otherwise we would get too much light."

Dr. Wild made the point very strongly that type III bursts need a radially directed magnetic field above the active center, and he thinks of them as starting fairly high in the corona. The postulated process fits those requirements excellently.

APPLICATIONS OF THE CONCEPT

It is possible here to mention only a few of the effects that appear to follow from this concept of the flare process; the reader will find that many other flare effects known to him can readily be fitted into the picture.

The Dark Filament

Dr. Kiepenheuer stressed the great importance of understanding the formation of the dark flare filament which seems to be intimately associated with the subsequent occurrence of a flare. The dark filament may form or become perceptibly darker only 1 hour before a flare takes place. When the flare occurs, sometimes the filament itself brightens, and sometimes bright flare filaments form one on each side of the more permanent dark filament. The dark filament usually seems to lie along a line (sometimes called the *magnetic axis* of the sunspot group) separating the areas of opposite polarity of the plage. This is a region of strong horizontal magnetic field and Kiepenheuer drew a sketch, Figure 54–4, conjecturing that the filament might be supported by dips in the magnetic lines of force, but he did not exhibit much confidence in this idea.

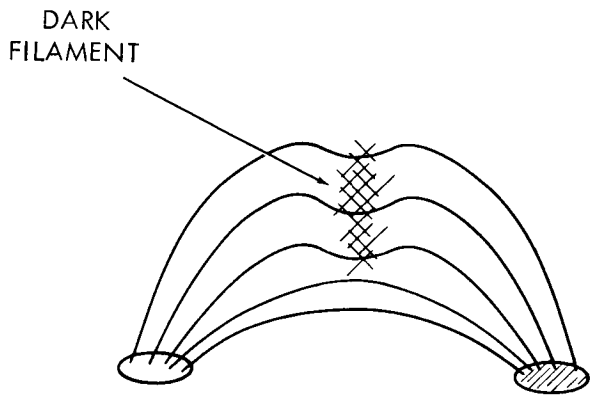

FIGURE 54–4.

In terms of the present concept, the filament is composed of matter falling back toward the the sun from between the vertical magnetic fields formed above the plage. This matter collects in the relatively field-free region that must exist, Figure 54–5, above the strong chromospheric arched field. The filament can remain supported by the underlying arched field and, should it be dissipated, it can readily form again in the same place so long as the same magnetic configuration persists.

The Location and Development of Flares

It is well known that large flares tend to start with the almost simultaneous appearance of several bright points at widely ($\approx$100,000 km) separated places. These points increase in size, slowly at first, then more quickly; and they finally coalesce into two thin bright filaments lying close to, and on each side of, the magnetic axis. The flash phase quickly follows, during which both the area and the brightness of the flare filaments increase rapidly and the Hα emission line undergoes a strong transitory broadening lasting for only a few minutes.

If the flare results from the descent of accelerated particles from a region high in the corona, where the opposed magnetic fields illustrated in Figures 54–2 and 54–3 are touching each other, it is not difficult to account for widely separated, simultaneous starting points and for the subsequent development of the flare in the

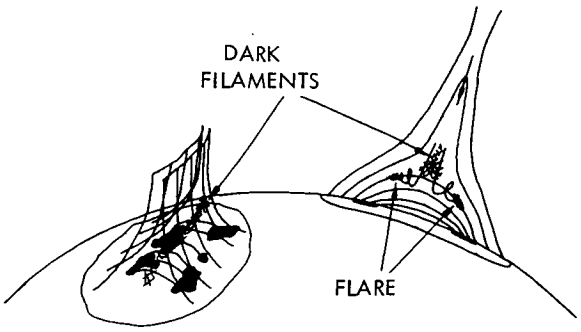

FIGURE 54–5.

form of two expanding and separating bright filaments. High-speed particles might be expected to gyrate down into the stronger underlying fields in just such a pattern and to penetrate into them and expand them as they dissipate their energy.

Occultation of Umbrae

It is reasonable to assume that the energies to which particles are accelerated on different occasions will vary. On some occasions when the energies are low, the particles may only brighten the dark filament or its extensions. Higher energy particles will penetrate farther into the chromospheric fields; on occasions when the energies are very great, particles will spiral into the strong field regions above the umbra of spots. Thus the well-established fact first noted by Mrs. Dodson-Prince that cosmic ray flares tend to cover umbra may be considered as good evidence that flares are indeed produced by accelerated particles.

Hα Broadening

It was mentioned by Dr. Kiepenheuer that the problem of Stark effect, or Doppler effect, as the cause of Hα broadening is not fully resolved. In this connection it is tempting to recall the classic investigations of Meinel showing Hα broadening in the aurora. The chromosphere consists principally of hydrogen atoms, large numbers of which should be knocked on by collisions with the energetic gyrating protons. Can sufficient numbers of hydrogen atoms, moving omnidirectionally with speeds of about 1000 km/sec, exist for a few minutes to explain the transitory broadening of the Hα line?

Disappearing Filaments

Mrs. Dodson-Prince showed how the temporary disappearance of an old filament near an active center at the time of a flare is caused by a downward and upward motion of the filament as a whole.

In terms of the concept we can think of the filament as hanging in the general radial magnetic field of the sun. This field near an active center will be severely distorted suddenly when a magnetic collapse leading to a flare occurs, because this corresponds to the sudden appearance of a large pressure void high in the corona. Hence a strong wavelike disturbance—not necessarily a shock wave—will travel down the magnetic field in which the filament is hanging, and move it down and up like a marionette on a string.

The Moreton Disturbance

The writer saw at the end of this Symposium for the first time the well-known motion picture studies of Moreton. The disturbance propagating across the visible surface of the sun and obviously triggering flares in active regions at a great distance from the original flare did not have the expected appearance of a shock wave, but it is difficult to understand how any other wave could travel at speeds in the 1000 km sec^{-1} range so low in the chromosphere. However, the impression was like looking at a field of grain over which an atmospheric disturbance was passing high in the air above.

In terms of the concept it is possible that a severe magnetic collapse out in the corona at a distance about a solar radius can generate a strong wave disturbance, not necessarily a shock wave, which can propagate with sufficient speed around the sun in the high corona and, on its way, disturb visible structures in the chromosphere in much the same manner as that of the disappearing filament. Also, whenever this wave passes the magnetic stalks above other active regions, it will tend to activate the collapse process and cause flares.

728–629 O—64——30

Type II Outbursts and Explosive Ejections

The ejections which some flares emit, which seem to be correlated with type II radio outbursts, occur while the flare is in progress and seem to be closely associated with the flash phase.

In terms of the concept, we like to think of these phenomena as an aftereffect of the flare process caused by a cutting and detachment of magnetic fields within the volume of the visible flare. This cutting perhaps can be caused by the high energy particles. In any case, once the lines are cut and suitably rejoined, the entrained matter is simply pulled upward by the field to give the characteristic appearance of a luminous cloud leaving the flare.

CONCLUSION

It is realized that the above conjectures probably include theoretically impossible suggestions, and it is also realized that the vast complexity of the phenomena associated with flares has not been sufficiently emphasized. However, the papers of the Symposium indicate that a generally acceptable concept of the flare process does not in fact exist at the present time.

The writer wishes to thank Mrs. Dodson-Prince for many hours of fascinating instruction.

REFERENCES

1. Carmichael, H., 1962, "*High Energy Solar Particle Events*," *Space Science Review*, 1: 28–61, p. 54.
2. Swann, W. F. G., 1962, *J. Phys. Soc. Japan*, 17, Suppl. AIII: 176.

SUMMARY OF A RECENT PUBLICATION BY E. E. DUBOV

Contributed by E. R. Mustel

Prof. Mustel has supplied the following summary of a recent Soviet publication for our use:

E. E. Dubov: *Doclady of Acad. of Sc. of the USSR*, 1963, 150: 1246; and *Izv. of Crimean Astroph. Obs.*, 1963, 29: 86.

It is shown that energy production due to ionization losses of fast particles, originating on the sun, is sufficient to explain flare emission and that the heating of the gas should take place during the relaxation time of energy balance in the flare. The dependence of ionis zation energy losses of fast particles on time is computed on the basis of existing conceptions of the spectra of fast particles. It is shown that this dependence is in agreement with the photometric curves in Hα obtained for flares. It also has been found that the emission increase in the Hα and Lα lines during flares should not be observed simultaneously.

APPENDIX

ATTENDEES AT THE SYMPOSIUM ON THE PHYSICS OF SOLAR FLARES

AARON, JULES
Chief, Radio Astronomy Branch
Air Force Cambridge Research Laboratories

AIKIN, ARTHUR C.
NASA Goddard Space Flight Center

ALEXANDER, JOSEPH K.
NASA Goddard Space Flight Center

ALSMILLER, R. G.
Oak Ridge National Laboratory

ATHAY, R. GRANT
Department of Physics, University of Utah

AXFORD, W. I.
Astronomy Department, Cornell University
Newman Laboratory

BADER, MICHEL
Chief, Physics Branch
NASA Ames Research Center

BAILEY, D. K.
Div. 87, C.R.P.L., National Bureau of Standards

BALLARIO, MARIA CRISTINA
Dottore in Matematica, Osservatorio Astrofisico di Arcetri

BAUER, S. J.
NASA Goddard Space Flight Center

BEHRING, W. E.
NASA Goddard Space Flight Center

BLUM, RONALD
NASA Institute for Space Studies

BOISCHOT, ANDRÉ
Observatoire de Paris, Section d'Astrophysique

BRADT, HALE VAN DORN
Massachusetts Institute of Technology

BRIDGE, HERBERT S.
Massachusetts Institute of Technology

BRUZEK, ANTON
Fraunhofer Institut and Sac. Peak Obs.

CAMERON, A. G. W.
NASA Institute for Space Studies

CHUBB, TALBOT
U.S. Naval Research Laboratory

CHUPP, E. L.
Department of Physics, University of New Hampshire

CLARK, JOHN F.
NASA Headquarters, Code SS

CLARK, LAURENCE H.
U.S. Weather Bureau
National Weather Satellite Center

CLINE, T. L.
NASA Goddard Space Flight Center

COATES, ROBERT J.
Chief, Advanced Development Division
NASA Goddard Space Flight Center

COHEN, MARSHALL H.
Arecibo Ionospheric Observatory

COMBS, SYDNEY S., Major
Kentucky Society

COVINGTON, ARTHUR E.
Radio and Electrical Eng. Division
National Research Council

DAVIS, L. R.
NASA Goddard Space Flight Center

DAVIS, LEVERETT, Jr.
Professor of Theoretical Physics
California Institute of Technology

DE FEITER, L. D.
Observatory, Theoretical Department
Sterrewacht "Sonnenborgh"

DICKINSON, HILLMAN, Major
High Altitude Program Manager, Office of the Secretary of Defense
Advanced Research Projects Agency

DOCKERY, JOHN
c/o Physics Department, Florida State University

DUBERG, JOHN
Technical Assistant to the Director
NASA Langley Research Center

DUBIN, MAURICE
NASA Headquarters

DUNGEY, J. W.
Physics Department, Imperial College

DUNKELMAN, LAWRENCE
NASA Goddard Space Flight Center

DUNN, RICHARD B.
Sacramento Peak Observatory

DYER, EDWARD
National Academy of Sciences

ELGAROY, ØYSTEIN
Institute of Theoretical Astrophysics
University of Oslo

ELSTE, DR.
Astronomy Department, University of Michigan

ELWERT, GERHARD
University of Tübingen

ERICKSON, WILLIAM C.
Physics and Astronomy Department, University of Maryland

ESHLEMAN, VON R.
Stanford University
Radioscience Laboratory

EVANS, JOHN W.
Director, Sacramento Peak Observatory
FAZIO, GIOVANNI G.
Smithsonian Astrophysical and Harvard College Observatories
FELLOWS, ROBERT F.
Chief, Chemistry Program
Office of Geophysics and Astronomy Programs
NASA Headquarters, Code SGC
FICHTEL, CARL E.
Head, Nuclear Emulsion Section
NASA Goddard Space Flight Center
FIHELLY, A.
NASA Goddard Space Flight Center
FIREMAN, EDWARD L.
Smithsonian Astrophysical Observatory
FIROR, JOHN W.
High Altitude Observatory
FIRTH, JOHN
Cambridge University
FLAMM, EILEEN J.
Research Geophysicist
University of California at Los Angeles
FLETCHER, JACK
North American Aviation Corporation
FOELSCHE, T.
NASA Langley Research Center
FREEMAN, JOHN W.
NASA Headquarters
FRIEDMAN, HERBERT
U.S. Naval Research Laboratory, Code 7100
FROST, KENNETH J.
AST Solar Studies
NASA Goddard Space Flight Center
GARWIN, Col.
Director of Technical Services, SCWT
AFSC–SCW Headquarters
Andrews Air Force Base
GERJUOY, EDWARD
Director, Plasma & Space Applied Physics
RCA–DEP, RCA Laboratories
GILL, JOCELYN R.
Chief, In-Flight Sciences
NASA Headquarters, Code SM
GIOVANELLI, R. G.
C.S.I.R.O. Division of Physics,
National Standards Laboratory
GLASER, HAROLD
Office of Naval Research
GOETT, HARRY J.
Director, NASA Goddard Space Flight Center
GOLD, THOMAS
Professor, Director of Center for Radiophysics and Space Research
Cornell University, Newman Laboratory
GOLDBERG, LEO
Professor of Astronomy, Harvard College Observatory
GREENSTADT, E. W.
Space Technology Laboratory
GUSS, DONALD E.
NASA Goddard Space Flight Center
HADDOCK, FRED
Director of Radio Astronomy Observatory
The Observatory, University of Michigan
HAGEN, JOHN P.
Pennsylvania State University
HALLAM, K. L.
NASA Goddard Space Flight Center
HALPERN, RICHARD E.
NASA Headquarters, Geophysics and Astronomy Programs
HARRIS, DAVID
Operations Evaluation Branch
NASA Goddard Space Flight Center
HARVEY, GLADYS A., Mrs.
Assistant Research Officer, Radio and Electrical Engineering Division
National Research Council
HAYASHI, CHUSHIRO
Research Associate of N.A.S., NASA Goddard Space Flight Center
HEDEMAN, RUTH, MISS
McMath-Hulbert Observatory
HEER, RAY R., Jr.
Research Administrator
Air Force Office of Scientific Research
HEPPNER, JAMES P.
NASA Goddard Space Flight Center
HESS, WILMOT N.
Chief, Theoretical Division
NASA Goddard Space Flight Center
HIEI, EIJIRO
Visiting Fellow, Joint Institute for Laboratory Astrophysics
University of Colorado
HIGGINS, PETER
NASA Manned Spacecraft Center
HINTEREGGER, HANS E.
Air Force Cambridge Research Laboratories
HOFFMAN, ROBERT A.
NASA Goddard Space Flight Center
HOFMANN, DAVID J.
Research Assistant, University of Minnesota
HONES, EDWARD W., Jr.
Institute for Defense Analyses
HORSTMAN, HENRY M., Jr.
NASA Goddard Space Flight Center
HOWARD, ROBERT
Mt. Wilson & Palomar Observatories
HULQUIST, BENGT
NASA Goddard Space Flight Center
JAGGI, R. K.
NASA Goddard Space Flight Center
JEFFERIES, J. T.
Joint Institute for Laboratory Astrophysics
JENSEN, CARL
UCLA Institute of Geophysics
JONAH, FRED C.
LTV Astro Division, Lingtemco Vought

JONES, FRANK C.
NASA Goddard Space Flight Center
KALIL, FORD
NASA Goddard Space Flight Center
KASTNER, S. O.
NASA Goddard Space Flight Center
KELLOGG, PAUL J.
Associate Professor, University of Minnesota
KESTER, WILLIAM L.
McDonnell Aircraft Corporation
KIEPENHEUER, K. O.
Direktor des Fraunhofer Institut
KILLEEN, JOHN
Lawrence Radiation Laboratory
KLECZEK, JOSIP
Sacramento Peak Observatory
KREPLIN, ROBERT W.
U.S. Naval Research Laboratory
KRISHNAN, T.
Radio Astronomy Institute
Stanford University
KROOK, MAX
Professor, Harvard University
KUNDU, MUKUL R.
Associate Professor, Astronomy Department
Cornell University
LEIGHTON, ROBERT B.
Professor of Physics, California Institute of Technology
LEVY, RICHARD H.
Principal Research Scientist, AVCO-Everett Research Laboratory
LEWIS, LUNN
Bendix Systems Division
LIDDEL, URNER
Asst. Director and Chief of Sciences, Lunar and Planetary Programs
NASA Headquarters
LINCOLN, J. VIRGINIA
Chief, Radio Warning Services
C.R.P.L., National Bureau of Standards
LINDSAY, JOHN
NASA Goddard Space Flight Center
LINGENFELTER, RICHARD E.
Institute of Geophysics and Planetary Physics
University of California
MAEDA, KAICHI
NASA Goddard Space Flight Center
MALITSON, HARRIET H.
NASA Goddard Space Flight Center
MALKUS, WILLEM V. R.
Professor of Geophysics, University of California
Institute of Geophysics and Planetary Physics
MALVILLE, JOHN M.
Asst. Professor, University of Michigan Observatory
MARAN, STEVE
Department of Astronomy, University of Michigan
MARTENS, C.
Melpar, Inc., Exploratory Research Laboratory
MAXWELL, A.
Project Director, Harvard Radio Astronomy Station
MCCRACKEN, CURTIS W.
NASA Goddard Space Flight Center
MCDONALD, FRANK B.
NASA Goddard Space Flight Center
MEAD, GILBERT
NASA Goddard Space Flight Center
MECHTLY, E. A.
Research Projects Laboratory
NASA Marshall Space Flight Center
MEEKINS, J. F.
Resident Physicist, U.S. Naval Research Laboratory
MEREDITH, L. H.
Chief, Space Sciences Division
NASA Goddard Space Flight Center
MEYER, FRIEDRICH
High Altitude Observatory
MODISETTE, JERRY L.
NASA Manned Spacecraft Center
MOORE, RICHARD L.
Douglas Aircraft Company
MORETON, GAIL
Solar Physics Laboratory
Lockheed California Company
MUSTEL, E. R.
Astronomical Council, U.S.S.R. Academy of Sciences
NAKADA, M. P.
NASA Goddard Space Flight Center
NAUGLE, J.
NASA Headquarters, Code SC
NESS, N. F.
NASA Goddard Space Flight Center
NEUPERT, W. M.
NASA Goddard Space Flight Center
NEWELL, H.
Director, Office of Space Sciences
NASA Headquarters
NEY, E. P.
Physics Department, University of Minnesota
NOBLE, L. M.
Space Technology Laboratory
NORTHROP, T.
University of California
Lawrence Radiation Laboratory
NOYES, J.
Head, Geoastrophysics Laboratory
Boeing Scientific Research Laboratory
OGILVIE, K. W.
NASA Goddard Space Flight Center
OLSON, ROGER H., Lt. Col.
Air Weather Service/ss
Scott Air Force Base
ORRALL, F. Q.
Sacramento Peak Observatory
OSTER, L.
Yale University Observatory

PALMEIRA, R. A. R.
NASA Goddard Space Flight Center
PARKER, E. N.
Institute for Nuclear Studies
University of Chicago
PETERSON, L. E.
University of California at San Diego
PETSCHEK, Harry
Avco-Everett Research Laboratory
PICKEN, J.
Radio Astronomy Institute
PIEPER, G.
NASA Headquarters
PIERCE, A. K.
Associate Director, Kitt Peak National Observatory
PORTER, J. R.
U.S. Naval Research Laboratory
PRINCE, H. D.
McMath-Hulbert Observatory
PURCELL, J. D.
U.S. Naval Research Laboratory
REED, S. G.
Office of Naval Research
REETZ, ARTHUR
Office of Advanced Research and Technology
NASA Headquarters
ROMAN, N.
NASA Headquarters
ROSENBLUTH, M.
General Atomic Division, General Dynamics Corporation
SCHARDT, A.
NASA Headquarters
SCHERB, F.
Assistant Professor of Physics, Massachusetts Institute of Technology
SCHMIDT, H.
Sacramento Peak Observatory
SHAKESHAFT, JOHN
Professor, University of Maryland
SHIPLEY, E. N.
Bellcom Inc.
SHORE, B.
Harvard College Observatory
SMERD, S. F.
Radiophysics Laboratory, C.S.I.R.O.
SMITH, ELSKA
Physics Department, University of Maryland
SMITH, HENRY J.
NASA Headquarters, Code SG
SMITH, SHELDON M.
NASA Ames Research Center
SNYDER, CONWAY
Jet Propulsion Laboratory
SONETT, CHARLES
NASA Ames Research Center
SPREITER, JOHN R.
Chief, Theoretical Studies Branch, Space Studies Division
NASA Ames Research Center
STERN, DAVID
Theoretical Division
NASA Goddard Space Flight Center
STOCKHAUSEN, RALPH
NASA Goddard Space Flight Center
STURROCK, PETER
Institute for Plasma Research, Stanford University
SUEMOTO, Z.
Tokyo Astronomical Observatory
SUGIURA, M.
NASA Goddard Space Flight Center
SWARUP, G.
Tata Institute of Fundamental Research
SWEET, P. A.
The University Observatory, Glasgow
TAKAKURA, T.
Tokyo Astronomical Observatory
TALWAR, S.
NASA Goddard Space Flight Center
TANDBERG-HANSSEN, E.
High Altitude Observatory
TESKE, RICHARD G.
Astronomy Department, University of Michigan
THOMAS, R. N.
Joint Institute for Laboratory Astrophysics
TILLES, DAVID
Astrophysical Observatory
TOUSEY, R.
U.S. Naval Research Laboratory
TOWNSEND, J. W., Jr.
Assistant Director
NASA Goddard Space Flight Center
TSUCHIYA, ATSUSHI
Radio Astronomy Observatory
Ohio State University
UCHIDA, YUTAKA
c/o Princeton University Observatory
VETTE, JAMES I.
Aerospace Corporation
WARWICK, CONSTANCE
Boulder Laboratories
National Bureau of Standards
WARWICK, JAMES
High Altitude Observatory
WASIELEWSKI, E.
NASA Goddard Space Flight Center
WEBBER, D. S.
Manager, Solar Physics Laboratory
Lockheed California Company
WEBBER, W. R.
Physics Department, University of Minnesota
WEDDELL, JAMES
Space and Information Systems Division
North American Aviation, Inc.

WENTZEL, DONAT
University of Michigan Observatory
WHITE, WILLIAM A.
NASA Goddard Space Flight Center
WIDING, K. G.
U.S. Naval Research Laboratory
WILCOX, JOHN M.
Lawrence Radiation Laboratory
WILD, J. P.
Radiophysics Laboratory, C.S.I.R.O.
WILSON, RAYMOND
NASA Headquarters
WINCKLER, J. R.
School of Physics, University of Minnesota
WINCKLER, S.
RCA, Astro-El. Division
WOLFF, C. L.
NASA Goddard Space Flight Center
WOOD, LOWELL
Institute of Geophysics
University of California
ZIRIN, HAROLD
High Altitude Observatory
ZIRKER, J. B.
Sacramento Peak Observatory
ZMUDA, ALFRED
Applied Physics Laboratory
Johns Hopkins University

U.S. GOVERNMENT PRINTING OFFICE: 1964--728-629